Evaluation of technology and energy vector combinations for decarbonising future subsonic long-range aircraft

Swapnil Sarjerao Jagtap

Department of Civil and Environmental Engineering

Imperial College London, United Kingdom

A thesis submitted as fulfilment of the requirements for the Degree of Doctor of Philosophy (PhD) and the Diploma of Imperial College London (DIC), submitted on 27th October 2022

Declaration of originality

The work presented in this thesis is that of the author and is completely original. Contributions made by others is referenced appropriately.

Copyright

Abstract

Global aviation demand and its climate impact are forecast to increase significantly in the next two decades. The broader aim of this thesis is to evaluate aircraft technology and low-carbon energy-vector combination(s) considering lifecycle effects for enabling climate-neutral subsonic long-range flight (14,000 km) of a large aircraft (~300 passengers) – a challenging domain to decarbonise. Firstly, using Breguet's range equation it is observed that liquid hydrogen (LH$_2$) and 100% synthetic paraffin kerosene (SPK) are the only two alternative fuels found suitable for this domain. Using present-day technology, the specific energy consumption (SEC in MJ/tonne-km) of LH$_2$ and 100% SPK aircraft are 11% higher and 0.2% lower relative to Jet-A, respectively. Secondly, a global sensitivity analysis is conducted using the range equation to study the impacts of four technologies – aerodynamics, lighter structures, cryo-tank weight, and overall efficiency (η_o) – on the design-point performance of a tube-wing LH$_2$ aircraft. Relative to the present-day technology, it is observed that for an LH$_2$ aircraft: (i) improving η_o and aerodynamics dramatically improves its SEC; and (ii) using the most optimistic technology development estimates, its SEC improves by 33% requiring a 22% longer fuselage. Thirdly, by using weight sizing methods and GasTurb simulation, it is observed that the SEC of a futuristic BWB aircraft powered by Jet-A, 100% SPK, and LH$_2$ decreases by 47.9%, 48% and 53.5% relative to the present-day Jet-A aircraft, respectively. Lastly, a comparative life-cycle analysis is conducted for these three BWB aircraft while quantifying both CO_2 and non-CO_2 effects. After examining over 100 manufacturing feedstocks/pathways for 100% SPK and LH$_2$, it is observed that only LH$_2$ could enable a climate-neutral long-range flight using fuel manufactured from biomass-based manufacturing unit employing carbon sequestration. The findings of this thesis could guide and enable more informed decision making in future aviation technology development and policy making.

Dedication

I dedicate this thesis to a few special people for their sacrifices. I am indebted to my mother Mrs. Shubhangi Jagtap and father Mr. Sarjerao Jagtap for all their love, support, care, and the sacrifices that they have made while raising and educating me. Also, a ton of thanks to both my elder sisters Dr. Sheetal Jagtap and Dr. Shilpa Jagtap, for their love, teachings, and contributions in my life, and loads of love to my nieces Eshal and Shreenika. I am grateful to my family, relatives, and community.

2022 is India's platinum jubilee year of independence. I am grateful to India's icons Chhatrapati Shivaji Maharaj, Dr. Ambedkar, M. K. Gandhi, and many others for their struggle and contributions to India. As an Indian, I am extremely grateful to all the freedom fighters who laid down their lives for making India independent, and servicemen (army, navy, air force, paramilitary, and police) who got injured/disabled or lost their lives for keeping Indians safe. I am forever grateful to my idols Sardar Bhagat Singh, Rajguru, Sukhdev, Chandrashekhar Azad, Mangal Pandey, and many others who gave supreme sacrifices for the country at a young age so that young people like me could taste freedom, get educated, prosper in life, and live a life that they once dreamt of but couldn't live. This thesis is dedicated to Indians or people of Indian origin located across the world, who have made or are making a name for themselves and for the country through their work.

A significant fraction of this work is based on the methods of Prof. Jan Roskam, who recently passed away. This thesis is also dedicated to him, and efforts are made in this thesis to take forward his legacy in aircraft design.

Acknowledgements

I am extremely thankful to my research supervisors Dr. Marc Stettler and Prof. Peter Childs for shaping me, encouraging me to be more ambitious towards my research, and fostering my all-round development. Both my research supervisors showed faith in me, and my ideas, and abilities. They provided a free and flexible environment which enabled creativity and innovation. Additionally, I am thankful to the President's PhD Scholarship which funded my PhD research. I am also thankful to my lab mates, the Civil and Environmental Engineering department, and everyone at Grantham Institute as I was an aligned doctoral student trainee of the 'Science and Solutions for a Changing Planet', Doctoral Training Partnership, Cohort 5. I am also thankful to Sarah Willis for being super supportive right from the day I made my scholarship and admission application to Imperial College London.

I have enjoyed the competitive and world-class atmosphere at Imperial College London, and this always kept me motivated. The vibes at Imperial College London fostered scientific temper and reasoning, and it enabled problem understanding and problem-solving at both micro and macro scale. My peers, like me, brought in a lot of diversity at Imperial College London. It was not only enriching to engage in a dialogue with such a diverse community, but it also kept on refining me as a global citizen.

I will cherish these four years I spent at Imperial College London for the rest of my life as I have grown both professionally and personally. In 2019, I got a US patent granted as a solo inventor and I went through this techno-legal process without a patent attorney and by raising funds via crowd funding. In 2020, I was

named as one of the 30 innovators, disruptors, and game-changers under the age of 30 by the Forbes Magazine in the 2020 Europe list in the 'manufacturing and industry' category. Additionally, in 2021, I was named in Georgia Institute of Technology's (my alma mater) 40 under 40 list of innovators, trend-setters, and people to watch. Moreover, in 2022, I was recognised in the MIT Technology Review Innovators Under 35 Europe list. I feel both honoured and humbled to be recognised for my PhD research, on these lists of individuals who are positively impacting the world at large. While it is obviously an ecstatic point in my career to be one of the very few individuals who made it to these lists, it is an emotional point as well. I have honestly enjoyed the struggle to reach where I am today, more than the awards. I have had my own fair share of failures and setbacks, but I have never let those stymie my instincts, passion, confidence, and ambitions. I just cannot emphasise the importance of failing – it builds a strong character and resilience. Additionally, this is also a point of acknowledging and thanking the contributions of everyone who have shaped me directly or indirectly – it takes a village to raise a child. When your dreams are big, you are never alone, and it is not just your hard work at play – people hope and root for you, they feel motivated by you. Lastly, such honours and distinctions put more responsibilities on your shoulders and invigorate you to stay focused, consistent, and dedicated towards the betterment and benefit of society and the environment, especially in a post-pandemic era.

The fourth year of my PhD has been the most rewarding year for me as I have worked on a long-time coming pursuit of mine along with my research work – weight loss and body building – which was hard. I am thankful to my friends who kept me motivated during my journey of losing 30 kg weight, especially the weight loss plateaus which are super frustrating to deal with.

I am especially thankful to Braden Lapp for all insightful discussions on aircraft design process. I am thankful to my friends Hitesh Chhabra, Abhinav Gavhane, Urvish Trivedi (Guruji), Sivaramakrishnan Vaidyanathan (SRK), Kshama Krishnan, Sachin Purohit, Sandesh Herekar, Aditya Shetty, Ravi Sikhwal, Vaidhishwaran Ramesh, Prachi Yadav, Shreyas Moolya, Snehal Avhad, Sarthik Shah, and Dr. Snehal Patil for their support and/or being my agony aunts. I am thankful to my friends Rishabh Parakh, Indervir Singh Banipal, Mohamed Asaad, and Ameya Gadiwan for nominating me for several awards. Special thanks to my friends in London – Prashant Nakil, Napameth Phantawesak, Peter Knapp, Carl Thomas, and Ramesh Penugonda, for their help.

I am grateful to my teachers, peers, and colleagues during my school days (at Pune Vidyarthi Griha's Pune Vidya Bhawan, Mumbai), my junior college (SIES, Mumbai), undergraduate institution (K. J. Somaiya College of Engineering, Mumbai), and master's education (at Georgia Institute of Technology, Atlanta), for building a strong foundation and instilling the right values in me. I am especially thankful to my mentors Prof. Sanjay Bhandari, Prof. Ramola Sinha, Prof. Prashant Yelpale, Prof. Ajay Gangrade, Mr. Ananth Anand, Mr. Devendra Shukla, Mr. Anand Khandekar, Mr. Vijay Shekhar, Mr. Ganesh Kohli, Mr. K.P. Singh, Prof. Prasanna Nambiar, Prof. Radhakanta Sarangi, and Prof. Timothy Lieuwen.

Lastly, I am thankful to the Almighty and time for being kind to me.

"तमसो मा ज्योतिर्गमय।"

May the light of knowledge remove the darkness of ignorance.

"विद्यां ददाति विनयं, विनयाद् याति पात्रताम्।
पात्रत्वात् धनमाप्नोति, धनात् धर्मं ततः सुखम्॥"

Knowledge gives humility, from humility one attains character (worthiness), character creates enrichment (wealth), enrichment leads to right conduct, and right conduct brings happiness (contentment).

"न चोरहार्यं न च राज्यहार्यं न भ्रातृभाज्यं न च भारकारि।
व्यये कृते वर्धत एव नित्यं विद्याधनं सर्वधनप्रधानम्॥"

It cannot be stolen by thieves, nor it can be taken away by kings (people with power). It cannot be divided among brothers/siblings and is not heavy to be carried. If spent (or shared) regularly (for the good of society and planet), it always keeps growing. The wealth of knowledge is the most superior wealth of all.

<div align="right">– Verses from the scriptures of Sanātana Dharma (Hinduism)</div>

Table of Contents

List of Figures

List of Tables

17

Nomenclature

A, a, b, c, d and e	Correlation constants for emission index based on hydrogen data		$f/_a$ or FAR	Fuel air ratio
A'	correlation constant for emission index based on Jet-A fuel		FCS	fuel cell systems
APU	Auxiliary power units			
AR	Aspect ratio		FCH	Fuel Cells and Hydrogen
ASTM	American Society for Testing and Materials		FF	Fuel fraction
ATJ	Alcohol-to-jet		FLOPS	Flight optimisation system
B.	Biological plant type		FPR	Fan pressure ratio
BC	Black carbon		FT	Fischer–Tropsch
BCC	Braided carbon composite		g	Acceleration due to gravity
BLI	boundary layer ingestion		GBD	Greener by design
BPR	Bypass ratio		GEMIS	Global Emission Model for Integrated Systems
BWB	blended wing body		GHG	Greenhouse gas
By-product Cl plant	H_2 produced as a by-product of chlorine manufacturing plant		GREET	Greenhouse Gases, Regulated Emissions, and Energy Use in Technologies
CAEP	Committee on Aviation Environmental Protection		GTF	Geared turbofan
C and D	Regression coefficients		GTOW	gross take-off weight
C_D	Total drag coefficient		GWP	Global warming potential
$C_{D,O}$	Zero-lift drag coefficient		h	Lower calorific value
CDM	Corn with dry mill		h'	Flight altitude (in feet)
CDMWE	Corn dry mill with extraction		H	Humidity correction factor
CDMWOE	Corn dry mill without extraction		HEFA	Hydro-processed esters and fatty acids
C_f	Skin friction coefficient		HPC	High pressure compressor
CH_4	Methane		HPT	High pressure turbine
C_L	Lift coefficient		HRJ	Hydro-processed renewable jet fuel
CMC	Ceramic matrix composite		HTE	High temperature electrolysis
CO	Carbon monoxide		HTGR	High temperature gas reactor
CO_2	Carbon dioxide		HTL	Hydrothermal Liquefaction
COG	Coke oven gas		HWB	Hybrid wing body
CORSIA	Carbon offsetting and reduction scheme for international aviation		IATA	International Air Transport Association
C_p	Molar heat capacity at constant pressure		ICAO	International Civil Aviation Organization
CUSM	Corn US mix		IF	Integrated fermentation
C_v	Molar heat capacity at constant volume		IGV	Inlet guide vane
CWEH	Catalytic with external H_2 plant type		ILUC	indirect land-use change
CWHBG	Catalytic with H_2 from biomass gasification plant type		IPC	Intermediate pressure compressor (Booster)
CWIH	Catalytic with in-situ H_2 plant type			
d_f	Fuselage diameter		ISA	International standard atmosphere
e	Oswald's Skin friction coefficient efficiency factor		LBIGCC	Liquefied using electricity from biomass integrated gasification combined cycle
EF	Energy forcing			
EI	Emission index		LCIGCC	Liquification using electricity from coal integrated gasification combined cycle
EPNLdB	Effective perceived noise levels in decibels		LCV	lower calorific value
ERA	Environmentally responsible aviation		LDI	Lean direct injection

l_f	Fuselage length		PTWa	Pump-to-wake
LFW-UDF	laminar-flow wing aircraft using un-ducted fan engine		PV	Photovoltaics
LH_2	Liquid hydrogen		P_3	Combustor inlet pressure (in MPa)
LNGCC	Liquification using power from natural gas combined cycle		R	Aircraft range
LPC	Low pressure compressor (fan)		R'	Universal gas constant
LPP	Lean Premixed Pre-vapourised		RF	radiative forcing
LPT	Low pressure turbine		RFI	Radiative Forcing Index
LTA	large twin aisle		RNG	Renewable natural gas
LTO	landing and take-off		RoC	Rate of climb
LUSME	Liquefication using US mix electricity		RQL	Rich-burn Quick-quench Lean-burn
L/D	lift to drag ratio		RR	Rate of reaction
L-Nuclear	Liquefication using electricity from nuclear energy		S	Wing area
L-Solar	Liquefication using electricity from solar energy		SC	Steam cracking
M	Flight Mach number		SEC	Specific energy consumption
MSW	Municipal solid waste		SELECT	Silent Efficient Low-Emissions Commercial Transport
MTOW	Maximum take-off weight		SFB	Specific fuel burn
MW	Molecular weight		SFC	Specific fuel consumption
$\dot{m}_f$	Fuel consumption rate		SLS	Sea level static
NAFG	North American flared gas		S_L^o	Laminar premixed flame speed
NANG	North American natural gas		SMR	Steam methane reformation
NASA	National Aeronautics and Space Administration		SN	Smoke number
NBC	Non-biogenic carbon		SOEC	Solid oxide electrolysis cell
NH_3	Ammonia		SO_x	Oxides of sulphur
NGL	Natural gas liquid		SO_2	Sulphur Dioxide
nmi	Nautical mile		SPK	Synthetic paraffinic kerosene
NO_x	Oxides of nitrogen		STJ	Sugar-to-jet fuel
N_2O	Nitrous oxide		SUGAR	Subsonic Ultra Green Aircraft Research
OC	Organic carbon		S_{wet}	Aircraft wetted area
OEM	Original equipment manufacturer		$S_{wet, Fuselage}$	Fuselage wetted area
OEW	Operating empty weight		T_{amb}	Ambient temperature (in K)
OH	Hydroxyl radical		TCCW	Thermochemical cracking of water
OML	Outer mould line		TeDP	Turboelectric Distributed Propulsion
OPR	Overall pressure ratio		TET	Turbine entry temperature
O_3	Ozone		TOC	Top of climb
p_{amb}	Ambient pressure (in Pa)		TSEC	Thrust specific energy consumption
p_{total}	Total pressure (in Pa)		TSFC	Thrust specific fuel consumption
PAH	polycyclic aromatic hydrocarbons		T_{total}	Total temperature (in K)
PAX	Passenger		T_3	Combustor inlet temperature (in K)
PEM	Proton exchange membrane		T_4/T_2	Ratio of turbine inlet temperature and fan inlet temperature
PFAD	Palm fatty acid distillate		t/c	thickness to chord ratio
PFR	Plug flow reactor		T/W	Thrust-to-weight ratio
PKT	passenger kilometre travelled		UCO	Used cooking oil
PM	Particulate matter		UHB	Ultra-high bypass ratio
PMC/Al-honeycomb	Polymer matrix composite-aluminium honeycomb core		V	Cruise speed of aircraft
PtL	Power-to-liquid		VLTA	very large twin aisle

VOC	Volatile organic compound
V_∞	Climb flight speed
$W_{aircraft}$	Aircraft weight in cruise
w CS	With carbon sequestration
$W_{F,block}$	Block fuel weight
W_{final}	End of cruise aircraft weight
$W_{Fuselage}$	Aircraft fuselage weight
$W_{F,total}$	Total fuel weight carried at mission start
$W_{initial}$	Initial cruise aircraft weight
W_p	Passenger payload weight
WSR	Well stirred reactor
WTWa	well-to-wake
w/o CS	Without carbon sequestration
α	Diffusive transport of energy (and species)
γ	Specific heat ratio (1.4 for air)
δ_{total}	Pressure correction factor
ΔL	Additional fuselage length for alternative liquid fuels
$\Delta P/P$	Fuel injector air flow pressure drop ratio
λ	Ratio of dry tank weight and cryogenic fuel weight
ω	Weight reduction factor for fuselage weight and OEW
η	Gravimetric index
η_o	Overall efficiency
Φ	Equivalence ratio
ϕ_{H_2}	Hydrogen equivalence ratio
τ	Combustor residence time
θ_{total}	Temperature correction factor
ρ	Fuel density
ρ_a	Density of air at cruise altitude

Chapter 1: Introduction

1.1   Background

The exhaust of an aircraft operating on conventional jet fuel includes: carbon dioxide (CO_2), water vapour, nitrogen oxides (NO_x), carbon monoxide (CO), unburned hydrocarbons, sulphur oxides (SO_x), traces of hydroxyl family and nitrogen compounds, small amounts of soot particles, and normal atmospheric oxygen and nitrogen [1]. Additionally, aircraft are also source of noise. The sustainability of any system is dependent on three fundamental dimensions: social, economic and environmental [2]. Using these three pillars of sustainability, the impacts of aviation sector are discussed below:

- Social:

    In year 2019, 2020 (lockdown year), 2021 and 2022 the aviation industry delivered services to approximately 4.5, 1.8, 2.2 and 3.8 billion passengers (PAX) respectively, and delivered 62, 55, 66 and 68 million metric tonnes of freight respectively [3]. Additionally, aviation has human health impacts (noise and air pollution), especially on community health in the airport vicinity. These human health impacts of aviation are detailed in the next chapter.

- Economic:

    In year 2019, 2020, 2021, and 2022, aviation contributed 838, 382, 506, and 782 billion USDs to the global economy, respectively [3].

- Environmental:

    Conventional jet fuel is manufactured from crude oil/petroleum, which is a resource impact of aviation. In 2019, 2020, 2021, and 2022, the global aviation sector emitted 905, 495, 577, and 809 million metric tonnes of CO_2 respectively, and consumed 360, 197, 227, and 318 billion litres of fuel, respectively [3].

    Aviation has climate change impacts, which can be classified into two categories: CO_2 effect and non-CO_2 effects. CO_2 effect is linearly dependent on the fuel burn. Presently, a Washington DC ↔ New Delhi return air-travel emits similar amount of carbon emissions an average car in the UK/~USA emits on an annual basis (calculated using [4]–[6]). The aviation sector contributes to 2% of the global man-made carbon dioxide (CO_2) emissions [1], [7]–[9]. The non-CO_2 effects comprise of: NO_x emission, sulphur compounds, soot, contrails and cirrus [1], [7]–[11]. The non-CO_2 effects are uncertain, difficult to quantify and complicated, as these are not linearly dependent on fuel burn. The non-CO_2 effects also depend on the atmospheric conditions, aircraft technology, and fuel type.

    Aircraft contrails have a climate impact. Under some meteorological conditions, they can last in the atmosphere in the form of 'cirrus' clouds, which can contribute to climate change. These clouds can have different warming and cooling effects, depending on flight times (night or day) [1], [7]–[11]. Overall, contrails and cirrus clouds have a net warming effect (ibid). Aviation has a greater effect than other sectors because of the altitude at which the emissions are released. The most significant greenhouse gas (GHG) CO_2 does not have any additional impact due to the difference in altitude. However, emissions like NO_x and water vapour can have amplified climate change impact at higher altitudes. During aircraft cruise, NO_x emitted from engine reacts with hydrocarbons/volatile organic compounds (VOC) in the presence of

sunlight to form ozone, which is a GHG [1], [7]–[11]. When non-CO_2 effects and their impacts are considered (including the effect of aircraft induced cirrus), it is estimated that currently aviation contributes to 3.5% of total man-made radiative forcing [12].

The aviation industry anticipates a doubling of air-traffic between 2021 and 2040 [13], despite the COVID-19 pandemic [13], [14] and therefore aviation's total contribution to anthropogenic radiative forcing is forecast to increase by 2050 [1], [7]–[11].

The environmental impacts mentioned above place challenges for the aviation industry to mitigate its climate change impact, while ensuring the supply of required quantity of fuel for the increasing air-travel demand. With rising aviation-related human and environmental health concerns, the aviation industry is exploring paths to make the air-transportation sector more sustainable. To reduce aviation's climate change impacts, the International Air Transport Association (IATA) has set three-goals and a four-pillar strategy to meet these goals [15]. IATA's 3 goals are as follows:

- An average improvement in fleet fuel-efficiency of 1.5% per year from 2009 to 2020 [15];
- Capping net aviation CO_2 emissions (carbon-neutral growth) from year 2020 [15]; and
- 50% decrease in net aviation CO_2 emissions by year 2050 as compared to year 2005 [15].

IATA's 4 pillar strategy comprises:

- Use of advanced technology, including the use of sustainable low-carbon fuels [15];
- Increasing the efficiency of aircraft operations [15];
- Improvements to infrastructure, including advanced air traffic management systems [15]; and
- A single global market-based action for addressing the remaining emissions gap [15].

The industry expectation is that the emission reduction share of the use of low-carbon alternative fuels and improved aircraft technologies to the carbon neutral growth could be 50%, and 30% respectively [16]. Thus, IATA strategies 1 and 2 combined could contribute to 80% of the efforts required for carbon neutral growth. It is to be noted that according to IATA [17], the 'sustainability' evaluation of aviation fuels comprise of life-cycle analysis (net emissions).

In-line with environmentally responsible aviation (ERA) program, National Aeronautics and Space Administration (NASA) initiated the concept of 'N+i' goals to reduce noise, fuel consumption and landing and take-off (LTO) NO_x emissions, and to improve aircraft performance [18]. This will encourage advanced aircraft concepts and technologies along with the use of alternative fuels. These are expected to enter service in a fixed timeframe in future. 'N+i' nomenclature is used to define the sequence of improving aircraft generations, where N specifies the present generation and 'i' represents a specific future generation beyond N (ibid). Each generation is an improvement over the previous one, in terms of LTO NO_x emissions, noise, fuel consumption, and performance.

Considering technology development, regional or short-range air travel could be powered by batteries and/or fuel cells, and medium range flight could be powered by hybrid-electric (battery or turbo) technologies along with fuel cells [19]–[22]. There are low-carbon technologies predicted for future travel, such as Hyperloop, which could be an alternative transport mode for short and medium distance (intra-continental) air-travel. The travel time predicted using Hyperloop is lesser than short and medium distance (range) air-

travel [23]. However, there is no alternative to air-transportation for 'quick' long intercontinental travel. Long-range travel of a large aircraft is a challenging domain to decarbonise as there are few alternative fuels that can match the energy density (both gravimetric and volumetric) of conventional jet fuel [24], [25]. Long-range aircraft are either large twin aisle (LTA) aircraft seating approximately 300 passengers over 14,000 km at design point, such as Boeing 777 and 787, and Airbus A350, or very large twin aisle (VLTA) aircraft seating at least 400 passengers for more than 14,000 km at design point such as Boeing 747 and Airbus A380. Long-range passenger aircraft in the airline operations (range > 5,000 km, seating approximately 250 passengers) contribute to 27% of the global aviation CO_2 emissions [26], [27]. More recent LTA aircraft have enabled 235 new point-to-point routes [28]. During the 2020 COVID-19 lockdown, a number of major airlines retired their VLTAs (A380 and/or B747) [29]–[31]. Therefore, it appears that LTAs will likely be the most common means of intercontinental or long-range travel in the coming decades.

1.2   Objectives

The broader aim and scope of this research is to evaluate future aircraft technologies and alternative fuels, which will be essential to evaluate feasible technology and energy vector combinations for future intercontinental or long-range 300-passenger aircraft (a challenging domain to decarbonise) considering lifecycle effects, towards the goal of sustainable aviation. This aim is in-line with IATA strategy #1 of the four-pillar strategy discussed above within its 'sustainability' definition.

The rationale for this aim is as follows. In the present setup, the aviation-related technology development and regulations are limited only to the use-phase or direct-use of aircraft. The present regulations are for noise and air-quality. In year 2016, International Civil Aviation Organization (ICAO) released CO_2 standard (kg/km) for new aircraft [32]. Moreover, not all alternative fuel pathways are energy efficient (considering the embodied emissions). For example, using the conventional perspective of looking at direct emissions, liquid hydrogen seems to be an excellent candidate for aviation use because of its higher energy density and zero-carbon emissions during aircraft operation, compared to the conventional Jet-A fuel. Using the Greenhouse Gases, Regulated Emissions, and Energy Use in Technologies (GREET) 2021 model [33], it is found that liquid hydrogen (LH_2) from coal has approximately 23 times more CO_2 emissions (g/MJ) compared to Jet-A in the fuel manufacturing phase, and has three times more CO_2 emissions than Jet-A on a lifecycle basis. GREET is a lifecycle assessment tool developed by Argonne National Lab, USA. The embodied energy/emissions associated with alternative fuel production also need to be considered for estimating greener production pathways. In general, a holistic approach needs to be used for evaluating the performance of future aircraft technology and energy vector combinations. In addition, the energy performance of LH_2 powered aircraft could be sensitive to aircraft and cryogenic tank technology [34], and thus requires further quantitative evaluation.

A review study by Pinheiro Melo et al. [35] establishes the need for an integrated methodological framework that should consider life-cycle impacts of aircraft performance towards the goal of sustainable aviation. Such a framework will enable a better understanding of the implications of future technologies considering the three sustainability parameters by coupling different scenarios and examining the interactions

between different designs, spatial differences, and product parameters. Additionally, novel methodologies are required to understand the implications of aviation technologies of the future, beyond the operational phase of the aircraft. Though advanced technologies and alternative fuels could provide solutions for mitigating aviation emissions, there might be new socio-economic and environmental challenges associated with these. Thus, the authors establish the need for diversifying environmental indicators beyond GHG emissions and the need to consider social and economic aspects. According to the authors, this approach can help engineers towards a more sustainable aircraft design and operation.

Considering the discussion so far (high-level research gaps) and above rationale with the defined scope for long-range 300 passenger LTA subsonic aircraft, the research aim can be achieved with the detailed objectives comprising:

1. Quantify the energy performance characteristics of LTA (tube-wing) aircraft powered by the shortlisted alternative fuels and identify the fuels that enable a typical long-range flight within the aircraft's structural limit; and evaluate the off-design energy performance of the LTA aircraft powered by identified alternative fuel(s) which meets the Jet-A design target range,

2. Perform a global sensitivity analysis to evaluate the effects of identified technology parameters for enabling an LH_2 powered long-range travel with an LTA (tube-wing) aircraft, within the maximum take-off weight (MTOW) limit of a baseline Jet-A aircraft,

3. Develop a model for estimating the performance metrics of the future aircraft powerplant using conventional and identified alternative fuels (separately),

4. Develop an operational energy consumption model for the future long-range LTA aircraft powered by conventional and identified alternative fuels (separately),

5. Develop a model for calculating the lifecycle GHG emissions and other unintended impacts mitigation potential of the aircraft technology and alternative fuel combinations. This requires:

    a. Development of a database of manufacturing phase energy, emissions, and materials inventory for identified alternative fuels produced from different pathways.

    b. Evaluation of the aircraft operational phase emissions.

The above five research objectives are high-level and are addressed in separate main chapters (discussed next) where a dedicated literature review is conducted. Each objective is accompanied by sub-objectives that result from the gaps in a literature (reviewed in specific chapters). These sub-objectives are discussed and listed in respective chapters. It is to be noted that the timeframe for 'future' in the overarching research aim and in objectives #3 and #4 get defined in Chapters 2, 5, 6, and 7.

1.3   Structure of thesis

The subsequent chapters of this thesis are organised as follows.

- Chapter 2 includes a comprehensive literature review with a summary of this review. Chapter 2 creates a context for the main research contributions of this thesis (Chapters 4 - 8), particularly with respect to the climate and human health impacts of aviation and solutions to minimise these. It also includes research

addressing the measures included in IATA's four-pillar strategy to mitigate the human and environmental health impacts.

- The overall research philosophy, methodology, and flow of thesis is presented in Chapter 3. This chapter provides a context and perspective to the reader for identifying the research theories or approaches that are employed in the individual research chapters and thesis. Additionally, overall methodology and thesis flow is discussed, with a glimpse of contents of the main research chapters.

- Chapter 4 includes energy performance evaluation of different alternative aviation fuels and helps in the identification of the fuels that enable a typical long-range flight within (tube-wing LTA) aircraft's maximum take-off (MTOW) limit. Chapter 4 addresses research objective #1.

- This is followed by a global sensitivity analysis in Chapter 5 to evaluate the effects of identified technology parameters for enabling a liquid hydrogen powered long-range travel with an LTA tube-wing aircraft, within the MTOW limit of a baseline present-day aircraft. Chapter 5 addresses research objective #2.

- Thereafter, in Chapter 6 engine modelling is presented. Chapter 6 includes the conceptual design methodology for engine performance simulation at on-design and off-design points for conventional jet fuel and identified fuels (separately). Chapter 6 addresses research objective #3.

- Chapter 7 includes the aircraft energy consumption modelling of a future technology aircraft powered by conventional jet fuel and identified fuels (separately), which is part of the conceptual aircraft design phase. Results of Chapters 6 and 7 are used for predicting the future aircraft's fuel consumption in one flight mission. Chapter 7 addresses research objective #4.

- Thereafter, in Chapter 8, lifecycle approach is considered that requires results of Chapters 4 – 7 towards aircraft's use phase energy and emissions. In addition to the results of Chapters 4 - 7, GREET model is used for obtaining the manufacturing phase information for different fuels and their manufacturing pathways, which enables the estimation of GHG emission (both CO_2 and non-CO_2 effects), and other unintended socio-environmental impacts including air quality, water use, and resource impact. Chapter 8 addresses research objective #5.

- The summary, conclusions, and the recommendations for future work from this thesis are included in Chapter 9, along with the limitations and significance of the present thesis.

Chapter 2: Literature review

2.1 Introduction and chapter structure

The literature review in this chapter develops the context for this research. The negative impacts of aviation are first reviewed in sub-section 2.2 to 2.5 to understand the problem at depth. Thereafter, a high-level review of technological solutions is conducted in sub-section 2.6 to 2.12, that could enable minimisation of the said impacts. This literature review is conducted along the lines of IATA's four-pillar strategy to mitigate the human and environmental health impacts of aviation, and it is divided into multiple sections. These are followed by the summary of the literature review.

2.2 Impact of aviation on climate

Aviation has climate impacts through gases and particulate emissions which change the 'greenhouse' properties of the atmosphere [8], [10]. This contributes to climate warming and climate change (ibid). Aviation has climate change impacts via CO_2 and non-CO_2 effects [10]. CO_2 is a key pollutant from aviation, and it is a well understood and quantified GHG. CO_2 has been assigned a 'very high' level of confidence in its share of net anthropogenic forcing (ibid). Aviation also has a number of significant non-CO_2 impacts through its emissions of water vapour, particles, and NO_x; affecting clouds, aerosols and atmospheric composition [8]. The primary metric used for attributing the contribution of the changes that has an impact on the global mean surface temperature is 'radiative forcing' (RF) [watts per square meter (W m^{-2})] [10]. The RF changes are approximately proportional to the anticipated (equilibrium) mean surface temperature changes of the planet. In the case of impacts of soot emission on cirrus cloud formation at high altitudes, both the sign (cooling or warming) and magnitude of the forcing are uncertain (ibid). In the case of impacts of aviation sulphur compound emissions on low-level clouds, even though the sign of the impact is known (cooling), the magnitude is still uncertain (ibid). There is a significant progress made on modelling the impacts of aviation NO_x emission, and the formation and impacts of linear contrails and contrail-cirrus (ibid). Overall, contrails and cirrus clouds have a net warming effect (ibid).

Aircraft NO_x emission causes the formation of atmospheric ozone (O_3), a radiatively active gas (a GHG), via complex atmospheric chemistry. NO_x emissions also result in the formation of the short-lived hydroxyl radical (OH), which is the principal reactant that leads to the removal of ambient methane (CH_4) by about 1-2%. Methane in the atmosphere is primarily from natural sources (e.g., wetlands) and anthropogenic sources (e.g., agriculture and industry). Therefore, the destruction of ambient CH_4 is a negative RF (cooling) and the formation of O_3 is a positive RF (warming). The net NO_x RF term is a combination of these two terms, but overall is a positive RF.

The non-CO_2 pollutants can have both negative and positive RF effects (cooling and warming), though scientific consensus puts the overall non-CO_2 effects of aviation as having a net positive (warming) RF effect, which in terms of RF is thought to be approximately two to three times that of the RF effect from aviation's historical CO_2 emissions [8], [10]. The 'Radiative Forcing Index' (RFI) is defined as the total RF from aviation

divided by the RF from historical aviation CO_2 emissions, and was introduced by the Intergovernmental Panel on Climate Change (IPCC) in their 1999 Special Report, 'Aviation and the Global Atmosphere' [8]. Global warming potential (GWP) is defined as the cumulative radiative forcing (direct and indirect effects) over a specified time period due to the emission of a unit mass of gas related to some reference gas [36]. It should be noted that the RFI is not an emissions metric for comparing effects of equivalent emissions to CO_2, like the GWP [10].

When non-CO_2 effects and their impacts are considered (including the effect of aircraft induced cirrus), it is estimated that currently aviation contributes to 3.5% of total man-made radiative forcing [12]. According to the study by Lee et al. [11], for 2018 the net aviation RF is +149.1 mWm^{-2} (5–95% likelihood range of (70, 229)) where CO_2 (34.3 mW m^{-2}), contrail cirrus (111.4 mW m^{-2}), and NO_x (8.2 mW m^{-2}) are major contributors. Non-CO_2 species cause a net positive (warming) RF that accounts for more than half (77%) of the aviation net RF in 2018.

A study by Grobler et al. [37] calculates aviation's marginal climate and air quality impacts per (metric) tonne of released species and considers the chemical composition, location, and altitude of emissions. The authors calculate the climate impacts using a reduced-order climate model. The study finds that three components are responsible for 97% of climate and air quality damages per unit aviation fuel burn. These are climate impacts of CO_2 at 25%, climate impacts of contrails at 14%, and air quality impacts of NO_x at 58%. The impacts of different air-pollutants and the findings of the study by Grobler et al. in the context of air-quality impacts are discussed next in detail.

2.3   Impact of aviation on air-quality

A review study by Pinheiro Melo et al. [35] establishes the need for diversifying aircraft impact indicators beyond GHG emissions and the need to consider social aspects (such as human health/air-quality). Air quality in the airport vicinity is important because of relatively high concentration of different pollutants which affect human-health. Aviation emissions are responsible for 16,000 premature deaths annually because of damage to the air quality [37]. This is approximately 0.4% of air-quality related premature deaths from all sources [38]. The human health impacts of some of the common emissions are as follows [39]:

a. CO:

At high levels CO causes drowsiness, headaches, slowed reflexes and nausea, and at very high levels it results in death. At low levels it can impair nervous system function and concentration, and it may cause heart pain in people with coronary heart disease.

b. NO_x:

NO_x impairs respiratory cell function, and damage cells of the immune system and blood capillaries. It may aggravate asthma and increase susceptibility to infection. In children, exposure may result in colds, coughs, breathing problems, phlegm, respiratory diseases including bronchitis, and chronic wheezing.

c. Particulate matter (PM):

PM is strongly related with a broad range of symptoms such as colds, coughs, chest pain, asthma, breathing problems, phlegm, respiratory diseases including bronchitis, chronic wheezing, sinus problems,

emphysema, and loss of lung efficiency. As many as 7% of chronic obstructive pulmonary disease and 15% of asthma cases in the urban population are estimated to be possibly associated with prolonged exposure to high concentrations of PM. Long term exposure to PM is associated with high risk of death from lung and heart diseases. It may carry carcinogens such as polycyclic aromatic hydrocarbons (PAHs), therefore may increase the risk of developing cancer.

d. VOC:

This type of pollutant includes thousands of various chemicals, many of which are hydrocarbons. VOC may cause breathing difficulties and skin irritation. Long term exposure to VOC may impair lung function. Many individual compounds are carcinogenic (including benzene). Benzene can cause leukaemia. Those most at risk are people exposed to benzene at work or who live or work in vicinity of vehicle activity.

e. Sulphur Dioxide (SO_2):

SO_2 is associated with chronic bronchitis and causes irritation of lungs. People suffering from asthma are particularly vulnerable and SO_2 exposure of few minutes may trigger an attack. However, the most serious effect occurs when SO_2 is absorbed by PM which is then inhaled deep into the lungs. Inhaling air with high concentrations of SO_2 can release sulfuric acid in the lungs (SO_2 reacts with moisture in lungs to form sulfuric acid). This can result in widespread illness and death. For example, it is likely to have been the main cause of the 4000 deaths during the notorious 1952 London smog.

f. O_3:

Ozone is formed when VOC reacts with NO_x in the presence of sunlight. Ground level ozone reduces lung function in healthy people as well as those with asthma. It may increase susceptibility to responsiveness and infection to allergens such as pollens and house dust mites. It may cause cough, nausea, headaches, chest pain and nose, eye and throat irritation, and loss of lung efficiency; and it increases the likelihood of asthma attacks.

For long-haul aircraft flight missions, the aircraft spends majority of flight time in cruise. Cruise emissions dominate global health impacts attributable to air pollution caused by aviation [37], [40]. The study by Grobler et al. [37] evaluates the air quality-related health impacts using marginal atmospheric sensitivities to emissions from the adjoint of the GEOS-Chem (global chemistry-transport model) along with the value of statistical life and concentration response functions. According to the authors, 64% of all damages are due to air quality impacts and about 90% of the impacts per unit of fuel consumption are due to cruise emissions. Three components are responsible for 97% of climate and air quality damages per unit aviation fuel burn. These are climate impacts of CO_2 at 25%, climate impacts of contrails at 14%, and air quality impacts of NO_x at 58%. The authors found that the air quality impacts of aviation emissions are significantly higher (1.7 to 4.4 times) than the climate impacts per unit of fuel burn. Cruise emissions, which are not regulated currently, should be explicitly considered in policy, and technology and operations development process for mitigating the air-quality impacts of air transportation [40].

Koo et al. [41] performed long-term (greater than one year) simulations with a global atmospheric chemistry-transport model with a focus on population exposure to fine particulate matter ($PM_{2.5}$) and associated risk of early death. Sensitivities relevant to high-altitude and intercontinental PM pollution are estimated for

aircraft emissions. Specifically, the sensitivities of premature mortality risk in different regions to SO_x, NO_x, VOC, CO, and primary $PM_{2.5}$ emissions as a function of location are calculated. They found that NO_x emissions are responsible for 93% of population exposure to aircraft attributable $PM_{2.5}$. Aircraft NO_x accounts for all aircraft-attributable nitrate exposure and 53% of aircraft attributable sulphate exposure due to the strong 'oxidative coupling' between aircraft NO_x emissions and non-aviation SO_2 emissions in terms of sulphate formation (ibid). Of the health risk weighted human $PM_{2.5}$ exposure attributable to aviation, 73% occurs in Asia and 18% in Europe. 95% of the air quality impacts of aircraft emissions in the US are incurred outside the US.

2.4   Environmental cost of aviation

Wolfe et al. [42] model the distribution of environmental damages and net cost from one year of aviation operations. They find that community staying at airport boundaries face damages between $5–16 per person per year from climate damages, and $100–400 per person per year from aircraft noise (in 2006 dollars). The expected damages from air quality depend on the number of operations at the airport. They range from $20 to over $400 per person per year with air quality damages approaching those of noise at high volume airports (ibid). The mean expected air quality and noise damages decay with distance from the airport, but for noise the range of expected damages at a given distance can be high. This depends on the orientation with respect to flight patterns and runways. Damages from climate change caused by aviation dominate those from degradation of local air quality and noise pollution further away from the airport (ibid). However, air-quality damages may exceed those from climate when considering the impact of cruise emissions on air-quality (ibid).

2.5   Systems-level measures and policies

In a study to examine the air-quality impacts of UK airports, Yim et al. [43] estimate that up to 65% of the health impacts of UK airports could be reduced by: desulfurizing jet fuel, avoiding use of auxiliary power units (APUs), electrifying ground support equipment, and using single engine taxiing.

The study by Sgouridis et al. [44] evaluates the impact of policies for reducing the emissions of commercial aviation. These policies include technological efficiency improvements, operational efficiency improvements, use of alternative fuels, demand shift, and carbon pricing (i.e., market-based incentives) (ibid). The evaluation of impacts of the said policies on total emissions, air transport mobility, airfares, and airline profitability, is carried out by using dynamics modelling approach (ibid). It is to be noted that this study takes rebound effect into account. The rebound effect in this case is the induced demand created because of decreasing operating costs (and thus average fares), which in turn stimulates demand (ibid). Sgouridis et al. observed that no single policy can maintain emissions levels steady while increasing projected air-transportation demand (ibid). A combination of policies that includes aggressive levels of operations and technological efficiency improvements, use of biofuels along with moderate levels of carbon pricing and short-haul demand shifts achieves a 140% increase in capacity in year 2024 over year 2004 while only increasing emissions by 20% over year 2004 (ibid). Additionally, airline profitability is moderately impacted (10%

decrease) in comparison with the other scenarios where profitability is reduced by over 50% which can impede necessary investments and the implementation of measures to reduce CO_2 emissions (ibid). A study by Grobler et al. [37] finds that CO_2 emissions, contrails, and cruise NO_x emissions are principal targets for future strategies to mitigate the atmospheric impacts of aviation emissions.

According to the study by Teoh et al. [45], 2.2% of flights contribute to 80% of the contrail energy forcing (EF) in the study region. A selective diversion of 1.7% of the fleet could decrease the contrail EF by up to 59.3% with a negligible penalty (0.014%) in total fuel consumption (and CO_2 emissions). Using a low-risk flight diversion strategy if there is no increase in fuel consumption (CO_2 emissions), then it would decrease contrail EF by 20.0%. Future or advanced engine combustor technologies are predicted to reduce black carbon (BC) particle emissions. Use of such advanced combustor technology could decrease 68.8% contrail EF. A combination of above strategies could decrease the contrail EF by 91.8%.

2.6   Alternative aviation fuels

One of the IATA strategies that can significantly reduce aviation sector's carbon footprint and potentially enable carbon-neutral growth, on a lifecycle or well-to-wake (WTWa) basis (raw material extraction to use of jet fuel in aircraft), is the use of low-carbon fuel [46]. Fuels such as synthetic jet fuel (fossil fuel based, biomass based, and power-to-liquid), hydrogen, natural gas, ammonia, ethanol, and methanol are explored in literature as alternative aviation fuels [47], [48]. Among these fuels, biomass derived jet fuel has been extensively explored in literature. Performance characteristics of an aircraft powered by natural gas, ammonia, ethanol, and methanol, especially for intercontinental travel are less published. These fuels require a separate viability examination for aviation application.

According to the study by Nygren et al. [49], the use of alternative fuels can be helpful in increasing the availability of fuel for growing aviation demand, but it is less likely to provide large contribution, considering that there is work-in-progress in this domain. The possibility of bio-jet fuels replacing conventional jet fuel is limited, but the development of bio-jet fuel is still significant for the future aviation sector (ibid).

On a WTWa basis, some bio-jet fuels have the potential to significantly reduce the GHG emission from the aviation sector, depending on the feedstock type/source [50]. A study by Hileman et al. [51] examines performance of bio-jet fuels based on a first-order approach using the Breguet-range equation. The results from this study show that the fleet-wide (hypothetical) use of pure (100%) synthetic paraffinic kerosene fuels (SPK), like fuels produced from hydro-processing of renewable oil sources or Fischer–Tropsch (FT) synthesis, can decrease aircraft energy consumption (in-flight) by 0.3% (ibid). A study by Blakey et al. [52] reveals that the use of FT-SPK can help in reducing the local air-quality as a result of reduced particulate matter release. Also, the use of correct alternative fuels has the potential to make the aviation sector carbon-neutral (ibid). A study by Daggett et al. [48] provides fuel solutions for the future to reduce the environmental impact of aviation. Daggett et al. propose 50/50 blend of FT-SPK/conventional jet fuel to be used in present day aero engines as a near-term solution; 0-50% HEFA-SPK (hydro-processed esters and fatty acids) with 100-50% FT-SPK to be used in advanced engines like inter-cooled recuperated engines, and ultra-high bypass ratio engines like geared

turbofan engines and un-ducted propfan as a mid-term solution; and LH_2 and/or liquid methane to be used in cryo-fuelled engine as a long-term solution to dramatically reduce aviation sector's GHG emissions (ibid).

Testing by Rolls Royce [22] provides a range of alternative fuels and propulsion technology towards making aviation more sustainable, which are similar to the above literature findings. The alternative fuels comprise of:

a. SPK produced from non-crude oil sources but fossil-fuel sources (typically using FT process)

b. Biomass derived SPKs (using FT, alcohol-to-jet, sugar-to-Jet-And HEFA manufacturing pathways) and

c. Fuel produced from renewable electricity.

In the first kind of alternative fuel, hydrotreated pyrolysis oil (from fossil fuel), coal (coal to liquid), natural gas, and/or flue gas (gas to liquid) are used for producing SPKs typically using FT synthesis [53]. Biofuels (second type of alternative fuel) produced from crops that compete with food are termed as first-generation biofuels, while those produced from non-food crops that require arable land for cultivation are termed as second generation or advanced biofuels. Biofuel produced from algae: a non-food 'aquatic' crop, is termed as third generation biofuel. The third type of alternative fuels comprise of fuels produced from electrochemical synthesis, where the manufacturing process uses electricity produced from renewable sources. Broadly, the third type of alternative fuels can be categorised into carbon-rich and carbon-lean fuels. Power to liquid fuel is a carbon rich fuel, as it is essentially an SPK which is chemically similar to the conventional jet fuel (Jet-A) [54]. Fuels which are rich in hydrogen content fall under the category of carbon-lean fuels. Hydrogen is a clean fuel because its combustion produces only water vapour and small amount of NO_x, and zero carbon emissions (operational phase) [55]. Hydrogen can be used as a fuel in form of compressed gas, LH_2, and hydrides. Methane and ammonia are examples of hydrides. However, it is to be noted that the methane combustion produces carbon emissions, and ammonia combustion cannot be called as a self-sustained combustion process (poor flammability characteristics) and produces higher NO_x [56]–[58]. These aspects will be further discussed in detail in section 2.6.3.1.

Hydrogen is a flexible energy vector, though it has major infrastructure implications [22]. According to Rolls Royce [22], small size and short range aircraft can be powered by hydrogen fuel by using proton exchange membrane (PEM) fuel cells. The range can further be extended by the use of batteries. This system of propulsion has better efficiency than small gas turbine engines and lithium-ion batteries (ibid). Additionally, for medium and long-range aircraft, direct combustion of hydrogen in gas turbine engine is the solution. However, with this system of hydrogen combustion NO_x is produced along with water vapour, which is not the case with fuel cell as it only produces water vapour. Storing hydrogen is a major challenge considering the lower volumetric density of compressed hydrogen gas and LH_2 (ibid). Additionally, all-electric propulsion can power a small aircraft with short range. This is typically a regional and single-aisle aircraft category. Moreover, hybrid-electric aircraft technology could be used for typical medium flight range aircraft, and potentially with its range extended to slightly higher range. Lastly, drop-in SPKs (like biofuels, FT fuel, power to liquid fuel) and hydrogen fuel could be used for medium to long range aircraft applications. 'Drop-in' fuels are the fuels that can be used in current aircraft and/or engines without modifying aircraft hardware [52].

A recent study by the World Economic Forum [25] provides insights into pathways that could make aviation climate neutral. This study explores for alternatives to Jet-A other than SPK. This study finds that for short-range travel, battery–electric aircraft utilising renewable electricity could be less carbon intense than conventional aircraft (<400 km in 2035 and <600 km in 2050). This study points out the need to improve battery life cycles and management, and advance battery-electric aircraft energy density. For medium-range flight, fuel cell (LH$_2$) powered aircraft could provide a low-carbon alternative to Jet-A powered aircraft (<2,000 km in 2035 and <4,000 km in 2050). This study emphasises the need to develop lighter fuel cell systems. Lastly, for long-range travel combustion-based LH$_2$ aircraft could cause lesser climate impacts than Jet-A fuel. Overall, for LH$_2$ as a fuel (fuel cell based and combustion-based), this study points out the need to: accelerate the introduction of green hydrogen, develop low weight cryogenic tanks, and redesign aircraft (not retrofit) for optimised hydrogen performance. Additionally, this study emphasises the need for more detailed research that would improve confidence levels of prediction of climate effect of contrails and mitigation strategies, especially for LH$_2$ fuel. The above findings in terms of technology roadmaps for every (aircraft range and size) domain is similar to Rolls Royce's testing [22].

2.6.1   Biomass derived jet fuels

Not all bio-jet fuels (i.e. fuel from different production pathways) can be directly used in the present aircraft (called 'drop-in' fuels), because some of fuel properties and chemical contents are not same as that of the conventional jet fuel [59]. Some systems within the aircraft are designed considering the properties of conventional jet fuel. For example: The aromatic content of conventional jet fuel causes rubber seals used in the high-pressure fuel system to swell, thereby preventing fuel leakage during aircraft operation at different altitudes; and synthetic paraffin kerosene (SPK) jet fuel cannot be used in neat form (100%) without modifications to aircraft or without addition of synthetic aromatics/additives [59]. The American Society for Testing and Materials (ASTM) has approved four bio-jet fuel pathways which can be used in aircraft as 'drop-in' fuels [60]. These are:

1. FT SPK (FT-SPK) with maximum 50% blend and syngas FT with aromatic alkylation (FT-SPK/A) with maximum 50% blend
2. Hydro-processed renewable jet fuel (HRJ) or HEFA (HRJ/HEFA-SPK) with maximum 50% blend
3. Bio-chem sugars or hydro-processed fermented sugars to synthetic iso-paraffins with maximum 10% blend (also referred to as sugar-to-jet fuel or STJ), and
4. Alcohol-to-jet (ATJ-SPK) fuel with maximum 50% blend (recently revised from 30% blending)

where the blending is done with the conventional jet fuel (ibid). 100% SPK (biomass-based and electro-fuel) is not strictly a drop-in fuel as it has not yet been approved.

A study by Wei et al. [61] reviews different bio-jet fuel types produced from different feedstocks. The authors carry out a comparison of holistic life cycle (WTWa) GHG emission for the fuel type and feedstock combinations, which is summarised in Table 2.1 (also includes use-phase GHG emissions [without the effect of contrails]). The GHG lifecycle analysis is carried out at an industrial level and the GHG emission comprise of following process components:

- Feedstock cultivation, harvesting, and transportation

- Land use effect

- Production and transportation of ancillary chemicals

- Refining

- Transport, distribution, storage, and the combustion of the fuel

Table 2.1. Comparison of GHG emission for the fuel type and feedstock combinations

Use-phase GHG emissions (without the effect of contrails) from GREET 2021 [33]		
Fuel		Use-phase GHG (g CO_2-eq/MJ)
Conventional jet fuel (petroleum)		73.2
100% SPK		70.4
WTWa GHG emissions (information source [61])		
Fuel		GHG (g CO_2-eq/MJ)
Conventional jet fuel (petroleum)		90
Fuel type	Feedstock	GHG (g CO_2-eq/MJ)
FT	Lignocellulose	−1.60 to 18.20
HEFA	Microalgae	27.00 to 38.00
	Camelina oil	3.06 to 53.10
	Waste oils and animal fat	16.80 to 21.40
	Jatropha	33.00 to 40.00
ATJ	Corn grain	47.5 to 117.50
	Sugar cane	−27.00 to 19.70
	Poplar	32.00 to 73.00
	Switchgrass	11.70 to 89.80
STJ	Sugar cane	22.00 to 80.00

Table 2.2. Cost comparison of fuel type and feedstock combinations (information source [61])

Fuel		Cost (€/litre)
Conventional jet fuel (petroleum)		0.47 (in 2018)
Fuel type	Feedstock	Cost MJSP (€/litre)
FT	Lignocellulose	1.24 – 1.51
HEFA	Microalgae	6.36
	Camelina oil	0.33 – 0.92
	Waste oils and animal fat	0.47 – 0.94
	Soybean oil	0.76 – 0.88
	Jatropha	1.1 – 1.15
ATJ	Lignocellulose (thermochemistry)	1.46 – 1.56
	Sugar cane (biochemistry)	0.73 – 1.61
	Corn grain (biochemistry)	0.77 – 1.32
	Lignocellulose (biochemistry)	0.86 – 2.17
STJ	Lignocellulose	3.61 – 4.86
	Sugar cane	1.43

Additionally, the authors carry out a cost comparison of some of the fuel type and feedstock combinations (from Table 2.1) and this is summarised in Table 2.2. It can be observed from Table 2.1 and

Table 2.2 i.e., considering both holistic life cycle GHG emission and fuel cost, that HEFA-camelina oil and HEFA-waste oils and animal fat are the preferred candidates of fuel type and feedstock combinations followed by ATJ-sugarcane (biochemistry) and ATJ-switchgrass (lignocellulose-biochemistry).

Another study by Pavlenko et al. [62] examines different alternative jet fuel types produced from different feedstocks. The authors use three different parameters that measure embodied carbon for a given fuel. The first measure is called direct lifecycle emissions (i.e., WTWa). This is attributable to upstream phase of fuel manufacturing (feedstock production and fuel conversion), transport, and the use-phase of the fuel. The second measure is indirect land-use change (ILUC) that comprises of indirect GHG emissions considering land-use effects. The ILUC emissions are associated with crop-based feedstocks. The ILUC emissions may also be attributable to by-products, waste, and residues if these are deflected from the present utilisation. Such impacts may be significant, especially if the economic relationships of the feedstocks are closely related with vegetable oils (ibid).

Table 2.3. Comparison of complete lifecycle GHG emissions (three measures) and levelized production cost for the fuel type and feedstock combinations (source [62])

Fuel		Carbon intensity (gCO$_2$-eq./MJ)			Approximate wholesale cost (€/litre)
Conventional jet fuel				87	0.4
Fuel type	Feedstock	Direct lifecycle emissions (WTWa)	ILUC emissions	Carbon intensity	Approximate levelized costs of production (€/litre)
		(gCO$_2$-eq./MJ)			
FT	Agricultural residue	6.3	–	6.3	1.75
	Municipal solid waste (MSW)	14.8	–	14.8	1.34
	Power-to-liquids (solar)	1.0	12.5*	13.5	2.35
	Energy crop	11.7	– 12.0	– 0.3	1.87
HEFA	Palm oil	30.8 to 36.5	231.0	216.8 to 267.5	1.01
	Palm fatty acid distillate (PFAD)	19.4	213.0	232.4	0.98
	Soy oil	27.9 to 34.9	150.0	177.8 to 184.9	1.09
	Used cooking oil (UCO)	19.4	–	19.4	0.88
ATJ	Agricultural residue	14.9	–	14.9	2.33
	Corn grain	65.0	14.0	79.0	1.67
	Sugarcane	48.1	17.0	65.1	1.65
	Energy crop	20.3	–	20.3	2.48
STJ	Molasses	47.0	–	47.0	3.85

* emissions attributable to infrastructure required for new renewable electricity generation

The third measure is called carbon intensity, which is a sum of the first and the second measure i.e. sum of direct lifecycle (WTWa) emissions and ILUC emissions [62]. Additionally, the authors carry out a cost comparison of some of the fuel type and feedstock combinations, where they compare the levelized cost of the production process. The levelized cost comprises of capital, feedstock, and operating cost. The comparison of

complete life cycle GHG emissions (three measures) and levelized production cost for the fuel type and feedstock combinations is summarised in Table 2.3.
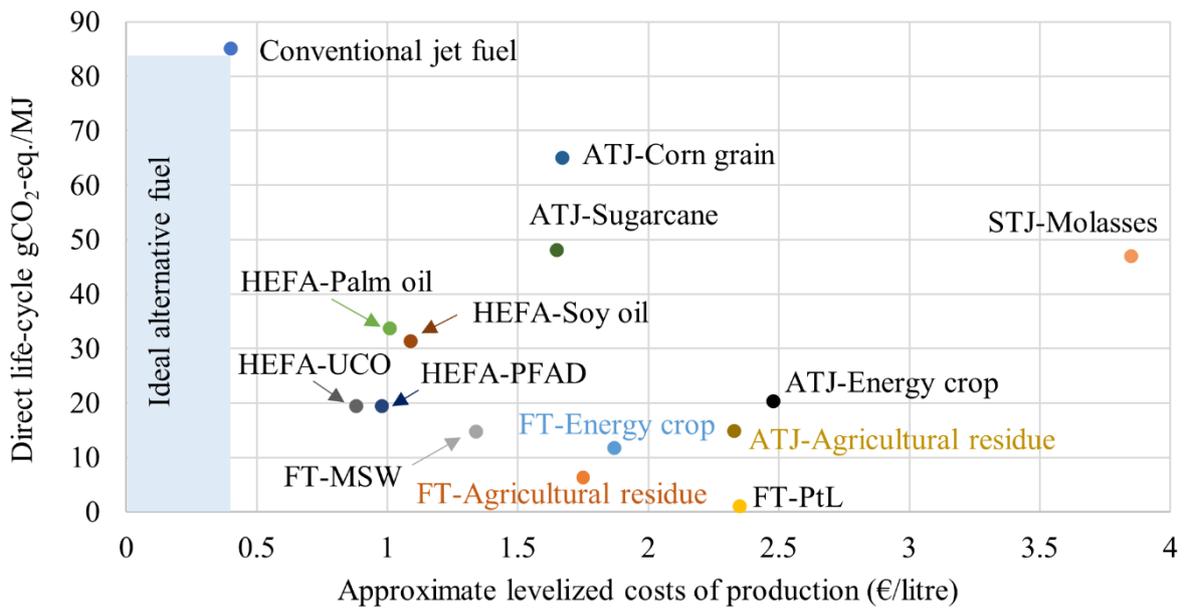
Figure 2.1. Comparison of feedstock and fuel type considering the levelized production cost and (WTWa) direct lifecycle emissions (data source [62])
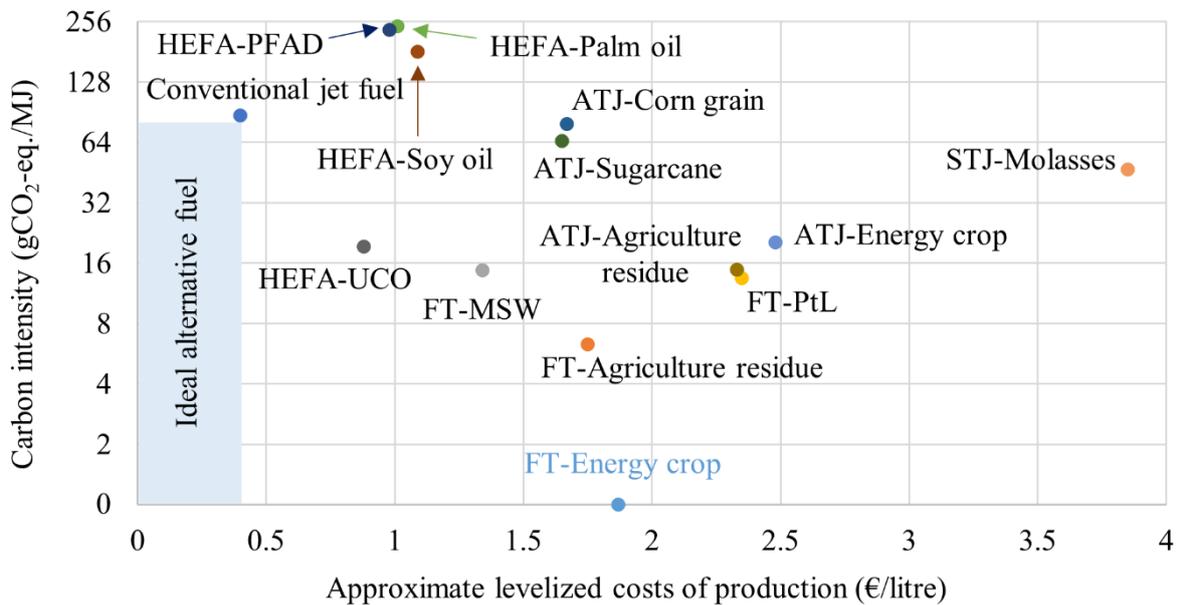
Figure 2.2. Comparison of feedstock and fuel type considering the levelized production cost and carbon intensity (data source [62])

The information in Table 2.3 is important, particularly considering the first and third measure. This information is helpful for analysing the 'sustainability' aspect of bio-jet fuels with the limited feedstocks evaluated in the study by Pavlenko et al. [62]. The levelized production cost and the first measure i.e., direct lifecycle emissions for feedstock and fuel type is analysed through Figure 2.1. Similarly, the levelized production cost and the third measure i.e., carbon intensity for feedstock and fuel type is analysed through

Figure 2.2. Figure 2.2 absorbs the unintended impacts of crop-based feedstocks i.e., ILUC emissions. Typically, ILUC emissions are not calculated in all lifecycle studies. It can be observed from Figure 2.1 and Figure 2.2 that none of the feedstock and fuel type combination fall in the 'ideal alternative fuel zone' (or sustainable alternative fuel zone) i.e., the combination that has lower GHG emission and cost compared to the conventional jet fuel. Referring to Figure 2.1, HEFA-UCO and HEFA-PFAD (food crop) are the preferred candidates of fuel type and feedstock combinations followed by HEFA-palm oil (food crop) and HEFA-soy oil (food crop). After considering the land-use impacts of the crop-based feedstocks i.e., Figure 2.2, particularly for food-crops, HEFA-PFAD (food crop), HEFA-palm oil (food crop) and HEFA-soy oil (food crop) are no longer preferred candidates. Referring to Figure 2.2, HEFA-UCO and FT-MSW are the top two preferred candidates. Figure 2.1 and Figure 2.2, especially the latter convey the importance of a holistic evaluation. Though 'direct lifecycle emission' or WTWa is a holistic measure, it does not capture the unintended impacts of certain feedstocks for fuel production, especially feedstocks that compete with food-crops.

2.6.2   Power-to-liquid fuel

A study by Schmidt et al. [63] demonstrates the development of a relatively novel fuel called 'power-to-liquid' (PtL) jet fuel. Electricity produced from renewable sources like solar and wind energy is used in the electrolysis of water for hydrogen production. After carbon (CO_2) capture, hydrogen and CO_2 undergo chemical process to form hydrocarbon fuel (PtL). This study provides information on different pathways of producing PtL fuel, and it estimates the life cycle GHG from the production pathways. PtL has significantly lower/near-zero lifecycle GHG emission and about 55% lower water consumption compared to conventional jet fuel. It is not currently approved for civil aviation. The lifecycle GHGs of PtL from two paths [54], [63]; are as follows:

  i.   PtL (wind/photovoltaics[PV] in Germany, renewable world embedding) = ~1 g/MJ
  ii.   PtL (wind/PV in Germany, today's energy landscape in material sourcing and construction) = 11 to 28 g/MJ

One of the processes involved in fuel refining is the FT process. It is to be noted that 50% blended FT jet fuel is approved by ASTM, and 50% blend of PtL from FT process can be used directly. It has higher fuel productivity per hectare land compared to all bio-jet fuels. Its thermo-physical and fuel handling properties are like conventional jet fuel, which means that PtL can be potentially used as a 'drop-in' fuel (ibid). This enables status-quo in aircraft powerplants. Presently, it costs 7.3 – 10 times more than conventional jet fuel. Similar information is revealed in the report by the German Environmental agency [54], where details of PtL fuel production, lifecycle GHG, and its current and year 2050 production costs are provided. In 2050, the cost of PtL is predicted to be 1.4 – 4.5 times the cost of conventional jet fuel [54], [63]. Table 2.3 and Figure 2.2 provide the ILUC emissions of PtL. The ILUC emissions are attributable to the infrastructure required for new renewable electricity generation. The direct lifecycle GHG emissions for PtL in future renewable energy landscape is 1 g/MJ and after considering the ILUC emission of 12.5 g/MJ results in a carbon intensity of 13.5 g/MJ for PtL. Referring to Table 2.3, the levelized cost of production of FT-PtL (using future energy landscape) is 5.9 times the present cost of the conventional jet fuel.

2.6.3   Hydrogen as fuel and the physical state of its storage

Hydrogen is a suitable energy storage medium which is carbon free and does not include other impurities [64]. Hydrogen as a fuel was enthusiastically examined during the last fuel crisis. Considering the previously discussed environmental impacts of aviation, hydrogen is again being studied as a long-term energy solution. Hydrogen is a versatile energy carrier and can be produced from a wide range of primary energy sources. It can potentially reduce the geopolitical tensions related to the high concentration of fossil fuel resources in a small geographical area (ibid). Therefore, it can enable a geographically decentralised system of fuel production and supply. Additionally, it can improve the fuel supply reliability for aviation [65]. Because of this versatility, its adoption might lead to a stability in fuel cost [66].

2.6.3.1   Physical state of hydrogen as a fuel

Hydrogen can be stored as: a pressurised gas, a hydride, LH_2, or slush or solid form. Examples of hydride include methane, ammonia, etc. Storage as slush or solid hydrogen demands high energy to sub-cool the fuel and its use only leads to nominal savings in tank volume and weight [66]. Hydrogen storage as a super-saturated (subcooled) liquid can cause high pressure fluctuations inside the tank thereby resulting in heavier tanks. Hydride and gaseous storage are impractical because of the excessive tank weight or volume resulting from carrying a fuel of low energy density per unit volume especially for 'gaseous' hydrogen [66], [67]. A first order evaluation of a small twin aisle aircraft (such as Boeing 767) with a flight range of 5,600 km suggests that LH_2 is preferred over liquid natural gas (LNG), liquid ammonia (LNH_3), ethanol, and methanol [47]. Additionally, LNG combustion releases CO_2, which is not wanted in this exercise. These fuels require a separate viability examination for aviation application. A more detailed examination compared to above, by Verstraete [68], shows that for a long-range (double-decker) aircraft the operational energy consumption reduces by 12% compared to conventional jet fuel operation. Therefore, hydrogen storage as a saturated liquid (LH_2) is preferred for aviation applications requiring a considerable fuel load.

Moreover, hydrides such as NH_3 have higher NO_x emission [56] considering a chemical kinetics viewpoint. NO_x formation by NH_3-air combustion can be understood via three mechanisms: prompt NO_x, thermal NO_x, and fuel-NO_x [57]. For hydrocarbon and hydrogen fuel, the third mechanism, NO_x formation (fuel-NO_x), does not apply because these fuels do not carry 'N' with them. Along with NO_x, the 'N' from the fuel has the potential to also make more nitrous oxide (N_2O) (a strong GHG) compared to other fuels. Additionally, combustion in engine is expected to be a self-sustaining process. NH_3 has low flammability [56] and complete combustion of NH_3 requires presence of a catalyst (viz. platinum). Experimental studies for NH_3 combustion are usually carried out in the presence of hydrogen [58] or CH_4, as these fuels increase the flame properties (radical and heat diffusion, flame speed, increases flammability of mixture etc.). Additionally, future combustors are expected to burn in fuel-lean region and NH_3 combustion in this regime results in higher NO_x formation [58]. Moreover, there are ultra-low NO_x combustors (compared to conventional jet fuel) such as 'lean direct injection' and 'micro-mix' combustors designed for combustion of hydrogen [64]. Therefore, LH_2 is the preferred form of storing hydrogen for aircraft use.

2.6.3.2 *LH₂ as aviation fuel*

LH_2 as an aviation fuel comes across as an interesting candidate, primarily because of its higher energy density (lower calorific value [LCV]) of 120 MJ/kg compared to conventional jet fuel's LCV of 43.2 MJ/kg [55], and because hydrogen combustion does not release emissions like CO_2, CO, VOC, PM, BC and organic carbon (OC), and SO_x during direct-use. The high energy density of LH_2 for aviation applications can be extracted via two ways: fuel cell powered and gas turbine engine powered aircraft. The study by Ashcraft et al. [18] finds that fuel-cells are unlikely to be ready for completely powering propulsion systems on large aircraft by year 2035 but they are more likely to be used for augmenting a primary power source. The fuel cell specific power metrics are typically reported for fuel cell stacks [69]. The specific power for fuel cell systems (FCS) includes important supporting and/or auxiliary components. This is based on the stack or site-specific requirements, e.g., hydrogen-, air-, water-, heat-, and system-management. They are integrated into a comprehensive fuel cell system package. FCS performance is based on the functioning of non-stack systems. In terms of modelling energy systems, FCS specific power is used. In a study by Delgado Gosálvez et al. [70], a small LH_2 fuel cell powered regional aircraft called the 'Greenliner' is designed. The range of 'Greenliner' is 500 nautical mile (nmi) or 926 km and it seats 19 passengers. The authors have assumed a specific power capacity for the FCS similar in magnitude (2.72 kW/kg) as that of the fuel cell stacks used in latest fuel cell powered car 'Toyota Mirai' (2 kW/kg). It is to be noted that the FCS specific power capacity of the fuel cell technology used in Toyota Mirai has a maximum value of 0.8 kW/kg. Additionally, the said aircraft is partially powered by lithium-sulphur battery. If the previous discussion on Rolls Royce's testing is recalled, then Rolls Royce's plan is much more ambitious (thrice the range) than 'Greenliner'. It is to be noted that this future plan despite being ambitious is limited to flight range of ~1,500 nmi (~2,800 km). This could be representative of a fuel-cell powered single-aisle aircraft seating approximately 150 passengers.

Recent studies also limit the application of fuel cell powered aircraft and/or turbo-electric aircraft (powered by LH_2) for regional/short- to mid-range application (small- to mid-sized aircraft). A study by Kasim et al. [71] models the performance of a regional aircraft (Cessna) retrofitted with fuel cell and hydrogen fuel systems. The maximum passenger seating reduces from 14 to 8, and the aircraft range is 350 km. A study by Nicolay et al. [72] examines the performance of a small/regional aircraft powered by fuel cell and hydrogen fuel systems. The maximum payload is 428 kg (or four passenger seating) with a range of 1,678 km. A study by Waddington et al. [73] models an LH_2 fuel cell powered aircraft called CHEETA of an unconventional airframe or architecture seating 180 passengers over 5,436 km range (similar to a class of Boeing 737). A thesis by Vonhoff [74] designs a regional aircraft powered by fuel cell and hydrogen systems. A study by Brelje et al. [75] designs a small fuel cell powered aircraft (range ~2,000 km), where the LH_2 fuel is stored in wings. The author conducts a detailed aero-structural analysis of the wings for the installation of LH_2 fuel tanks. A study by Marciello et al. [76] provide conceptual design of a fuel cell powered regional aircraft with a design range of 926 km seating 19 passengers. A study by Pastra et al. [77] models a hybrid hydrogen fuel cell and battery powered regional turboprop aircraft with a design range of 2,035 km seating 74 passengers. A study by Dietl et al. [78] designs a turbo-electric aircraft called Polaris which is powered by LH_2 fuel (stored

in foam based tanks) employing N+3 technology and an unconventional aircraft architecture with open rotor engines. This aircraft seats 150 passengers with 2,780 km at design point. A study by Druot et al. [79] models turbo-electric aircraft fleet powered by LH$_2$ fuel by employing different configurations of fuel tank integration. The study finds that such a propulsion technology enables range and payload combination only for a single aisle type of aircraft with short-range application.
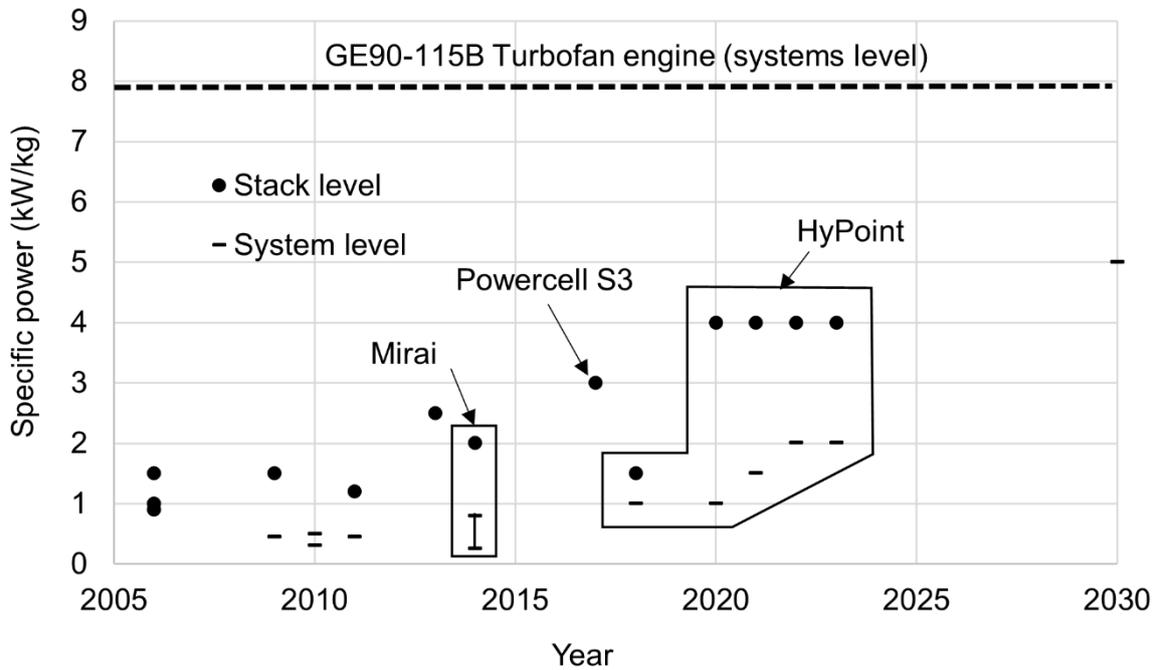
Figure 2.3. Trend of specific power of fuel cell technology and comparison with the specific power of a gas turbine engine used on Boeing 777-200LR aircraft (data source [69], [80]–[82])

Figure 2.3 shows the trend of fuel cell technology development (with time until year 2030) on both stack level and systems level. On a Boeing 777-200LR aircraft, two GE90 engines are used. The fuel flow rate at take-off is known to be 4.32 kg/s from the ICAO emissions databank while using conventional jet fuel (gravimetric energy density of 43.2 MJ/kg) [83]. The overall efficiency is known to be 0.37 [84]. Additionally, the engine weight is known to be 8,761 kg [85]. The specific power of this engine (system level) is calculated to be (4.32 x 43,200 x 0.37/8,761 =) 7.88 kW/kg. Therefore, from Figure 2.3 and previous discussions it can be concluded that fuel-cells do not appear to be a technological solution for future large aircraft with a long range. In terms of hydrogen use, according to World Economic Forum's report and Rolls Royce's tests discussed previously, long range large aircraft need to be powered by direct combustion of hydrogen in gas turbine engines.

The products of hydrogen combustion include water vapour and NO$_x$, and therefore it has the potential to make aviation cleaner and carbon-neutral in the use-phase. LH$_2$ as an aviation fuel has gravimetric energy density or LCV of 120 MJ/kg as compared to 43.2 MJ/kg for the conventional jet fuel [55]. However, conventional jet fuel is about 11.4 times denser (by mass) than LH$_2$ [47]. Therefore, the volumetric energy density (MJ/litre) of the conventional jet fuel is about 4.1 times as that of LH$_2$. This implies that the fuel tanks on LH$_2$ powered aircraft will require more volume storage (bigger tanks with insulation), which will further

increase aircraft weight and penalty due to drag. To maintain the same payload capacity, it is necessary to re-design the aircraft (fuselage and wing-loading for a conventional tube-wing aircraft) accounting extra fuselage and fuel tank weight, and form factor for the fuel tanks. The increase in aircraft weight and size, increases the drag on the aircraft. Verstraete [68] models the use of LH_2 in different sizes of aircraft (conventional tube-wing architecture) and finds that use of LH_2 shows energy consumption improvements only in long-range aircraft. For short and mid-range aircraft, there is an increase in energy use. The use of LH_2 in long-range (double-decker) aircraft mission leads to an improvement in energy efficiency of up to 12% (ibid). Therefore, LH_2 is an excellent candidate as an alternative fuel for long-range large aircraft. Current aircraft structures (tube-wing) are designed to accommodate jet fuel and gas turbines allowing a limited retrofitting only. New designs such as the blended wing body (BWB), also known as hybrid wing body (HWB), enable a more flexible integration of new storage technologies and energy converters such as cryogenic hydrogen tanks due to higher internal volume as compared to a tube-wing architecture [34], [86]. On similar lines, a study by Rompokos et al. [87] qualitatively examine morphologies of short-to-medium range and long-range LH_2 aircraft that enable shortlisting or selection of concepts for a more detailed study. A tube-wing aircraft with extended wing roots is selected for short-to-medium range application and a BWB design is selected for the long-range application. Therefore, a dedicated literature review on BWB aircraft architecture is deemed necessary and is conducted in sub-section 2.12. As discussed, this promising and new aircraft architecture is expected to provide benefits in terms of LH_2 storage.

2.7   Heat recovery in aircraft engines for improving efficiency

Heat recovery in aircraft (thrust-powered and shaft-powered) has been pursued for a long-time, especially in the past two decades, to improve the overall efficiency of aircraft. With such systems, there is always a balancing act between efficiency improvement and weight addition. A patent application by Fonseca [88], [89] reveals a heat recovery system for a thrust-powered aircraft engine (i.e. turbofan engine in this case). A design-optimisation study based on this system, by Perullo et al. [90], shows that the addition of this heat recovery system will have thrust-specific fuel consumption improvement of 0.9 – 2.5%. In a granted patent, Jagtap [91],[92] reveals a heat recuperation system for the family of shaft-powered aircraft gas turbine engines (turbo-shaft and turbo-prop engines) which increases the engine performance and life. A study based on this patent, Jagtap [93] presents the conceptual design of a novel compact heat-exchanger for application within annular fluid-flow path.

The study by Misirlis et al. [94] reveals an intercooled recuperated aero-engine of MTU Aero Engines AG. This engine uses an alternative thermodynamic cycle with intercooling and heat recuperation, where the heat recovery system comprises of heat exchangers installed in its exhaust nozzle (ibid). The intercooled recuperated aero-engine reduces the specific fuel consumption by 9.1 – 13.1 % depending on the selected heat exchanger type (ibid).

2.8 Air-to-air refuelling

The civil-aviation sector's fuel efficiency can be increased by implementing air-to-air refuelling and reducing short-haul flights. A study by McRoberts et al. [95] shows that air-to-air refuelling can give up to 14% fuel-burn and 12% operating-cost savings, when compared to a similar technology-level aircraft concept without aerial refuelling, which represents up to 26% in fuel burn and 25% in total operating cost over the existing operational model, at present standard fleet performance and technology. However, these potential savings are not uniformly distributed throughout the network, and the system is highly sensitive to the routes serviced, with decrease in revenue-generation potential observed throughout the network for air-to-air refuelling operations due to decrease in passenger revenue [95]. Another study on air-to-air refuelling by Nangia [96] shows that aerial refuelling can have 15 – 30% improvement in fuel burn. A research thesis by Verhagen [97] finds that shape formation/flocking can have up to 4% fuel improvement. Aerial refuelling reduces aviation-related noise and emissions (local and global air quality) with energy reduction in ground system at airport [96]. Medium-range flights (approximately 3,000 nmi or 5,555 km) will be efficient with air-to-air refuelling (ibid). For passenger aircraft, safety is the paramount concern, and safety issues with air-to-air refuelling persists with defence sector aircraft. Air-to-air refuelling is not yet certified for civil aviation use. Moreover, for a sector which contributes to 3.5% of total man-made radiative forcing, if short-haul flights are removed, then the transportation load on ground and rail transportation will increase, which already contribute significantly to climate impacts. Also, the proposed removal of short-haul flights will cause inconvenience to people in the need of travel emergency. For example: The distance between Seattle, USA and Miami, USA is approximately 2,800 nmi (5,185 km) [98], which approximately represents the maximum (diagonal) distance in USA. According to Nangia [96], medium-range aircraft will be efficient with air-to-air refuelling. If short-haul flights are removed to support it, then the domestic aviation sector in USA could collapse i.e., it could have economic as well as social impacts. For air-to-air refuelling to succeed (after certification), it is required to re-design aircraft, re-structure air-traffic system, routing revisions, and development of automated systems for air-to-air refuelling.

2.9 Infrastructure, supply chain, and lifecycle analysis of aviation systems

A comprehensive and detailed lifecycle energy and emissions assessment of passenger transportation has been carried out by Chester et al. [99] to help the decision makers in appropriately developing technology and policies for mitigating environmental impacts of transportation. For aviation sector, depending on the type of aircraft (small, midsize, or large), active operations account for 69 – 79% and inactive operations account for 2 – 14% of air travel lifecycle energy (ibid). Aircraft have the largest ratios of operational energy to the total lifecycle energy due to their large fuel requirements per passenger kilometre travelled (PKT) and relatively small infrastructure (as aircraft is in cruise for majority of the flight-time) (ibid). During the life cycle of an aircraft, majority of SO_2 emissions come from the non-operational phase (primarily from the electricity required during individual paths in aircraft's life cycle), majority of NO_x comes from operational phase of aircraft, and majority of CO emissions come from vehicle manufacturing and infrastructure operation

(ground support equipment) (ibid). Therefore, technological advancements for improving fuel economy and switching to lower-carbon fuels are the most effective measure for improving the environmental performance of the aviation sector (ibid). Additionally, the use of alternative fuels/green energy instead of diesel or gasoline equipment, or stronger emission controls can reduce aircraft's total lifecycle CO emissions via ground support equipment operations and truck transport (ibid).

2.10 Recent efforts towards cleaner aviation

In the past few years, there have been efforts in terms of implementing unconventional aviation propulsion systems (prototype or for pilot-use/small-scale); and using alternative fuel and renewable energy. Test flights using biofuels (SPK) from algae and camelina were successfully conducted which marks the beginning of using alternative fuel in aviation [59], [100]–[102]. Additionally, Lufthansa successfully completed a six-month flight-operation using 50% blended biofuel on Airbus A321 between Hamburg and Frankfurt, without any technical problems or operational inconsistencies [59], [100], [103]. In recent years many test flights have been conducted on regional jets (ATR aircraft) [104], business jets [105], and LTA (A350), and VLTA (A380) [106], powered by 100% SPK primarily from HEFA pathway using waste biomass. From these test flights, no major issues were reported. Cochin airport in the Kerala state of India, is the world's first airport to be powered 100% by solar energy [107]. Solar impulse [108], is the world's first solar-powered aircraft with a seating capacity of one passenger. This solar-powered aircraft has successfully toured the globe (ibid). Researchers at the University of Cambridge have developed a single-seater hybrid-electric aircraft and have flown it successfully [109]. In 2016, the world's first four-seater passenger aircraft (range of up to 1,500 km) powered by fuel cells and battery system called 'HY4' made its first flight [110]. An ion-based propulsion method has been applied to a model aircraft (no passengers) by researchers at MIT, and test flights have been conducted [111]. In September 2022, Alice, the first all-electric passenger aircraft (Eviation company) made its maiden flight [112]. This is a nine-seater aircraft with a design range of 250 nmi (460 km). The above efforts are in-line with the measures suggested to mitigate the impacts of aviation, via advancements in aircraft technology, and use of alternative fuels and/or improved airport energy systems.

2.11 Future aircraft technology

A thesis by Cullen [113] examines the energy efficiency of various energy systems. The analysis also includes the possible improvements to energy systems for increasing their efficiencies. In the chapter on aircraft, the author finds that significant fuel efficiency improvements can be made via structural/airframe, aerodynamics, and propulsion systems. The author conducts comparison of presently used swept-wing aircraft and a future laminar-flow wing aircraft using un-ducted fan engine (LFW-UDF). LFW-UDF is essentially a combination of improved structural/airframe, aerodynamics, and propulsion systems. The LFW-UDF particularly uses boundary layer suction for maintaining laminar flow over the complete airframe and employs engine with improved propulsive efficiency. This analysis is based on the specific fuel burn model from the

greener by design (GBD) report [114]. The study by Cullen finds that approximately 46% fuel efficiency improvement can be achieved with the LFW-UDF configuration.

Table 2.4. NASA N+i subsonic fixed wing aircraft technology goals [115]

Corners of the trade space	N+1 (service entry year 2020 and beyond) technology benefits relative to a single aisle reference configuration (Boeing 737/CFM 56)	N+2 (year 2025 and beyond) technology benefits relative to a large twin aisle reference configuration (Boeing 777/GE 90)	N+3 (year 2030 and beyond) technology benefits
Noise	-32 dB	-42 dB	-71 dB
LTO NO_x emissions (below Committee on Aviation Environmental Protection 6)	-60%	-75%	Better than -75%
Performance (Aircraft fuel burn)	-33%	-50%	Better than -70%

A study by Benzakein [115] guides the readers through the future technologies for commercial aviation until year 2050. The discussion in this study is primarily about NASA N+i concepts[1], especially the propulsion systems involved in these concepts (ibid). Table 2.4 lists the NASA N+i subsonic fixed-wing aircraft technology goals (ibid). N+1 (year 2020 and beyond) will have advanced turbofan engines with high bypass ratios (BPR), and N+2 (year 2025 and beyond) will have ultra-high BPR (UHB) turbofan engines (open-rotor and/or ducted geared turbofans [GTF]), via improvement in the thermal efficiency by increasing the overall pressure ratio (OPR) [18],[115]. The N+3 generation (year 2030 and beyond) will include ultra-high BPR propulsion (net effective BPR), hybrid engines, alternative cycles, integrated propulsion, variable cycle engine, and/or engines with inter-cooling (ibid). The technological improvements in N+1 category include: improving the current aerodynamics and structure (tube and wing body) and using efficient turbofans (high BPR) [116]. Also, advancements in the N+2 category include use of advanced form of tube and wing body and unconventional aircraft body; efficient turbofans (UHB/GTF); low NO_x combustor concepts for high OPR environment; improved thermal efficiency of engines (or high operating temperatures) without increasing NO_x emissions (ibid). Overall, the N+2 category engines will have cleaner combustion, partial pre-mixed and lean direct multi-injection, lightweight ceramic matrix composite (CMC) liners to handle higher temperatures associated with higher OPR, advanced instability control, improved fuel-air mixing to minimise hot spots that create additional NO_x, and will have the flexibility to implement emerging alternative fuels [116].

A study by Ashcraft et al. [18] provides a systems-level review of the N+3 aircraft concepts which include Boeing's SUGAR (Subsonic Ultra Green Aircraft Research) concepts (more specifically Boeing SUGAR Volt concept); MIT's Double-bubble; Northrop Grumman SELECT (Silent Efficient Low-Emissions Commercial Transport); General Electric concept developed in partnership with Cessna and Georgia Tech;

---

[1] For N+i technology description and nomenclature, please refer Chapter 1

and NASA's N3-X Turboelectric Distributed Propulsion (TeDP) concept. Additionally, a study by Jagtap [117] conducts a systems-level assessment of subsonic hybrid-electric propulsion concepts for NASA N+3 goals with conceptual aircraft sizing (300 passengers). This comparative study is conducted using systems engineering methods to select the best concept from Boeing SUGAR Volt, MIT Double-bubble, Northrop Grumman SELECT, and NASA N3-X TeDP [117]. This study is helpful in phase one of such a project. The Georgia Tech Integrated Product-Process Development method is used in the study by Jagtap [117] to conceive a commercial aircraft which meets the rigorous N+3 goals set by NASA. The benefits of such a study are that it enables design changes to be made in early life of the project, thereby decreasing lifecycle costs (ibid). This study evaluates the NASA N3-X TeDP concept (BWB airframe) to be the best of the four concepts under consideration (ibid).

The N+1 technology is almost similar in architecture (tube and wing body) and in propulsion type, to most of the present-day aircraft. The N+1 technology can be thought of as an improvement in performance relative to the present-day aircraft, which is majorly a result of using high BPR engines, improved aerodynamics, and reduced weight of the aircraft. The aircraft concepts under N+1 are currently undergoing development-manufacturing (example Boeing 777X). The N+3 aircraft concepts have their own set of technology challenges to make them feasible for entering service in the targeted year. The study by Ashcraft et al. [18] shows feasibility criteria and constraints for N+3 hybrid-electric aircraft. For N+3 aircraft concepts, the electric motors and boundary layer ingestion (BLI) require significant technological developments (ibid). The BLI affects the propulsion system design due to flow distortion, and it has to be accurately included within the propulsion system design and optimisation via high-fidelity multi-physics approach [118]. As discussed in sub-section 2.6.3.2, fuel-cells are unlikely to be ready for powering propulsion systems on large aircraft by year 2035 but they are more likely to be used for augmenting a primary power source.

Additionally, according to the study by Ashcraft et al. [18], considering past battery development cycles, it is unlikely that new chemistries will be available for year 2035 advanced concepts. NASA N3-X TeDP concept uses novel propulsion system, which utilises superconducting electrically driven, distributed low-pressure-ratio (1.35) fans with power provided by two remote superconducting electric generators [119]. The turbogenerators are located at the wing tips, while the fans are positioned at the rear of the planform where they ingest the boundary layer. NASA N3-X TeDP concept has the potential to reduce fuel consumption by 70-72% (ibid). For this concept it is assumed that the required power density of the generators and motors is achieved from wound rotor synchronous machines with superconductor windings on stator and rotor. For keeping the required cooling capacity within acceptable limits, the stator conductors must be engineered carefully for reducing the alternating current losses. The required filament size for enabling this presently appears achievable only for the superconductor MgB_2. The critical temperature (the highest temperature at which it is superconducting) for MgB_2 is only 39 K, and it must be below 30 K for producing useful current density (ibid). Although Bismuth Strontium Calcium Copper Oxide cannot be manufactured presently with acceptable alternating current losses, a future development is assumed which makes it possible. Motors and generators with a hypothetical fine-wire Bismuth Strontium Calcium Copper Oxide are assumed. Additionally, according to Ashcraft et al. [18], superconducting electric motors are extremely important to the success of

NASA's N3-X TeDP concept. The limitations of using the said superconducting system is the increased system complexity. Along with the electric motors, other components such as a compressor, cryocooling system, inverter, and power source would also need to be added (ibid). The viability is closely related to the development of boundary layer ingestion and superconducting electric motor/generators that will eliminate mechanical connections for power distribution.

Other future aircraft concepts (LTA or VLTA) include the aircraft from the CENTRELINE project [120], Airbus' MAVERIC aircraft [121], KLM - TU Delft V-shaped aircraft [122], and MIT's H3.2 BWB aircraft [123]. The aircraft from the CENTRELINE project [120] has two UHB engines that power an electric fuselage BLI fan that reduces drag and improves the aerodynamic performance. This concept has the potential to reduce the fuel consumption by 27% seating 340 passengers with a design range of 12,000 km in comparison with a reference aircraft of year 2000 technology. Airbus' MAVERIC aircraft [121] is predicted to reduce 20% fuel consumption as compared to an unknown reference aircraft. KLM - TU Delft V-shaped aircraft [122] can potentially reduce the fuel consumption by 20% seating 314 passengers compared to the latest Airbus A350 aircraft. The design details and other performance characteristics of Airbus' MAVERIC aircraft and KLM - TU Delft V-shaped aircraft are not published so far. Lastly, MIT's H3.2 BWB aircraft [123] can enable travel of 354 passengers over 14,075 km with 53.7 % payload fuel energy intensity improvement for the podded-engine version as compared to B777 aircraft.

Studies on electric aircraft (turbo-electric, battery electric – hybrid and/or full electric) [18], [19], [117], [119], [124]–[128], [20]–[22], [25], [78], [79], [109], [110] suggest that these technologies are infeasible for typical long-range Mach 0.85 flight of an LTA aircraft, considering future technology development trend.

Figure 2.4 provides the specific energy of different battery technologies as compared with the energy density of kerosene/conventional jet fuel. It is to be noted that this figure is on a log-scale, and there is an order of magnitude difference between the specific energy of the best battery technology and conventional jet fuel. A study by Grönstedt et al. [124] finds that aircraft fuel is currently 50-100 times more power dense than batteries and historical improvement rate of 2-3% makes it uncertain whether batteries will reach the power density required for (approximately) year 2050 timeframe. Brelje et al. [125] raise safety concerns, as batteries are a known aviation hazard and have much less service experience, and fail in seemingly more-complex modes. The design of economically viable fixed-wing electric-aircraft demands high-end technology (ibid). According to studies by Pornet et al. [126] and Voskuijl et al. [19], the current technology is not ready, and significant development in battery technology is required for hybrid-electric aircraft, especially for a long-range 300 passenger aircraft.

The current battery energy density is 100-200 Wh/kg. Pornet et al. [126] investigated the use of batteries as energy source alongside conventional jet fuel as a retrofit for short-to-medium range single-aisle turbofan aircraft. They conclude that the use of batteries with an energy density of 1,500 Wh/kg, as an energy source, can provide a block fuel reduction (of 16%) on short-range missions. Further analysis by Pornet et al. demonstrates that batteries with an energy density below 1,000 Wh/kg provide no significant fuel savings at all. Voskuijl et al. [19] examine the use of 1,000 Wh/kg energy density batteries for powering a 70 passenger regional turbo-prop aircraft with a range of 1,528 km, comprising of 34% electric shaft power. The authors do

not account for the turbo-prop noise effects in this study. This arrangement results in 28% reduction in mission fuel, but it comes at the expense of a larger aircraft in terms of weight and wing area. In a study by Friedrich et al. [20], a Boeing 737–800 aircraft was retrofitted with a hybrid electric propulsion system. Assuming a specific energy of 750 Wh/kg, 10.4% fuel saving was computed on a two-hour mission. The study by Schäfer et al. [21] uses battery packs of 800 Wh/kg for an aircraft completely powered by batteries. This full-electric aircraft seats 150 passengers for a range of up to 1,111 km. The authors find that this full-electric aircraft has the potential to decrease net CO_2 emissions by 15%. Additionally, this full-electric aircraft can decrease the airport NO_x emissions by 40% (ibid). For the 2040 timeframe, DLR researchers are developing a 70 seater hybrid-electric aircraft (battery energy density unknown) with a range of 2,000 km [110].
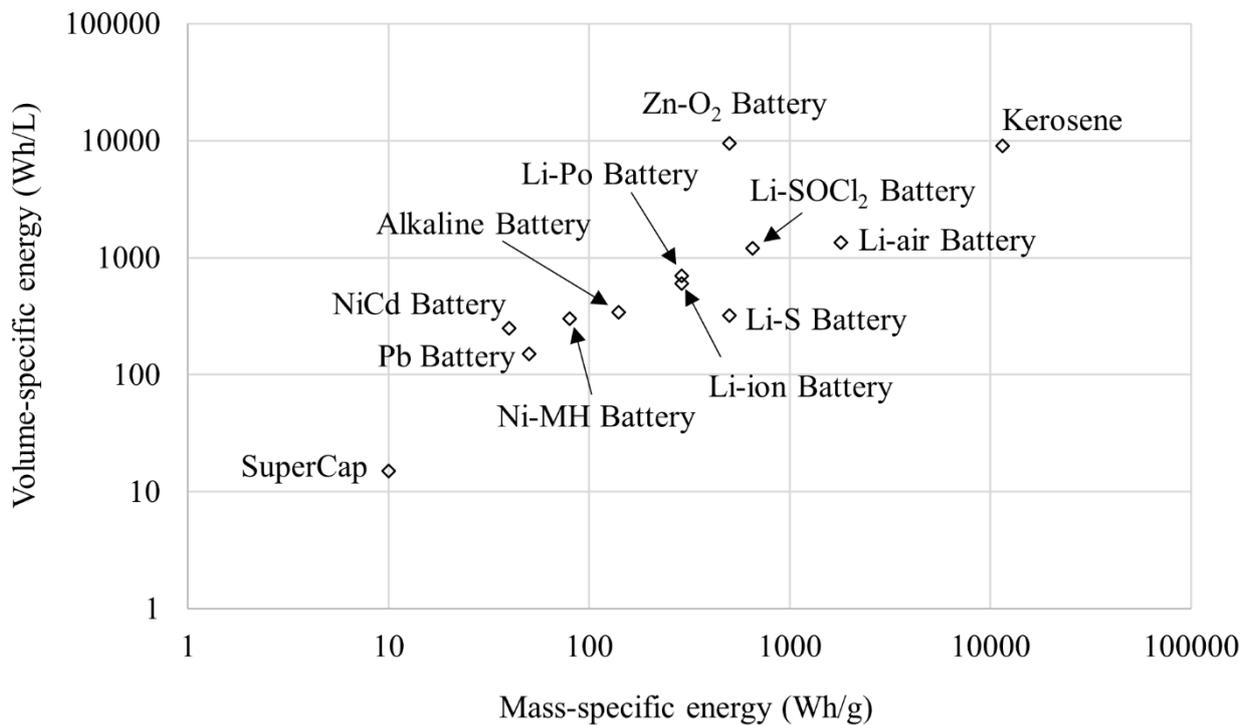
Figure 2.4. Specific energy of different battery technologies as compared with the energy density of kerosene/conventional jet fuel (data source [129])

Overall, with the assumption of battery energy density reaching 4-8 times the present capacity, the maximum fuel consumption reduction of 28% is observed in a turbo-prop aircraft. Additionally, if lifecycle effects are taken into consideration, the savings in fuel consumption come at the expense of extra electricity production or emissions elsewhere which is also sensitive to the energy-mix of a country/region (thermal vs renewable power production).

The N+2 aircraft concepts and the studies based on it, show the potential to meet the set targets. Some of these concepts include advanced tube-wing body, BWB, and box-wing body aircraft versions by different companies/organizations. These concepts use an UHB, direct-drive, or open-rotor/un-ducted turbofan or GTF engine. From Table 2.5, it can be observed that the N+2 goals have significant fuel savings (50% reduction) compared to the present fuel consumption. This is achieved through technological advancements in aircraft concepts, architecture, and propulsion systems, including the unconventional aircraft architecture like

blended/hybrid wing body (BWB or HWB). The blended/hybrid wing body is also a part of the N+3 concept (NASA N3-X TeDP), as discussed previously. Additionally, the use of UHB engines/propulsion system will be started with N+2 technology. A study by Nickol et al. [130] (NASA) models a fleet of advanced N+2 aircraft and conducts their performance evaluation. The fleet comprise of regional jet/RJ (small-range), single aisle/SA (mid-range), very large twin aisle/VLTA (long-range), small twin aisle/STA (long-range) and large twin aisle/LTA (long-range); with at least 2 options of aircraft for each aircraft type.

LTA options have both tube-wing and BWB architecture using UHB engines. Only the BWB concept with UHB shows the potential of tending towards NASA N+2 noise, fuel consumption (of ~47% reduction compared to the 2005 level baseline aircraft), and LTO NO$_x$ reduction goals. Overall, N+2 is a generation where technology starts transitioning significantly and rapidly. N+2 concepts appear to be technologically feasible as indicated by studies. In the context/scope of this work that considers LTA aircraft, the NASA concepts and their features are summarised in Table 2.5.

Table 2.5. Summary of NASA's LTA concepts for 301 passengers (source [130])

Features	Concepts				
	Tube-wing 301 – direct-drive	Tube-wing 301 – GTF	BWB 301 – direct-drive	BWB 301 – GTF	Mid fuselage nacelle 301 – GTF
Architecture	Tube-wing	Tube-wing	BWB	BWB	Tube-wing
Engine drive	Direct	Geared	Direct	Geared	Geared
Tail type	Conventional	Conventional	-	-	T-tail
Engine location	Below the wing	Below the wing	Aft of airframe	Aft of airframe	Mid fuselage

2.12 BWB aircraft

BWB is a category of aircraft between conventional and all-wing (example: Horten wing) aircraft configurations [131]. It is characterised by a low aspect ratio high thickness ratio inboard wing, a high aspect ratio outboard wing, and basic verticals (ibid). The lift to drag ratio (*L/D*) at cruise can be improved up to 25% compared to a similar passenger capacity tube-wing aircraft, and the installed thrust and fuel savings are even higher (ibid). Figure 2.5 shows a typical large/very-large BWB aircraft with two podded UHB engines.

2.12.1 Benefits of BWB aircraft configuration

2.12.1.1 Aero-structure

The BWB weight is distributed more optimally along the span, and has lower reduced structural weight as compared to a conventional tube-wing aircraft [132]–[136]. The integration of the thick centre-body with the outer wing in a BWB decreases the bending moments (ibid). The BWB has lower total wetted area and such an architectural integration allows for a long wingspan [132], [133], [137]. This results in the optimal aspect ratio of the outer wing being slightly higher than that of a tube-wing aircraft [132], [138]. Therefore, BWB has a higher lift-to-drag ratio and is structurally efficient than a tube-wing aircraft [132], [133], [138].

Top view

Front view

Side view
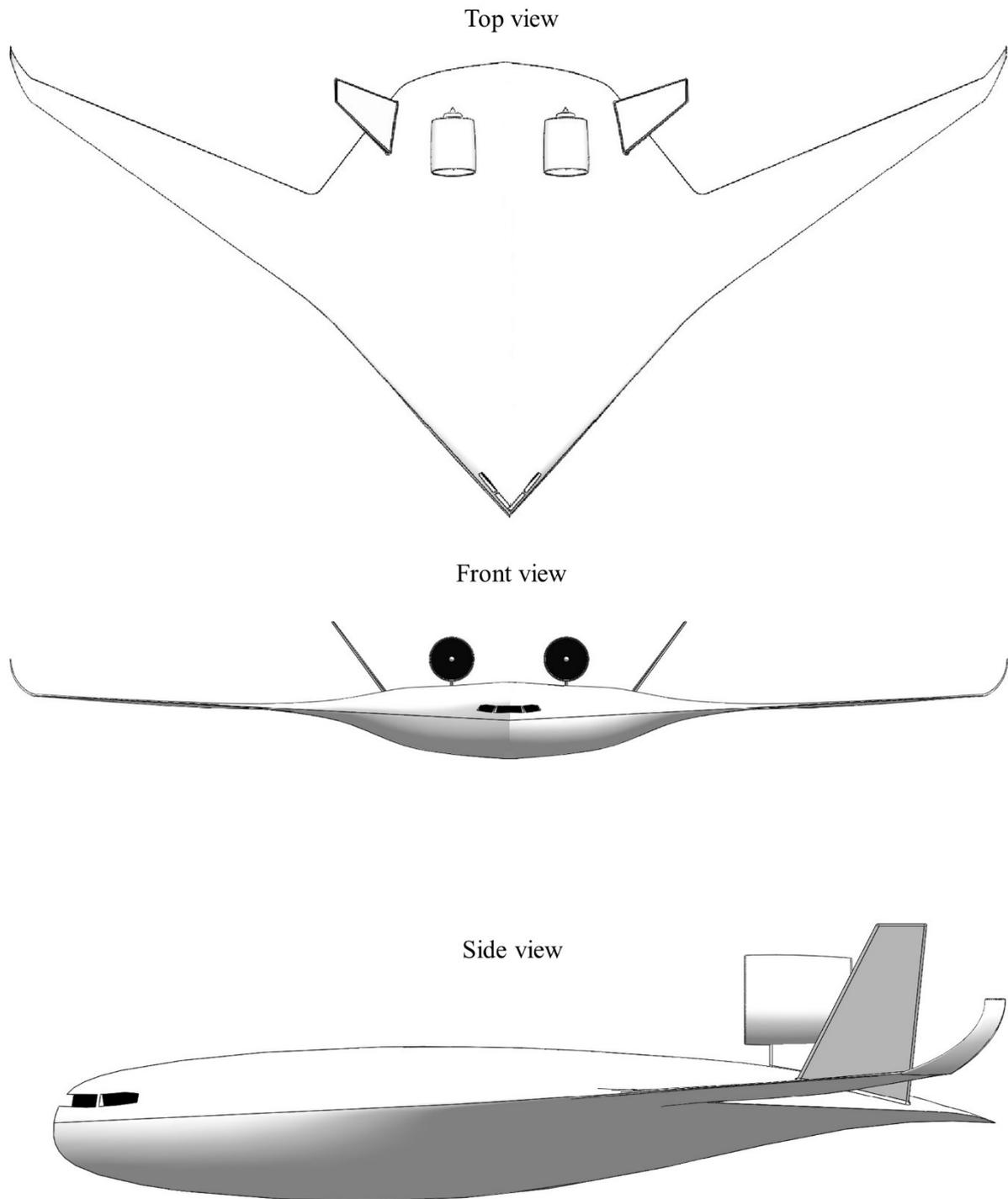
Figure 2.5. Graphical representation of a typical large BWB aircraft

2.12.1.2 Aerodynamics and propulsion

Considering the aerodynamics, the BWB architecture inherently follows the area-rule and thus can potentially enable higher cruise Mach numbers without the need to modify the basic shape [132], [139], [140]. The variation of cross-sectional area in BWBs is similar to that of the body of minimum wave drag due to volume i.e. the Sears-Haack body, which results into decrease in wave drag at transonic speeds [132], [139], [140]. A crucial feature of the BWB is its lift-generating centre-body that provides benefit over the tubular fuselage of a tube-wing aircraft [132], [136], [141], [142]. This enhances the aerodynamic performance by

decreasing the wing loading. Additionally, the reduction in wetted area through a smaller outer wing as compared to a similar sized present-day tube-wing aircraft results into an improved lift-to-drag ratio as it is proportional to the wetted aspect ratio. The wetted aspect ratio improves because it its inversely proportional to the wetted area [132], [133], [139], [143], [144]. The elimination of horizontal tail compared to a tube-wing aircraft, implies a decrease in the associated penalties due to friction and induced drag, causing further improvement in *L/D* [132], [138]. This causes the BWB shape to be more streamlined. The additional benefits are lesser wetted area to volume ratio for larger BWBs compared to a tube-wing aircraft. The interference drag decreases because of the reduction and/or elimination of surface-intersections/junctions between the fuselage and wings of a tube-wing aircraft [132], [134]–[136], [141], [143], [145].

In terms of the interaction of aerodynamics and propulsion system, some BWB aircraft concepts have engines partially embedded in the aft section of the BWB. With such an arrangement, the BLI technology can be used. The BLI can be done from a portion of the centre-body upstream of the engine inlet BLI results in the ram drag reduction which improves propulsive efficiency [132], [133], [139], and resultantly decreases the required thrust and fuel burn [146]. The aft installation of engine offsets the weight of the furnishings, payload, and other systems, and effectively balances the airframe. Additionally, this maximises the benefits from BLI because the boundary layer is completely developed towards the aft of wing [132], [146]. There is a potential for further reduction in drag via active and passive laminar flow control through laminar flow technology and wing shaping, on the lifting surfaces and engine nacelle. This can significant decrease skin friction drag [132], [143]. The BWB is an appropriate aircraft for the use of such technologies.

2.12.1.3 Noise

The BWB configuration inherently has the potential to produce lesser noise than a tube-wing aircraft type [132], [139], [146]. The BWB features that contribute to its low-noise characteristics are smooth lifting-surfaces, no tail, and minimally exposed cavities and edges (ibid). In the current tube-wing aircraft (mostly) the engines are installed/positioned below the wing. Whereas, for BWB the engines are installed on the aft side of its upper surface. The BWB airframe shields noise (fan and exhaust), from passengers and community, as compared to a current tube-wing aircraft (ibid).

2.12.1.4 Flight control and stability

According to Liebeck [133], a complicated high-lift system is not needed for the Boeing design due to the low-effective wing loading. The author discusses the reconfigurability and redundancy of the trailing edge flight controls. This decreases the secondary power requirement of the control system [132], [147].

2.12.1.5 Passenger safety

The pressure vessel because of its unique structural needs, and the requirement to handle pressure loads and wing bending, should be robust and have substantial crashworthiness [132], [133], [139]. The aft position of engines on the BWB displaces the shrapnel from engine failure behind the flight controls devices,

the pressure vessel, and systems and fuel tanks. In some BWB designs, broad cargo bays separate the fuel systems and the passenger section [132], [133].

2.12.1.6 Manufacturing, modularity, economics, and marketing

BWB design eliminates the need of mechanical joints of highly-loaded structures at 90° to each other and fillets [132], [139], [147]. Additionally, there is a significant reduction (order of 30%) in the total number of parts (ibid). Considering the aspect of passenger-comfort levels, the vertical cabin walls in the BWB might offer a more spacious experience than the curved walls of a tube-wing aircraft [132], [139]. The direct operating costs per seat/mile for the BWB are forecast to be 15% lesser than a tube-wing aircraft [132], [138].

In terms of design and reconfiguration, the BWB aircraft can be used for military and civil aviation applications; and it can be stretched laterally that will increase the span and wing, and resultantly the payload [132], [139], [147]. These benefits are not possible with a tube-wing aircraft as they are longitudinally stretched for increasing the payload. The commonality between 450-passenger and 250-passenger versions has been assessed, with the nose/cockpit section and outer wings being common members of this family of aircraft. The modular centre-bodies are aerodynamically balanced and smooth. The required fuel volume in the outer wing is sufficient for all the members of the family. This commonality offers 12% and 23% reduction in recurring costs and non-recurring costs respectively, compared to the stand-alone cases of the 450-passenger and 250-passenger versions. This decrease in cost is anticipated to increase if more sizes of BWB are considered viz. a 350-passenger version [132], [139], [147]. With the Boeing cabin design, this commonality between families holds good even with the interior, as the cabin cross-sections would be similar for all aircraft. From the perspective of airline companies, this would translate to advantages which are: a potential decrease in the manufacturing learning-curve penalties; fleet mix needs can be readily accommodated; and increased savings in maintenance and lifecycle cost. These can be achieved by variation of the wing area and span with weight, for maintaining the aerodynamic efficiency [132], [139]. This benefit is only possible with the BWB aircraft (ibid). As discussed before, the BWB architecture inherently follows the area-rule. This can decrease the manufacturing costs associated with a tube-wing aircraft that must be manufactured with a variable cross-section, commonly referred as called 'coke-bottle' fuselage to obtain the area-rule [132], [147]. So BWB aircraft has the potential to perform at higher speeds and at lower costs.

2.12.1.7 Operations

The likely advantages of BWB in terms of operations include effect on the off-loading and loading times due to the smaller fuselage length on a mid-sized BWB (200-passenger) [132], [148]. Additionally, BWB requires smaller take-off field-length without the necessity of complicated high-lift devices [132], [142]. As a result, in future, with the wider use BWB in the fleet (or fleet of 100% BWB) will cause airport to use lesser land-space (land-use effects of aviation).

2.12.2 Challenges/current limitations of BWB aircraft

2.12.2.1 Structures

The BWB's non-cylindrical pressure vessel poses an important challenge [132]. This pressure vessel has to weigh less, and it should bear the cabin pressure loads and the wing bending loads. The stress associated with a box-type BWB fuselage could be about an order of magnitude greater than the stress in a cylindrical pressurised fuselage [132], [149]. The increased stresses in such a pressure vessel results in increased structural weight [132], [133], [150].

2.12.2.2 Propulsion

There are challenges associated with aft-mounted engines and airframe-propulsion integration aspect in BWB, because this type of integration impacts multiple aspects of BWB more directly compared to a tube-wing aircraft [132], [133], [151]. Moreover, the interaction between the control surfaces, wing, and propulsion system increase design complexity [132], [137]. A recent study by Flamm et al. [152] focusses on the UHB engine integration for BWB technology demonstration located within the ERA vehicle systems integration' sub-project. This study addresses the ERA technical challenge to show decreased noise-level resulting to 42 EPNdB to Stage 4 noise margin for the aircraft system and simultaneously minimise the integration and weight penalties to provide 50% fuel savings (ibid). This study examines the UHB's engine operability aspect where this engine is mounted on the upper surface of the aircraft; and it optimises the high lift system for increasing *L/D* and improving noise performance (ibid). The authors observe that all inlet distortion case-studies within BWB's operating boundary have allowable blade stresses and engine operability. Systems-level examinations show that the BWB aircraft scaled-model obtained reduction of 53% in fuel consumption as compared to the reference configuration (ibid). The authors infer from the certification noise level examination that the cumulative margin below Stage 4 is 38.4 dB for the vehicle including chevron nozzle technologies and landing gear fairing (ibid).

2.12.2.3 Aerodynamics

Unconventional transonic air-foils with high thickness to chord ratio (t/c) of about 17% according to the Boeing designs [139] are needed to hold the landing gear, cargo and passengers on-board. Additionally, this t/c must be retained along a substantial section of the BWB, which is a challenge if low drag is to be maintained [132], [137], [139], [151]. Moreover, because of the deck angle restrictions, the centre-body air-foils should be designed to produce the required lift at angles of attack that are consistent with the deck angle requirements [132], [137], [139], [144]. The supersonic flow on the lower surface of the BWB is another challenge, which is not observed in a tube-wing aircraft [132], [137]. A smooth transition from the thicker centre-body air-foils to the thinner outer-wing air-foils might be problematic [132], [142]. This could be problematic specifically for the medium-sized 200-passenger BWBs as such transition might be more abrupt for such smaller vehicles (ibid). Lastly, though embedded engines and BLI technologies are promising, difficulties persist with the airframe-engine integration and with the inclusion of these technologies that

comprise of turbomachinery integration, design of low-loss inlet system, and distortion control of inlet flow [132], [146]. The manufacturing constraints should be considered within the aerodynamic design of the aircraft [132], [137], [139]. The complex 3D shapes which might be difficult and expensive to manufacture can be replaced with simple and smooth curved surfaces (ibid). Additionally, other challenges include landing approach speed, and stall-buffet aspects [132], [139], [144]. There are other studies of BWB having engines installed on pylons under the wing, which would take away a lot of the advantages previously discussed in terms of drag and noise reduction [132], [138].

2.12.2.4 *Flight control and stability*

As discussed previously, the BWB is an integrated aircraft configuration with no tail. This implies that interactions between aerodynamic loads, inertial forces, elastic deformations and the flight control system responses may significantly impact the aircraft's stability and performance [132], [139], [150], [153]. The aircraft should be balanced and simultaneously it is to be ensured that the control deflections do not negatively impact the drag and span-load [132], [151]. For bigger BWBs, the control surface hinge moments are considerable [132], [144]. Therefore, in case of aircraft instability and that the aircraft is dependent on the active flight controls, then the secondary power requirements can be restrictive [132], [139], [144], [151].

2.12.2.5 *Passenger safety and certification*

The certification of the BWB might be impacted due to the requirement of efficient emergency exit [132], [139]. This might be more challenging for larger BWBs because of the increased distance between exits [132], [138]. The shortage of clear views of the different exit doors on larger BWBs will be difficult for cabin crew passengers during evacuation [132], [154]. However, according to both Liebeck [139] and Bolsunovsky et al. [138], procedures that are compliant with federal aviation regulation 25 can be incorporated. Liebeck suggests that passengers have a direct view of at least one exit-door(s), and they do not need turn 90 degrees from the aisle to get access to the door. This is supported by the Boeing design that includes a main cabin door directly ahead of every aisle and an exit via the aft pressure bulkhead at the back end of every aisle. Moreover, four spanwise aisles cross the longitudinal aisles [132], [139]. The full-scale evacuation tests and computer simulations were carried out by Galea et al. [154] for BWB aircraft with more than one thousand passengers. The authors observed that the aircraft-layout awareness and enhanced visual access, are important for efficient exit during evacuation. The fire simulations resulted in 12 fatalities which were deemed inevitable, but independent of the cabin architecture (ibid). In a worst-case scenario, the BWB can be used only for cargo application (civil and military).

2.12.2.6 *Ergonomics and marketing*

The BWB presents a more spacious environment, however, there are some aspects that can make the marketing this configuration challenging viz. passenger acceptance [132]. Firstly, having only one window in each main cabin door and no windows on the cabin walls of BWB, the passengers might feel uncomfortable. A proposed solution to this challenge is installing display screens connected to a series of digital video cameras

for making every seat a window seat [132], [139]. Secondly, considering the lateral offset from the aircraft's centre of gravity, the quality of flight experience might degrade, especially in the outer sections of the BWB, as compared to a tube-wing aircraft flight experience. A series of flight simulation tests was conducted by Boeing for the B747-400 and BWB-450 with the flight profile and participation by same pilots. The NASA Jacobsen ride quality model was used to estimate the passenger satisfaction for the worst and seats on both aircraft [132], [139], [147]. The authors observed that the ride quality only reduced slightly by approximately 4%. Okonkwo et al. [155] recommend that the BWB should be designed for maximum productivity, because profitability and safety are the main needs of commercial aviation. This implies creating BWBs with good ride and handling quality; and determining the optimal altitude and cruise speed that improves operating efficiency and minimises fuel burn (ibid). The good handling quality could be achieved by setting the best combination of planform variables (aerodynamic and geometric twist, sweep angles, etc.) that improves aircraft controllability and trimmability, and simultaneously the ride-quality is enhanced by minimising the impact of gust and increasing passenger comfort (ibid).

2.13 Summary and arising insights from the literature review

The literature review provides insights into the social and environmental impacts of aviation, and different technologies, alternative fuels and pathways of making aviation more sustainable, along with feasibility consideration of future technologies and passenger safety within the definition of 'sustainability'. 'N+i' technology, in general, is in-line with the four-pillar strategy of IATA for mitigating the impacts of aviation. Overall, N+i is inclusive of aircraft technology improvements and the use of alternative fuels, which will offer significant fuel savings/reduction in emissions. Overall, the review suggests that the research efforts agree with each other and are in-line with the IATA strategies for making future aviation more sustainable.

Solar-electric and ion propulsion technology appear to be infeasible currently and require dramatic improvement for enabling typical long-range Mach 0.85 flight of ~300 passengers with passenger safety considerations. Battery, fuel cell, and hybrid- and turbo-electric technology development trend could enable passenger travel only for a small short-range to medium-range aircraft. Different approved blends of drop-in SPKs are currently the alternative to Jet-A fuel. Based on the literature review, methanol, ethanol, 100% SPK, LH_2, LNG, and LNH_3 'appear' to be future alternatives to the conventional Jet-A fuel based on their properties.

N+2 is identified as the aircraft technology level that provides significant energy consumption improvements, and it appears to be technologically feasible as indicated by studies. Also, several alternative aviation fuels are identified via literature review, that are widely studied, and these include: ASTM approved sugar-to-jet (STJ) SPK (10% blending), and (50% blending) HRJ-SPK, ATJ-SPK and FT-SPK; PtL; and LH_2. Additionally, 100% SPK is also found to provide negligible energy efficiency benefit in the use-phase, though it is not a drop-in fuel currently. The performance characteristics of an aircraft powered by LNG, LNH_3, ethanol, and methanol, especially for intercontinental travel are less published. These fuels require a separate viability examination for aviation application along with LH_2 and 100% SPK. Moreover, in a life cycle of a conventional aircraft, active operation (direct fuel-use) dominates lifecycle energy and GHG emissions (~75% of the total lifecycle energy), followed by fuel production (~10% of the total lifecycle energy). Hence, a

lifecycle approach is deemed necessary for the alternative and conventional jet fuel, to be used in the future aircraft concepts. Additionally, not all alternative fuels mentioned above are 'drop-in' fuels, therefore it is required to examine the operability issues and the interaction between alternative fuels and aircraft. For example: LH_2 has lower density than conventional jet fuel, so it requires more volume storage on aircraft.

In terms of airframe selection, the literature review on BWB aircraft suggests that BWBs have higher internal volume storage capacity for the same passenger capacity compared to a conventional tube-wing aircraft architecture. In other words, BWBs have higher volume to wetted area ratio, which means that they provide same drag for higher internal volume compared to a tube-wing architecture. This enables storage of extra-large and bulky fuel tanks, especially for using LH_2 fuel, which might not require re-designing/re-structuring of aircraft as required in the case of a tube-wing architecture. LH_2 use will have maximum benefits if used on BWB because of its higher aircraft volume storage for same payload and wetted area/drag, compared to a tube-wing architecture. Therefore, BWBs enable a more flexible and efficient integration of new storage technologies such as LH_2 fuel storage tanks. However significant technical and operational challenges remain for BWB concepts ranging from structural integrity, manufacturing, and aerodynamics to whether it is possible to evacuate such a passenger aircraft safely.

From the literature review it is found that CO_2 emissions, contrails, and cruise NO_x emissions, are the three components that are responsible for 97% of climate and air quality damages per unit aviation fuel burn. Thus, these are principal targets for future strategies to mitigate the atmospheric impacts of aviation emissions. In terms of methodological approaches (high-level), multiple studies are identified which are relevant to this research. The methodological approach used in this study is a combination of the following studies. The study by Chester [99] conducts lifecycle assessment (LCA) of present passenger aircraft fleet using conventional jet fuel. It finds that fuel life cycle GHG/energy dominates (~85% of) aircraft's life cycle GHG/energy. However, the effects of improvement in aircraft design/architecture, alternative fuel, and source/feedstock for alternative fuel production on aircraft's lifecycle energy, are not explored. Thesis/study by Cullen [113] uses model from GBD report [114], to evaluate (current and future) aircraft's direct fuel use, via a simple computational model called the SFB model. These studies do not consider alternative aviation fuels except LH_2, and their lifecycle effects. A recent review study by Pinheiro Melo et al. [35] establishes the need for an integrated methodological framework that should consider lifecycle impacts of aircraft performance towards the goal of sustainable aviation. This framework will enable a better understanding of the implications of future novel technologies considering the three sustainability parameters by coupling different scenarios and examining the interactions between different designs, spatial differences, and product parameters.

Considering the above identified gaps, this research will also examine N+2 BWB aircraft technology for 300 passengers along with technologically advanced tube-wing aircraft, and the use of various alternative fuels from different feedstocks/pathways, on a fuel lifecycle basis, along with the assessment of operability issues and the interaction between alternative fuels and aircraft. In the next chapter (Chapter 3), the research philosophy and overall methodology of the thesis is discussed. In addition to the philosophical and methodological approach, the novelty of this research is underscored by the computation models developed towards the research objectives which are discussed in Chapters 4 – 8.

Chapter 3: Research philosophy and overall methodology

3.1   Introduction and chapter structure

In this chapter the research philosophy, and overall thesis research methodology along with flow of information in this thesis are discussed. The discussion on philosophy of research in section 3.2 provides a context and perspective to the reader for identifying the research theories or approaches that are employed in the individual research chapters and thesis. In addition, the overall methodology and thesis flow is discussed with a glimpse of contents of main research chapters, in section 3.3.

3.2   The philosophy of research

Figure 3.1 shows the schematic of the research 'onion', which includes different research philosophies, research approaches, methodological choices, strategies, time horizon, and techniques and procedures [156]. The research philosophy – forms a research basis by delineation of ontology – nature of reality, epistemology – nature, sources of knowledge or facts and axiology – values, beliefs and ethics of the research [156], [157].

In an inductive approach, the research begins with observation and data collection, moving to discussion and analysis for forming a theory [156], [157]. In a deductive approach the research begins with an existing theory, then putting forward a question or hypothesis and data collection for rejecting or confirming the hypothesis. With an abductive approach, the observation of an empirical phenomena is followed by the research using a best guess or inference based on available evidence. A deductive approach is applied for existing theory testing and an inductive approach is generally used in developing a theory or in research areas with lesser research on a topic. An abductive approach generally begins with a surprising fact and moves between deductive and inductive approaches for finding the most likely explanation (ibid). A deductive research approach is typically used in scientific examinations [158]. The inference from a deductive approach is guaranteed to be true, whereas the inference from inductive and abductive approach are 'probably true' and 'best guess' respectively.

The research philosophies of interpretivism (interviews, ethnography, and grounded theory) and post-modernism (discourse analysis and visual methods) are used for pure qualitative evaluations. Critical realism (archival research and historical analysis) and pragmatism (any strategy) take an abductive approach and are used for quantitative and/or qualitative evaluations. Positivism primarily reflects the philosophical stance of a natural scientist [156], [157]. Its ontology is based on objectivist assumptions that "entities are observed, atomistic events, existing external to social actors, therefore only observation and empirical data may be referred to as 'credible'" (ibid). Knowledge is acquired by observation and finding event regularities that are based on law-like, functional, and causal relations. Positivism uses a deductive approach, and it is used for pure quantitative evaluations (experiments, surveys, etc.).
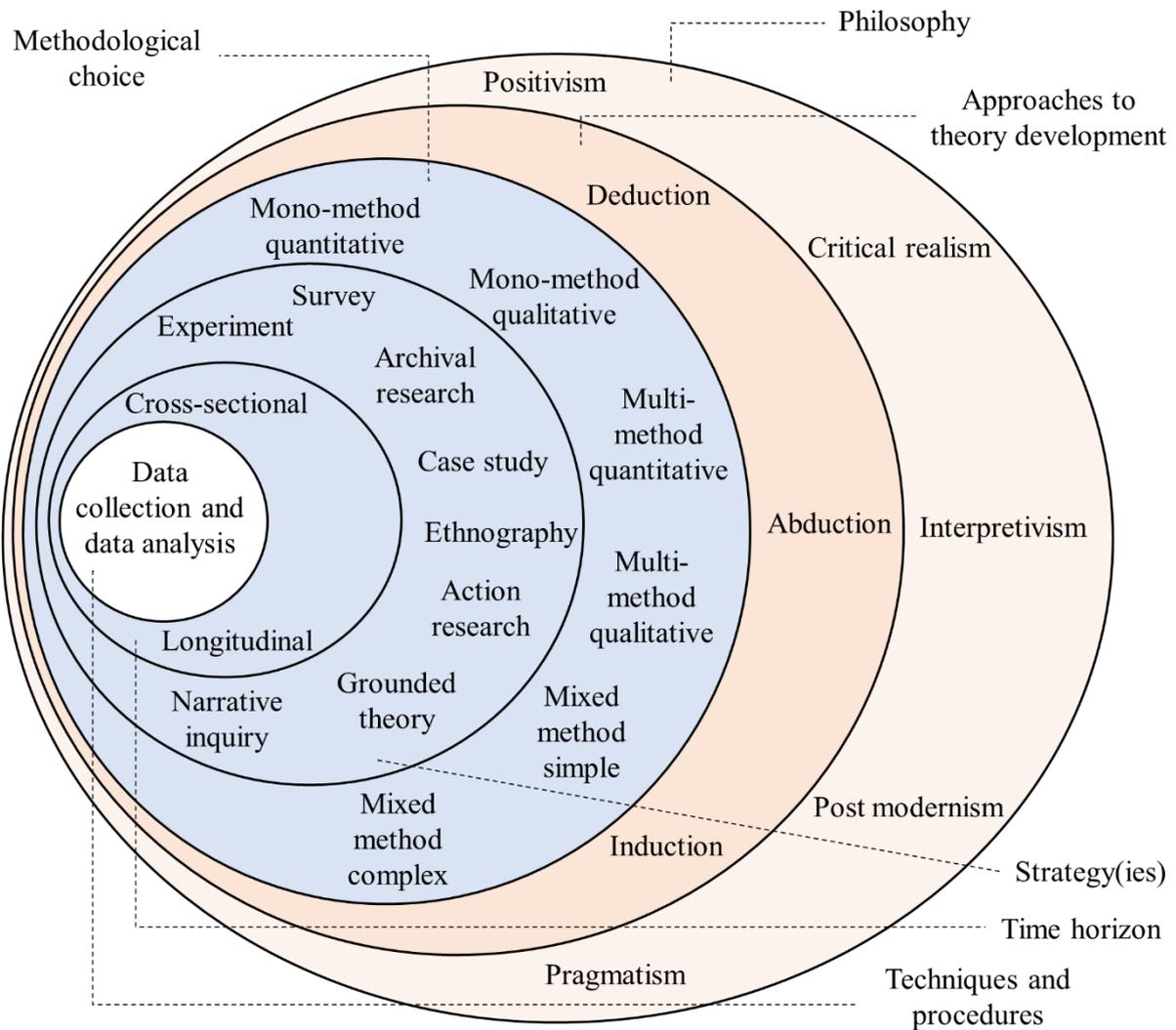
Figure 3.1. Schematic of the research 'onion' (data source [156])

The research in the present thesis is a 'quantitative' assessment of low-carbon technology and energy vector combinations for future intercontinental passenger aircraft. Considering the above discussion, the research philosophy of 'positivism' is relevant and is thus used in this research, which uses deductive approach. Table 3.1 lists the research routes and associated risks and benefits using the philosophy of positivism while employing a deductive approach. Referring to Table 3.1, routes 1 – 3 would employ mix methods (quantitative and qualitative) towards the overall thesis.

In the context of the thesis, research route #4 is chosen based on the risk and benefit analysis listed in Table 3.1. Each main chapter (Chapters 4 – 8) in this thesis would use a mono quantitative method (numerical experiment). Overall, this thesis would employ multi-method quantitative research approach with the philosophy towards the research aims and objectives.

Table 3.1. Different research routes and associated risks and benefits using the philosophy of positivism while employing a deductive approach

	Route I	Route II	Route III	Route IV
Chapter 4	Mono-method qualitative (survey based)	Mono-method quantitative (numerical experiment)	Mono-method qualitative (survey based)	Mono-method quantitative (numerical experiment)
Chapter 5	Mono-method quantitative (numerical experiment)	Mono-method quantitative (numerical experiment)	Mono-method quantitative (numerical experiment)	Mono-method quantitative (numerical experiment)
Chapter 6	Mono-method quantitative (numerical experiment)	Mono-method quantitative (numerical experiment)	Mono-method quantitative (numerical experiment)	Mono-method quantitative (numerical experiment)
Chapter 7	Mono-method quantitative (numerical experiment)	Mono-method quantitative (numerical experiment)	Mono-method quantitative (numerical experiment)	Mono-method quantitative (numerical experiment)
Chapter 8	Mono-method qualitative (survey based)	Mono-method qualitative (survey based)	Mono-method quantitative (numerical experiment)	Mono-method quantitative (numerical experiment)
Overall thesis	Mixed method (quantitative and qualitative)	Mixed method (quantitative and qualitative)	Mixed method (quantitative and qualitative)	Multi-method (quantitative)
Risk	A qualitative methodology with survey strategy inherently bring in biases and not everyone in the sample set would be willing to share all information. Such an approach for Chapter 4 (which forms a basis for the thesis), and Chapter 8 would ignore other emerging alternative fuel candidates and their production pathways, respectively	A qualitative methodology with survey strategy inherently bring in biases and not everyone in the sample set would be willing to share all information. Such an approach for Chapter 8 would ignore other emerging alternative fuel production pathways	A qualitative methodology with survey strategy inherently bring in biases and not everyone in the sample set would be willing to share all information. Such an approach for Chapter 4 (which forms a basis for the thesis) would ignore other emerging alternative fuel candidates	The accuracy of quantitative methods depend on the order (or fidelity level) of analysis
Benefit	Likelihood to get more hints into unpublished or on-going research on emerging/novel alternative fuel candidates and their production pathways	Likelihood to get more hints into unpublished or on-going research on emerging/novel alternative fuel production pathways	Likelihood to get more hints into unpublished or on-going research on emerging/novel alternative fuel candidates	Scientific backing to the (first-hand experimental) results as compared to second- or third-hand opinions that could have biases

3.3 Overall methodology and flow of information in thesis

The scope of the quantitative evaluation in this thesis is limited to a long-range 300 passenger LTA subsonic aircraft. The high-level research methodology for individual chapters in this thesis are discussed next based on research route #4. The overall process or thesis information flow schematic is provided in Figure 3.2, where each of the research objectives discussed previously are addressed in individual chapters.
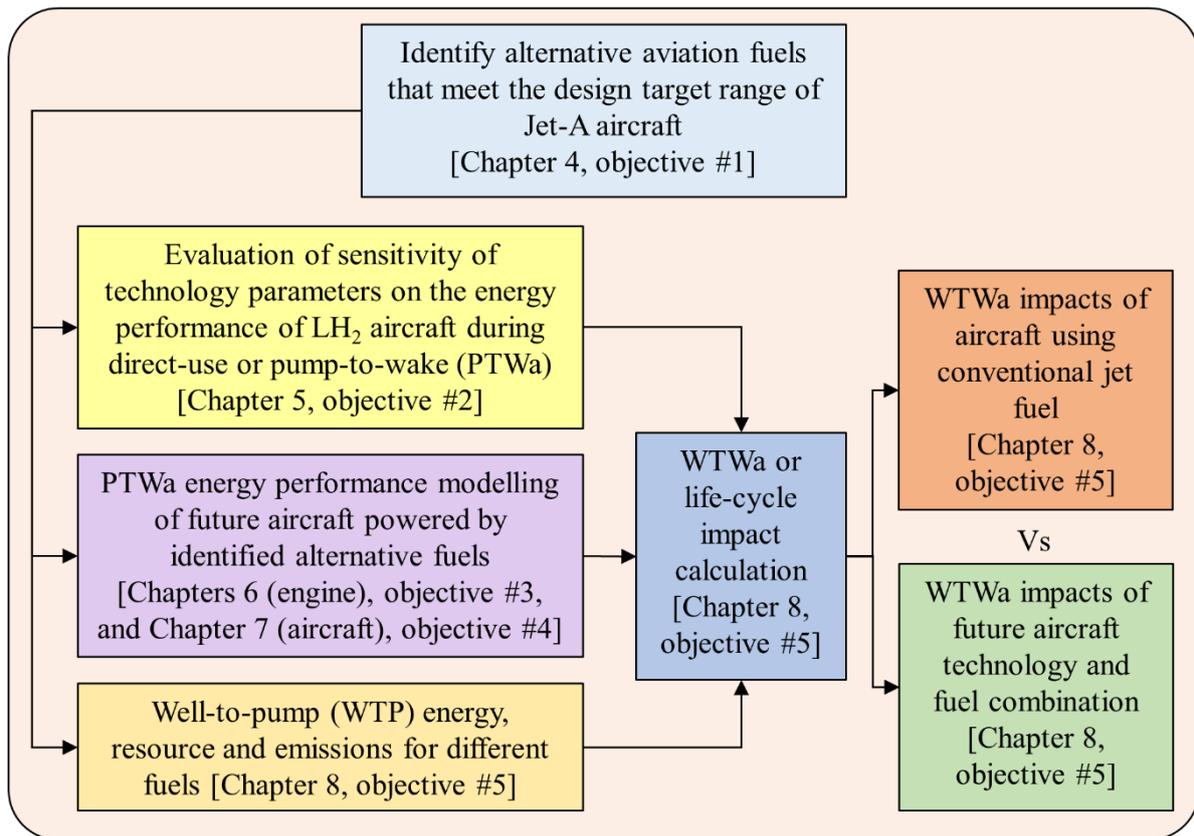
Figure 3.2. Schematic of the overall process or thesis information flow

In Chapter 4, six alternative fuels (methanol, ethanol, 100% SPK, LH$_2$, LNG, and LNH$_3$) are examined to check whether they could enable a typical long-range flight of an LTA aircraft within MTOW limit, and fuels that can enable such a flight are identified. In Chapter 4 the operational (pump-to-wake [PTWa]) energy performance of a long-range tube-wing LTA aircraft powered by six alternative fuels is modelled. This is followed by a global sensitivity analysis of technology parameters on the operational (PTWa) energy performance of an LH$_2$ aircraft, in Chapter 5, using the model developed in Chapter 4. Additionally, the work in Chapters 6 and 7 combined, enables the estimation of operational (PTWa) energy performance of a future (N+2 timeframe) BWB aircraft powered by fuels identified in Chapter 4. Chapter 6 includes the conceptual design methodology for (N+2 timeframe) (UHB) engine performance simulation at on-design and off-design points for conventional jet fuel and identified fuels (separately). Chapter 7 includes the aircraft energy consumption modelling of a future (N+2 timeframe) BWB technology aircraft powered by conventional jet fuel and identified fuels (separately), using conceptual design methods. Overall, the operational (PTWa)

energy performance modelling of an LTA aircraft powered by identified fuels is conducted in Chapters 4 – 7, and this enables the estimation of emissions in the aircraft use-phase. Thus, knowing the fuel manufacturing emissions, WTWa or lifecycle emissions can be calculated. In Chapter 8 the life cycle or WTWa performance or impacts are evaluated for different long-range LTA aircraft powered by identified alternative fuels, where each of them are manufactured from different feedstocks and/or pathways. This WTWa performance is compared with the Jet-A LTA aircraft performance, to evaluate which alternative fuel(s) and associated manufacturing route(s) could enable zero/negative GHG emissions long-range flight.

In general, low-order quantitative modelling methods are used in Chapters 4 – 8. Particularly, for aircraft energy consumption modelling in Chapters 4 – 7, the analysis doesn't consider detailed structural/stress and stability analysis, and the fuel manufacturing database in Chapter 8 is primarily based on GREET 2021 model (US specific data).

In the next chapter, a quantitative energy performance evaluation of the six alternative liquid fuels – methanol, ethanol, 100% SPK, LH_2, LNG, and LNH_3 – is conducted to evaluate whether they could enable design target long-range (similar to Jet-A) travel considering realistic effects on aircraft design. Additionally, off-design point analysis of the aircraft powered by the identified fuels is conducted as airlines rarely operate at aircraft design point.

Chapter 4: Energy performance evaluation of alternative energy vectors for subsonic long-range tube-wing aircraft

4.1 Introduction

4.1.1 Background

Different alternative energy vectors were reviewed in Chapter 2 (sections 2.6 and 2.11), and it is observed that methanol, ethanol, 100% SPK, LH_2, LNG, and LNH_3 appear to be the six principal future alternatives to the Jet-A fuel. Among these fuels, both 100% SPK and LH_2 have been extensively reviewed. Performance characteristics of an aircraft powered by LNG, LNH_3, ethanol, and methanol, especially for intercontinental travel are less published and thus require a separate viability examination for aviation application. This is the motivation for the present chapter, which quantitatively evaluates the performance of these six fuels to determine if they could enable long-range travel considering their realistic effects on aircraft design. The aim of this chapter is to evaluate the energy performance characteristics of six alternative fuels using Breguet's range equation to identify fuels that enable design target long-range (similar to Jet-A) for future LTA aircraft. Breguet's range equation is a very fundamental equation in aeronautics which estimates the flight range, where the flight range is influenced by aircraft aerodynamics, engine overall efficiency, aircraft structure and material, and calorific value of fuel. Additionally, off-design point analysis is conducted as aircraft rarely operate at design point.

The broader objectives of this chapter are to quantify the energy performance characteristics of LTA aircraft powered by the six alternative fuels and identify the fuels that enable a typical long-range flight within the aircraft's structural limit; and evaluate the off-design energy performance of the LTA aircraft powered by identified alternative fuel(s) which meets the Jet-A design target range. This is research objective #1 of the thesis as discussed in Chapter 1. The present chapter is a low-order evaluation of the aircraft energy performance using different fuels. The detailed objectives of this chapter are formulated based on the literature review in section 4.2.

4.1.2 Chapter structure

The studies that explore the performance characteristics of an aircraft powered by 100% SPK, LH_2, LNG, LNH_3, ethanol, and/or methanol are first reviewed in section 4.2. Thereafter, a comparative assessment of the performance characteristics of the six alternative fuels is conducted using the standard Breguet's range equation using the methodology described in section 4.3 and the results are discussed in section 4.4. Lastly, based on these findings a further examination is conducted on the retired VLTA aircraft such as Airbus A380.

4.2 Literature review on alternative fuel powered aircraft

Bicer et al. [47] examined small twin aisle aircraft of conventional tube-wing architecture (like Boeing 767) with a mid-range flight of 5,600 km, where the aircraft is operated by Jet-A, LH_2, LNG, LNH_3, ethanol, and methanol. The authors found that only LH_2 aircraft consumes less energy relative to Jet-A. However, it is

unclear how the volumetric energy density of these alternative fuels and the subsequent impacts on aircraft design and energy performance were accounted for. The above five alternative fuels and 100% SPK appear to be principal future alternatives to Jet-A fuel. However, there is a need to quantitatively evaluate the performance of these six fuels to determine if they could enable long-range travel with an LTA aircraft considering their realistic effects on aircraft design.

Among the six principal fuels identified through review, 100% SPK has been extensively reviewed in literature [48], [51], [52], [59]. Hileman et al. [51] evaluated the performance of 100% SPK based on a first-order approach using Breguet's range equation. The authors found that a hypothetical fleet-wide scenario using pure (100%) SPK could decrease aircraft energy consumption by 0.3% as compared to a Jet-A aircraft. Similarly, a study by Proesmans et al. [159] found that a 100% SPK aircraft had similar energy consumption as that of a Jet-A aircraft.

LH_2 is an attractive fuel because of its high gravimetric energy density and its potential to emit zero carbon emissions in the use-phase. There is a growing interest in LH_2 as an aviation fuel and the aviation industry has begun R&D and investments on conceptualising aircraft design, cryogenic tank testing, and fuel infrastructure [160]–[164].

Studies on combustion based LH_2 aircraft [165]–[170] model the energy performance of a regional/small- to mid-size aircraft for a short- to medium-range application. Other literature based on combustion based LH_2 aircraft: (i) is designed for different (smaller) payload and range combination compared to the reference long-range LTA aircraft [171], [172]; (ii) LH_2 aircraft cruises at lower Mach and/or altitude and has different aircraft design characteristics compared to the typical baseline long-range LTA aircraft [159], [173]; (iii) aircraft is not completely powered by LH_2 (powered 33% by biofuel) [174]. These above studies are discussed below.

A study by Prewitz et al. [165] simulates the performance of a regional hydrogen powered aircraft (ATR-72) that has a design range of 1,324 km (715 nautical miles) for maximum payload of 7,050 kg. A study by Yang et al. [166] models a small single aisle LH_2 aircraft (range 5,480 km with 177 passengers) and examines the environmental impact of a fleet of this LH_2 aircraft on a world-wide network. The authors use the Fleet-Level Environmental Evaluation Tool (FLEET) tool to model different scenarios and estimate equivalent carbon emissions and LH_2 cost. The study finds that that by introducing a (small) single aisle LH_2 aircraft (in 2035) could reduce fleet-level carbon emission by 9.96% in comparison with a baseline with no liquid hydrogen aircraft.

A thesis by Svensson [167] simulates a medium range LH_2 aircraft that seats 185 passengers over a range of 7,400 km. The design of this aircraft is carried out in a design environment called PIANO (and also referencing to the Cryoplane study [175]). The energy consumption of this LH_2 aircraft increases by 10% compared to a reference Jet-A aircraft.

A study by Silberhorn et al. [168] designs LH_2 aircraft seating 165 passengers with range of 5,740 km. The authors design three LH_2 aircraft, each having a distinct cryogenic tank installation configuration – aft of fuselage, on top of fuselage (best energy performance), and wing podded. Depending on the type of tank installation, the energy consumption of the LH_2 aircraft increases by 6.5 – 7.5% compared to the baseline Jet-

64

A aircraft. Another study by Silberhorn et al. [176] models the energy performance of LH_2 aircraft seating 261 passengers over 7,220 km using advanced aircraft technology. The energy consumption of this LH_2 aircraft decreases by 37.6% compared to present-day Jet-A aircraft and increases by 2% compared to same technology Jet-A aircraft. A study by Lammen et al. [170] simulate the energy performance of a 300 passenger LH_2 aircraft having 3,704 km range, using advanced aircraft technology.

A study by Cipolla et al. [171] designs LH_2 powered small– and medium–range aircraft, where a box-wing aircraft concept is a reference aircraft that has 5,722 km range seating 308 passengers. The authors primarily consider two fuselage/cabin layouts (for installing LH_2 tanks) that affect the passenger seating and range. For one of the layouts the passenger seating is 308 but the range (<=4,000) reduces. However, for the other layouts the passenger seating is between 164 and 196, and their corresponding ranges are 6,000 km and 4,000 km respectively.

A study by Gomez et al. [172] models the performance of an LH_2 powered tube-wing aircraft. The reference aircraft seats 296 passengers with range of 6,500 km. The modified version of this aircraft for LH_2 use seats 194 passengers with range of 9,000 km, and the fuselage length is equal to the reference aircraft. For this LH_2 powered tube-wing aircraft, the cryogenic tank η is 0.826 for the rear tank and 0.741 for the forward tank. The authors conduct a detail structural and stress analysis of the cryogenic tanks, where the tanks are of integral type made of Aluminium alloy employing polyurethane insulation.

A study by Grewe et al. [174] examines the climate impact of a futuristic multi-fuel BWB aircraft seating 300 passengers for design range of 14,000 km. For this aircraft 33% of energy is provided by bio-kerosene and 67% energy either comes from LNG or LH_2. It is to be noted that this aircraft design performance is based on an extremely simple model as it does not take into account details such as the cryogenic storage requirements and the associated drag and weight penalty. The study finds that LNG – bio-kerosene has lower climate impacts compared to LH_2 – bio-kerosene and the conventional aircraft.

Troeltsch et al. [173] designed an LH_2 aircraft (range 11,853 km with 400 passengers) with foam-based tanks (front and aft). In contrast to other studies on LH_2 aircraft design, the authors choose to reduce the cruise Mach speed from 0.82 of the reference Jet-A aircraft to 0.7, and this LH_2 aircraft shows a 9% increase in energy consumption compared to the reference aircraft. Proesmans et al. [159] conducted a pareto-optimal design examination of LH_2 and 100% SPK (separately) powered aircraft for short-, medium- and long-range aircraft, where each fuel and aircraft type was designed separately to minimise climate impact or operating costs. When minimising climate impact, for a long-range LTA aircraft, the optimal cruise altitude (6.1 km) and cruise Mach (0.6) are similar for their Jet-A, LH_2, and 100% SPK. However, these are lower than is typical for present-day Jet-A aircraft, which cruise at an altitude of ~10.5-12.8 km and cruise Mach of up to ~0.9. The energy performance of their Jet-A and 100% SPK aircraft were identical. Their LH_2 aircraft had a 7.6% lower gross take-off weight (GTOW), 22.8% higher operating empty weight (OEW), 41.1% longer fuselage, and 12.9% higher energy consumption compared to the baseline Jet-A aircraft.

A study by Onorato et al. [177] designs LH_2 aircraft of three different sizes – regional/small (72 passengers, 926 km), medium-sized (150 passengers, 4,560 km), and large aircraft (295 passengers, 7,674 km) – while considering five different tank installation configurations for each aircraft size. For a large LH_2 aircraft,

the authors find that the front and aft tank installation in both single deck and double deck seating type provides energy consumption improvement of 4.2% (37.1% increase in fuselage length) and 7% respectively, compared to a single-deck Jet-A aircraft. Additionally, studies by Huete et al. [178], [179] examine the performance of (double-decker) large aircraft (different range and payload combinations). The authors design four large aircraft: 232 passengers with 10,370 km range, 332 passengers with 8,890 km range, 388 passengers with 6,112 km range, and 720 passengers with 3,334 km range. However, the energy performance characteristics are unknown from these studies.

Verstraete [68] modelled the use of LH$_2$ in different aircraft size/types including a long-range double-decker (greater fuselage diameter) aircraft (conventional tube-wing architecture) with 14,000 km range. The study considered the additional structural weight resulting from integral LH$_2$ fuel tank systems and changes in aerodynamic performance resulting from a longer fuselage length, required to accommodate LH$_2$, and found a 12% improvement in operational energy efficiency for a 400-passenger double-decker tube-wing aircraft. Brewer [180] evaluated different aircraft size/types, including a 400 passenger very long-range (18,500 km) tube-wing double-decker aircraft powered by LH$_2$, and found that the block fuel energy (kJ/seat-km) improved by 33% relative to a baseline Jet-A aircraft.

An analysis of LH$_2$ powered aircraft from the Airbus Cryoplane study [181], which adopts a minimal change approach to the aircraft wing planform and engine design for a hydrogen aircraft [182], showed a 9% increase in specific energy consumption (SEC) (energy/passenger-nautical mile) for a LH$_2$ powered double-decker (greater fuselage diameter) long-range large aircraft (14,000 km design range seating approximately 300 passengers) [175]. This increase in the SEC is primarily attributable to the larger wetted area of the LH$_2$ powered aircraft required to accommodate LH$_2$ tanks.

It is clear from the above discussion that there is a need to examine and compare the aircraft performance of the six identified alternative fuels to check whether they could enable a typical long-range flight with an LTA aircraft while considering both gravimetric and volumetric energy density effects on aircraft design (associated weight, aerodynamics, and energy performance penalties), especially for cryogenic fuels like LH$_2$, LNG, and LNH$_3$. Furthermore, there is a scarcity of literature on the design an LTA long-range single-decker aircraft completely powered by the combustion of LH$_2$, to the same design specification as that of the baseline Jet-A aircraft.

The use of low-carbon energy vectors and/or alternative fuels is critical to the mitigation of aviation's climate impact. The objectives of this work are to: (i) quantitatively evaluate the energy performance characteristics of six alternative fuels – methanol, ethanol, 100% SPK, LH$_2$, LNG and LNH$_3$ – to identify fuels that enable the typical design target for future single-decker LTA aircraft (similar to Jet-A); (ii) conduct off-design point analysis for the identified fuel(s) and evaluate sensitivity of SEC (in MJ/tonne-km) to range and payload combinations, especially for LH$_2$ aircraft; and (iii) quantify the relationship between the OEW and GTOW for combustion based LH$_2$ aircraft based on regression analysis of the data obtained from the present work and literature to inform future studies on LH$_2$ aircraft weight sizing. The above analysis will be conducted using Breguet's range equation.

The present chapter is a low-order evaluation of the aircraft energy performance using different fuels. The methodology for the performance evaluation is detailed in section 4.3 followed by the results and discussion in section 4.4. Details omitted from the main text are included in the Appendix A.

4.3 Methodology

Breguet's range equation is used for the performance evaluation of methanol, ethanol, 100% SPK, LH_2, LNG, and LNH_3. Breguet's range equation is dependent on aspects such as fuel type, aircraft aerodynamics, overall efficiency, and structural weight [183]. The Airbus A350-1000 aircraft is used as a baseline, and it is modified for the use of the six fuels accounting for both volumetric and gravimetric energy density effects of each fuel on the aircraft aerodynamics and structure. It is assumed that typical cruise Mach number, altitude, and necessary fuel reserves are maintained.

4.3.1 Breguet's range equation

Breguet's range equation, represented by equation 4.1 (source [183]), is a fundamental equation in aeronautics which estimates the aircraft range given the LCV of the fuel (h), L/D, overall efficiency (η_0), and aircraft initial and final weight. The range, R, of an aircraft is given by,

$$R = \left(\frac{h}{g}\right)\left(\frac{L}{D}\right) \eta_o \ln\left(\frac{W_{initial}}{W_{final}}\right). \tag{4.1}$$

where g is gravitational acceleration, and $W_{initial}$ and W_{final} are the aircraft weight at the beginning and end of cruise, respectively. The Breguet range equation is applicable to cases where η_o, L/D, and flight speed are constant over the flight and can therefore be used to give a first order estimate for typical cruise conditions [183]. The accuracy of Breguet's range equation is evaluated by predicting the performance characteristics of two in-service aircraft (Airbus A320-200 and Boeing B767-300F), and this validation is included in Appendix A, where the aircraft range is predicted for two separate payload cases for both aircraft types. The performance characteristics predicted using the range equation for these four points are in reasonable agreement with the published data (within ±5%, a criterion defined for low-order aircraft performance modelling [184], [185] in Appendix A).

4.3.2 Overall efficiency and lost-fuel factors

4.3.2.1 Overall efficiency

Table 4.1 lists the properties of different alternative fuels that are considered in this chapter. The ratio of fuel consumption rate of Jet-A fuel and fuel consumption rate of a given fuel ($\dot{m}_{f,Jet-A}/\dot{m}_f$) for Jet-A, 100% SPK, LH_2, and LNG, are calculated at engine design point using GasTurb 13 software.

GasTurb 13 is a software tool that estimates the performance and optimisation of gas turbine engines [186]–[189]. It can perform zero-dimensional (thermodynamic cycle performance and weight estimation) and one-dimensional gas turbine analysis, which at least fall within the ambit of the conceptual engine design phase. In GasTurb 13, the details needed for professional gas turbine performance are estimated along with the engine

thermodynamics. This tool also has the feature of conducting optimisation of the engine thermodynamic cycle. Additionally, turbine cooling and secondary air system can be analysed with this tool. The calculations in GasTurb are based on the engine design and performance methods and Euler turbomachinery equations [187], [189], [190]. GasTurb functioning and calculation procedures are detailed in [187], [189]. Additionally, the author of GasTurb 13, simulates three different gas turbine engines i.e. J57-19W, CFM56-3 and F107-WR-400, in their book in reference [189].

For the research in this chapter, a turbofan engine in GasTurb 13 is operated for same thrust production (equal to Jet-A) at typical cruise altitude and Mach (35,000 ft [10.67 km] at Mach 0.85) using 100% SPK, LH_2 and LNG (separately), and the said ratios are calculated. Additionally, for LH_2 this ratio is also known from literature [191]. Ethanol, methanol, and LNH_3 are unavailable fuels in GasTurb 13 software. For methanol and LNH_3 the said ratios are known from literature [192]. The ratio $\dot{m}_{f,Jet-A}/\dot{m}_f$ is not known for ethanol from literature. This ratio is calculated for ethanol as described below after assuming the ratio of overall efficiency for a given fuel case and overall efficiency for Jet-A ($\eta_{o,f}/\eta_{o,Jet-A}$). η_o is defined as the ratio of the propulsive power (product of thrust and velocity) to the fuel power ($\dot{m}_f h_f$) [183]. It is assumed that the thrust production and flight speed remain same for all fuel cases. The ratio $\eta_{o,f}/\eta_{o,Jet-A} = (\dot{m}_{f,Jet-A} h_{Jet-A})/(\dot{m}_f h_f)$, for same thrust production and flight speed. Except for ethanol, this ratio is calculated from the known values and are listed in Table 4.1. The value of h for ethanol is greater than that for methanol but less than h of Jet-A. The ratio $\eta_{o,f}/\eta_{o,Jet-A}$ increases from 99.93% (methanol) to 100% (Jet-A). Therefore, for ethanol this ratio must be between 99.93% and 100%. A value of 99.95% is assumed and the ratio $\dot{m}_{f,Jet-A}/\dot{m}_f$ is calculated for ethanol to be 0.63 as listed in Table 4.1. η_o for the aircraft (Jet-A) considered in this chapter is discussed in section 4.3.7. Knowing this and the $\eta_{o,f}/\eta_{o,Jet-A}$ ratio for all fuels, the η_o is calculated for all alternative fuels to be used on the said aircraft. A sanity check is further conducted on the ratio $\dot{m}_{f,Jet-A}/\dot{m}_f$ for all alternative fuels, which is calculated by using the above approach, using a simple thermodynamic cycle analysis of a turbofan engine (further details in Appendix A section A.1). It is observed that the ratio $\dot{m}_{f,Jet-A}/\dot{m}_f$ for all alternative fuels calculated using both methods are similar.

Table 4.1. Properties of different alternative fuels

Fuel	h (MJ/kg)	Density ρ (kg/m^3)	$\dot{m}_{f,Jet-A}/\dot{m}_f$	$\eta_{o,f}/\eta_{o,Jet-A}$ (%)
Jet-A	43.2 [47]	808 [47]	1.00	100.00
100% SPK	44.1 [33]	757 [33]	1.02 *	99.97
LH_2	120.0 [47]	71[47]	2.86 *,[191]	103.14
LNG	50.0 [47]	424 [47]	1.16 *	100.42
LNH_3	18.6 [47]	730 [47]	0.40 [192]	92.90
Methanol	19.9 [47]	796 [47]	0.46 [192]	99.93
Ethanol	27.2 [47]	794 [47]	0.63 ***	99.95 **

* Calculated using GasTurb 13

** is assumed value and *** is calculated based on it

Equation 4.1 estimates the aircraft range and the estimation of the fuel consumed in non-cruise phases is conducted using the lost fuel factor, which represents a percentage of the aircraft GTOW and varies for different fuels [114], [193]. The lost fuel factor for Jet-A and LH_2 fuel is 2.2% and 1.4% of the GTOW of the aircraft [114], [193]. Using the findings listed in Table 4.1, the lost fuel factor for other alternative fuels is calculated as a percentage of the (same) MTOW. For example, the MTOW of the Airbus A350-1000 aircraft is 316 (metric) tonnes. The lost fuel factors for other alternative fuels are listed in Table 4.2. Using the lost fuel factor of 2.2% of MTOW (316 tonnes for the A350-1000) Jet-A aircraft, the lost fuel is calculated (to be 6,952 kg). For the same period of operation, $\dot{m}_{f,Jet-A} / \dot{m}_f$ calculated in Table 4.1 equals $M_{f,Jet-A} / M_f$ listed in Table 4.2. Knowing $M_{f,Jet-A} / M_f$ ratios for other alternative fuels and $M_{f,Jet-A}$ (6,952 kg) for Jet-A, the M_f for each of these alternative fuels is calculated. The lost fuel for each alternative fuel is then listed as a percent of the MTOW (316 tonnes). As can be observed from Table 4.2, the alternative fuels with gravimetric energy densities lesser than Jet-A, such as LNH_3, methanol, and ethanol have higher lost fuel factor i.e., more of the respective fuel is consumed. This is an expected trend.

Table 4.2. Lost fuel factor for alternative fuels

Fuel	$M_{f,Jet-A} / M_f$	Lost fuel (kg)	% of MTOW (lost fuel)
Jet-A	1	6,952	2.20 [114], [193]
100% SPK	1.02	6,812	2.16
LNG	1.16	5,981	1.89
LNH_3	0.40	17,380	5.5
Methanol	0.46	15,103	4.78
Ethanol	0.63	11,041	3.49

4.3.3 Flight mission profile and iteration process

Figure 4.1 and Figure 4.2 show the process schematic of the range equation analysis for the Jet-A fuel case and alternative liquid fuel (cryogenic and non-cryogenic) cases respectively. SEC (in MJ/tonne-km) is calculated for the different fuels as it is an important performance parameter that facilitates the calculation of direct operating costs. The A350-1000 aircraft (Jet-A) is the baseline case, and all alternative fuels will be evaluated for the same payload weight and design target range. The passenger payload weight (W_p) and other A350-1000 aircraft (Jet-A) data is included in section 4.3.7. The total fuel weight carried at mission start ($W_{F,total}$), determines the volume needed to store that fuel and therefore OEW of the aircraft. The aircraft GTOW is the sum of the OEW, W_p, and $W_{F,total}$. It is chosen to constrain the aircraft GTOW to be less than or equal to the MTOW limit of the baseline aircraft structure, which is 316 tonnes (weight breakdown in section 4.3.7). This constraint is applied since a detailed structural analysis is not conducted in this chapter. Therefore, the MTOW determines the design limit on the $W_{F,total}$. In other words, for the alternative fuel cases, the $W_{F,total}$ is iterated and estimated such that the aircraft GTOW does not exceed the MTOW. For the baseline Jet-A aircraft, the MTOW, OEW, and $W_{F,total}$ are known for a given W_p (see section 4.3.7). For alternative fuel cases, the wing planform (area, span, and/or AR) is maintained from the baseline aircraft, which is similar to the approach used

in the Cryoplane study [182]. To accommodate greater volumes of fuel that could be required for alternative fuels, extensions of the fuselage length is allowed in this chapter. Additional fuselage length penalises aircraft fuel/energy performance via increased wetted area, drag, and weight (via increased OEW). For cryogenic fuels (LH$_2$, LNG, and LNH$_3$), $W_{F,total}$ needs to be stored in cryogenic tank systems that are installed in the fuselage. For non-cryogenic fuels (100% SPK, methanol, and ethanol), a substantial fraction of $W_{F,total}$ fits inside the existing tank in the wings of the baseline aircraft. The remainder of the fuel (if any) must be accommodated in the (additional) fuselage. These calculations are discussed in further detail in section 4.3.4 and 4.3.5. The sum of the fuel consumed during non-cruise and cruise operation in a typical mission is defined here as block fuel consumption. For all fuels a ratio of 0.9 of the block fuel weight ($W_{F,block}$) and $W_{F,total}$ is maintained, which accounts for reserve or additional fuel, as used by Nickol et al. for both tube-wing and blended wing body long-range LTA aircraft [130]. The SEC is calculated from the $W_{F,block}$ for each fuel case [SEC = ($W_{F,block}$ h) / (W_p R)].
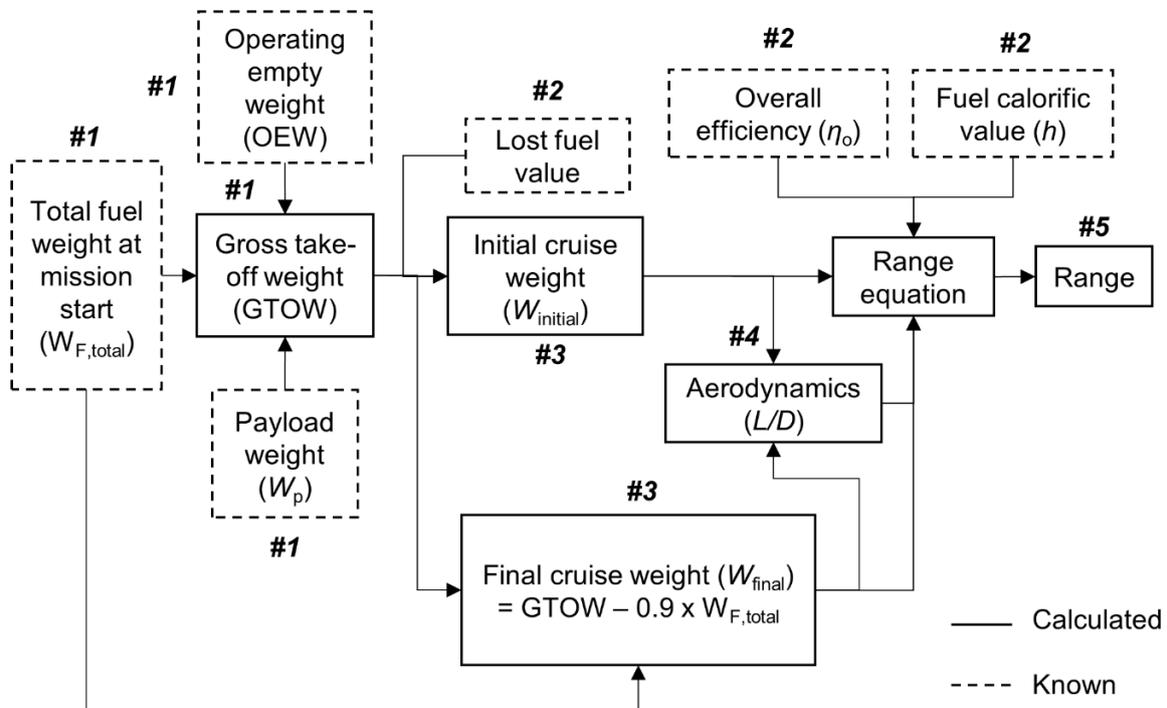
Figure 4.1. Process schematic of the range equation analysis for Jet-A (baseline) case. Boxes with dashed borders represent known values, boxes with solid border represent a calculation step, and # represent the calculation step number

The lift to drag ratio for all fuel cases are calculated using method described in section 4.3.4. Using the lost fuel factors for different fuels, the aircraft weight at the beginning of cruise [$W_{initial}$ = (1 − lost fuel factor) x GTOW] is calculated. The aircraft weight at the end of cruise [W_{final} = GTOW − 0.9 x $W_{F,total}$] is calculated by subtracting 90% of $W_{F,total}$ from the GTOW. Therefore, all parameters of equation 4.1 are known and the aircraft range can be calculated. The stepwise procedure of the range equation analysis for the baseline and alternative fuel cases is described in Appendix A section A.2 (referencing the step numbers shown in Figure 4.1 and Figure 4.2).
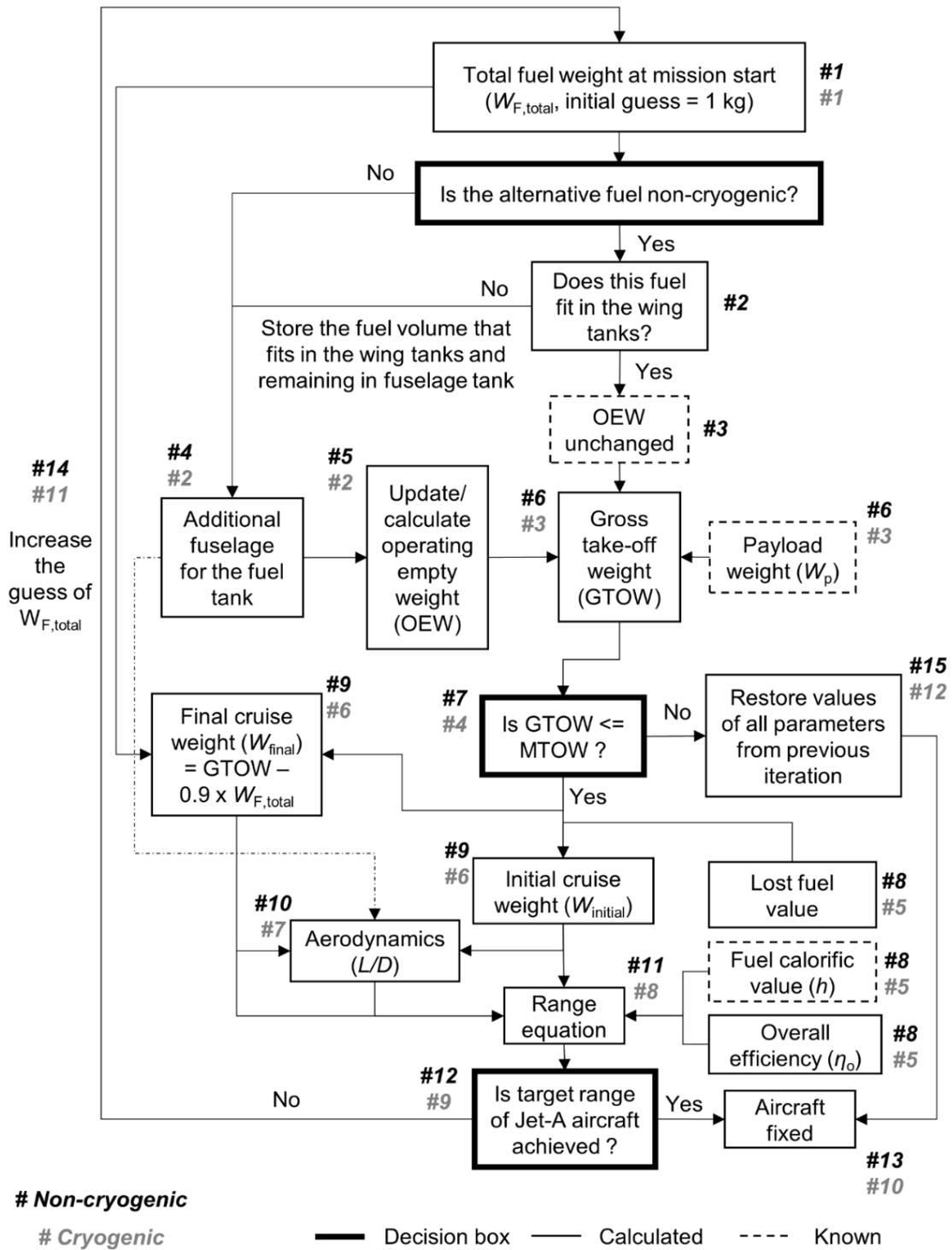
Figure 4.2. Process schematic of the range equation analysis for alternative fuel cases. Boxes with dashed borders represent known values, boxes with thin solid border represent a calculation step, boxes with solid thick border represent a decision box, and # represent the calculation step number. Grey and black colours are used for cryogenic and non-cryogenic fuel cases, respectively

4.3.4 Aerodynamics and additional fuselage structure

4.3.4.1 L/D ratio

The drag coefficient (C_D) is estimated using equation 4.2, assuming that it is the sum of the zero-lift drag coefficient and lift-induced drag coefficient, and that there is no wave drag,

$$C_D = C_{D,0} + \frac{C_L^2}{\pi \, AR \, e}, \tag{4.2}$$

$$\text{where } C_{D,0} = \frac{C_f \, S_{wet}}{S}, \text{ and} \tag{4.3}$$

$$C_L = \frac{W_{aircraft}}{0.5 \, \rho_a \, S \, V^2}. \tag{4.4}$$

$C_{D,0}$ is the coefficient of zero-lift drag, C_L is the coefficient of lift, AR is the AR for a given aircraft (see section 4.3.7), and e is the Oswald's efficiency factor – a correction factor that is representative of change in drag with lift of a 3D wing in comparison with an ideal wing that has same AR with an elliptical lift distribution. An LTA aircraft such as the B777 has an 'e' value of 0.85 and this is used in the present chapter for the baseline aircraft [194]. C_f is the skin friction coefficient, which for today's large transport jets is typically 0.003 [195], [196]. S is the wing area known from aircraft data (see section 4.3.7). The wetted area (S_{wet}) is calculated separately using the model described in the next section. Assumed values for the airspeed (V) and air density (ρ_a) are known from aircraft data (see section 4.3.7). $W_{aircraft}$ is the aircraft weight at cruise, calculated as the average of the weight at the start and end of cruise. The wave drag modelling is a high order or high-fidelity analysis, which is beyond the scope of this chapter. For a present-day long-range sub-sonic aircraft like B787, the contribution of the wave drag (compressibility effects) to the total drag is small (2.9% at cruise altitude of 37,000 ft and Mach 0.85) [197]. After both C_L and C_D are calculated, the *L/D* (C_L/C_D) is calculated for cruise.

4.3.4.2 Wetted area and fuselage weight prediction model

Aircraft wetted area prediction

As observed from equations 4.2 and 4.3, S_{wet} is required for estimating the C_D. For a tube-wing aircraft, S_{wet} is calculated from using an empirical equation from Roskam [198] that relates S_{wet} to GTOW,

$$\log_{10}(S_{wet} \, [ft^2]) = D \log_{10}(GTOW \, [lb]) + C, \tag{4.5}$$

where the coefficients C and D are 0.0199 and 0.7531 respectively, for transport jets [198]. A validation of equation 4.5 is conducted for two cases, a Boeing 787 [197] and a tube-wing aircraft of future [199], and gives agreement to within ±5% (< + 2%) (see Appendix A section A.4.2).

Fuselage wetted area and weight prediction

For alternative fuels that are being studied here, a fraction of (for non-cryogenic fuels) or the entire fuel tanks (for cryogenic fuels) are installed in the fuselage. The increase in the fuselage length increases the aircraft wetted area, drag and weight, and resultantly the fuel consumption. Therefore, the S_{wet} of the alternative fuel powered aircraft is the sum of the S_{wet} of baseline aircraft and the wetted area of the additional fuselage required to store the alternative fuel. The fuselage wetted area ($S_{\text{wet,Fuselage}}$) is calculated as [200],

$$S_{\text{wet,Fuselage}} \, [\text{ft}^2] = \pi \, d_F \, l_F \left(1 - \frac{2 \, d_F}{l_F}\right)^{\frac{2}{3}} \left(1 + \left(\frac{d_F}{l_F}\right)^2\right), \qquad (4.6)$$

where the parameters d_F and l_F represent the cylindrical fuselage diameter and length (in ft). The fuselage weight (W_{Fuselage}) is then calculated as [201], [202],

$$W_{\text{Fuselage}} [\text{lb}] = 5 \, S_{\text{wet,Fuselage}} \, [\text{ft}^2]. \qquad (4.7)$$

Validations of equations 4.6 and 4.7 are included in Appendix A section A.4.3, where $S_{\text{wet,Fuselage}}$ and W_{Fuselage} of a Boeing 787 predicted using this method are within ±5% of their known values.

4.3.5   Additional systems weight for alternative fuels

In all cases of alternative fuels studied here, the OEW of the aircraft is expected to change because of the need for additional fuel storage, or fuel tank systems and the structure required to support these tank systems. The additional fuselage length for all alternative fuels is estimated from the fuel volume that need to be stored in the fuselage tanks.

4.3.5.1   Non-cryogenic fuels

For non-cryogenic fuels, a substantial fraction of the $W_{\text{F,total}}$ fits inside the existing tanks in the wings based on the tank volume of the baseline aircraft. The remainder of the fuel must be accommodated in the (additional) fuselage. There are two components of additional weight considered for non-cryogenic fuels: the additional tank weight required to hold the remaining fuel that cannot fit in the wing tanks and the additional fuselage weight required to accommodate this additional tank. The additional fuselage weight is calculated according to the approach described in section 4.3.4.

To estimate the additional tank weight for non-cryogenic fuels that have similar mass densities as Jet-A (100% SPK, ethanol, and methanol), the findings of Goraj [203] are used, who reported that the structural weight of a conventional fuel tank is ~1/70 of the fuel weight. Thus, the OEW calculation for non-cryogenic fuels ($OEW_{\text{non-cryogenic}}$) is given by,

$$\text{OEW}_{\text{non-cryogenic}}$$

$$= \text{OEW}_{\text{baseline}}(1 - \omega)$$

$$+ \frac{1}{70}\left(W_{\text{F,total,non-cryogenic}} - \frac{\rho_{\text{non-cryogenic}} \; W_{\text{F,total,baseline}}}{\rho_{\text{Jet-A}}} \right) \qquad (4.8)$$

$$+ \left(W_{\text{Fuselage,non-cryogenic}} - W_{\text{Fuselage,baseline}} \right)(1 - \omega),$$

where $W_{\text{F,total,non-cryogenic}}$ and $W_{\text{F,total,baseline}}$ are the total fuel weights of the non-cryogenic fuel and Jet-A fuel respectively at mission start; $\rho_{\text{non-cryogenic}}$ and $\rho_{\text{Jet-A}}$ are the densities of the non-cryogenic fuel and Jet-A fuel respectively; and $W_{\text{Fuselage,non-cryogenic}}$ is the fuselage weight of the non-cryogenic aircraft. ω is the weight reduction factor for fuselage weight and OEW (in percentage), which is dependent on technology improvement. It is zero by default for all non-cryogenic fuel cases during the performance evaluation of different alternative liquid fuels considered in this chapter.

4.3.5.2   Cryogenic fuels

For cryogenic fuels (LH$_2$, LNG, and LNH$_3$), in addition to the extra fuselage weight, the weight of cryogenic tank systems is added to the structural weight required to support the cryogenic tank system, to the OEW of the aircraft.

The gravimetric index, gravimetric efficiency, or gravimetric storage density (η), is defined as the ratio of cryogenic fuel weight to the sum of the dry tank weight and cryogenic fuel weight [34], [66], [86], [191]. The tank weight is dependent on the type of the insulation system used in its design [64]. Therefore, η is an important technology parameter that determines the feasibility of cryogenic-fuelled aircraft [34]. Advances in lighter and stronger composite materials have recently shown LH$_2$ cryogenic tank $\eta = 0.92$ for manufactured tanks [204] (which could improve in future), and that too for a small size tank (diameter 1.2 m and length 2.4 m). A study by Sjöberg et al. [205] models a light weight LH$_2$ tank (4.7 m length and 3 m diameter) using composite materials with $\eta = 0.94$ for a full tank, in comparison with metallic tank having $\eta = 0.71$. For the LH$_2$ fuel case in the present chapter, an integral type of cryogenic tank with foam-based insulation is selected in this study. An average value of η of 0.78 for long-range LH$_2$ aircraft is selected with an insulation thickness of 8.1 cm according to the study by Verstraete et al. [66]. There is significant uncertainty in the value of η. For example, foam based integral tanks are known to have higher η compared to other tank types, especially for larger tank volumes (on the order of 75%) [66], whereas a value of $\eta = 0.38$ was assumed to represent a double-wall evacuated tank with multi-layer insulation for a large long-range aircraft by the Clean Sky 2 - Fuel Cells and Hydrogen (FCH) joint project [34], [206]. In this chapter, an optimistic value is used and the sensitivity due to this uncertainty is explored in Chapter 5. For LNG, two cases are analysed, where the fuel tank is integral to the fuselage structure. The first LNG case uses a hypothetical value of $\eta = 0.78$, similar to LH$_2$ case. In the second LNG case, a present-day (best) value of $\eta = 0.63$ is used, which is similar to the values used in transportation of LNG fuel via trucks [207]. For LNH$_3$, the fuel the tank is assumed to be integral to the fuselage structure. The weight of cryogenic tank (assumed to be made of steel) is a quarter of the weight of required fuel (or $\eta = 0.8$) as a thumb rule according to Dincer et al. [208]. To calculate the tank internal volume, with

the outer diameter constrained by the fuselage diameter, the insulation thickness of 8.1 cm is assumed for the LH$_2$ case [66] and it is also applicable to the LNH$_3$ and LNG cases.

For all three cryogenic fuels (LH$_2$, LNG, and LNH$_3$) to be installed in the fuselage, a structural support weight for the integral cryogenic tanks is added which is 6% of the fuselage weight according to the study by Verstraete et al. [66]. While this weight penalty was defined for a LH$_2$ aircraft, it is assumed that the same penalty applies to both LNG and LNH$_3$ aircraft since there are less published studies on these fuels. Therefore, the OEW calculation for cryogenic fuels is,

$$\text{OEW}_{\text{cryogenic}} = \text{OEW}_{\text{baseline}} (1 - \omega) + \frac{(1 - \eta) \ W_{\text{F,total,cryogenic}}}{\eta} + 0.06 \ W_{\text{Fuselage,baseline}}(1 - \omega) + \left(W_{\text{Fuselage,cryogenic}} - W_{\text{Fuselage,baseline}} \right)(1 - \omega), \tag{4.9}$$

where $\text{OEW}_{\text{baseline}}$ is the baseline aircraft OEW, $W_{\text{F,total,cryogenic}}$ is the total fuel weight of the cryogenic fuel at mission start, and $W_{\text{Fuselage,cryogenic}}$ and $W_{\text{Fuselage,baseline}}$ are the fuselage weight of the cryogenic and baseline aircraft respectively. ω is dependent on technology improvement and it is zero by default for all cryogenic fuel cases in this chapter.

4.3.6   Off-design analysis
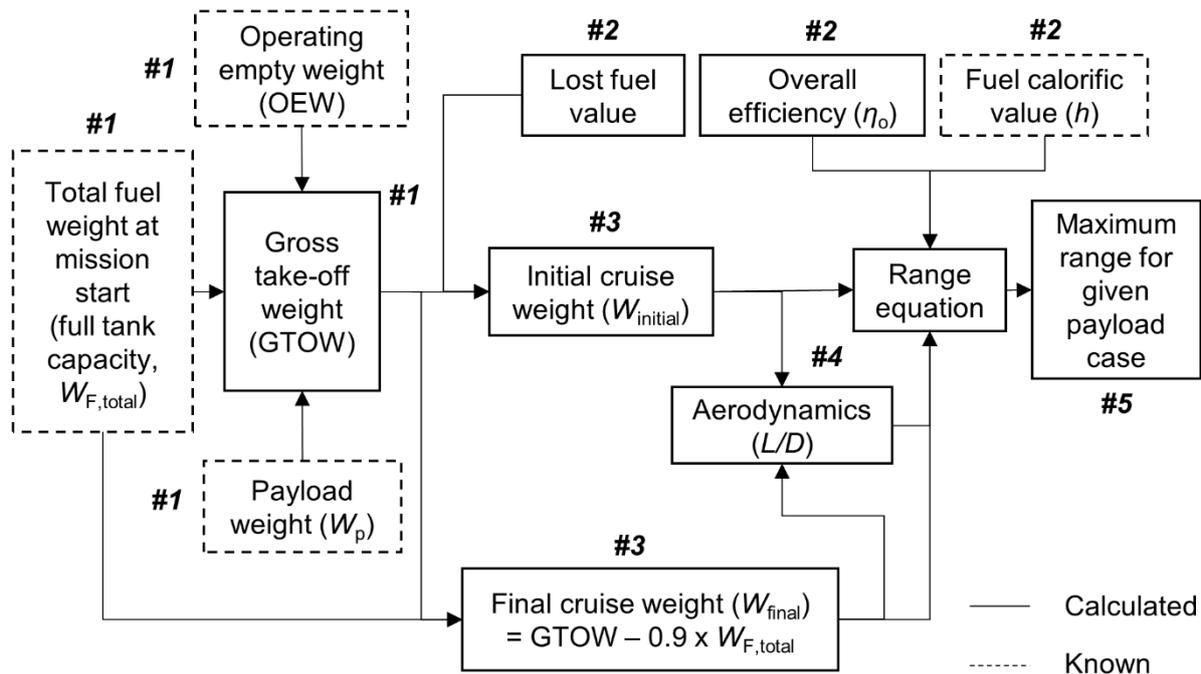
Figure 4.3. Schematic for the estimation of the maximum permissible range with full fuel tank for a given payload case. Boxes with dashed borders represent known values, boxes with solid border represent a calculation step, and # represent the calculation step number

By using the methodology discussed in sections 4.3.1 to 4.3.5 for Breguet's range equation analysis, the aircraft performance at design point is known for different fuel cases. The aircraft now becomes a 'fixed'

aircraft with fixed OEW, fuselage length, and maximum fuel capacity for each fuel under consideration. However, in real world applications, airlines do not always operate their aircraft with full design payload capacity, design range, and/or full fuel tank. For example, with a full fuel tank and reduced payload or load factor (compared to design payload i.e., 100% load factor), the aircraft can fly greater distance compared to the design range. Such operation is known as the off-design point performance of the aircraft.
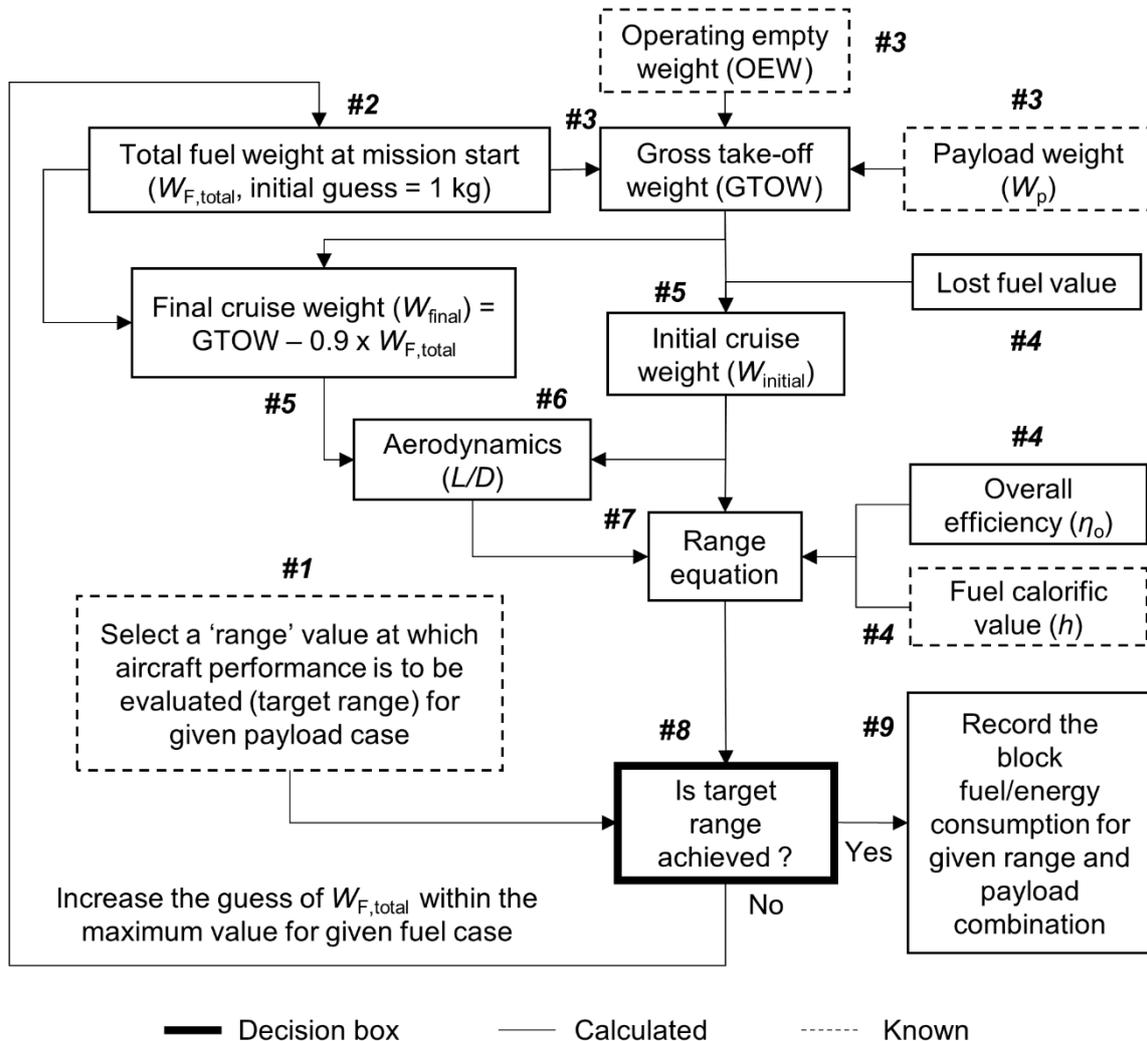
Figure 4.4. Schematic for the estimation of the $W_{F,block}$ of an aircraft for given range and payload combination. Boxes with dashed borders represent known values, boxes with thin solid border represent a calculation step, boxes with solid thick border represent a decision box, and # represent the calculation step number

In this chapter, after identifying the alternative fuels that meet the design target range of the baseline Jet-A aircraft within the MTOW limit, the off-design aircraft performance for such fuel(s) is evaluated for typical range and payload (load factor) combinations for long-range flights. Three off-design passenger – load factor cases are considered for A350-1000 aircraft, other than its design reference point (366 passengers, 34.8 tonnes passenger payload): (i) 200 passengers (19 tonnes passenger payload, 55% load factor); (ii) 250 passengers (23.8 tonnes passenger payload, 68% load factor); and (iii) 301 passengers (28.6 tonnes passenger payload, 82% load factor). These different payload cases are evaluated for aircraft range between 5,000 km

and the maximum range for a given load factor case flying with full tank capacity. The flowchart/schematic for the estimation of the maximum range with full fuel tank for a given load factor case using Breguet's range equation is shown in Figure 4.3. Additionally, Figure 4.4 shows the schematic for the estimation of the $W_{F,block}$ of an aircraft for given range and payload combination using Breguet's range equation. The stepwise process in Figure 4.3 and Figure 4.4 is detailed in Appendix A section A.3.

4.3.7 Known and calculated aircraft data

Table 4.3. Airbus A350-1000 Jet-A aircraft data and cruise conditions

Parameters	Units	Value
Aircraft data (Airbus A350-1000)		
Maximum take-off weight (MTOW)	kg	316,000 [209]
Maximum PAX in a 3-class configuration	-	366 [209]
Average weight of one passenger	kg	95 [209], [210]
Passenger payload weight (W_p)	kg	34,770 (= 366 x 95)
Total fuel weight ($W_{F,total, Jet-A}$) at mission start	kg	126,101 [209]
Operating empty weight ($OEW_{Baseline}$) (= MTOW $- W_{F,total, Jet-A} - W_p$)	kg	155,129
Overall efficiency (η_o)	-	0.4 [211]
Fuselage length (l_f)	m	72.25 [209]
Fuselage width (d_f)	m	5.96 [209]
Fuselage fineness ratio (l_f/d_f)	-	12.12
Wing area	m^2	465 [212] [213]
Span	m	65 [209]
Aspect ratio AR (= span^2/wing area)	-	9.12
Typical cruise conditions for large transport jets		
Altitude	ft	35,000
	m	10,668
Airspeed at 35,000 ft (10,668 m)	knots	490 [214]
	m/s	252.1
Mach number	-	0.85 [214]
Air density ρ_a at 35,000 ft	kg/m^3	0.38 [215]
Calculated data		
$S_{wet,Fuselage}$	m^2	1,208
	ft^2	13,000
$W_{Fuselage}$	kg	29,484 kg
$S_{wet,Fuselage}$	m^2	2,445
	ft^2	26,320

The Airbus A350-1000 aircraft is chosen as the baseline aircraft for the comparative assessment of the performance characteristics of the 100% SPK, LH$_2$, LNG, LNH$_3$, ethanol, and methanol in comparison with the performance of Jet-A. Table 4.3 lists the A350-1000 aircraft data which will be used for the aircraft performance modelling using Breguet's range equation. η_o for the A350-1000 aircraft (Jet-A) is known to be

0.4. Knowing this and the $\eta_{o,f}/\eta_{o,Jet\text{-}A}$ ratio for all fuels (known from section 4.3.2), the η_o is calculated for all alternative fuels to be used on the aircraft.

The validation of equations 4.1, 4.5, 4.6, and 4.7 is conducted Appendix A section A.4. The accuracy of the Breguet range (equations 4.1) is evaluated by predicting the performance characteristics of two in-service aircraft (Airbus A320-200 and Boeing B767-300F), and this validation is included in section A.4.1. A validation of equation 4.5 is conducted in section A.4.2 for two cases, a Boeing 787 and a tube-wing aircraft of future. Validation of equations 4.6 and 4.7 is included in section A.4.3, where $S_{wet,Fuselage}$ and $W_{Fuselage}$ of a Boeing 787 is predicted. Lastly, an attempt is made to validate the long-range LH_2 aircraft design in the Clean Sky 2 - Fuel Cells and Hydrogen (FCH) joint project [34], and this is included in section A.4.4. The performance prediction using respective equations are in reasonable agreement with the published data (within ±5%, a criterion defined for low-order aircraft performance modelling [184], [185] in Appendix A section A.4).

4.4   Results and discussion

The results of the performance evaluation of the six fuels at design point are analysed in section 4.4.1 and the off-design performance analysis results of the identified alternative fuels that meet the baseline aircraft range within the MTOW limit are discussed in section 4.4.2. Lastly, section 4.4.3 presents the relationship between OEW and GTOW for LH_2 aircraft.

4.4.1   Performance evaluation of alternative liquid fuels at design point

Figure 4.5 shows the comparison of different alternative fuels for their SEC and range performance within the MTOW limit of the baseline Jet-A aircraft carrying 366 passenger-payload (34,770 kg). It is to be noted that 100% SPK fuel has similar properties as that of Jet-A fuel, and thus its SEC is similar to Jet-A. The SEC points for 100% SPK and Jet-A fuel overlap, thus in Figure 4.5 these two points are combined together and labelled as 'Jet fuel'. It can be observed from Figure 4.5 that of the six alternative fuels only 100% SPK and LH_2 powered LTA aircraft (single decker tube-wing) enable the typical long-range flight distance as that of the Jet-A aircraft (baseline) of 13,870 km for 366 passenger-payload of 34,770 kg, within the limit of MTOW (of 316 tonnes). Thus, 100% SPK and LH_2 powered aircraft are quantitatively identified alternative liquid fuels from this chapter that enable a long-range air travel with an LTA aircraft. Further details of the performance characteristics of the baseline aircraft modified for the use of six alternative liquid fuels (for same payload of 34,770 kg i.e., 366 passenger payload) is included in Appendix section A.5. Additionally, Appendix section A.5 includes details of comparison of the aircraft and systems characteristics (such as fuselage length, wing loading, etc. for similar tank η) for LH_2 aircraft with other studies in literature.

Table 4.4 shows the SEC performance of identified alternative liquid fuels that enable long-range travel with an LTA aircraft. A study by Proesmans et al. [159] found that a 100% SPK aircraft had similar energy consumption as that of a Jet-A aircraft. Similarly, according to the findings of Hileman et al. [51], 100% SPK offers a 0.3% improvement in energy consumption relative to Jet-A while considering that the fuel gravimetric energy density is a significant aspect compared to the volumetric energy density. In the present

chapter, both gravimetric and volumetric energy densities are considered to be equally important. Considering this, the energy consumption benefits due to slightly better gravimetric energy density performance of 100% SPK gets reduced due to its slightly poor volumetric energy density performance (increase of fuselage length by 0.25 m or by 0.3%), compared to Jet-A. It can be observed from Table 4.4 that 100% SPK offers an insignificant (net) improvement (of 0.17%) in energy consumption as compared to Jet-A, which is similar to the findings of Hileman et al. For non-cryogenic fuel, especially 100% SPK it is observed that the fuselage length increases insignificantly (by 0.3%) to store additional fuel and this fuel could be accommodated in future aircraft designs with minor changes to the aircraft wing design instead of storing the fuel in fuselage as considered in this chapter.
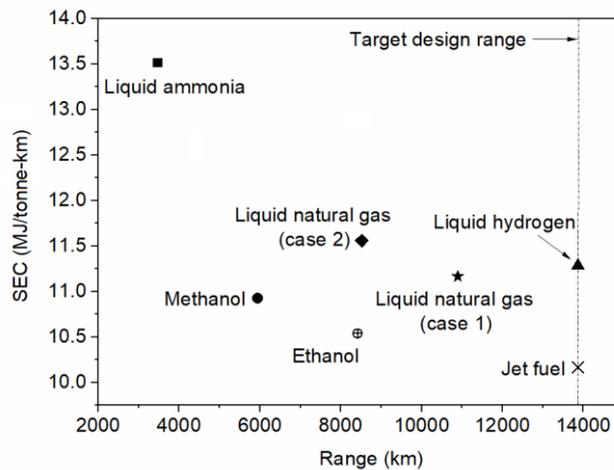
Figure 4.5. Comparison of different alternative fuels for their SEC and range performance within the MTOW limit of the baseline Jet-A aircraft carrying 366 passenger-payload (34,770 kg)

Table 4.4. Nominal SEC of LTA aircraft at 13,870 km range for payload of 34,770 kg with Jet-A, 100% SPK and LH$_2$

Fuel	ΔL (%)	$W_{F,block}$ (kg)	L/D	GTOW (kg)	OEW/GTOW	Wing loading at take-off (kg/m^2)	SEC (MJ/tonne-km)
Jet-A	-	113,491	18.63	315,999	0.49	679.6	10.17
100% SPK	0.3	110,988	18.57	313,404 (-0.82%)	0.50	674.0	10.15 (-0.17%)
LH$_2$	37.2	45,338	16.09	268,516 (-15%)	0.68	577.5	11.28 (+10.97%)

It can be observed from Table 4.4 that LH$_2$ aircraft consumes more energy than Jet-A aircraft due to its poor volumetric energy density performance compared to Jet-A and higher OEW due to cryogenic systems requirements, thereby resulting in longer and heavier fuselage (negative impact on L/D). The LH$_2$ aircraft fuselage length increases by 26.87 m (or by 37.2%) compared to Jet-A case. This finding is similar to the observation made in the study by Verstraete [68] where there is 38.2% increase in fuselage length for a single-decker 300 passenger LH$_2$ aircraft (using similar cryogenic tank η) but has a shorter design range of 9,000 km.

In terms of absolute value, for a single decker 400 passenger aircraft with a design range of 14,000 km, the study by Verstraete [68] finds that the LH_2 aircraft (similar cryogenic tank η) fuselage length is greater than 95 m which is of the similar order as that of the finding of this chapter (of approximately 99 m). More design details of this single decker 400 passenger aircraft by Verstraete [68] are not known in sufficient detail to enable further comparison. Moreover, according to a study by Onorato et al. [177], for a large LH_2 aircraft (295 passengers, 7,674 km), the authors find that there is a 37.1% increase in fuselage length (similar to the findings of the present chapter), compared to a single-deck Jet-A aircraft.

The cryogenic tank η used by Brewer [172], [180], [191] ($\eta = 0.836$) is of the similar order used in this chapter ($\eta = 0.78$). According to the book by Brewer [180], the LH_2 aircraft will have lower wing loading. Brewer [172], [180], [191] evaluates a double-decker 400 passenger LH_2 aircraft (18,500 km range). The wing (area) is subjected to modifications (wing structural weight and loading). The wing loading of the Jet-A and LH_2 aircraft are calculated to be 681.6 kg/m^2 and 569.3 kg/m^2, respectively (details in Appendix section A.5.1). Therefore, the wing loading (at take-off) of the double-decker 400 passenger LH_2 aircraft (18,500 km range) evaluated by Brewer [180] reduces by 16.5%, compared to the baseline Jet-A aircraft. In this chapter, the wing planform (area, span, and/or AR) is maintained constant for different fuel cases. This is similar to or in-line with the approach used in the Cryoplane study of minimal change to the wing planform. As observed from Table 4.4, the wing-loading of the LH_2 aircraft at take-off (577.5 kg/m^2) modelled in this chapter reduces by 15% (similar to 16.5% reduction observed by Brewer), in comparison with the wing-loading of the Jet-A aircraft (679.6 kg/m^2).

The significant reduction in the GTOW of LH_2 aircraft is of importance during emergency landing situations as a lighter aircraft will not necessitate jettison of a highly flammable LH_2 fuel (details in Appendix section A.5.2). For LH_2 aircraft, it is observed that relative to the baseline Jet-A aircraft, for a high energy dense (by weight) LH_2 fuel there is a net reduction in the aircraft GTOW of 15% (OEW/GTOW = 0.683) and 10.97% increase in SEC (for $\eta = 0.78$). These findings are similar to the observations made in the Cryoplane study which uses foam based insulation tanks (exact tank η not known but is expected to be of the similar order used in this chapter), where the SEC of the long-range LH_2 powered aircraft (using conventional tube-wing architecture) increases by 9% and GTOW reduces by 14.8% (OEW/GTOW = 0.68) relative to the Jet-A aircraft [175].

4.4.2 Off-design performance analysis

Figure 4.6 shows the SEC comparison of different fuel cases at different range and payload (load factor) combinations. The SEC for 100% SPK is similar to Jet-A and thus it is not shown in Figure 4.6 due to overlapping points (can be observed from Figure A.2 included in Appendix A section A.5.3). It can be observed that reducing the load factor increases the maximum aircraft range for all fuels (points on extreme right). Additionally, for any given load factor, the trend of SEC variation with range and the absolute values of SEC for Jet-A and 100% SPK are similar. For both fuels, it can be observed that there is a minimum point at ~7,000 km. On an absolute scale, the LH_2 aircraft ($\eta = 0.78$) consumes more energy than Jet-A aircraft at all combinations of range and load factor. For LH_2 aircraft, the SEC decreases with increasing range, though SEC

variation with range is less sensitive beyond ~10,000 km. Increasing the load factor improves SEC, for all three fuels. The difference in SEC variation with range for Jet-A (and 100% SPK) and LH$_2$ aircraft is due to the high OEW/GTOW ratio for LH$_2$ aircraft. The high OEW and lighter GTOW of the LH$_2$ aircraft than Jet-A case makes LH$_2$ aircraft consume more energy at lower range. Further details on the OEW/GTOW and aerodynamic performance variation with range for different load factor cases are included in Appendix section A.5.3.
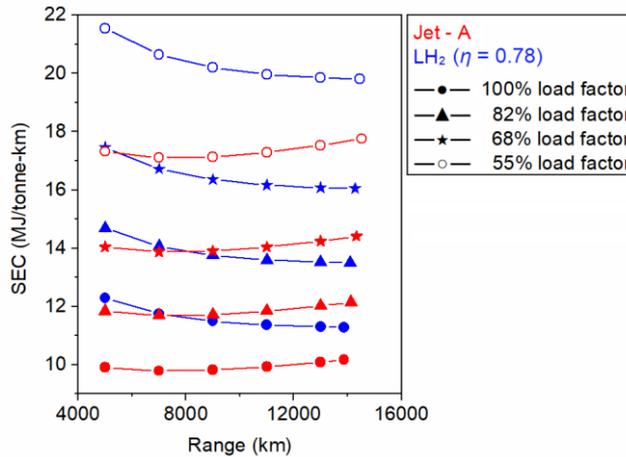
Figure 4.6. SEC comparison for Jet-A (and/or 100% SPK) and LH$_2$ aircraft ($\eta = 0.78$) at different range and payload (load factor) combinations
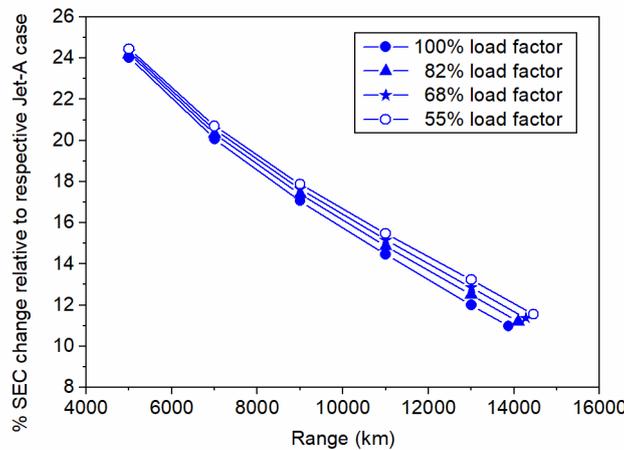
Figure 4.7. Comparison of percent change in SEC for LH$_2$ aircraft ($\eta = 0.78$) relative to the Jet-A aircraft at different range and payload (load factor) combinations

Figure 4.7 shows the comparison of percent change in SEC for LH$_2$ aircraft ($\eta = 0.78$) relative to the Jet-A aircraft at different range and payload (load factor) combinations. The percent difference in SEC between LH$_2$ and Jet-A aircraft decreases with increasing range for all load factor cases, and this reduction is greater at higher load factor cases. In other words, the effect of load factor on the percent difference in SEC between LH$_2$ and Jet-A aircraft increases with increasing range. For 100% SPK the percent difference in SEC relative to Jet-A aircraft is insignificant and is constant for all load factor and range combinations. Thus, 100% SPK is not included in Figure 4.7, and the said insignificant change in SEC can be observed from Figure A.3 included

in Appendix section A.5.3. In summary, 100% SPK can be used across all range and load factor combinations with similar SEC as that of Jet-A, whereas the SEC of LH$_2$ is lower at higher range and greater load factor combination though it is always greater than the SEC of Jet-A for all load factor cases i.e., tube-wing single-decker LH$_2$ aircraft is less energy efficient than Jet-A aircraft at all combinations of payload (load factor) and range.

Based on the findings in this section and section 4.4.1, a separate study is undertaken for a modified seating of A350-1000 to 301 passengers (in Appendix section A.6), and modification and use of retired aircraft (by major airlines during 2020 lockdown) such as Airbus A380 (in Appendix section A.7). This is in-line with recent efforts from Airbus to convert retired A380 aircraft into an LH$_2$ aircraft [216]. The SEC of these different LH$_2$ aircraft modelled are compared in Appendix section A.8. It is observed that due to a high ratio of OEW and W_p, for both LH$_2$ versions of A350-1000 (301 passengers) and A380 aircraft (seating 312 passengers), the SEC values are significantly greater (i.e., the direct operating costs could be significantly greater), especially for A380 LH$_2$ aircraft, than the SEC observed for A350-1000 (366 passengers). The inference from this separate study is that a custom designed double-decker tube-wing aircraft with large fuselage diameter (similar to A380) could not provide a better SEC performance for long-range travel of ~300 passengers compared to a single-decker tube-wing aircraft like A350-1000.

4.4.3   Relationship between OEW and GTOW for LH$_2$ aircraft

Figure 4.8 shows the relationship between OEW and GTOW of tube-wing LH$_2$ aircraft from the present study and literature (Brewer [180], Verstraete [68], Troeltsch et al. [173], Beck et al. [217], Proesmans et al. [159], Gomez et al. [172], Silberhorn et al. [168] (2019), Silberhorn et al. [176] (2022), Lammen et al. [170], Onorato et al. [177], and Huete et al. [178]). For data from Proesmans et al. [159], 'ATR' and 'COC' denote LH$_2$ aircraft optimised for average temperature response and cash operating cost, respectively. Additionally, in the study by Silberhorn et al. [168] (2019), the authors design three versions of LH$_2$ aircraft, where each version has a distinct tank installation location (rear, top, and pod) and these are included in Figure 4.8.

It can be observed from Figure 4.8 that the relationship between OEW and GTOW for the LH$_2$ aircraft designed in this research and earlier literature follow a consistent trend, which can be approximated by a power law. This trend (of 31 LH$_2$ aircraft) could facilitate a more rapid weight sizing studies on LH$_2$ aircraft designs using low-order modelling approaches. Similarly, an equation is developed (in Appendix section A.5.1) which provides a relationship between OEW and GTOW of 100% SPK from the present chapter and aircraft in service.

The chart plots OEW (kg) versus GTOW (kg) on logarithmic axes, with the fitted relationship:

$$y = 0.41x^{1.05}$$
$$R^2 = 0.99$$

Legend:
- This study (366 PAX 13,870 km)
- Brewer (130 PAX 2,778 km)
- Brewer (200 PAX 5,556 km)
- Brewer (400 PAX 5,556 km)
- Brewer (400 PAX 10,186 km)
- Brewer (400 PAX 18,520 km)
- Verstraete (150 PAX 4,000 km)
- Verstraete (300 PAX 9,000 km)
- Verstraete (400 PAX 14,000 km)
- Proesmans et al. ATR (67 PAX 2,410 km)
- Proesmans et al. COC (67 PAX 2,410 km)
- Proesmans et al. ATR (130 PAX 3,200 km)
- Proesmans et al. COC (130 PAX 3,200 km)
- Proesmans et al. ATR (253 PAX 10,800 km)
- Proesmans et al. COC (253 PAX 10,800 km)
- Silberhorn et al. (2019) (165 PAX 5,740 km) Rear tank
- Silberhorn et al. (2019) (165 PAX 5,740 km) Top tank
- Silberhorn et al. (2019) (165 PAX 5,740 km) Pod tank
- Airbus Cryoplane (185 PAX 7,400 km)
- Gomez et al. (194 PAX 9,000 km)
- Beck et al. BWB (524 PAX 11,408 km)
- Silberhorn et al. (2022) (261 PAX, 7,220 km)
- Lammen et al. (300 PAX, 3,704 km)
- Troeltsch et al. (400 PAX 11,853 km)
- Onorato et al. (72 PAX, 926 km)
- Onorato et al. (150 PAX, 4,560 km)
- Onorato et al. (295 PAX, 7,674 km)
- Huete et al. (232 PAX, 10,370 km)
- Huete et al. (332 PAX, 8,890 km)
- Huete et al. (388 PAX, 6,112 km)
- Huete et al. (720 PAX, 3,334 km)

Figure 4.8. Relationship between OEW and GTOW of LH₂ aircraft from the literature [except Beck et al. data point (BWB), all aircraft are tube-wing] and present study (Brewer [180], Verstraete [68], Troeltsch et al. [173], Beck et al. [217], Proesmans et al. [159], Gomez et al. [172], Silberhorn et al. [168] (2019), Silberhorn et al. [176] (2022), Lammen et al. [170], Onorato et al. [177], and Huete et al. [178])

4.4.4 Discussion

Firstly, the significant increase in the LH_2 aircraft fuselage length observed in this work could be a potential challenge associated with the use of LH_2 in the conventional tube-wing architecture, as this likely has structural and stability implications. Additionally, longer tube-wing LH_2 aircraft might not be readily compatible with the current airport design and layout. Secondly, for a significantly lighter LH_2 aircraft observed in this work (~15% GTOW reduction), aircraft design optimisation is necessary considering that a lighter aircraft would have reduced thrust requirement for maintaining the same thrust to weight (T/W) ratio, which could further decrease the SEC of the LH_2 aircraft. Thirdly, 100% SPK and LH_2 should be manufactured from less carbon intense or renewable energy pathways (considering lifecycle effects) that will enable a truly near-zero carbon air travel. Lastly, from the Breguet range equation it is known that the aircraft energy performance depends on aircraft technologies like aerodynamics, structures, and propulsion, and it is observed in this chapter that cryogenic tank η affects the aircraft energy performance. The effect of these four technology aspects on the long-range LH_2 powered LTA aircraft performance (such as its SEC) could be explored via a sensitivity analysis, which motivates Chapter 5. The above aspects are further elaborated in Appendix A section A.9.

4.4.5 Limitations of the present chapter

The present chapter is a low-order modelling of aircraft performance characteristics using Breguet's range equation for different fuels. The L/D ratio during cruise is based on the average aircraft weight during cruise. Also, in the estimation of the drag coefficient, wave drag is considered to be negligible which is typically considered in high-fidelity analysis. The evaluation of the aircraft performance characteristics in this chapter is limited to the aircraft use-phase only and these include the aerodynamics, weight, and energy performance. Low carbon fuels with more hydrogen content compared to Jet-A fuel, such as LNH_3, LH_2, LNG, etc. are expected to produce more water vapour at typical cruise altitude and could increase contrails, which are known to have a net warming effect on climate. However, significant uncertainties remain as to the contrail induced climate effects of hydrogen aircraft, and it might be possible to implement operational avoidance strategies, such as avoiding ice-supersaturated regions [45], [167]. The emissions and contrail performance, and effect of varying altitude on LH_2 aircraft, are not included in this chapter. Additionally, aircraft structural/stress and stability examination are not considered in this chapter (particularly resulting from increase in fuselage length), and these could be crucial for LH_2 powered aircraft where the aircraft fuselage length increases significantly (~30%). The present chapter does not conduct rigorous design and optimisation of aircraft employing different fuels. Lastly, the effect of cryogenic tank is not considered in detail and is based on other studies. Ideally, a separate design model for cryogenic tank is required that accounts both internal and external mechanical and thermal stresses.

4.5 Chapter summary and conclusions

This chapter evaluated low-carbon energy vectors for long-range LTA passenger aircraft and used the standard Breguet range equation to perform a comparative assessment for the characteristics of six alternative liquid fuels (methanol, ethanol, 100% SPK, LH_2, LNG, and LNH_3). Considering the realistic gravimetric and volumetric energy density effects, LH_2 and 100% SPK are the alternative liquid fuels that could enable typical long-range flight of approximately 14,000 km (or 7,500 nautical miles) in a conventional tube-wing aircraft for a 366 passenger-payload within the MTOW limit of the baseline Jet-A LTA aircraft. Additionally, by using present-day aircraft technology, the SEC (MJ/tonne-km) of the aircraft powered by LH_2 and 100% SPK (separately) could change by +10.97% and -0.17% respectively, compared to the Jet-A aircraft. A potential challenge associated with the use of LH_2 in the conventional tube-wing architecture is the significant increase in the fuselage length (~30%), as this could have structural and stability implications. Additionally, significantly long tube-wing LH_2 aircraft might not be readily compatible with the current airport in terms of aircraft operations such as taxi, landing, and take-off. Another inference from this chapter is that a custom designed double-decker tube-wing aircraft with large fuselage diameter (similar to A380 [greater OEW]) could not provide a better SEC performance for long-range travel of ~300 passengers compared to a single-decker tube-wing aircraft like A350-1000.

Moreover, this chapter conducts off-design point analysis that is of interest to airlines, using different range and payload (load factor) combinations for aircraft (separately) powered by LH_2 and 100% SPK. It is observed that for any given load factor, the SEC of LH_2 aircraft is higher than SEC of Jet-A aircraft at all range. The SEC of LH_2 aircraft decreases with increasing range but is less sensitive to range beyond 10,000 km. Additionally, the difference in SEC between LH_2 and Jet-A aircraft decreases with increasing range for all load factor cases, and this reduction is greater at higher load factor. Overall, 100% SPK can be used across all range and load factor combinations with similar SEC as that of Jet-A, whereas the SEC of LH_2 is lower at higher range and greater load factor combination though it is always greater than the SEC of Jet-A for all load factor cases. Additionally, an equation is developed in this chapter that relates the OEW and GTOW for LH_2 aircraft at design point, based on the present chapter and literature. This equation will facilitate low-order modelling or weight sizing of LH_2 aircraft. The aircraft energy consumption estimation in this chapter for both 100% SPK and LH_2 fuel should inform future studies on the estimation of: (i) feedstocks and/or pathways that could decarbonise long-range civil aviation on a lifecycle basis; and (ii) ticket pricing as the fuel cost is dependent on the energy consumption of aircraft and fuel manufacturing process. Lastly, it was observed that the four technology parameters like engine efficiency, structures (materials), aerodynamics, and cryogenic tank storage density could impact LH_2 aircraft energy performance and fuselage length. This motivates the next chapter on the global sensitivity analysis of technology parameters on energy performance of a (subsonic) tube-wing LH_2 long-range LTA aircraft.

Chapter 5: Global sensitivity analysis for examining the effects of technology on subsonic liquid hydrogen long-range tube-wing aircraft

5.1   Introduction

5.1.1   Background

In Chapter 4, it was observed that for a present-day aircraft technology there are only two alternatives to Jet-A fuel such as 100% SPK and LH_2 fuel for a typical long-range flight of 14,000 km (7,500 nmi) using an LTA tube-wing aircraft. 100% SPK aircraft performance is similar to Jet-A due to similar fuel properties but LH_2 aircraft consumes more energy than Jet-A. The energy performance of an LH_2 aircraft is dependent on different technologies. It is known from Chapter 4 that Breguet's range equation predicts the aircraft performance metrics from the fuel type (calorific value), and three aircraft technology aspects such as aircraft aerodynamics, η_o (propulsion), and aircraft weight (structures). Additionally, it was observed in Chapter 4 that cryogenic tank η affects the aircraft energy performance. The effects of these four technology parameters on the long-range LH_2 powered LTA aircraft performance (such as its SEC) is explored in this chapter via a global sensitivity analysis. The learnings of Chapter 4 motivate the present chapter.

The present chapter is a low-order evaluation of LH_2 aircraft performance. The aim of this chapter is to evaluate the effects of technology development on the performance of future subsonic LH_2 long-range LTA aircraft, towards the goal of sustainable aviation. The broader objective of this chapter is to perform a global sensitivity analysis to evaluate the effects of identified technology parameters for enabling a LH_2 powered long-range travel (~14,000 km) with an LTA aircraft, within MTOW limit of a baseline present-day LTA aircraft that seats 366 passengers. This chapter addresses research objective #2 discussed in Chapter 1. The detailed objectives of this chapter are formulated based on the literature review in section 5.2

5.1.2   Chapter structure

The studies that explore the performance characteristics of an LH_2 aircraft and their cryogenic tank η, are first reviewed in section 5.2. Thereafter, a global sensitivity analysis is performed to evaluate the effects of identified technology parameters for enabling an LH_2 powered long-range travel with an LTA aircraft, within MTOW limit of a baseline present-day LTA aircraft that seats 366 passengers using the methodology described in section 5.3 and the results are discussed in section 5.4.

5.2   Literature review on impact of technology development on aircraft performance

100% SPK has been extensively studied in literature [48], [51], [52], [59], and the findings of Chapter 4 are similar to studies by Hileman et al. [51] and Proesmans et al. [159], where we observe that 100% SPK offers negligible energy consumption benefits in the use-phase. The literature on the operational energy consumption or SEC of LH_2 aircraft, however, is very limited. LH_2 as an aircraft fuel is garnering interest because its gravimetric energy density is 2.78 times greater than Jet-A and its potential to emit zero carbon emissions in the use-phase [218]. However, the volumetric energy density of LH_2 is one-fourth that of Jet-A,

which poses challenge to LH_2 powered tube-wing aircraft design in terms of fuel storage. The aviation industry has initiated R&D and investments on cryogenic tank testing, fuel infrastructure, plans of fuel testing in aircraft, and conceptualizing aircraft design [160]–[164].

Studies on pure combustion based (thrust-powered gas turbine engines) LH_2 aircraft [165]–[170], [176], [177] simulate only the performance characteristics for regional/short- to medium-range aircraft. Following are the other studies focussed on pure combustion based LH_2 aircraft: (i) aircraft is partially powered by LH_2 (powered 67% by LH_2 and remaining by bio-kerosene) [174]; (ii) LH_2 aircraft is modelled for different range and (lesser) payload combination in comparison with the reference long-range LTA aircraft [171], [172]; (iii) LH_2 aircraft operates at lower cruise altitude and/or cruise Mach and has different aircraft design features in comparison with the typical reference long-range LTA aircraft [159], [173].

For tube-wing LH_2 aircraft, the fuselage length could increase by one-third of the baseline Jet-A aircraft fuselage length for accommodating the fuel thereby penalizing the aircraft SEC [34], [159], [218], and this is also observed in Chapter 4. As discussed before, the Breguet range equation shows that the aircraft performance depends on the type of fuel used and advancements in aircraft technology such as use of energy efficient engines, lighter materials, and improved aerodynamics, and thus it could be employed to examine the effects of the above three advancements in aircraft technology, especially on the long-range LH_2 powered LTA aircraft performance such as its SEC.

LH_2 cryogenic tank weight is an important technology parameter which is reported in literature either as: (i) the gravimetric index, gravimetric efficiency, or gravimetric storage density (η), which defined as the ratio of cryogenic fuel weight to the sum of the dry tank weight and cryogenic fuel weight [34], [66], [86], [191]; or (ii) the ratio of dry tank weight and cryogenic fuel weight (λ). The integral type of tank is part of the basic airframe structure. Thus, it must withstand fuselage bending, shear and axial stresses along with bearing fuel containment load. Non-integral tanks only carry the fuel, and they are mounted inside or outside the fuselage [64], [66]. Therefore, with a non-integral tank type, the tank's role is only to bear the loads resulting from the fuel containment such as internal tank pressure, aircraft acceleration, fuel weight, and fuel sloshing because of vibrations and manoeuvres. Non-integral tank design is heavier than integral tanks [64], [66]. The cryogenic tank weight is dependent on the type of the insulation system used in its design [64].

Different studies on LH_2 powered aircraft have been extensively reviewed and these are listed in Table 5.1 along with their tank gravimetric index. It can be observed from Table 5.1 that η is dependent on the type of insulation and it improves with increasing aircraft size or range. For example, foam based integral tanks are known to have higher η as compared to other tank types, especially for long-range travel (on the order of 75%) [66], whereas $\eta = 0.38$ for a double-wall evacuated tank with multi-layer insulation used for a large long-range aircraft by the Clean Sky 2 - FCH joint project [34], [206]. Additionally, a recent study by Huete et al. [178] examines the effect of η on aircraft range. The authors find that for short range aircraft the effect of η improvement on range is not as significant as the sensitivity observed for long-range aircraft. The authors find that for long-haul flights improving η from 0.3 to 0.85 increases the range from 7,400 km to 12,960 km respectively, however, the other performance metrics such as energy consumption are not known from this study. Therefore, from the above discussion and Table 5.1, it is observed that η is a significant technology

aspect that determines the feasibility of LH₂ powered aircraft. In Chapter 4, a nominal value of $\eta = 0.78$ is used for a foam based integral tank installed in an LH₂ aircraft employing present-day single decker tube-wing aircraft technology. This value of $\eta = 0.78$ is based on the study by Verstraete et al. [66] for long-range LTA aircraft. However, based on observations from Table 5.1 and above discussion, there is a need to evaluate the effect of cryogenic tank technology parameter η i.e., impact of different insulation material and/or tank type, on the (energy) performance of long-range LH₂ powered LTA aircraft. Further details on some of the studies in Table 5.1 is included in Appendix B section B.5 (Table B.4).

Table 5.1. Different studies on LH₂ powered aircraft and the cryogenic tank gravimetric index used

Study	Application	Tank type	η
Multi-layer insulation system			
Cleansky 2 [34], [206]	19 passengers with 500 km range	Integral	0.25
Cleansky 2 [34], [206]	80 passengers with 1,000 km range	Integral	0.30
Cleansky 2 [34], [206]	165 passengers with 2,000 km range	Integral	0.35
Cleansky 2 [34], [206]	250 passengers with 7,000 km range	Integral	0.37
Cleansky 2 [34], [206]	325 passengers with 10,000 km range	Integral	0.38
Foam insulation			
Huete et al. [178], [179]	232 passengers with 10,370 km range, 332 passengers with 8,890 km range, 388 passengers with 6,112 km range, and 720 passengers with 3,334 km range	Integral	0.45
Huete et al. [178]	232 passengers with 7,400 km range	Integral	0.3
Huete et al. [178]	232 passengers with 12,960 km range	Integral	0.85
Cryoplane [175], [181]	All aircraft categories	Integral	-
Winnefeld et al. [86]	General application of cylindrical tanks	Non-integral	$0.6 - 0.7$
Brewer's work summarised by Verstraete [191]	-	Non-integral	0.9
NACA/NASA [219], [220]	High-altitude (20 km) reconnaissance aircraft	Integral	0.881 feasible
Delgado Gosálvez et al. [70]	19 passengers with 926 km range	Non-integral	0.5
Verstraete et al. [66]	32 passengers with range of 2,100 km	Integral	$0.66 - 0.71$
Gomez et al. [172]	197 passengers with 9,000 km range	Integral	$0.74 - 0.83$
Brewer's work summarised by Gomez et al. and Verstraete [172], [180], [191]	400 passengers with 10,190 km range	Integral	0.84
Beck et al. [217]	VLTA blended wing body aircraft for 531 passengers with 11,400 km range	Non-integral	0.77
Verstraete et al. [66]	550 passengers with 13,890 km range	Integral	$0.76 - 0.79$

A study by Prewitz et al. [165] models the performance of a regional hydrogen aircraft (ATR-72) having a design range of 1,324 km for maximum payload of 7 metric tonnes. The authors evaluate the critical value of η of $0.33 - 0.35$ for flight operations to be more economic, while the required value of η to enable design target range is 0.19 (the current technology surpass the value needed). As discussed in the previous paragraph, the tank η depends on the aircraft type and range, and it is very likely that the critical value of η also depends on

these factors and the aircraft technology used. A study that estimates the critical value of η for a long-range LTA aircraft is missing in literature.

Studies by Verstraete et al. [66], Verstraete [68], Brewer [180], Airbus Cryoplane [181], Clean Sky 2 - Fuel Cells and Hydrogen joint project [34], [206], Troeltsch et al. [173], Proesmans et al. [159], and Huete et al. [178], [179] have modelled long-range LH_2 powered LTA aircraft but have not conducted a detailed sensitivity analysis which evaluates the impact of uncertainties in technology improvements on the LH_2 aircraft design and energy performance. There is a need for a global sensitivity analysis which quantitatively evaluates the potential technology improvements and outstanding uncertainties, in terms of the performance of long-range LTA aircraft powered by LH_2. Such an analysis would estimate the impact of uncertainties in technology improvements on the LH_2 aircraft design characteristics and energy performance, which directly impacts the direct operating costs, and lifecycle energy and emissions. Additionally, the use of advanced technologies could reduce the additional fuselage length resulting from LH_2 storage tanks and SEC. Lastly, this global sensitivity analysis will enable to estimate the critical value of tank η for a long-range LTA aircraft for the present-day and futuristic aircraft technologies. There are no studies in literature that conduct such a sensitivity analysis with the above pointed dimensions to the study. Considering the gaps pointed out in the previous paragraphs, none of the above three items are quantitively explored in literature. This is a first of its kind study that quantitively addresses the identified research gaps via an up-to-date literature review.

The aim of this chapter is to evaluate the effects of technology development on the performance of future subsonic LH_2 long-range LTA aircraft, towards the goal of sustainable aviation. The objectives of this chapter are to:

- Perform a global sensitivity analysis to evaluate the effects of identified technology parameters for enabling a LH_2 powered long-range travel with an LTA aircraft with low SEC, within MTOW limit of a baseline present-day LTA aircraft,
- Evaluate the critical value of cryogenic tank η for a long-range LTA aircraft, and
- Identify the technology parameters that could cause a dramatic improvement in SEC of an LH_2 powered long-range LTA aircraft.

The methodology for the global sensitivity analysis is detailed next in section 5.3 followed by results and discussion in section 5.4. Details omitted from the main text are included in Appendix B.

5.3 Methodology

Breguet's range equation is used for the aircraft performance evaluation towards the sensitivity analysis. The Airbus A350-1000 aircraft is used as a baseline, and it cruises at a typical Mach and altitude with required reserves. This aircraft is modified for the use of LH_2 where both gravimetric and volumetric energy density effects of this fuel are considered on the aircraft structure, propulsion, and aerodynamics.

5.3.1 Breguet's range equation

Breguet's range equation is given by equation 4.1 (Chapter 4 section 4.3.1) and it calculates the aircraft range from the *L/D*, aircraft weight, lower calorific value of the fuel, and η_o. The Breguet range equation is

employed to flight operations where the flight speed, L/D, and η_o are constant over the flight segment (example cruise) [183].

5.3.2 Flight mission profile and iteration process

In this chapter, Breguet's range equation analysis methodology is similar to the analysis at design point for LH_2 as conducted in Chapter 4. Following is summary of the approach. The Airbus A350-1000 aircraft (Jet-A) is selected as a sector-relevant baseline case, and LH_2 is evaluated for the same payload weight and design target range. For Jet-A baseline aircraft, the MTOW, OEW, and $W_{F,total}$ are known for a given W_p (366 passenger-payload), and this information and other data of A350-1000 aircraft (Jet-A) can be found in Chapter 4 section 4.3.7. For storing LH_2 fuel in the cryogenic tank systems, we allow for the extension of the fuselage, recognising that this would represent a significant engineering undertaking. The additional fuselage results in penalty on the aircraft performance through increased drag/wetted area and OEW. $W_{F,total}$ governs the volume requirement to store LH_2 fuel and thus OEW of the aircraft. The aircraft GTOW is the summation of W_p, $W_{F,total}$, and OEW. A constraint is set on the aircraft GTOW, and it should be less than or equal to the MTOW limit of 316 tonnes (metric) for the baseline aircraft (weight breakdown can be found in Chapter 4 section 4.3.7). This MTOW constraint is employed in this chapter since a detailed aircraft structural examination isn't conducted in this chapter. Thus, the MTOW governs the design limit on $W_{F,total}$ i.e., for LH_2, $W_{F,total}$ is iterated and calculated such that the aircraft GTOW $\leq$ MTOW. For LH_2 fuel, the wing design (AR, span, and planform area) is unchanged from the baseline aircraft, and this is similar to the procedure employed in the Airbus Cryoplane study [182]. The detailed methodology (design process schematic and equations) for calculating the OEW and L/D of the LH_2 aircraft which accounts for the performance penalty due to installation of cryogenic tank (weight) and the resulting increase in fuselage length and associated increase in fuselage structural weight can be found in Chapter 4 section 4.3. The cryogenic tank η, and OEW and ω are absorbed in the equation for the estimation of OEW of the LH_2 aircraft (i.e., equation 4.9 in Chapter 4). Additionally, C_f is absorbed in the equation for the estimation of the drag coefficient (or L/D calculation) (i.e., equation 4.3 in Chapter 4).

Equation 4.1 calculates the distance or range travelled during cruise. The fuel consumed in non-cruise operations is estimated using a lost fuel factor, which varies for different fuels and is represented as a percentage of the GTOW [114], [193]. The block fuel consumption (weight) $W_{F,block}$ is the sum of the fuel consumed during cruise and non-cruise operations of a typical mission. For both Jet-A and LH_2, a value of 0.9 is maintained for the ratio of $W_{F,block}$ and $W_{F,total}$, and it accounts for additional or reserve fuel, according to the study by Nickol et al. [130] for both blended wing body and tube-wing long-range LTA aircraft. The SEC (in MJ/tonne-km) is a pertinent performance parameter as it is an important service unit for airlines which helps in the estimation of the direct operating costs. The SEC for both baseline and LH_2 aircraft is calculated from the $W_{F,block}$ [SEC = $(W_{F,block}\, h) / (W_p\, R)$].

The aircraft weight at the beginning of cruise [$W_{initial} = (1 - \text{lost fuel factor}) \times \text{GTOW}$] is calculated using the lost fuel factor. The lost fuel factor for Jet-A and LH_2 is 2.2% and 1.4% respectively [114], [193]. The estimation of $\eta_{o,LH2}$ (overall efficiency of the LH_2 aircraft) from the known $\eta_{o,Jet-A}$ (overall efficiency of the baseline Jet-A aircraft) is detailed in Chapter 4 section 4.3.2. The ratio $\eta_{o,LH2} / \eta_{o,Jet-A}$ i.e., the ratio of overall

efficiency of the LH$_2$ aircraft and baseline Jet-A aircraft is calculated to be 1.0314 in Chapter 4 section 4.3. Therefore, knowing $\eta_{o,Jet-A}$ of the baseline A350-1000 aircraft, $\eta_{o,LH2}$ of the modified aircraft powered by this alternative fuel can be estimated. Additionally, the aircraft weight at the end of cruise [W_{final} = GTOW – 0.9 x $W_{F,total}$] is calculated by subtracting 90% of $W_{F,total}$ from the GTOW. Lastly, h for Jet-A and LH$_2$ are taken to be 43.2 MJ/kg and 120 MJ/kg respectively [47]. Thus, all parameters (or the calculation process) of equation 4.1 are known and the aircraft range can be evaluated.

5.3.3 Global sensitivity analysis

The effects of four technology parameters on the LH$_2$ aircraft performance are evaluated by simultaneously varying all four input parameters, using the Breguet's range equation: η, C_f, η_o, and ω. The ranges for each of these four parameters applied in the global sensitivity analysis are listed in Table 5.2. The ranges in Table 5.2 for four technology parameters are discussed further in this section.

The range for η (0.35 – 0.881) is directly based on multiple studies that model LH$_2$ aircraft for different range and passenger seating capacity, and these are included in Table 5.1 and this index is absorbed in equation which calculates the OEW of the LH$_2$ aircraft (i.e., equation 4.9 in Chapter 4). A study by Sjöberg et al. [205] simulates a light weight LH$_2$ tank (3 m diameter and 4.7 m length) employing composite materials with η = 0.94 for a full tank, compared with a metallic tank having η = 0.71. Recent advances in stronger and low-weight composite materials have enabled LH$_2$ cryogenic tank η = 0.92 for manufactured tanks [204] for a small sized tank (length 2.4 m and diameter 1.2 m), that might improve in future. The tank design specifics and application for both tanks revealed above are not known completely from respective studies, and thus they aren't listed in Table 5.1 and the maximum limit for the sensitivity analysis the remains unchanged (0.881).

Table 5.2. Input ranges for different technology parameters for the global sensitivity analysis

Input parameter	Minimum value	Maximum value	Reference
η	0.35	0.881	[34], [219], [220]
C_f	0.0025	0.003	[195], [196], [221]
η_o	0.4 for Jet-A	0.5 for Jet-A	[211], [222]
	0.413 for LH$_2$ (calculated)	0.516 for LH$_2$ (calculated)	
ω	0%	15%	[130]

C_f enables the estimation of the aircraft L/D. For the present large transport jets the value of C_f is 0.003 [43], [44]. For advanced/modern (N+2 and N+3 technology) large transport jets, C_f is projected to improve to 0.0025 [221], as futuristic aircraft could employ drag reducing devices/technologies. η_o of Jet-A powered present-day aircraft viz. A350-1000 is 0.4, and for future Jet-A aircraft engine this value is expected to increase to 0.455 [130] and 0.5 [211], [222] for N+2 and N+3 technology (2050 timeframe) respectively. According to Chapter 4, $\eta_{o,LH2}$ / $\eta_{o,Jet-A}$ is 1.0314. Using this ratio for the LH$_2$ powered A350-1000 (present-day), $\eta_{o,LH2}$ is calculated to be 0.413, and for the N+2 and N+3 technology (N+i)^2 LH$_2$ powered aircraft engine $\eta_{o,LH2}$ is calculated to be 0.464 and 0.516, respectively. In a futuristic aircraft design by Nickol et al. [130] using

---

[2] For N+i technology description and nomenclature, please refer Chapter 1

advanced technologies and materials for a LTA tube-wing aircraft, the fuselage weight (using stitched and resin-infused composite) and OEW of the Jet-A aircraft reduces by 15%. Thus, ω which is absorbed in the calculation of the OEW of the LH$_2$ aircraft (i.e., equation 4.9 in Chapter 4), varies from 0% (present technology) to 15% (N+2 and N+3 technology).

5.4 Results and discussion

The range of the baseline Jet-A aircraft is calculated to be 13,870 km (approximately 7,500 nautical miles), which is the target range for the LH$_2$ aircraft that has same MTOW limit of 316 tonnes (metric tonnes) at design point, as that of baseline Jet-A aircraft for the same passenger payload of 34,770 kg (366 passengers-payload) [218]. The following sections evaluate the sensitivity of LH$_2$ aircraft range, fuselage length, GTOW, and SEC, to the range of possible values for η, C_f, η_o, and ω.

5.4.1 Aircraft range and critical value of η
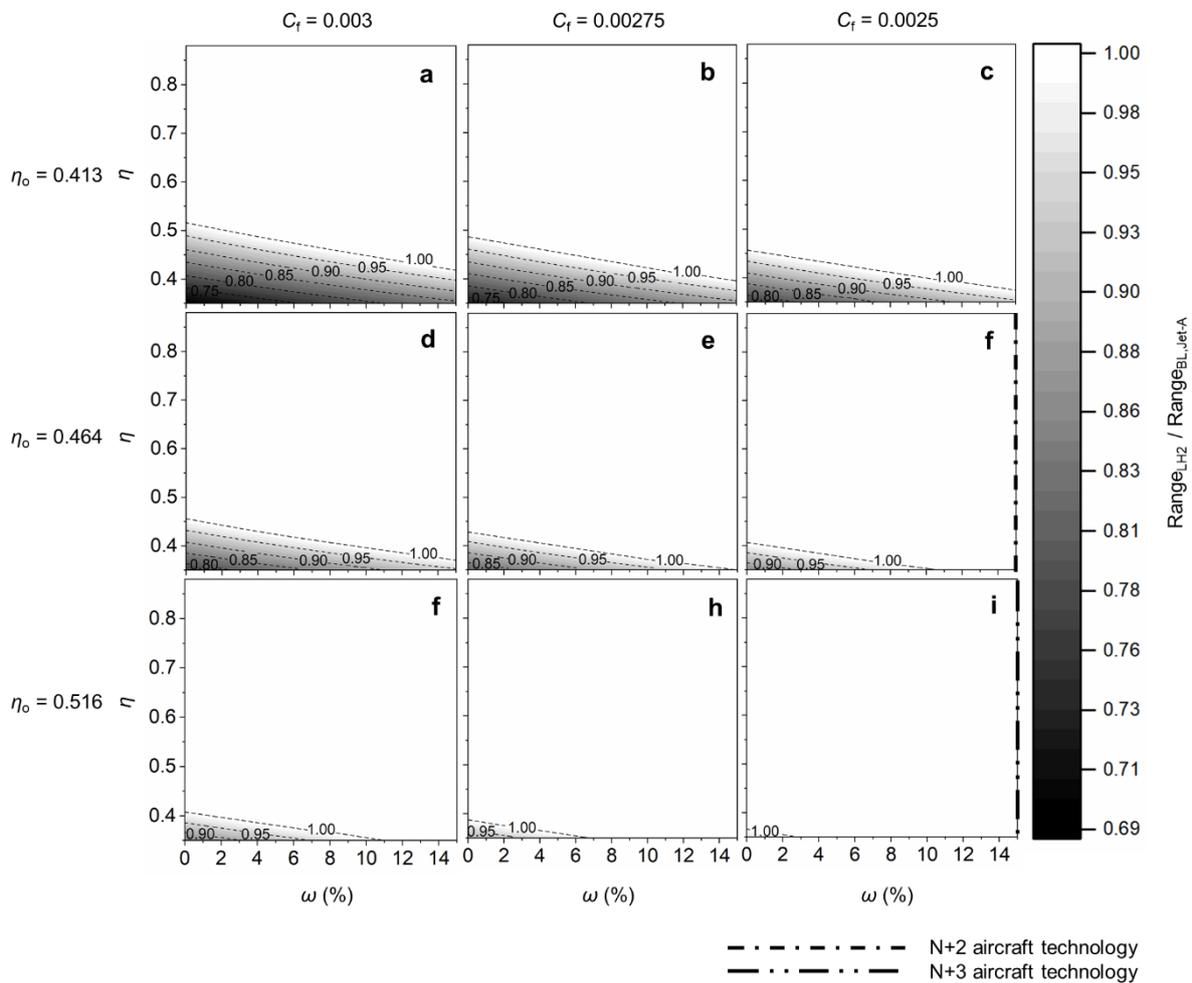
Figure 5.1. Effect of η, C_f, η_o, and ω on the LH$_2$ aircraft range relative to the (present-day) baseline (BL) Jet-A aircraft range

Figure 5.1 shows the effect of η, C_f, η_o, and ω on the LH$_2$ aircraft range relative to the (present-day) baseline Jet-A aircraft. In summary, the LH$_2$ aircraft range matches that of the baseline aircraft for higher η,

η_o, and ω and lower values of C_f. The different panels in Figure 5.1 represent different combinations of discrete values of η_o and C_f, and in each the relative range is shown for continuous values of η and ω for the range summarised in Table 5.2. For a given combination of η_o and C_f, the critical values of η and ω can be determined that would enable an LH$_2$ aircraft range on par with the baseline aircraft.

For today's values of $C_f = 0.003$ and $\eta_o = 0.413$ (plot a in Figure 1) and $\omega = 0$, $\eta_{critical}$ can be observed to be 0.52. Alternatively, if LH$_2$ storage tank weight were greater, and $\eta = 0.38$, the relative aircraft range would be limited to 75% (i.e., 10,000 km) and no reasonable values of ω would enable the aircraft to match the baseline range. For the best-case improvements to $C_f = 0.0025$ and $\eta_o = 0.516$ (plot i in Figure 5.1), it can be observed that baseline aircraft range would be matched for $\eta > 0.38$ if $\omega = 0$, and $\eta > 0.35$ if $\omega > 2.5\%$. Adding future aircraft technology reference points to the discussion, the single-dot-dashed and two-dot-dashed line represent N+2 ($\omega = 15\%$, $C_f = 0.0025$ and, $\eta_o = 0.464$) and N+3 ($\omega = 15\%$, $C_f = 0.0025$, and $\eta_o = 0.516$) technology, respectively. In Figure B.1 (in Appendix B) the effect of varying design target range and required $\eta_{critical}$ is shown for N+2 values of η_o and C_f at $\omega = 0$, and $\eta > 0.6$ is required for a design range of 20,000 km. Additionally, in Figure B.2 (in Appendix B) the effect of varying design target range and required $\omega_{critical}$ is shown for N+2 values of η_o and C_f at $\eta = 0.35$, and $\omega > 11\%$ is required for a design range of 14,000 km.

For the present-day aircraft technology, the critical value of η is 0.52 i.e., a minimum cryogenic tank η of 0.52 for enabling a (14,000 km) long-range LTA LH$_2$ aircraft (seating 366 passengers). Similarly, using N+2 and N+3 technology for the same payload and range combination, the (expected) critical value of $\eta <$ 0.35 and $\eta \ll 0.35$, respectively, for a long-range LTA LH$_2$ aircraft.

5.4.2   Fuselage length

Figure 5.2 shows how the fuselage length is dependent on η and ω for different values of C_f and η_o. The relative increase in the LH$_2$ aircraft fuselage length is calculated with reference to the baseline Jet-A aircraft. In general, increasing η and/or ω would reduce the required additional fuselage length. However, for lower values of η and ω, the design range is not achieved (due to the MTOW constraint) and consequently the LH$_2$ aircraft fuselage length increases and peaks once the critical values of these two parameters are reached. Then as η and ω increase further, the fuselage length decreases due to reductions in the cryogenic tank weight and aircraft structural weight respectively. As a result, the $W_{F,total,LH2}$ and associated OEW, and the aircraft GTOW reduce non-linearly with increasing η and/or ω after the critical point. At a given higher η (beyond critical value), increasing ω reduces the LH$_2$ aircraft fuselage length (and associated drag) as the aircraft OEW reduces, which improves the energy consumption.

Additionally, LH$_2$ aircraft fuselage length can be represented in terms of the fineness ratio, which is defined as the ratio of fuselage length and fuselage diameter [223] and/or in terms of $W_{F,total,LH2}$. The trends of the effect of η, C_f, η_o, and ω on $W_{F,total,LH2}$ and fineness ratio are shown in Figure B.3 and Figure B.4 respectively (Appendix B). These trends are similar to the trends observed in Figure 5.2.
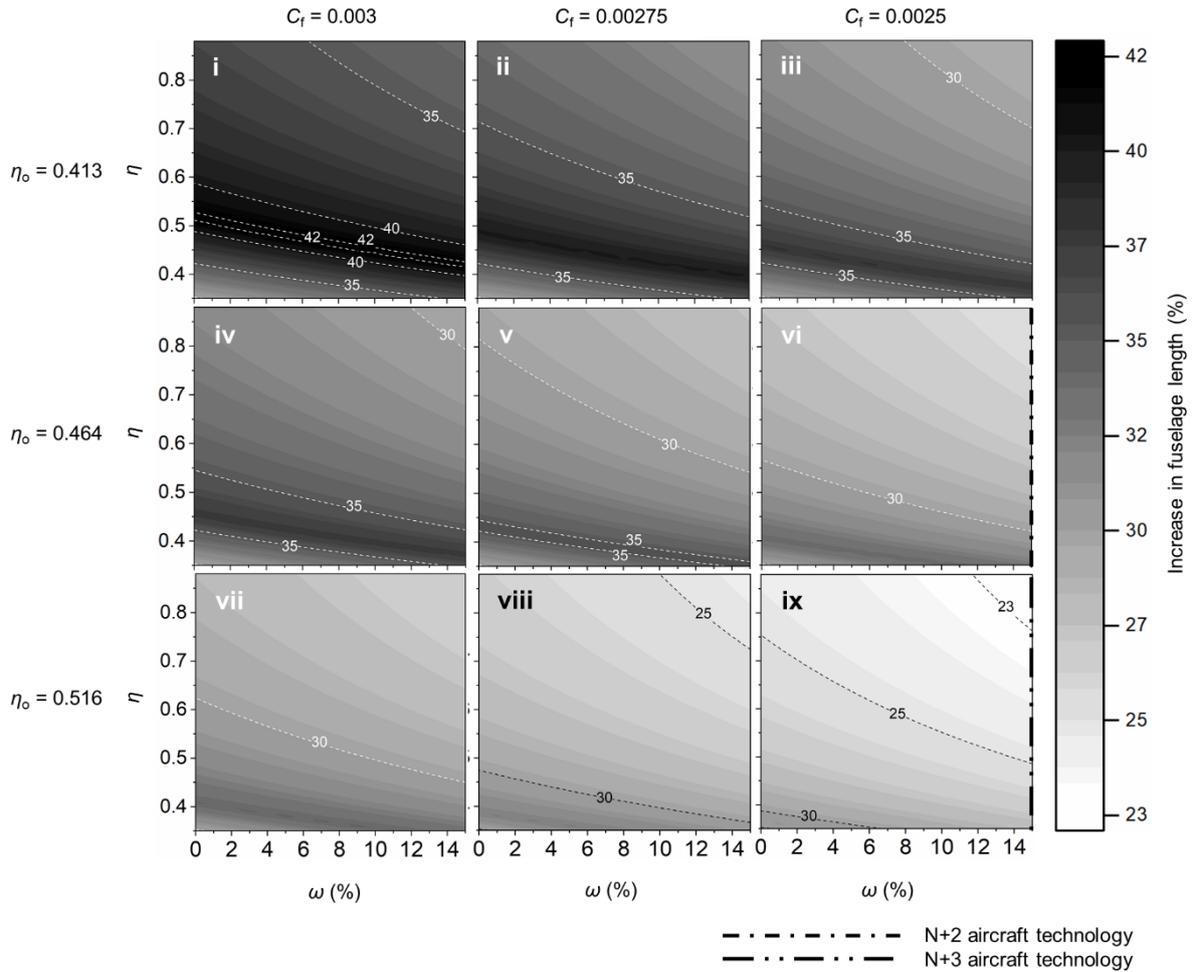
Figure 5.2. Effect of η, C_f, η_o, and ω on the percent increase in LH$_2$ aircraft fuselage length with reference to the (present-day) baseline Jet-A aircraft fuselage length

It can be observed from Figure 5.2 (with plot i in Figure 5.2 as a reference) that reducing C_f (from 0.003 to 0.0025) and/or increasing η_o (from 0.413 to 0.516) reduces the increase in the LH$_2$ aircraft fuselage length. Decreasing C_f reduces the drag coefficient (increases L/D), and/or increasing η_o improves the energy efficiency, thereby reducing the energy/fuel consumption or requirement and resultantly reducing the increase in the LH$_2$ aircraft fuselage length with reference to plot i in Figure 5.2. As a result, the LH$_2$ aircraft fuselage weight decreases with decreasing C_f and/or increasing η_o, and this can be observed from Figure B.5 provided in Appendix B. For present-day aircraft technology at $\eta = 0.52$, highest increase in LH$_2$ aircraft fuselage weight of 47% is observed. Additionally, for N+2 and N+3 aircraft technology, 10 – 15% and 6 – 10% increase is observed (for different η) in LH$_2$ aircraft fuselage weight, respectively.

Within the range defined in this chapter for the four technology parameters, the maximum increase in the LH$_2$ aircraft fuselage length is observed to be 42.1% (at $\eta_{critical}$ ridge in plot i in Figure 5.2). Additionally, N+2 aircraft technology leads to an increase in LH$_2$ aircraft fuselage length in the range of 27 – 33% (for different η). Lastly, the minimum increase in the LH$_2$ aircraft fuselage length is observed to be 22.5% (plot ix in Figure 5.2), where η, η_o, and ω have the maximum values and C_f has the minimum value i.e., N+3 aircraft technology with highest η ($\eta = 0.881$).

In the regime of η and ω combinations where the GTOW of the LH$_2$ aircraft equals MTOW, increasing ω reduces the aircraft structural weight, and therefore more LH$_2$ fuel quantity can be accommodated until the MTOW limit is reached. As a result, increasing ω increases the cryogenic tank weight in this regime. Increasing η and/or ω beyond their critical point reduces the cryogenic tank weight non-linearly (as $W_{F,total,LH2}$ decreases non-linearly from earlier discussion). These trends can be observed from Figure B.6 provided in Appendix. At a given higher η (beyond the critical value), increasing ω reduces the cryogenic tank weight as the aircraft gets lighter which improves the energy consumption. Additionally, reducing C_f and/or increasing η_o decreases the energy consumption/requirement (and $W_{F,total,LH2}$) and thus reduces the cryogenic tank weight. The lowest cryogenic tank weight is observed for both N+2 and N+3 aircraft technology at $\eta > 0.85$.

5.4.3   GTOW
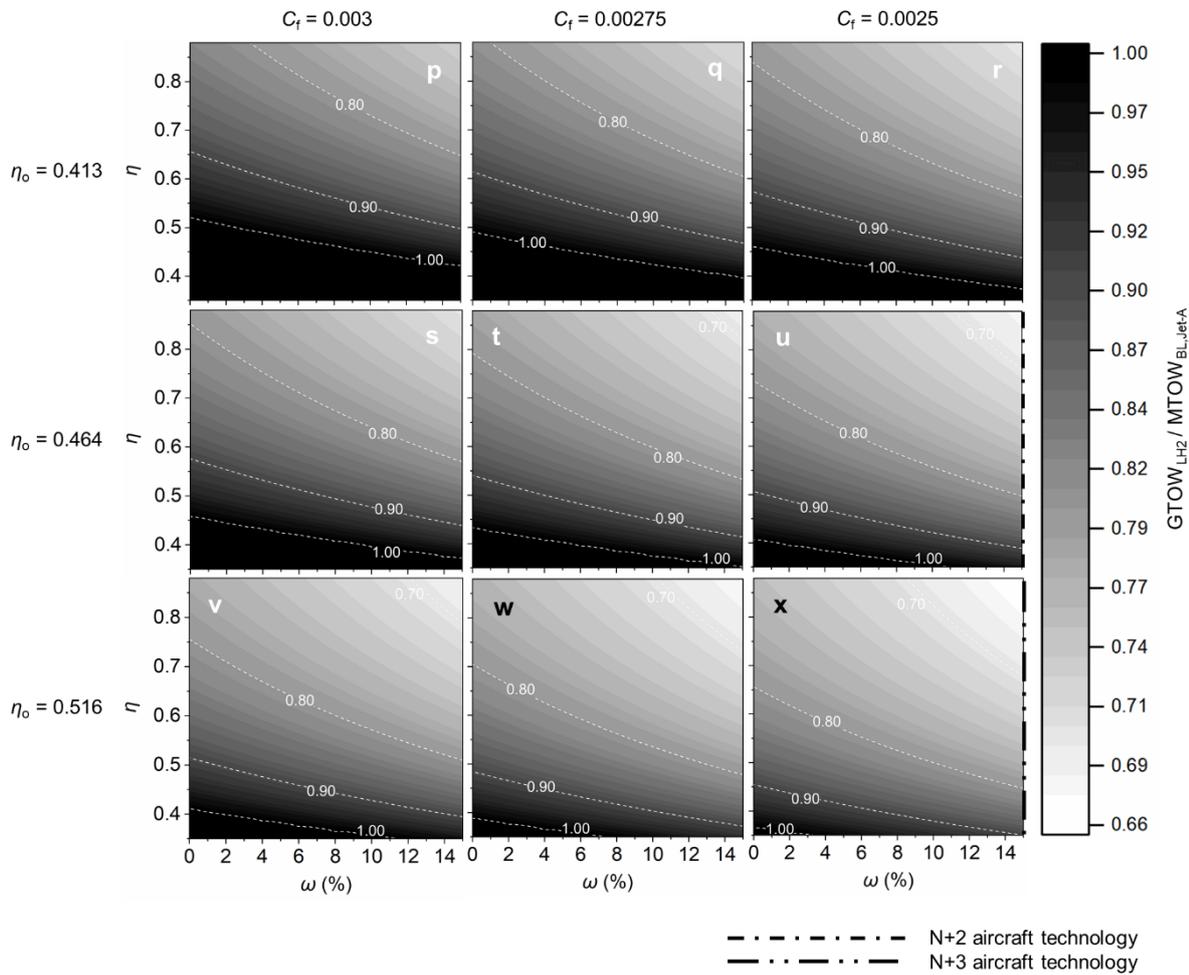
Figure 5.3. Effect of η, C_f, η_o, and ω on the ratio of the GTOW of the LH$_2$ aircraft (GTOW$_{LH2}$) and the MTOW of the (present-day) baseline Jet-A (MTOW$_{BL, Jet-A}$) aircraft

Figure B.7 provided in Appendix shows the effect of η, C_f, η_o, and ω on the ratio of OEW of the LH$_2$ aircraft (OEW$_{LH2}$) and the OEW of the (present-day) baseline (BL) Jet-A (OEW$_{BL, Jet-A}$) aircraft. It is observed that increasing ω decreases LH$_2$ aircraft OEW, which is expected as per the definition of ω. As discussed earlier, increasing η reduces the cryogenic tank weight. Particularly, increasing η after the critical point reduces the cryogenic tank weight and LH$_2$ aircraft fuselage weight non-linearly. As a result, the LH$_2$ aircraft OEW

reduces non-linearly with increasing η after the critical point. Additionally, reducing C_f and/or increasing η_o decreases the fuel/energy consumption and thus reduces the LH$_2$ aircraft fuselage weight and cryogenic tank weight, thereby reducing the LH$_2$ aircraft OEW. As expected, it is observed that lowest OEW$_{LH2}$ occurs at $\eta >$ 0.8 for both N+2 and N+3 aircraft technology.

Figure 5.3 shows the effect of η, C_f, η_o, and ω on the ratio of GTOW of the LH$_2$ aircraft (GTOW$_{LH2}$) and the MTOW of the (present-day) baseline Jet-A (MTOW$_{BL, Jet-A}$) aircraft. The (dark) regime of η and ω combinations where the GTOW of the LH$_2$ aircraft equals MTOW (i.e., GTOW$_{LH2}$/MTOW$_{BL, Jet-A}$ = 1) can be observed from Figure 5.3. After the critical point, increasing η reduces the LH$_2$ aircraft GTOW (= W_p + OEW$_{LH2}$ + $W_{F,total,LH2}$) non-linearly as both LH$_2$ aircraft OEW and $W_{F,total,LH2}$ reduce non-linearly (discussed earlier). At higher η (beyond critical value), increasing ω reduces the GTOW as the aircraft OEW reduces. Additionally, reducing C_f and/or increasing η_o decreases the fuel/energy consumption (and $W_{F,total,LH2}$ and the LH$_2$ aircraft OEW), and thus reduces LH$_2$ aircraft GTOW. For N+2 aircraft technology with $\eta > 0.8$, LH$_2$ aircraft GTOW reduces by approximately 30%. Within the range defined in this chapter for the four technology parameters, the maximum reduction in the LH$_2$ aircraft GTOW is observed to be 34% (plot x in Figure 5.3), where η, η_o, and ω have the maximum values and C_f has the minimum value i.e., N+3 aircraft technology with $\eta > 0.8$.

The effect of the four technology parameters on the L/D performance can be observed from Figure B.8 provided in Appendix B. Overall, the effect of C_f reduction on L/D performance is more pronounced than the effect of improvement in the other three technology parameters. The lift coefficient varies with the aircraft weight. Increasing η and/or ω reduce the GTOW or the aircraft weight (and lift coefficient) after critical point as discussed earlier, thereby reducing L/D. Additionally, reducing C_f reduces the zero-lift drag coefficient, thereby improving L/D performance. Similarly, increasing η_o decreases the fuel/energy consumption (or reduces LH$_2$ fuselage length and the associated zero-lift drag), and thus improves the L/D performance.

5.4.4   SEC and the sensitivity of technology parameters to it

The impact of the four technology parameters on different aircraft aspects discussed above affect the aircraft's energy consumption. Figure 5.4 shows the effect of η, C_f, η_o, and ω on the ratio of SEC in MJ/tonne-km of the LH$_2$ aircraft (SEC$_{LH2}$) and SEC of the (present-day) baseline Jet-A (SEC$_{BL,Jet-A}$) aircraft. As η increases, especially beyond the critical point (where design target range is met), LH$_2$ aircraft SEC decreases non-linearly due to the non-linear decrease in $W_{F,total,LH2}$ and OEW. Increasing ω reduces LH$_2$ aircraft weight and thus decrease the SEC, and this reduction is greater at higher η (beyond critical point). Additionally, reducing C_f and/or increasing η_o improves L/D and/or energy efficiency respectively, thereby reducing the LH$_2$ aircraft SEC. Within the range defined in this chapter for the four technology parameters, the maximum LH$_2$ aircraft SEC is observed to be 28.7% higher than the (present-day) baseline Jet-A aircraft (plot A in Figure 5.4, at low η with C_f = 0.003, η_o = 0.413 and ω = 0). Table 5.3 lists the performance characteristics of tube-wing LTA aircraft of different technologies and fuels for a design range of 13,870 km and carrying passenger payload of 34,770 kg. For N+2 aircraft technology (with $\eta > 0.8$) the SEC reduction for the LH$_2$ aircraft is of the order of 25% compared to the (present-day) baseline Jet-A aircraft (plot F in Figure 5.4) [or ~6% increase

in SEC compared to N+2 Jet-A aircraft (details in Table 5.3)]. Moreover, the N+3 technology (with $\eta > 0.8$) leads to a highest reduction in LH$_2$ aircraft SEC of approximately 33% than the (present-day) baseline Jet-A aircraft (plot I in Figure 5.4) [or ~6% increase in SEC compared to N+3 Jet-A aircraft (details in Table 5.3)]. This finding is very similar to the findings of the study by Silberhorn et al. [176], which models the energy performance of LH$_2$ aircraft seating 261 passengers over 7,220 km using 2035 (N+3) aircraft technology. The energy consumption of this N+3 LH$_2$ aircraft decreases by 37.6% compared to present-day Jet-A aircraft.
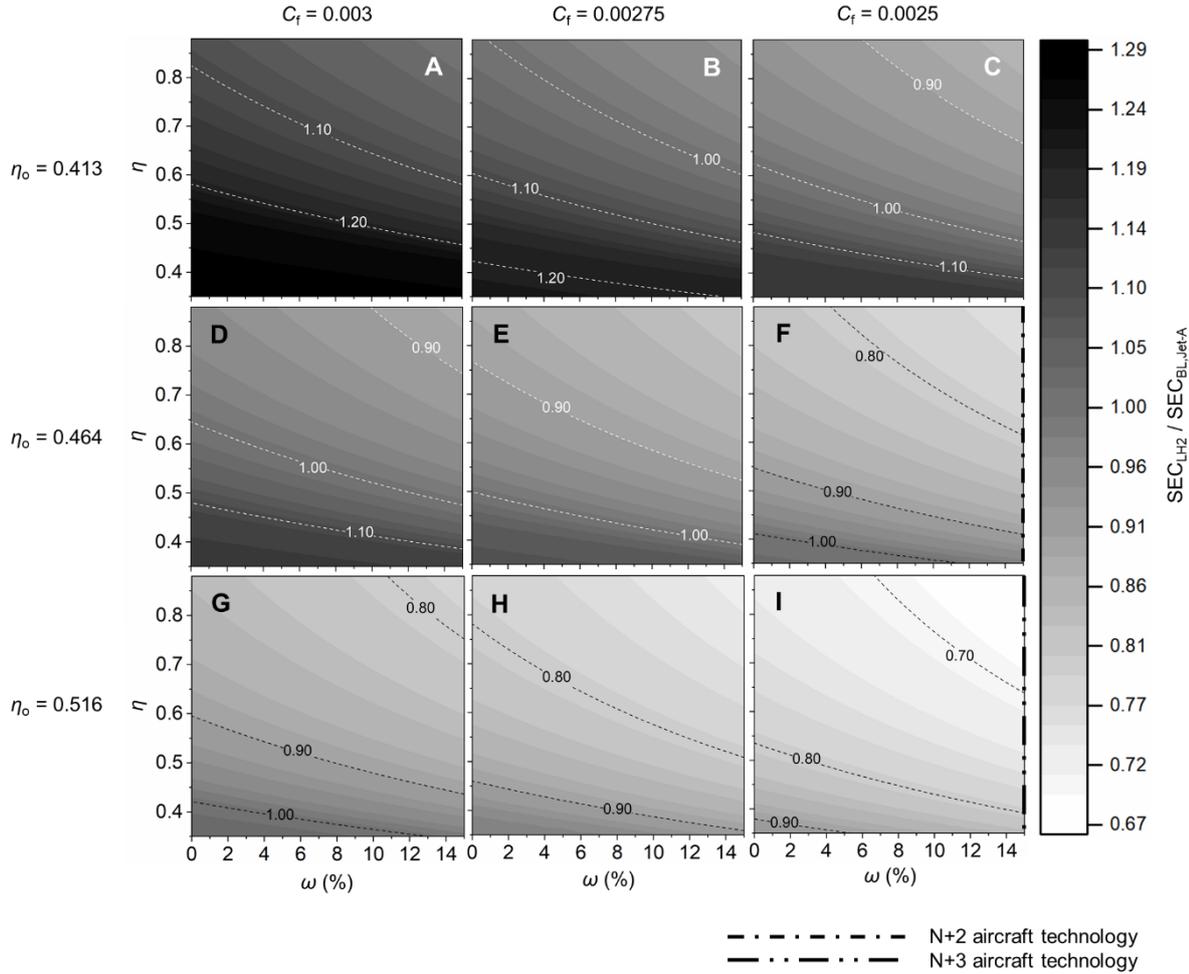
Figure 5.4. Effect of η, C_f, η_o, and ω on the ratio of SEC of the LH$_2$ aircraft (SEC$_{LH2}$) and SEC of the (present-day) baseline Jet-A (SEC$_{BL, Jet-A}$) aircraft

Table 5.3. Performance characteristics of tube-wing LTA aircraft of different technologies for a design range of 13,870 km and carrying passenger payload of 34,770 kg

Aircraft/fuel	η	$W_{F,total}$ (kg)	Fuselage length (m)	OEW (kg)	η_o	L/D	GTOW (kg)	SEC (MJ/tonne-km)
Jet-A (A350)		126,101	72.25	155,129	0.40	18.63	316,000	10.17
N+2 Jet-A		89,256	72.25	131,859	0.45	19.74	255,886	7.20
N+3 Jet-A		79,791	72.25	131,859	0.50	19.55	246,420	6.43
LH$_2$ (A350)	0.88	49,226	98.51	175,532	0.41	15.88	259,528	11.02
N+2 LH$_2$	0.88	34,058	90.42	144,321	0.46	17.31	213,149	7.63
N+3 LH$_2$	0.88	30,433	88.48	143,155	0.52	17.33	208,358	6.82

Figure 5.5 shows surface plots for comparing the effects of η, C_f, η_o, and ω on the ratio of SEC of the LH$_2$ aircraft and SEC of the (present-day) baseline Jet-A aircraft. Overall, it can be clearly observed from Figure 5.5 that the effects of varying ω and/or η on LH$_2$ aircraft SEC are weaker than the effects observed for varying C_f and/or η_o. At higher values of η, increasing ω by 15% causes a significant reduction in LH$_2$ aircraft SEC compared to the effects observed at lower values of η. At higher values of η (beyond $\eta = 0.7$), LH$_2$ aircraft SEC is less sensitive to η variation. This ($\eta > 0.7$) is the typical regime observed for foam-based insulation tanks for long-range travel in large aircraft (from Table 5.1).

Referring to Figure 5.5 and using same plot names from Figure 5.4 (viz. plots A, C, G, and I), for a fixed C_f and η_o, and constant η, increasing ω by 15% causes a maximum reduction of LH$_2$ aircraft SEC by approximately 8%. Additionally, for a fixed C_f and η_o, and constant ω, increasing η from 0.35 to 0.881 causes a maximum reduction of LH$_2$ aircraft SEC by approximately 21%. For a constant η_o, reducing C_f from 0.003 to 0.0025 reduces LH$_2$ aircraft SEC by approximately 14% (moving from surface A to surface C). For a fixed C_f, increasing η_o from 0.413 to 0.516 (25% increase) reduces LH$_2$ aircraft SEC by approximately 22.5% (moving from surface A to surface G). Surface plot I in Figure 5.5 has highest and lowest values of η_o and C_f respectively, used in this chapter, and it also includes the N+3 aircraft technology (not shown in Figure 5.5 but shown in Figure 5.4). The lowest LH$_2$ aircraft SEC is found on surface plot I in Figure 5.5, at highest η and ω.
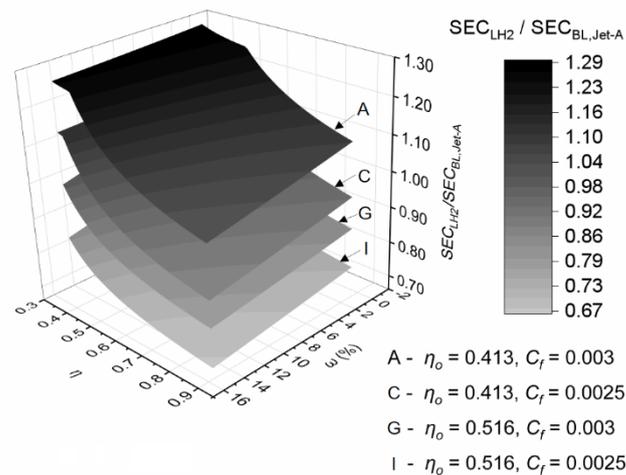
Figure 5.5. Surface plots for comparing the effects of η, C$_f$, η$_o$, and ω on the ratio of SEC of the LH$_2$ aircraft (SEC$_{LH2}$) and SEC of the (present-day) baseline Jet-A (SEC$_{BL, Jet-A}$) aircraft

5.4.5   Synthesis of results towards chapter objectives

It is observed via the global sensitivity analysis that all four technology parameters – η_o, C_f, ω, and η – impact the long-range LTA LH$_2$ aircraft performance. The aircraft design performance characteristics studied quantitatively (in section 5.4.1 to 5.4.4) are the aircraft range, fuselage length extension for LH$_2$ storage, aircraft GTOW, and SEC and the sensitivity of technology parameters to it.

For the present-day aircraft technology, the critical value of η is 0.52 for a long-range LTA LH$_2$ aircraft. For N+2 and N+3 technology, the (expected) critical values of η are $\eta < 0.35$ and $\eta \ll 0.35$, respectively, for a long-range LTA LH$_2$ aircraft. Regardless of the aircraft technology, η should be maximised

for reducing the SEC of the LH$_2$ aircraft. Lastly, it is observed that by increasing the target design range, the critical value of η also increases.

From the global sensitivity analysis and discussion, it is clear that the technology parameters that provide reduction in LH$_2$ aircraft SEC, in decreasing order of impact, are η_o, C_f, ω, and η. Ideally, all four technology parameters have to be improved in the future in order to enable a more energy efficient long-range travel with an LTA aircraft powered by LH$_2$ fuel. Particularly, η_o and C_f (or improved aerodynamics) provide a similar but significant order of reduction in LH$_2$ aircraft SEC, indicating that improving the overall efficiency and aircraft aerodynamics should be the priorities.

5.4.6   Discussion

Firstly, similar to the findings of Chapter 4 and discussion in section 4.4.4, it is observed that the LH$_2$ aircraft fuselage length increases significantly which could pose a challenge for LH$_2$ use in the conventional tube-wing airframe, since it could have stability and structural implications. The fineness ratio of the LH$_2$ aircraft modelled in Chapter 4 is (99.12/5.96 =) 16.63 (37.2% increase in fuselage length compared to the baseline Jet-A aircraft). From the global sensitivity analysis, the maximum and minimum fineness ratios are 17.23 (42.1% increase in fuselage length from baseline) and 14.85 (22.5% increase in fuselage length from baseline), respectively. Secondly, it is observed that the LH$_2$ aircraft could have significantly lower GTOW (<34% reduction) and thus optimisation is required for a lighter aircraft as the required thrust for maintaining the same thrust to weight (T/W) ratio reduces. This optimisation would further decrease the SEC of the LH$_2$ aircraft. Thirdly, from the sensitivity analysis it is found that improving aircraft aerodynamics is one of the ways to dramatically improve the energy efficiency of an LH$_2$ aircraft. The use of a BWB aircraft architecture could be a promising solution for LH$_2$ use as it is expected to provide benefits in terms of significantly better integration of LH$_2$ storage due to its higher internal volume and highly improved L/D performance [34], compared to tube-wing aircraft. Lastly, LH$_2$ should be produced from pathways that have low embodied carbon emissions or renewable energy pathways (considering lifecycle effects) that would contribute towards a near-zero carbon flight. The above aspects are further elaborated in Appendix B section B.2.

5.4.7   Limitations of the present research

The current chapter is a low-order modelling of LH$_2$ aircraft performance characteristics using Breguet's range equation for the sensitivity analysis. The L/D ratio during cruise is based on the average aircraft weight during cruise. Also, in the estimation of the drag coefficient, wave drag is considered to be negligible which are typically considered in high-fidelity analysis. This examination is restricted only to the operational or use-phase of the aircraft and lifecycle impacts are not considered. The effect of cryogenic tank is not considered in detail and is based on other studies. Ideally, a separate design model for cryogenic tank is required that accounts both internal, and external mechanical and thermal stresses. The combustion of LH$_2$ fuel would release more water vapour at typical cruise altitude and could produce more contrails, and other non-CO$_2$ effects [128]. Moreover, aircraft stability and stress/structural evaluation are not conducted in this chapter (especially due to increase in fuselage length), and these could be important for LH$_2$ powered aircraft

which is expected to have significantly greater fuselage length (~30% increase). The LH_2 aircraft could be significantly lighter (~30%) and thus optimisation (airframe and engine) is necessary as this aircraft would have reduced thrust requirement for maintaining similar *T/W* as that of the baseline aircraft (or same aircraft class/type). The current chapter does not carry out rigorous aircraft design and optimisation of LH_2 powered aircraft.

The other aircraft technology aspect that is important to the design of LH_2 powered long-range aircraft and the sensitivity analysis is the deck configuration or the fuselage diameter (single versus double deck). The volume of fuselage cryogenic fuel tank varies with the square of the diameter of the fuselage (for a tube-wing aircraft). Therefore, a large diameter (or equivalent diameter) fuselage similar to the Airbus A380 (double-decker VLTA) can prevent large increases in fuselage length. This is also observed in the study by Verstraete [68] that uses FLOPS (flight optimisation system) software for aircraft performance modelling. The effect of fuselage diameter or cross-section is not investigated in the present chapter because this chapter is developed mostly using publicly available data. There is not a single aircraft in the present/past fleet that has full double-decker configuration in the LTA aircraft type which is the scope of this research work.

5.5 Chapter summary and conclusion

In this chapter, a global sensitivity analysis is performed to evaluate the effects of four technology aspects – improved aerodynamics, use of lighter materials, cryogenic tank weight, and improved overall efficiency – on the performance of subsonic LH_2 powered tube-wing LTA aircraft for 14,000 km range (or 7,500 nmi) seating 366 passengers at the design point, while considering the realistic gravimetric and volumetric energy density effects of LH_2 fuel on aircraft design within the MTOW limit of the baseline Jet-A LTA aircraft. It is observed that the aircraft fuselage length increases significantly (~30%). This could pose challenges associated with the use of LH_2 in the conventional tube-wing architecture in terms of aircraft stability and structural design, and the compatibility of significantly long tube-wing LH_2 aircraft with the present airport infrastructure especially during aircraft operations such as LTO. It is observed that for the present-day technology, the critical value of η is 0.52 for a long-range LTA LH_2 aircraft. For N+2 and N+3 technology, the (expected) critical values η are $\eta < 0.35$ and $\eta \ll 0.35$, respectively, for a long-range LTA LH_2 aircraft, but regardless of the aircraft technology used η should be maximised for reducing the SEC of the LH_2 aircraft. Additionally, it is observed that by increasing the target design range, the critical value of η also increases. Moreover, it is observed that improving the η_o and aircraft aerodynamics could contribute dramatically towards a more energy efficient LH_2 powered long-range aircraft compared to the present-day Jet-A aircraft. Using the most optimistic estimates for technology development, the SEC of the LH_2 tube-wing aircraft could be up to 33% lower than a present-day Jet-A aircraft, requiring at least 22% increase in fuselage length. Considering the above, the use of a BWB architecture could be a promising solution for LH_2 use as it is expected to provide benefits in terms of better integration of LH_2 storage due to its higher internal volume and highly improved aerodynamics performance, compared to a tube-wing aircraft. This motivates Chapters 6 and 7. In Chapter 6, N+2 technology UHB engine is modelled fuelled by Jet-A, LH_2, and 100% SPK, and Chapter 7 provides operational phase energy performance modelling of N+2 BWB aircraft. Lastly, the results

of this chapter should inform further studies on the holistic lifecycle impacts of different LH_2 production pathways on LH_2 aircraft operation, which is explored in Chapter 8. This will enable informed decision making towards the selection of alternative fuels and its production pathway, for a truly climate neutral long-range air travel.

Chapter 6. Modelling of ultra-high bypass ratio engine

6.1   Introduction

6.1.1   Background

In Chapter 4, LH$_2$ and 100% SPK were identified as the alternative liquid fuels for typical long-range flight in a conventional tube-wing LTA aircraft. In Chapter 5, it was observed that improving η_o and aircraft aerodynamics could contribute dramatically towards a more energy efficient LH$_2$ powered long-range aircraft compared to the present-day Jet-A aircraft. Along these lines, it was discussed in Chapter 5 that the use of a BWB architecture could be a promising solution for LH$_2$ use as it is expected to provide benefits in terms of better integration of LH$_2$ storage due to its higher internal volume and highly improved aerodynamic performance, compared to a tube-wing aircraft. In both Chapters 4 and 5, it was observed that the GTOW of LH$_2$ aircraft significantly reduces (or thrust requirement reduces) which necessitates a more detailed design and optimisation of an LH$_2$ aircraft for meeting *T/W* of the aircraft. The above findings and limitations of previous chapters motivate Chapters 6 and 7.

The combined objective of Chapters 6 and 7 is to develop energy consumption models of a future (N+2 timeframe) energy efficient aircraft using conventional jet fuel, LH$_2$ fuel, and 100% SPK, separately. Additionally, the results of Chapters 6 and 7 are useful to meet research objectives 3 and 4, respectively, that are discussed in Chapter 1. The scope of these chapters is limited to the conceptual design phase of a long-range 300 passenger LTA aircraft using N+2 BWB aircraft technology, as per the discussion (and summary) in Chapter 2. The future N+2 technology used for modelling the aircraft (and sub-systems) are well established and supported through publications. Chapters 6 and 7 address the propulsion aspect and aircraft weight sizing aspect of the conceptual aircraft design process, respectively. In Chapter 6 and Chapter 7, an engine model and aircraft's operational energy consumption model are developed, respectively, for conventional jet fuel, LH$_2$ fuel, and 100% SPK. In this chapter, a model of a future (N+2 timeframe) UHB GTF engine is developed using conceptual design approach, and this model is applied to design engines powered by Jet-A, LH$_2$, and 100% SPK (separately). The engine design and optimisation is conducted using commercial software called as GasTurb 13 [188], which is widely used for performance modelling and analysis of gas turbine engines for aircraft and ground-based power production. GasTurb 13 software is capable of zero-dimensional (thermodynamic cycle performance and weight estimation), and one-dimensional gas turbine analysis, which at least fall within the ambit of the conceptual engine design phase.

A literature review directly related and specific to the current chapter is carried out in section 6.2. There are no prior studies that specifically design hydrogen powered BWB aircraft with the design of an aircraft UHB GTF engine, for a long-range travel of 300 passengers. The proposed model is further used to develop engine designs of the future (N+2 timeframe) for conventional jet fuel, LH$_2$ fuel, and 100% SPK, in section 6.5, that are useful to meet the objectives of both Chapter 6 and Chapter 7 and to meet the set design specifications. There are validation cases that establish a confidence in the model, and these are included in Appendix C section C.1. According to the book by Kundu et al. [184] and thesis of Kirby [185], a prediction

difference of ±5% is acceptable in the conceptual design phase. Therefore, for the two validation cases considered in this chapter, this criteria of ±5% difference on engine metrics is used as a basis for establishing confidence in the model.

6.1.2 Chapter structure

The present chapter begins with a literature review on next generation propulsion systems, hydrogen powered engines, and on the design process of a gas turbine engine and aircraft, which is included in section 6.2. Thereafter, more details of the selected future aircraft and engine (UHB GTF) technology are listed and discussed comprehensively in section 6.3. Based on this discussion, design requirements are set for the aircraft and engine design. Because this chapter is focussed specifically on the conceptual engine design, the engine design data is then listed and discussed thoroughly considering future technological improvements for individual components in the aircraft engine. This is followed by the research methodology in section 6.4, where an engine model has been proposed and is developed using advanced materials and future component efficiencies. The engine model developed using GasTurb 13 in this chapter is comprehensively discussed, where the details comprise of data known from literature/publications, design requirements/specifications and the model inputs. The validation of the engine model is conducted in Appendix C section C.1. After discussing the methodology, the engine designs of the future for conventional jet fuel, LH_2 fuel, and 100% SPK are developed, and details are provided in section 6.5. The results comprise of performance analysis at on-design point and off-design points. Lastly, 'model' and 'design' can be used interchangeably, but with respect to this chapter, model refers to a generic engine parametric setup, whereas 'design' refers to a more specific version of the model with well-defined parameters.

6.2 Literature review on future propulsion and fuel systems

6.2.1 NextGen propulsion system and fuels

A study by Bijewitz et al. [224] design a UHB GTF engine powered by conventional jet fuel for future aviation application, using GasTurb 11 software. However, this study is limited to the on-design point, and the off-design points are not considered in the engine and/or aircraft performance estimation. This study is used in the first validation case (in Appendix C section C.1) as sufficient data for a replication study is supplied by the authors.

A study by Greitzer et al. [123] design a futuristic UHB engine powered by conventional jet fuel. The authors use NPSS software developed by NASA for on-design point analysis and GasTurb software for off-design analysis. The authors use this engine in a BWB aircraft of the future. There are primarily two important cases in the said study: BWB with BLI, and BWB without BLI. The N+2 BWB aircraft technology that is considered in the present chapter does not have BLI and the engines are podded.

Both studies (Bijewitz et al. [224] and Greitzer et al. [123]) cannot be directly compared to the present model since they have a different BPR-OPR combination, but are relevant to the present chapter. Moreover, the propulsion system in the study by Greitzer et al. [123] has four fans driven by two engine core compared

to a single fan driven via a gearbox by one engine core in the current chapter. Therefore, these studies cannot be used for direct comparison. In the present proposed model, the future component efficiencies are used and these come from the study by Greitzer et al. [123] and it also provides ratio of burner exit temperature and fan inlet temperature (T_4/T_2), which gives some reference point for temperature comparison (between future technologies).

A study by Kestner et al. [225] designed a N+2 UHB engine powered by conventional jet fuel. The authors use NPSS software in their analysis. The authors use this engine in a BWB aircraft of the future. There are two main cases: BWB with BLI, and BWB without BLI (podded engines). The N+2 BWB aircraft technology that is considered in the current chapter does not have BLI and the engines are podded. Additionally, the published engine and aircraft performance data by the authors of the said study is very limited and sparse, which neither enables a direct comparison of results nor encourages a replication/validation study.

In another study by Beck et al. [217], a first order examination of an LH_2 powered BWB aircraft (combustion-based) is developed. The aircraft design developed is a large quad or VLTA BWB aircraft type, which has a capacity similar to a Boeing 747 aircraft. Additionally, the BWB uses high BPR engines partially embedded into the airframe for implementing BLI. In terms of engine modelling, which is the scope of this chapter, the authors do not actually model the LH_2 powered engine. Instead, they calculate the specific fuel consumption (SFC) by scaling the SFC of the engine powered by the conventional jet fuel, by using the ratio of gravimetric energy densities of hydrogen and conventional jet fuel. Similar to the above studies, even this study cannot be used for a direct comparison.

A study by Corchero et al. [226] simulate the performance of a low BPR direct-drive turbofan engine powered by hydrogen using GasTurb 8. Even though the engine specification considered by the author is much different, some of the findings are useful towards thermodynamic cycle and performance comparison of conventional jet fuel and hydrogen powered engine designed in the present chapter. Because Corchero et al. only simulate a low BPR engine performance (compared to the UHB GTF currently studied) without its installed performance on aircraft, it cannot be used for direct comparison of results of this thesis.

Only the study by Nickol et al. [130] on N+2 aircraft technology is directly relevant to the proposed model since this study is selected as a reference case. This study is used for aircraft technology selection (as discussed in Chapter 2), and it sets the design requirements for the present study. This study is also used as the second validation case (Appendix C section C.1). The details of engine and aircraft data of N+2 BWB aircraft is discussed in section 6.3.

6.2.2   Hydrogen powered gas turbine engine

6.2.2.1   *Combustion physics of hydrogen*

Hydrogen is a promising alternative aviation fuel because of its high LCV of 120 MJ/kg compared to 43.2 MJ/kg of conventional jet fuel (kerosene/Jet-A) [55]. There are other aspects in terms of combustion physics that must be considered for the use of hydrogen as a fuel in gas turbine engines. There is a need to first

understand few relevant terms and mechanisms before proceeding with the analysis of the fuel switch from Jet-A to hydrogen in gas turbine engines.

First and foremost, it is important to understand the respective combustion chemistry/chemical reaction mechanism of Jet-A-air and hydrogen-air combustion. The equivalence ratio (Φ) is defined as the ratio of actual fuel-air ratio (FAR) and the stoichiometric FAR and is represented by equation 6.1. Φ is given by,

$$\Phi = \frac{FAR_{actual}}{FAR_{stoichiometric}} \tag{6.1}$$

where $FAR_{stoichiometric} = \frac{Molecular\ weight_{fuel}}{a'\left(1+\frac{0.79}{0.21}\right)Molecular\ weight_{air}}$. \hfill (6.2)

A 'major combustion species' model is presented below in equation 6.3 (source [227]), which provides a generic combustion reaction of fuel C_xH_y with typical major products of combustion. It is given by,

$$C_xH_y + a'\left(O_2 + \frac{0.79}{0.21}N_2\right) \rightarrow b'\ CO_2 + c'\ CO + d'\ H_2O + e'\ H_2 + f'O_2 + \frac{0.79}{0.21}a'\ N_2 \tag{6.3}$$
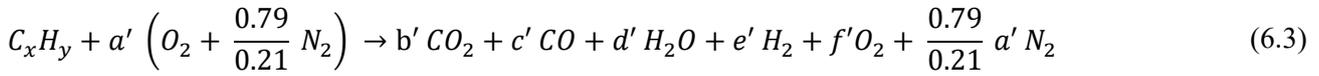
For fuel lean and stoichiometric condition i.e. $\Phi \leq 1$, equation 6.3 transforms to equation 6.4 (source [227]) as the reactant mixture is air rich and there will not be excess fuel to produce CO (c = 0) and H_2 (e = 0), as the combustion products, and this is represented by,

$$C_xH_y + a'\left(O_2 + \frac{0.79}{0.21}N_2\right) \rightarrow b'\ CO_2 + d'\ H_2O + f'O_2 + \frac{0.79}{0.21}a'\ N_2 \tag{6.4}$$
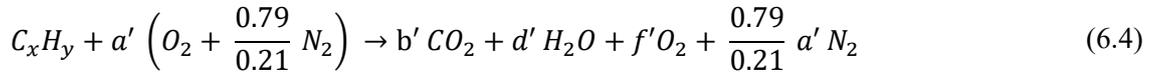
Similarly, for fuel rich conditions i.e. $\Phi > 1$, equation 6.3 transforms to equation 6.5 (source [227]) as the reactant mixture is fuel rich and there will not be excess oxidizer (especially oxygen, as nitrogen is considered to stay unreacted in this simple major species model) left over by the end of the combustion process. This transformation is given by,

$$C_xH_y + a'\left(O_2 + \frac{0.79}{0.21}N_2\right) \rightarrow b'\ CO_2 + c'\ CO + d'\ H_2O + e'\ H_2 + \frac{0.79}{0.21}a'\ N_2 \tag{6.5}$$
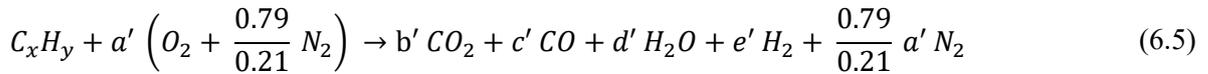
Future aircraft combustors are expected to burn in the fuel-lean regime because of improved efficiency as a result of high overall pressure ratio and bypass ratios [228]. Henceforth, for all analytical purposes only equation 6.4 is useful and relevant. It is important to note that the composition of air used in the equations below is 79% nitrogen and 21% oxygen, which is used for simplicity and is a theoretical composition typically used for analytical purposes. The resulting molecular weight is 28.85 g/mol. However, the composition of air is slightly different than the theoretical composition. In reality, air additionally includes other inert and non-inert gases resulting in a molecular weight of air of 28.97 g/mol [229]–[231]. The coefficients in equation 6.4 viz. are a', b', d', and f', are represented by equation 6.6 and these are given by,

$$a' = \frac{x+\frac{y}{4}}{\Phi}\ ;\ b' = x\ ;\ d' = \frac{y}{2}\ and\ f' = \frac{(1-\Phi)}{\Phi}\left(x+\frac{y}{4}\right) \tag{6.6}$$

Knowing the actual FAR, Φ can be calculated using equations 6.1, 6.2, and 6.6 for a given fuel-air combination. In this chapter, the actual FAR is predicted by GasTurb 13 [188] for both conventional jet fuel and hydrogen fuel. Jet-A fuel/kerosene is represented by the molecular formula of $C_{11.6}H_{22}$ (molecular weight of 161.5 g/mol) [232]. Therefore, x is 11.6 and y is 22 in equations 6.2 to 6.6. The combustion equation for Jet-A fuel for $\Phi < 1$ is represented by equation 6.7, and this is assumed to also apply to 100% SPK. The resulting equation 6.7 is arranged for 1 mole of air in the reactant, and is given by,

$$\frac{0.21\Phi}{17.1} C_{11.6}H_{22} + (0.21 O_2 + 0.79 N_2)$$
$$\rightarrow \frac{2.436\Phi}{17.1} CO_2 + \frac{2.31\,\Phi}{17.1} H_2O + 0.21(1-\Phi)\,O_2 + 0.79\,N_2 \tag{6.7}$$
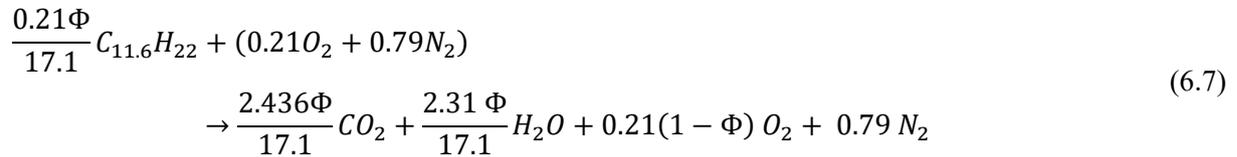
Similarly, for H_2, x = 0 and y = 2 equations 6.2 to 6.6, thereby b = 0. Therefore, the combustion equation for hydrogen fuel for $\Phi < 1$ is represented by equation 6.8, which is arranged for 1 mole of air in the reactant, and this is represented by,

$$0.42\Phi\,H_2 + (0.21\,O_2 + 0.79\,N_2) \rightarrow 0.42\Phi\,H_2O + 0.21(1-\Phi)O_2 + 0.79\,N_2 \tag{6.8}$$
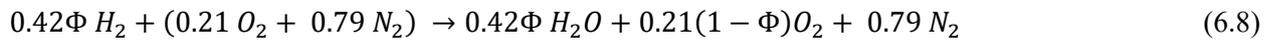
Therefore, if the Φ is known, the mass and molecular weight of both reactants and products can be calculated, for both Jet-A and hydrogen (mass is conserved). Both equations 6.7 and 6.8 are highly simplified because these do not include typical minor species like NO, NO_2, OH, etc. However, from analytical viewpoint both equations 6.7 and 6.8, are very helpful to predict mass and molecular weight of products. These equations are used in the results section (in section 6.5.2) for estimating the product mass and molecular weight of the products of combustion. This is very helpful in understanding the energy efficiency improvement in hydrogen engines, especially for same thrust production as that of Jet-A engine, where the actual fuel to air ratios are known. An interesting fact is that the molecular weight of products of combustion of gas turbine engines powered by Jet-A/kerosene is similar to the molecular weight of air, in the typical regime of engine operation [231], [233].

The reaction rate of hydrogen is seven times as that of conventional jet fuel [228]. This significant difference between the reaction rates of the two fuels can be explained from fundamental sciences. From kinetic theory of gases, the root mean squared speed, most probable speed, and mean speed of gas is inversely related to its the molar mass [234]. Comparing the properties of hydrogen (molecular weight of 2 g/mol) and kerosene (molecular weight of 161.5 g/mol) it is clear that the molar mass of the former case is significantly lower. This results in high speeds of hydrogen molecules. Rate of a reaction can be understood from kinetic theory of gases through the molecular collision frequency [235]. Collision frequency is proportional to the speed of gases [234]. Therefore, because of significantly higher speeds of hydrogen gas relative to kerosene (heavier molecule), the rate of reaction is higher for hydrogen compared to kerosene. Another simple reasoning for the seven times higher rate of reaction of hydrogen compared to kerosene is the significant difference in the number of bonds to be broken during combustion. Kerosene which is typically represented by $C_{11.6}H_{22}$, is a heavier hydrocarbon (molecular weight of 161.5 g/mol) which has multiple bonds, compared to H_2

(molecular weight of 2 g/mol). Due to the significantly lower number of bonds to be broken during the combustion of H_2, compared to kerosene, hydrogen has a higher rate of reaction.

The comparison of laminar premixed flame speeds (S_L^o) between different fuels can be done using equation 6.9 (source [236]), and it is given by,

$$S_L^o \propto \sqrt{\alpha \, RR} \qquad\qquad (6.9)$$

where α is the diffusive transport of energy (and species) from reaction zone into unburned gases and RR is the rate of reaction. Hydrogen is lighter compared to kerosene, and therefore it can diffuse quickly or has higher diffusion relative to kerosene. Additionally, as discussed above, the rate of reaction of hydrogen is seven times higher than kerosene. Therefore, as per equation 6.9 the flame speed of hydrogen is greater than that for kerosene.

For a flow channel (like a tube), if the diameter is smaller than some critical value, then the flame will not propagate in the tube even if the gas velocity in the tube is lower than the adiabatic flame speed. This critical diameter value is called as the quenching diameter which can be inversely scaled with the flame speed for analytical purpose [237]. Therefore, the quenching diameter for hydrogen (higher flame speed) is lower than that of kerosene. Flashback is an uncontrolled propagation of the flame upstream of combustion chamber because of a local imbalance in the flame speed and flow velocity [227]. If hydrogen is used directly in the gas turbine engines with same fuel lines designed for Jet-A then hydrogen will flash-back with flame propagation that can reach the fuel tank. Therefore, fuel systems must be designed that establish reliability and redundancy.

6.2.2.2 *Flame characteristics and emissions*

Figure 6.1 represents a comparison of flame temperature variation with equivalence ratio between kerosene (Jet-A) and hydrogen and their respective lean blowout points (data source [181]). It can be observed that even though hydrogen has a higher temperature at its stoichiometry compared to kerosene, it can stably combust at significantly leaner equivalence ratio regime. In the leaner equivalence ratio regime, the mixing intensity should be increased for: preventing the creation of local hotspots and effective mixing of reactants. Combustion of hydrogen demands modifications to the combustor for preventing high temperatures and for enabling effective mixing such that significant benefits of hydrogen's performance at leaner conditions (relative to kerosene) can be completely utilised.

The products of combustion of conventional jet fuel are: CO_2, CO, water vapour, SO_x, PM 10 (size up to 10 micrometre), NO_x, PM 2.5 (size up to 2.5 micrometre), VOC, CH_4, BC, OC, and N_2O [53], [238], [239]. On the other hand, combustion of hydrogen produces only water vapour and small quantity of NO_x [55]. If Jet-A combustor is used directly for hydrogen combustion, it will generate high temperature flames that results into higher NO_x emission. This can be observed from Figure 6.2 (data source [64], [240]) which provides a comparison of NO_x emission for an APU powered by conventional jet fuel and hydrogen fuel in conventional combustor. As discussed above, hydrogen has higher flame speed compared to kerosene. Thus, in a conventional combustor which is designed for kerosene, the combustor length is shorter thereby causing non-uniform mixing and creation of local high NO_x spots. Therefore, considering the above discussion, combustors

must be designed specifically for hydrogen use. A review of other aspects of hydrogen use in aviation is included in Appendix B section B.3. These include hydrogen fired combustors (lean direct injection [LDI] and micro-mix combustors), safety aspects of LH_2 use, airport systems design and operations, and engine operational issues for hydrogen use.
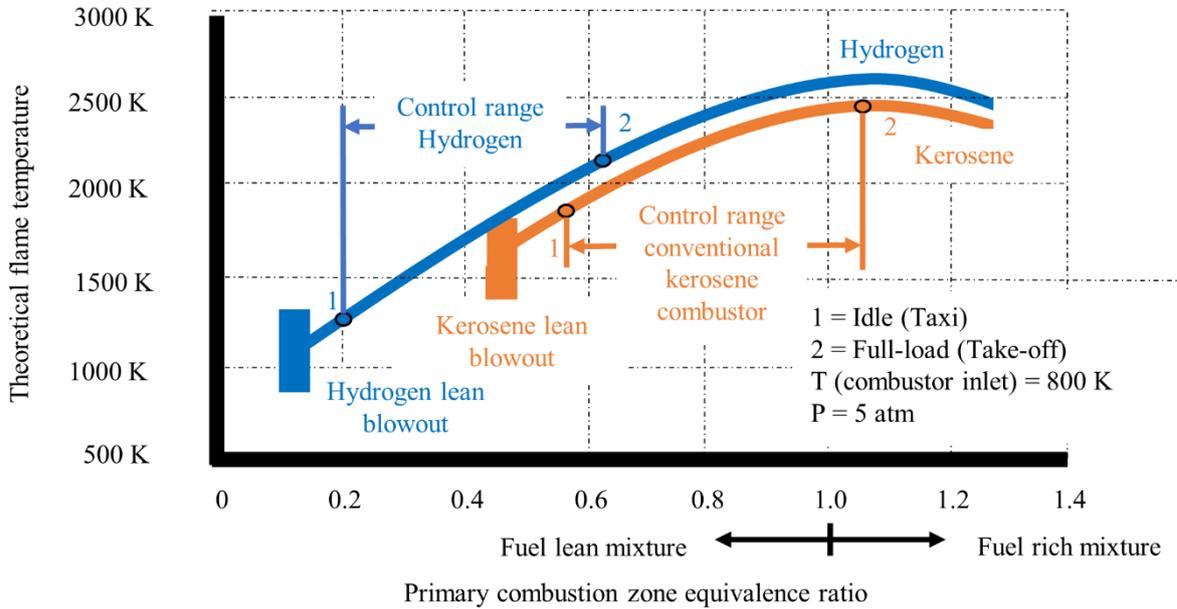
Figure 6.1. Comparison of flame temperature variation with equivalence ratio between kerosene (Jet-A) and hydrogen and their respective lean blowout points (data source [181])
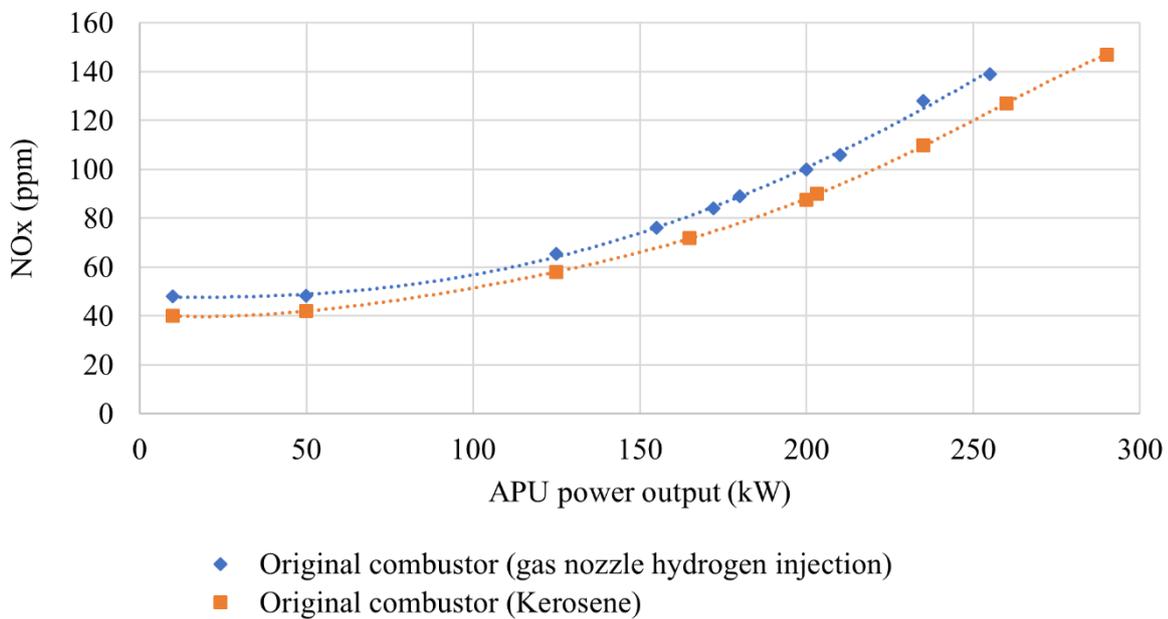
Figure 6.2. Comparison of NO_x emission for APU powered by conventional jet fuel and hydrogen fuel in conventional combustor (data source [64], [240])

108

Additionally, similar to the review of studies on the effect of hydrogen on aircraft and engine operation that is conducted above, a literature review on fuel properties of SPK and their operational impact (qualitative analysis) on aircraft and engine is included in Appendix B section B.3.

6.2.3 Review of aircraft and engine design process

In the current section, the approaches for the gas turbine engine design and aircraft design process are reviewed, as both processes are very important towards the research goals. This section reviews the design approaches used for aircraft performance modelling. It is imperative to first understand and get familiarised with the practiced process of gas turbine engine design and aircraft design, before developing the models in Chapters 6 and 7 respectively. These processes are first studied in detail and based on the published approaches individual models are developed in the respective chapters considering the research scope.

6.2.3.1 *Aircraft design process*

The aircraft design process can be categorised into three main phases: conceptual, preliminary and detailed design according to Raymer [201], Sadraey [241], Fielding [242], Kirby [185], Torenbeek [243], and Kundu et al. [184], and this is represented in Figure 6.3 in the form of a schematic. Original equipment manufacturers (OEMs) have differing approaches to aircraft design and so Figure 6.3 represents an aggregate of some commonly used methods.
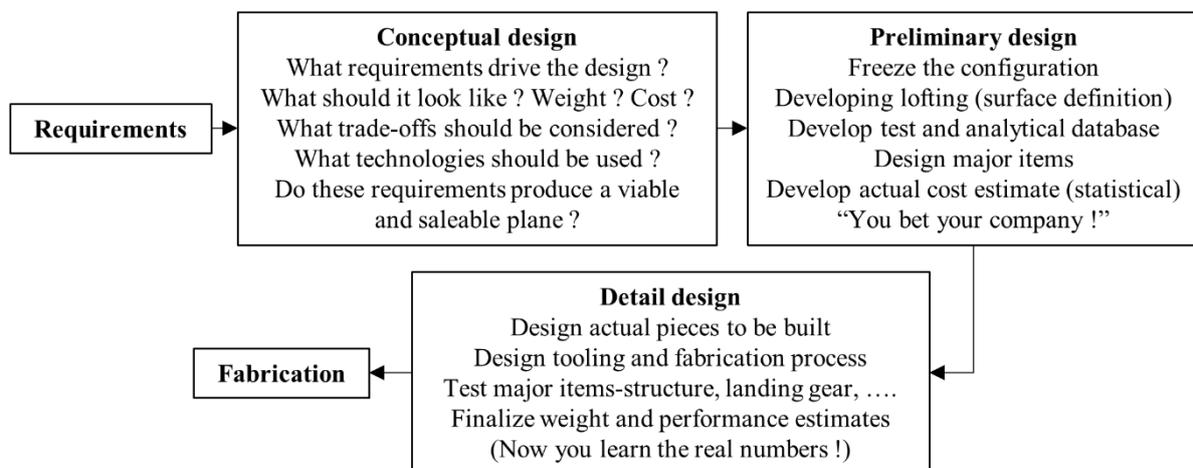
Figure 6.3. Phases of aircraft design process (source [201])

6.2.3.1.a Conceptual design

Following the schematic indicated in Figure 6.3, designers would consider and examine a wide range of aircraft architecture concepts, perform trade studies of the designs and the requirements, and then finalise a best design, and with significant customer input, finalise a well-balanced list of requirements. The conceptual design stage is a fluid process, and it answers the fundamental questions of configuration arrangement, weight and size, and performance. The customer requirements are addressed in this step, and sometimes the customer may wish to relax the requirements. As a design is assessed in increasing detail, novel ideas and problems

emerge. Every time the recent design is evaluated and sized, it must be updated and re-sketched to reflect the latest parameters such as gross weight, wing size, fuel weight, engine size, and other updates. Early wind-tunnel experiments frequently reveal problems requiring some modifications to the configuration [184], [185], [201], [241]–[243].

6.2.3.1.b Preliminary design

Preliminary design may start when the major modifications are completed, and important design questions have been resolved. In this stage, the finalised concept from the previous stage is refined and studied in sufficient detail. The configuration/arrangement can be anticipated to remain similar to the current drawings, but minor revisions may occur. In late stages of preliminary design, even minor modifications are stopped after it is decided to freeze the configuration. During this stage, the specialists in areas such as control systems, structures, etc. will design and investigate their section of the aircraft. Testing begins in the areas like structures, propulsion, aerodynamics, and stability and control. A mock-up may be manufactured at this stage. A crucial activity during this design stage is 'lofting', which is the mathematical modelling of the outer skin (or airframe) of the aircraft with sufficient accuracy. This ensures proper fit of different components, even if they are designed and manufactured by different designers in different locations. The ultimate purpose of preliminary design is to prepare the company for the next step i.e., the detail design stage, which is also referred to as full-scale development. Therefore, the completion of preliminary design usually comprises of a full-scale development proposal. Preliminary design should establish a confidence that the aircraft can be manufactured on time and at the estimated cost [184], [185], [201], [241]–[243].

6.2.3.1.c Detail design

With a favourable decision for entering a full-scale development, the detail design phase is started. It comprises of designing the actual components and their sub-components in detail, which will be fabricated. Another crucial step in the detail design is called as production design, where the specialists determine how the aircraft will be fabricated. This begins with the simplest and smallest assemblies of sub-components and then building up to the final assembly process. The production designers often wish to change the design considering the aspect of manufacturing ease, which may have a significant impact on the weight and/or performance. Minor modifications are unavoidable, but the design should meet the original requirements. During this design stage, the testing efforts intensifies. The actual aircraft structure is manufactured and tested. The control laws for the flight control system are tested. These tests are conducted on a detailed working model of the flight control surfaces and actuators. Both company and customer test-pilots fly on the developed flight simulators. This design stage ends with aircraft manufacturing [184], [185], [201], [241]–[243].

6.2.3.2 *Aircraft engine design process*

In general, the engine design process comprises of three stages: conceptual, preliminary, and detailed design [190], [244], [245]. Figure 6.4 from NASA's 'A Manual for Preliminary Design of Gas Turbine Engines, Volume I: Overview', depicts this design process, which is reported by Hendricks [244]. As can be

observed from Figure 6.4, the level of detail to the engine definition in each phase, increases from phase 1 to 3. In Figure 6.4, FPR is the engine fan pressure ratio. The entire engine design process is only conducted completely by the engine manufacturers. Every engine manufacturer has their individual perspective of this overall process, which is a well-guarded industry secret for gaining a competitive advantage over their rival manufacturers. Therefore, it is difficult to state an exact layout of the industry used engine design process. However, different authors with extensive industrial experience have published their perspective of the overall engine design process [190], [245], [246].

	Phase 1: Conceptual design		Phase 2: Preliminary design	Phase 3: Detailed design
Known	• Basic mission requirements • Duty cycle • Material limits (thermal, mechanical, cost)		• Aero-elastic requirements • Fatigue requirements • Flutter requirements • Overall strength requirements	• Local strength requirements • Producibility • Functional requirements

Results	Thermodynamic cycle
	• BPR
	• OPR
	• FPR
	• Pressure and temperature
	• Airflow
		Design objectives
		• Performance
		• Weight goals
		• Cost goals
			• Flow-path geometry
			• Weights
			• Major loads, stresses, deflections
				• Detail design
				  - Mechanisms
				  - Joints, attachments
				• Production drawings

Figure 6.4. Aircraft engine design process (data source [244])

Books on gas turbine engine design by Saravanamuttoo et al. [246], Mattingly [245], and Walsh and Fletcher [190], provide their engine design schematic. Consideration of off-design performance in the engine design is important for the engine to meet the performance requirements at all off-design points in the flight mission. The engine design schematic by Saravanamuttoo et al. [246] identifies a critical engine design path in the engine design process and it excludes the off-design performance from this critical path. Saravanamuttoo et al. [246] state that the off-design analysis can be conducted separately from the critical design path. This limits the ability to effectively meet the performance requirements at off-design points. Therefore, only the engine design schematics by Mattingly [245] (discussed below), and Walsh and Fletcher [190] (discussed in

section 6.2.4) are considered in this chapter which consider the off-design process towards an effective engine design.

Mattingly [245] presents a preliminary propulsion design sequence which is depicted in Figure 6.5. T_{SL}, W_{TO}, and S, in Figure 6.5 are the thrust at sea level, take-off weight, and wing area, respectively. This sequence provides the engine design process within the context of the overall aircraft design process. Thus, it starts with determining the aircraft specifications and associated drag polar, and thereafter conducting the constraint and mission analysis. When the process ends, the engine design is used to evaluate the performance of the aircraft, which can potentially result in a return to the mission analysis for performing iteration(s) of the engine design. This sequence comprises of design point or on-design analysis, and off-design analysis. After selecting the engine cycle and evaluating the entire off-design performance envelope, the size of engine and design of components is carried out. The component design is thus conducted before the end of the process and requires iteration(s) when the performance does not meet the assumptions made in prior steps.
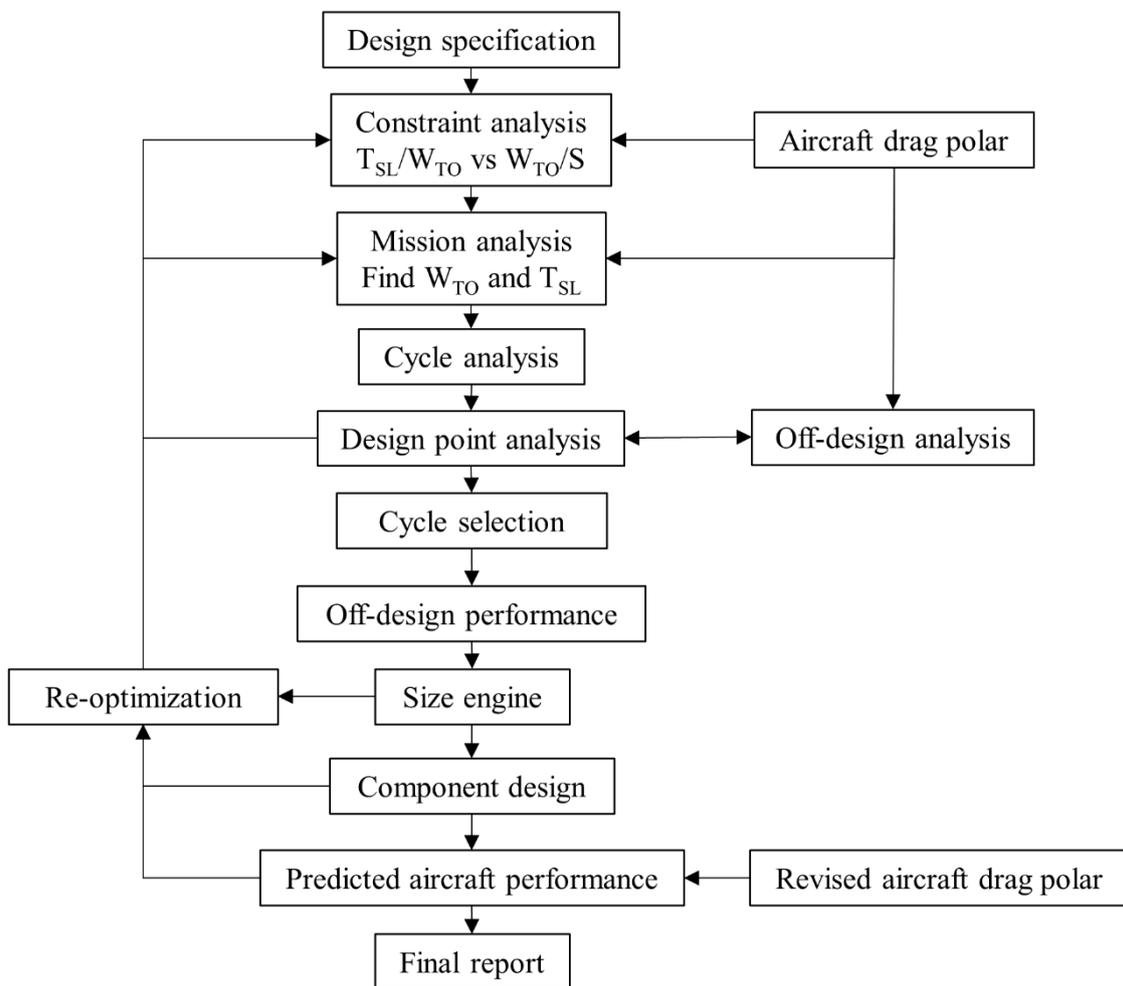
Figure 6.5. Preliminary propulsion design sequence (data source [245])

112

6.2.4 Review of aircraft engine conceptual design process

It is imperative to first understand and get familiarised with the practiced process of conceptual aircraft engine design, before developing an engine model using this design approach. This process is first studied in detail and based on the published approaches a model is developed.

Walsh and Fletcher [190] discuss the engine design steps focussed on the conceptual design stage. This is synthesised and reported by Hendricks [244] as a schematic, and is shown in Figure 6.6. This schematic is useful in defining the boundaries of the conceptual engine design process, which is the scope of the present chapter. In general, these steps are similar to those presented by Mattingly [245] (as seen in Figure 6.5). However, the order of the design steps, is different. The on-design cycle analysis and component design are the steps considered earlier in the process by Walsh and Fletcher [190]. The off-design assessment of both the cycle and component performance come at a later stage in the process. An extra step to examine the engine operability is included in the scheme, for which the author mentions that this step is frequently skipped. The are many iteration loops identified which should be executed when the cycle and component performance do not match, or when the overall engine performance does not match the constraints and requirements.
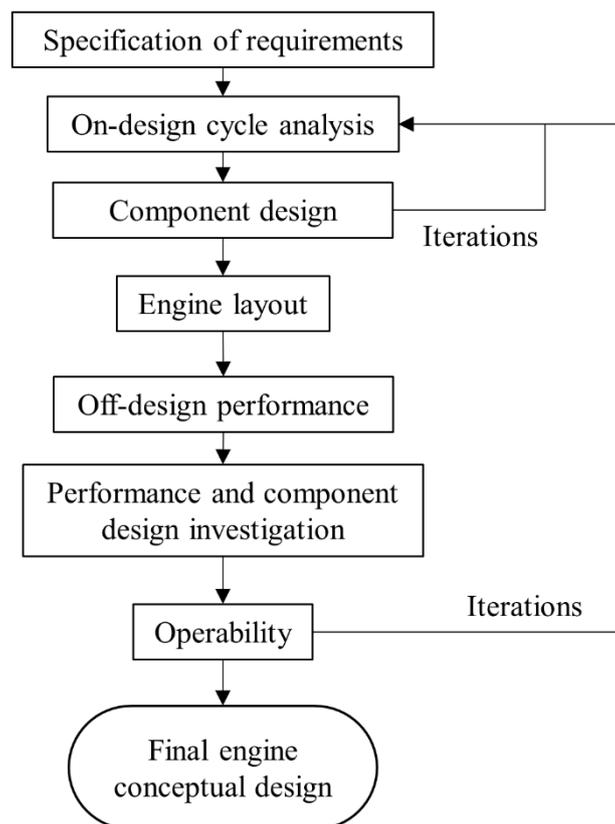
Figure 6.6. Aircraft engine conceptual design process (source [244])

The engine design and optimisation scheme used in this chapter is along the lines of the schematic of Walsh and Fletcher [190] shown in Figure 6.6 as it is more holistic and specific to the conceptual engine design phase as compared to the engine design schematic of Mattingly [245]. The engine design and optimisation

methodology are discussed in detail in the section 6.4, followed by engine design results specific to the design requirements.

6.3 Design requirements and known data

6.3.1 Future engine and aircraft design data from literature

Table 6.1. NASA N+2 BWB 301-GTF and B777-200LR aircraft data (source [130])

Characteristics	Value
Boeing 777-200LR	
Block fuel consumption	125,706 kg
NASA's N+2 BWB 301-GTF aircraft	
Range	7,500 nautical-miles (nmi) or 13,890 km
Passengers	301
Powerplant	2 geared turbofan engines
Fuel type	Conventional jet fuel
Cruise Mach	0.84
GTOW	242,441 kg
OEW	114,907 kg
Payload weight	53,570 kg
Wingspan	76.2 m
Wing area	944.73 m^2
AR	6.1
Total jet fuel at mission start, $W_{F,total}$	73,965 kg
Block fuel consumption	66,683 kg
Saving in block fuel consumption relative to B777-200LR	47%

Table 6.2. Engine data of NASA N+2 BWB 301-GTF aircraft (source [130])

Parameters	Units	Top of climb (TOC)	Sea Level Static (SLS)
Mach and altitude	- , m	0.8 at 10,668 m	0, 0 m
Net thrust	kN	55.603	299.9
Specific fuel consumption	g/kN-s	13.15	5.62
OPR	-	60.0	47.1
BPR	-	17.65	20
FPR	-	1.35	1.25
Bare engine weight	kg	6,789.37	6,789.37
Accessories weight	kg	835.06	835.06
Engine mount weight	kg	137.44	137.44
Total engine weight	kg	7,761.87	7,761.87
Nacelle and inlet weight	kg	776.15	776.15
Fan diameter		132.4 inches or 3.36296 m	132.4 inches or 3.36296 m
Power off-take	kW	150	150
Bleed		Zero	Zero

In terms of the future aircraft configuration, NASA N+2 BWB/HWB with UHB GTF for 301 passengers [130] is selected here as technology reference. The aircraft technology selection is discussed and

summarised in Chapter 2. Moreover, a significant amount of information on the engine and aircraft design for conducting a conceptual design study is available from NASA's studies [130], [247]–[249].

The design characteristics of the long-range NASA N+2 BWB-GTF aircraft and Boeing 777-200LR (datum used by NASA), for 301 passengers are listed in Table 6.1. Additionally, the engine data of NASA N+2 BWB 301-GTF aircraft is provided in Table 6.2. Based on the information in Table 6.1 and Table 6.2, design targets are set for the engine (Chapter 6) and aircraft design (Chapter 7) respectively. The graphical representation of this NASA N+2 BWB 301-GTF aircraft configuration can be found in resource [130].

6.3.2   Specification of requirements

The design requirement/specification is a necessary step for initiating the design process which can be observed from Figures 6.3 to 6.6. In the current chapter, the design requirement is to carry out a conceptual design of an LTA BWB aircraft for transporting 301 passengers over a range of 7,500 nmi or 13,890 km. This aircraft should be powered by LH_2 for zero direct-carbon emissions (operational phase) and 100% SPK, separately. For developing a model (and design) of LH_2 aircraft and SPK aircraft, a baseline case is required where this BWB aircraft is powered by conventional jet fuel. Modifications to the baseline case are made for the use of LH_2 fuel and 100% SPK (separately), where the modifications are based on published literature. The aircraft design requirements are listed in Table 6.3, and these are based on Table 6.1. It is to be noted that the GTOW and OEW from Table 6.1 are not listed in Table 6.3 because these are expected to change since the engine weight might change because of the use of next generation lighter materials. For uniformity with the NASA N+2 BWB aircraft study [130] (reference study as discussed before), the ratio of $W_{F,block}$ to $W_{F,total}$ is kept unchanged for modelling the use of conventional jet fuel, LH_2 fuel, and 100% SPK. For the BWB conventional jet fuel (baseline) case, except for the engine weights, there is no other change expected. In case of LH_2 fuel, modifications are required to the aircraft which changes the total aircraft weight. For 100% SPK, slight modifications are required to the baseline aircraft for accommodating a slightly less dense fuel (as learnt from Chapter 4) which changes the OEW and GTOW. The aircraft design requirements will be revisited in Chapter 7, which is completely focussed on aircraft energy consumption modelling.

In the context of engine design, which is the scope of this chapter, the design requirements are listed in Table 6.4. The listed parameters in Table 6.4 are set as design requirement since the NASA N+2 BWB aircraft has been tested for noise assessment. It is assessed at 40.3 effective perceived noise levels in decibels (EPNLdB) cumulative 'below' the Stage 4 certification level. The parameters in Table 6.4 viz. thrust (exhaust velocity) and FPR (with fan diameter), significantly contribute to noise emission. The OPR changes as FPR changes, and therefore is considered as a design requirement here. The high engine BPR can be perceived as a technology metric which has an impact on noise emission reduction.

Table 6.3. Aircraft design requirements

Characteristics	Value
Range	7,500 nautical-miles (nmi) or 13,890 km
Passengers	301
Powerplant	Two geared turbofan engines
Fuel type	1. Conventional jet fuel
	2. Liquid hydrogen (LH$_2$)
	3. 100% SPK
Cruise Mach and altitude	0.84 at 10,668 m (35,000 ft)
Payload weight	53,570 kg
Wingspan	76.2 m
Wing area	944.73 m^2
Aspect ratio	6.1

Table 6.4. Engine design requirements

Parameters	Units	TOC	SLS
Mach and altitude	- , m	0.8 at 10,668 m	0, 0 m
Net thrust	kN	55.603	299.9
OPR	-	60.0	47.1
BPR	-	17.65	20
FPR	-	1.35	1.25
Fan diameter*		132.4 inches or 3.36296 m	132.4 inches or 3.36296 m
Power off-take	kW	150	150
Bleed	-	Zero	Zero
Drive and engine type	-	Geared turbofan engine	Geared turbofan engine

* is a design requirement only for baseline (BWB conventional jet fuel) case, LH$_2$ case 1, and 100% SPK

For LH$_2$ fuel, there are three different cases that are analysed. These are as follows:

- Case 1 is where the aircraft thrust production remains the same as that of the conventional jet fuel case. Since LH$_2$ fuel is more energy dense than conventional jet fuel, lesser mass of LH$_2$ fuel is required at the start of the mission. Therefore, for similar *T/W*, the thrust requirements reduce. Dincer [250], Verstraete [191], and Nojoumi [55] support that for a LH$_2$ powered aircraft, the thrust requirement reduces and that the engine becomes smaller in size. This thrust requirement reduction is not considered in this case but is considered in the next case.

- Therefore, Case 2 is where the aircraft thrust requirement and engine size reduces for maintaining similar *T/W* as that of conventional jet fuel (Jet-A) case.

- Case 3 is essentially Case 2 without engine cooling flows, since the engine is expected to run colder relative to the baseline case because of reduced thrust requirement, where (as mentioned before) the engine uses advanced materials for withstanding high temperatures in baseline case (Jet-A), Case 1, and Case 2.

Overall, the engine design requirements in Table 6.4 remain the same for conventional jet fuel, Case 1 of LH$_2$ fuel, and 100% SPK. For Case 2 and Case 3 of LH$_2$ fuel, the engine diameter requirement is taken off as suggested by Dincer [250], Verstraete [191], and Nojoumi [55].

6.3.3   Data for engine design

Considering the design requirements set above, a discussion is required on the data known from literature. This data comprises of engine design and technology used currently and planned to be used in the future, which can be useful for meeting the set engine design requirements. The objective of this chapter is to design a UHB GTF engine that meets the requirements listed in Table 6.4. The engine data in terms of component efficiencies, stage count, advanced materials, cooling flows, and combustor technology, are discussed as follows. These form the basis of most inputs to the engine model developed in this chapter.

6.3.3.1   *Component efficiencies*

The engine design and optimisation will be conducted using commercial software called as GasTurb 13 [188] (reviewed in section 4.3.2.1). Table 6.5 and Table 6.6 below list gas turbine engine's component polytropic efficiencies for the present and future technology, respectively. In Table 6.5 the component efficiencies are taken from GasTurb 13 [188] and in Table 6.6 component efficiencies for all operating point except 'climb' come from NASA's study [123] for the H3.2 aircraft. The H3.2 aircraft is a BWB aircraft having propulsion systems installed aft of the aircraft, similar to the aircraft design requirement set in this chapter. The component efficiencies during climb in Table 6.6 is calculated by taking an average of respective component efficiencies at take-off and top-of-climb for the H3.2 aircraft from NASA's study [123].

Table 6.5. Engine component polytropic efficiencies presently (source [188])

Component		Value (%)
Fan	Inner	91.00
	Outer	90.37
Intermediate pressure compressor		92.01
High pressure compressor		91.00
High pressure turbine		89.00
Low pressure turbine		92.16

Table 6.6. Future engine component polytropic efficiencies

Component		SLS [123]	TOC [123]	Cruise [123]	Climb
		(in %)	(in %)	(in %)	(in %)
Fan	Inner	92.1	92.8	94.4	94.1
	Outer				
Intermediate pressure compressor		92.6	92.5	93.0	92.2
High pressure compressor		92.1	91.2	93.0	92.8
High pressure turbine		93.6	94.4	93.5	94.4
Low pressure turbine		94.1	95.6	93.8	95.6

6.3.3.2   *Turbomachinery stage count*

The stage count of the turbomachinery in a gas turbine engine is an important aspect. Depending on the turbomachinery stage-loading, the distribution of work between stages of this machine is determined.

Therefore, for a fixed engine geometry, if a compressor with standard stage loading is used to do the required work, but with lower stage count, then the compressor might not be able to carry out the required compression, as it isn't designed for these conditions. On the other hand, if more stages of a turbomachinery are selected, then it can increase the engine weight. Therefore, selection of turbo-machinery stage count is very crucial.

In this chapter, the selection of stage counts for compressor and turbines is based on three studies: Kestner et al. [225], Bijewitz et al. [224], and Pratt and Whitney's GTF engine PW1100G [251]. The engine compression system includes intermediate pressure compressor (IPC) and high-pressure compressor (HPC), and expansion system includes a high-pressure turbine (HPT) and low pressure turbine (LPT). Kestner et al. [225] and Bijewitz et al. [224] design turbofan engines for future applications. Table 6.7 lists the stage count of GTF engine compressor and turbines from the three studies. It also provides the stage counts used in this chapter. It can be observed from Table 6.7 that the stage counts between the three studies are very similar except the stage counts for the HPC and LPT.

Kestner et al. [225] use stage count of 10 for the HPC citing the GEnx engine (used on the latest Boeing 787 aircraft), which has same number of stages. PW1100G engine [251] has a stage count of 8 for the HPC. Bijewitz et al. [224] arrives at a value of stage count of 9 for the HPC based on trade studies that take into consideration stage loading and feasible stage pressure ratios. Moreover, the design parameters of the study by Bijewitz et al. [224] is almost similar to the current chapter. Therefore, stage count of 9, similar to the study by Bijewitz et al. [224], for the HPC is selected here.

Table 6.7. Stage counts of GTF engine compressors and turbines

Component	Stage count			
	Kestner et al. [225]	Bijewitz et al. [224]	PW 1100 G [251]	Present chapter
Fan	1	1	1	1
IPC	3	3	3	3
HPC	10	9	8	9
HPT	2	2	2	2
LPT	3	4	3	3

In case of LPT stage count, the value of 3 is selected, similar to the study by Kestner et al. [225] and to the PW1100G engine [251]. Firstly, it is observed later in the methodology section (section 6.4) that the gear ratio is one of the optimisation design variables. Gear ratio is linked to the low-pressure spool speed. The low-pressure spool speed along with the stage loading determine the stage count. Secondly, low pressure turbines are large components compared to the high-pressure systems, hence have more weight. Considering both these points, especially the weight aspect, stage count of 3 similar to the study by Kestner et al. [225] and to the PW1100G engine [251], is used here for LPT.

6.3.3.3 *Engine materials*

Most advanced materials (with advanced component manufacturing process) that are planned to be used in future aircraft engines are currently expensive. Therefore, use of these materials is cost prohibitive currently. The use of these materials provides benefits during the engine operation. The examples of these benefits are engine weight reduction due to use of lighter materials, high operating temperatures due to the use

of CMC, implementation of materials with excellent strength for reducing mechanical and thermal stresses in components, improved component and engine life, etc.

There are primarily four NextGen engine materials that have the potential to improve the operating conditions, safety, and performance. These four materials include:

- Ti-6Al-4V (titanium alloy):

  The benefits of this material is that it is lighter and stronger than conventional materials [252]. It can be used in engine components with low operating temperature such as fan and booster (IPC). The technology readiness level for this material's manufacturing is high, and it is implemented currently in engines. However, the use is limited because of the high costs (ibid). In future, using advanced manufacturing techniques, the production cost is expected to decrease [252], [253].

- Braided carbon composite (BCC):

  Braided composites find application to the engine casings. Specifically, in terms of application, they are best suited for casings of fan and IPC. They create lighter and more fuel-efficient engine casing, that is stronger and safer compared to the conventional materials [254], [255]. The manufacturing is matured currently and is cost-effective, and overall facilitates reduction of engine cost [254].

- Polymer matrix composite-aluminium honeycomb core (PMC/Al honeycomb):

  This is attractive for aero-engine applications because of its properties such as low weight, high strength, and low cost for manufacturing complex-shaped components. It can be used in the fan section of the engine [256].

- CMCs:

  There has been a significant progress made in the development and application of CMCs consisting of silicon carbide (SiC) based matrices reinforced by small diameter continuous-length SiC-based fibres [257]. The SiC/SiC composites are currently in the early stages of implementation into hot-end components of aero gas turbine engines for civil aviation application. In comparison with the traditional materials, they offer multiple advantages because of their lighter weight and higher temperature structural capability (ibid). There is a variety of SiC-based fibres, some of which are listed below in Table 6.8 with their densities and maximum allowable/operable temperatures. It can be seen from Table 6.8 that with SiC fibre Tyranno SA, the operable temperature can be as high as 1900°C or 2173K. Considering the trend of turbofan engine development, the engines are becoming hotter over the time with the increase in the OPR [258]. With higher OPR, the thermal efficiency of the engine will be higher. Therefore, for the higher turbine temperatures in future engines, the use of these SiC based CMC is helpful and is required. In this chapter, such CMCs will be used in the hot-end components, depending on the location and need of the components. For example: Tyranno SA will be used for the combustor cans and the high-pressure turbines because these components are in direct contact with extremely hot gases. Hence, the best quality SiC fibre is selected. On the other hand, for the combustor casing (outer to the cans), CMCs are required but not the high-end SiC fibres like Tyranno SA (which can also minimise the cost). A Tyranno TE (standard) type fibre will be used for the combustor casing.

Table 6.9 provides a comparison of conventional and advanced/NextGen material densities for the engine's important components. Additionally, Table 6.10 provides a comparison of conventional and advanced/NextGen material densities for the engine's miscellaneous components. Moreover, Table 6.11 provides a comparison of mass to power ratio of conventional and advanced/NextGen gearbox. The information in Table 6.9, Table 6.10, and Table 6.11 will be used as inputs to the future engine model developed in this chapter and in the validation cases (in Appendix C section C.1), using GasTurb 13 software.

Table 6.8. Some key properties of SiC-based fibres

SiC fibre	Density (kg/m^3)	Maximum temperature (K)
Tyranno TE	2,550 [259], [260]	1,673 [260], [261]
Hi-Nicalon	2,740 [259]	1,723 [257]
Hi-Nicalon Type-S	3,110 [259]	1,923 [257]
Tyranno SA	3,110 [259]	2,173 [257]

Table 6.9. Comparison of conventional and advanced/NextGen material densities for engine's important components

Component	Conventional		Advanced/NextGen	
	Material	Density (kg/m^3)	Material	Density (kg/m^3)
Fan casing	Ti-6Al-4V	4,429 [256], [262], [263]	BCC	1,520 [255]
Fan bypass vane	Ti-6Al-4V	4,429 [256], [262], [263]	PMC/Al honeycomb	1,533 [256]
Fan Blades and disk	Titanium-alloy (Hollow core)	2,000 [188], [264]	PMC/Al honeycomb	1,533 [256]
IPC Blades and disks	Ti-6Al-4V	4,429 [256], [262], [263]	Ti-6Al-4V	4,429 [256], [262], [263]
IPC-HPC Duct casing	Inconel 718	8,221 [265]	BCC	1,520 [255]
HPC Blades and disks	Inconel 718	8,221 [265]	Inconel 718	8,221 [265]
Combustor casing material	Inconel 718	8,221 [265]	SiC CMC (Tyranno TE)	2,550 [259]
Combustor can material	Inconel 718	8,221 [265]	SiC CMC (Tyranno SA)	3,100 [259]
HPT Blades and disks	Inconel 718	8,221 [265]	SiC CMC (Tyranno SA)	3,100 [259]
LPT Blades and disks	Inconel 718	8,221 [265]	Inconel 718	8,221 [265]

Table 6.10. Comparison of conventional and advanced/NextGen material densities for engine's miscellaneous components

Component	Density (kg/m³)	
	Conventional	Advanced/NextGen engine
Shaft	4,429 [256], [262], [263]	3,204 [266]
Engine inlet casing	4,429 [188], [256], [262], [263]	1,602 [266]
Containment ring (Fan)	800 [188]	321 [266]
Inlet guide vane (IGV) of IPC	4,429 [188], [256], [262], [263]	1,602 [266]
Casing (IPC)	4,429 [188], [256], [262], [263]	1,602 [266]
IGV (HPC)	4,429 [188], [256], [262], [263]	4,429 [188], [256], [266]
Outer casing (HPC)	4,429 [188], [256], [262], [263]	4,429 [188], [256], [266]
HPC casing	4,429 [188], [256], [262], [263]	4,429 [188], [256], [266]
Outer casing (HPT)	8,221 [188], [265]	1,922 [266]
HPT casing	8,221 [188], [265]	1,922 [266]
Turbine inter-duct (HPT-LPT)	8,221 [188], [265]	3,204 [266]
LPT casing	8,220.93 [188], [265]	4,428.785 [188], [256], [266]
Exhaust casing	8,220.93 [188], [265]	4,428.785 [188], [256], [266]
Bypass casing	4,428.785 [188], [256], [262], [263]	1,601.85 [266]
Nozzle	8,220.93 [188], [265]	1,922.22 [266]

Table 6.11. Comparison of mass to power ratio of conventional and advanced/NextGen gearbox

Component	Conventional	Advanced/NextGen engine
Gearbox mass to power ratio (kg/kW)	3E-2 [188]	4.83E-3 [266]

Turbomachinery disks: Table 6.9 lists advanced material for 'disks' of compressors and turbines. These are usually the most massive components of any gas turbine engine. Disks are structurally critical, and they experience very high stresses and loads in the engine. Disk failure (disk burst) can be catastrophic as such failures are not containable. The turbomachinery disks will also be considered within the engine design-optimisation space in GasTurb 13. Using the advanced materials, a check is made such that the disks are not overstressed at different points in the flight envelope and that disks weigh lesser compared to the case of conventional materials.

6.3.3.4 *Cooling flows*

It is to be noted that through all cases, advanced materials are used (as reasoned and discussed previously). Therefore, especially for hot components (combustor and HPT) the ability of advanced materials to bear high temperatures is greater compared to conventional materials. 20% cooling flows for HPT are used through all cases except Case 3 of LH_2 where the turbine cooling flow requirement is relaxed owing to the condition that the engine runs colder relative to the baseline case (Jet-A), Case 1, Case 2, 100% SPK, and more importantly the material's high-temperature withstanding limit. The value of 20% cooling flows for high pressure turbine is selected based on NASA's study [123] and study by Bijewitz et al. [224]. Furthermore, the engine design characteristics and thrust requirement of the study by Bijewitz et al. [224] is similar to the design requirements of this chapter. Therefore, the selection of 20% cooling flows in this chapter, for HPT, is well

supported. Additionally, the study by Bijewitz et al. [224] sets design temperature limit of 1,350 K on LPT, to allow it to remain uncooled i.e. zero cooling flows. Similar condition is set in the current chapter, such that the LPT doesn't require cooling. In other words, if the temperature at the inlet of the low-pressure turbine exceeds 1,350 K, cooling flows are required. Cooling flows affect the fuel consumption since the air required for turbine cooling is extracted from the compressor. Higher the cooling flows, more is the fuel consumption.

6.3.3.5   *Combustor technology*

LDI combustor uses lean combustion and is a promising low emissions combustor for aero-engines, especially for those with high OPR [267]. A continuous rise in engine OPR and turbine entry temperature (TET) because of performance requirements, results in the increase of NO_x formation. Combustors which can simultaneously meet ICAO LTO NO_x emissions regulations, achieve high efficiency and low SFC, are highly demanded. Other low emission technologies such as rich-burn quick-quench lean-burn (RQL) have been developed and are tested to be successful. In comparison with other low emission combustors, the LDI is shorter in length and has the potential to achieve further reduction in NO_x compared to RQL combustor. It is less likely to suffer from combustion instabilities and flashback compared to the lean premixed pre-vapourised (LPP) combustor. The use of LDI combustor is advantageous because of its lean combustion, where the flame temperature is decreased by fuel combustion far (lean) from stoichiometric condition. The fuel is directly injected into the flame zone instead of being pre-vapourised and premixed with air. Therefore, the LDI combustors are less likely to suffer from auto-ignition and flashback compared to LPP combustors. The fuel injector design is thus crucial for LDI combustors to enable the required level of atomisation and homogeneous fuel-air mixing (ibid).

In this chapter, hydrogen is also being explored as the potential alternative to the conventional jet fuel. A review of combustors for hydrogen use is included in Appendix B section B.3. The need to use hydrogen in liquid form, and in combustion systems is discussed in Chapter 2. One of the important technology challenges for using hydrogen in gas turbine engines is its compatibility and performance in the present combustion system, particularly the current fuel injectors. Marek et al. [228] conduct experiments with a series of novel LDI injectors for hydrogen as a potential gas turbine fuel candidate. All these injectors for hydrogen are based on LDI technology with multiple injection points and quick mixing. Flashback is one challenge to hydrogen based premixing combustion systems because hydrogen's reaction rate is about seven times that of conventional jet fuel (Jet-A). To mitigate the risk of flashback, the mixing times were designed to be short and velocities to be high. All LDI configurations for hydrogen combustion performed well and were stable, and these resulted in low levels of NO_x. No autoignition or flashback phenomena were encountered during the experiments (ibid). LDI combustor is found to be suitable for the use of both conventional jet fuel and hydrogen based on the above discussion. For hydrogen, C4 type of combustor configuration is preferable according to the discussion in Appendix B section B.3. In this thesis LDI combustors (for Jet-A, 100% SPK, and LH_2 [C4 type]) will be used for the emissions assessment, which is covered in detail in Chapter 8.

6.4 Methodology

The design and optimisation of the GTF engine will be conducted using commercial software called GasTurb 13 [188]. As discussed in section 6.2.4, the overall process for engine design will be similar to Figure 6.6 i.e., process schematic from literature. An overview of the GasTurb 13 software is provided below.

6.4.1 Overview of GasTurb 13

6.4.1.1 *On-design point calculation*

During the design process of the gas turbine engine, a thermodynamic cycle will be calculated and selected for the on-design point [186]–[189]. The total temperatures, total pressures, and mass flows, at the entry and exit of all engine components are calculated. The Mach numbers and hub-tip ratios for the components determine the crucial engine dimensions considering the aero-thermodynamics. Thus, through the selection/calculation of the cycle design point (on-design point), the flow-annulus geometry and the engine weight are determined (ibid). In addition to the engine geometry, the disk stresses are calculated.

At this point in GasTurb 13, the flow annulus geometry, disks of turbines and compressors, and engine cross section, are designed. Thus, as compared to pure zero-dimensional/cycle analysis, more details on engine simulation are known and the quality of the design analysis is improved significantly (ibid). Additionally, more insights are obtained on the interaction between component aerodynamics, thermodynamics, and the mechanical design of the gas turbine engines.

6.4.1.2 *Off-design point calculation*

At off-design points, the performance of a gas turbine engine with a given/fixed geometry (from the on-design point) is evaluated. During the initiation of an off-design point analysis, the component design points should be correlated with the component maps. This can be carried out automatically via standard GasTurb maps and the standard design point settings in these maps. The maps are scaled (by GasTurb) to size at the initiation of the off-design point calculations in such a manner that the maps are consistent with the on-design point [186]–[189].

6.4.1.3 *Standard Maps*

For every turbine and compressor there is one standard map [186]–[189]. These maps are taken from open literature for axial flow turbo machinery, and these are physically sound depiction of real turbomachines (ibid).

6.4.1.4 *Selected Maps*

The accuracy of the off-design estimation is dependent on the validity of the component maps on whether or not they reflect the component performance [186]–[189]. The selected maps have a catalogue of pre-selected maps which provide numerous and different maps for different components, where each of them

depicts a common turbine or compressor design. This enables the selection of the most suitable component maps and resultantly improving the accuracy of the off-design performance (ibid).

6.4.1.5 *Cycle optimisation algorithms*

In GasTurb 13, any cycle output parameter can be chosen as an objective function or figure of merit which can be minimised or maximised [186]–[189]. There are different optimisation algorithm/process available in GasTurb: random new start search, adaptive random search, endless random search, and systematic search. Whichever strategy is used initially for the optimisation should be complemented with other search strategies for ensuring that the estimated optimum point is global and not local. The 'random new start' will initiate a random search by shifting away from the previous optimum point towards the estimation of the new optimum. In the 'adaptive random search' algorithm, random numbers are used for the optimisation variables which are concentrated in the vicinity of the best prior optimum. The systematic search strategy is a gradient based search. The best optimum point estimated during all searches is the final outcome of an endless random search. The endless random search is the ideal for cases where there are numerous optimisation variables and constraints, making the optimisation problem more complex. If the similar optimum point is obtained using multiple strategies, then it is clear that the point is the global optimum (ibid).

6.4.1.6 *Disk design and optimisation*

During the off-design mode, information such as engine geometry and the disk stress at any operational point can be obtained, however, the engine geometry cannot be modified [186]–[189]. Disk design and optimisation can be carried out in the off-design mode.

After the engine performance analysis, the disk dimensions and the disk stress should be analysed at both on- and off-design points, such that the disks are not overstressed at any operating point. GasTurb recommends that the disks should be optimised one by one, via several optimisation attempts for every disk. The optimisation should be initiated from different disk-shape points. During the disk optimisation, both the systematic search and random search should be used (ibid).

6.4.2 Model description

As described in section 6.3.2, the design cases that will be considered in this chapter are baseline case that uses conventional jet fuel in the UHB GTF, three cases of LH_2 fuel, and 100% SPK fuel. The overview of conditions in the three cases of LH_2 fuel that are analysed are as follows:

- Case 1 is where the aircraft thrust production remains the same as that of the conventional jet fuel case.
- Case 2 is where the aircraft thrust requirement reduces for maintaining similar thrust to weight ratio as that of conventional jet fuel case (baseline).
- Case 3 is essentially Case 2 without engine cooling flows, since the engine is expected to run colder relative to the baseline case because of reduced thrust requirement, where (as mentioned before) the engine uses advanced material for withstanding high temperatures in baseline case (Jet-A), Case 1, and Case 2.

The design-optimisation parameters are discussed below. The model inputs are discussed in section 6.4.3. Some of these inputs change between baseline case, 100% SPK case, and three cases of LH$_2$ fuel, and the changes are identified/reported accordingly.

6.4.2.1 *Design-optimisation parameters*

The overall engine design requirements and performance targets are known (as listed in Table 6.4), along with the referenced future engine data (Table 6.2). The data on engine technology and its components, has been listed and discussed in section 6.3. However, some engine design data (or approximate values) such as the pressure ratio of the compressors, gearing ratio, burner temperature, tip speeds of fan and high-pressure compressor, and engine inlet mass flow rate, are unknown. These parameters can be estimated using the optimisation process. The optimisation objective or figure of merit is to minimise the thrust specific fuel consumption (TSFC, which is the ratio of rate of fuel consumption and thrust). With this set objective, the design variables and constraints considered in this chapter, are as listed in Table 6.12 and Table 6.13 respectively. Referring to Table 6.12, the design variables and their extreme values are selected very carefully, either directly from literature or via educated guess considering prior studies.

The study by Bijewitz et al. [224], which has almost similar design requirements as that of the present chapter, uses a maximum gear ratio of 4.5:1, and their actual design gear ratio is 4:1. The design gear ratio in the study by Kestner et al. [225] is 2.88:1, while the design gear ratio for the Pratt and Whitney's engine PW1100G is expected to be 3:1 [268]. Therefore, the minimum, start-guess, and maximum values are selected to be 2.5, 3, and 4.5, respectively.

Table 6.12. Design variables in the engine design-optimisation process

Variable		Units	Minimum value	Starting guess value	Maximum value
Gearing ratio		-	2.5:1	3:1 [268]	4.5:1 [224]
Mass flow rate (inlet standard corrected flow)		kg/s	1,400	1,700	1,800
TET (T$_4$)		Kelvin (K)	1,400	1,750 [224]	2,173 [257]
FPR	Inner	-	1.1	1.33	1.35 [130]
	Outer		1.1	1.34	1.35 [130]
IPC pressure ratio		-	1.1	3	10
HPC pressure ratio		-	1.1	15	25
Fan tip speed		m/s	300	380	411.48 [266]
HPC tip speed		m/s	250	360	382.84 [266]

Table 6.13. Design constraints/target values in engine design-optimisation process

Variable	Value
OPR	60
Thrust	55.603 kN (at least)
Fan diameter*	3.36296 m
* is a design constraint only for baseline (conventional jet fuel) case, 100% SPK case, and LH$_2$ case 1	

For the inlet standard corrected flow of engine, the extreme values are based on an educated guess. Halliwell [266] estimates the inlet standard corrected flow value of ~ 1,443 kg/s for Trent XWB engine which has a BPR of 9.3 and fan diameter of ~ 3.18 m. The design target of the current engine is BPR of 17.65 at TOC, and fan diameter of ~ 3.36 m. The inlet standard corrected flow is directly related to the fan diameter. Therefore, for a higher fan diameter and significantly higher BPR compared to the Trent XWB model by Halliwell [266], the inlet standard corrected flow has to be greater than 1,443 kg/s. The minimum, start-guess, and maximum values are selected to be 1,400, 1,700, and 1,800 kg/s, respectively. Additionally, the fan diameter value of ~ 3.36 m is set as a constraint (in Table 6.13) in the optimisation process of the current chapter as per the set design targets. The other constraint considered in this chapter (in Table 6.13), which is directly related to the inlet standard corrected flow, is the thrust. It is observed later (in the result section) that the value of inlet standard corrected flow for the baseline (Jet-A) case is ~ 1,663 kg/s, after optimisation.

The burner exit or TET design variable has been discussed before. Since CMCs are selected for the design of hot-end components, the maximum limit is set to be 2,173 K (Tyranno SA SiC fibre) [257]. The start-guess value is 1,750 K, which is a design TET in the study by Bijewitz et al. [224]. A realistic minimum value of 1,400 K is selected as the minimum temperature limit here, though it can be set to zero as lower TETs are preferred. The optimisation constraint used here (in Table 6.13), which is directly linked to the design variable of TET (T_4), is the thrust.

The minimum value of pressure ratio of any compressor must be greater than 1 for it to be called a compressor. Therefore, the minimum value of pressure ratio of fan, IPC, and HPC is set to 1.1. One of the constraints considered in this chapter (in Table 6.13) is OPR of 60, which is directly related to the pressure ratios of compressors. It is important to note that OPR is dependent on the FPR, and IPC and HPC pressure ratios. The design requirement states that the FPR must be 1.35, which is set as the maximum limit. The FPR is considered as a design variable primarily to try to achieve as low value as possible (<1.35) towards the set design requirements. This also results in lesser noise production, though noise evaluation is not considered in the design process explicitly throughout this chapter. Halliwell [266] uses a pressure ratio of 6.3 for the IPC in their turbofan engine model of an 8 stage IPC. Since, OPR of 60 (at TOC) as per the engine design requirement, is higher in comparison to the OPR of 50 in the study by Halliwell [266], a maximum value of 10 is used for the design variable of IPC pressure ratio. The number of stages of the IPC is previously selected to be 3 (Table 6.7), so assuming uniformly distributed compression in each stage similar to the Halliwell study [266], the start-guess value of 3 is used. The maximum value of the pressure ratio of the HPC is set to 25 considering that the study by Kestner et al. [225] used a pressure ratio of 23 for the HPC. The product of the pressure losses (discussed in the model inputs), FPR, and IPC and HPC pressure ratios, equals OPR. Since the engine OPR of 60 must be modelled and all values in the above-mentioned product except the HPC pressure ratio are known, a value of 15 suffices this product and is considered as a start-guess value for the pressure ratio of HPC.

The tip speeds of fan and HPC from the study by Halliwell [266] are used as maximum values for tip speeds for fan and HPC in this chapter. Tip speeds are linked to spool speeds. Since the engine currently under consideration is a geared turbofan, only the fan design speeds are expected to be different than the study by Halliwell [266] (direct-drive turbofan). Additionally, BPR and the fan diameter in the current chapter are

greater than the study by Halliwell [266]. Therefore, the fan speeds can be expected to be very different from the study by Halliwell. The HPC speed in this chapter is expected to remain similar to the values in the study by Halliwell [266]. The minimum values and the start-guess values are based on the above estimation. Additionally, because the maximum values of tip speeds have been set with realistic design speeds, the spool speed has indirectly been set to realistic values. Therefore, there is an indirect design constraint considered here. This prevents high engine shaft speeds which can cause vibrations, and very high shaft speeds can lead to a phenomenon called as 'whirling' of shafts, which is a violent shaft vibration that could lead to shaft failure.

6.4.2.2 *On-design point and off-design point*

Based on the process learnt from Figure 6.6 (as discussed in section 6.2.4), a simple schematic focussed only the engine design and optimisation process (not explicitly stating the aircraft drag polar here) is created as shown in Figure 6.7.
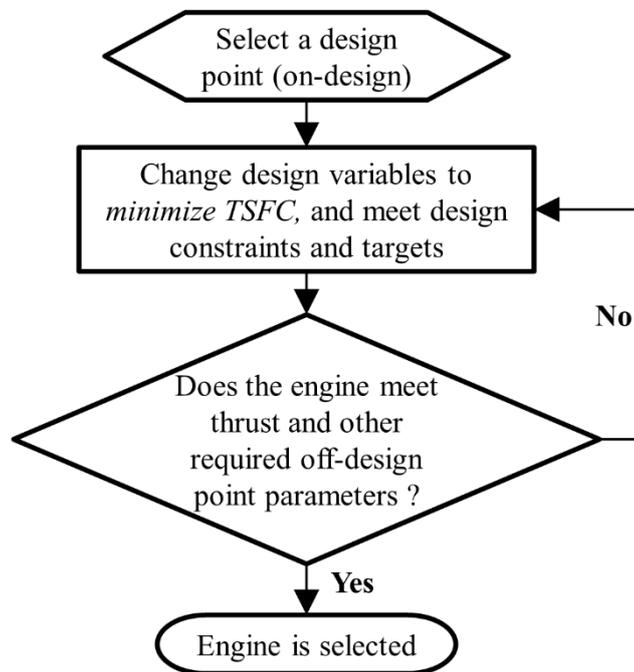
Figure 6.7. Engine design-optimisation schematic used in this chapter

Referring to Figure 6.7, the design and optimisation process starts with the selection of the design point (on-design). The TOC condition is the on-design point because maximum engine inlet corrected flow is at this point [224]. There are inputs in the engine model such as engine/component design parameters, component efficiencies, cooling flows, materials, component stage counts, etc., the details of which are discussed in section 6.3.3.

After the engine model is ready with these inputs, design variables for the optimisation process are identified. There is an initial guess value assigned to each of the design variables for initiating the optimisation process. For example: T_4 is set as a design variable and at the design point its value is unknown. A realistic value of 1,750 K is input to the model as a starting guess, which later gets optimised. CMCs are used for the hot end components, and thus a maximum value of 2,173 K is provided to the design variable. After selecting the design variables, design constraints are identified. For example: thrust is one of the constraints in the

design-optimisation process, where minimum required value must be met for the aircraft to fly. For the baseline case using conventional jet fuel, at TOC condition it is necessary to produce at least 55.603 kN of thrust as per the design requirements listed in Table 6.4. The figure of merit or the objective of the optimisation process is to minimise the TSFC. During optimisation process in GasTurb 13, the design variables are perturbed within their specified limits such that the specified design constraints are met for minimising the TSFC. Once this process is finished, the turbomachinery of this engine configuration is checked for a satisfactory aerodynamic performance of individual turbomachinery stages (aerodynamic and geometrical factors) using standard/GasTurb 13 default turbomachinery inputs (degree of reaction, flow coefficient, and stage loading). Once a satisfactory aerodynamic performance of the turbomachinery is obtained, the engine performance at different off-design points is evaluated using GasTurb 13. Only if the engine meets the off-design parameters including the thrust requirements, the engine is selected as a final candidate.

6.4.2.3 *Disk optimisation and engine weight*

The finalised engine model is then checked for shape and stress in all disks, and at all points in the flight envelope. An 'I-section' for the disk's shape is preferred. 'I-section' has excellent resistance to high bending and shear forces acting on it [269]. The disk optimisation is done in GasTurb 13 using similar process as shown in Figure 6.7, where the software flags overstressed disks. At the design point, the disk shape and stress for each stage of each turbomachine is analysed for satisfactory mechanical performance and minimisation of weight. After this is fulfilled, the mechanical performance of each disk of all turbomachines is analysed at all off-design points in the flight envelope considered in this chapter (to be discussed in detail in Chapter 7). If some disks remain overstressed at some off-design points, then those disks must be redesigned at the on-design point and later checked for its off-design point mechanical performance. This process goes on until all disks have satisfactory mechanical performance at on-design point and all off-design points through the flight envelope considered in this chapter.

The engine materials data are input into the model at the beginning of the on-design analysis. Once the disk design-optimisation is completed, the engine weight is evaluated. This is the bare engine weight without accessories (like control unit), engine-mount, and nacelle. The bare engine weight includes the engine's principal components (considered in Table 6.9 and Table 6.10), and supplementary components such as nuts, bolts, washers, seals, piping, and pumps. The weight of the principal engine components is estimated from the material densities input into GasTurb 13. The weight of the above-mentioned supplementary components is estimated by using a mass-factor (multiplication factor) to the principal engine weight. Halliwell [270] uses a mass factor of 1.2 and GasTurb 13's default mass factor value is 1.3. An average mass factor value of 1.25 is used in this model to estimate the bare engine weight. The bare engine weight, and TSFCs at on-design point and different off-design points, are estimated using the above process. The summation of weights of nacelle, accessories, and engine-mount, with the engine bare weight equals the total engine pod weight. The weights of nacelle, accessories and engine-mount is not calculated separately, and is used as it is from Table 6.2.

6.4.2.4 *Comments*

It is to be noted that the engine weight, and TSFCs obtained from the above engine model at on-design point and different off-design points are input to the aircraft weight sizing model (Chapter 7). This in-turn determines the thrust requirements at various points in the aircraft mission. The aircraft design is an iterative and interactive process, and it continues until the thrust value evaluated after the aircraft weight sizing process converges with the thrust produced by the engine in the present iteration of engine design-optimisation. Therefore, it is a coupled process between two models, but dealt separately in two chapters – Chapter 6 and Chapter 7. In this chapter, for avoiding confusion, only the calculated thrust values for engine design are considered for the multiple cases discussed here. The process for thrust requirement calculations is discussed in detail, in Chapter 7.

6.4.3   Model inputs

Most of the model inputs are similar for baseline Jet-A fuel, 100% SPK, and all three cases of LH_2 fuel. Some of the model inputs change between baseline case and three cases of LH_2 fuel. To differentiate these changes, inputs are listed separately.

Table 6.14. Atmospheric data input at off-design point of sea level static

Input parameters	SLS
Pressure	101.325 kPa [271]
Temperature	288.15 K [271]
Relative humidity	50% [271]

Table 6.15. Atmospheric data input at on-design point of top-of-climb, and off-design point of cruise, loiter and climb

Input parameters	Top of climb (TOC)	Cruise	Loiter	Climb (mid-way and average climb speed)
Altitude (m)	10,668	10,668	1,500 [272]	5,334
Relative humidity (%)	10 [273]	10 [273]	60 [273]	60 [273]
Mach number	0.8	0.84	0.6 [272]	0.47

Table 6.14 lists the atmospheric data input into the engine model at off-design point of SLS. Table 6.15 lists the atmospheric data input at on-design point of TOC, and off-design point of cruise, loiter, and climb. It is to be noted that all five points, realistic values of humidity (from literature) are used, which is not used in the international standard atmosphere (ISA)standards. Humidity acts as a real-world penalty on the engine thrust, and thus it is required to consider a worse case thrust in the engine design-optimisation, compared to ISA. The temperature and pressure at SLS condition are standard. The altitude (35,000 ft or 10,668 m), and Mach number at cruise and TOC points are as per the design requirements discussed before (Table 6.1 – Table 6.4). Standard transport jet (civil aircraft) loiter altitude (5,000 ft or 1,500 m) and Mach number are used (from literature). Because this chapter uses first order modelling methods, for climb an average climb speed of 290 knots (149.19 m/s), similar to present day efficient aircraft like Airbus A350-900 and Boeing

787, is considered mid-way (5,334 m) of complete climb, for estimating the engine TSFC at climb [274], [275]. At the mid-way climb altitude of 5,334 m, the speed of sound is 319 m/s. Therefore, at this point 290 knots is equal to Mach number of 0.47.

Table 6.16. Inputs for different engine components and different engine design cases (square brackets indicate reference number)

Input parameters	Value
Basic inputs for all cases (Jet-A, all three LH$_2$ cases, and 100% SPK)	
Intake pressure ratio	0.99 [276]
Core inlet duct pressure ratio	0.99 [188], [277]
IPC-HPC inter-duct pressure ratio	0.98 [188]
Bypass duct pressure ratio	0.992322 [188]
Turbine inter-duct reference pressure ratio	0.98 [188]
Design bypass ratio	17.65
Burner design efficiency	0.9995 [188]
Overboard bleed	0 kg/s
Power off-take	150 kW
High pressure spool mechanical efficiency	0.995 [188]
Low pressure spool mechanical efficiency	0.992 [188]
Burner pressure ratio	0.96 [266]
Turbine-exit duct pressure ratio	0.99 [188]
Fuel heating value (MJ/kg)	43.2 [1], 120 [2,3,4], 44.1 [5] [33], [55]
Cooling flows	
High pressure turbine section	20% [1,2,3,5] (source [123], [224]), 0% [4]
Low pressure turbine section	0% [1-5] (source [224])
Fan inputs for all cases (Jet-A, all three LH$_2$ cases, and 100% SPK)	
Inlet radius ratio	0.28 [188]
Inlet Mach number	0.6 [188]
HPC inputs	
Inlet radius ratio	0.423 [1,2,5], 0.448 [3], 0.46 [4]
Inlet Mach number	0.5 [1,2,5], 0.52 [3], 0.53 [4]

Inputs to be selected as per the respective case considered:
[1] Baseline case (Jet-A), [2] Case 1 of LH$_2$, [3] Case 2 of LH$_2$, [4] Case 3 of LH$_2$, [5] 100% SPK

Table 6.17. Inputs for engine nozzle section for different operating points and different engine design cases

Input parameters	Value
SLS (Jet-A, all three LH$_2$ cases and 100% SPK)	
Core and Bypass thrust coefficient	0.9 [278]
Core and bypass discharge coefficient	1 [278]
On-design (TOC), climb, cruise and loiter (Jet-A, all three LH$_2$ cases and 100% SPK)	
Core and bypass thrust coefficient	1 [279]–[281]
Design core nozzle angle	20 [266]
Design bypass nozzle angle	30 [266]

Some of the model inputs have already been listed and discussed which include a. future engine component efficiencies (Table 6.6); b. Turbomachinery stage count (Table 6.7); c. Engine materials (Table 6.9

130

and Table 6.10); d. Gearbox weight to power ratio (Table 6.11); e. Engine design variables i.e., start-guess values (Table 6.12). In this chapter, new engine design of the future for conventional jet fuel, 100% SPK, and LH_2 fuel (three cases), are developed using advanced material and future component efficiencies (respective inputs to the GasTurb 13 engine model), where the design requirements are set using literature. In some of the validation cases only (in Appendix C section C.1) conventional material and conventional component efficiencies will be input to the GasTurb 13 engine model. There are other inputs to the engine model which are listed and discussed next.

At the design point i.e., TOC, the design requirement values of BPR, bleed, and power off-take are 17.65, 0 kg/s, and 150 kW respectively, which are input to the engine model. These along with other inputs i.e., standard values from literature and GasTurb 13, are listed in Table 6.16. Recalling the discussion on OPR from section 6.4.2.1, OPR is a product of pressure losses, FPR, and IPC and HPC pressure ratios. The pressure losses that count towards OPR comprise of loss in engine intake and in ducts between two consecutive compressors (fan included).
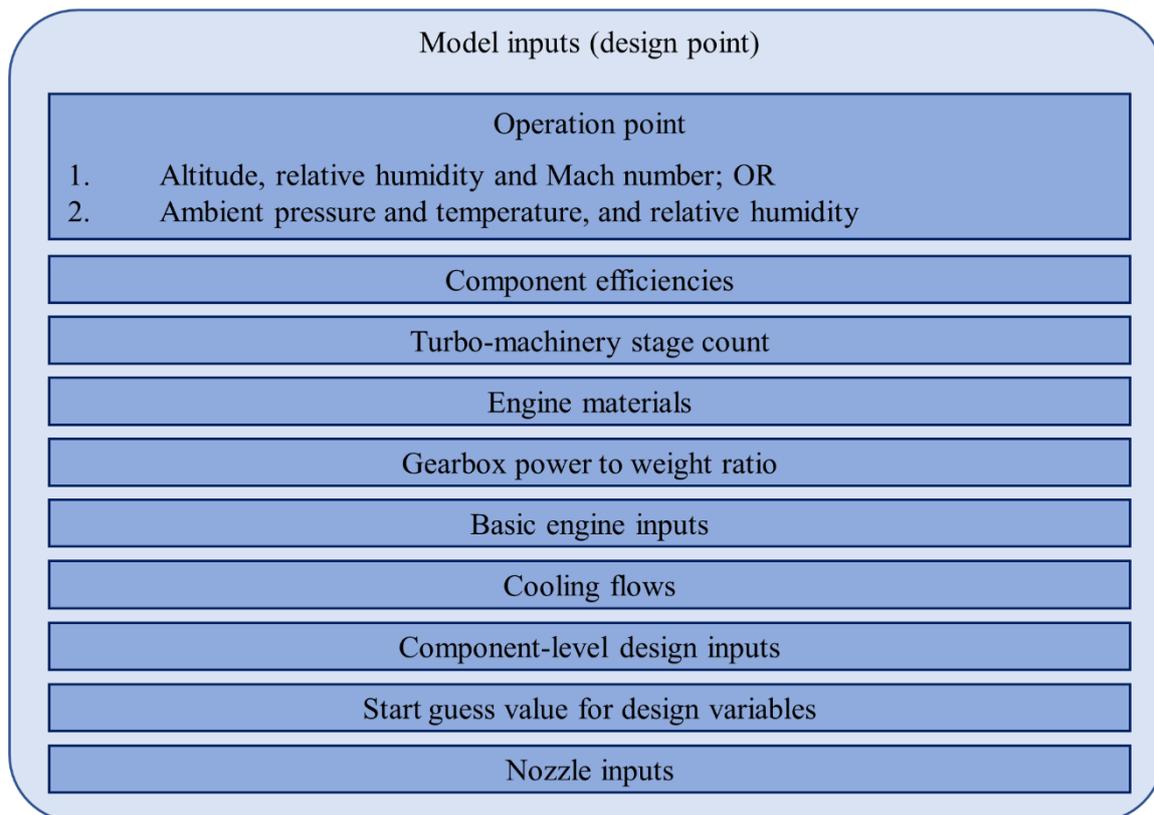
Figure 6.8. Engine model inputs

The aspect of cooling flows (input in Table 6.16) has been discussed in detail in section 6.3.3.4. While most inputs remain the same for all design cases (Jet-A, 100% SPK, and three cases of LH_2), the HPC inputs viz. the HPC inlet radius ratio and HPC inlet Mach number change slightly between cases. It is to be noted that these two inputs are similar to the standard/default inputs in GasTurb 13 [188]. These are changed primarily to obtain satisfactory aerodynamic performance of the turbomachinery (details discussed earlier in section 6.4.2.2). It can be observed from Table 6.16 that both HPC inlet radius ratio and HPC inlet Mach

number remain same for Jet-A, 100% SPK, and Case 1 of LH$_2$, since there is no change in engine thrust production between these cases. However, during the optimisation of Case 2 and Case 3 of LH$_2$, the thrust requirement and fan diameter reduces (because of lighter aircraft), which changes the shape of the HPC for maintaining the required design bypass ratio of 17.65 and thus both HPC inlet radius ratio and HPC inlet Mach number increases.

Table 6.17 lists the inputs for engine nozzle section for different operating points. These inputs remain same for all design cases. Gamble et al. [282] suggest that fixed-nozzles (of gas turbine engines) have highest thrust coefficient at their design point. To account for a drop in nozzle performance at off-design point, specifically at ground conditions, an average/moderate thrust coefficient value of 0.9 is considered at SLS (off-design point) based on the study by Manneville [278], which makes this evaluation at take-off condition (approximated to SLS for the present chapter). All above-mentioned model inputs have been summarised and listed in Figure 6.8.

On- and off-design point model inputs analysis:

All inputs for on- and off-design analysis have been listed and discussed in this section. The model description has been discussed in detail in section 6.4.2. Conducting on-design analysis using the above discussed inputs is straight-forward.

Table 6.18. Off-design modifiers-iteration variables and target

Variable	Target	Design requirement is met for:
Component efficiencies		
Δ outer LPC (fan) efficiency	outer LPC (fan) efficiency	LPC (fan) efficiency
Δ inner LPC (fan) efficiency	inner LPC (fan) efficiency	
Δ IPC efficiency	IPC efficiency	IPC efficiency
Δ HPC efficiency	HPC efficiency	HPC efficiency
Δ HPT efficiency	HPT efficiency	HPT efficiency
Δ LPT efficiency	LPT efficiency	LPT efficiency
Design parameters		
HPC spool speed	OPR	OPR
Δ LPC capacity	Outer fans exit pressure	FPR
Δ Bypass pressure	BPR	BPR

The off-design analysis is conducted with the help of maps, which is a standard procedure. In the current chapter, this is done in GasTurb 13 software. 'Standard maps' are selected in GasTurb 13 for climb, cruise and loiter points, for conducting off-design analysis at these points. The data of ambient conditions at these points from Table 6.15, are input to the model. A feature in GasTurb 13 of off-design modifiers through iteration of parameters, is used for the turbomachinery parameters such that every turbomachine operates at their efficiencies listed in Table 6.6 at respective points of climb, cruise, and loiter. The identified iteration variables and their target parameters are listed in Table 6.18, along with the respective design requirements met. For loiter, there is no separate column of component efficiencies. In this chapter, loiter is essentially treated as additional cruise and therefore efficiencies of cruise point are selected. Thus, every turbomachine

operates at their respective efficiency (published values) during climb, cruise, and loiter. It is to be noted that for all off-design points except SLS, only the target component efficiencies are known, and are set as a design requirement. The design requirements are not set for BPR, OPR, and FPR at these points, as per data known from Table 6.1 – Table 6.4. Therefore, the 'design parameter' section of Table 6.18 is not used in the off-design iteration for climb, cruise, and loiter.

SLS is a special off-design point in this chapter where not only turbomachinery efficiencies but also the performance/design requirements are to be met (such as BPR, FPR, OPR, thrust, etc.). For SLS condition, the option of 'selected map' is chosen in GasTurb 13. After choosing it, map option for a 'single-stage fan, sub-sonic IPC/booster, high pressure ratio for HPC, two-stage HPT, and medium pressure ratio LPT' is selected in GasTurb 13. Similar to the above discussed process, the off-design modifiers feature through iteration of parameters. In GasTurb 13 off-design case is used such that the target SLS turbomachinery efficiencies listed in Table 6.6 and all performance/design requirements at SLS, are met (such as BPR, FPR, OPR, thrust, etc.). The above complete the methodology section of this chapter. In Appendix C section C.1, validation cases of the developed model, are included. These establish a confidence in the proposed model, and the engine designs for the different cases (Jet-A baseline case, 100% SPK, and three cases of LH_2 fuel) are developed and analysed next in section 6.5.

6.5   Results and discussion

An aircraft engine model has been proposed in the methodology section (section 6.4). The model has been described in detail, where the details comprise of: data known from literature, design requirements/specification, and the model inputs. In this chapter, with the help of this model, new engine designs of the future for conventional jet fuel, LH_2 fuel (three cases), and 100% SPK, are developed using advanced materials and future component efficiencies, where the design requirements are set using literature. These design requirements are listed in Table 6.4. Firstly, two engine cases from literature are considered and the respective engine designs (with case specific design targets) were successfully replicated with satisfactory accuracy as per the set criteria, and therefore the proposed engine model is validated (see Appendix C section C.1). In this section, the results of the engine model for the set research objectives and design requirements (in Table 6.4) are considered. The results comprise of performance analysis at on-design point and all off-design points (listed before).

6.5.1   Jet-A engine

Table 6.19 shows on-design performance of the present model. Also, there are other studies listed in Table 6.19 (also discussed in section 6.2.1), which have a unique engine configuration and are relevant to this chapter, though not used for direct comparison. A study by Kestner et al. [225] on N+2 aviation technology is listed in this table. However, the point of engine operation is not known. It is listed as a reference point for engine weight, though the materials used in the said study are not disclosed by the authors.

Table 6.19. Engine performance of the present model and other studies [123], [130], [224], [225] using Jet-A fuel at TOC condition

Parameters	Units	Operating point unknown Kestner et al. [225]	TOC Greitzer et al. [123]	Bijewitz et al. [224]	Nickol et al. [130]	Present design
Mach, altitude	- , m	Unknown	~0.8 at 10,668 m	0.78 at 10,668 m	0.8 at 10,668 m	0.8 at 10,668 m
Engine mass flow	kg/s	-	512	674.6	-	638.1
Net thrust	kN	-	44	56	55.603	55.603
TSFC	g/kN-s	14.333	14.47	12.67	13.1543	12.3997
Fuel consumption	kg/s	-	0.637	0.71	0.731	0.689
OPR	-	46	55.2	60	60	60
BPR	-	20.29	19.44	19.4	17.65	17.65
FPR	-	1.353	1.46	-	1.35	1.35
Fan diameter	m	3.079	-	3.35	3.36296	3.36296
Bare engine weight	kg	4,515	-	7,648*	6,789	4,411
Gear ratio	-	2.88	-	4	-	3.5
Cooling flow	%	-	20	20	-	20
T_4/T_2	-	-	7	7.12	-	6.84
Power off-take	kW	-	-	0	150	150
LPT inlet temperature	K	-	-	< 1,350	-	1,139

* it is total propulsion system weight and not bare engine weight

Table 6.20. Engine performance of the present model and other studies [123], [130] using Jet-A fuel at SLS condition

SLS parameters	Units	Greitzer et al. [123]	Nickol et al. [130]	Present design
Engine mass flow	kg/s	1,119	-	1,527
Net thrust	kN	261.4	299.9	303.9
TSFC	g/kN-s	6.12	5.62	5.12
Fuel consumption	kg/s	1.6	1.69	1.56
OPR	-	52.8	47.1	47.1
BPR	-	18.86	20	20
FPR	-	1.43	1.25	1.25
Cooling flow	%	20	-	20
T_4/T_2	-	6.60	-	6.16
Power off-take	kW	-	150	150
LPT inlet temperature	K	-	-	1,213

A study by Bijewitz et al. [224] is also listed in Table 6.19, and it is used in the first validation case. Another study by Greitzer et al. [123] is also listed in Table 6.19. Both studies (Bijewitz et al. [224] and Greitzer et al. [123]) cannot be directly compared to the present model since they have a different BPR and OPR combination, but are relevant. Moreover, the propulsion system in the Greitzer et al. study [123] has four fans driven by two engine core compared to a single fan driven by one engine core via gearbox in the current chapter. Therefore, these studies cannot be used for direct comparison. In the present proposed model, the

future component efficiencies are used and these come from the study by Greitzer et al. [123] and it also provides T_4/T_2 value (T_2 is the fan inlet temperature), which gives some reference point for temperature values of future (efficient) engine technologies. Only the study by Nickol et al. [130] is directly relevant to the proposed model since this study sets the design requirements for the present chapter (listed in Table 6.4). This study is used in the second validation case.

It can be observed from Table 6.19 that the Jet-A engine design resulting from the proposed model meets all design requirements at the TOC condition, which are set in Table 6.4. The effect of high values of future component efficiencies is reflected in the lower TSFC and/or fuel consumption values of the present Jet-A engine design, in comparison with the study by Nickol et al. [130]. In line with this effect, the TET of the present chapter is also lower than the studies by Bijewitz et al. [224] and Greitzer et al. [123].

If the second validation case (Appendix C section C.1) is recalled, then by using conventional materials in the engine except the combustor and HPT, slightly higher engine weight (of 200-380 kg, depending on the case considered) is obtained, compared to the study by Nickol et al. [130]. As observed from Table 6.19, the use of advanced materials throughout the engine has resulted in significant reduction (~35%) in engine weight compared to the study by Nickol et al. [130]. The present Jet-A engine weight estimated by using the proposed model is similar to the engine weight of the study by Kestner et al. [225].

Table 6.21. Engine performance of the present model and other studies [123], [130] using Jet-A fuel at cruise condition

Cruise parameters	Units	Greitzer et al. [123]	Nickol et al. [130]	Present design
Mach, altitude	- , m	0.83 at ~10,668 m	0.84 at 10,668 m	0.84 at 10,668 m
Engine mass flow	kg/s	484	-	649.7
Net thrust	kN	36.9	-	51.6
TSFC	g/kN-s	14	13.455	12.667
Fuel consumption	kg/s	0.517	-	0.654
Cooling flow	%	20	-	20
T_4/T_2	-	6.60	-	6.57
Power off-take	kW	-	150	150
LPT inlet temperature	K	-	-	1,107

Table 6.22. Engine performance of the present engine model using Jet-A fuel at loiter and climb conditions

Parameters	Units	Present Jet-A engine design	
		Loiter	Climb (mid-way and average climb speed)
Mach, altitude	- , m	0.6 at 1,500 m	0.47 at 5,334 m
Engine mass flow	kg/s	1,488.32	904.96
Net thrust	kN	114.67	94.94
TSFC	g/kN-s	12.175	9.798
Fuel consumption	kg/s	1.396	0.931
Cooling flow	%	20	20
T_4/T_2	-	5.741	6.315
Power off-take	kW	150	150
LPT inlet temperature	K	1,167	1,129

Table 6.20 lists the off-design engine performance (SLS condition) of the present Jet-A engine design and of other studies. It can be observed from Table 6.20 that the present Jet-A engine design meets all design requirements at the SLS condition, which are set in Table 6.4. The effect of high values of future component efficiencies is reflected (at SLS as well) in the lower TSFC and/or fuel consumption values of the present Jet-A engine design, in comparison with the study by Nickol et al. [130]. On similar lines, TET of engine in the present chapter is also lower than the study by Greitzer et al. [123].

Table 6.21 shows the off-design engine performance (cruise condition) of the present Jet-A engine design and of other studies. It can be observed from Table 6.21 that the impact of high values of future component efficiencies can be seen at cruise conditions also. The use of very high efficiency turbomachinery components have resulted in lower engine TSFC and/or fuel consumption values in the present Jet-A engine design compared to the study by Nickol et al. [130]. On similar lines, the TET of the present design is also lesser compared to the study by Greitzer et al. [123]. An LTA aircraft spends 90+% of the flight time in cruise. The lower TSFC value is expected to result into significant savings in fuel consumption over one flight mission. For cruise condition, the lift force equals aircraft weight, and thrust is equal to drag force. In cruise, T/W is equal to the reciprocal of the L/D ratio of the aircraft. The calculation of the L/D ratio is done separately through aerodynamic equations, and the aircraft weight is estimated in the aircraft weight sizing process. This calculates the unknown value of required thrust. The process for thrust requirement calculations is discussed in detail, in Chapter 7. In Table 6.21, the engine produces 51.61 kN of thrust where the minimum required thrust is calculated to be 42.25 kN.

Table 6.22 shows the off-design engine performance of the present Jet-A engine design at points of loiter and climb. There are no studies that can be used either for comparison or providing some reference values. It is to be noted that the LPT inlet temperatures at all points (on-design and off-design) in the present Jet-A engine design listed in Table 6.19 – Table 6.22, are lower than 1,350 K which was required for having uncooled LPT. This design choice was successful primarily because of the use of future component efficiencies. Figure 6.9 shows the cross-sectional view of the Jet-A powered GTF engine designed from the proposed/present model. This figure also shows the diameter of the fan (a design requirement) and length of the engine. The 'I-section' of the turbomachinery disk, a design choice, can be noticed in Figure 6.9.

Overall, the use of future component efficiencies in the present Jet-A engine design, has improved the fuel efficiency of the engine at all operational points considered in this chapter, which is as per expectation. A significant reduction (~35%) in engine weight (compared to the study by Nickol et al. [130]) is observed primarily because of two reasons: use of advanced materials, and the turbo-machinery stage count selection process (section 6.3.3.2) along with satisfactory aerodynamic performance of turbomachinery (section 6.4.2.2). The TSFC values in Table 6.19 – Table 6.22 of the present Jet-A engine design at different/all operational points considered in this chapter, are inputs to the aircraft weight sizing process discussed in Chapter 7. This enables the estimation of fuel burn of the aircraft over one mission. The above discussion concludes the Jet-A UHB GTF engine on-design and off-design analysis. In the next section, three cases of the LH_2 engine are discussed along with their performance comparison with Jet-A engine at on-design point and different off-design points.
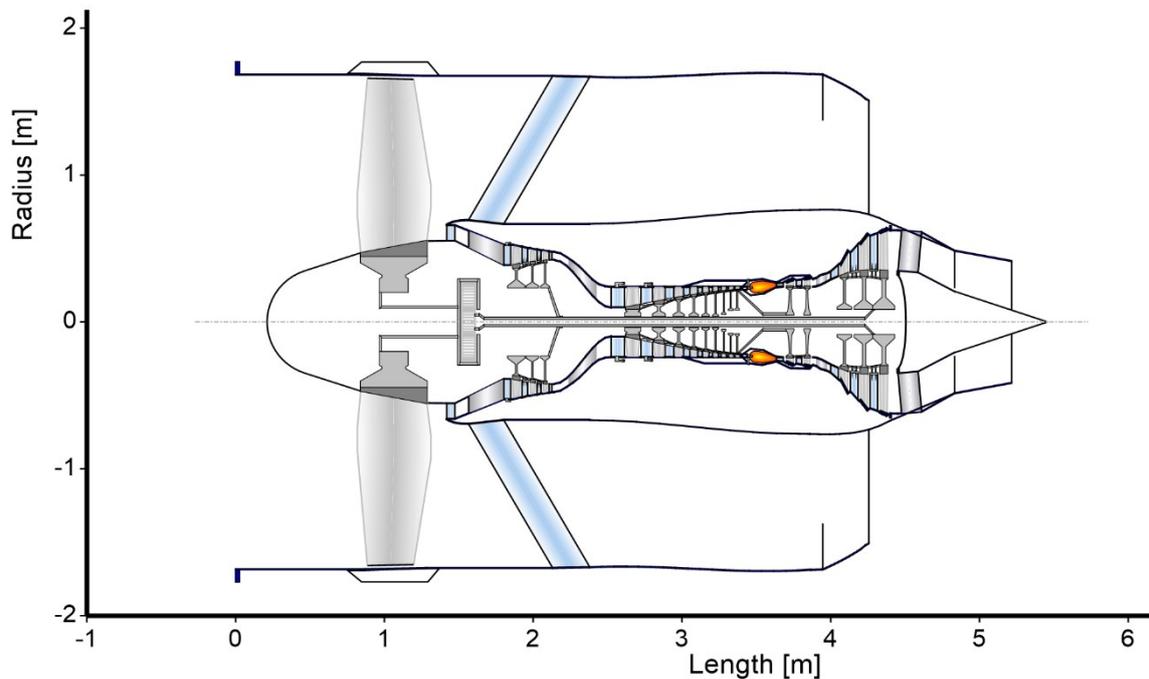
Figure 6.9. Cross-sectional view of the Jet-A powered GTF engine designed using the proposed model

6.5.2 LH$_2$ engine

The energy density per unit mass of LH$_2$ is 2.78 times the energy density per unit mass of Jet-A. Therefore, lower mass of LH$_2$ must be carried at the beginning of the flight mission, and the LH$_2$ aircraft weight at different points in flight mission is lesser than the Jet-A case (also observed in Chapter 4 and 5). *T/W* is defined for an aircraft structure. Since in this chapter the outer aircraft structure remains the same for both Jet-A and LH$_2$, *T/W* should ideally be similar. Thus, to maintain the same *T/W* for a lower aircraft weight, the thrust requirement reduces. The process for thrust requirement calculations is discussed in detail, in Chapter 7. To account these impacts of LH$_2$ use in aircraft, three different cases are considered, as discussed in methodology. In this section, only the LH$_2$ engine performance will be discussed. It is to be noted that Case 2 and Case 3 have the effect of lighter aircraft for LH$_2$ use, absorbed in them and hence the thrust requirement in the analysis below have considered these effects. The process for thrust requirement calculations is discussed in detail, in Chapter 7.

Tables 6.23, 6.25, 6.26, 6.27 and 6.28 list the comparison of engine performance using Jet-A and LH$_2$ (three cases), at TOC (on-design point), SLS, cruise, climb, and loiter points, respectively. Also, Table 6.24 provides comparison of combustion product species, mass, momentum, and total energy between LH$_2$ Case 1 and Jet-A engine at design point/TOC condition (same thrust production). It is to be noted that the Jet-A engine performance has already been discussed in the previous section. It is listed here for a comparative engine-performance assessment with the three cases of the LH$_2$ engine. Also, the values of thrust required mentioned in Table 6.23, Tables 6.25, and Table 6.26, are calculated through an iterative and interactive process between the proposed/present engine model and the aircraft weight sizing process. The process for thrust requirement calculations is discussed in detail, in Chapter 7.

137

It can be observed from Table 6.23, Tables 6.25, and Table 6.26 that the engine designs successfully meet the design requirements/targets as set in Table 6.4. In Table 6.23, Tables 6.25, and Table 6.26, the engine designs meet the required thrust values for all three cases of LH_2 fuelled engine, at said mission points considered in these tables. These thrust requirements are calculated through the aircraft weight sizing process (details in Chapter 7).

Table 6.23. Comparison of engine performance at TOC condition using LH_2 fuel (three cases) and Jet-A, using the proposed model

TOC parameters	Units	Jet-A	LH₂		
			Case 1	Case 2	Case 3
Mach, altitude	- , m	0.8 at 10,668 m	0.8 at 10,668 m	0.8 at 10,668 m	0.8 at 10,668 m
Engine mass flow	kg/s	638.06	638.06	571.92	558.79
Thrust required	kN	55.603	46.29	46.02	45.66
Thrust produced	kN	55.603	55.603	46.354	46.12
TSFC	g/kN-s	12.399	4.328	4.284	4.160
TSEC	kJ/kN-s	535.67	519.36	514.06	499.14
TSEC % difference compared to Jet-A	%	-	-3.04	-4.03	-6.82
Fuel consumption	kg/s	0.689	0.241	0.199	0.192
Fuel-air ratio (FAR)	-	0.025191	8.7927E-3	8.0942E-3	6.4021E-3
Equivalence ratio (Φ)	-	0.37	0.30	0.28	0.22
OPR	-	60	60	60	60
BPR	-	17.65	17.65	17.65	17.65
FPR	-	1.35	1.35	1.35	1.35
IPC pressure ratio	-	3.296	3.296	3.296	3.296
HPC pressure ratio	-	13.9	13.9	13.9	13.9
Cooling flow	%	20	20	20	Zero
Combustor length	m	0.1981	0.1981	0.18723	0.18505
Combustion gas velocity	m/s	235.68	238.45	234.29	223.6
Residence time	ms	0.841	0.831	0.8	0.826
P_3	kPa	2,159.4	2,159.4	2,159.4	2,159.4
T_3	K	859.4	859.5	859.5	859.5
T_4	K	1,689.61	1,642.39	1588.50	1,452.50
T_4/T_2	-	6.844	6.653	6.434	5.883
Bare engine weight	kg	4,411	4,381	4,084	3,636
Gear ratio	-	3.5	3.5	3.11	3.11
Fan diameter	m	3.36296	3.36296	3.1839	3.14713
LPT inlet temperature	K	1,139	1,111	1,060	1,054
Power off-take	kW	150	150	150	150

Table 6.24. Comparison of combustion product species, mass, momentum, and total energy between LH₂ Case 1 and Jet-A engine at TOC condition (same thrust production)

Baseline Jet-A FAR = 0.025191 (in equation 6.7), at TOC condition					
	CO_2	H_2O	O_2	N_2	Total
Molecular weight (kg/k-mol)	44	18	32	28	-
Number of moles	0.0522	0.0495	0.1330	0.7900	1.025
Mole fraction	0.0509	0.0483	0.1298	0.7709	1
Molar heat capacity C_p (J/mol-K)	3.5 R'	4 R'	3.5 R'	3.5 R'	-
Mass (kg)	2.297	0.892	4.257	22.131	*29.577*
Molar heat capacity C_p of combustion products (J/mol-K)					3.524 R'
Molecular weight of combustion products (kg/k-mol)					28.863
Mass flow rate at combustor exit (kg/s) [from GasTurb 13]					28.06
Time consumed by ~ *29.577 kg* of combustion products to flow (sec)					1.054
Fuel flow rate (kg/s) [from GasTurb 13]					0.689
Fuel mass combusted by one k-mol of air (kg) [using equation 6.7]					0.727
Time taken for the combustion of ~0.727 kg fuel (sec)					1.054
Total pressure at combustor exit (kPa) [from GasTurb 13]					2,073.06
Total enthalpy at combustor exit (MJ/kg) [from GasTurb 13]					1.63
Specific heat capacity c_p at total temperature at combustor exit (J/kg-K) [from GasTurb 13]					1,287.22
Emission index of H_2O (kg H_2O per kg fuel)					1.23
Case 1 H_2 FAR = 8.7927×10^{-3} (in equation 6.8), at TOC condition					
	CO_2	H_2O	O_2	N_2	Total
Molecular weight (kg/k-mol)	44	18	32	28	-
Number of moles	0	0.1258	0.1471	0.7900	1.063
Mole fraction	0	0.1184	0.1384	0.7432	1
Molar heat capacity C_p (J/mol-K)	-	4 R'	3.5 R'	3.5 R'	-
Mass (kg)	0	2.267	4.706	22.131	*29.104*
Molar heat capacity C_p of combustion products (J/mol-K)					3.559 R'
Molecular weight of combustion products (kg/k-mol)					27.381
Mass flow rate at combustor exit (kg/s) [from GasTurb 13]					27.611
Time consumed by ~ *29.104 kg* of combustion products to flow (sec)					1.054
Fuel flow rate (kg/s) [from GasTurb 13]					0.241
Fuel mass combusted by one k-mol of air (kg) [using equation 6.8]					0.254
Time taken for the combustion of ~0.254 kg fuel (sec)					1.054
Total pressure at combustor exit (kPa) [from GasTurb 13]					2,073.06
Total enthalpy at combustor exit (MJ/kg) [from GasTurb 13]					1.63
Specific heat capacity c_p at total temperature at combustor exit (J/kg-K) [from GasTurb 13]					1,343.13
Emission index of H_2O (kg H_2O per kg fuel)					8.937
* R' is the universal gas constant					

According to the study by Corchero et al. [226], T_4 in hydrogen-based gas turbine engines decreases by approximately to 37 K compared to Jet-A engines for same thrust production at SLS, which translates into a significantly longer engine life. As can be observed from Table 6.25, at SLS point, for same thrust production (case 1) the LH₂ engine operates at about 46 K lower T_4 compared to Jet-A engine. This is similar to the findings of Corchero et al. Additionally, study by Verstraete [65] reports a drop in T_4 of 60 K at take-off (absorbing the

modifications to a double-decker tube-wing aircraft for the use of LH_2). However, the engine performance modelling in the present work does not consider take-off point separately since the aircraft energy consumption during smaller segments is based on (fuel fractions) weight sizing methods (Chapter 7) and thus comparison at take-off cannot be made. The reason for the reduction in T_4 is discussed below with the consideration of combustion chemistry.

When a fluid mass flows through a control volume, it is accompanied by its energy. These include four types of energy: internal energy, kinetic energy, potential energy, and flow work [283]. Therefore, any given fluid flow through a control volume is analysed by the mass, momentum, and total energy equations between the entry point and the exit point of the control volume.

Referring to Table 6.23 i.e., the design point/TOC, it can be observed that for same thrust production, the TSFC value of Jet-A is 2.865 times the TSFC value for LH_2 Case 1, whereas the energy density per unit mass of LH_2 is 2.78 times the energy density per unit mass of Jet-A. This (TSFC of LH_2 Case 1 vs Jet-A) can also be observed at off-design/other points in Table 6.25 – Table 6.28. For same thrust production, Verstraete [191] observes a similar relation between TSFC of Jet-A and the TSFC for LH_2 ($TSFC_{Jet-A} = 2.86$ x $TSFC_{LH2}$). This reduction in TSFC is attributable to difference in the combustion chemistry of the two fuels, in totality, which comprise of two effects: energy densities of two fuels, and mass and species conservation. As observed from Figure 6.1 (section 6.2.2.2), for same flame temperature, hydrogen burns 'leaner' than Jet-A. Additionally, as described above, burner temperature (T_4) of Case 1 of LH_2 engine for same thrust production is about 47 K lower than that for Jet-A engine. Thus, for producing the same thrust, lesser LH_2 fuel is required or hydrogen burns 'much leaner' than expected, compared to Jet-A.

The physics can further be understood through Table 6.24, which provides a comparison of combustion product species, mass, momentum, and total energy between LH_2 Case 1 and Jet-A engine at TOC condition (same thrust production). The mass of the product species is calculated using equations 6.7 and 6.8 (section 6.2.2.1) for Jet-A and hydrogen respectively (with FAR for Jet-A and LH_2 Case 1 from Table 6.23). As discussed before in section 6.2.2.1, these equations are based on a simplistic major species model. It can be observed that the mass of combustion products/gas for both Jet-A and LH_2 Case 1 is similar. This is despite the fact that hydrogen combustion does not produce any CO_2. Hence for achieving the same mass of combustion products/gas, which can impart same momentum on the turbines (for same thrust production), hydrogen burns much leaner than Jet-A. The extra air from the leaner combustion, especially oxygen, contribute to the mass requirement of the combustion product/gas. This can be observed from Table 6.24, where the mass of oxygen (heavier gas relative to air) in the combustion products of hydrogen combustion is greater than that for Jet-A combustion. Moreover, this extra oxygen also contributes to the formation of higher mass of water for hydrogen engine compared to Jet-A engine. This can be observed from Table 6.24, where the mass of water in the combustion products of hydrogen combustion is significantly greater than that for Jet-A combustion. In terms of emissions index (EI), the EI (H_2O) for Jet-A and LH_2 are calculated to be 1.23 kg/kg-fuel and 8.937 kg/kg-fuel respectively. These calculated values are very similar to the EI reported in literature of 1.24 kg/kg-fuel [284] and 8.937 kg/kg-fuel [285] for Jet-A and LH_2, respectively.

Therefore, lean combustion of hydrogen enables the inclusion of more heavy gas molecules such that the mass of the combustion products is similar to the combustion products of Jet-A, and both cases thus result in similar momentum of combustion products. It can be observed from Table 6.24, that both Jet-A and LH_2 Case 1 engines have same total pressure at combustor exit. The 'total pressure' (static and dynamic) is a measure of the momentum. Lastly, both Jet-A and LH_2 Case 1 engines have same 'total enthalpy' (measure of energy) of 1.63 MJ/kg. Additionally, using equations 6.7 and 6.8, and GasTurb 13, it can be observed from Table 6.24 that both cases have: similar time scales for consumption of respective fuel mass with respective fuel consumption rate; and time taken by the mass of combustion products to flow with respective flow rate. Therefore, at the combustor exit point, both Jet-A and LH_2 Case 1 engines have similar mass, momentum, and energy, which enables both engines to produce same thrust. Thus, as observed from Table 6.23, for same thrust production, the TSFC value of Jet-A is 2.865 times the TSFC value for LH_2 Case 1. In summary, the ratio of energy density per unit mass of LH_2 and Jet-A is 2.78, and it is a primary contributor to the above ratio of TSFC of 2.865 (ratio of TSFC of Jet-A and LH_2), and the difference in mass and species conservation in combustion chemical reaction of the two different fuels (discussed above) is the secondary contributor to this (2.865) ratio. According to the study by Verstraete [65], the drop in T_4 is also due to the increased heat capacity of combustion products of hydrogen for same thrust production. This aspect can also be observed in Table 6.24, where the specific heat capacity c_p of combustion products at total temperature of Case 1 of LH_2 engine is higher than Jet-A engine. The increase in the heat capacity can be understood from statistical mechanics. From statistical mechanics, the molar heat capacity is a measure of momentum/kinetic energy [286]. The molar heat capacity (J/mol-K) for an ideal gas, through equipartition principle can be represented by the translational, rotational, vibrational, and other modes of kinetic energy. For typical gas turbine operational temperatures (< 2,000 K), only translational and rotational energies are completely activated (ibid). According to equipartition principle, (the molar heat capacity at constant volume C_v), $C_{v,translational}$ is nR'/2 and $C_{v,rotational}$ is mR'/2, where n and m are translational and rotational degrees of freedom respectively, and R' is the universal gas constant. For an ideal gas the molar heat capacity at constant pressure $C_P = R' + C_v$. For a linear molecule (CO_2, O_2, and N_2), there are three translational and two rotational modes/degrees of freedom (one redundant) i.e., C_v = 2.5 R' and C_P = 3.5 R', and for a non-linear molecule (H_2O), there are three translational and three rotational modes/degrees of freedom i.e., C_v = 3 R' and C_P = 4 R'. The molar C_p of the combustion products of Jet-A and Case 1 of LH_2 are calculated to be 3.524 R' and 3.559 R', respectively, as listed in Table 6.24.

The above reasons are therefore responsible for the ~ 47 K drop in burner temperature (T_4) of Case 1 of LH_2 engine compared to Jet-A engine, for same thrust production. In other words, for same thrust production one would expect that the T_4 for both Jet-A and hydrogen engine would be similar, and for a given flame temperature in Figure 6.1 (section 6.2.2.2), hydrogen burns at a 'leaner' FAR. It is further observed that in the hydrogen engine for same thrust production, the T_4 is about 47 K lower than Jet-A engine, and this further reduces the FAR or hydrogen burns 'much leaner' than expected, and this is attributable to the difference in mass and species conservation of Jet-A and hydrogen (as discussed above).

The TSFC in Table 6.23, Table 6.25 – Table 6.28 is converted to thrust specific energy consumption (TSEC) by multiplying every case with the energy density of the respective fuel considered. The reduction in

TSFC is attributable to difference in the combustion chemistry of the two fuels, in totality, which comprise of two effects: energy densities of two fuels, and mass and species conservation. As observed from Table 6.23, hydrogen engine (case 1) is 3% more energy efficient than Jet-A engine, for same thrust production. The study by Verstraete [191] observes a similar (3%) reduction in hydrogen engine TSEC compared to Jet-A engine (for same thrust production).

Table 6.25. Comparison of engine performance at SLS condition using LH$_2$ fuel (three cases) and Jet-A, using the proposed model

SLS parameters	Units	Jet-A	LH$_2$ Case 1	LH$_2$ Case 2	LH$_2$ Case 3
Mach, altitude	- , m	0 at 0 m	0 at 0 m	0 at 0 m	0 at 0 m
Engine mass flow	kg/s	1,526.97	1,528.70	1,356.61	1,331.98
Thrust required	kN	299.9	251.1	249.6	247.7
Thrust produced	kN	303.9	304.5	263.8	261.1
TSFC	g/kN-s	5.124	1.778	1.761	1.690
TSEC	kJ/kN-s	221.37	213.34	211.34	202.78
TSEC % difference compared to Jet-A	%	-	-3.63	-4.53	-8.40
Fuel consumption	kg/s	1.557	0.541	0.465	0.441
FAR	-	0.026912	9.346E-3	9.0383E-3	6.9941E-3
Φ	-	0.39	0.32	0.31	0.24
OPR	-	47.1	47.1	47.1	47.1
BPR	-	20	20	20	20
FPR	-	1.25	1.25	1.25	1.25
IPC pressure ratio	-	3.028	3.044	2.890	2.945
HPC pressure ratio	-	12.769	12.702	13.391	13.031
Cooling flow	%	20	20	20	Zero
Combustor length	m	0.1981	0.1981	0.1872	0.1851
Combustion gas velocity	m/s	241.78	244.57	243.21	230.82
Residence time	ms	0.82	0.81	0.77	0.80
P$_3$	kPa	4,724.8	4,724.5	4,724.7	4,724.7
T$_3$	K	914	914	914	912
T$_4$	K	1,776	1,720	1,698	1,539
T$_4$/T$_2$	-	6.163	5.97	5.892	5.342
LPT inlet temperature	K	1,213	1,179	1,152	1,135
Power off-take	kW	150	150	150	150

Additionally, it can be observed from Table 6.23, Table 6.25 – Table 6.28 that all three cases of LH$_2$ engine operate at a lower T$_4$ compared to the Jet-A engine. Especially, for case 1 of LH$_2$ engine i.e., for similar thrust production, the T$_4$ is lower (as described above) compared to Jet-A engine because H$_2$ burns much leaner than Jet-A. Additionally, it can be observed from Table 6.23, Table 6.25 – Table 6.28 that the thrust values drops between Case 1 and Case 3 of LH$_2$, because the effect of lighter LH$_2$ aircraft weight is considered. Therefore, T$_4$ drops between Case 1 and Case 3 of LH$_2$, which is expected. In Case 3 of LH$_2$, there are no cooling flows (at on-design and all four off-design points) because the engine is operating at significantly lower T$_4$ (approximate reduction of 200 K) and the design decision to consider this case specifically in the

study, is well supported. Because there are no cooling flows, the engine must consume lesser fuel compared to Case 2 of LH_2. The drop in thrust values as discussed above for Table 6.23, Table 6.25 – Table 6.28, along with the effect of zero cooling flows in Case 3 of LH_2, both are attributable to the TSFC drop between Case 1 and Case 3 of LH_2. Overall, these above discussed effects (lower T_4 and FAR or Φ, lighter aircraft or thrust reduction, and reduction in cooling flows) result in the reduction in TSEC for LH_2 Case 1 (of ~ 3-4%) and Case 3 (of 6-8%), compared to Jet-A engine, which can be observed from Table 6.23, Table 6.25 – Table 6.28.

Table 6.26. Comparison of engine performance at cruise condition using LH_2 fuel (three cases) and Jet-A, using the proposed model

Cruise parameters	Units	Jet-A	LH_2		
			Case 1	Case 2	Case 3
Mach, altitude	- , m	0.84 at 10,668 m	0.84 at 10,668 m	0.84 at 10,668 m	0.84 at 10,668 m
Engine mass flow	kg/s	649.7	649.8	602.9	569.7
Thrust required	kN	42.25	40.24	40.15	40.02
Thrust produced	kN	51.61	51.68	51.09	43.12
TSFC	g/kN-s	12.667	4.424	4.351	4.278
TSEC	kJ/kN-s	547.2	530.9	522.1	513.4
TSEC % difference compared to Jet-A	%	-	-2.98	-4.59	-6.16
Fuel consumption	kg/s	0.654	0.229	0.222	0.185
FAR	-	0.024099	8.4241E-3	7.9129E-3	6.0565E-3
Φ	-	0.35	0.29	0.27	0.21
Propulsive efficiency	-	0.863	0.863	0.855	0.868
Core efficiency	-	0.605	0.626	0.631	0.641
Overall efficiency	-	0.455	0.469	0.477	0.485
Transmission efficiency	-	0.872	0.869	0.884	0.871
Combustion gas velocity	m/s	231.99	234.68	234.00	219.89
Residence time	ms	0.854	0.842	0.801	0.842
P_3	kPa	2,108.29	2,110.35	2,473.61	2,162.54
T_3	K	838	838	876	843
T_4	K	1,640	1,597	1,588	1,410
T_4/T_2	-	6.567	6.394	6.359	5.645
Cooling flow	%	20	20	20	Zero
LPT inlet temperature	K	1,107	1,081	1,066	1,025
Power off-take	kW	150	150	150	150

As observed from Table 6.23, the engine weight of Case 1 of LH_2 is lower than Jet-A engine by approximately 30 kg for same thrust production despite both cases having same stage counts of turbomachinery and same advanced materials. This is primarily attributable to lower T_4 (-47 K) of LH_2 Case 1, which results in lower aero-thermal and mechanical loading of LPT section in GasTurb 13. In other words, Jet-A engine has higher T_4 compared to LH_2 Case 1. Therefore, the LPT section loading of Jet-A engine is slightly higher than LH_2 Case 1, which results in ~ 30 kg higher weight. Additionally, the engine weight decreases from Case 1 to

Case 3 of LH$_2$. Jet-A and all three cases of LH$_2$ use the same stage counts of turbomachinery and same advanced materials. Referring to Table 6.23 i.e., the design point/TOC, it can be observed that the fan diameter decreases from Case 1 to Case 3 of LH$_2$. The drop in engine weight is primarily attributable to this decreasing fan diameter (huge component in the engine) from Case 1 to Case 3 of LH$_2$. In Case 2 and Case 3 of LH$_2$, as described before, the fan diameter is removed as a design constraint/target since Dincer [250], Verstraete [191], and Nojoumi [55] mention that for an LH$_2$ powered aircraft, the thrust requirement reduces and that the engine becomes smaller in size. In Case 2 and Case 3 of LH$_2$, this chapter is specifically trying to optimise the engine as per the thrust requirement of the aircraft and based on the suggestions of above literature. Thus, the fan diameter is removed as a design constraint/target. Case 2 and Case 3 of LH$_2$ have the effect of lighter aircraft (lower: thrust requirement, engine weight, fan size, and cooling flows) for LH$_2$ use absorbed in them, compared to Case 1 of LH$_2$ and Jet-A.

Table 6.27. Comparison of engine performance at climb condition using LH$_2$ fuel (three cases) and Jet-A, using the proposed model

Climb parameters	Units	Jet-A	LH$_2$		
			Case 1	Case 2	Case 3
Mach, altitude	- , m	0.47 at 5334 m	0.47 at 5,334 m	0.47 at 5,334 m	0.47 at 5,334 m
Engine mass flow	kg/s	904.96	906.71	857.06	798.62
Thrust produced	kN	94.94	95.54	96.96	82.58
TSFC	g/kN-s	9.798	3.413	3.389	3.266
TSEC	kJ/kN-s	423.26	409.58	406.73	391.91
TSEC % difference compared to Jet-A	%	-	-3.23	-3.91	-7.41
Fuel consumption	kg/s	0.930	0.326	0.329	0.270
FAR	-	0.024524	8.5724E-3	8.0763E-3	6.2803E-3
Φ	-	0.36	0.29	0.28	0.21
Combustor length	m	0.1981	0.1981	0.1872	0.1851
Combustion gas velocity	m/s	234.28	237.10	237.14	223.33
Residence time	ms	0.846	0.836	0.79	0.829
P$_3$	kPa	2,978.50	2,989.01	3,632.44	3,093.35
T$_3$	K	861	862	910	868
T$_4$	K	1672	1628	1628	1450
T$_4$/T$_2$	-	6.315	6.149	6.152	5.478
Cooling flow	%	20	20	20	Zero
LPT inlet temperature	K	1,129	1,102	1,096	1,054
Power off-take	kW	150	150	150	150

It is to be noted that the LPT inlet temperatures at all points (on-design and off-design) in engine designs listed in Table 6.23, Table 6.25 – Table 6.28, are lesser than 1,350 K which was required for having uncooled LPT. This design choice was successful primarily because of the use of future component efficiencies. Figure 6.10 shows the Jet-A powered GTF engine overlapped with the three cases of LH$_2$ powered GTF engine designed using the proposed model. This figure also shows the diameter of the fan (a design

requirement) and length of the engine. The 'I-section' of the turbomachinery disk, a design choice, can be noticed in Figure 6.10. LH_2 engines are, in general, lighter, and colder than baseline or Jet-A engine as seen observed from Figure 6.10 and/or Table 6.23. Especially, the optimised LH_2 engines (Case 2 and Case 3) are smaller, shorter, colder, and lighter than Jet-A engine or LH_2 Case 1 engine.

Table 6.28. Comparison of engine performance at loiter condition using LH_2 fuel (three cases) and Jet-A, using the proposed model

Loiter parameters	Units	Jet-A	LH₂		
			Case 1	Case 2	Case 3
Mach, altitude	- , m	0.6 at 1500 m	0.6 at 1500 m	0.6 at 1500 m	0.6 at 1500 m
Engine mass flow	kg/s	1,488.32	1,490.63	1,403.87	1,307.75
Thrust produced	kN	114.67	115.46	120.05	98.02
TSFC	g/kN-s	12.175	4.234	4.195	4.067
TSEC	kJ/kN-s	525.94	508.03	503.35	487.98
TSEC % difference compared to Jet-A	%	-	-3.41	-4.30	-7.22
Fuel consumption	kg/s	1.397	0.489	0.504	0.399
FAR	-	0.024892	8.6933E-3	8.0066E-3	6.3186E-3
Φ	-	0.36	0.30	0.27	0.22
Combustor length	m	0.1981	0.1981	0.1872	0.1851
Combustion gas velocity	m/s	237.44	240.26	239.83	226.44
Residence time	ms	0.835	0.825	0.781	0.818
P_3	kPa	4,486.2	4,499.9	5,715.1	4,624.2
T_3	K	905	906	967	911
T_4	K	1,713	1,667	1,665	1,486
T_4/T_2	-	5.741	5.586	5.579	4.977
Cooling flow	%	20	20	20	Zero
LPT inlet temperature	K	1,167	1,139	1,133	1,087
Power off-take	kW	150	150	150	150

Overall, three important effects are noted about the impacts of properties hydrogen on the engine performance. The first effect is the 2.78 times higher energy density per unit mass of LH_2 in comparison with Jet-A. This effect is directly observed in the combustion chamber through TSFC. The second effect is that the reduction in TSFC is also attributable to difference in the mass and species conservation in the two different fuels. The first two effects are observed for LH_2 case 1 engine (same thrust production), where $TSFC_{Jet-A}$ = 2.865 x $TSFC_{LH2}$. The third effect is an indirect effect of the higher energy density per unit mass of LH_2 compared to Jet-A, resulting in lower aircraft weight for LH_2 use in the same aircraft structure (*T/W* aspect) powered by Jet-A. This effect results in lower thrust requirement, engine weight, and fan size. All three effects are observed in Case 2 and Case 3 of LH_2 engine. Along with these, the reduced thrust requirement enables the engine to run colder than Jet-A, Case 1 of LH_2 and more importantly the maximum allowable temperatures of the CMC used (as advanced material) in the hot-end components. Such low temperatures do not require

cooling flows (Case 3 of LH$_2$), and therefore the TSFC further drops. This impact of cooling flows is included in Case 3 of LH$_2$.

	Engine weight	Fan diameter
Baseline (Jet A)	4412 kg	3.36296 m
LH$_2$ Case 1	4381 kg	3.36296 m
LH$_2$ Case 2	4085 kg	3.1839 m
LH$_2$ Case 3	3636 kg	3.14713 m
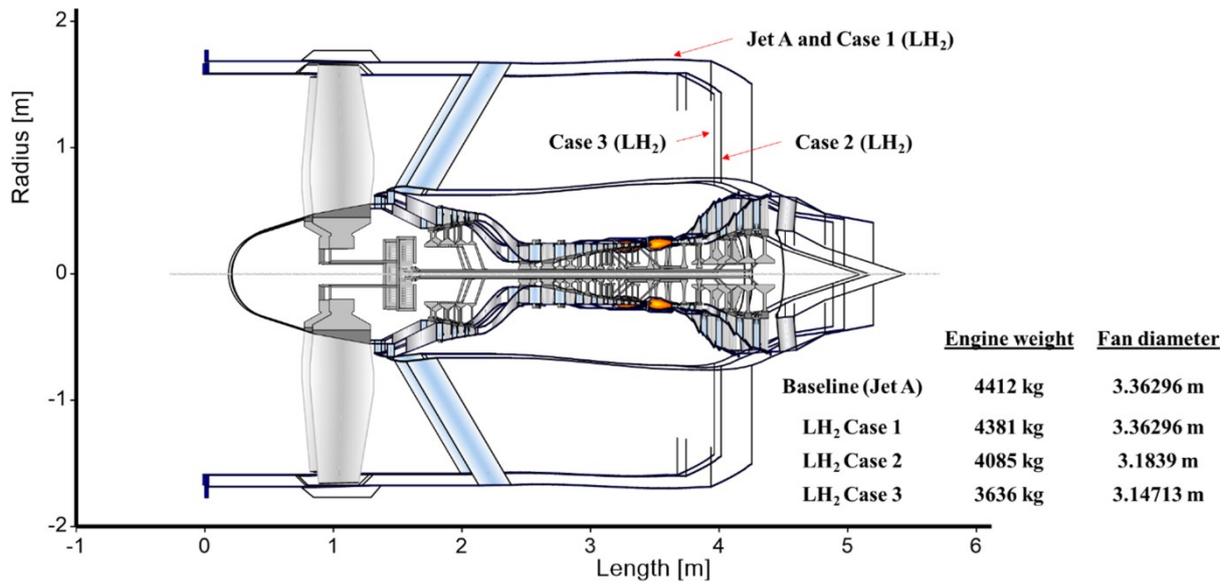
Figure 6.10. Cross-sectional view of the Jet-A powered GTF engine overlapped with the three cases of LH$_2$ powered GTF engine designed using the proposed model

The TSFC values in Table 6.23, Table 6.25 – Table 6.28 for Jet-A engine case and all three cases of LH$_2$ engine, developed using the present/proposed model at different/all operational points considered in this chapter, are inputs to the aircraft weight sizing process discussed in Chapter 7. This enables the estimation of fuel burn of the aircraft over one mission. The above discussion concludes the LH$_2$ powered GTF engine on-design and off-design analysis.

6.5.3   SPK engine

In this section 100% SPK fuel is being investigated. The LCV of 100% SPK fuel is known to be 44.1 MJ/kg, as compared to LCV of Jet-A of 43.2 MJ/kg. Therefore, slightly lesser mass of SPK fuel must be carried at the beginning of the flight mission. Therefore, the SPK aircraft weight at different points in flight mission is lesser than the Jet-A case resulting in slight efficiency improvement (discussed in Chapter 7), which is also observed in Chapter 4. The process for thrust requirement calculations is discussed in detail, in Chapter 7. Tables 6.29, 6.30, 6.31, 6.32, and 6.33 list the comparison of engine performance using Jet-A and 100% SPK, at TOC (on-design point), SLS, cruise, climb, and loiter points, respectively. It can be observed from Table 6.29 – Table 6.31 that the thrust requirement for 100% SPK at TOC, SLS, and cruise is insignificantly lesser than Jet-A case. Therefore, the thrust production for the 100% SPK is kept similar to Jet-A case.

It can be observed from Table 6.29 – Table 6.31 that the engine designs successfully meet the design requirements/targets set in Table 6.4. In Table 6.29 – Table 6.31, the engine designs meet the required thrust values for 100% SPK, at said mission points considered in these tables. These thrust requirements are calculated through the aircraft weight sizing process (details in Chapter 7).

Table 6.29. Comparison of engine performance at TOC condition using 100% SPK and Jet-A, using the proposed model

TOC parameters	Units	Jet-A	100% SPK
Mach, altitude	- , m	0.8 at 10,668 m	0.8 at 10,668 m
Engine mass flow	kg/s	638.1	638.1
Thrust required	kN	55.603	55.24
Thrust produced	kN	55.603	55.603
TSFC	g/kN-s	12.40	12.15
TSEC	kJ/kN-s	535.68	535.82
Fuel consumption	kg/s	0.689	0.676
Fuel-air ratio (FAR)	-	0.025191	0.024684
Equivalence ratio (Φ)	-	0.37	0.36
OPR	-	60	60
BPR	-	17.65	17.65
FPR	-	1.35	1.35
IPC pressure ratio	-	3.296	3.296
HPC pressure ratio	-	13.9	13.9
Cooling flow	%	20	20
Combustor length	m	0.1981	0.1981
Combustor gas velocity	m/s	235.68	235.80
Residence time	ms	0.841	0.841
P_3	kPa	2159.43	2159.43
T_3	K	859	859
T_4	K	1,690	1,691
T_4/T_2	-	6.844	6.850
Bare engine weight	kg	4,411	4,410
Gear ratio	-	3.5	3.5
Fan diameter	m	3.36296	3.36296
LPT inlet temperature	K	1,139	1,140
Power off-take	kW	150	150

The slight increase in LCV (as detailed above) of 100% SPK as compared to Jet-A, improves its TSFC. This can be observed from Table 6.29 – Table 6.33. The slightly higher LCV of 100% SPK as compared to Jet-A, causes an insignificant rise in their respective T_4 which can be observed from Table 6.29 – Table 6.33. It can be observed from Table 6.29 – Table 6.33 that the TSEC of both Jet-A and 100% SPK are similar. Additionally, it is to be noted that the LPT inlet temperatures at all points (on-design and off-design) in engine designs listed in Table 6.29 – Table 6.33, are lower than 1,350 K which was required for having uncooled LPT. This design choice was successful primarily because of the use of future component efficiencies. The engine diameter doesn't change between Jet-A case and 100% SPK (design constraint as per Table 6.4). The bare engine weight is similar for Jet-A case and 100% SPK as listed in Table 6.29.

Table 6.30. Comparison of engine performance at SLS condition using 100% SPK and Jet-A

SLS parameters	Units	Jet-A	100% SPK
Mach, altitude	- , m	0 at 0 m	0 at 0 m
Engine mass flow	kg/s	1,526.97	1,526.89
Thrust required	kN	299.9	301.8
Thrust produced	kN	303.9	303.9
TSFC	g/kN-s	5.124	5.022
TSEC	kJ/kN-s	221.36	221.47
Fuel consumption	kg/s	1.557	1.526
FAR	-	0.026912	0.026371
Φ	-	0.39	0.38
OPR	-	47.1	47.1
BPR	-	20	20
FPR	-	1.25	1.25
IPC pressure ratio	-	3.028	3.028
HPC pressure ratio	-	12.769	12.768
Cooling flow	%	20	20
Combustor length	m	0.1981	0.1981
Combustor gas velocity	m/s	241.78	241.91
Residence time	ms	0.82	0.82
P_3	kPa	4,724.82	4,724.26
T_3	K	914	914
T_4	K	1,776	1,777
T_4/T_2	-	6.163	6.168
LPT inlet temperature	K	1,213	1,213
Power off-take	kW	150	150

Table 6.31. Comparison of engine performance at cruise condition using 100% SPK and Jet-A

Cruise parameters	Units	Jet-A	100% SPK
Mach, altitude	- , m	0.84 at 10,668 m	0.84 at 10,668 m
Engine mass flow	kg/s	649.65	649.67
Thrust required	kN	42.25	42.16
Thrust produced	kN	51.61	51.61
TSFC	g/kN-s	12.667	12.411
TSEC	kJ/kN-s	547.21	547.33
Fuel consumption	kg/s	0.654	0.641
FAR	-	0.024099	0.023613
Φ	-	0.35	0.34
Combustor length	m	0.1981	0.1981
Combustor gas velocity	m/s	231.99	232.11
Residence time	ms	0.854	0.854
P_3	kPa	2,108.3	2,108.4
T_3	K	838	838
T_4	K	1640	1641
T_4/T_2	-	6.567	6.572
Cooling flow	%	20	20
LPT inlet temperature	K	1,107	1,108
Power off-take	kW	150	150

Table 6.32. Comparison of engine performance at climb condition using 100% SPK and Jet-A, using the proposed model

Climb parameters	Units	Jet-A	100% SPK
Mach, altitude	- , m	0.47 at 5,334 m	0.47 at 5,334 m
Engine mass flow	kg/s	904.96	904.99
Thrust produced	kN	94.94	94.95
TSFC	g/kN-s	9.798	9.599
TSEC	kJ/kN-s	423.27	423.32
Fuel consumption	kg/s	0.930	0.912
FAR	-	0.024524	0.02403
Φ	-	0.36	0.35
Combustor length	m	0.1981	0.1981
Combustor gas velocity	m/s	234.3	234.4
Residence time	ms	0.846	0.846
P_3	kPa	2,978.5	2,978.8
T_3	K	861	861
T_4	K	1672	1673
T_4/T_2	-	6.315	6.321
Cooling flow	%	20	20
LPT inlet temperature	K	1,129	1,129
Power off-take	kW	150	150

Table 6.33. Comparison of engine performance at loiter condition using 100% SPK and Jet-A, using the proposed model

Loiter parameters	Units	Jet-A	100% SPK
Mach, altitude	- , m	0.6 at 1,500 m	0.6 at 1,500 m
Engine mass flow	kg/s	1,488.32	1,488.41
Thrust produced	kN	114.67	114.70
TSFC	g/kN-s	12.175	11.929
TSEC	kJ/kN-s	525.96	526.07
Fuel consumption	kg/s	1.396	1.368
FAR	-	0.024892	0.024394
Φ	-	0.36	0.36
Combustor length	m	0.1981	0.1981
Combustor gas velocity	m/s	237	237.6
Residence time	ms	0.835	0.834
P_3	kPa	4,486	4,487
T_3	K	905	905
T_4	K	1,713	1,715
T_4/T_2	-	5.741	5.746
Cooling flow	%	20	20
LPT inlet temperature	K	1,167	1,167
Power off-take	kW	150	150

6.5.4   Trend of engine technology development

Figure 6.11 shows the trend of engine technology development with different efficiency metrics during cruise for engines entered in service till date (data source [211]) and engines modelled in this chapter. The

effective propulsive efficiency is the product of propulsive efficiency and transmission efficiency, and the core efficiency represents the engine thermal efficiency. The overall efficiency is the product of the effective propulsive efficiency and core efficiency. The said efficiency metrics at cruise for all engines designed in this chapter are listed in Table 6.26. According to a study by Benzakein [115], UHB engine are expected to have overall efficiency in the range of 0.4 – 0.48 (depending on the BPR and OPR combinations). It can be observed from Figure 6.11 that the overall efficiencies of the UHB engines modelled in this chapter (UHB GTF powered by Jet-A, 100% SPK, and three LH$_2$ cases) are similar to the expected values. It is to be noted that the UHB GTF Jet-A and 100% SPK engines in Figure 6.11 are represented by the same point (similar efficiencies as expected). The different efficiency metrics during cruise for all aircraft engines in Figure 6.11 are included in Appendix B.6 in Table B.5.
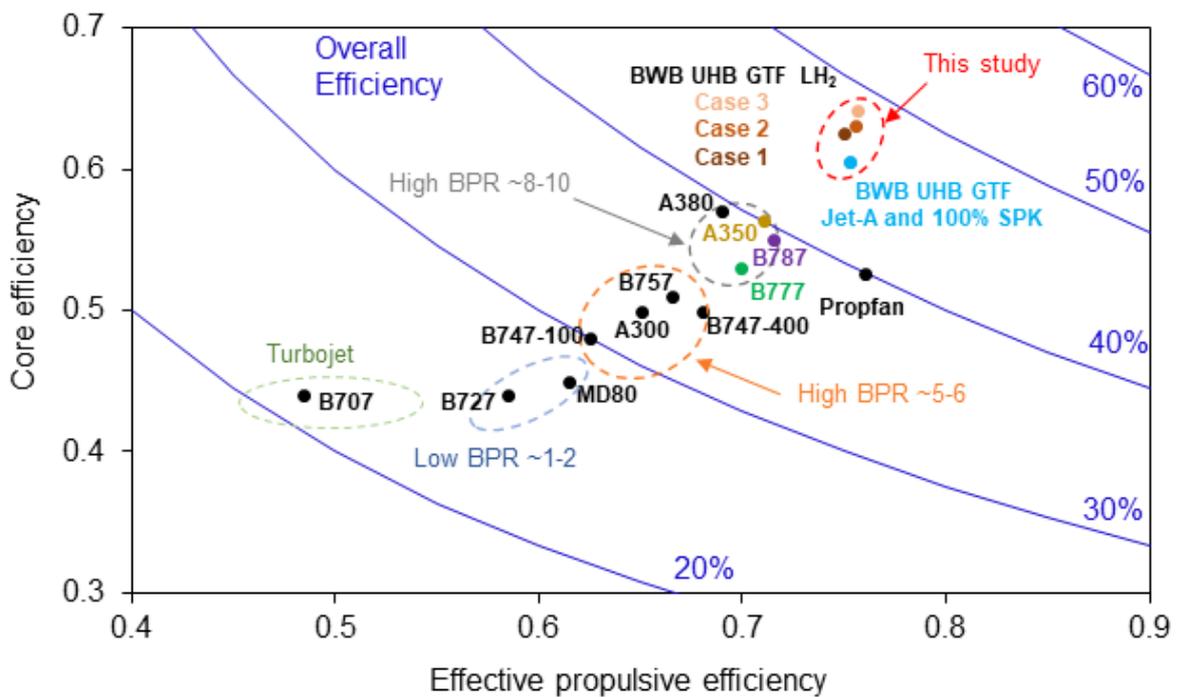
Figure 6.11. Trend of engine technology development with different efficiency metrics during cruise for engines entered in service till date (data source [211]) and engines modelled in this chapter

6.5.5   Limitations of the present chapter

The estimation of the engine performance (TSFC, weight, thermodynamic properties, etc.) is conducted using GasTurb (zero-dimensional and/or one-dimensional analysis). Such level of analysis use simplistic loss models for the performance analysis. In high-fidelity analysis of engine performance, performance loss due to shock waves and air-foil geometry (used in turbomachinery) are also accounted. These affect the engine performance and geometry (weight). Additionally, the engine performance during climb, cruise, and loiter, are considered to be average performance values. Overall, the engine performance estimation in this chapter is a low-fidelity analysis and errors in engine performance metrics are expected.

6.6   Chapter summary and conclusion

The present chapter begins with a literature review on NextGen propulsion systems and fuel systems, hydrogen powered engines, and aircraft and gas turbine engine design process. Thereafter, more details of the NASA N+2 BWB aircraft and engine technology are discussed. Based on these discussions, design requirements are set for the aircraft and engine design. Because this chapter is focussed specifically on the conceptual engine design, the engine design data is then listed and discussed thoroughly considering future technological improvements for individual components in the aircraft engine. In the research methodology, a UHB GTF engine model has been proposed and developed using GasTurb 13 software. After the model/methodology is proposed, the model is validated using two engine cases from literature. This establishes model's accuracy and builds a scientific confidence in the model.

After conducting the model validation, the results of the UHB GTF engine design for the set research objectives and design requirements are considered. In this chapter, engine designs of the future (N+2 timeframe) for conventional jet fuel, LH_2 fuel, and 100% SPK (separately), are developed using advanced material and future component efficiencies. The results comprise of performance analysis at on-design point and all off-design points. For Jet-A and 100% SPK, the results at on-design point and all off-design points are similar, as expected since their properties are similar. Three important effects of LH_2 fuel properties on the engine TSFC relative to Jet-A are observed. The first effect is due to the higher gravimetric energy density during combustion. The second effect is due to the difference in mass and species conservation that governs the specific heat of combustion products. The third effect is an indirect effect of the higher gravimetric energy density of LH_2 (compared to Jet-A), resulting in lower LH_2 aircraft weight (reduced thrust requirement, engine weight, and fan size) for meeting the *T/W* of the baseline Jet-A aircraft structure. The first two effects are applicable to case 1 LH_2 engine (same thrust production as that of Jet-A, where $TSFC_{Jet-A} = 2.865$ x $TSFC_{LH2}$) and all three effects are applicable to case 2 and 3 LH_2 engines. The TSEC for optimised (case 3) LH_2 engine is 6-8% lesser than Jet-A.

Along with these, the reduced thrust requirement enables the engine to run colder than Jet-A, Case 1 of LH_2 and more importantly the maximum allowable temperatures of the CMC used in the hot-end components. These low temperatures do not require cooling flows, and therefore the TSFC further drops. This impact of cooling flows is included in Case 3 of LH_2. Additionally, it was observed that with LH_2 engine reaching its optimised design case i.e., from Case 1 to Case 3 of LH_2, the TSFC drops further, along with a reduction in engine length, fan diameter, and bare engine weight. The results show that LH_2 engines are, in general, lighter and colder than baseline or Jet-A engine as. More specifically, it is seen that the optimised LH_2 engines (Case 2 and Case 3) are smaller, shorter, colder, and lighter than Jet-A engine or LH_2 Case 1 engine.

In this chapter, hydrogen powered gas turbine engine cycle (with above cases and findings) is studied in great detail. Additionally, a simple 'major species' combustion model quantitatively explains the reasons behind the drop in hydrogen combustor temperature or increase in the specific heat of combustion products of hydrogen, for same thrust production, compared to Jet-A. Thus, this chapter has significantly expanded the

pool of knowledge on hydrogen powered gas turbine engines, and it is likely to guide future research on hydrogen engines, and emissions and contrails modelling.

Lastly, with respect to 100% SPK, the effect of slightly higher LCV compared to Jet-A (TSFC improvement and lighter aircraft) was primarily observed via improved TSFCs, where the engine designs successfully meet the design requirements/targets. The thrust production and engine size/weight for 100% SPK was similar to Jet-A case, as thrust requirements were similar.

In the next chapter, aircraft weight sizing is conducted (or mission fuel burn analysis) for Jet-A, 100% SPK, and three cases of the LH_2 engines, using TSFC values and engine weights for respective fuel and aircraft operating/mission points in the future BWB LTA long-range aircraft.

Chapter 7. Operational energy consumption modelling of a BWB aircraft

7.1   Introduction

7.1.1   Background

As discussed in Chapter 6, the scope of the present chapter is limited to the conceptual design phase of a long-range 300 passenger aircraft using futuristic BWB aircraft technology. The engine to be used on the BWB aircraft is discussed in Chapter 6 and aircraft data is detailed in this chapter. The aircraft design process has been reviewed in Chapter 6 section 6.2.3. The present chapter comprises of the conceptual design of the future (N+2 timeframe) BWB aircraft. In this context, conceptual design in this chapter is limited to the aircraft weight sizing (reviewed in section 7.2.2) for the estimation of the aircraft operational energy consumption. This chapter does not conduct detailed aircraft structural and stability examination.

A literature review directly related and specific to the current chapter is carried out in section 7.2. The literature review includes review on: LH_2 powered aircraft studies and conceptual aircraft design process. The review on SPK fuel performance characteristics has been conducted in Chapter 4 and review on SPK fuel properties is conducted in Appendix B.4. There are no prior studies that specifically model the performance of a BWB aircraft completely powered by LH_2 fuel and 100% SPK (separately), for long-range (14,000 km) travel of ~300 passengers. In both Chapters 4 and 5, it was observed that the GTOW of LH_2 aircraft significantly reduces (or thrust requirement reduces) which necessitates a more detailed design and optimisation of an LH_2 aircraft for meeting *T/W* of the aircraft.

The above findings and limitations of previous chapters motivate chapters 6 and 7. As discussed, the combined objective of Chapter 6 and the current chapter is to develop energy consumption models of an LTA long-range BWB aircraft using conventional jet fuel, 100% SPK, and LH_2 fuel, separately. Additionally, the results of Chapters 6 and 7 are useful to meet research objective 3 and 4, respectively, that are discussed in Chapter 1. The future technologies used for modelling the aircraft (and sub-systems) are well established and supported through publications. Chapter 6 and the current chapter address the propulsion aspect and aircraft weight sizing aspect of the conceptual aircraft design process, respectively. In Chapter 6 and in the current chapter, an engine model and aircraft's operational energy consumption model are developed, respectively, for conventional jet fuel, 100% SPK, and LH_2 fuel. In Chapter 6, a model of a future (N+2 timeframe) UHB GTF engine is developed and is further used to develop designs of the future for conventional jet fuel, 100% SPK, and LH_2 fuel, which are useful to meet the objectives of both Chapter 6 and the current chapter and to meet the set design specifications.

7.1.2   Chapter structure

This chapter is focussed specifically on the conceptual design of a BWB aircraft. The current chapter begins with a literature review in section 7.2 on LH_2 powered aircraft studies, and the conceptual aircraft design process. Thereafter, more details of the selected future (N+2 timeframe) BWB aircraft is listed and discussed comprehensively in section 7.3. Based on this discussion and the discussion from Chapter 6, the design

requirements are set for the aircraft. After the design requirements are set, data such as structural weights of different components/systems of BWB aircraft, and BWB aircraft geometry are then listed and discussed thoroughly along with flight mission profile, LH_2 tank design model from literature, and the physics-based equation for service ceiling aircraft thrust requirement calculation. This is followed by the aircraft weight sizing methodology, which is discussed comprehensively in section 7.4. Thereafter, BWB aircraft design details of the future (N+2 timeframe) powered by conventional jet fuel, 100% SPK, and three cases of LH_2 fuel are included in results and discussion in section 7.5. Additionally, the BWB aircraft powered by conventional jet fuel, 100% SPK, and LH_2 fuel (three cases) are operated at different off-design cases of typical range and payload combinations for typical long-range LTA aircraft. Thereafter, a final evaluation i.e., a sanity check is conducted where the relationship between the OEW and GTOW is analysed for the aircraft designed in this thesis, literature, and aircraft that have already entered in service (for conventional jet fuel, 100% SPK, and LH_2 fuel).

7.2 Literature review on conceptual aircraft design process and LH_2 aircraft performance

7.2.1 LH_2 powered BWB aircraft

Studies on LH_2 powered long-range tube-wing LTA aircraft have been reviewed in Chapters 4 and 5. The study by Beck et al. [217] conducts an examination of a LH_2 powered BWB aircraft (combustion based). The aircraft design developed is a large quad or VLTA BWB aircraft type, which has a capacity similar to a Boeing 747 aircraft. Additionally, the BWB uses high BPR engines partially embedded into the airframe for implementing BLI. The authors do not actually model the LH_2 powered engine. Instead, they calculate the SFC by scaling the SFC of the engine powered by the conventional jet fuel, by using the ratio of gravimetric energy densities of hydrogen and conventional jet fuel. This study cannot be used for a direct comparison because the authors design a large quad or VLTA BWB aircraft (capacity similar to a Boeing 747) using high BPR engine with BLI, whereas the current chapter considers an LTA aircraft (capacity similar to a Boeing 777) using UHB GTF engines podded on the aircraft i.e., without a BLI. Therefore, because of this difference, no direct comparison can be made.

7.2.2 Review of aircraft conceptual design process

The initial stage of the aircraft design process is called as 'conceptual design process' and 'preliminary sizing' by Raymer [201] and Roskam [198] respectively. In most cases, the conceptual design begins with specific design requirements. These are set by a company-generated models, market research/survey, or by the prospective customer, towards the future needs of the customers. The design requirements comprise parameters like the aircraft range, payload, speed requirements, etc. for civil or military applications. Figure 7.1 depicts the conceptual design process in more detail. In some cases, a design may be initiated as an innovative idea instead of a response to a given requirement. For example: the aircraft project called 'flying wings' was not conceived in response to a requirement. It was a product of Northrop's idea of a 'better

airplane'. Before initiating a new aircraft design, a decision has to be made as to what technologies will be used depending on the timeframe in which the aircraft is expected to enter in service [184], [201].

The effort for the actual conceptual design begins with a conceptual sketch. This is a rough illustration of what the design might look like. A good conceptual sketch will include the approximate geometries, shape, and locations of the major aircraft components (ibid). The conceptual sketch may be used to evaluate the weight fractions and aerodynamics by comparing it to prior designs. These approximate evaluations are helpful for providing a first estimate of the necessary fuel weight and total weight for performing a designed mission, by a process known as 'sizing'. The conceptual sketch might not be even required for the initial sizing if the design resembles a prior design (ibid). The initial sizing gives the specific data required for developing an initial design layout, which is a three-view engineering drawing completed with geometries, shapes, and locations of the major aircraft components, and any other internal components that are large enough to affect the overall shaping of the aircraft. It is used to verify that everything fits [201].
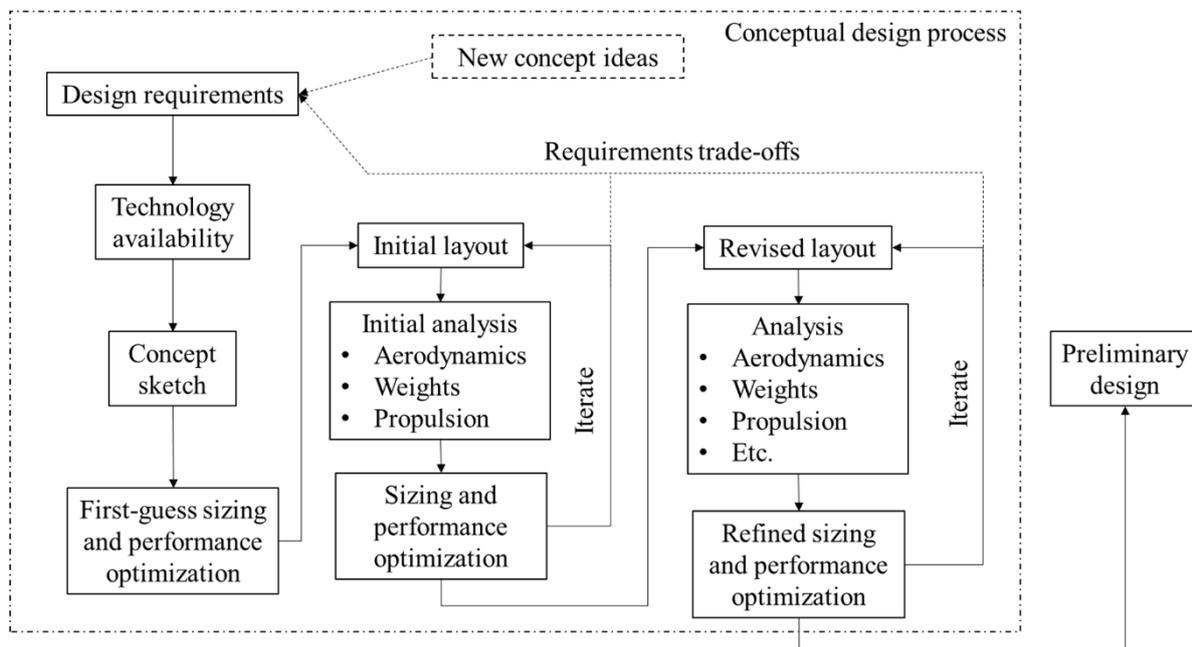
Figure 7.1. Conceptual aircraft design process (source [201])

This initial layout is examined to find out whether it will perform the mission as predicted by the first-order sizing. The actual weights, aerodynamics, and installed propulsion features are examined and are subsequently used for carrying out a detailed sizing calculation. Moreover, the performance capabilities of the design are estimated and compared to the mentioned requirements. Optimisation is used to find the lightest aircraft that will perform the design mission while meeting all performance requirements. The outcome of the optimisation comprises a better estimate of the necessary fuel weight and total weight for meeting the design mission. These also include necessary revisions to the wing and engine sizes. This often would require a fresh or revised design layout within which the designer implements these modifications and other changes recommended by other efforts. The revisions to the drawing, after some iterations, are then evaluated in detail by specialists, where they ensure that the design under consideration meets the requirements of their specialty. The final product of these efforts will be an aircraft design which can confidently be handed over to the next

155

phase i.e., the preliminary design stage. Although further changes can be expected in the preliminary design phase, significant revisions will not take place if the efforts in the conceptual design phase have been successful (ibid).

7.3 Design requirement and known data

7.3.1 Design requirement

The design requirement/specification is a necessary step for initiating the design process which can be observed from Figure 7.1, and Figures 6.3 to 6.6 (in Chapter 6). In terms of the future aircraft configuration, NASA N+2 BWB aircraft powered by UHB GTF engine for 301 passengers is selected. The aircraft technology selection is discussed in Chapters 2 and 6. Additionally, a significant amount of data on the aircraft design for conducting a conceptual design study is available from NASA's studies [130], [199], [247]–[249], [287]. The design characteristics of the long-range NASA N+2 BWB-GTF aircraft and Boeing 777-200LR (datum used by NASA), for 301 passengers are listed in Table 6.1 and discussed in Chapter 6, and based on this discussion, design requirements are set for the conceptual design of the BWB aircraft listed in Table 6.3 (in Chapter 6).

It is to be noted that the length or the aircraft geometric details of the NASA N+2 BWB-GTF aircraft are not known directly from NASA's study [130]. NASA's project has evolved over a period of ten years and this project has been published through a series of publications that can be found in resources [130], [199], [247]–[249], [287]. A study by June et al. [288] reveals a three-view engineering drawings of the NASA N+2 BWB-GTF aircraft that seats 301 passengers. Knowing the aircraft span, the other geometric information of the aircraft will be estimated via reverse engineering. Using the three-view engineering drawing, the outer mould line of the aircraft is developed in SolidWorks 2019 (discussed ahead). Additionally, the wetted area of the NASA N+2 BWB-GTF aircraft is not known through studies [130], [199], [247]–[249], [288]. Therefore, this will be calculated from the geometric model developed in SolidWorks 2019 in this chapter.

Table 7.1. BWB aircraft design requirements

Characteristics	Value
Range	7,500 nmi or 13,890 km
Passengers	301
Powerplant	two GTF engines
Fuel type	1. Conventional jet fuel
	2. LH_2
	3. 100% SPK
Cruise Mach and altitude	0.84 at 10,668 m (35,000 ft)
Payload weight	53,570 kg
Wingspan	76.2 m
Length	37.465 m
S	944.73 m^2
AR	6.1

In the current chapter, the design requirement is to carry out a conceptual design of an LTA BWB aircraft for transporting 301 passengers over a range of 7,500 nmi or 13,890 km. This aircraft should be powered by LH_2 fuel and 100% SPK (separately).

For developing the design of the 100% SPK and LH_2 aircraft, a baseline case is required where this BWB aircraft is powered by conventional jet fuel. Modifications to the baseline case are made for the use of 100% SPK and LH_2 fuel, where the modifications are based on published literature. The BWB aircraft design requirements are summarised in Table 7.1, and these are based on Table 6.1 and Table 6.3 (in Chapter 6). It is to be noted that the GTOW and OEW from Table 6.1 are not listed in Table 7.1 because these are expected to change since the weights of the two engines have reduced as observed in Chapter 6 (use of lighter materials and future component efficiencies). The ratio of $W_{F,block}$ to $W_{F,total}$ of the Jet-A NASA N+2 BWB aircraft is 0.9 [130]. In this chapter, similar value for the said ratio is used during the iteration process of the weight sizing process for estimating the aircraft operational energy consumption (discussed in section 7.4). For the BWB conventional jet fuel (baseline) case of this chapter, except for the engine weights and $W_{F,total}$, there is no other change compared to the Jet-A BWB aircraft [130] (data in Table 6.1 and Table 6.3 in Chapter 6). In case of 100% SPK and LH_2 fuel, modifications are required to the aircraft which change the GTOW, which are discussed later.

7.3.2 Flight mission profile
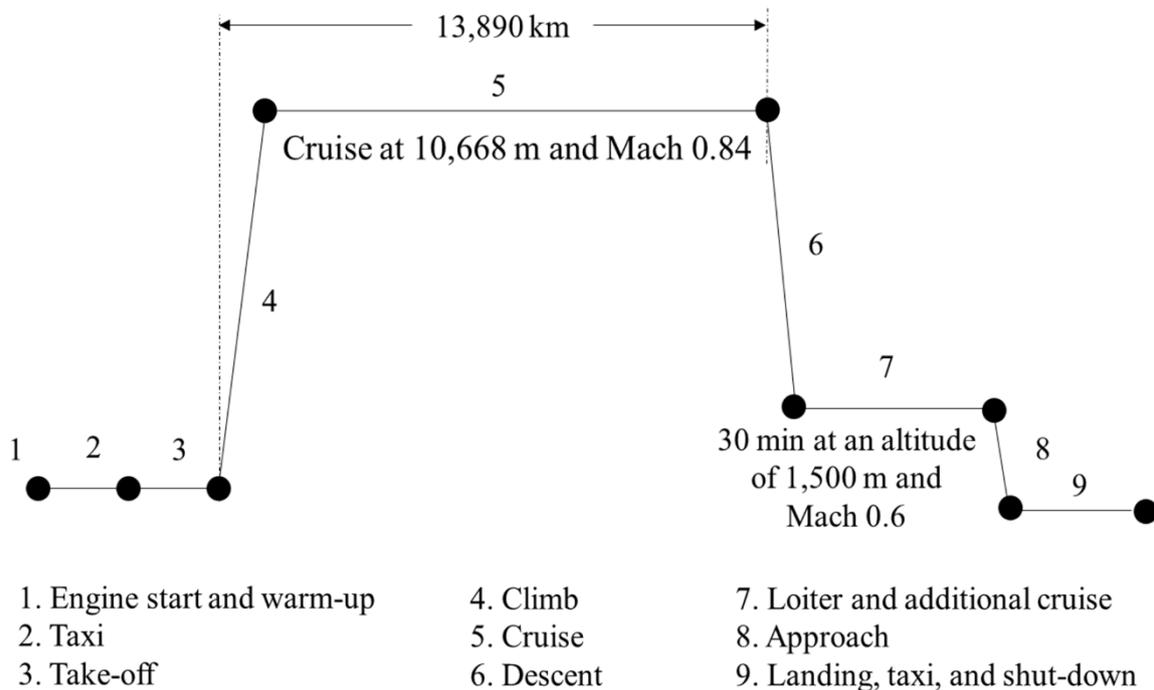
Figure 7.2. Multi-segment flight mission profile

A simple multi-segment flight mission profile is considered in this chapter, which is represented in Figure 7.2. The mission begins with engine start and warm-up followed by taxi-out. Thereafter, the aircraft takes-off from the runway and climbs to the design cruise altitude of 10,668 m (or 35,000 ft as per set design requirements in Table 7.1). The mission design range is 13,890 km as discussed earlier, which is covered only

during climb and cruise (primarily in cruise). After cruising, the aircraft descends to a loiter altitude. A standard value of 30 minutes loiter (or additional cruise) at an altitude of 5,000 feet (~1,500 m) at Mach 0.6 [272], [289], is considered in this chapter. The resulting loiter range is ~362 km as per calculations. After the loiter is completed, the aircraft approaches the runway for landing. Once the aircraft lands, it is taxied into the gate followed by engine shutdown. Overall, in this chapter, the contribution of flight range or distance to the total design range during flight segments except climb and cruise, is considered negligible. The loiter phase is an additional flight operation outside of the design range because it is carried out only when the aircraft has to wait for receiving clearance to land on the runway. This flight mission profile is used for the calculation of $W_{F,block}$ i.e., aircraft's block fuel consumption.

7.3.3 Service ceiling thrust equation

The service ceiling for a transport jet is defined as the altitude at which the maximum rate of climb (RoC) is 500 ft/min (2.54 m/s) for jet powered aircraft [290]. In the current chapter, the engine thrust requirement at TOC point for the LH$_2$ BWB aircraft is based on two separate calculations. The first method is using the service ceiling thrust equation i.e., equation 7.1 below, and the second method is using T/W of the baseline (conventional jet fuel) BWB aircraft. Both predictions are found to be of similar magnitude, however, the maximum of the two values is selected as the thrust required to be produced by the engines at TOC point. Chapter 6 and the current chapter are interdependent as mentioned before, and the TOC thrust requirement calculation process is one of the links between these two chapters. The derivation of the service ceiling thrust equation (based on resource [290]) is included in Appendix C (section C.2). The aircraft thrust (T) at service ceiling is given by,

$$T = W \left(\frac{RoC}{V_\infty} + \frac{\sqrt{1 - \left(\frac{RoC}{V_\infty}\right)^2}}{(L/D)_{max}} \right) \tag{7.1}$$

where V_∞ is flight speed and W is aircraft weight at service ceiling.

As discussed before, in this chapter equation 7.1 will be used as one of the two methods for estimating the TOC thrust requirement. It can be observed from equation 7.1 that the thrust equation depends on four parameters: aircraft weight, rate of climb, flight speed, and the maximum lift to drag ratio i.e. $(L/D)_{max}$ of the aircraft. Because this chapter uses first order modelling methods, for climb:

- An average climb speed of Mach 0.47 (calculation discussed in section 6.4.3 in Chapter 6).
- The aircraft weight is an average weight of aircraft during climb (between the 'end-point of take-off' and 'beginning-point of cruise'). This aircraft weight and $(L/D)_{max}$ are known from the weight sizing process.
- The RoC at service ceiling conditions for a transport jet, by definition (discussed above), is 500 ft/min (2.54 m/s).

7.3.4 Data known

7.3.4.1 Structural weight of different BWB aircraft sections

Even though OEW, payload weight, and GTOW of N+2 BWB-GTF aircraft (301 passengers) is known from resource [130], the structural weight of different components or sections of the NASA N+2 BWB-GTF aircraft is required in the LH_2 aircraft design process primarily for restructuring the aircraft for the installation of LH_2 tank and insulation. NASA's study [130], which is used as a reference study for setting the design requirements for the current chapter, uses the 'Hybrid wing body Conceptual Design and structural optimisation' (HCDstruct) tool for modelling the BWB structure. The structural weights of different sections of NASA N+2 301 passenger BWB aircraft using HCDstruct is published in resource [247], which is summarised in Table 7.2. The resource [247] includes the structural analysis of the NASA N+2 301 passenger BWB aircraft which is based on a model validated with two separate BWB design cases. The structural addition to the BWB aircraft due to the LH_2 integral tank systems, comes in the form of a weight penalty. Verstraete [65] uses a weight penalty of 6% of the fuselage weight (of a tube-wing aircraft) to account for the additional structure required for attaching the structure of the integral LH_2 tank systems with the fuselage structure. In the current chapter, for the BWB aircraft the LH_2 tanks are installed in the inner wings and aft body. Therefore, the additional structural weight for installing the integral LH_2 tank systems is calculated to be 1,632 kg which is 6% of 27,220 kg (cumulative weight of the wings and aft body).

Table 7.2. Structural weights of different sections of NASA N+2 301 passenger BWB aircraft [247]

System	BWB aircraft section	Weight (kg)
1	Centre body	22,703
2	Cockpit	905
3	Aft body	4,074
4	Wing	23,146
5	Additional structural weight for installing integral LH_2 tank systems	1,633
		[= 6% of 27,220 (3+4)]

7.3.4.2 Structural weight of the conventional jet fuel and 100% SPK tank in BWB

The structural weight of the conventional jet fuel tank is important because this weight must be subtracted from the baseline BWB aircraft (powered by conventional jet fuel) and at the same time adding the LH_2 tank systems weight, while modelling the LH_2 aircraft. The structural weight of the conventional jet fuel tank in NASA N+2 301 passenger BWB aircraft is not known from any of NASA's studies [130], [199], [247]–[249], [287]. Goraj [203] conducts design and optimisation of fuel tanks for BWB aircraft. Through their BWB aircraft design, Goraj finds that the weight of the conventional jet fuel tank systems is 284 tonnes (fuel weight and structural weight of tank) for fuel mass of 280 tonnes. Therefore, the structural weight of the conventional jet fuel tank is 4 tonnes for 280 tonnes of fuel mass. Referring to Table 6.1 $W_{F,total}$ (of conventional jet fuel) for NASA N+2 301 passenger BWB aircraft is 73,965 kg. Therefore, for maintaining the same non-dimensional

ratio of fuel weight and structural weight of tank of the study by Goraj, the structural weight of conventional jet fuel tank of the NASA N+2 301 passenger BWB aircraft is calculated to be 1,057 kg (~1.057 metric tonne).

Additionally, for 100% SPK there is a need for extra tank system. The additional tank weight will be estimated using the findings of the study by Goraj [203] discussed above. It will be observed in section 7.5 that this additional increase in tank weight for accommodating 100% SPK at mission start i.e., $W_{F,total}$ (slightly less mass dense as discussed in Chapters 4 and 6), at start is insignificant (19 kg increase).

7.3.4.3 LH_2 tank systems weight

A study by Khandelwal et al. [64] reviews different types of hydrogen tanks for aviation applications (configuration, shape, insulation, and tank materials). Another study by Verstraete et al. [66] examines different types of tank and insulation materials for hydrogen tanks for sub-sonic aviation application. Both studies suggest that integral type of hydrogen tanks of cylindrical shape with elliptical caps/heads are preferred for aviation applications. Aluminium alloy is the preferred tank wall material. An external tank insulation configuration using foam as the insulating material is preferable for the LH_2 tank to be used on a sub-sonic aircraft. These findings are used towards the selection of hydrogen tank type in this chapter.

It is observed from Table 5.1 (Chapter 5) that foam-based cryogenic tanks for LH_2 aircraft with range greater than 9,000 km have $0.74 < \eta < 0.881$. The study by Beck et al. [217] models an LH_2 powered BWB VLTA aircraft (design range 11,400 km for 531 passengers) that has tank $\eta = 0.77$. Advances in lighter and stronger composite materials have recently shown LH_2 cryogenic tank $\eta = 0.92$ for manufactured tanks [204] (which could improve in future), and that too for a small size tank (diameter 1.2 m and length 2.4 m). A study by Sjöberg et al. [205] model a light weight LH_2 tank (4.7 m length and 3 m diameter) using composite materials with $\eta = 0.94$ for a full tank, in comparison with metallic tank having $\eta = 0.71$. For LH_2 cases in this chapter, an average $\eta = 0.78$ with insulation thickness of 8.1 cm is used according to the study by Verstraete et al. [66] towards the estimation of the cryogenic tank systems weight for given $W_{F,total}$. Using $\eta = 0.78$ for a given (capacity) $W_{F,total}$, the unknown i.e., tank weight, can be estimated.

7.3.4.4   BWB aircraft geometry

7.3.4.4.1   Selection of BWB air-foils

In terms of aircraft geometry, the data for NASA N+2 BWB-GTF aircraft is not completely known from (NASA) study by Nickol et al. [130] (used as a reference study for setting design requirements in the current chapter). One of the designers/authors of NASA's BWB known from resource [130], was associated with Garmendia's PhD thesis [291], where the t/c of the BWB 301 is revealed.

The t/c ratio of the transonic air-foils used for BWB geometric modelling in this chapter is provided in Figure 7.3. Figure 7.3 shows the comparison of the t/c from the study by Garmendia and t/c used in this chapter. At the aircraft root 11.5% t/c is recommended by Garmendia and the same t/c is used here (air-foil coordinates source [292]). At the end of cabin (y/semi-span of 18%), 15% t/c is recommended by Garmendia and 15.5% t/c is used here as this is the closest available transonic air-foil in open literature (air-foil coordinates

source [293]). For outer wings 8% t/c is recommended by Garmendia and the same t/c is used here (air-foil coordinates source [294]).
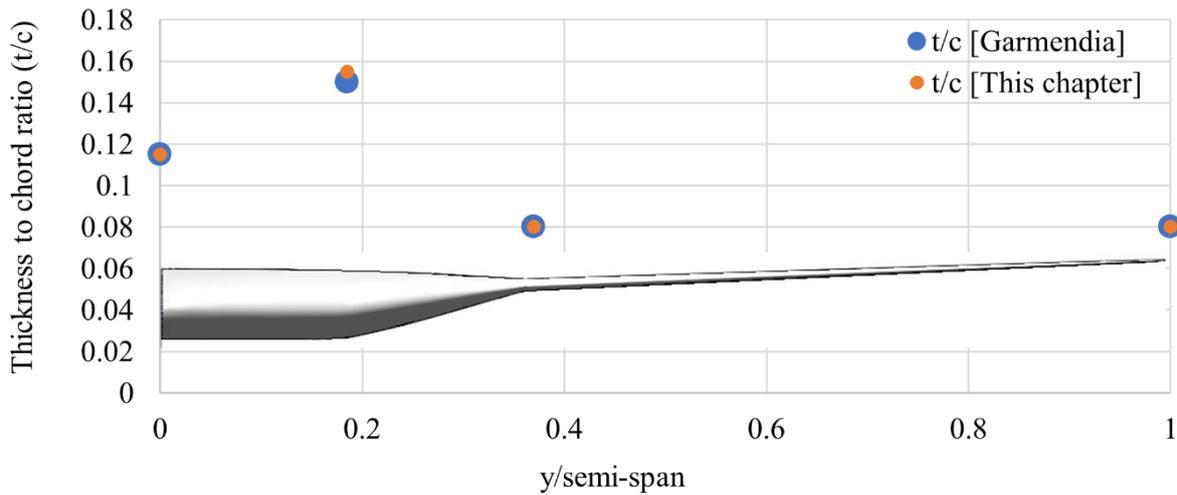
Figure 7.3. Thickness to chord (t/c) ratio of the transonic air-foils along the span for BWB geometric modelling (using data from [291])

7.3.4.4.2 Other geometric dimensions

Figure 7.4. Cabin layout of NASA N+2 BWB aircraft for 301 passengers where dimensions are in inches (source [287], Copyright: work of the US government and public use is permitted)

In terms of the geometric dimensions, except the span no other dimension are known for the NASA N+2 BWB-GTF aircraft from resources [130], [199], [247]–[249], [287]. The span of the aircraft under design consideration is known to be 76.2 m. Recently, a study by June et al. [288] reveals a three-view engineering

drawings of the NASA N+2 BWB-GTF aircraft that seats 301 passengers. Knowing the aircraft span, the other geometric information of the aircraft will be estimated via a reverse engineering approach. Using the three-view engineering drawing, the outer mould line of the aircraft will be developed in SolidWorks 2019. Figure 1 in resource [288] shows the three-views of NASA N+2 BWB-GTF aircraft for 301 passengers. From the top view of this figure, the aircraft outer mould line (OML) can be traced in SolidWorks 2019 by setting the aircraft span to 76.2 m. Once the OML is traced with the known span as reference, the remaining geometric information can be obtained. Based on the front and top view of the aircraft, the air-foils are positioned along the spanwise direction (known from section 7.3.4.4.1). Figure 7.4 shows the cabin layout of NASA N+2 BWB aircraft for 301 passengers. It is to be noted that the dimensions in the said figure are in inches. The length of the cabin is 23.67 m, and the maximum cabin width is 14.11 m.

7.4   Aircraft weight sizing methodology

The aircraft weight sizing process is not only iterative but also there is interaction between the different systems of aircraft with each other (viz. aerodynamics, propulsion, weight, etc.). The schematic/methodology is based on the sizing method of Raymer [201] and Roskam [198]. In this chapter, three cases of LH_2 fuel (as discussed in Chapter 6) are analysed.

Figure 7.5 shows the weight sizing process schematic for aircraft powered by conventional jet fuel, 100% SPK, and LH_2 (all three cases). In the case of aircraft powered by conventional jet fuel, the sizing is straightforward using the methods of Raymer [201] and Roskam [198] because of data availability. For using LH_2, there are modifications required to be made to the baseline (conventional jet fuel) aircraft structure. Therefore, the LH_2 aircraft sizing has some new sub-components within the process schematic as observed from Figure 7.5, though it includes the steps covered in the sizing of conventional jet fuel aircraft. It can be observed that Figure 7.5 includes *T/W* consideration in the iteration process for the two hydrogen aircraft cases, which isn't included for case 1 LH_2, as per definition of each LH_2 aircraft case. Additionally, in Figure 7.5, for 100% SPK minor modifications to tank system are required as the density of 100% SPK is slightly lesser than Jet-A as discussed in Chapter 6 and in section 7.3.4.2. The sub-components of Figure 7.5 are discussed below in detail case by case.
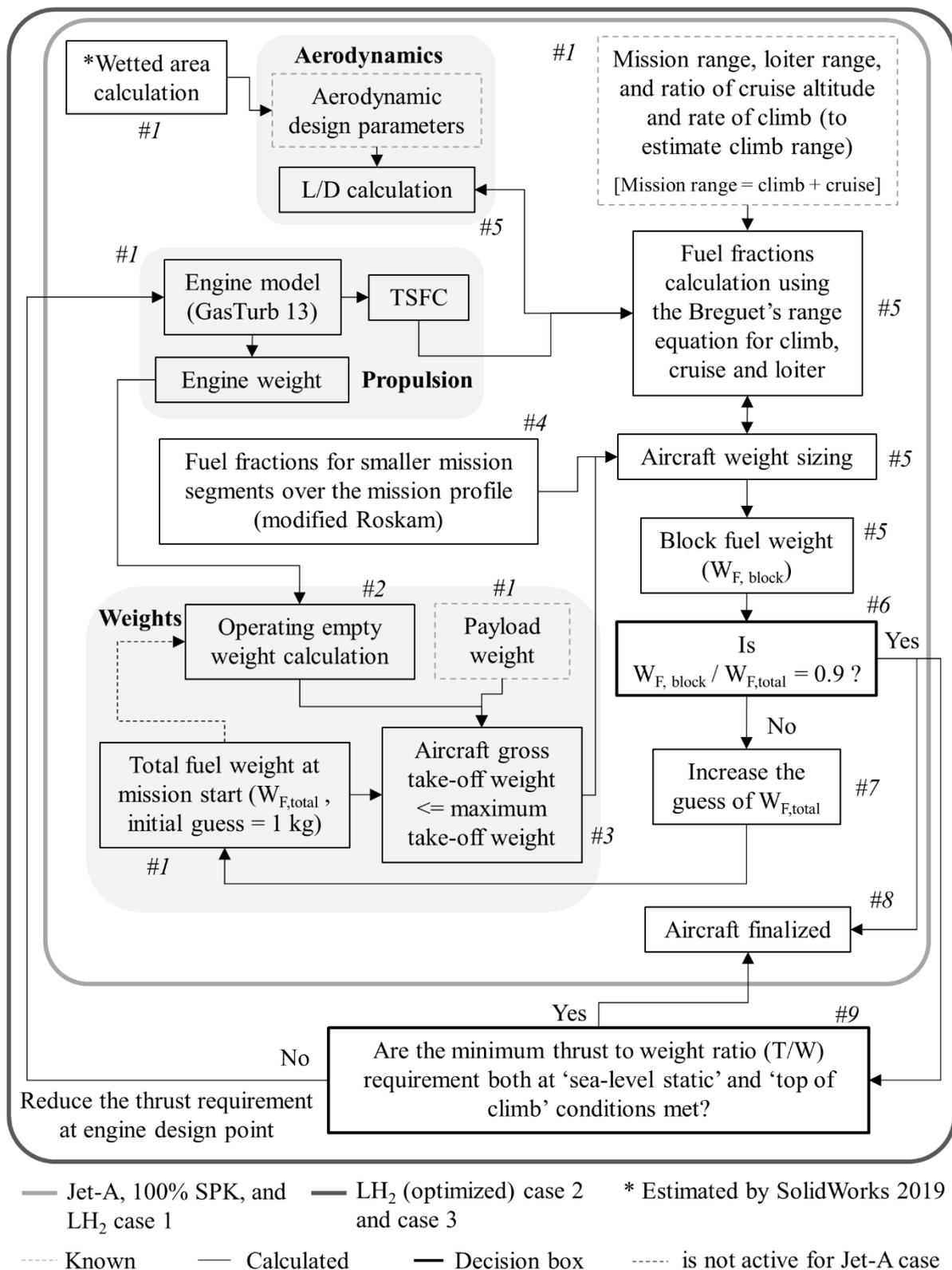
Figure 7.5. Weight sizing process schematic for aircraft powered by conventional jet fuel, 100% SPK, and liquid hydrogen (all three cases)

7.4.1 Propulsion

The propulsion aspect of the weight sizing process is described in detail in Chapter 6. UHB GTF engines are designed for the set research objectives and design requirements, which powers the BWB aircraft using conventional jet fuel, 100% SPK, and LH_2 fuel (separately). The results for engines fired by conventional jet fuel, 100% SPK, and LH_2 fuel comprise of performance analysis at on-design point and all off-design points, along with the engine weight. The TSFC at all points in the flight mission profile (discussed in section 7.3.2) are input to the weight sizing process. More specifically, they are inputs to Breguet's range equation (discussed ahead in detail) which is used for estimating the fuel mass consumed during the aircraft operation. Additionally, the engine weights are inputs to the aircraft weight sizing process, as these contribute to GTOW of the aircraft which determines the fuel consumed over the flight mission.

7.4.2 Aerodynamics

In terms of aerodynamics, *L/D* is calculated using standard equations at three operating conditions: climb, cruise, and loiter. The drag is estimated using equation 4.2 and 4.3 (in Chapter 4) assuming there is no wave drag. The wave drag modelling is a high order or high-fidelity analysis, which is beyond the scope of this chapter and thesis. AR, e, and C_f are respectively known to be 6.1 (Table 7.1), 0.85 (for LTA aircraft [194]), and 0.0025 (modern/advanced large transport jets [221]). S_{wet}, is estimated from the aircraft geometric model developed in SolidWorks 2019. S is known from Table 7.1 to be 944.73 m² for the NASA N+2 BWB-GTF aircraft. GTOW can be calculated once the weights of all aircraft systems are known. The lift coefficient is given by equation 4.4 (Chapter 4). Knowing the Mach number and altitude for climb, cruise, and loiter, both V and ρ_a are known. The aircraft weight at climb, cruise, and loiter, is the average weight (of start and end of each operation) of the aircraft during each of the three conditions, estimated from the weight sizing process. After both the lift coefficient and drag coefficient are calculated, *L/D* is calculated for the climb, cruise, and loiter. In cruise, *T/W* ratio is equal to the reciprocal of the *L/D* ratio of the aircraft. The (minimum) thrust requirement at cruise is calculated from the estimated *L/D* and aircraft weight, as both are known from the weight sizing process.

7.4.3 Fuel fraction for Jet-A, SPK and LH_2

The fuel fraction (FF) is a measure of the fuel consumed during a given aircraft operation. For example: FF value of 0.995 for taxi-out operation means that the weight of fuel consumed during taxi-out operation is (1-0.995 =) 0.5% of the aircraft weight at the beginning of taxi-out operation. FF can be used for individual aircraft mission segments such as taxi, cruise, descent, etc. and/or for the entire mission. The product of FFs for all mission segments represents the FF of the aircraft over the entire mission. For example: If the product of all FFs is 0.8 then it means that the weight of fuel consumed during entire mission is (1-0.8 =) 20% of the aircraft weight at the beginning of the mission.

Table 7.3. Fuel fraction provided by Roskam [198] with recommended modifications to Roskam's FFs for Jet-A, and FFs recommended for LH₂

Segment	Operation	Roskam's FFs (Jet-A) [198]	Modified FFs (Jet-A)	FFs (LH₂)
1	Engine start and warmup	0.99	0.9964	0.9987
2	Taxi-out	0.99	0.9964	0.9987
3	Takeoff	0.995	0.9982	0.9994
4	Climb	0.98	$M_{ff,climb}$	$M_{ff,climb}$
5	Cruise	$M_{ff,cruise}$	$M_{ff,cruise}$	$M_{ff,cruise}$
6	Descent	0.99	0.9964	0.9987
7	Loiter	$M_{ff,loiter}$	$M_{ff,loiter}$	$M_{ff,loiter}$
8	Land, taxi-in, engine shutdown	0.992	0.9971	0.9989
	Overall FF	Product (1-8)	Product (1-8)	Product (1-8)

Table 7.4. Fuel fraction (FF) provided by Roskam [198] with recommended modifications to Roskam's FFs for Jet-A, and FFs recommended for 100% SPK

Segment	Operation	Modified FFs (Jet-A)	FFs (100%SPK)
1	Engine start and warmup	0.9964	0.9965
2	Taxi-out	0.9964	0.9965
3	Takeoff	0.9982	0.9982
4	Climb	$M_{ff,climb}$	$M_{ff,climb}$
5	Cruise	$M_{ff,cruise}$	$M_{ff,cruise}$
6	Descent	0.9964	0.9965
7	Loiter	$M_{ff,loiter}$	$M_{ff,loiter}$
8	Land, taxi-in, engine shutdown	0.9971	0.9972
	Overall FF	Product (1-8)	Product (1-8)

Roskam [198] provides the FFs for a transport jet using conventional jet fuel (Jet-A). Roskam's FFs for all mission segments except cruise and loiter, are provided in Table 7.3. For a long-range LTA aircraft that is considered in this chapter, the fuel expenditure in non-cruise and non-loiter phases is significantly lesser as compared to that in cruise and loiter phases. The product of these FFs (not including cruise and loiter FFs) by Roskam is approximately 0.936, which means that weight of fuel consumed in these mission segments is 6.143% of GTOW of the aircraft. For cruise and loiter, the FFs can be calculated using Breguet's range equation. The range equation has been discussed in Chapter 4.

The FF for climb, cruise, and loiter can be calculated using equations 7.2, 7.3, and 7.4 respectively (discussed next). However, Roskam's FFs are based on historical data (older aircraft before 1990s). The fuel efficiency of aircraft introduced in the past two decades have improved significantly. Therefore, there is a need for modifying the FFs provided by Roskam, based on the recent literature. The GBD report of the Royal Aeronautical Society [114] and the study by Kenway et al. [193], both model the aircraft performance using the modified Breguet's range equation. For all operations except cruise and loiter, both studies model the weight of fuel consumed to be 2.2% of GTOW (also discussed in Chapter 4). This weight of fuel consumed (2.2% of GTOW) during all operations except cruise and loiter is 64.19% less than the fuel weight predicted

using Roskam's FF (6.143%). As mentioned before, the Roskam's FF are based on historical aircraft and thus modifications are recommended. The modified FF (64.19% improvement to Roskam's FF) for Jet-A are listed in Table 7.3. For example: FF value of 0.99 for taxi-out operation means that the weight of fuel consumed during taxi-out operation is (1-0.99 =) 1% of the aircraft weight at the beginning of taxi-out operation. The improvement of 64.19% means that instead of 1% GTOW, only 35.81% of 1% GTOW was the amount of fuel consumed. Therefore, the FF is 0.9964. It is to be noted that for the 'climb' operation, Roskam provides a defined value of FF for historical aircraft. In this chapter, modifications are not made to the defined value by Roskam (FF) for climb phase as the performance during the climb operation will be modelled using Breguet's range equation as represented by equation 7.2 (discussed next). The reason for this is that compared to the other operations except cruise and loiter, the effects of better aircraft aerodynamics of a BWB is prominently observed during climb.

If the GTOW is 300,000 kg for a Jet-A aircraft and the modified Roskam's FF for 'engine start and warmup' operation is 0.9964 (from Table 7.3), then the fuel consumed during this aircraft operation is [300,000 x (1-0.9964) =] 1,080 kg and the aircraft weight at the end of this operation or in the beginning of (the next operation) take-off is [300,000 – 1,080 =] 298,920 kg. Similarly, for each of the other mission segments the aircraft weight and fuel consumption for respective mission segments, are calculated. $W_{F,block}$ is the summation of the fuel consumption weights in all segments in the mission.

For LH_2 powered BWB aircraft, the FFs are different compared to Jet-A case. This is because for same work output if 1 kg of LH_2 fuel is used, then 2.865 kg of Jet-A is consumed equivalently (as studied in Chapters 4 and 6). Therefore, this results in weight reduction of 65.1% and lesser fuel mass of LH_2 need to be carried on the aircraft. This effect is reflected through the FFs as shown in Table 7.3. The FF calculation for LH_2 is as follows. For example: The modified FF for Jet-A during the taxi-out operation is 0.9964, which means that the fuel weight consumed during the taxi-out operation is 0.36% of aircraft weight at the start of the taxi-out stage. For the same energy content during the taxi-out stage, accounting the 65.1% reduction in fuel weight (described above) while switching from Jet-A to LH_2, the FF for LH_2 is calculated to be [0.9964 + (1-0.9964) x (1-(1/2.865)) =] 0.9987 i.e., LH_2 fuel weight is 0.13% of aircraft weight at the start of the taxi-out stage. Similarly, the other FFs are calculated and listed in Table 7.3 for LH_2 powered aircraft. This is similar to the approach used by Beck et al. [217] for their LH_2 powered VLTA BWB aircraft.

The FFs of 100% SPK powered aircraft are expected to be slightly different than the FFs of Jet-A aircraft since SPKs have slightly higher gravimetric energy density than Jet-A. Recalling the results of Chapter 6, for same thrust production, the energy released by 1 kg Jet-A is equal to energy released by 0.98 kg of 100% SPK (2% fuel weight saving). This effect is reflected through the FFs as shown in Table 7.4. The FF calculation for different SPKs is as follows. For example: The modified FF for Jet-A during the taxi-out operation is 0.9964, which means that the fuel weight consumed during the taxi-out operation is 0.36% of aircraft weight at the start of the taxi-out stage. For the same energy content during the taxi-out stage, accounting 2% reduction in fuel weight (described above) while switching from Jet-A to 100% SPK, the FF for 100% SPK is calculated to be [0.9964 + (1-0.9964) x (1-0.98) =] 0.9965. Similarly, the other FFs are calculated and listed in Table 7.4 for different SPK powered aircraft.

For each of the mission segments, the FF determines the fuel consumed during that mission segment for known aircraft weight at the beginning of that mission segment. Therefore, using FF the aircraft weight at end of a mission segment or beginning of the next mission segment can be calculated, for a known mission profile. The FF during climb ($M_{ff,climb}$) is calculated from Breguet range equation with the form seen in equation 7.2, and is given by,

$$M_{ff,climb} = \frac{1}{e^{\left[\left(\frac{endurance}{60}\right)*TSFC\middle/\left(\frac{L}{D}\right)\right]}},$$ (7.2)

where endurance during climb is calculated in minutes [and equals the ratio of cruise altitude and RoC]. The RoC used is 3,000 ft/min [295] or 914.4 m/min (standard value used for transport jets) to a cruise altitude of 10,668 m (or 35,000 ft in the current chapter as per design requirements or mission profile discussed in section 7.3). For the cruise and loiter (additional cruise), the method is similar. Instead of using endurance in the equation, both range and velocity are input (values are known from section 7.3.2). The FF during cruise ($M_{ff,cruise}$) is calculated from Breguet range equation with the form seen in equation 7.3, and is given by,

$$M_{ff,cruise} = \frac{1}{e^{\left[cruise\,range*TSFC\middle/V*\left(\frac{L}{D}\right)\right]}},$$ (7.3)

and the FF during loiter ($M_{ff,loiter}$) is calculated from Breguet range equation with the form seen in equation 7.4, and is given by,

$$M_{ff,loiter} = \frac{1}{e^{\left[loiter\,range*TSFC\middle/velocity*\left(\frac{L}{D}\right)\right]}}.$$ (7.4)

The product of all FFs in the mission gives the FF value for the entire mission. The TSFC values for climb, cruise, and loiter come from the engine model developed in GasTurb 13 software tool [188] (Chapter 6), and *L/D* calculation as described in section 7.4.2.

The average aircraft weight during climb, cruise, or loiter, is absorbed in equations 4.2 to 4.4 (Chapter 4) that enable the estimation of *L/D*. After GTOW is estimated, using the above FFs, the aircraft weight at beginning of climb can be calculated but the aircraft weight at the end of climb is unknown and so is the *L/D*. Both *L/D* and aircraft weight at the end of climb are calculated through simple iteration looping, as they are linked via weight sizing process. Similar approach is used for cruise and loiter for the estimation of *L/D* and aircraft weight at the end, of respective aircraft operation.

7.4.4   Aircraft systems weight

In the current chapter, three separate BWBs are considered for design analysis. The first is powered by conventional jet fuel (Jet-A), the second is powered by LH_2 and the third is powered by 100% SPK fuel. Table 7.5 lists the aircraft systems weight for Jet-A BWB aircraft (baseline) and LH_2 BWB aircraft. Similarly, Table 7.6 lists the aircraft systems weight for Jet-A BWB aircraft (baseline) and 100% SPK BWB aircraft.

As discussed in section 7.3, the ratio of $W_{F,block}$ and $W_{F,total}$ of the Jet-A NASA N+2 BWB aircraft is 0.9 [130]. In this chapter, similar value for the said ratio is used during the iteration process of the weight sizing process for estimating the aircraft operational energy consumption. For the BWB conventional jet fuel (baseline) case of this chapter, except for the engine weights and $W_{F,total}$, there is no other change compared to the Jet-A BWB aircraft [130].

Table 7.5. Aircraft systems weight for Jet-A BWB aircraft (baseline) and LH$_2$ BWB aircraft

System	Aircraft system	Weight (kg)	Source
1	Total propulsion systems weight [2 x (weight of bare engine + nacelle + inlet + mounting + accessories)]	17,076	[130]
2	OEW (NASA BWB)	114,907	[130]
3	Weight of the conventional jet fuel tank	1,057	Calculated in section 7.3.4.2
4	OEW without propulsion systems and tank	96,774	= 2-1-3
5	Payload weight (design)	53,570	[130]
6	$W_{F,total}$ (Jet-A)		Calculated iteratively using ratio of 0.9 of $W_{F,block}$ and $W_{F,total}$
7	GTOW of NASA N+2 BWB-GTF (301 passengers) Jet-A aircraft	242,441	[130] or (2+5+6)
8	Total propulsion systems weight in the present thesis [2 x (weight of bare engine + nacelle + inlet + mounting + accessories)]		Based on Chapter 6 (Jet-A and/or LH$_2$ engines)
9	GTOW of Jet-A BWB aircraft (baseline) [current chapter]		= 2-1+8+5+6
10	Weight of LH$_2$ tank systems		Calculated using model described in section 7.3.4.3
11	Additional structural weight for installing integral LH$_2$ tank systems	1,633	Calculated in section 7.3.4.1
12	$W_{F,total}$ for LH$_2$ BWB aircraft		Calculated iteratively using ratio of 0.9 of $W_{F,block}$ and $W_{F,total}$
13	GTOW of LH$_2$ BWB aircraft [current thesis]		= 4+8+5+10+11+12

The total propulsion systems weight comprises of weight of the bare engine, nacelle, inlet, mounting, and accessories, for two engines. GTOW of Jet-A BWB aircraft is essentially OEW from the Nickol et al. [130] study minus the total propulsion systems weights predicted by Nickol et al., and adding the total propulsion systems weights estimated from Chapter 6, the design payload weight and $W_{F,total}$ (calculated iteratively) as indicated in Table 7.5. Therefore, for Jet-A BWB aircraft, beginning with a guess of $W_{F,total}$, all inputs are known for estimating the mission fuel burn. Knowing GTOW, the aerodynamics (section 7.4.2), the FFs (modified FFs and FFs based on Breguet's range equation for Jet-A, from section 7.4.3), and TSFCs at different points in flight mission (Chapter 6), $W_{F,block}$ for Jet-A BWB aircraft can be calculated iteratively according to the flowchart shown in Figure 7.5 until the ratio of $W_{F,block}$ and $W_{F,total}$ of 0.9 is met.

7.4.4.2   LH₂ BWB aircraft

The weight sizing process that calculates the mission/block fuel consumption, is more iterative for LH$_2$ BWB aircraft as compared to Jet-A BWB aircraft. This is because LH$_2$ BWB aircraft has addition of new components like the LH$_2$ tank systems and additional structural weight for installing the integral LH$_2$ tank systems, along with the LH$_2$ fired propulsion systems.

Table 7.6. Aircraft systems weight for Jet-A BWB aircraft (baseline) and 100% SPK BWB aircraft

System	Aircraft system	Weight (kg)	Source
1	Total propulsion systems weight [2 x (weight of bare engine + nacelle + inlet + mounting + accessories)]	17,076	[130]
2	OEW (NASA BWB)	114,907	[130]
3	Weight of the conventional jet fuel tank	1,057	Calculated in section 7.3.4.2
4	OEW without propulsion systems and tank	96,774	= 2-1-3
5	Payload weight (design)	53,570	[130]
6	$W_{F,total}$ (Jet-A, NASA)	73,965	[130]
7	$W_{F,total}$ (calculated in this chapter)		Calculated iteratively using ratio of 0.9 of $W_{F,block}$ and $W_{F,total}$
8	GTOW of NASA N+2 BWB-GTF (301 passengers) Jet-A aircraft	242,441	[130] or (2+5+6)
9	Total propulsion systems weight in present chapter [2 x (weight of bare engine + nacelle + inlet + mounting + accessories)]		Based on Chapter 6 (Jet-A and/or SPK engines)
10	GTOW of Jet-A BWB aircraft (baseline) [current chapter]		= 2-1+9+5+7
11	Additional weight of 100% SPK tank systems		Calculation described in section 7.3.4.2
12	$W_{F,total}$ for SPK BWB aircraft		Calculated iteratively using ratio of 0.9 of $W_{F,block}$ and $W_{F,total}$
13	GTOW for 100% SPK BWB aircraft [current thesis]		= 2-1+9+5+11+12

The hydrogen fuel systems for an aircraft comprise of storage tanks, a feed and distribution system, and an interface fuel panel [296]. The feed and distribution system consists of all lines, valves, pressure and temperature sensors, heat exchangers, pumps, and regulators needed to create a safe cryogenic fuel system (ibid). As discussed in Chapter 6, considering that hydrogen has higher flame speeds as compared to Jet-A fuel, the diameter of the hydrogen fuel lines is expected to be lesser than that for Jet-A. This has a potential to reduce the weight of fuel lines. The effect of above-mentioned hydrogen fuel systems except the fuel storage tank, on aircraft weight is assumed to be negligible in this chapter.

GTOW of the LH$_2$ powered aircraft will be different than that of the conventional jet fuel powered aircraft because of lesser weight of hydrogen fuel to be carried on-board, addition of LH$_2$ tank systems, and additional structural weight for installing the integral LH$_2$ tank systems in the BWB aircraft, along with the LH$_2$ fired propulsion systems. As shown in Table 7.5, GTOW of LH$_2$ BWB aircraft is calculated by: subtracting

the total weight of Jet-A propulsion system (17,076 kg) [Nickol et al. [130] study] and the weight of conventional jet fuel tank (1,057 kg) from the OEW of NASA N+2 BWB-GTF (301 passengers) Jet-A aircraft (of 114,907 kg), and then adding: the total LH_2 fired propulsion systems weight (based on Chapter 6), the payload weight (53,570 kg), the weight of LH_2 tank systems (calculation described in section 7.3.4.3), the additional structural weight for installing the integral LH_2 tank systems (1,633 kg, calculated in section 7.3.4.1), and $W_{F,total}$ (calculated iteratively for maintaining the same ratio of $W_{F,block}$ and $W_{F,total}$, as that for Jet-A BWB aircraft, of 0.9). The iterative process for LH_2 BWB aircraft is discussed in detail in section 7.4.5.

7.4.4.3   SPK BWB aircraft

100% SPK case requires insignificant modification to tank system as the density of 100% SPK is slightly lesser than Jet-A as discussed in Chapter 6 and in section 7.3.4.2. GTOW of 100% SPK powered aircraft will be different than that of the conventional jet fuel powered aircraft because of slightly lesser fuel weight of 100% SPK fuel (as this fuel has slightly high gravimetric energy density) to be carried on-board compared to Jet-A case. As shown in Table 7.6, GTOW of 100% SPK BWB aircraft is calculated by: subtracting the total weight of Jet-A propulsion system (17,076 kg) [Nickol et al. [130] study] from the OEW of NASA N+2 BWB-GTF (301 passengers) Jet-A aircraft (of 114,907 kg), and then adding: the total SPK fired propulsion systems weight (based on Chapter 6), the payload weight (53,570 kg), and $W_{F,total}$ of 100% SPK carried on the aircraft (calculated iteratively for maintaining the same ratio of $W_{F,block}$ and $W_{F,total}$, as that for Jet-A BWB aircraft, of 0.9). Additionally, for 100% SPK case there is an (insignificant) addition of extra tank system for accommodating a slightly less dense fuel than Jet-A. The iterative process for 100% SPK BWB aircraft is discussed in detail in section 7.4.5.

7.4.5   Iteration conditions during the weight sizing process

7.4.5.1   Convergence criteria

Referring to Figure 7.5, for the Jet-A BWB aircraft case, the weight sizing process that estimates the aircraft operational energy consumption, a convergence criterion for the ratio of $W_{F,block}$ and $W_{F,total}$, is set to 0.9. The weight sizing process begins with a guess value of $W_{F,total}$ (other inputs are discussed in section 7.4.4.1), and $W_{F,block}$ is calculated from it. The guess value of $W_{F,total}$ is iterated until the said ratio equals 0.9. This determines the GTOW of the Jet-A BWB aircraft, which is set as MTOW for 100% SPK and three cases of LH_2.

It is chosen to constrain the aircraft GTOW of 100% SPK and LH_2 fuel, to be less than or equal to the MTOW limit of the baseline aircraft structure (observed in Figure 7.5). This constraint is applied since a detailed structural analysis is not conducted in this chapter. Therefore, the MTOW determines the design limit on the $W_{F,total}$ for both fuels.

Similarly, for the 100% SPK BWB aircraft case, the weight sizing process that estimates the aircraft operational energy consumption, a convergence criterion for the ratio of $W_{F,block}$ and $W_{F,total}$ is set to 0.9. 100% SPK case require insignificant modification to tank system as the density of 100% SPK is slightly lesser than

Jet-A as discussed in Chapter 6 and in section 7.3.4.2. The weight sizing process begins with a guess value of $W_{F,total}$ (other inputs are discussed in section 7.4.4.3), and $W_{F,block}$ is calculated from it. The guess value of $W_{F,total}$ is iterated until the said ratio equals 0.9. For the 100% SPK case, based on the guessed value of $W_{F,total}$, the corresponding (insignificant) increase in tank weight is estimated (based on discussion in section 7.3.4.2) for accommodating a slightly less dense fuel than Jet-A, which adds to the aircraft OEW and resultantly the GTOW.

Recalling the three cases of LH$_2$ fuel (from Chapter 6) which are analysed in this chapter are as follows:

- Case 1 is where the aircraft thrust production remains the same as that of the conventional jet fuel case.

- Case 2 is where the aircraft thrust requirement reduces for maintaining similar thrust to weight ratio as that of conventional jet fuel case (baseline). The fan diameter is no longer a design constraint as considered in Case 1.

- Case 3 is essentially Case 2 without engine cooling flows, since the engine is expected to run colder relative to the baseline (conventional jet fuel) case (as observed in Chapter 6) because of reduced thrust requirement, where the engine uses advanced material for withstanding high temperatures in baseline case, Case 1, and Case 2.

For all three cases of LH$_2$ aircraft considered in this chapter, the ratio of $W_{F,block}$ and $W_{F,total}$ (of 0.9) is set as the convergence criteria for the weight sizing process. Using the calculation process discussed in section 7.3.4.3, the weight of LH$_2$ tank systems is calculated. The LH$_2$ tank systems must be adapted to the internal available space of the BWB aircraft in the inner wings and in aft body (not affecting the aircraft cabin discussed in section 7.3.4.4). The LH$_2$ tank systems are expected to be a tapered cylindrical tank, similar to the tapered cylindrical tank design or frustum-shaped tank design by Verstraete et al. [66] for the tube-wing aircraft. Verstraete et al. study is used for the design of the LH$_2$ fuel tank in this chapter (discussed in section 7.3.4.3). The geometric model of the BWB aircraft is developed in SolidWorks 2019 [297], using the BWB geometry data discussed in section 7.3.4. For the LH$_2$ aircraft cases, the geometric model is used for ensuring that the tanks fit inside the BWB. Post-convergence, knowing the total LH$_2$ fuel weight at the beginning of the mission from the weight sizing process and the mass-density of LH$_2$ fuel (71 kg/m^3), the (minimum) required volume of LH$_2$ fuel is calculated. Using the insulation thickness (8.1 cm for η of 0.78) and the (minimum) volume of LH$_2$ fuel required to be stored at the beginning of the mission, a tapered cylindrical tank is modelled in SolidWorks 2019, which is integral to the structure of and inside the BWB aircraft. Since the cross-sectional area of a BWB aircraft is variable both in the spanwise and lengthwise direction, the tapered cylindrical LH$_2$ tank must be designed in a piece-wise manner for making maximum use of the internal space in the wings of a BWB aircraft. The tapered cylindrical LH$_2$ tank shape can be considered as multiple small-tapered cylinders joined together. The tapered cylindrical shape resulting in this chapter could have negative structural and heat-transfer implications. The tank design volume is the volume formed by the 'inner tank wall'. The inner tank wall is separated from the outer tank surface by insulation. Therefore, care must be taken while designing the LH$_2$ tank systems such that the effect of the insulation thickness on volume calculation is accounted. The weight sizing iteration continues until the end of convergence. The effect of T/W ratio of the aircraft is

171

important during the convergence. However, it depends on the type of LH$_2$ aircraft case considered, which is discussed below.

7.4.5.2   *Aircraft T/W constraint*

Referring to Figure 7.5, for Case 1 of the LH$_2$ aircraft, the sizing process begins with a guess weight of $W_{F,total}$, where the guess value of $W_{F,total}$ is 1 kg. Based on this guess value and weight sizing process, $W_{F,block}$ for Case 1 LH$_2$ aircraft is calculated iteratively. Using the above discussed process and convergence criteria, $W_{F,block}$ of LH$_2$ fuel and $W_{F,total}$ are calculated such that their ratio is 0.9. As discussed before, in case 1 the thrust production remains unchanged and therefore *T/W* is not a constraint in the weight sizing process. The *T/W* ratios at SLS and TOC are estimated using the thrust produced by engines (similar to Jet-A BWB aircraft case/design requirements) and the aircraft weight estimated from the weight sizing process. An aircraft powered by LH$_2$ fuel will be lighter as compared to an aircraft powered by Jet-A considering only the effect of LH$_2$'s higher gravimetric energy density, resulting in lower thrust requirement. Since in Case 1 the thrust production remains the same as the baseline case (Jet-A BWB aircraft), the resulting *T/W* ratios at SLS and TOC will be greater than the baseline case. After the convergence criteria is met in the weight sizing process, the aircraft design is finalised. The main effect that is anticipated in Case 1 is the effect of lighter aircraft on the block fuel (energy) consumption reduction.

Referring to Figure 7.5 in Case 2 of LH$_2$, the fan diameter is no longer a design constraint that is considered in Case 1 and thus the fan/engine diameter reduces (engine and aircraft weight reduces) because of lesser thrust requirement (due to a lighter aircraft because of lesser weight of high gravimetric energy density fuel and reduction in engine weight). Case 2 of LH$_2$ aircraft begins with the (guess value of) $W_{F,total}$ similar to Case 1. The convergence criteria for the weight sizing process remain similar to the process described for Case 1. However, the *T/W* ratio is an important factor considered in Case 2. The *T/W* ratio of the BWB-GTF Jet-A aircraft after the weight sizing process is calculated at SLS and TOC. The thrust value at on-design point is iteratively changed and the engine is designed along with its off-design performance. This is done in such a way that the *T/W* ratio at SLS and TOC is at least the respective calculated value for BWB-GTF Jet-A aircraft, or slightly higher. As discussed in section 7.3.3, in the current chapter the engine thrust requirement at TOC for the LH$_2$ BWB aircraft is based on two separate calculations. The first method is using the service ceiling thrust equation, and the second method is using the *T/W* ratio of the baseline case (Jet-A BWB aircraft). Both predictions are of similar magnitude, however, the maximum of the two values is selected as the thrust required to be produced by engines at TOC point. It is to be noted that because this chapter designs aircraft at a conceptual level, the *T/W* ratios do not reach the exact values (as calculated for Jet-A BWB aircraft). Nevertheless, they are similar in magnitude to or are slightly higher than the *T/W* values for Jet-A BWB aircraft. Typically, during high-order modelling or high-fidelity analysis, a multi-point design and optimisation is carried out in a flight mission, such that the *T/W* are identical to the target values. While the thrust is iterated, the convergence criteria in the weight sizing process along with the sizing of the LH$_2$ fuel tank and its integration (structural penalty) within the BWB aircraft, remain same as described earlier. As thrust changes, the following weights change along with it: the propulsion systems weights (smaller engine as compared to

Case 1), the LH$_2$ fuel tank weight, $W_{F,total}$ for LH$_2$ fuel, and GTOW of the aircraft (with aerodynamic parameters), as compared to Case 1. This interaction between different components of the weight-sizing process is shown in Figure 7.5. Only after the convergence criteria and the T/W ratio constraints are met, the aircraft design for Case 2 LH$_2$ aircraft is finalised.

Similarly, Case 3 of LH$_2$ aircraft is essentially Case 2 without engine cooling flows, because the engine operates colder and is smaller than the baseline (Jet-A) engine due to reduced thrust requirement. This further improves the TSFC, reduces propulsion systems weight, and therefore reduces $W_{F,block}$ (as compared to Case 2). For the set convergence criteria and T/W ratio constraints, this results in reduction in $W_{F,total}$, the LH$_2$ fuel tank weight, propulsion systems weights, and GTOW of the aircraft (with effect on aerodynamics), as compared with Case 2. This interaction between different components of the weight-sizing process is shown in Figure 7.5. The methodology (including the convergence criteria and T/W effects) remains similar to Case 2, as discussed above. Only after the convergence criteria and the T/W ratio constraints are met, the aircraft design for Case 3 LH$_2$ aircraft is finalised. The main effects that are anticipated in both Case 2 and Case 3 on block fuel (energy) consumption reduction are due to: the use of a high gravimetric energy density (LH$_2$) fuel that reduces the aircraft weight; the effect of thrust requirement reduction due to a lighter aircraft; and the effect of engine weight reduction (smaller engines due to thrust requirement reduction) on the aircraft weight; all of which result in block fuel (energy) consumption reduction.

As can be observed, the conceptual design phase of the aircraft is not only iterative but also there is interaction between the different systems of aircraft with each other (viz. aerodynamics, propulsion, weight, etc.). In the context of this thesis, the conceptual design phase of the aircraft is iterative and interactive between Chapter 6 and the present chapter.

7.4.6 Off-design performance of aircraft
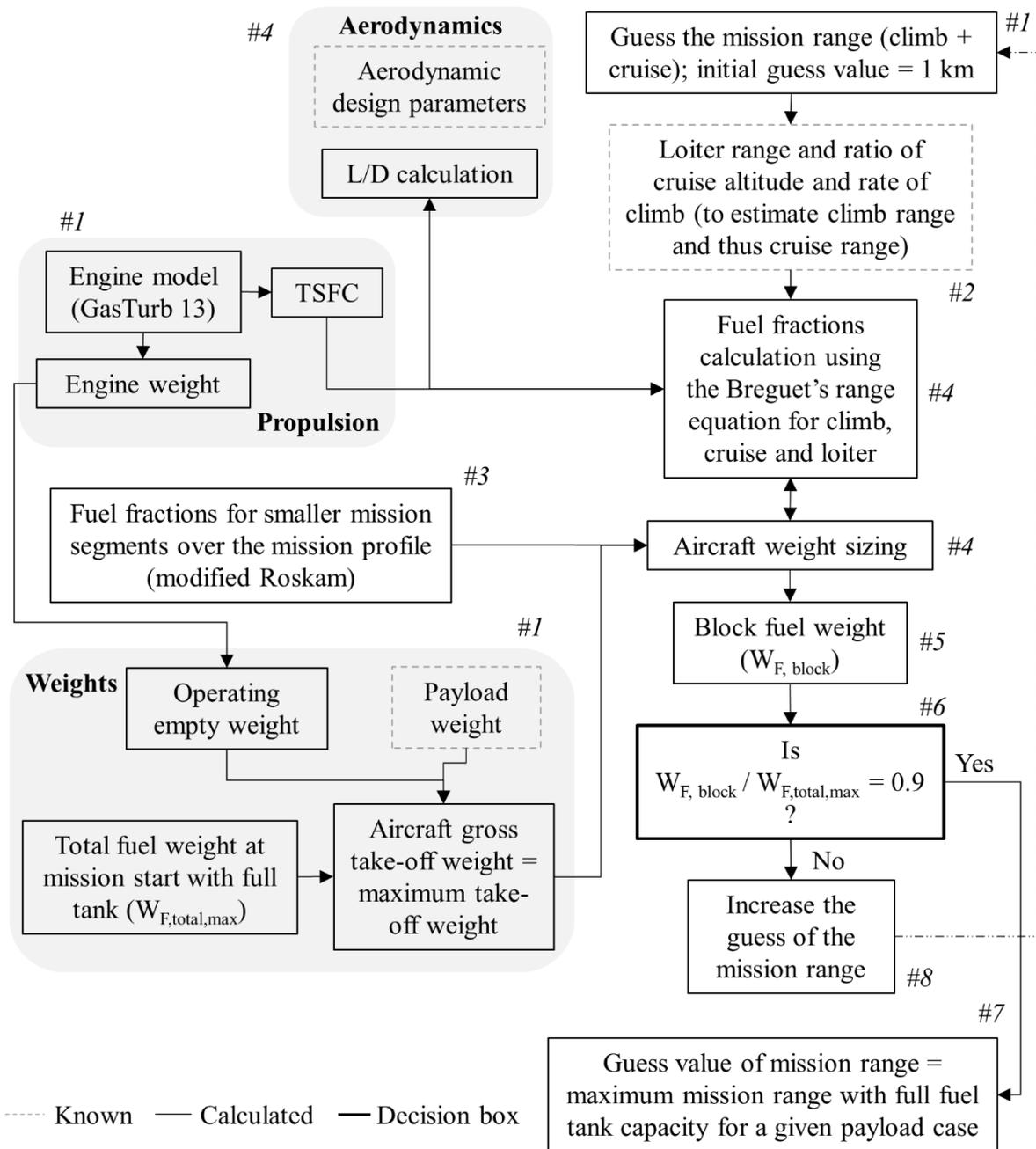
Figure 7.6. Schematic for the estimation of the maximum permissible range for a given payload case
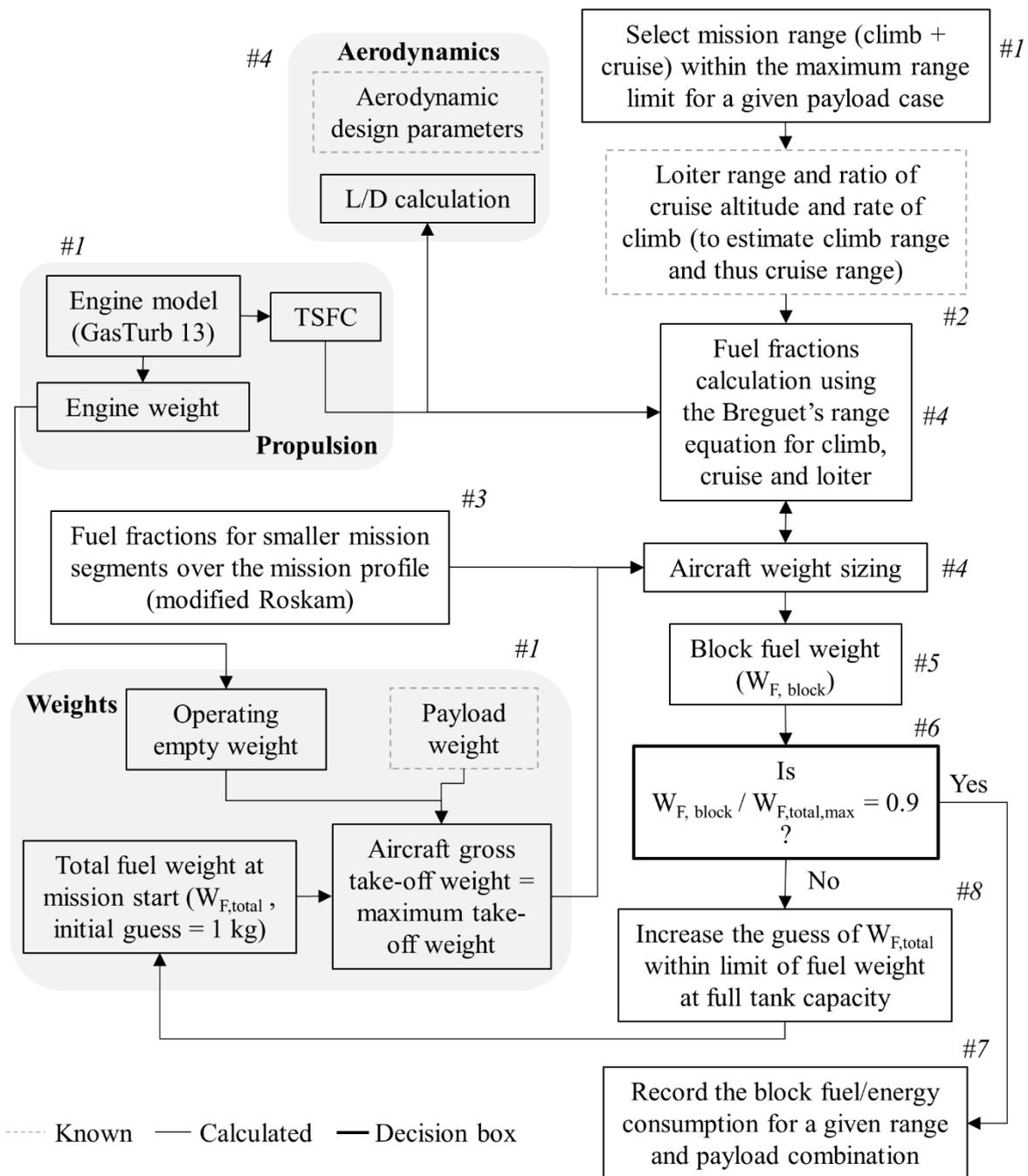
Figure 7.7. Schematic for the estimation of the operational energy consumption of an aircraft for given range and payload combination

For all fuel cases considered in this chapter, after following the aircraft weight sizing methodology described in previous sections, the aircraft performance for each fuel case at design point is known. The aircraft now becomes a 'fixed' aircraft. In real world applications, aircraft do not always fly with full design payload capacity, full fuel tank, and/or at design range. In this chapter, the performance of each of the aircraft powered by different fuels is evaluated for typical range and payload combinations for long-range flights. Three payload cases are considered: 66.5% load factor (200 passengers or 35.59 tonnes), 83.1% load factor (250 passengers or 44.49 tonnes), and 100% load factor (301 passengers or 53.57 tonnes). The three load factor cases are evaluated for aircraft range between 5,000 km and the maximum permissible range for a given load factor case

flying with full tank capacity. The flowchart/schematic for the estimation of the maximum permissible range for a given load factor with full fuel tank is represented by Figure 7.6. Additionally, Figure 7.7 shows the flowchart/schematic for the estimation of the operational energy consumption of an aircraft for given range and load factor combination.

7.5   Aircraft weight sizing results

7.5.1   SolidWorks geometric model of the BWB aircraft

Using the BWB aircraft geometry data such as air-foils and the process of estimation of other dimensions as discussed in section 7.3.4.4, the BWB aircraft geometric model is developed. Figure 7.8 provides the pictorial representation of this aircraft. It is to be noted that Jet-A, three cases of LH_2, and 100% SPK aircraft have the same outer BWB frame/skin (outer mould) as illustrated by Figure 7.8. The aircraft length is estimated to be 35 m and S_{wet} is calculated to be 2,132 m^2 (22,944 ft^2) using the SolidWorks 2019 geometric model.
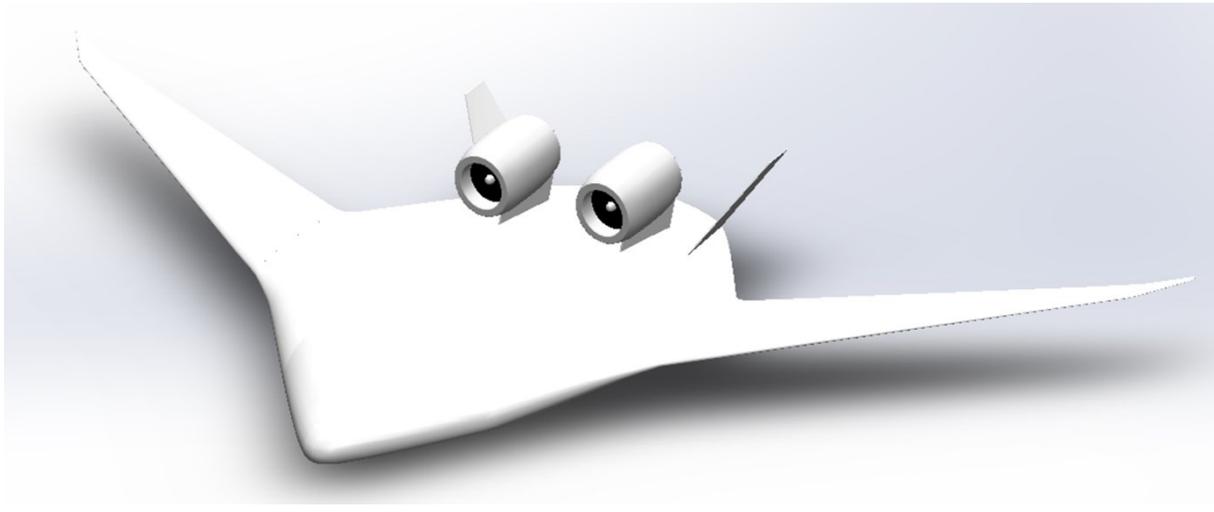
Figure 7.8. Geometric model of BWB aircraft simulated in this chapter

7.5.2   Iteration parameters for LH_2 aircraft cases

Table 7.7. Convergence criteria and T/W ratio constraints for LH_2 aircraft cases during the iteration of the weight sizing process

Parameter	Value
Convergence criteria* (Ratio of $W_{F,block}$ and $W_{F,total}$)	0.9
Minimum T/W at TOC**	0.04851
Minimum T/W at SLS**	0.262
* For all three cases of LH_2 aircraft	
** Only for case 2 and 3 of LH_2 aircraft (as described in section 7.4.5)	

For the Jet-A BWB aircraft case, using the weight sizing process, the ratio of $W_{F,block}$ and $W_{F,total}$ is calculated to be 0.9. For 100% SPK and three cases of LH_2 considered in this chapter, the above ratio of $W_{F,block}$

and $W_{F,total}$ (of 0.9) is set as the convergence criteria for the weight sizing process, according to the methodology described in section 7.4.5.

Additionally, using the weight sizing process for the Jet-A BWB aircraft and known data, the *T/W* ratios at SLS and TOC are calculated to be 0.262 and 0.04851 respectively. These two *T/W* ratios are set as constraints (minimum values to be met) in the weight sizing process for both Cases 2 and 3 of LH$_2$ aircraft, according to the methodology described in section 7.4.5. Case 1 of LH$_2$ aircraft, by the problem formulation, remains unaffected by the lighter aircraft (LH$_2$ use) and its engines produce the same thrust as produced by the engines of Jet-A BWB aircraft. Similarly, 100% SPK BWB aircraft remains unaffected by the slightly lighter aircraft and their engines produce the same thrust as produced by the engines of Jet-A BWB aircraft. Therefore, the *T/W* ratio (minimum) constraints at SLS and TOC (0.262 and 0.04851 respectively) is not considered for iteration purposes in the weight sizing process for case 1 of LH$_2$ aircraft and 100% SPK. Resultantly, *T/W* at SLS and TOC for case 1 of LH$_2$ aircraft is greater than Jet-A BWB aircraft, and case 2 and 3 of LH$_2$ aircraft, because it is an unoptimized case where the engines are producing more thrust than required, for a lighter aircraft. Similarly, *T/W* at SLS and TOC for 100% SPK aircraft is slightly greater than Jet-A BWB aircraft. The convergence criteria and *T/W* constraints are summarised in Table 7.7.

7.5.3   Aerodynamics

The BWB wingspan, *S*, and AR in this chapter (for Jet-A use, 100% SPK use, and LH$_2$ use [all three cases]) are 76.2 m, 944.73 m^2, and 6.1, respectively, as discussed in section 7.3.1. S_{wet} (for Jet-A use, 100% SPK use, and LH$_2$ use [all three cases]) is calculated to be 2,132 m^2 (22,944 ft^2) using the SolidWorks 2019 geometric model as discussed in section 7.3.4.4.

The cruise *L/D* ratio of the NASA N+2 BWB aircraft (Jet-A) is 23.7 [130]. In this chapter, through the weight sizing process of the BWB the cruise *L/D* ratio for Jet-A, Case 1 LH$_2$, Case 2 LH$_2$, Case 3 LH$_2$, and 100% SPK are 23.7, 22.51, 22.45, 22.36, and 23.66 respectively. It can be observed that the cruise *L/D* ratio of the Jet-A and 100% SPK BWB case are similar to values for the NASA N+2 BWB aircraft (Jet-A).

7.5.4   Propulsion

7.5.4.1   *TOC thrust prediction*

As discussed before, the required thrust at the TOC point is predicted by two methods. The first method is using the service ceiling thrust equation (equation 7.1), and the second method is using the *T/W* ratio of the baseline (Jet-A BWB aircraft) case. The inputs to the service ceiling equation come from the weight sizing process and the *T/W* ratio at TOC for the (baseline) Jet-A BWB aircraft is calculated to be 0.04851 (as discussed before). The aircraft weight at the end of climb is known from the weight sizing process and using the known *T/W* ratio of 0.04851, the required thrust can be calculated. The maximum of thrust values calculated using the above two methods becomes the thrust required to be produced.

Table 7.8. Prediction of TOC thrust using the service ceiling equation and the constraint of T/W ratio of 0.04851 for LH₂ aircraft cases

TOC thrust prediction (per engine) using:	Jet-A (kN)	LH₂ (kN)		
		Case 1	Case 2	Case 3
1. Service ceiling equation (section 7.3.3)	54.83	46.17	45.94	45.63
2. *T/W* ratio of 0.04851	*	46.29	46.02	45.66
Thrust produced (Chapter 6)	55.603	55.603**	46.35	46.12

*For Jet-A case, the thrust at TOC is known to be 55.603 kN as per the design requirements set by using Nickol et al. [130] study

** Case 1 is where thrust production remains unchanged (not optimised)

Table 7.9. Prediction of TOC thrust using the service ceiling equation and the constraint of T/W ratio of 0.04851 for 100% SPK aircraft

TOC thrust prediction (per engine) using:	Jet-A (kN)	100% SPK
1. Service ceiling equation (section 7.3.3)	54.83	54.46
2. *T/W* ratio of 0.04851	*	55.24
Thrust produced (Chapter 6)	55.603	55.603

*For Jet-A case, the thrust at TOC is known to be 55.603 kN as per the design requirements set by using Nickol et al. [130] study

The comparison of thrust prediction using the two methods is summarised in Table 7.8 and Table 7.9. It is to be noted that the thrust per engine is known to be 55.603 kN, which is a design requirement. Hence this thrust value determines the *T/W* ratio at the TOC point. Thus, this thrust value is not listed corresponding to the second method that uses the TOC *T/W* ratio of 0.04851, and the above discussion is noted in Table 7.8 and Table 7.9. Additionally, LH₂ Case 1 is where thrust production remains unchanged, by problem definition, despite the thrust requirement being lesser as the aircraft is lighter due to use of high gravimetric energy density LH₂ fuel.

As can be observed from Table 7.8 and Table 7.9, the required thrust predicted by using both the service ceiling equation (equation 7.1) and the *T/W* ratio, are very similar. This builds a confidence in the model developed. Additionally, the thrust per engine is known to be 55.603 kN from the design requirement based on Nickol et al. [130] study, for Jet-A case. The service ceiling equation, which takes inputs from the weight sizing process discussed in this chapter predicts thrust per engine of 54.83 kN. It is to be noted that this difference is because the Jet-A engines used in Jet-A BWB aircraft are significantly lighter than engines used in Nickol et al. [130] study and $W_{F,total}$ is calculated to be lesser than Nickol et al. study. The total propulsion systems weight comprises of the weight of bare engine, nacelle, inlet, mounting, and accessories, for two engines. The total propulsion systems weight of Nickol et al. [130] study and the Jet-A BWB aircraft in this chapter are 17,076 kg and 12,319 kg, respectively. The Jet-A BWB aircraft designed in this chapter is lighter than NASA N+2 BWB-GTF aircraft by Nickol et al. [130], which results in lesser thrust requirement. Therefore, this difference in the thrust is anticipated. Despite this non-uniformity, the thrust prediction between the two methods is similar. As LH₂ aircraft gets more optimised (case 2 and 3), the thrust requirement reduces as compared to case 1, which is anticipated.

7.5.4.2   Propulsion systems performance and weight

The inputs (performance parameters) to the weight sizing process for Jet-A and the three cases of LH$_2$ are summarised in Table 7.10, and for Jet-A and 100% SPK are summarised in Table 7.11. These are selected parameters that are relevant to the weight sizing process. The reader is advised to see Chapter 6 to find other parameters related to the propulsion systems (not relevant to the discussion in this chapter). The total propulsion systems weight of Nickol et al. [130] study is 17,076 kg. It can be observed from Table 7.10 that the total propulsion systems weight of Nickol et al. study is significantly greater than Jet-A case (and 100% SPK) of the current chapter (by ~4.7 tonnes) and all three cases of LH$_2$ (by ~4.8 tonnes, ~5.4 tonnes and ~6.3 tonnes for case 1, 2, and 3, respectively). The discussion on the reasons for the propulsion systems weight reduction is detailed in Chapter 6. Additionally, it can be observed from Table 7.11 for 100% SPK case the total propulsion systems weight is similar to the for Jet-A case of this chapter.

Table 7.10. Performance of propulsion system at different points in the flight mission profile for Jet-A and LH$_2$ fuel (three cases) and their weights

Parameters		Units	Jet-A	LH$_2$		
				Case 1	Case 2	Case 3
Total propulsion systems weight		kg	12,319	12,259	11,666	10,769
Performance characteristics per engine						
TOC	Mach, altitude	- , m	0.8 at 10,668 m	0.8 at 10,668 m	0.8 at 10,668 m	0.8 at 10,668 m
	TSFC	g/kN-s	12.400	4.328	4.284	4.160
	Thrust required	kN	55.603	46.29	46.02	45.66
	Thrust produced	kN	55.603	55.603	46.354	46.12
Cruise	Mach, altitude	- , m	0.84 at 10,668 m	0.84 at 10,668 m	0.84 at 10,668 m	0.84 at 10,668 m
	TSFC	g/kN-s	12.667	4.424	4.351	4.278
	Thrust required	kN	42.25	40.24	40.15	40.02
	Thrust produced	kN	51.61	51.68	51.09	43.12
SLS	Mach, altitude	- , m	0 at 0 m	0 at 0 m	0 at 0 m	0 at 0 m
	TSFC	g/kN-s	5.124	1.778	1.761	1.690
	Thrust required	kN	299.9	251.09	249.62	247.69
	Thrust produced	kN	303.89	304.53	263.83	261.14
Climb	Mach, altitude	- , m	0.47 at 5,334 m	0.47 at 5,334 m	0.47 at 5,334 m	0.47 at 5,334 m
	TSFC	g/kN-s	9.798	3.413	3.389	3.266
	Thrust produced	kN	94.94	95.54	96.96	82.58
Loiter	Mach, altitude	- , m	0.6 at 1,500 m	0.6 at 1,500 m	0.6 at 1,500 m	0.6 at 1,500 m
	TSFC	g/kN-s	12.175	4.234	4.195	4.067
	Thrust produced	kN	114.67	115.46	120.05	98.02

Table 7.11. Performance of propulsion system at different points in the flight mission profile for Jet-A and SPKs (three cases) and their and weights

Parameters		Units	Jet-A	100% SPK
Total propulsion systems weight		kg	12,319	12,319
Performance characteristics per engine				
TOC	Mach, altitude	- , m	0.8 at 10,668 m	0.8 at 10,668 m
	TSFC	g/kN-s	12.400	12.150
	Thrust required	kN	55.603	55.24
	Thrust produced	kN	55.603	55.603
Cruise	Mach, altitude	- , m	0.84 at 10,668 m	0.84 at 10,668 m
	TSFC	g/kN-s	12.667	12.411
	Thrust required	kN	42.25	42.16
	Thrust produced	51.61kN	51.61kN	51.61kN
SLS	Mach, altitude	- , m	0 at 0 m	0 at 0 m
	TSFC	g/kN-s	5.124	5.022
	Thrust required	kN	299.9	301.83
	Thrust produced	kN	303.89	303.85
Climb	Mach, altitude	- , m	0.47 at 5,334 m	0.47 at 5,334 m
	TSFC	g/kN-s	9.798	9.600
	Thrust produced	kN	94.94	94.95
Loiter	Mach, altitude	- , m	0.6 at 1,500 m	0.6 at 1,500 m
	TSFC	g/kN-s	12.175	11.929
	Thrust produced	kN	114.67	114.70

7.5.5   Characteristics of LH$_2$ tank systems

Figure 7.9 shows the LH$_2$ tank integration with BWB aircraft for Case 1 LH$_2$ aircraft (semi-span). This is a generic view without any tank dimensions. For all three LH$_2$ aircraft cases, three fuel tanks are placed on each of the two sides of the cabin and the three fuel tanks are placed aft of the cabin. The tank dimensions and fuel volume for all three LH$_2$ aircraft cases are provided in Table 7.12.

Table 7.12 shows the LH$_2$ tank geometry and dimensions for three cases (semi-span) considered in the current chapter. The total fuel requirement for case 1 at the beginning of the mission is calculated iteratively to be 24.25 tonnes (341.56 m^3) in the weight sizing process, which is the highest of the three LH$_2$ cases because it is an unoptimized case. This means that the volume of the tank required will be the highest of the three cases. The tank is designed in a piece-wise manner as discussed in section 7.4.5. The radius and the length for each piece of the tapered cylinder/frustum are listed in Table 7.12. Considering the total aircraft, for case 1, the total designed tank volume is calculated to be 341.66 m^3. The weight of the total tank system is calculated to be 6,840 kg for case 1. Similarly, the total fuel requirement for case 2 at the beginning of the mission is calculated iteratively to be 23.82 tonnes (335.47 m^3) in the weight sizing process (tank dimensions shown in Table 7.12). Considering the total aircraft, for case 2, the total designed tank volume is calculated to be 336.86 m^3. The weight of the total tank system is calculated to be 6,718 kg for case 2. Additionally, the total fuel requirement for case 3 at the beginning of the mission is calculated iteratively to be 23.35 tonnes (328.84 m^3) in the weight

sizing process (tank dimensions shown in Table 7.12). Considering the total aircraft, for case 3, the total designed tank volume is calculated to be 329.32 m^3. The weight of the total tank system is calculated to be 6,586 kg for case 3.

Cockpit and passenger cabin

7.05 m

23.67 m

35 m

Hinge-line of Elevons
(constraint during LH$_2$ tank installation)

38.1 m
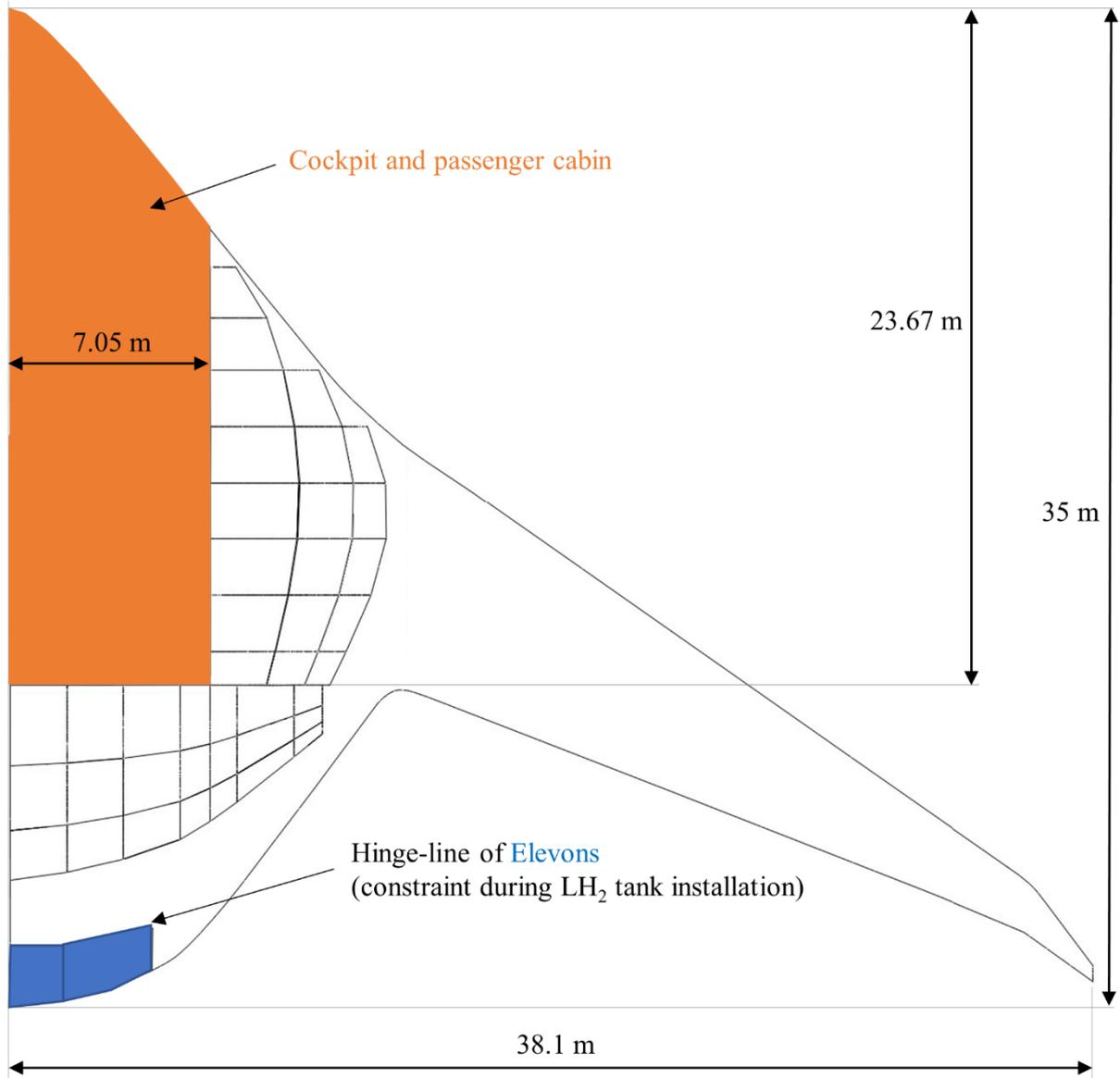
Figure 7.9. LH$_2$ tank integration with BWB aircraft for Case 1 LH$_2$ aircraft (semi-span)

Table 7.12. LH$_2$ tank geometry and dimensions for three cases considered in the current chapter
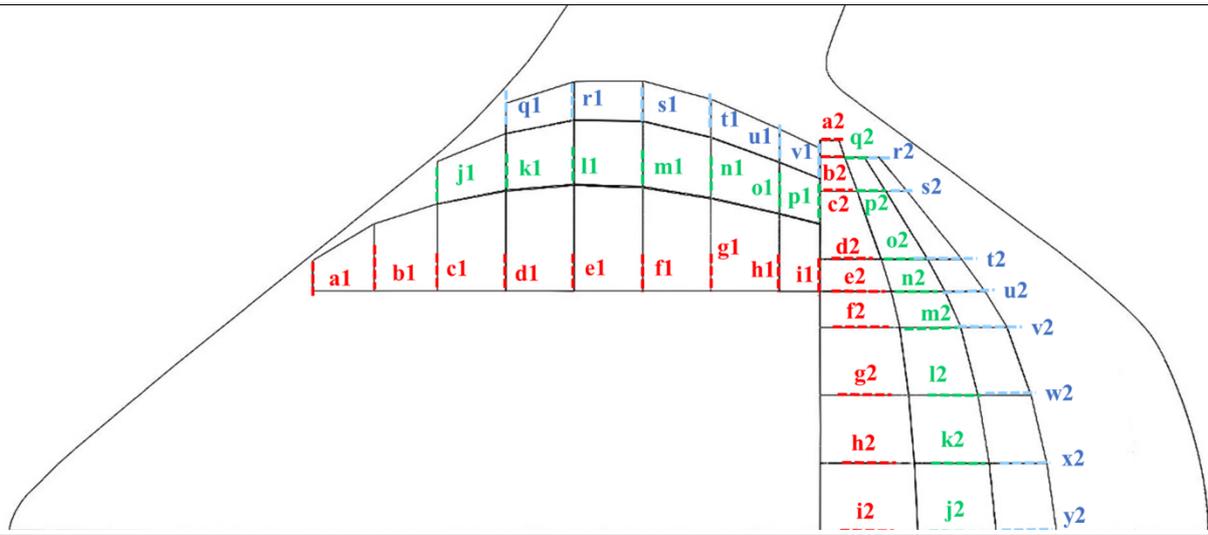
Case 1, Case 2, and Case 3 (Common tank systems to three cases)							
Section	Outer radius (m)	Piece length (m)	Section	Outer radius (m)	Piece length (m)	Section	Outer radius (m)	Piece length (m)
a1	0.45	0	j1	0.6275	0	q1	0.448	0
b1	0.9975	1.8	k1	0.8485	2	r1	0.57	2
c1	1.29	1.85	l1	0.964	2	s1	0.6	2
d1	1.49	2	m1	0.9825	2	t1	0.57	2
e1	1.5775	2	n1	0.905	2	u1	0.495	2
f1	1.543	2	o1	0.765	2	v1	0.4475	1.1855
g1	1.3795	2	p1	0.675	1.1855			
h1	1.15	2						
i1	1	1.1855						

Case 1 (remaining tank systems)							
Section	Outer radius (m)	Piece length (m)	Section	Outer radius (m)	Piece length (m)	Section	Outer radius (m)	Piece length (m)
a2	0.275	0	j2	1.144	0	r2	0.215	0
b2	0.36	0.5	k2	1.094	2	s2	0.31	1
c2	0.549	1	l2	1.0125	2	t2	0.5	2
d2	0.9	2	m2	0.893	2	u2	0.5895	0.95
e2	1.045	0.95	n2	0.7825	1.05	v2	0.677	1.05
f2	1.17	1.05	o2	0.674	0.95	w2	0.775	2
g2	1.3	2	p2	0.4175	2	x2	0.84	2
h2	1.385	2	q2	0.29	1	y2	0.8825	2
i2	1.435	2						

Case 2 (remaining tank systems)								
Section	Outer radius (m)	Piece length (m)	Section	Outer radius (m)	Piece length (m)	Section	Outer radius (m)	Piece length (m)
c2	0.549	0	j2	1.144	0	u2	0.5895	0
d2	0.9	2	k2	1.094	2	v2	0.677	1.05
e2	1.045	0.95	l2	1.0125	2	w2	0.775	2
f2	1.17	1.05	m2	0.893	2	x2	0.84	2
g2	1.3	2	n2	0.7825	1.05	y2	0.8825	2
h2	1.385	2	o2	0.674	0.95			
i2	1.435	2	p2	0.4175	2			
Case 3 (remaining tank systems)								
Section	Outer radius (m)	Piece length (m)	Section	Outer radius (m)	Piece length (m)	Section	Outer radius (m)	Piece length (m)
c2	0.549	0	j2	1.144	0	v2	0.677	0
d2	0.9	2	k2	1.094	2	w2	0.775	2
e2	1.045	0.95	l2	1.0125	2	x2	0.84	2
f2	1.17	1.05	m2	0.893	2	y2	0.8825	2
g2	1.3	2	n2	0.7825	1.05			
h2	1.385	2						
i2	1.435	2						

7.5.6 Design point performance of the BWB aircraft powered by Jet-A, 100% SPK, and LH$_2$

The results of the different components/sub-systems of the weight sizing process, for Jet-A BWB aircraft, BWB LH$_2$ aircraft (all three cases), and BWB 100% SPK aircraft, have been discussed so far. The aircraft performance over one flight mission is summarised below in comparison to the present-day aircraft i.e., Boeing 777-200 LR. The performance data for Boeing 777-200 LR is included in Chapter 6 (Table 6.1). The aircraft weight and fuel consumption breakdown over flight mission for the BWB aircraft powered by different fuels are included in Appendix C section C.3.

It can be observed from Table 7.13 that *T/W* ratio at SLS and TOC for BWB LH$_2$ aircraft tend towards the *T/W* ratios of BWB-GTF Jet-A aircraft at SLS and TOC, from case 1 to case 3 (from the unoptimized to the optimised aircraft). In all three cases of BWB LH$_2$ aircraft the minimum required *T/W* at SLS and TOC are met, for a flight to be possible with the same airframe used for Jet-A BWB aircraft (and NASA N+2 BWB-GTF 301 passenger [PAX] aircraft).

The NASA N+2 BWB-GTF 301 PAX (Jet-A) aircraft provides 47% reduction in block fuel energy consumption as compared to Boeing 777-200LR, which is known from Nickol et al. [130] study. The Jet-A BWB aircraft (designed in this chapter) is (1.74%) more efficient than NASA N+2 BWB-GTF 301 PAX (Jet-A). This energy efficiency improvement is attributable to TSFC improvement (high component efficiencies, discussed in Chapter 6), and engine weight reduction (discussed in Chapter 6) that reduces the GTOW.

Table 7.13. Performance comparison of Boeing 777-200 LR and future aircraft [Jet-A BWB aircraft and BWB LH₂ aircraft (all three cases)] over one flight mission

Aircraft range: 13,890 km (Current scenario)		
Aircraft	Jet-A block fuel consumption (kg)	Jet-A block fuel energy consumption (TJ)
Boeing 777-200LR	125,705	5.43

				Aircraft range: 13,890 km (Future scenarios)		
Parameters	Units	Nickol et al. [130]	Jet-A BWB aircraft	BWB LH₂ aircraft		
				Case 1	Case 2	Case 3
GTOW	kg	242,441	236,398	195,325	194,177	192,677
OEW	kg	114,907	110,150	117,505	116,790	115,760
Payload weight	kg	53,570	53,570	53,570	53,570	53,570
Cryogenic tank η	-	-	-	0.78	0.78	0.78
$W_{F,total}$	kg	73,965	72,678	24,250	23,817	23,347
Ratio of GTOW and GTOW$_{NASA}$	-	*1*	*0.975*	*0.806*	*0.801*	*0.795*
$W_{F,block}$	kg	66,683	65,523	21,863	21,473	21,049
Block fuel energy	TJ	2.88	2.83	2.62	2.58	2.53
Block fuel energy reduction as compared to Boeing 777-200LR	%	47%	47.88%	51.69%	52.55%	53.49%
Block fuel energy reduction as compared to Jet-A BWB aircraft	%		-	7.31%	8.97%	10.76%
$(L/D)_{cruise}$	-	23.7	23.7	22.51	22.45	22.36
Block fuel weight/total fuel weight	-	0.9	0.9	0.9	0.9	0.9
T/W (SLS)	-	0.252	0.262	0.318	0.277	0.276
T/W (TOC)	-	-	0.04851	0.058	0.0487	0.0489
Structurally (average) permissible ratio of aircraft landing weight and GTOW, for transport jet		0.84 (according to Roskam [198])				

The Jet-A BWB aircraft provides 47.88% reduction in the block fuel energy consumption as compared to Boeing 777-200LR. The performance of BWB LH₂ aircraft is better than both NASA N+2 BWB-GTF 301 PAX (Jet-A) aircraft and Jet-A BWB aircraft (present chapter). Case 1, 2, and 3 of BWB LH₂ aircraft provide 51.69%, 52.55%, and 53.49% reduction, respectively, in the block fuel energy consumption as compared to Boeing 777-200LR. It is important to note that the LH₂ fuel tank systems fit inside the BWB aircraft primarily because of the consideration of future aircraft technology that significantly reduces the fuel weight and fuel volume to be carried on the aircraft. For example: as discussed above, BWB LH₂ aircraft (all three cases) provides energy-efficiency improvement of approximately 50% as compared to Boeing 777-200LR. Had there been no energy efficiency improvement due to the use of aircraft technology, the LH₂ fuel volume required would be approximately twice the volume of fuel required by the current BWB LH₂ aircraft cases. The use of

future aircraft technology (engine and airframe) enables successful and efficient use of LH_2 fuel in the aircraft. In Chapter 5, the N+3 tube-wing LH_2 aircraft shows 33% improvement in energy consumption compared to A350 Jet-A aircraft. Using the same baseline case (A350 Jet-A aircraft) instead of Boeing 777-200LR, the energy consumption of N+2 BWB LH_2 aircraft improves by 48.5%. Therefore, from this analysis it can be clearly observed that a BWB airframe has energy consumption benefits for LH_2 use (despite lagging by one technology generation) compared to a tube-wing aircraft.

Table 7.14. Performance comparison of Boeing 777-200 LR and future aircraft [Jet-A BWB aircraft and BWB 100% SPK aircraft] over one flight mission

Aircraft range: 13,890 km (Current scenario)			
Aircraft	Jet-A block fuel consumption (kg)		Jet-A block fuel energy consumption (TJ)
Boeing 777-200LR	125,705		5.43

Aircraft range: 13,890 km (Future scenarios)			
Parameters	Units	Nickol et al. [130]	Jet-A BWB aircraft	BWB 100% SPK aircraft
---	---	---	---	---
GTOW	kg	242,441	236,398	234,798
OEW	kg	114,907	110,150	110,169
Payload weight	kg	53,570	53,570	53,570
$W_{F,total}$	kg	73,965	72,678	71,059
GTOW / GTOW$_{NASA}$	-	1	0.975	0.968
$W_{F,block}$	kg	66,683	65,523	64,065
Block fuel energy	TJ	2.88	2.83	2.82
Block fuel energy reduction as compared to Boeing 777-200LR	%	47%	47.88%	47.97%
Block fuel energy reduction as compared to Jet-A BWB aircraft	%		-	0.187%
$(L/D)_{cruise}$	-	23.7	23.7	23.656
Block fuel weight/total fuel weight	-	0.9	0.9	0.9
T/W (SLS)	-	0.252	0.262	0.264
T/W (TOC)	-	-	0.04851	0.04883
Structurally (average) permissible ratio of aircraft landing weight and GTOW, for transport jet		0.84 (according to Roskam [198])		

Compared to the Jet-A BWB aircraft, BWB LH_2 aircraft case 1, 2, and 3 provide 7.31%, 8.97%, and 10.76% reduction, respectively, in the block fuel energy consumption. As discussed before, the improvement in the block fuel energy consumption in all three cases of BWB LH_2 aircraft is primarily due to the improved TSFCs (details in Chapter 6) and due to the aircraft weight reduction. In case 2 and 3 of BWB LH_2 aircraft the reduction in the thrust requirement [leading to engine weight reduction and therefore the reduction of aircraft GTOW] is an additional reason for the improved energy efficiency. It was observed in Chapters 4 and 5, that tube-wing LH_2 aircraft requires increase in fuselage length to accommodate LH_2 fuel tanks which negatively impacts L/D and therefore the aircraft energy consumption, for maintaining same range and payload as that of baseline case. This negative impact is not observed for BWB (N+2 aircraft technology) because of their higher internal volume that enable storage of LH_2 tanks.

The significant reduction in the GTOW of LH_2 aircraft observed from Table 7.13 (greater than 19% reduction in GTOW depending on case) is of importance during emergency landing situations as a lighter aircraft will not necessitate jettison of a highly flammable LH_2 fuel (details in Appendix section C.4). A similar analysis is conducted for tube-wing LH_2 aircraft in Chapter 4. It is to be noted that the reduction in GTOW and take-off wing-loading (from baseline) is observed to be greater for N+2 BWB LH_2 aircraft in this chapter (~20%) and N+3 tube-wing aircraft in Chapter 5 (~34%), as compared to the tube-wing aircraft of present technology fuelled by LH_2 fuel in Chapter 4 (~15%). Lastly, it is to be noted that unlike Chapter 4 there are no comparisons made in terms of take-off wing-loading with literature as the data is not available. Study by Beck et al. is the only study that models a BWB LH_2 aircraft (VLTA) and their reference aircraft is B747 which is a tube-wing aircraft. The said study does not have a Jet-A version of the BWB to enable a comparison of change in wing-loading switching from Jet-A to BWB.

Table 7.14 provides the performance comparison of Boeing 777-200 LR and future aircraft (Jet-A BWB aircraft and BWB 100% SPK aircraft) over one flight mission. BWB 100% SPK aircraft has similar performance metrics as that of BWB Jet-A aircraft. BWB 100% SPK case has insignificant energy efficiency improvement of 0.19%. This is similar to the findings of Hileman et al. [51] (0.3% improvement in energy efficiency), Proesmans et al. [159] (similar energy consumption), and that of Chapter 4 (0.17%), for tube-wing aircraft. Additionally, for the 100% SPK BWB aircraft there is an insignificant increase in the OEW (of 19 kg in fuel tank weight) to accommodate slightly less mass-dense (100% SPK) fuel than Jet-A. It is to be noted that 100% SPK is not a drop-in fuel presently.

7.5.7   Off-design point performance of the BWB aircraft powered by Jet-A, 100% SPK, and LH_2

The methodology/flowchart for the aircraft off-design point performance estimation has been discussed in section 7.4.6. Three payload (load factor) cases are considered: 66.5% load factor (200 passengers or 35.59 tonnes), 83.1% load factor (250 passengers or 44.49 tonnes), and 100% load factor (301 passengers or 53.57 tonnes). The three load factor cases are evaluated for aircraft range between 5,000 km and the maximum permissible range for a given load factor case flying with full tank capacity. Figures 7.10, 7.11, and 7.12 show the variation of SEC with range for BWB aircraft powered by different fuels ($\eta = 0.78$ for all three LH_2 cases) for 66.5% load factor, 83.1% load factor, and 100% load factor, respectively. In all three figures same trend is observed for SEC vs range i.e., with increasing range, the SEC decreases for each of the fuel case.
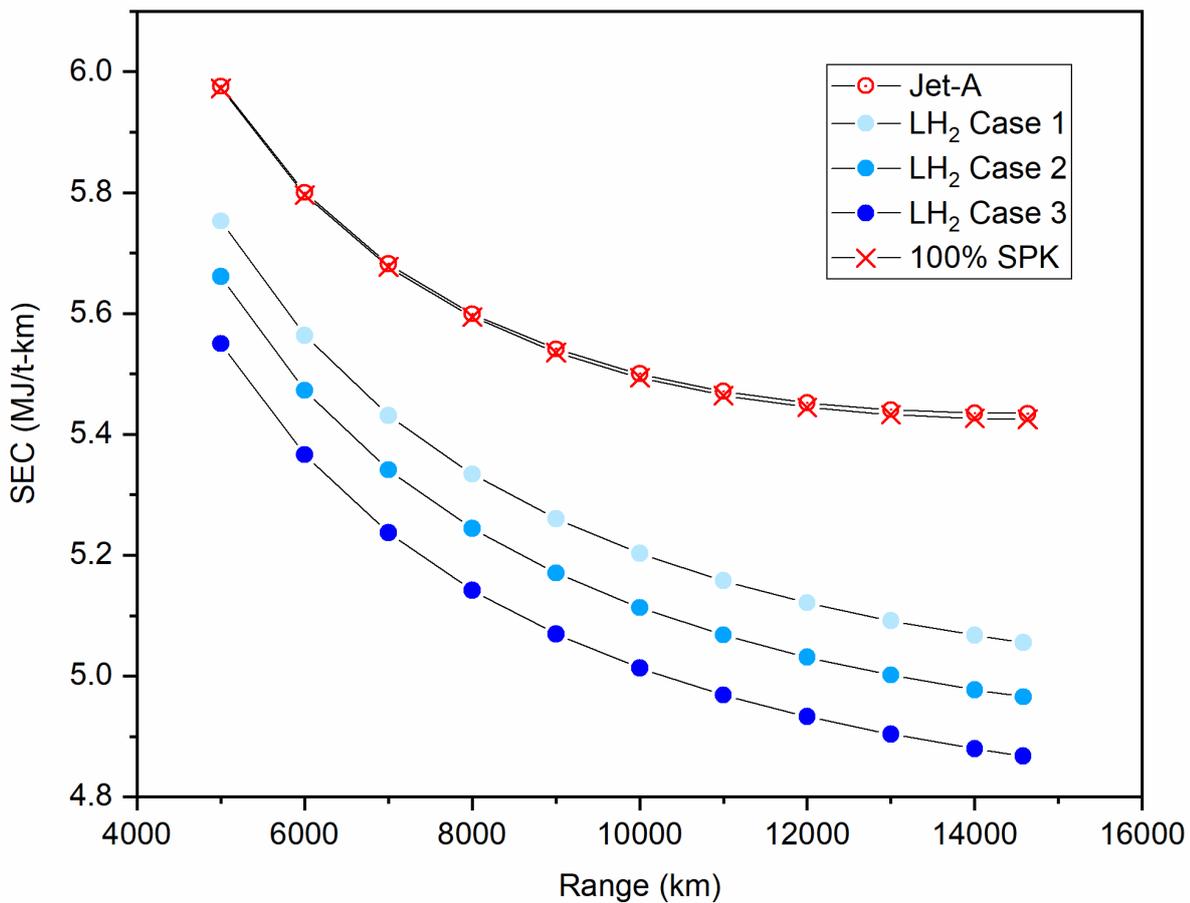
Figure 7.10. Variation of SEC with range for BWB aircraft powered by different fuels (η = 0.78 for all three LH$_2$ cases) for 66.5% load factor

Additionally, at any given range, by increasing the load factor the absolute value of SEC decreases for each of the fuel case. BWB LH$_2$ aircraft (all three cases, η = 0.78) are more efficient at greater range and the SEC curve appears to keep dipping with increasing range as compared to Jet-A. This (for BWB LH$_2$ aircraft) contrasts with the observations made in Chapter 4, where the SEC of LH$_2$ 'tube-wing' aircraft, though decreases with range, is less sensitive beyond (the range of) 10,000 km. SEC of both Jet-A and 100% SPK BWB cases appear to be less sensitive to range beyond ~13,000 km. Of the three BWB LH$_2$ aircraft cases, Case 3 offers the best energy efficiency at all range and load factor combinations.
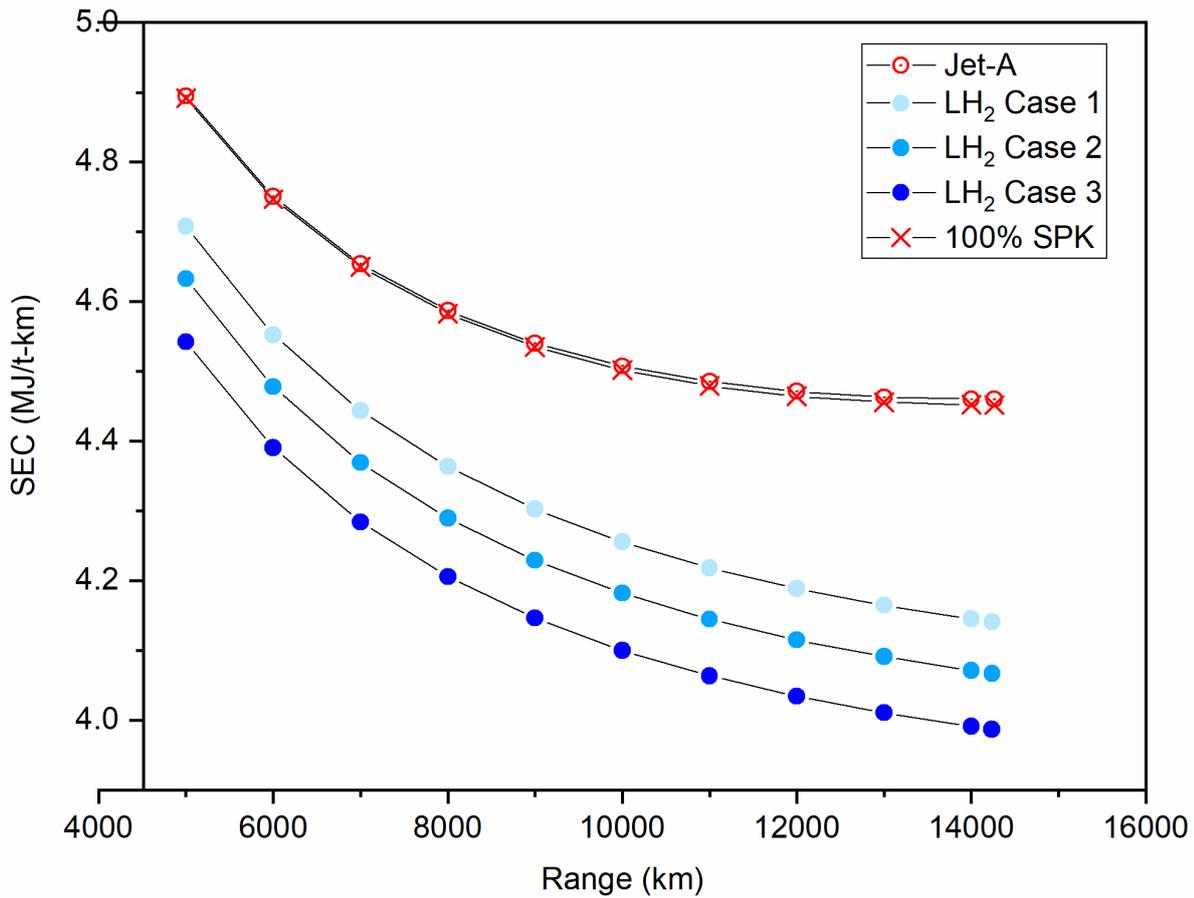
Figure 7.11. Variation of SEC with range for BWB aircraft powered by different fuels ($\eta = 0.78$ for all three LH$_2$ cases) for 83.1% load factor

The findings of Figures 7.10, 7.11, and 7.12 can be summarised through a single plot i.e., Figure 7.13 which demonstrates the energy efficiency improvement of BWB powered by different fuel cases ($\eta = 0.78$ for all three LH$_2$ cases) as compared to Jet-A BWB aircraft for varying range and load factor combinations. For a given fuel case, with increasing load factor, the maximum range that can be travelled decreases. Additionally, for a given fuel case, increasing the load factor improves the energy efficiency compared to a Jet-A BWB aircraft. Moreover, for a given fuel and load factor case, the energy efficiency improves with increasing range compared to a Jet-A BWB aircraft. This increase in energy efficiency is observed prominently for all three cases of BWB LH$_2$ aircraft compared to the Jet-A BWB aircraft. The BWB LH$_2$ Case 3 aircraft is the most efficient aircraft at all range and load factor combinations compared to the Jet-A BWB aircraft.
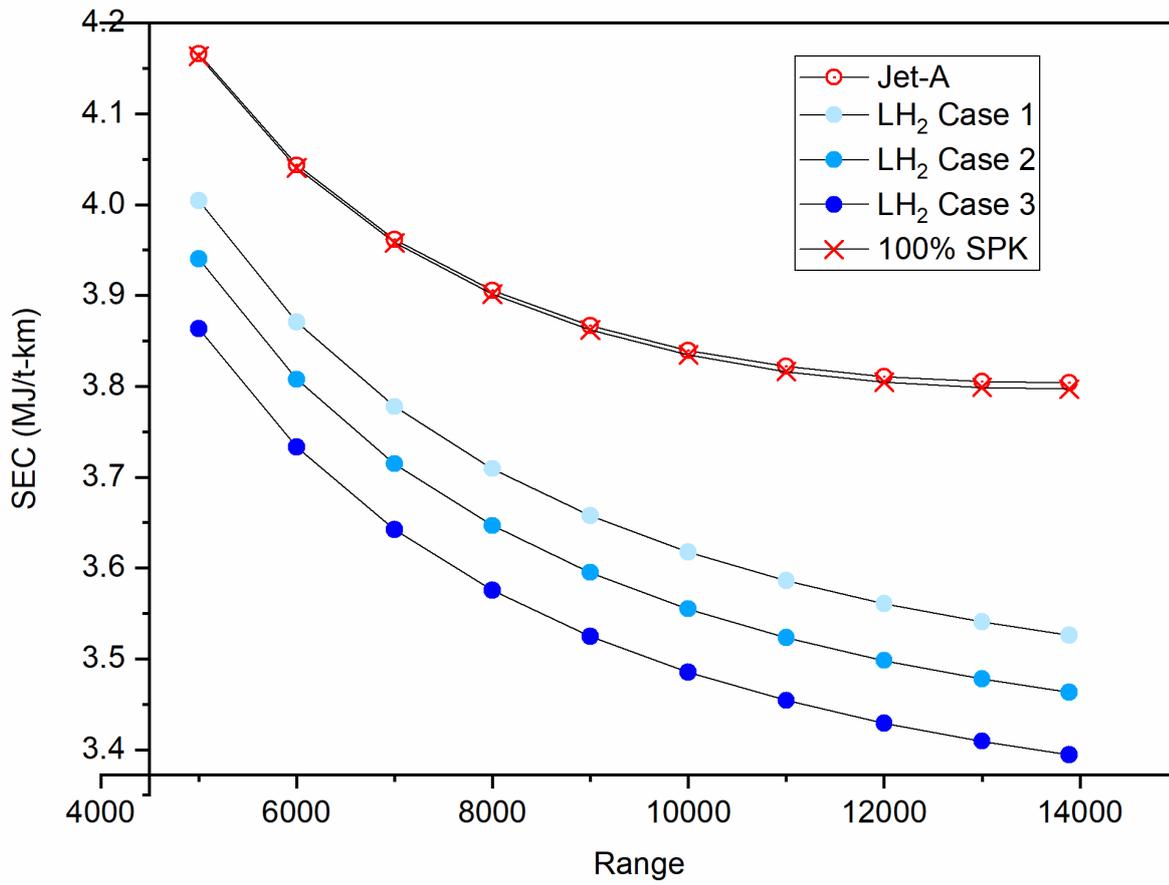
Figure 7.12. Variation of SEC with range for BWB aircraft powered by different fuels ($\eta = 0.78$ for all three LH$_2$ cases) for 100% load factor
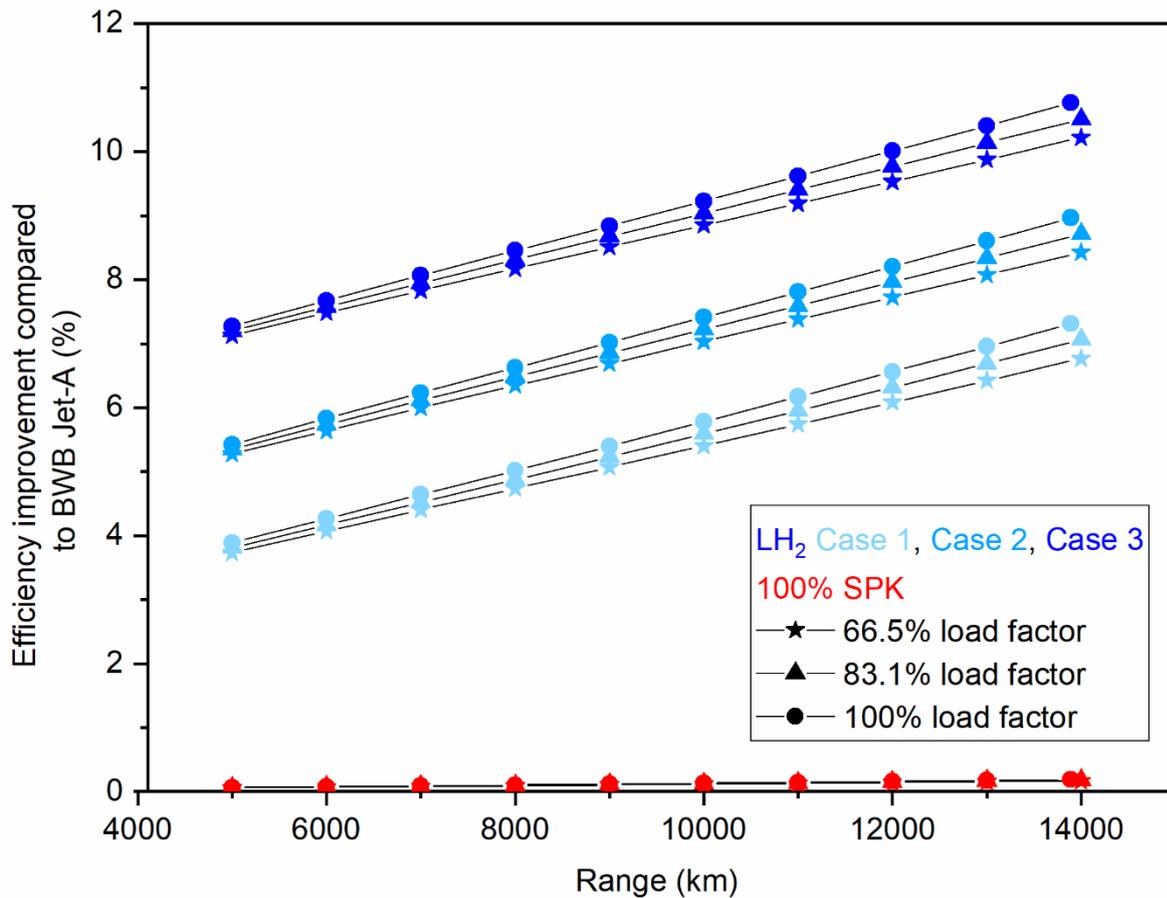
Figure 7.13. Energy efficiency improvement of BWB powered by different fuel cases ($\eta = 0.78$ for all three LH$_2$ cases) as compared to Jet-A BWB aircraft for varying range and load factor combinations

7.5.8   Relationship between OEW and GTOW for LH$_2$ aircraft

The engine designs in Chapter 6 and the aircraft designs in the current chapter are based on data and design approaches from literature. It is important to conduct a final evaluation i.e., a sanity check, by analysing the relationship between OEW and GTOW for the transport aircraft designed in this chapter and the transport aircraft that have already entered in service and/or in literature. Historical aircraft data and literature is used for the regression analysis, where the data is of different sizes of aircraft (ranging from small aircraft like Boeing 737-200 to large quads or VLTAs like Airbus A380-800). Table 7.15 lists the OEW and GTOW of aircraft already into service, in literature, and aircraft designed in this thesis. Overall, 70 aircraft are listed in Table 7.15. 34 aircraft are included from literature and from present thesis in the regression analysis to estimate the relation between OEW and GTOW for LH$_2$ aircraft. 27 present-day aircraft (Jet-A) and nine futuristic aircraft (Jet-A and 100% SPK) are included in the regression analysis to estimate the relation between OEW and GTOW of Jet-A and/or 100% SPK aircraft.

The equation shown in the figure:

$$y = 0.46 \, x^{1.04}$$
$$R^2 = 0.99$$

Legend:
- This study (366 PAX 13,870 km)
- Brewer (130 PAX 2,778 km)
- Brewer (200 PAX 5,556 km)
- Brewer (400 PAX 5,556 km)
- Brewer (400 PAX 10,186 km)
- Brewer (400 PAX 18,520 km)
- Verstraete (150 PAX 4,000 km)
- Verstraete (300 PAX 9,000 km)
- Verstraete (400 PAX 14,000 km)
- Proesmans et al. ATR (67 PAX 2,410 km)
- Proesmans et al. COC (67 PAX 2,410 km)
- Proesmans et al. ATR (130 PAX 3,200 km)
- Proesmans et al. COC (130 PAX 3,200 km)
- Proesmans et al. ATR (253 PAX 10,800 km)
- Proesmans et al. COC (253 PAX 10,800 km)
- Silberhorn et al. (2019) (165 PAX 5,740 km) Rear tank
- Silberhorn et al. (2019) (165 PAX 5,740 km) Top tank
- Silberhorn et al. (2019) (165 PAX 5,740 km) Pod tank
- Airbus Cryoplane (185 PAX 7,400 km)
- Gomez et al. (194 PAX 9,000 km)
- Silberhorn et al. (2022) (261 PAX, 7,220 km)
- Lammen et al. (300 PAX, 3,704 km)
- Troeltsch et al. (400 PAX 11,853 km)
- Onorato et al. (72 PAX, 926 km)
- Onorato et al. (150 PAX, 4,560 km)
- Onorato et al. (295 PAX, 7,674 km)
- Huete et al. (232 PAX, 10,370 km)
- Huete et al. (332 PAX, 8,890 km)
- Huete et al. (388 PAX, 6,112 km)
- Huete et al. (720 PAX, 3,334 km)
- Beck et al. BWB (524 PAX 11,408 km)
- This study BWB LH2 Case 1 (301 PAX 13,890 km)
- This study BWB LH2 Case 2 (301 PAX 13,890 km)
- This study BWB LH2 Case 3 (301 PAX 13,890 km)

Figure 7.14. Relationship between OEW and GTOW of LH$_2$ aircraft (34 aircraft) from the present chapter and literature (all are tube-wing except four BWB as indicated) (Brewer [180], Verstraete [68], Troeltsch et al. [173], Beck et al. [217], Proesmans et al. [159], Gomez et al. [172], Silberhorn et al. [168] (2019), Silberhorn et al. [176] (2022), Lammen et al. [170], Onorato et al. [177], and Huete et al. [178], and Chapter 4)

Figure 7.14 shows the relationship between OEW and GTOW of LH_2 aircraft (34 aircraft) from the present chapter and literature (all are tube-wing except four BWB as indicated) (Brewer [180], Verstraete [68], Troeltsch et al. [173], Beck et al. [217], Proesmans et al. [159], Gomez et al. [172], Silberhorn et al. [168] (2019), Silberhorn et al. [176] (2022), Lammen et al. [170], Onorato et al. [177], and Huete et al. [178], and tube-wing [A350-1000] LH_2 aircraft modelled in Chapter 4 [366 PAX 13,870 km]). It can be observed that the relationship between OEW and GTOW for the aircraft designed in this chapter is similar to the LH_2 aircraft designs in literature, and the developed equation would facilitate weight sizing studies on LH_2 aircraft design. The equation developed in Figure 7.14 will enable low-order modelling or weight sizing of LH_2 aircraft.
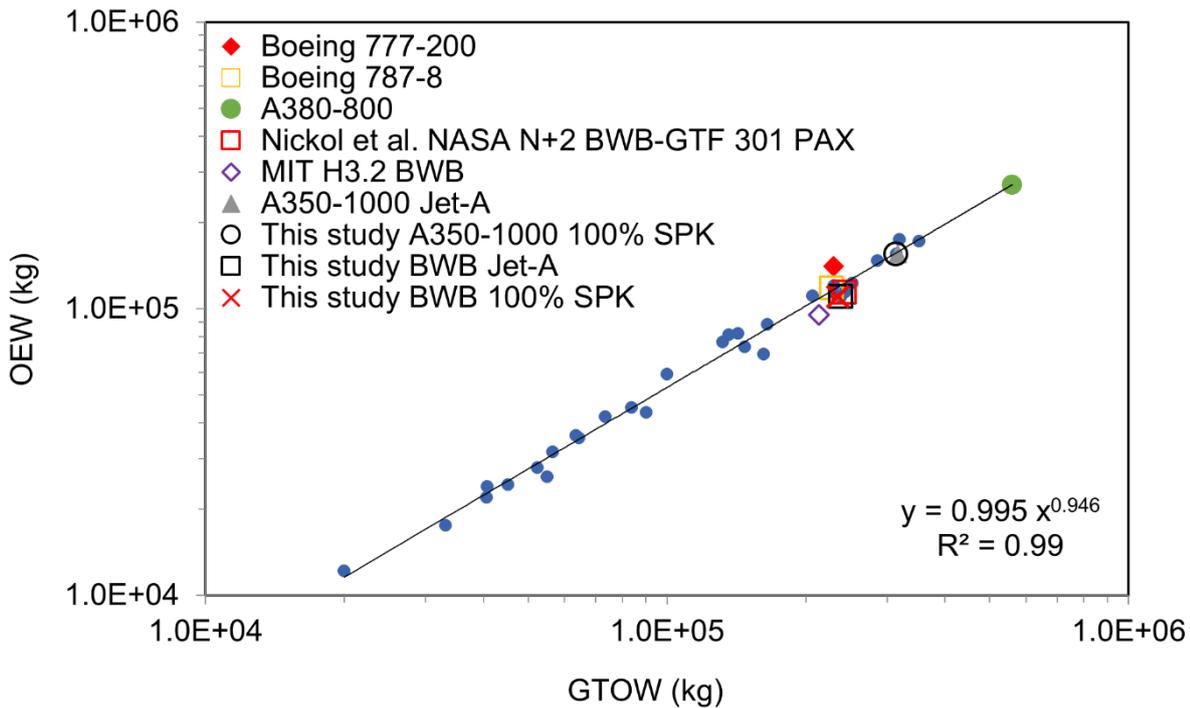
Figure 7.15. Relationship between OEW and GTOW of aircraft in service, of future (other studies) and future aircraft designed in this chapter (only Jet-A and 100% SPK) (see Table 7.15 for source of data)

Figure 7.15 shows the relationship between OEW and GTOW of aircraft in service, of future (other studies), and future aircraft designed in this chapter (only Jet-A and 100% SPK) (readers are advised to see Table 7.15 for source of aircraft data). It is to be noted that Figure 7.15 also includes the tube-wing [A350-1000] 100% SPK aircraft modelled in Chapter 4. It can be observed from Figure 7.15 that the relationship between OEW and GTOW for the aircraft designed in this chapter is very similar to that of aircraft that have already entered in service. GTOW is an indirect measure of the structural weight of the aircraft, payload, and the fuel weight ($W_{F,block}$ and $W_{F,total}$). 100% SPK aircraft cases have similar (magnitude of) OEW and GTOW as that of BWB Jet-A case, hence these lie in the vicinity of the BWB Jet-A case. For compactness, only the names of recent aircraft in service and the aircraft designed in this chapter (along with reference aircraft) are mentioned in Figure 7.15.

Table 7.15. OEW and GTOW of aircraft already into service, in literature and aircraft designed in this thesis

Aircraft	GTOW (kg)	OEW (kg)
27 Aircraft already into service ([198], [209], [298], [299])		
727-200	83,824	45,359
737-200	52,390	27,955
737-300	56,472	31,720
747-200B	351,534	172,365
747-SP	285,763	147,417
757-200	99,790	59,157
767-200	136,078	81,230
DC8-Super 71	147,417	73,799
DC9-30	54,885	25,941
DC9-80	63,503	36,177
DC10-10	206,384	111,086
DC10-40	251,744	122,952
Lockheed L1011-500	231,332	111,357
Fokker F28-4000	33,112	17,546
Rombac-111-560	45,200	24,386
VFW-Fokker 614	19,958	12,179
BAe 146-200	40,596	21,999
A300-B4-200	164,999	88,500
A310-202	131,995	76,616
Ilyushin-Il-62M	162,000	69,400
Tupolev-154	90,000	43,499
A330-200	229,998	120,499
Airbus A320	73,498	42,100
Boeing 777-200	229,518	140,659
A380-800	559,993	270,012
Boeing 787-8	227,930	117,707
A350-1000	316,000	155,129
Nine futuristic aircraft (Jet-A and 100% SPK) [123], [130]		
Over wing nacelle 98 – direct drive engine	40,728	23,977
Over wing nacelle 160 – GTF	64,350	35,551
BWB 216 – GTF	142,364	82,169
BWB 400 – GTF	318,661	174,793
MIT H3.2 BWB	213,445	95,243
Nickol et al. NASA N+2 BWB-GTF 301 PAX	242,441	114,349
This study A350-1000 100% SPK Chapter 4	313,404	155,314
This study BWB Jet-A	237,685	110,151
This study BWB 100% SPK	234,798	110,169

34 LH$_2$ aircraft [68], [159], [217], [168], [172], [173], [176]–[180]		
Brewer tube-wing (130 PAX 2,778 km)	45,510	29,780
Brewer tube-wing (200 PAX 5,556 km)	79,600	51,540
Brewer tube-wing (400 PAX 5,556 km)	143,330	90,340
Brewer tube-wing (400 PAX 10,186 km)	168,740	103,300
Brewer tube-wing (400 PAX 18,520 km)	249,400	149,840
Verstraete tube-wing (150 PAX 4,000 km)	78,000	58,200
Verstraete tube-wing (300 PAX 9,000 km)	175,700	122,900
Verstraete tube-wing (400 PAX 14,000 km)	250,100	161,600
Proesmans et al. ATR (67 PAX 2,410 km)	32,200	20,500
Proesmans et al. COC (67 PAX 2,410 km)	33,100	21,500
Proesmans et al. ATR (130 PAX 3,200 km)	63,600	41,200
Proesmans et al. COC (130 PAX 3,200 km)	64,500	42,600
Proesmans et al. ATR (253 PAX 10,800 km)	244,000	156,000
Proesmans et al. COC (253 PAX 10,800 km)	248,000	163,000
Gomez et al. (194 PAX 9,000 km)	133,676	108,897
Airbus Cryoplane (185 PAX 7,400 km)	87,600	61,200
Silberhorn et al. (2019) (165 PAX 5,740 km) Rear tank	67,819	44,334
Silberhorn et al. (2019) (165 PAX 5,740 km) Top tank	66,045	42,605
Silberhorn et al. (2019) (165 PAX 5,740 km) Pod tank	64,584	41,084
Silberhorn et al. (2022) (261 PAX, 7,220 km)	128,670	92,245
Lammen et al. (300 PAX, 3,704 km)	164,900	128,600
Onorato et al. (72 PAX, 926 km)	22,900	14,600
Onorato et al. (150 PAX, 4,560 km)	77,000	52,000
Onorato et al. (295 PAX, 7,674 km)	210,000	141,000
Huete et al. (232 PAX, 10,370 km)	309,000	238,000
Huete et al. (332 PAX, 8,890 km)	303,000	299,000
Huete et al. (388 PAX, 6,112 km)	273,000	200,000
Huete et al. (720 PAX, 3,334 km)	287,000	194,000
Troeltsch et al. (400 PAX 11,853 km)	196,000	128,000
Beck et al. BWB (524 PAX 11,408 km)	288,994	201,003
This study (366 PAX 13,870 km) Chapter 4	268,516	183,371
This study BWB LH$_2$ Case 1 (301 PAX 13,890 km)	196,339	118,194
This study BWB LH$_2$ Case 2 (301 PAX 13,890 km)	195,206	117,501
This study BWB LH$_2$ Case 3 (301 PAX 13,890 km)	193,732	116,505

Referring to Figure 7.15, the data points on left (GTOW< 1.0E+5), centre (1.0E+5<GTOW<4.0E+5), and right (GTOW>4.0E+5) are primarily of small aircraft (short range), LTA and small twin aisle aircraft (medium and long range), and VLTA (large quads and long range), respectively. All these data points used for creating both Figure 7.14 and Figure 7.15, are listed in Table 7.15. Additionally, by using the developed equation in Figure 7.15, and knowing either OEW or GTOW, the GTOW or OEW can be estimated for low-order modelling.

7.5.9 Other results and comments

It was observed through the findings of Chapter 4 (details in Appendix C) that LNG aircraft showed a potential in terms of getting closer to the design target range (10,895 km for LNG case 1 compared to target

of 13,870 km). Since this chapter considers weight sizing of a BWB aircraft that has greater internal volume as compared to a tube-wing aircraft, it is a good exercise to also examine the performance of LNG fuel in a BWB. The details of the LNG aircraft weight sizing process are included in Appendix C section C.5. Similar to Chapter 4, two LNG cases (of cryogenic tank η of 0.78 and 0.63) are considered here for BWB powered by LNG. For LNG case of $\eta = 0.78$, which has highest cryogenic tank η of the two cases, the aircraft reaches a range of 12,052 km. Therefore, LNG is not identified as an alternative fuel even for use in an N+2 BWB aircraft (since target design range of 13,890 km is not met).

7.5.10   Limitations of the present chapter

The effect of cryogenic tank is not considered in detail and is based on other studies. Ideally, a separate design model for cryogenic tank is required that accounts both internal and external mechanical and thermal stresses. The estimation of the aircraft's operational energy consumption is based on a simplified (multi-segment) mission in the weight sizing process, where the energy consumption in smaller flight segments is calculated using the modifications to Roskam's fuel fraction. Additionally, *L/D* ratios during climb, cruise, and loiter are average values for respective segments based on the aircraft weight during respective segment's beginning and end. Moreover, in the estimation of the drag coefficient, wave drag is considered to be negligible which is typically considered in high-fidelity analysis. Overall, the weight sizing process is a low-order or low-fidelity analysis and errors in aircraft performance metrics are expected.

7.6   Chapter summary and conclusion

The present chapter begins with a literature review on LH_2 powered aircraft studies, and the conceptual aircraft design process. Thereafter, more details of the selected future NASA N+2 aircraft (BWB) is listed and discussed comprehensively (as per the discussion and selection in Chapter 2), considering that this chapter is focussed specifically on the conceptual aircraft design. Based on this discussion and the discussion from Chapter 6, the design requirements are set for the aircraft.

After the design requirements are set, the data such as structural weights of different components/systems of the BWB aircraft and BWB aircraft geometry are then listed and discussed comprehensively along with the flight mission profile, LH_2 tank model from literature, and the physics-based equation for service ceiling aircraft thrust requirement calculation. This is followed by the aircraft weight sizing methodology, which is discussed thoroughly. Additionally, aircraft off-design point performance estimation methodology is discussed. The details of the aircraft weight sizing process comprise of the propulsion aspect, aerodynamics, fuel fractions, aircraft systems weight, and the iteration conditions during the sizing process of the BWB LH_2 aircraft (three cases) considered in this chapter.

Thereafter, BWB aircraft designs of the future (N+2 timeframe) for conventional jet fuel, 100% SPK case, and three cases of LH_2 fuel are developed. The results of this design process comprise of the geometric model, iteration parameters during the sizing process, propulsion aspect (summarised using the results from Chapter 6), aerodynamics, characteristics of LH_2 tank systems for BWB aircraft powered by LH_2, weight of the aircraft and fuel consumed during different points in the aircraft flight mission for aircraft powered by the

conventional jet fuel, 100% SPK case, and LH$_2$ fuel (three cases), and the overall performance (design and off-design points) of the BWB aircraft powered by the conventional jet fuel, 100% SPK case, and LH$_2$ fuel (three cases).

The *T/W* ratios at SLS and TOC for BWB LH$_2$ aircraft tend towards the *T/W* ratios of Jet-A BWB aircraft at SLS and TOC, from case 1 (unoptimized) to case 3 (optimised). In all three cases of BWB LH$_2$ aircraft, the minimum required *T/W* at SLS and TOC are met, for a flight to be possible with the same airframe used for Jet-A BWB aircraft (and NASA N+2 BWB-GTF 301 PAX aircraft). The NASA N+2 BWB-GTF 301 PAX (Jet-A) aircraft provides 47% reduction in block fuel energy consumption as compared to Boeing 777-200LR, which is known from Nickol et al. [130] study. The Jet-A BWB aircraft (modelled in this chapter) is more efficient (by 1.74%) than the NASA N+2 BWB-GTF 301 PAX (Jet-A) aircraft. The Jet-A BWB aircraft provides 47.88% reduction in the block fuel energy consumption as compared to Boeing 777-200LR at the design point. The performance of BWB LH$_2$ aircraft is better than both NASA N+2 BWB-GTF 301 PAX (Jet-A) aircraft and Jet-A BWB aircraft. Case 1, 2, and 3 of BWB LH$_2$ aircraft provide 51.69%, 52.55%, and 53.49% reduction, respectively, in the block fuel energy consumption as compared to Boeing 777-200LR at the design point. BWB 100% SPK case has similar performance metrics as that of BWB Jet-A aircraft at the design point. BWB 100% SPK cases has insignificant energy consumption improvement of 0.19%.

It is important to note that the LH$_2$ fuel tank systems fit inside the BWB aircraft primarily because of the consideration of future aircraft technology that significantly reduces the fuel weight and fuel volume to be carried on the aircraft. This effect was observed in Chapter 5, where the N+3 tube-wing LH$_2$ aircraft SEC improved by 33% requiring a fuselage length increase of 22%, compared to A350-1000 Jet-A aircraft. For the LH$_2$ aircraft modelled in Chapter 4 using present-day aircraft technology, the SEC increased by 11% requiring 37% increase in fuselage length, compared to present-day Jet-A aircraft. BWB LH$_2$ aircraft (case 3) provides energy consumption improvement of approximately 53.5% as compared to Boeing 777-200LR or 48.5% compared to A350-1000 Jet-A aircraft. Had there been no energy consumption improvement due to the use of future aircraft technology, the LH$_2$ fuel volume required would be significantly greater than the fuel volume required in the BWB LH$_2$ aircraft cases modelled in this chapter. The use of future (N+2 timeframe) aircraft technology (engine and airframe) enables successful and efficient use of LH$_2$ fuel in the aircraft. Compared to the Jet-A BWB aircraft, BWB LH$_2$ aircraft case 1, 2, and 3 provide 7.31%, 8.97%, and 10.76% reduction, respectively, in the block fuel energy consumption. As discussed before, the improvement in the block fuel energy consumption in all three cases of BWB LH$_2$ aircraft is primarily due to the improved TSFCs and reduction in GTOW. In case 2 and 3 of BWB LH$_2$ aircraft the reduction in the thrust requirement is an additional reason for the improved energy efficiency.

With BWB LH$_2$ aircraft (all three cases) there is no need to conduct fuel jettison of a highly flammable hydrogen fuel in the event of an emergency landing, because its GTOW is lesser than the average permissible landing weight considering its structure (MTOW). This finding is of great significance considering the safety issue associated with LH$_2$ use in an aircraft. Thereafter, a final evaluation i.e., a sanity check is conducted where the relationship between the OEW and GTOW is analysed for the LH$_2$, and Jet-A and 100% SPK aircraft. It is observed that the relationship between OEW and GTOW for the aircraft designed in this chapter

is similar to the LH_2 aircraft designs in literature, and the developed equation would facilitate future weight sizing studies on LH_2 aircraft design. Similar (OEW vs GTOW) observations are made for Jet-A and 100% SPK.

At off-design points, for a given fuel case, with increasing load factor, the maximum range that can be travelled decreases. Additionally, for a given fuel case, increasing the load factor improves the energy efficiency compared to a Jet-A BWB aircraft. Moreover, for a given fuel case and load factor, the energy efficiency improves with increasing range compared to a Jet-A BWB aircraft. This increase in energy efficiency is observed prominently for all three cases of BWB LH_2 aircraft compared to the Jet-A BWB aircraft. The BWB LH_2 Case 3 aircraft is the most efficient aircraft at all range and load factor combinations compared to the Jet-A BWB aircraft.

Overall, purely based on energy efficiency performance, the BWB LH_2 aircraft appears to be a preferred LTA aircraft type for long-range travel considering all LH_2 aircraft performance observed from Chapters 4 to 7. The BWB LH_2 aircraft does have an advantage over both Jet-A BWB aircraft and BWB 100% SPK aircraft in terms of energy consumption (use-phase) and that this BWB LH_2 aircraft would emit only water vapour and small amount of NO_x. However, this and previous chapters do not consider the lifecycle emissions of Jet-A, 100% SPK, and LH_2 aircraft. Thus, this need for a holistic assessment of lifecycle emissions due to the use of Jet-A, 100% SPK and LH_2 aircraft motivates the next chapter, where different manufacturing pathways and feedstocks of these fuels will be explored. This analysis would help in the estimation of the fuel pathway(s) and/or feedstock(s) that could enable climate neutral long-range flight with a N+2 BWB LTA aircraft.

Chapter 8: Lifecycle comparative performance assessment of different aircraft and fuel combinations

8.1   Introduction

8.1.1   Background

The lifecycle emissions attributable to the fuel performance of an aircraft is the summation of emissions during the operational phase of the aircraft and fuel manufacturing stage (raw material extraction to fuel in storage tank). In the present setup, the operational phase GHG emissions from aircraft contribute to ~70% of the total aircraft GHG emissions [99].

In this study, the operational energy performance modelling of an LTA aircraft powered by LH_2 and 100% SPK (separately) is conducted in Chapters 4 – 7, and this enables the estimation of emissions in the aircraft use-phase. Thus, knowing the fuel manufacturing emissions, the WTWa or lifecycle emissions can be calculated. This motivates the current chapter where the life cycle or WTWa performance is evaluated for a long-range LTA aircraft powered by LH_2 and 100% SPK (separately) manufactured from different feedstocks and/or pathways.

Firstly, in the current chapter, an inventory of fuel manufacturing phase CO_2 equivalent emissions is created using the GREET model [33] and literature. GREET model is a lifecycle assessment tool developed by Argonne National Lab, USA. Secondly, the use-phase CO_2 emissions are modelled in this chapter for a future (N+2 timeframe) BWB aircraft (which is identified in Chapter 7 as efficient and suitable for LH_2 fuel systems integration), along with the quantification of other non-CO_2 emissions. These enable the estimation of WTWa CO_2 equivalent emissions.

In this chapter, the life cycle or WTWa performance is evaluated for future (N+2 timeframe) long-range BWB LTA aircraft powered by LH_2 and 100% SPK (separately) manufactured from different feedstocks and/or pathways. The objective of this chapter is to identify the aircraft technology and fuel (feedstock and/or pathway) combination(s) that enable a climate-neutral long-range flight of an LTA aircraft. This addresses the fifth and last research objective discussed in Chapter 1. In addition to the CO_2 equivalent emissions, this work also quantifies some of the unintended effects due to the use of LH_2 and 100% SPK (separately) that are manufactured from different feedstocks and/or pathways. These unintended effects comprise of fossil fuel use, water consumption, and other emissions.

8.1.2   Chapter structure

The studies that explore the WTWa emissions performance of aircraft (separately) powered by Jet-A, 100% SPK, and LH_2, are first reviewed in sub-section 8.2. Thereafter, a comparative WTWa emissions assessment of the above fuels is conducted using the methodology described in section 8.3, and the results are discussed in section 8.4.

8.2 Well-to-wake literature review

A preliminary or high-level literature review on synthetic jet fuels such as biomass-based fuels and PtL has been conducted in Chapter 2, which enables the understanding of the potential of these fuels in terms of carbon emissions reduction on a WTWa basis. These fuels are further reviewed in detail in this chapter along with LH_2, towards their WTWa emissions performance.

Table 8.1. WTWa CO_2 equivalent values for different renewable jet pathways (source [300])

Technology	Feedstock	CO_2 equivalent (g/MJ)
FT	Forestry residues	6
	Poplar	-6 to 10
	Corn Stover	13
	Willow	0
HEFA	Camelina	44 to 47
	Used cooking oil	28
	Jatropha	21 to 55
STJ (10% blend)	Sugarcane	47 to 49
STJ (increased blend level)	Sugarcane	76 to 79
ATJ	Sugarcane	31
	Corn Stover	22 to 35
	Corn	54 to 71
Pyrolysis (in situ)	Forestry residues	22
Pyrolysis (ex situ)	Forestry residues	37 to 41
Hydrothermal Liquefaction (HTL) (in situ)	Forestry residues	18
HTL (ex situ)	Forestry residues	21

A study by De Jong et al. [300] carries out WTWa CO_2 equivalent emission performance of several renewable jet fuel pathways and analyses the effect of different co-product allocation process. The WTWa CO_2 equivalent values for different renewable jet pathways are summarised in Table 8.1. The authors find that FT pathway enables the highest reduction of GHG emission (86 – 104%) compared to conventional jet fuel. The authors highlight that renewable jet fuel could significantly reduce aviation-related GHG emissions if correct pathways and/or feedstock are used. Additionally, the authors note that the GHG emission performance of renewable jet fuel could be further improved by employing carbon capture and storage, and using sustainable hydrogen sources, in the fuel production.

In 2021, ICAO published/updated the default life cycle emissions values for carbon offsetting and reduction scheme for international aviation (CORSIA) eligible fuels [301], based on study [302]. For these CORSIA values, three different parameters are used that measure embodied carbon for a given fuel. The first measure is called direct or core lifecycle emissions which is attributable to upstream phase of fuel manufacturing (feedstock production and fuel conversion), transport, and the use-phase of the fuel. The second measure is indirect land-use change or ILUC that comprises of indirect GHG emissions considering land-use effects. The ILUC emissions are associated with crop-based feedstocks which maybe attributable to by-products, waste, and residues if these are deflected from the present utilisation. Such effects may be important, especially if the economic relationships of the feedstocks are closely related with vegetable oils. The third

measure is called carbon intensity or net emissions, which is a sum of the first and the second measure i.e., sum of direct lifecycle emissions and ILUC emissions. These default values are calculated based on the core lifecycle emissions and ILUC emissions, for selected feedstocks and pathways in different country, region and/or globally, and are summarised in Table 8.2. The lowest net emissions (WTWa) are observed for FT fuel (-22.5 g/MJ CO_2 equivalent) produced from miscanthus in the USA.

A review study by Kolosz et al. [303] compares the WTWa performance metrics of different studies on 'drop in' fuels which include biofuels (first, second, and third generation) and different fossil fuel based jet fuel (from coal, oil sands, oil shale, natural gas, etc.). The review study highlights the uncertainty during fuel production and combustion at high altitudes. The study points out next generation fuels such as oleaginous yeasts, alcohols, and low-carbon fuels – LH_2, LNG, and LNH_3, and the need to examine these fuels on WTWa basis, in future studies.

A report by Van Der Sman et al. [304] reviews cost of sustainable aviation fuels (biofuels and PtL) and their carbon reduction potential in EU, in addition to reviewing literature on other industry strategies for decarbonising aviation. The authors report that PtL has higher embodied carbon reduction potential as compared to biofuels but has significantly higher cost. For example, jet fuel produced from used cooking oil (HEFA) and hydrothermal liquefaction (separately) will cost 1.9 – 2.7 times higher and PtL will cost 2.2 – 6.4 times higher, compared to Jet-A.

The study by Koroneos et al. [305] (based on the Cryoplane project) conducted a comparative WTWa performance examination of a small aircraft from the A320 family (3,360 km range, 124 passengers) powered by LH_2 and Jet-A (separately) considering effects such as greenhouse, acidification, eutrophication, and winter smog. This analysis is conducted using GEMIS (global emission model for integrated systems) database. The authors examine a smaller aircraft, though it is relevant to this chapter (LTA aircraft) in terms of high-level objectives, is less recent (early 2000s) and considers fewer ways of producing LH_2. Also, the authors do not consider the effect of contrails cirrus in their WTWa analysis. The authors consider energy source like solar photovoltaics, solar thermal, wind, biomass, hydropower, and natural gas, for hydrogen production. The authors emphasise the significance of producing LH_2 from renewable energy sources such as wind energy and hydropower, especially considering their negligible environmental impacts. However, the authors also point the need to produce LH_2 from these sources cost-effectively while ensuring the fuel demands are met.

A study by Pereira et al. [296] compares LH_2, LNG, and Jet-A on a WTWa basis, where LH_2 is produced from four separate pathways – steam methane reformation, solar PV, wind energy, and hydropower. This comparison is carried out for both small (A320 type) and large aircraft (A340 type). The authors use a combination of existing models (GREET and GEMIS) for the WTP phase emissions modelling and existing EMEP/EEA dataset for the PTWa phase. The methodology does not consider the poor volumetric energy density characteristics of LH_2 which penalises aircraft energy performance. The aircraft use-phase energy consumption and/or emissions have a significant impact on the WTWa performance. Also, the authors do not consider the effect of contrails cirrus in their WTWa analysis. The authors observe that renewable hydrogen is the less polluting option, particularly from hydropower or wind energy. Additionally, manufacturing LH_2 from renewable energy sources has benefits both in terms of WTWa energy consumption, and environmental and

social impacts. The authors point out the need to examine renewable LH$_2$ production cost, since the market penetration of this fuel depends on its cost effectiveness.

Table 8.2. CORSIA default values based on the core lifecycle emissions and indirect land use change emissions (source [301], [302])

Fuel Conversion Process	Region	Fuel Feedstock	Core LCA Value	Indirect land use change LCA Value	Net emissions (gCO$_2$e/MJ)
HEFA	Global	Tallow	22.5	0	22.5
	Global	Used cooking oil	13.9		13.9
	Global	Palm fatty acid distillate	20.7		20.7
	Global	Corn oil (from dry mill ethanol plant)	17.2		17.2
	USA	Soybean oil	40.4	24.5	64.9
	Brazil	Soybean oil	40.4	27	67.4
	EU	Rapeseed oil	47.4	24.1	71.5
	Malaysia and Indonesia	Palm oil – closed pond	37.4	39.1	76.5
	Malaysia and Indonesia	Palm oil – open pond	60	39.1	99.1
	Brazil	Brassica carinata (grown as a secondary crop that avoids other crops displacement)	34.4	-20.4	14
	USA	Brassica carinata (grown as a secondary crop that avoids other crops displacement)	34.4	-21.4	13
FT	Global	Agricultural residues	7.7	0	7.7
	Global	Forestry residues	8.3		8.3
	Global	Municipal solid waste (MSW), 0% non-biogenic carbon (NBC)	5.2		5.2
	Global	MSW (NBC given as a percentage of the non-biogenic carbon content)	NBC*170.5 + 5.2		NBC*170.5 + 5.2
	USA	Poplar (short-rotation woody crops)	12.2	-5.2	7

	USA	Miscanthus (herbaceous energy crops)	10.4	-32.9	-22.5
	EU	Miscanthus (herbaceous energy crops)	10.4	-22	-11.6
	USA	Switchgrass (herbaceous energy crops)	10.4	-3.8	6.6
Alcohol (ethanol) to jet (ETJ)	Brazil	Sugarcane	24.1	8.7	32.8
	USA	Corn grain	65.7	25.1	90.8
	Global	Agricultural residues (standalone conversion design)	39.7	0	39.7
	Global	Agricultural residues (integrated conversion design)	24.6		24.6
	Global	Forestry residues (standalone conversion design)	40		40
	Global	Forestry residues (integrated conversion design)	24.9		24.9
	USA	Miscanthus (herbaceous energy crops) standalone conversion design	43.3	-42.6	0.7
	USA	Miscanthus (herbaceous energy crops) integrated conversion design	28.3	-42.6	-14.3
	EU	Miscanthus (herbaceous energy crops) standalone conversion design	43.3	-23.3	20
	EU	Miscanthus (herbaceous energy crops) integrated conversion design	28.3	-23.3	5
	USA	Switchgrass (herbaceous energy crops)	43.9	-10.7	33.2

		standalone conversion design			
	USA	Switchgrass (herbaceous energy crops)	28.9	-10.7	18.2
		integrated conversion design			
Alcohol (isobutanol) to jet (ATJ)	Global	Agricultural residues	29.3	0	29.3
	Global	Forestry residues	23.8		23.8
	Brazil	Sugarcane	24	7.3	31.3
	USA	Corn grain	55.8	22.1	77.9
	USA	Miscanthus (herbaceous energy crops)	43.4	-54.1	-10.7
	EU	Miscanthus (herbaceous energy crops)	43.4	-31	12.4
	USA	Switchgrass (herbaceous energy crops)	43.4	-14.5	28.9
Synthesised iso-paraffins	Brazil	Sugarcane	32.8	11.3	44.1
	EU	Sugar beet	32.4	20.2	52.6

Bicer et al. [47] conducts a WTWa evaluation of a small twin aisle aircraft of conventional tube-wing architecture (such as the Boeing 767) with a flight range of 5,600 km, where the aircraft is operated by Jet-A, LH_2, LNG, LNH_3, ethanol, and methanol (separately). It is to be noted that the authors use SimaPro software (with Ecoinvent database), which is a lifecycle assessment software, for their analysis. The methodology does not consider the poor volumetric energy density characteristics of LH_2 which penalises aircraft energy performance that has a significant impact on the WTWa performance. Also, the authors do not consider the effect of contrails cirrus in their WTWa analysis. The fuels are examined considering aspects such as land use, GWP, ozone layer depletion, abiotic depletion, and human toxicity. For both LH_2 and LNH_3, the authors evaluate renewable energy sources for fuel manufacturing that include hydropower, geothermal, solar, and wind energy, and for LH_2 the production pathway of underground coal gasification with carbon capture storage is also examined. The authors find that LH_2 when manufactured from geothermal energy could be preferred route than LNH_3 (from geothermal), other alternatives, and Jet-A on WTWa basis in terms of GWP.

Similarly, a study by Ratner et al. [306] provides the WTWa performance of a small aircraft (1,667 km range, 190 passengers) powered by battery and fuel cell (separately), where the electricity and LH_2 are produced from different sources. The authors use Ecoinvent LCA dataset for their analysis and it is unclear (not explicit) whether the (negative) volumetric effects of LH_2 are considered in the aircraft energy modelling. The methodology is either not clear from the information supplied or do not consider the poor volumetric energy density characteristic of LH_2 which penalises aircraft energy performance. The aircraft use-phase energy consumption and/or emissions have a significant impact on the WTWa performance. Also, the authors

do not consider the effect of contrails cirrus in their WTWa analysis. The authors provide comparison of 13 different alternative cases with metrics such as oxidation and eutrophication potential, climate impact, ecotoxicity, and land use, along with their cost. The authors find that electric aircraft powered by electricity produced from wind energy could reduce the aircraft's climate impact, compared to Jet-A, while being the most cost-effective solution of all alternatives and of similar magnitude as that of Jet-A. The analysis is simplistic in nature and is limited to fewer pathways/sources of producing electricity and LH_2, for a small aircraft with short range.

A study by Siddiqui et al. [307] conducts comparative WTWa performance examination of a passenger aircraft (range and passengers not known) powered by LH_2, LNH_3, ethanol, methanol, dimethyl ether, biodiesel, and Jet-A (separately). The fuels are examined considering aspects such as greenhouse effect, ionising radiation potential, terrestrial acidification, freshwater eutrophication, photochemical ozone formation, particulate matter, freshwater ecotoxicity, human carcinogenic toxicity, and land use occupation. For LH_2 and LNH_3, the authors examine renewable energy sources for fuel production such as hydropower, geothermal, solar, and wind energy. This analysis is conducted using SimaPro software using Ecoinvent database. The methodology is either not clear from the information supplied or do not consider the poor volumetric energy density characteristic of LH_2 which penalises aircraft energy performance. The aircraft use-phase energy consumption and/or emissions have a significant impact on the WTWa performance. Also, the authors do not consider the effect of contrails cirrus in their WTWa analysis. The authors find that LH_2 when produced from geothermal energy, performs better than LNH_3 (from geothermal), other alternatives, and Jet-A, on WTWa basis in terms of greenhouse effect. The authors point out the need of manufacturing LH_2 from renewable energy sources cost-effectively while simultaneously ensuring that the required fuel demand is met.

In a thesis by Miller [308], a slightly more detailed WTWa analysis of alternative aviation fuels (LH_2 and biofuels) is conducted, compared to above studies. The metrics used for this comparative WTWa analysis are climate impacts and air quality, water consumption in fuel manufacturing stage, and in non-use phase it estimates acidification, eutrophication, respiratory effects, and smog. This study encompasses aircraft and airport emissions (construction and use-phase) and considers a simplistic estimation of effect of contrails toward climate impacts. The methodology of the thesis for the WTWa emissions analysis is eclectic as the authors use published models for different segments of the lifecycle. For example, the author uses GREET model for the fuel manufacturing phase emissions. The author uses all available LH_2 production pathways in GREET, and for biofuel only FT, HEFA, and ATJ are used. The study by Miller, though is slightly more detailed compared to the above studies as it consider tens of several feedstocks and/or pathways for LH_2 and biofuels along with the effect of contrails cirrus in WTWa analysis, it misses out on PtL or electro-fuels and STJ fuel, and the WTWa results are limited only to short or medium range aircraft. The author provides analysis in the use-phase for different aircraft size at 930 km range (500 nmi) and further examines a Boeing 787-800 type for a 6,500 km range (3,500 nmi), for its WTWa performance. The author observes that the WTWa performance of combustion based LH_2 aircraft is strongly dependent on the fuel production pathway. LH_2 produced from renewable energy sources (wind, hydroelectric, and geothermal) are strong contenders but scalability is a concern. Additionally, the author points out the need for further evaluation of contrail cirrus

effect of LH$_2$ aircraft to refine the WTWa estimates and help decision making towards LH$_2$ powered aviation investments.

A study by Mukhopadhaya et al. [127] evaluates the performance of regional and small range LH$_2$ aircraft along with cost analysis and embodied carbon. The authors model the LH$_2$ aircraft while considering its poor volumetric energy density characteristic along with the effect of cryogenic tank gravimetric index, which penalises the energy performance. The authors compare the embodied carbon and cost per revenue passenger km of LH$_2$ (blue and green) and e-kerosene (PtL) with Jet-A for 2035 and 2050 timeframe in EU and USA. However, the authors consider fewer ways of LH$_2$ production and do not consider the effect of contrails cirrus in their WTWa analysis for the fuels considered. The authors find that the cost of powering aircraft with green hydrogen is expected to be more than Jet-A but lesser than e-kerosene or blue hydrogen. Also, if carbon pricing is included then green LH$_2$ could be cost competitive with Jet-A or cost lesser. Additionally, to maximise the climate impact reduction potential for LH$_2$ aircraft and enable successful penetration of green hydrogen (low embodied carbon) in aviation, there is a need to account the life cycle effects appropriately along with policies. Moreover, for LH$_2$ aircraft to be successful, the above efforts need to be complemented with supportive government policies such as low-carbon fuel standards, alternative fuel mandates to bridge the cost gap with Jet-A, carbon pricing, and/or bolstering fuel efficiency policies, to enable required investments for fostering R&D, design, testing, and establishing infrastructure for LH$_2$ production, distribution, and storage.

The FlyZero report [128] studies different fuels and propulsion type (with technology improvement in 2040 timeframe) and compares them on WTWa basis, for regional short-range to midsize medium range aircraft. In terms of fuels and propulsion type, the study examines LH$_2$ (fuel cell and combustion based, considering performance penalty due to installation of cryogenic tank), PtL, and biofuel. The study reports the climate impact due to contrail cirrus along with the climate impacts due to NO$_x$, H$_2$O, and CO$_2$ in the use-phase, and emissions in the fuel manufacturing phase. The study uses a combination of models for the lifecycle analysis which includes use of SimaPro software (hydrogen) and CORSIA values (for biofuels). The FlyZero report accounts the performance penalty due to cryogenic tank installation and the impact of contrail cirrus in their WTWa analysis of LH$_2$, PtL, and biofuel for small to mid-size aircraft. However, their analysis is limited to a few selected feedstocks and/or pathways of manufacturing LH$_2$, PtL, and biofuel. LH$_2$ is assumed to be produced only from renewable electricity and biofuels manufactured using a mix of feedstocks from CORSIA eligible fuels (limited feedstocks only). Overall, the study finds that both combustion-based and fuel-cell powered LH$_2$ aircraft are preferred candidates as their WTWa CO$_2$ equivalent emissions are lesser than other alternatives and Jet-A fuel, except for very-short range where electric aircraft would be preferred vehicles.

The above limitations in literature further motivate this chapter. These gaps are addressed in this chapter where a WTWa analysis of an LTA long-range aircraft is conducted. The energy consumption modelling for future (N+2 timeframe) BWB aircraft powered by LH$_2$ and 100% SPK (biofuel and PtL) (separately) is conducted in Chapters 6 and 7, where the performance penalty due cryogenic tank installation is considered for LH$_2$ aircraft modelling. In this chapter, over 100 different ways in total for producing LH$_2$, PtL, and biofuel are examined. The methodology is discussed in the next section.

8.3 Methodology

The WTWa emissions or performance of any fuel is the summation of emissions during the fuel manufacturing stage (from raw material extraction stage to its transportation and storage at fuel pump) and the operational phase of the aircraft. The fuel manufacturing stage is referred to as WTP and operational phase of aircraft is referred to as PTWa. In this chapter, its assumed that for all fuels the pump to aircraft tank emissions and/or leakages are zero. Figure 8.1 shows the schematic of WTWa emissions calculation process from WTP and PTWa emissions, used in this chapter. Referring to Figure 8.1, the latest WTWa CORSIA default values (2021), are available directly from literature and these are listed in Table 8.2 (in section 8.2). It is to be noted that the CORSIA default values are limited to a few feedstocks and/or pathways for biofuels. The methodology for WTWa emissions calculation is split into WTP and PTWa as separate models or estimation procedures are required. The methodology for estimating WTP and PTWa is discussed separately in section 8.3.1 and 8.3.2, respectively.
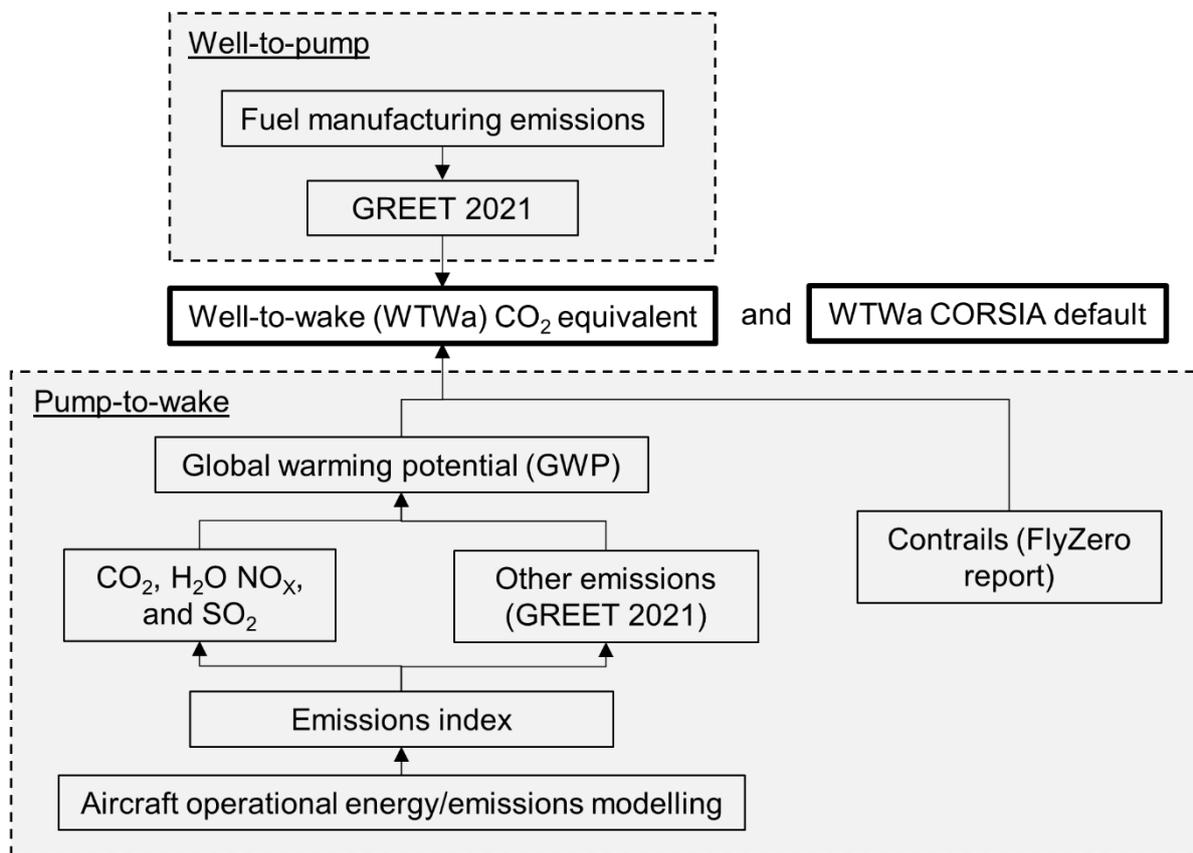
Figure 8.1. Schematic of WTWa emissions calculation process from WTP and PTWa emissions

8.3.1 Fuel production phase (WTP) emissions

Referring to Figure 8.1, the GREET 2021 model is used for making a database of fuel manufacturing phase emissions for LH_2 and 100% SPK (biofuel and PtL). The GREET model is documented extensively in literature (report, articles, manual, etc.) and the list of publications can be found in resource [309]. It is to be noted that the GREET model is USA specific, and thus is a limitation of this work. For both LH_2 and 100% SPK, a wide range of manufacturing pathways and/or feedstocks are examined. For a fuel under consideration,

not all feedstocks and/or pathways are considered for whole WTWa analysis. Most feedstocks and/or pathways are screened out based on their WTP performance for computational compactness and ease. Additionally, a few parameters are identified from literature to which the WTP emissions are sensitive, and these parameters are varied in GREET, for each fuel type under examination, and these are discussed in detail next.

8.3.1.1   LH$_2$

Table 8.3 lists the different feedstock and/or pathways for producing hydrogen at centralised manufacturing unit with or without carbon sequestration facility and type of liquefication used. These are in total 59 different ways LH$_2$ can be produced from centralised manufacturing units in the USA as simulated using GREET 2021 model [33].

There are two assumptions/models for hydrogen production in GREET 2021: (a) H2A model of National Renewable Energy Lab, USA (b) Industry data. 59 cases (and Jet-A) are simulated for both hydrogen production assumptions, wherever applicable and available. For example: Industry data assumptions are applicable/available in GREET 2021 for all 59 cases except four cases: (a) North American natural gas (NANG) with carbon sequestration (w CS) and hydrogen liquefication using US mix electricity (LUSME); (b) renewable natural gas (RNG) w CS LUSME; (c) NANG w CS and liquification using power from natural gas combined cycle (LNGCC); (d) RNG w CS LNGCC. Similarly, H2A model assumptions are applicable/available in GREET 2021 for all 59 cases except 18 cases: six feedstocks each (willow, poplar, switchgrass, corn stover, forest residue, and miscanthus) for biomass manufacturing plant type w CS for both LUSME type and hydrogen liquefied using electricity from biomass integrated gasification combined cycle (LBIGCC), and six feedstocks (same as above) with integrated fermentation manufacturing plant type w CS.

In the results section (8.4), for each of the 59 manufacturing cases, the sensitivity of the selection of model assumptions (H2A or industry data) is reflected as a range of values. This is the first sensitivity parameter. Additionally, each of the 59 manufacturing cases (and Jet-A) with respective manufacturing model assumptions is simulated for year 2020 and 2050. This is essentially to check the sensitivity of US energy mix, the second sensitivity parameter, on LH$_2$ WTWa emissions. The energy mixes for both 2020 and 2050 are listed in Table 8.4. According to Table 8.4, the USA energy mix in 2050 is expected to be dominated by more renewable energy sources, especially solar energy (photovoltaics). The different processes of manufacturing LH$_2$ and 100% SPK routes are discussed in Appendix D (section D.1).

The objective of this thesis is to find solutions for making long-range flight climate neutral. Thus, after examining 59 cases, only the LH$_2$ manufacturing options that provide near-zero and/or negative CO$_2$ equivalent emissions are considered for further WTWa analysis.

Table 8.3. List of different feedstocks and/or pathways of producing hydrogen at centralised manufacturing unit with or without carbon sequestration facility and type of liquefication used

Type of LH$_2$	Pathways/Feedstock	Carbon sequestration (CS)	Liquefication type
Grey	Coal	Without (w/o) CS	Liquefied using US mix electricity (LUSME)
			Liquification using electricity from coal integrated gasification combined cycle (LCIGCC)
		With (w) CS	LUSME
			LCIGCC
	Coke oven gas (COG)	-	LUSME
			LCIGCC
Blue	North American Natural Gas (NANG)	w/o CS	LUSME
			Liquification using power from natural gas combined cycle (LNGCC)
		w CS	LUSME
			LNGCC
	H$_2$ as a by-product of natural gas liquid (NGL) steam cracking (SC)	-	LUSME
Green	Renewable natural gas (RNG)	w/o CS	LUSME
			LNGCC
		w CS	LUSME
			LNGCC
	Solar photovoltaics (PV)	-	LUSME
		-	Liquefication using electricity from solar energy (L-Solar)
	Nuclear thermochemical cracking of water (TCCW)	-	Liquefication using electricity from nuclear energy (L-Nuclear)
	Nuclear high temperature gas reactor (HTGR)	-	LUSME
			L-Nuclear
	Biomass Willow	w/o CS	LUSME
	Poplar		
	Switchgrass		
	Corn stover		
	Forest residue		
	Miscanthus		
	Biomass Willow		Liquification using electricity from biomass integrated
	Poplar		
	Switchgrass		

			gasification
	Corn stover		combined cycle
	Forest residue		(LBIGCC)
	Miscanthus		
Biomass	Willow	w CS	LUSME
	Poplar		
	Switchgrass		
	Corn stover		
	Forest residue		
	Miscanthus		
Biomass	Willow		LBIGCC
	Poplar		
	Switchgrass		
	Corn stover		
	Forest residue		
	Miscanthus		
Integrated	Willow	w/o CS	LUSME
fermentation	Poplar		
(Biomass)	Switchgrass		
	Corn stover		
	Forest residue		
	Miscanthus		
	Willow	w CS	
	Poplar		
	Switchgrass		
	Corn stover		
	Forest residue		
	Miscanthus		
High temperature electrolysis with solid oxide electrolysis cell (HTE SOEC) using electricity from Nuclear HTGR for electrolysis		-	LUSME
HTE SOEC using electricity from natural gas combined cycle (NGCC) for electrolysis			
H_2 produced as a by-product of chlorine manufacturing plant (By-product Cl plant)			

Table 8.4. US energy mix in 2020 and 2050 – share of different energy sources for electricity production (stationary use)

2020 USA energy mix [33]				2050 USA energy mix [310]			
Source	%	Others source	%	Source	%	Others source	%
Residual oil	0.4	Hydroelectric	38.1	Residual oil	0.0%	Hydroelectric	13.0%
Natural gas	39.6	Geothermal	2.1	Natural gas	36.0%	Geothermal	2.0%
Coal	20.0	Wind	45.9	Coal	11.0%	Wind	34.0%
Nuclear power	20.4	Solar PV	11.4	Nuclear power	11.0%	Solar PV	47.0%
Biomass	0.3	Miscellaneous	2.5	Biomass	0.0%	Miscellaneous	4.0%
Others	19.4			Others	42.0%		

8.3.1.2   100% SPK

8.3.1.2.1   Preliminary shortlisting of feedstocks and pathways

In this section, four SPK fuel pathways are examined using the GREET 2021 model, where the 100% SPK fuel is produced from different feedstocks and manufacturing schemes. These are ATJ, STJ, HRJ or HEFA, and FT. For each of the four SPK fuel pathways, different feedstocks and manufacturing schemes are evaluated. Table 8.5 and Table 8.6 list different feedstocks and manufacturing schemes for 100% SPK produced from ATJ (18 cases) and STJ (24 cases), and FT (eight cases) and HEFA (four cases each of food and non-food crops) pathways, respectively.

Table 8.5. List of different feedstocks and manufacturing schemes for 100% SPK produced from ATJ and STJ pathways

ATJ schemes and feedstocks (18 cases)		STJ schemes and feedstocks (24 cases)	
Feedstocks in standalone (S.) scheme	Feedstocks in distributed (D.) scheme	STJ manufacturing schemes	Feedstocks for each of the four STJ manufacturing schemes
Corn with dry mill (CDM)	Corn US mix (CUSM)	Biological plant type (B.)	Poplar
Poplar	Corn dry mill without extraction (CDMWOE)	Catalytic with external H_2 plant type (CWEH.)	Forest residue
Forest residue	Corn dry mill with extraction (CDMWE)	Catalytic with in-situ H_2 plant type (CWIH.)	Miscanthus
Miscanthus	Corn wet mill (CWM)	Catalytic with H_2 from biomass gasification plant type (CWHBG.)	Switchgrass
Switchgrass	Poplar		Willow
Willow	Forest residue		Corn stover
Corn stover	Miscanthus		
	Switchgrass		
	Willow		
	Corn stover		
	Solid waste		

Table 8.6. List of different feedstocks and manufacturing schemes for 100% SPK produced from FT and HEFA pathways

FT feedstocks (8 main cases)	HEFA feedstocks (8 cases)
North American (NA) natural gas (NANG),	Food-crops
Non-NA natural gas (non-NANG)	Soybean
Non-NA flared gas (non-NAFG)	Palm FFB (fresh fruit bunch)
Biomass*	Canola
Coal	Corn oil
Coal (50%) + biomass* (50%) (share by mass)	Non-food feedstocks
Natural gas (50%) + biomass* (50%) (share by mass)	Algae
Electro-fuel (or PtL)	Camelina
*Poplar, forest residue, miscanthus, switchgrass, willow, corn stover	Jatropha
	Carinata

For HEFA, though there are eight feedstocks in total that are considered purely as an academic exercise in Table 8.6, only four non-food crops will be considered as feedstocks for fuel production in this chapter for further consideration. This is because there is a social aspect attached to using food crops for fuel production. In total there are 54 different ways (58 ways if food crops are included) in which 100% SPK can be produced using the above four pathways and feedstock combinations. These 54 manufacturing options are examined and only the options that provide lowest or negative CO_2 equivalent emissions for each of the four pathways are considered for sensitivity analysis (discussed next) and further WTWa analysis.

8.3.1.2.2 Manufacturing emissions sensitivity to identified parameters

According to the study by Pavlenko et al. [311], hydrogen is one of the important component required in the SPK fuel manufacturing process and therefore it contributes significantly to the lifecycle GHG emissions of SPKs, especially for HEFA and STJ pathways. Additionally, the use of green hydrogen for producing SPKs could be useful to reduce the lifecycle greenhouse gas emissions (ibid). From the exercise on LH_2 discussed in section 8.3.1.1, the feedstocks/pathways that enable a near-zero or negative emissions fuel production are used for this sensitivity analysis. For example, if solar-PV and biomass routes of hydrogen production are shortlisted via the approach detailed in section 8.3.1.1, then these routes will be used for producing the required hydrogen in the manufacturing process of a given SPK pathway. In the results section (8.4), for each of the shortlisted SPK fuel manufacturing case, the sensitivity of the hydrogen production route for manufacturing SPK fuel, is reflected as a range of values. The hydrogen production route for manufacturing SPK fuel is the first sensitivity parameter.

Additionally, similar to the exercise for LH_2, the WTP emissions for SPKs are simulated for year 2020 and 2050 (more renewable energy sourcing), and this is useful in the estimation of the sensitivity of US energy mix, the second sensitivity parameter, on 100% SPK WTWa emissions.

8.3.2 Operational phase (PTWa) emissions

Chapters 4 to 7 provide four LH_2 aircraft employing different aviation technologies (present and future) and their energy consumption metrics. These are as follows:

- LH_2 aircraft 1 (tube-wing) – 29% more SEC compared to the A350 Jet-A aircraft (baseline) (known from global sensitivity analysis in Chapter 5)
- LH_2 aircraft 2 (tube-wing) – 11% more SEC than A350 Jet-A aircraft (nominal case from Chapter 4)
- LH_2 aircraft 3 (tube-wing) – 33% less SEC than A350 Jet-A aircraft (from global sensitivity analysis in Chapter 5)
- LH_2 aircraft 4 (BWB) – 53.5% less SEC than B777 Jet-A or 48.5% less SEC than A350 Jet-A aircraft (from Chapter 7). This is case 3 or most optimised LH_2 aircraft in Chapter 7

The WTWa emission would be reduced the most using aircraft 4 (modelled in Chapter 7) as the aircraft shows highest SEC reduction compared to the baseline, in addition to the reduction in associated direct operating or fuel costs. Additionally, the engine cycle parameters required for PTWa emissions modelling are

known for the aircraft. Therefore, for the PTWa emissions estimation the BWB aircraft (Jet-A, 100% SPK, and LH$_2$) modelled in Chapter 7 will be considered.

8.3.2.1   NO$_x$

As discussed in Chapter 6, the LDI combustor type is used in the BWB aircraft (Jet-A, 100% SPK, and LH$_2$). In terms of NO$_x$ emission modelling, EI estimation process for NO$_x$ is known from the study by Marek et al. [228], which is based on experiments conducted by NASA. The $EI_{NOx,Jet-A}$ (grams NO$_x$ per kg fuel) i.e., emissions index for Jet-A LDI combustor is given by equation 8.1,

$$EI_{NOx,Jet-A} = A'(143P_3)^{0.594}e^{\left((T_3-255)/194\right)}\left(\frac{f}{a}\right)^{1.6876}\left(100\frac{\Delta P}{P}\right)^{-0.56}, \tag{8.1}$$

where A', P_3 (MPa), T_3 (K), $\frac{f}{a}$, and $\frac{\Delta P}{P}$ (%) are correlation constant for emission index based on Jet-A fuel, combustor inlet pressure, combustor inlet temperature, fuel to air ratio, and fuel injector air flow pressure drop ratio, respectively. A' is 14 for advanced LDI technology, and P_3, T_3, and $\frac{f}{a}$ are known from Chapter 6 (GasTurb engine modelling for engines powered by different fuels). A nominal value of 4% for $\frac{\Delta P}{P}$ is used for the combustor design (for both Jet-A and hydrogen) as reported by Marek et al. [228] and is used in this chapter for NO$_x$ modelling. It is assumed in this chapter that equation 8.1 is also applicable to 100% SPK, and respective P_3, T_3, and $\frac{f}{a}$ are used (known from Chapter 6).

For hydrogen, C4 type of LDI combustor configuration (refer Chapter 6 section 6.3.3.5 and Appendix B section B.3 for details about all configurations) is used in this chapter for emissions modelling, as according to Marek et al. [228], it was the only configuration that performed the best from a low NO$_x$ and durability criteria. For hydrogen, NO$_x$ is estimated is in terms of ppm_{NOx} in the study by Marek et al. [228]. The calculation of ppm_{NOx} for hydrogen LDI combustor is given by equation 8.2,

$$ppm_{NOx} = A(143P_3)^a\left(\phi_{H_2}\right)^b(\tau)^c e^{\left((1.8T_3-460)/d\right)}\left(\frac{\Delta P}{P}\right)^e, \tag{8.2}$$

where A, a, b, c, d, and e are correlation constants for emission index based on hydrogen data, and ϕ_{H_2} and τ are hydrogen equivalence ratio and combustor residence time, respectively. For C4 configuration, the values of A, a, b, c, d, and e are known to be 9.355, 0.275, 4.12, 0.455, 211, and -0.288 respectively. ϕ_{H_2} is calculated from the fuel to air ratio according to the definition in Chapter 6. The fuel to air ratio and τ are known from Chapter 6 (GasTurb engine modelling). The generic equation for the estimation of EI_{NOx} from ppm_{NOx} is given by equation 8.3,

$$EI_{NOx} = \frac{1}{1000}\frac{MW\ of\ NO_2}{MW\ of\ combustion\ products}\frac{(1+f/a)}{f/a}ppm_{NOx} \tag{8.3}$$

where MW is the molecular weight for respective species. The MW of NO_2 is 46 and for the combustion products it is calculated using the 'major species' combustion model as described in Chapter 6. Therefore,

once ppm_{NOx} is calculated using equation 8.2, the EI_{NOx} can be estimated using equation 8.3 for a given fuel case where the f/a is known.

It is to be noted that equations 8.1 and 8.2 that estimate NO_x are applicable to typical temperature and pressure combination during cruise, according to Marek et al. [228]. Therefore, using equation 8.1, and equations 8.2 – 8.3 the cruise EI_{NOx} for Jet-A (and 100% SPK) and LH_2 aircraft can be calculated, respectively.

For estimating EI_{NOx} at other points in the flight mission, the 'DLR fuel flow correlation' method [312] is used which is dependent on pressure, temperature, and Mach number, for respective flight segment. After calculating cruise EI_{NOx}, the EI_{NOx} at SLS ($EI_{NOx,SLS}$) point can be calculated using the DLR method, where both EI_{NOx} are related by parameters that depend on flight altitude, ambient pressure and temperature, and flight Mach number. Thus, now knowing the $EI_{NOx,SLS}$, the EI_{NOx} at other flight points like engine start and warm up, taxi out, take-off, climb, descent and approach, loiter, landing, taxi in, and shutdown, can be calculated knowing the respective flight altitude, ambient pressure and temperature, and flight Mach number. The relation between $EI_{NOx,SLS}$ and EI_{NOx} at other flight points is given by equation 8.4,

$$EI_{NOx} = EI_{NOx,SLS} \, \delta_{total}^{0.4} \, \theta_{total}^3 e^H \, , \tag{8.4}$$

$$\text{where } \delta_{total} = \frac{p_{total}}{101325 \, Pa} , \tag{8.5}$$

$$\theta_{total} = \frac{T_{total}}{288.15 \, K} , \tag{8.6}$$

$$H = -19 \left(-0.00634 + 0.001 \, e^{-0.0001426 \, (h'-12900)} \right) , \tag{8.7}$$

$$p_{total} = p_{amb} \left(1 + \frac{(\gamma-1)}{\gamma} M^2 \right)^{\gamma/(\gamma-1)}, \text{ and} \tag{8.8}$$

$$T_{total} = T_{amb} \left(1 + \frac{(\gamma-1)}{\gamma} M^2 \right). \tag{8.9}$$

$p_{amb}, p_{total}, T_{amb}, T_{total}, M, \gamma, \delta_{total}, \theta_{total}, EI_{NOx,SLS}, H,$ and h' are ambient pressure (in Pa), total pressure (in Pa), ambient temperature (in K), total temperature (in K), flight Mach number, specific heat ratio (1.4 for air), pressure correction factor, temperature correction factor, NO_x emission index at SLS, humidity correction factor, and flight altitude (in feet), respectively.

$W_{F,block}$ (kg) for Jet-A, 100% SPK, and LH_2 (case 3) is known from Chapter 7 at different flight segments such as engine start and warm up, taxi out, take-off, climb, cruise descent and approach, loiter, landing, taxi in, and shutdown. After calculating EI_{NOx} for these segments, the quantity of NO_x (kg) emitted can be calculated. Table 8.7 lists the engine parameters required to estimate EI_{NOx} during cruise (in equations 8.1 – 8.3) for different fuel cases. Table 8.8 provides the operational conditions and fuel burn for different fuels at various flight segments needed for estimating EI_{NOx} (using equations 8.4 – 8.9). For estimating the speed of the aircraft during taxi out (20 knots [313]), take-off (150 knots [314], [315]), descent (average descent 250 knots [314]), and landing (155 knots approach-landing speed [314], [316]), the speed of present-day LTA aircraft are used (values in SI system in Table 8.8).

Table 8.7. Engine parameters required to estimate EI_{NOx} during cruise for different fuels (source: Chapter 6)

BWB fuel cases	P_3 (MPa)	T_3 (K)	f/a	ϕ	τ (ms)	MW of combustion products
Jet-A	2.11	838	0.0241	0.351	0.854	28.86
100% SPK	2.11	838	0.0236	0.343	0.854	
LH$_2$ (case 3)	2.16	843	0.0061	0.206	0.842	27.45

Table 8.8. Operational conditions and fuel burn for different fuels at various flight segments

	Altitude (m)*	p_{amb} (Pa)**	T_{amb} (K)**	Speed (m/s)	Mach**	Fuel burn (kg)***		
						Jet-A	100% SPK	LH$_2$
Engine start and warm-up	0	101,325	288.15	0	0	847	824	241
Taxi-out	0	101,325	288.15	10.29 [313]	0.03	844	821	241
Take-off	0	101,325	288.15	77.17 [314], [315]	0.23	420	409	120
Climb	5,334	51,652	253.48	149.19*	0.47	584	568	162
Cruise	10,668	23,842	218.81	248.10*	0.84	59,035	57,727	19,003
Descent and approach	5,334	51,652	253.48	128.61 [314]	0.44	626	612	216
Loiter	1,500	84,556	278.40	200.85*	0.60	2,678	2,623	894
Land, taxi-in and shutdown	0	101,325	288.15	79.74 [314], [316]	0.23	491	481	172

*known from Chapter 6

**calculated using source [317] for given altitude known from Chapter 6

***known from Chapter 7

8.3.2.2 CO$_2$, H$_2$O, sulphur dioxide, other emissions, and contrails

Table 8.9 lists the emission index of different species and contrails for the three fuels under consideration. CO$_2$, H$_2$O, and SO$_2$ emission vary linearly with fuel burn. The production of species like VOC, CO, PM$_{10}$ and PM$_{2.5}$, SO$_x$ (total), BC, OC, CH$_4$, and N$_2$O, after Jet-A and 100% SPK fuel combustion is not linearly dependent on fuel burn and its estimation requires detailed combustion physics-based modelling.

Future LDI combustors are expected to have significantly lesser emission index of these species. In this chapter, it is assumed that the emission index for these species in the future (N+2 timeframe) BWB remains similar to the present-day emission index listed in Table 8.9 for LTA aircraft. Similarly, contrail modelling requires detailed physics-based simulation which should capture the effects of nucleation particles and/or lubrication oil from the aircraft engine acting as nuclei for ice formation, presence of nucleation particles in atmosphere (concentration expected to vary with time), and interaction of engine wake and wing-tip vortices. In this chapter, the CO$_2$ equivalent (g/MJ) from the FlyZero report [128] for the three fuels is used and is listed in Table 8.9. The FlyZero report [128] provides the aircraft performance, inclusive of contrails, in 2040 technology timeframe for the three fuels.

Table 8.9. Emission index of different species and contrails for the three fuels

Species	Emission index (g/kg fuel)			Reference
	Jet-A	LH_2	100% SPK	
CO_2	3,158 [33]	0	3,092 [33]	[33]
H_2O	1,240 [284]	8937 [285]	1,370 [318]	[284], [285], [318]
SO_2	0.8 [284]	0	0 [33]	[33], [284]
VOC	0.17	0	0.17	[33]
CO	1.49	0	1.51	[33]
PM_{10}	0.20	0	0.02	[33]
$PM_{2.5}$	0.20	0	0.02	[33]
SO_x (total)	1.40	0	0.00	[33]
BC	0.06	0	0.00	[33]
OC	0.06	0	0.00	[33]
CH_4	1.18E-03	0	1.21E-03	[33]
N_2O	2.31E-03	0	2.37E-03	[33]
g/MJ				
Contrails	65	40	50	[128]

8.3.3 Global warming potential

Table 8.10. GWP of NO_x and H_2O at different mission segments

	Altitude (m)	GWP	
		NO_x	H_2O
Engine start and warm-up	0	-11 [33], [167]	0 [167]
Taxi-out	0	-11 [33], [167]	0 [167]
Take-off	0	-11 [33], [167]	0 [167]
Climb	5,334	9.17 [167]	0 [167]
Cruise	10,668	114 [11]	0.06 [11]
Descent and approach	5,334	9.17 [167]	0 [167]
Loiter	1,500	-11 [33], [167]	0 [167]
Land, taxi-in and shutdown	0	-11 [33], [167]	0 [167]

Table 8.10 lists GWP of NO_x and H_2O at different mission segments. The GWP of NO_x increases from a negative value at zero altitude to a positive value at 11 km altitude [167]. A thesis by Svensson [167] provides the variation of GWP of NO_x and H_2O with altitude. The GWP of H_2O is zero until 9 km (from zero altitude) and increases thereafter (ibid). For cruise the most recent GWP values for NO_x and H_2O from the study by Lee et al. [11] are used in this chapter and are listed in Table 8.10. At zero and low altitudes (< 2 km), the GWP of NO_x provided by GREET 2021 model [33] is used here. For altitude between 2 km and 10.67 km (cruise), the NO_x GWP provided in Svensson's thesis [167], is used in this chapter. Table 8.11 provides the GWP of all emissions in the WTP and PTWa phase.

Table 8.11. GWP of all emissions in the WTP and PTWa phase

Species	GWP	
	WTP	PTWa
NO_x	-11 [33]	Variable (see Table 10)
H_2O	0 [167]	Variable (see Table 10)
BC	900 [33]	1166 [11]
SO_2	-	-226 [11]
CO_2	1 [33]	1 [33]
VOC	5 [33]	5 [33]
CO	3 [33]	3 [33]
OC	-69 [33]	-69 [33]
CH_4	30 [33]	30 [33]
N_2O	265 [33]	265 [33]

8.3.4   Other unintended environmental and social impacts

In addition to the CO_2 and non-CO_2 effects of aircraft on climate, there are other metrics that should be considered and quantified. These include the use of fossil fuels, water consumption, and WTWa emissions that affect air-quality. The emissions that are considered include VOC, CO, NO_x, PM_{10}, $PM_{2.5}$, SO_x, BC, and OC. These emissions affect both the environmental and human health. It is assumed that the emission index for VOC, CO, PM_{10}, $PM_{2.5}$, SO_x, BC, and OC for the future (N+2 timeframe) BWB remains similar to the present-day emission index listed in Table 8.9 (section 8.3.2.2) for LTA aircraft. The use of fossil fuels (natural resource) has an environmental impact, and water consumption has both environmental and social impact. The WTWa data for VOC, CO, PM_{10}, $PM_{2.5}$, SO_x, BC, and OC is directly obtained from GREET 2021 model. WTWa NO_x is calculated from WTP NO_x obtained from GREET 2021, and PTWa NO_x calculated from methodology described in section 8.3.2. The data for use of fossil fuels and water consumption is directly obtained from GREET 2021 model.

8.4   Results and discussion

8.4.1 LH_2

Figure 8.2 shows the WTWa comparison of different LH_2 feedstocks and/or pathways (59 manufacturing cases) for 2020 and 2050 US energy mix (with only CO_2 emissions in PTWa phase). In this figure, for the WTP stage all greenhouse gas emissions are considered but for PTWa only CO_2 emissions are included. The other emissions and contrails are included in later in section 8.4.3. As discussed in section 8.3.1.1, sensitivity to two parameters is analysed. For each of the 59 manufacturing cases, the sensitivity of the selection of model assumptions (H2A or industry data) is reflected as a range of values. This is the first sensitivity parameter.
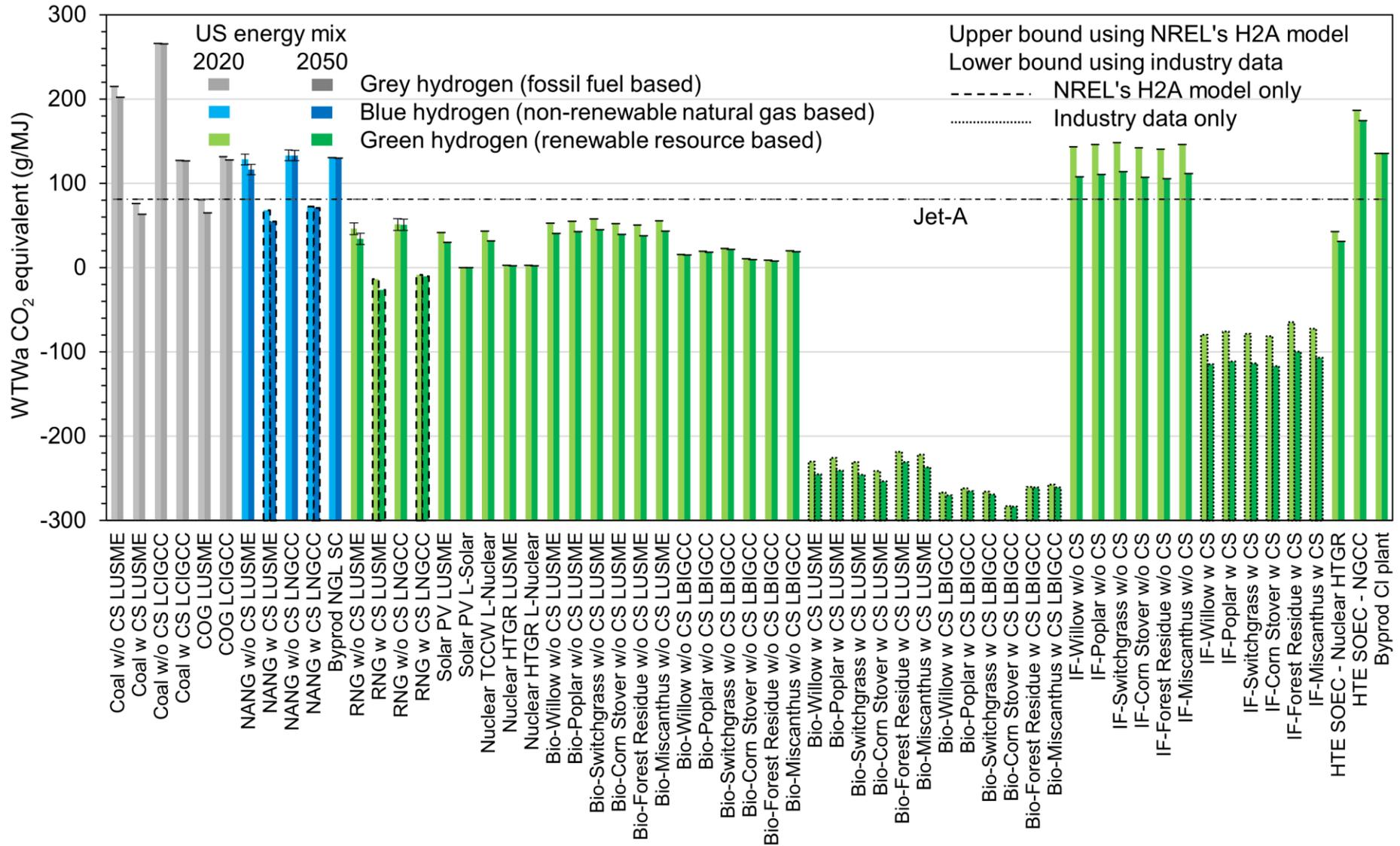
Figure 8.2. WTWa comparison of different LH₂ feedstocks and pathways for 2020 and 2050 (with only CO₂ emissions in PTWa phase)

217

Additionally, each of the 59 manufacturing cases (and Jet-A) with respective manufacturing model assumptions is simulated each for year 2020 and 2050 to check the sensitivity of US energy mix - the second sensitivity parameter, on LH_2 WTWa emissions.

It can be observed from Figure 8.2 that grey and blue hydrogen WTWa emissions are of the similar magnitude as that of Jet-A or more, regardless of the hydrogen production assumptions used or the energy mix type. Additionally, not all green hydrogen manufacturing cases have near zero or sub-zero WTWa CO_2 equivalent emissions. Certain manufacturing schemes like IF w/o CS, HTE SOEC – NGCC, and By-prod Cl plant have higher WTWa CO_2 equivalent emissions than Jet-A.

As discussed in section 8.3.1.1, only the LH_2 manufacturing options that provide near-zero and/or negative CO_2 equivalent emissions are considered for further WTWa analysis (including other emissions in PTWa and contrails). The LH_2 manufacturing cases that have near-zero and/or negative CO_2 equivalent emissions are RNG w CS LUSME, RNG w CS LNGCC, solar PV L-solar, nuclear HTGR LUSME, biomass w/o CS LBIGCC, biomass w CS LUSME, biomass w CS LBIGCC, and IF w CS. These eight cases will be considered for further WTWa analysis in section 8.4.3, that includes other emissions in PTWa and contrails.

8.4.2   100% SPK

8.4.2.1.1   Preliminary shortlisting of 100% SPK feedstocks and pathways
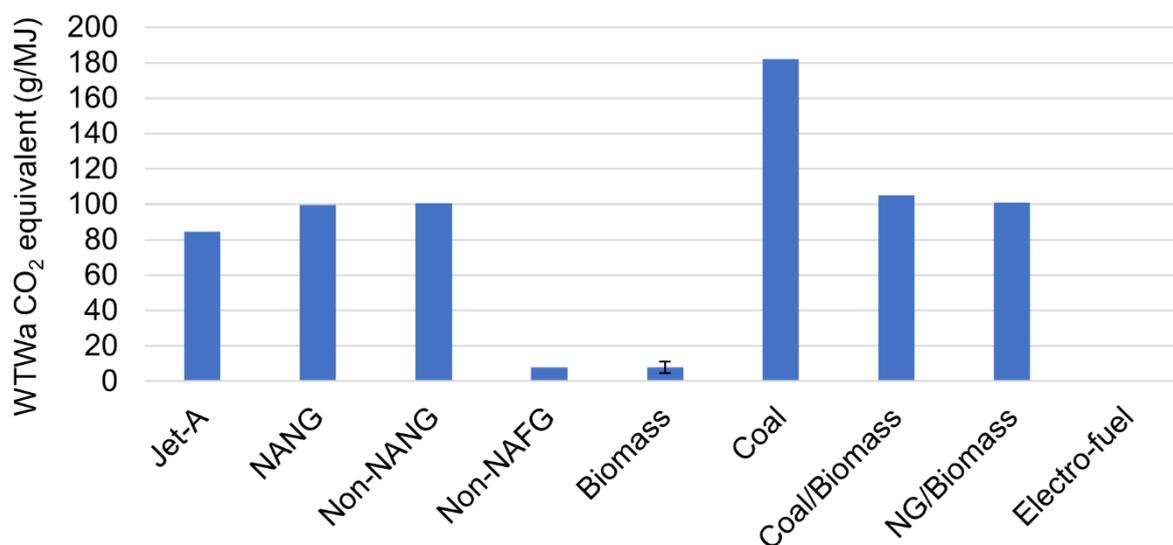
Figure 8.3. WTWa CO_2 equivalent emission comparison of different FT feedstocks for 2020 (with only CO_2 emissions in PTWa phase)

Figure 8.3, Figure 8.4, Figure 8.5, and Figure 8.6 provide the WTWa comparison of different FT, HEFA, ATJ, and STJ feedstocks, respectively, for 2020 (with only CO_2 emissions in PTWa phase). It can be observed from Figure 8.3 that electro-fuel (E-fuel) and biomass are the two feedstocks that have lowest (almost zero) WTWa CO_2 equivalent emissions and are shortlisted for further analysis. For biomass case, six feedstocks are considered that include willow, poplar, switchgrass, miscanthus, corn stover, and forest residue.

This is included as a range in Figure 8.3. Switchgrass has a poor performance whereas forest residue provides a greater reduction in WTWa CO_2 equivalent emissions and is thus considered as the default FT biomass-based feedstock for further analysis.
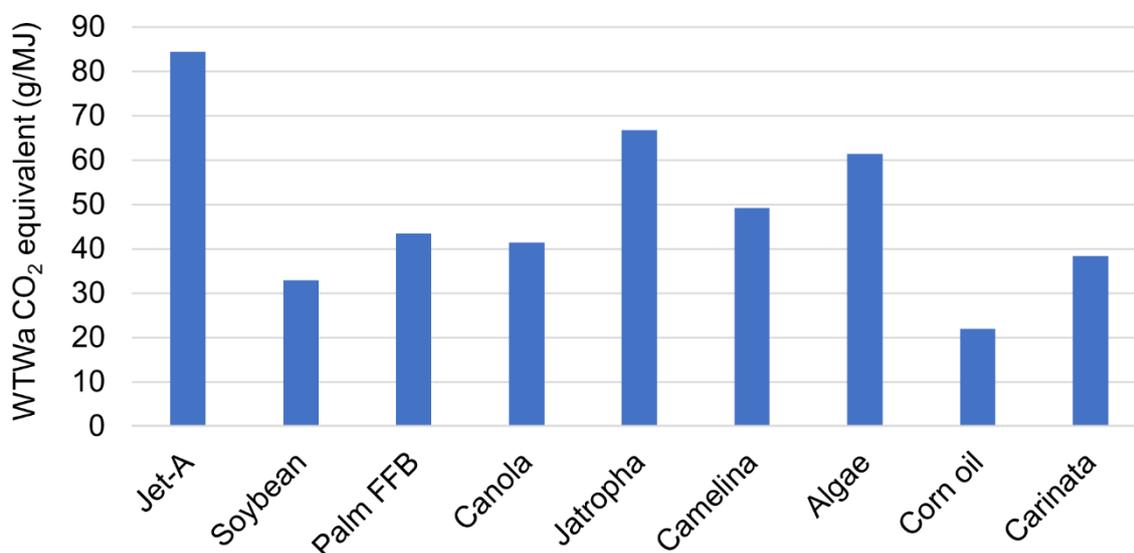
Figure 8.4. WTWa CO_2 equivalent emission comparison of different HEFA feedstocks for 2020 (with only CO_2 emissions in PTWa phase)

Similarly, it can be seen from Figure 8.4 that Carinata is the only non-food crop that has lowest WTWa CO_2 equivalent emissions of all HEFA feedstocks and is thus considered for further analysis. Ideally, corn oil has the lowest emissions but as discussed in section 8.3.1.2.1 only non-food crops are considered for analysis (due to the social impacts).

Referring to Figure 8.5, Miscanthus is the feedstock which provides lowest WTWa CO_2 equivalent emissions in both standalone and distributed ATJ production schemes (S.Miscanthus and D.Miscanthus) and are therefore shortlisted for further analysis. Similarly, it can be observed from Figure 8.6 that Miscanthus provides negative WTWa CO_2 equivalent emissions in three STJ production schemes – biological, catalytic with in-situ H_2 plant type, and catalytic with H_2 from biomass gasification plant type (B.Miscanthus, CWIH.Miscanthus and CWHBG.Miscanthus, respectively), and are thus considered for further analysis. It is to be noted that the above shortlisting of FT, HEFA, ATJ, and STJ feedstock/pathways (for further analysis) also takes into consideration latest WTWa CORSIA default values (2021) in Table 8.2 (section 8.2). The feedstock/pathways shortlisted from analysis in Figure 8.3, Figure 8.4, Figure 8.5, and Figure 8.6 have significantly lesser WTWa than the CORSIA data.
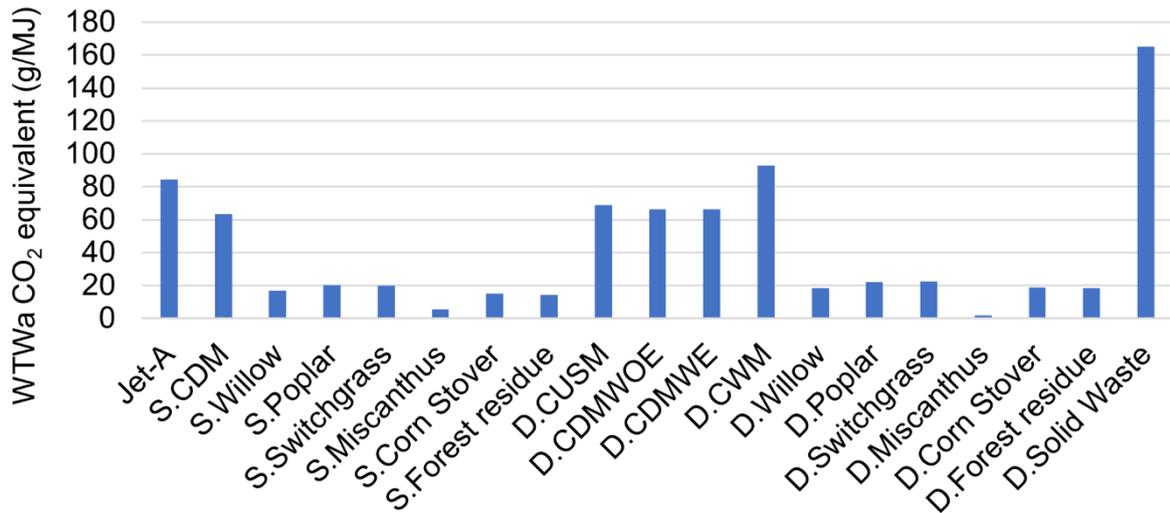
Figure 8.5. WTWa CO₂ equivalent emission comparison of different ATJ feedstocks for 2020 (with only CO₂ emissions in PTWa phase)
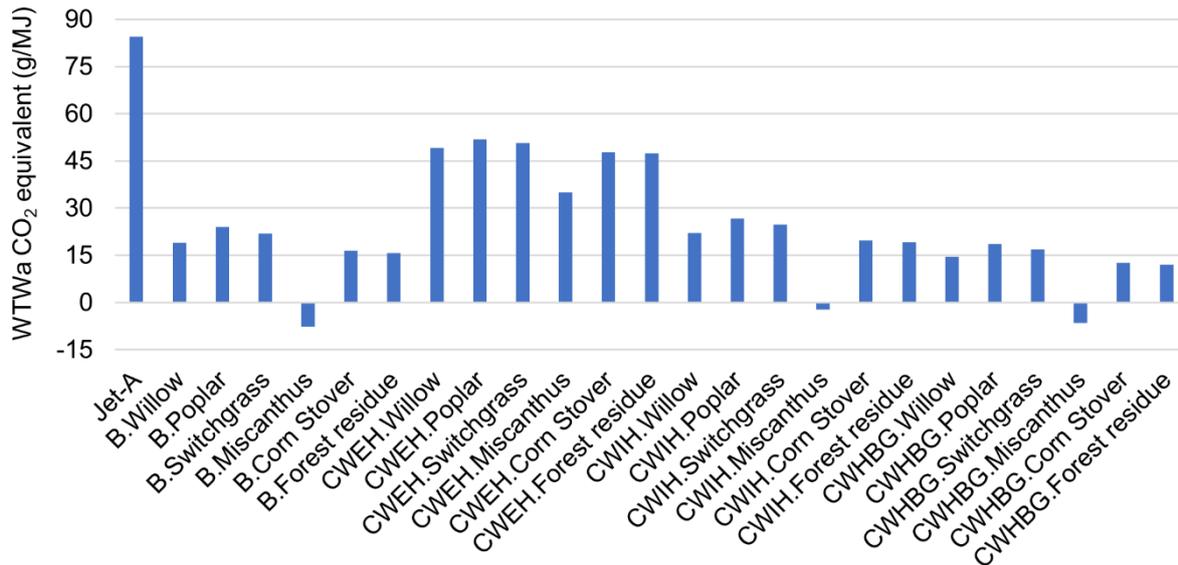
Figure 8.6. WTWa CO₂ equivalent emission comparison of different STJ feedstocks for 2020 (with only CO₂ emissions in PTWa phase)

8.4.2.1.2   Manufacturing emissions sensitivity to identified parameters

From section 8.4.1, RNG w CS, Solar PV, Nuclear HTGR, Biomass, and IF (biomass) LH_2 production pathways are found to provide near-zero or sub-zero WTWa CO_2 equivalent emissions. For each of the shortlisted 100% SPK fuel manufacturing cases in section 8.4.2.1.1, the sensitivity of selection of the hydrogen production route (discussed above) and the US energy mix type (year) for manufacturing SPK fuel on the WTWa CO_2 equivalent emissions is analysed. Figure 8.7 provides the WTWa comparison of low-carbon 100% SPK feedstocks and pathways for 2020 and 2050 US energy mix scenarios using hydrogen produced from less carbon intense scheme (with only CO_2 emissions in PTWa phase). It can be observed that HEFA (Carinata),

both ATJ distributed and standalone schemes using miscanthus, and miscanthus STJ biological production type are sensitive to the hydrogen manufacturing route. This is because hydrogen input to the production of these 100% SPK routes are greater than other routes for fuel production (i.e., greater dependency on hydrogen), in GREET 2021. Also, it can be observed that for ATJ distributed and standalone schemes using miscanthus, and miscanthus STJ biological production type, the WTWa CO_2 equivalent emissions increase between 2020 to 2050, opposite to the trend observed for other 100% SPK cases. This is primarily due to the higher use of fossil fuels via these routes and the need for fossil fuels in the 2050 US energy mix which has a greater share of renewable energy as discussed in section 8.3.1.2.1. The effect of use of fossil fuels is further discussed in section 8.4.4.
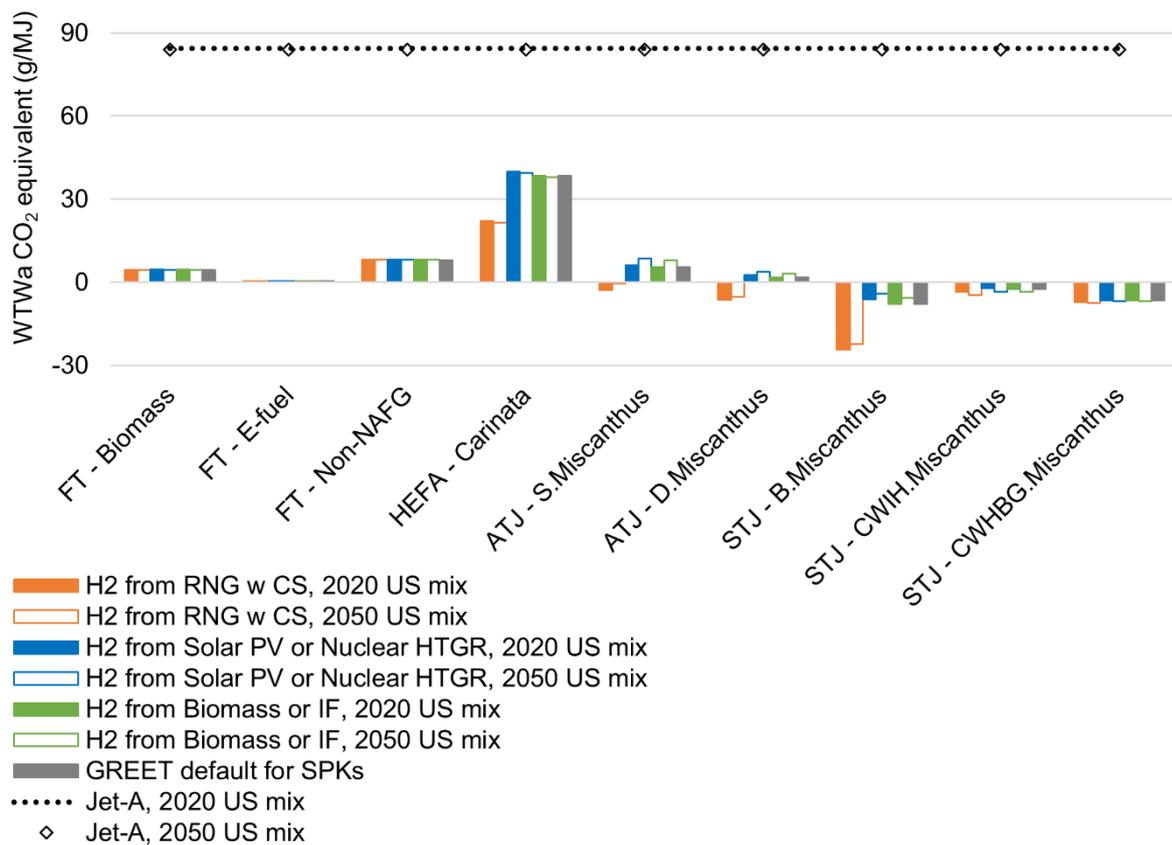
Figure 8.7. WTWa CO_2 equivalent emission comparison of low-carbon 100% SPK feedstocks and pathways for 2020 and 2050 US energy mix scenarios using hydrogen produced from less carbon intense scheme (with only CO_2 emissions in PTWa phase)

8.4.3   Comparative WTWa analysis with all emissions and contrails

Figure 8.8 shows the WTWa CO_2 equivalent emission comparison for different LH_2 and 100% SPK feedstock and pathways for 2020 and 2050 US energy mix scenarios, including non-CO_2 effects. Referring to Figure 8.8, the error bars reflect a range of values in the WTP phase. For LH_2 cases, the error bars show a range of values arising from the use of different biomass feedstocks. Similarly, for 100% SPK cases, the error

bars show a range of values due to the sensitivity because of using hydrogen produced from different low-carbon source for producing 100% SPK (see Figure 8.7 and discussion).
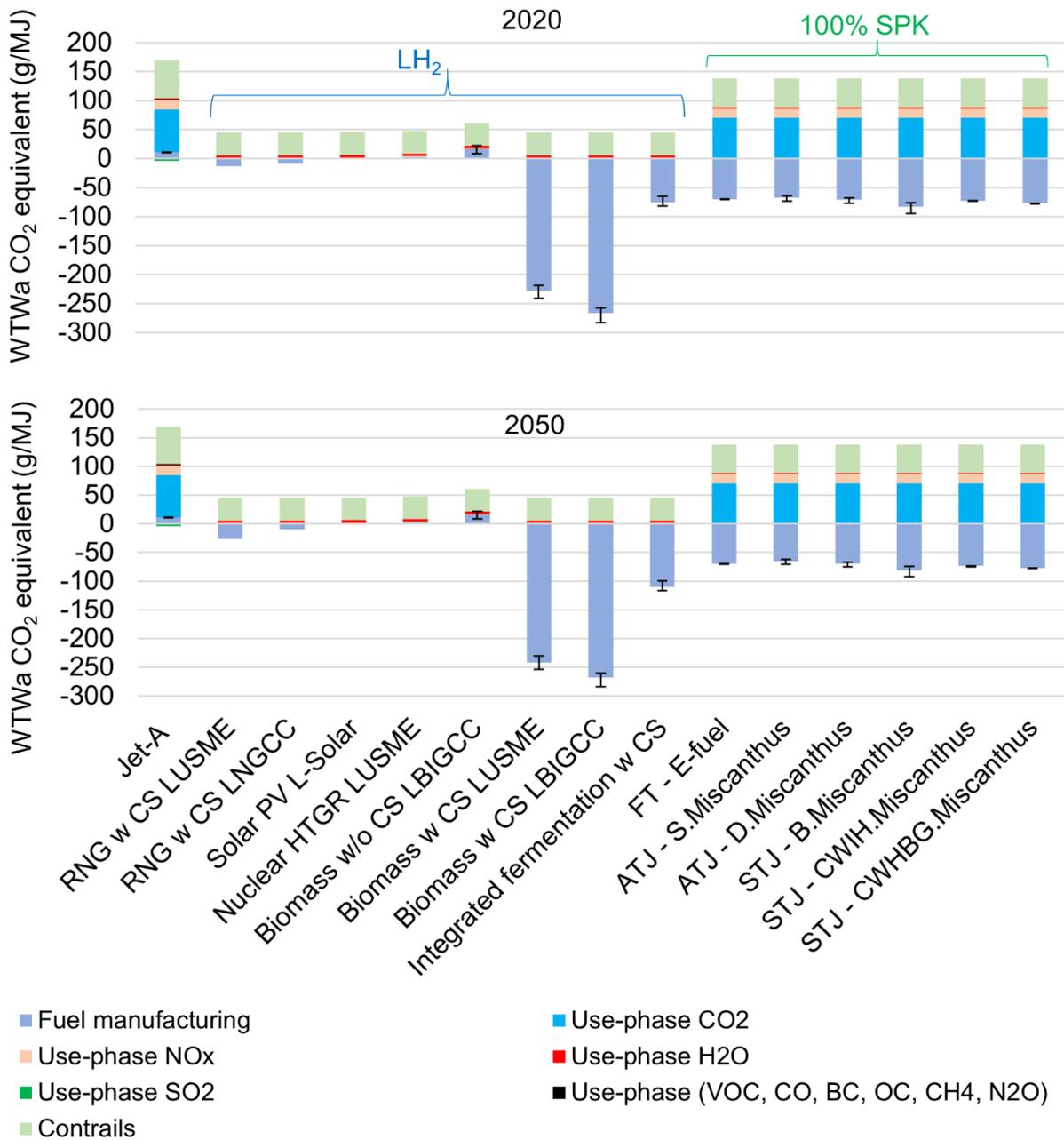
Figure 8.8. WTWa CO₂ equivalent emission comparison for different LH₂ and 100% SPK feedstock and pathways for 2020 and 2050 US energy mix scenarios including non-CO₂ effects

It can be observed that only LH₂ fuel could enable net zero or negative WTWa CO_2 equivalent emissions long-range flight of 300 passengers where LH₂ fuel is produced from Biomass w CS LUSME, Biomass w CS LBIGCC, and/or integrated fermentation (IF) w CS. The WTWa CO_2 equivalent emission (g/MJ) for Jet-A, Biomass w CS LUSME, Biomass w CS LBIGCC, and IF w CS in 2020 is 165, -184 (212% reduction), -225 (236% reduction), and -27 (116% reduction) g/MJ, respectively, and in 2050 these could be 165, -197 (219% reduction), -227 (236% reduction), and -63 (138% reduction) g/MJ, respectively.

Further, it can be observed from Figure 8.8 that for all fuels there is a reduction in WTWa CO_2 equivalent emissions from 2020 to 2050, which is expected due to increase in the use of renewable energy sources in the US energy mix. Also, for Jet-A and 100% SPK cases, the contribution of emissions like VOC, CO, BC, OC, CH_4, and N_2O to the WTWa CO_2 equivalent emission is negligible. It is to be noted that the emission indices for these emissions were assumed to be similar to the present-day aircraft technology for respective fuels. Using the N+2 technology the emission indices are bound to reduce due to lean burning combustors, thereby further reducing the WTWa CO_2 equivalent emissions contribution. Additionally, for Jet-A and 100% SPK cases, the use-phase non-CO_2 effects are of the similar magnitude or greater than the use-phase CO_2 effects. Moreover, for LH_2 fuel cases, the contribution of contrails is ~90% of use-phase effects, though the net WTWa CO_2 equivalent emission is significantly lesser than Jet-A.

As summarised in the literature review section (8.2), most studies do not take into account the effect of contrails, especially for LH_2 fuel. If the effect of contrails is ignored in this chapter, then all the feedstocks/pathways shortlisted for LH_2 fuel could enable a near-zero or negative net carbon emissions according to Figure 8.8. However, the climate impact of contrails is significant to the net WTWa CO_2 equivalent emissions, especially for LH_2 fuel. Therefore, the use of only advanced technology and low-carbon fuel (like LH_2) enable near-zero WTWa CO_2 equivalent emissions long-range flight, but these are insufficient strategies to reduce the effect of contrails. Similar to Jet-A aircraft, for LH_2 powered aircraft, operational strategies such as avoiding ice-supersaturated regions to prevent contrail formation could be used [45], [319]. However, this strategy has implications on the thrust production, aerodynamic performance, and fuel consumption.

The perspective used to select three feedstock and/or pathways for LH_2 fuel identified above only take into consideration the WTWa CO_2 equivalent emissions. However, for commercial aviation, the fuel cost, and the resulting direct operating cost (inclusive of carbon tax exemption) are significant aspects which should be accounted for identifying fuel manufacturing pathways for both LH_2 and 100% SPK. In this chapter, cost analysis is not conducted. The accuracy of fuel cost analysis depends primarily on the accuracy of simulation of the fuel manufacturing process, year of simulation, government incentives and market penetration of a fuel, and scale of fuel manufacturing and/or fuel manufacturing process technology readiness level. Additionally, there are fuel cost fluctuations due to externalities. For example: economic uncertainties due to pandemic like COVID-19, instability in middle eastern countries, and events such as the 2022 Ukraine war directly affect the global energy cost. The aspect of fuel production capacity is addressed in section 8.4.5. Overall, the success of LH_2 powered aviation requires appropriate: airport infrastructure, aircraft design, air-traffic or operations management, safety, fuel supply chain/manufacturing efficiency and capacity to meet the required fuel demand, fuel cost and direct operating cost, and policy.

8.4.4   Other unintended environmental and social impacts

In the previous section LH_2 is identified as the fuel that has the potential to make long-range flight emit near-zero and/or negative WTWa CO_2 equivalent emissions, where LH_2 is manufactured from Biomass

w CS LUSME, Biomass w CS LBIGCC and integrated fermentation (IF) w CS feedstock/pathways. Table 8.12 provides a summary of other unintended lifecycle environmental and social impacts for these three LH_2 production routes in comparison with Jet-A. These three routes are compared with Jet-A for aspects like indirect use of fossil fuels, water consumption, and WTWa VOC, CO, NO_x, PM_{10}, $PM_{2.5}$, SO_x, BC, and OC emissions. A colour coded ranking system is used for simplicity and this is indicated in Table 8.12. Similar data for remaining LH_2 production routes and 100% SPK cases are provided in Appendix D for completeness (Figure D.1 to Figure D.10). Further details on the aspects listed in Table 8.12 are provided in Appendix D sections D.2 and D.3.

Table 8.12. Summary of other unintended lifecycle environmental and social impacts

Ranking colour scheme			
1	2	3	4

Aspects	Jet-A	LH2		
		Biomass w CS LUSME	Biomass w CS LBIGCC	IF w CS
Fossil fuel use	1 (green)	3 (salmon)	2 (light green)	4 (red)
Water consumption	1 (green)	3 (salmon)	2 (light green)	4 (red)
WTWa VOC	1 (green)	2 (light green)	3 (salmon)	4 (red)
WTWa CO	3 (salmon)	2 (light green)	1 (green)	4 (red)
WTWa NOx	4 (red)	2 (light green)	1 (green)	3 (salmon)
WTWa PM10	2 (light green)	3 (salmon)	1 (green)	4 (red)
WTWa PM2.5	3 (salmon)	2 (light green)	1 (green)	4 (red)
WTWa SOx	1 (green)	2 (light green)	3 (salmon)	4 (red)
WTWa BC	4 (red)	1 (green)	2 (light green)	3 (salmon)
WTWa OC	3 (salmon)	2 (light green)	1 (green)	4 (red)

It can be observed from Table 8.12 that the three LH_2 production routes perform poorly in terms of use of fossil fuels (indirectly) and water consumption, compared to Jet-A. For WTWa CO, NO_x, PM_{10}, $PM_{2.5}$, BC, and OC emissions, Biomass w CS LBIGCC route performs the best. Jet-A performs best for VOC and SO_x emission (effect of lesser use of fossil fuels). The IF w CS route performs poorly on most of the aspects studied in Table 8.12, though this route provides a net negative WTWa CO_2 equivalent emissions compared to Jet-A (due to carbon sequestration). Therefore, it is important to examine the unintended environmental and social impacts of a selected route i.e., widening the boundary for analysis than just focusing on climate impacts. This is supported by a review study by Pinheiro Melo et al. [35], where the authors observe that though advanced technologies and alternative fuels could provide solutions for mitigating aviation emissions, there might be new socio-economic and environmental challenges associated with these. Thus, they establish the need for diversifying environmental indicators beyond GHG emissions and the need to consider social and economic aspects.

The above is the significance of this section and these aspects are not considered in the studies reviewed in section 8.2. It is important to minimise the (indirect) use of fossil fuels (resource impact) and water. The aspect of greater use of fossil fuels can be addressed by increasing the share of renewable energy

sources in the energy mix and increasing the efficiency of fuel manufacturing processes/plants and fuel supply chain. The water consumption aspect could be addressed by using ocean or wastewater and treating it to be used for fuel production. This entails accounting for water treating energy and emissions in WTWa analysis.

8.4.5 Fuel manufacturing capacities

Table 8.13. Production capacities of different fuels and production feedstocks/pathways (per plant)

Fuel	Feedstock/pathway	tonne/day	Source
H_2 (gas)	Steam methane reformation (SMR) with CS (H-vision initiative)	360 – 480	[320]
	Solar PV (hypothetical case estimation)	1,233	[320]
	Renewable source (solar, wind), plant for 2025	650	[321]
	Nuclear HTGR	230	[322]
	Biomass	2,000	[323]
Global hydrogen liquefaction capacity 290 tonnes/day [322]			
100% SPK	Neste/HEFA	933	[62]
	EU sub-group (HEFA)	1,348	[62]
	FT	456	[62]
		187	[62]
		249	[62]
	ATJ	477	[62]
	STJ	127	[62]
Jet-A (2019, Global)	Petroleum	7,90,165	[3]

Table 8.13 lists the production capacities of different fuels and production feedstocks/pathways per plant. It is to be noted that only shortlisted pathways of LH$_2$ and 100% SPK from section 8.4.3 are listed in this table. The IF manufacturing capacities are not known. In Table 8.13 the global manufacturing capacity for Jet-A is listed for 2019 (normal operations prior to the pandemic). It can be observed from Table 8.13 that for both LH$_2$ and 100% SPK the manufacturing units and capacities and liquefication capacity must be ramped up significantly, if these fuels have to replace Jet-A fuel.

8.4.6 Limitations of the present chapter

The fuel WTP emissions database used in this chapter is primarily based on the GREET model which is US specific. The WTP emissions are sensitive to country's energy mix, availability of raw materials (location wise) and the number of such locations in the country (determines the transportation emissions), transportation mode used (emissions and efficiency, viz. rail vs trucks, electricity/battery vs diesel, etc.), transportation network and its efficiency (direct connectivity between two points, terrain type of the transportation network, etc.), and fuel manufacturing plant efficiency. Additionally, for LH$_2$ fuel it is assumed that the pump to tank emission is zero. This assumption is simplistic and there could be some emissions associated in terms of energy/emission required to maintain the cryogenic temperature and pressure while filling LH$_2$ fuel in the

aircraft tank, transportation used (depending on the location of the fuel storage at or away from airport), and fuel losses while filling LH_2 fuel in aircraft tank. Also, the NO_x estimation in this chapter is based on a simplified (multi-segment) mission where the energy consumption in smaller flight segments is calculated using the modifications to Roskam's fuel fraction. Moreover, the GWP values used in this chapter for use-phase emissions like NO_x, H_2O, and contrails are based on other studies. The uncertainties from those studies will add up in the results of this chapter. Lastly, this chapter doesn't conduct cost analysis for aircraft mission powered by different fuels produced from various feedstocks and/or pathways.

8.5   Chapter summary and conclusion

In this chapter, the life cycle or WTWa performance is evaluated for long-range LTA aircraft powered by LH_2 and 100% SPK (separately) manufactured from different feedstocks and/or pathways. The GREET 2021 model is used for making a database of fuel manufacturing phase emissions for LH_2 and 100% SPK (biofuel and PtL), and the use-phase emissions are modelled separately in this chapter. After examining over 100 different ways in total for producing LH_2 and 100% SPK, it is observed that only LH_2 fuel could enable net zero or negative WTWa CO_2 equivalent emissions long-range (BWB) flight of 300 passengers where LH_2 fuel is produced from Biomass w CS LUSME (212 – 219 % reduction), Biomass w CS LBIGCC (236 – 238 % reduction), and/or IF w CS (116 – 138 % reduction). Also, it is found that the climate impact of contrails (based on low fidelity modelling done in the source study) is significant to the net WTWa CO_2 equivalent emissions, especially for LH_2 fuel, and operational strategies need to be employed for reducing contrail formation. It is to be noted that the effect of contrails from hydrogen aircraft is uncertain and more research work is required. The WTWa CO_2 equivalent emissions of 100% SPK long-range (BWB) flight of 300 passengers could be reduced by 60 – 80%, where the fuel should be produced from B.Miscanthus route.

The perspective used to select three feedstock and/or pathways for LH_2 fuel identified in this chapter, only take into consideration the WTWa CO_2 equivalent emissions. However, for commercial aviation the fuel cost and the resulting direct operating cost (inclusive of carbon tax exemption) are significant aspects which also needs to be accounted for identifying fuel manufacturing pathways for both LH_2 and 100% SPK, which are not considered in this chapter. Additionally, the above three selected LH_2 production pathways have unintended consequences in terms of significantly greater (indirect) fossil fuel use and water consumption compared to Jet-A, and these should be reduced by increasing the share of renewables in the energy mix and improving the energy efficiency of the fuel manufacturing process and supply chain, for making LH_2 an environmentally and socially benign aviation fuel. In summary, the success of LH_2 powered aviation requires appropriate airport infrastructure, aircraft design, air-traffic or operations management, safety, and fuel supply chain/manufacturing capacity and energy efficiency, to meet the required fuel demand, fuel cost and direct operating cost, and policy.

Chapter 9: Conclusions and future work

9.1   Summary, conclusions, and significance

Global aviation is responsible for 3.5% of the total anthropogenic radiative forcing. The world-wide aviation demand is expected to double in the next two decades (2021 – 2040) while considering the effects of COVID-19. As a result, the climate impact of aviation would increase with the growing demand. The industry strategy of using advanced aviation technology and low-carbon fuels could itself contribute to 80% of the efforts required for carbon neutral growth. In addition, the boundary of defining fuels as low-carbon should not be just restricted to the use-phase and the embodied (life cycle) emissions should also be accounted. Considering the developments in recent years and the impacts of COVID-19 on the aviation industry, it appears that LTAs will likely be the most common means of long-range travel in the next two decades. A high-level technology review in Chapter 1 suggested that long-haul aviation is tough to decarbonise. The broader aim of this thesis was to evaluate aircraft technology and low-carbon energy-vector combination(s) considering lifecycle effects for enabling climate-neutral subsonic long-range flight (14,000 km) of an LTA aircraft (~300 passengers).

It is observed through a detailed literature review and preliminary quantitative analysis in Chapter 2 that decarbonising long-range flight of an LTA aircraft is extremely challenging because there are a limited alternative energy vectors that can match the energy density (both gravimetric and volumetric) of Jet-A fuel. After this literature review six candidate fuels – methanol, ethanol, LNG, 100% SPK, LH_2, and LNH_3 – are identified for further quantitative evaluation, and feasible aircraft technologies and airframe are identified for further consideration.

Before beginning with the quantitative evaluation for addressing the five research objectives, the research philosophy of this thesis is discussed in Chapter 3 using the 'research onion' model. The research philosophy of 'positivism' is relevant and is thus used in this research, which uses deductive approach for quantitative research. In the context of the present research, each main chapter (Chapters 4 – 8) uses a mono quantitative method (numerical experiments). Overall, this thesis uses multi-method quantitative approach towards the research aim and objectives. Overall, in terms of the limitations, this thesis estimates the performance of aircraft using low-fidelity methods and these are computationally inexpensive. Errors are inherently introduced with such methods that involve simple assumptions. For each of the main research contributions/chapters (Chapters 4 – 8), the limitations are detailed at the end of every chapter.

The thesis has met the five research objectives established in Chapter 1, as follows :

1. *Quantify the energy performance characteristics of LTA aircraft powered by the shortlisted alternative fuels and identify the fuels that enable a typical long-range flight within the aircraft's structural limit; and evaluate the off-design energy performance of the LTA aircraft powered by identified alternative fuel(s) which meets the Jet-A design target range.*

     Using Breguet's range equation analysis in Chapter 4 for examining six alternative fuels, it is observed that LH_2 and 100% SPK are the only two alternative fuels that meet the design target range for a long-

range LTA tube-wing aircraft. Using the present-day tube-wing technology, the SEC of LH_2 and 100% SPK aircraft are 11% higher and 0.2% lower relative to Jet-A, respectively. At off-design points, the SEC of 100% SPK and LH_2 are always similar to and greater than Jet-A, respectively. LH_2 aircraft SEC decreases with increasing range and is less sensitive beyond 10,000 km. Thus, the first research objective is met. In a first, an equation is developed that relates the OEW and GTOW of (31) LH_2 aircraft through regression analysis of data from this thesis and literature. This equation will enable future studies on LH_2 aircraft weight-sizing.

2. *Perform a global sensitivity analysis to evaluate the effects of identified technology parameters for enabling an LH_2 powered long-range travel with an LTA aircraft, within the MTOW limit of a baseline Jet-A aircraft,*

A global sensitivity analysis is conducted in Chapter 5 using Breguet's range equation to study the impacts of four technologies – aerodynamics, lighter structures, cryo-tank weight, and overall efficiency (η_o) – on the design-point performance of a tube-wing LH_2 aircraft. Relative to the present-day technology, it is observed that for an LH_2 aircraft: (i) improving η_o and aerodynamics dramatically improves its SEC; and (ii) using the most optimistic technology development estimates, its SEC improves by 33% requiring a 22% longer fuselage. Thus, the second research objective is met. It is observed that for the present-day technology, the critical value of η is 0.52 for a long-range LTA LH_2 aircraft. For N+2 and N+3 technology, the (expected) critical values of η are $\eta < 0.35$ and $\eta \ll 0.35$, respectively, for a long-range LTA LH_2 aircraft, but regardless of the aircraft technology used η should be maximised for reducing the SEC of the LH_2 aircraft.

3. *Develop a model for estimating the performance metrics of the future aircraft powerplant using conventional and identified alternative fuels (separately),*

4. *Develop an operational energy consumption model for the future long-range aircraft powered by conventional and identified alternative fuels (separately),*

By using GasTurb a future (N+2 timeframe) UHB GTF engine is simulated in Chapter 6 and using aircraft weight sizing methods a performance model of a future (N+2 timeframe) BWB is developed in Chapter 7 which is powered by Jet-A, 100% SPK, and LH_2 (separately). It is observed that the SEC of a futuristic BWB aircraft powered by Jet-A, 100% SPK, and LH_2 decreases by 47.9%, 48%, and 53.5% relative to the present-day Jet-A aircraft, respectively. At off-design points, for a given fuel case, with increasing load factor, the maximum range that can be travelled decreases. Additionally, for a given fuel case, increasing the load factor improves the energy efficiency compared to a Jet-A BWB aircraft. Moreover, for a given fuel case and load factor, the energy efficiency improves with increasing range compared to a Jet-A BWB aircraft. This increase in energy efficiency is observed prominently for all three cases of BWB LH_2 aircraft compared to the Jet-A BWB aircraft. The BWB LH_2 Case 3 aircraft is the most efficient aircraft at all range and load factor combinations compared to the Jet-A BWB aircraft and the (N+3 timeframe) tube-wing LH_2 aircraft performance observed in the global sensitivity analysis. Thus, the third and fourth research objectives are met via Chapters 6 and 7 respectively. Furthermore, the equation

developed in Chapter 4 that relates the OEW and GTOW of LH_2 aircraft is refined by adding the three BWB LH_2 aircraft modelled in Chapter 7 to the regression analysis of (now) 34 tube-wing and BWB (data from this thesis and literature).

5. *Develop a model for calculating the lifecycle GHG emissions and other unintended impacts mitigation potential of the aircraft technology and alternative fuel combinations. This requires:*

   a. *Development of a database of manufacturing phase energy, emissions, and materials inventory for identified alternative fuels produced from different pathways,*

   b. *Evaluation of the aircraft operational phase emissions.*

Lastly, a comparative lifecycle analysis is conducted in Chapter 8 for these three BWB aircraft while quantifying both CO_2 and non-CO_2 effects. After examining over 100 manufacturing feedstocks/pathways for 100% SPK and LH_2, it is observed that only LH_2 could enable a climate-neutral long-range flight using fuel produced from biomass where the manufacturing setup employs carbon sequestration. Also, it is found that the climate impact of contrails is significant to the net WTWa CO_2 equivalent emissions, especially for LH_2 fuel, and operational strategies need to be employed for reducing contrail formation. The WTWa CO_2 equivalent emissions of 100% SPK long-range (BWB) flight of 300 passengers could be reduced by 60 – 80%, where the fuel should be produced from B.Miscanthus route. The perspective used to select feedstock and/or pathways for LH_2 fuel identified in this study only take into consideration the WTWa CO_2 equivalent emissions. However, for commercial aviation the fuel cost and the resulting direct operating cost (inclusive of carbon tax exemption) are significant aspects which also needs to be accounted for identifying fuel manufacturing pathways for both LH_2 and 100% SPK, which are not considered in this study. Additionally, the identified LH_2 production pathways have unintended consequences in terms of significantly greater (indirect) fossil fuel use and water consumption, and these should be reduced by increasing the share of renewables in the energy mix and improving the energy efficiency of the fuel manufacturing process and supply chain, for making LH_2 an environmentally and socially benign aviation fuel. Thus, the fifth and the last research objective is met.

Overall, the findings of this thesis could guide and enable more informed decision making in future aviation technology development and policy making (detailed below in 9.1.1 – 9.1.4). The success of these alternative fuels, especially LH_2, mandates development of suitable airport infrastructure, aircraft design, air-traffic or operations management, safety, and fuel supply chain/manufacturing capacity and energy efficiency, to meet the required fuel demand, fuel cost and direct operating cost, policy, and relevant investments.

9.1.1 Modifications to aircraft and aviation sub-systems

100% SPK and LH_2 are the only two alternative fuels (quantitatively) identified from this study that enable a long-range air travel. In terms of modifications required to the aircraft sub-systems, LH_2 use requires significant changes to the aircraft sub-systems which primarily include installation of cryogenic tank (negative effect on aerodynamic and structural performance), modifications to fuel lines and engine/combustor (improve flame characteristics and reduced emissions of oxides of nitrogen), and installation of a heat exchanger (for

enabling phase change of hydrogen before injecting it into the combustor and component cooling). These modifications and the aspects such as LH_2 aircraft safety and refuelling, and changes to airport infrastructure for hydrogen powered aviation are reviewed in Appendix B.3. It was observed that the future (N+2 timeframe) BWB aircraft did not require increase in wetted area from its baseline Jet-A version, as compared to a future (N+3 timeframe) tube-wing aircraft case, primarily because of the higher internal volume and better aerodynamic performance.

Compared to LH_2 aircraft, 100% SPK requires insignificant modifications (due to similar fuel properties as that of Jet-A) such as minor increase in fuel tank volume, change of seals in the high-pressure fuel systems (due to absence of aromatic content), etc. The effect of fuel properties of 100% SPK and required modifications are reviewed in Appendix B.4. Due to the significant modifications required for the LH_2 aircraft, its acquisition cost is expected to be more than Jet-A and 100% SPK.

9.1.2 Airline decision-making

It is observed in this work that for a long-range tube-wing LTA aircraft, compared to Jet-A, an LH_2 aircraft using present-day aircraft technology consumes more energy for all range and payload combinations. Purely based on the energy performance, it is observed from the off-design performance that for a given payload, LH_2 aircraft offers a stable SEC at greater range (>10,000 km). However, for Jet-A the SEC for a given payload decreases with increasing range and minimises at ~7,000 km and thereafter it increases with increasing range. Employing future (N+3 timeframe) aircraft technology, SEC of LH_2 aircraft could be improved by 33% compared to present-day Jet-A (A350-1000) aircraft at the design point. In contrast, a future (N+2 timeframe) BWB LH_2 aircraft consumes 48.5% less energy compared to present-day Jet-A (A350-1000) aircraft, at the design point. At off-design points for a given payload, SEC of this BWB LH_2 aircraft keeps decreasing with increasing range. This is an important observation for airline operations and selection of airframe (tube-wing vs BWB), that may favour LH_2 aircraft for long-haul flights, but this will ultimately be driven by fuel costs and aircraft availability.

9.1.3 Aircraft design and compatibility with airport

The significant increase in the LH_2 aircraft fuselage length observed in this work could be a potential challenge associated with the use of LH_2 in the conventional tube-wing architecture, as this likely has structural and stability implications. Longer tube-wing LH_2 aircraft and/or BWB LH_2 aircraft might not be readily compatible with the current airport design and layout, which may require modifications to airport aprons, in addition to new refuelling infrastructure. This thesis has identified the significance of optimisation of LH_2 aircraft to meet the *T/W* which further reduces its SEC. More rigorous multi-point optimisation of engine and aircraft along with the examination of deck configurations, would improve the fidelity level of aircraft design.

9.1.4 Fuel and life-cycle costs

100% SPK and LH_2 should be manufactured from less carbon intense or renewable energy pathways (considering life-cycle effects) that will enable truly climate-neutral air travel. It was observed in this thesis that the selected (three) climate-neutral LH_2 production pathways have unintended consequences in terms of significantly greater (indirect) fossil fuel use and water consumption compared to Jet-A. In terms of fuel manufacturing, these unintended consequences could be reduced by improving the energy efficiency of the fuel manufacturing process and supply chain and increasing the share of renewables in the energy mix.

Additionally, effects of contrails and other non-CO_2 emissions need to be considered. In the use phase, LH_2 combustion theoretically emits zero emissions except water vapour and oxides of nitrogen whereas combustion of 100% SPK emits similar quantity of greenhouse emissions as that of Jet-A.

The pathways and/or feedstocks used for manufacturing both these fuels would determine their benefits in terms of lifecycle emissions and fuel costs. The fuel costs also depend on the scale of manufacturing, technology advancements, efficiency and effectiveness of the fuel supply chain, and governmental incentives (carbon abatement). Using the results of this thesis, a study on the social, environmental and climate costs of using different fuels could be conducted. Using this cost, fuel production cost, and aircraft's operational energy consumption, the mission cost for respective fuel could be estimated. Overall, this would enable appropriate policy making for aviation. Suitable aviation and energy policies could be formulated based on this thesis and above discussion to quantify, translate, and accommodate the (climate/environmental and societal) benefits of manufacturing green LH_2 and its use (viz: incentives to fuel manufacturers and/or airlines)

9.2 Future work

In terms of aircraft and engine design, for both conventional tube-wing airframe and unconventional airframes (like BWB), accounting the limitations and learnings from Chapters 4 – 7, a more detailed and rigorous design-optimisation study could be conducted that considers:

- Stability and structural analysis:

  The number (and size) of cryogenic tanks and their positioning inside the aircraft determines the centre of gravity during different points during an aircraft mission and affects the vehicle's stability. As a result, this needs an examination of the criteria for positioning of the landing gear and an evaluation on the required take-off and landing speeds to avoid tail-strikes. Considering flight dynamics perspective, the empennage and control surfaces must be redesigned and/or recalibrated for stability. The installation of cryogenic tanks, particularly for a tube-wing aircraft, affects the structural stress in the longitudinal direction.

- Effects of deck configurations:

  A double deck or novel seating configurations (like stack seating) having larger fuselage diameter or size than conventional single deck fuselage, are expected to provide energy efficiency benefits for LH_2 use for same passenger seating and design range.

- Multi-point optimisation of engine and aircraft, and use of better engine loss models:

  The engine modelling in this thesis falls at least under zero-dimensional modelling that uses simple turbo-machinery loss models. High fidelity analysis enables the accurate estimation of performance loss in turbomachinery (profile [including shock], trailing edge, secondary, and tip clearance loss). In addition, engine and aircraft should be optimised considering typical off-design points in a given mission, for improving the aircraft's energy consumption.

- Hydrogen aircraft systems:

  The effect of cryogenic tank is not considered in detail in this thesis and is based on other studies. A separate design model should be integrated within the aircraft design process for cryogenic tank modelling that accounts both internal and external mechanical and thermal stresses on the cryogenic tank. Additionally, an important operational problem associated with combustion based LH_2 aircraft is the phase change from liquid (tank) to gas (combustor). This aspect has not been considered in open literature so far in LH_2 aircraft design. A heat exchange apparatus could be designed for enabling this LH_2 phase change, where LH_2 cools a working fluid and changes to gaseous hydrogen. If air is the working fluid, then it could be used directly for cabin air conditioning and/or turbine cooling. The other alternative for enabling the said phase change is the use of electric heating. A study is required that compares these two and other alternatives for the said phase change and their impacts on aircraft energy performance.

It was observed in this thesis that the selected (three) climate-neutral LH_2 production pathways have unintended consequences in terms of significantly greater (indirect) fossil fuel use and water consumption compared to Jet-A. In terms of fuel manufacturing, these unintended consequences could be reduced by improving the energy efficiency of the fuel manufacturing process and supply chain and increasing the share of renewables in the energy mix.

In terms of lifecycle analysis, a more holistic examination could be conducted that considers different regions or continents (effect of energy mix) for different fuel production (emissions) from various feedstocks and pathways, along with costs. Moreover, other unintended environmental and social impacts such as fossil fuel, water consumption, and other emissions, need to be considered. Such a study could enable the estimation of cost-effective and climate-neutral fuel production pathways for different regions/continents. Additionally, using the results of this thesis, a study on the social, environmental and climate costs of using different fuels could be conducted. Using this cost, fuel production cost, and aircraft's operational energy consumption, the mission cost for respective fuel could be estimated. Therefore, a more detailed comparative lifecycle emissions and cost analysis could be conducted for different fuels at a global level.

High- or systems-level:

In general, it is observed through this thesis that the success of LH_2 powered aviation, at a high-level, requires appropriate: airport infrastructure, aircraft design, air-traffic or operations management, safety, and fuel supply chain/manufacturing capacity and energy efficiency, to meet the required fuel demand, fuel cost and direct operating cost, policy, and relevant investments.

This thesis has particularly identified that BWB airframe employing futuristic aviation technologies enables an energy efficient and effective use of LH_2 compared to a tube-wing airframe of similar technology, for long-range LTA aircraft. Additionally, LH_2 need to be manufactured from green routes that also employ carbon sequestration. One route that was identified to be climate-neutral was LH_2 produced from biomass where the manufacturing setup employs carbon sequestration. However, this route has a poor performance in terms of (indirect) fossil fuel use and water consumption, compared to Jet-A. This is primarily due to poor fuel manufacturing process and supply chain energy efficiency, and greater contribution of fossil fuel to the energy mix. In addition, light-weight cryogenic tank development is significant to the success of LH_2 as a long-range aviation fuel.

LH_2 fuel (combustion based) is more likely to replace Jet-A fuel as an alternative for long-range travel. However, there are a lot of uncertainties in terms of contrail formation, emissions of oxides of nitrogen, and GWP of water vapour (at high altitude). The contribution share of contrails to the climate impact of LH_2 aircraft on a lifecycle basis is significant and therefore operational strategies (like avoiding ice-supersaturated regions for preventing contrail formation) need to be formulated.

The high- or systems-level recommendations of this thesis are that: (i) further R&D and investments should go in the direction of the above identified dimensions (fuel manufacturing for different regions/continents, its cost and lifecycle effects; cryogenic tank development; aircraft design-optimisation; and contrails) for making LH_2 powered travel more cost-effective and climate-neutral; and (ii) appropriate aviation and energy policies need to be formulated to quantify, translate, and accommodate the (climate/environmental and societal) benefits of manufacturing green LH_2 and its use (example: incentives to fuel manufacturers and/or airlines). These recommendations are completely in-line with and similar to the recommendations of study by the World Economic Forum [25] (reviewed in section 2.6), and quantitative evaluations by Mukhopadhaya et al. [127] and FlyZero report [128] (reviewed in section 8.2).

More information:

First author's other research work can be found in [53], [91], [325]–[334], [92], [335]–[342], [93], [100], [117], [218], [238], [239], [324].

References

[1] ATAG, "Aviation and climate change," *Air Transport Action Group*, 2020. https://aviationbenefits.org/media/167159/fact-sheet_2_aviation-and-climate-change.pdf (accessed Oct. 01, 2024).

[2] R. Hansmann, H. A. Mieg, and P. Frischknecht, "Principal sustainability components: empirical analysis of synergies between the three pillars of sustainability," *Int. J. Sustain. Dev. World Ecol.*, vol. 19, no. 5, pp. 451–459, Oct. 2012, doi: 10.1080/13504509.2012.696220.

[3] International Air Transport Association, "Industry Statistics Fact Sheet 2024," *International Air Transport Association*, 2024. https://www.iata.org/en/iata-repository/pressroom/fact-sheets/industry-statistics/ (accessed Oct. 02, 2024).

[4] A. Doherty, "Flying Is Bad for the Planet. You Can Help Make It Better," *The New York Times*, Jul. 27, 2017. Accessed: Apr. 27, 2019. [Online]. Available: https://www.nytimes.com/2017/07/27/climate/airplane-pollution-global-warming.html

[5] "Flight carbon footprint calculator." https://calculator.carbonfootprint.com/calculator.aspx?lang=en-GB&tab=3 (accessed Apr. 27, 2019).

[6] "Distance calculator." https://www.distance.to/ (accessed Apr. 27, 2019).

[7] International Civil Aviation Organization Secretariat, "Aviation's Contribution to Climate Change," 2010. https://www.icao.int/environmental-protection/Documents/EnvironmentReport-2010/ICAO_EnvReport10-Ch1_en.pdf (accessed Oct. 01, 2024).

[8] IPCC, "IPCC SPECIAL REPORT AVIATION AND THE GLOBAL ATMOSPHERE: Summary for Policymakers Aviation and the Global Atmosphere," 1999. https://archive.ipcc.ch/pdf/special-reports/spm/av-en.pdf (accessed Oct. 01, 2024).

[9] IATA, "Climate Change," *International Air Transport Association*, 2024. https://www.iata.org/contentassets/d13875e9ed784f75bac90f000760e998/fact_sheet_on_climate_change.pdf (accessed Oct. 01, 2024).

[10] D. S. Lee, "The current state of scientific understanding of the non-CO2 effects of aviation on climate," *Manchester Metropolitan University*, 2018. https://assets.publishing.service.gov.uk/government/uploads/system/uploads/attachment_data/file/813342/non-CO2-effects-report.pdf (accessed Jan. 02, 2020).

[11] D. S. Lee *et al.*, "The contribution of global aviation to anthropogenic climate forcing for 2000 to 2018," *Atmos. Environ.*, vol. 244, p. 117834, Jan. 2021, doi: 10.1016/J.ATMOSENV.2020.117834.

[12] D. S. Lee *et al.*, "The contribution of global aviation to anthropogenic climate forcing for 2000 to 2018," *Atmos. Environ. (1994).*, vol. 244, p. 117834, Jan. 2021, doi: 10.1016/J.ATMOSENV.2020.117834.

[13] Boeing, "COMMERCIAL MARKET OUTLOOK 2024–2043," 2024. https://www.boeing.com/commercial/market/commercial-market-outlook#overview (accessed Oct. 02, 2024).

[14] IATA, "2021-2039 CURRENT TRENDS," 2021. https://www.iata.org/contentassets/e938e150c0f547449c1093239597cc18/pax-forecast-infographic-2020-final.pdf

[15] "IATA - Climate Change." https://www.iata.org/en/programs/environment/climate-change/ (accessed Jan. 08, 2019).

[16] J. Hupe, "Setting the Scene-Aviation and Climate Change," *ICAO_Aviation_Green_Recovery_Seminar*, 2020. https://www.icao.int/Meetings/GreenRecoverySeminar/Documents/1.1 ICAO AGR - Setting the scene.pdf (accessed Jun. 05, 2021).

[17] "Carbon Markets, Low Carbon and Sustainable Aviation Fuels with ATAG 2019 Global Sustainable Aviation Forum," *International Air Transport Association*, 2019. http://aozhounum.buzz/contentassets/d13875e9ed784f75bac90f000760e998/training-talg84-carbon-saf-atag.pdf (accessed Apr. 19, 2020).

[18] S. W. Ashcraft, A. S. Padron, K. A. Pascioni, G. W. Stout, and D. L. Huff, "Review of propulsion technologies for N+3 subsonic vehicle concepts (Report # 20110022435)," 2011. https://ntrs.nasa.gov/citations/20110022435

[19] M. Voskuijl, J. van Bogaert, and A. G. Rao, "Analysis and design of hybrid electric regional turboprop aircraft," *CEAS Aeronaut. J.*, vol. 9, no. 1, pp. 15–25, Mar. 2018, doi: 10.1007/s13272-017-0272-1.

[20] C. Friedrich and P. A. Robertson, "Hybrid-Electric Propulsion for Aircraft," *J. Aircr.*, vol. 52, no. 1, pp. 176–189, Jan. 2015, doi: 10.2514/1.C032660.

[21] A. W. Schäfer *et al.*, "Technological, economic and environmental prospects of all-electric aircraft," *Nat. Energy*, vol. 4, no. 2, pp. 160–166, Feb. 2019, doi: 10.1038/s41560-018-0294-x.

[22] A. Newby, "Toward Sustainable Aviation," *Keynote at AIAA Propulsion and Energy Forum 2019*. American Institute of Aeronautics and Astronautics, 2019. Accessed: Jan. 02, 2020. [Online]. Available: https://livestream.com/AIAAvideo/PropEnergy2019/videos/195347621

[23] R. Walker, "Hyperloop : Cutting through the hype," 2018. https://trl.co.uk/sites/default/files/Hyperloop white

paper.pdf (accessed Aug. 02, 2020).

[24]   "Accelerating the transition of long-haul aviation towards net zero : Aviation: Benefits Beyond Borders," 2021. https://aviationbenefits.org/newswire/2021/10/accelerating-the-transition-of-long-haul-aviation-towards-net-zero/ (accessed Nov. 15, 2021).

[25]   World Economic Forum, "Target True Zero Unlocking Sustainable Battery and Hydrogen-Powered Flight - Insight Report," 2022. Accessed: Aug. 05, 2022. [Online]. Available: https://www3.weforum.org/docs/WEF_Target_True_Zero_Aviation_ROUND_2022.pdf

[26]   B. Graver, K. Zhang, and D. Rutherford, "CO 2 emissions from commercial aviation, 2018," *INTERNATIONAL COUNCIL ON CLEAN TRANSPORTATION*, 2019. http://sustainablehighworth.co.uk/wp-content/uploads/2020/10/ICCT_CO2-commercl-aviation-2018_20190918.pdf (accessed Sep. 10, 2021).

[27]   H. Ritchie, "Short-haul vs. long-haul; rich vs. poor countries: where do global CO2 emissions from aviation come from? - Our World in Data," *Our World in Data*, 2020. https://ourworldindata.org/breakdown-co2-aviation (accessed Sep. 10, 2021).

[28]   Boeing, "Boeing: 787 Dreamliner," *Boeing*, 2016. https://www.boeing.com/commercial/787/ (accessed Aug. 05, 2020).

[29]   M. Clinch, "British Airways retires its entire fleet of Boeing 747 jets," *CNBC*, 2020. https://www.cnbc.com/2020/07/17/british-airways-retires-its-entire-fleet-of-boeing-747-jets.html (accessed Aug. 05, 2020).

[30]   R. Qubein, "Lufthansa Retires Airbus A380 From Frankfurt Schedule, But Munich Flights Possible By 2022," *Forbes*, 2020. https://www.forbes.com/sites/ramseyqubein/2020/06/19/lufthansa-retires-airbus-a380-from-frankfurt-schedule-but-munich-flights-possible-by-2022/#2d7ba9df5489 (accessed Aug. 05, 2020).

[31]   G. Polek, "Air France-KLM Accelerates Airbus A380 Retirements," *Air Transport News: Aviation International News*, 2020. https://www.ainonline.com/aviation-news/air-transport/2020-05-20/air-france-klm-accelerates-airbus-a380-retirements (accessed Aug. 05, 2020).

[32]   International Council on Clean Transportation, "International Civil Aviation Organization CO2 standard for new aircraft," 2017. https://theicct.org/sites/default/files/publications/ICCT-ICAO_policy-update_revised_jan2017.pdf (accessed Jan. 02, 2020).

[33]   ANL, "GREET 2021," *Argonne National Laboratory*, 2021. https://greet.es.anl.gov/

[34]   CleanSky2-FCH, "Hydrogen-powered aviation," *CleanSky2 - Fuel Cell Hydrogen*, 2020. https://www.fch.europa.eu/sites/default/files/FCH Docs/20200720_Hydrogen Powered Aviation report_FINAL web.pdf (accessed May 03, 2021).

[35]   S. Pinheiro Melo *et al.*, "Sustainability Assessment and Engineering of Emerging Aircraft Technologies— Challenges, Methods and Tools," *Sustainability*, vol. 12, no. 14, p. 5663, Jul. 2020, doi: 10.3390/su12145663.

[36]   "Global Warming Potential - an overview | ScienceDirect Topics." https://www.sciencedirect.com/topics/earth-and-planetary-sciences/global-warming-potential (accessed Jul. 11, 2022).

[37]   C. Grobler *et al.*, "Marginal climate and air quality costs of aviation emissions," *Environ. Res. Lett.*, vol. 14, no. 11, 2019, Accessed: Aug. 06, 2020. [Online]. Available: https://iopscience.iop.org/article/10.1088/1748-9326/ab4942

[38]   "New LAE study quantifies air quality and climate impacts of aviation – MIT LAE." https://lae.mit.edu/2019/11/08/new-study-finds-aviation-emissions-impacts-on-air-quality-to-be-larger-than-than-on-climate/ (accessed Aug. 06, 2020).

[39]   N. Low, B. Gleeson, and Palgrave Connect (Online service), *Making urban transport sustainable*. Palgrave Macmillan, 2003. Accessed: Mar. 11, 2019. [Online]. Available: https://books.google.co.uk/books?id=CwuBDAAAQBAJ&pg=PA122&lpg=PA122&dq=increases+susceptibility+to+infection+and+aggravates+asthma.+In+children+exposure+may+result+in+coughs,+colds,+phlegm,+shortness+of+breath,+chronic+wheezing+and+respiratory+diseases+in

[40]   S. R. H. Barrett, R. E. Britter, and I. A. Waitz, "Global Mortality Attributable to Aircraft Cruise Emissions," *Environ. Sci. Technol.*, vol. 44, no. 19, pp. 7736–7742, Oct. 2010, doi: 10.1021/es101325r.

[41]   J. Koo, Q. Wang, D. K. Henze, I. A. Waitz, and S. R. H. Barrett, "Spatial sensitivities of human health risk to intercontinental and high-altitude pollution," *Atmos. Environ.*, vol. 71, pp. 140–147, Jun. 2013, doi: 10.1016/J.ATMOSENV.2013.01.025.

[42]   P. J. Wolfe, S. H. L. Yim, G. Lee, A. Ashok, S. R. H. Barrett, and I. A. Waitz, "Near-airport distribution of the environmental costs of aviation," *Transp. Policy*, vol. 34, pp. 102–108, Jul. 2014, doi: 10.1016/J.TRANPOL.2014.02.023.

[43]   S. H. L. Yim, M. E. J. Stettler, and S. R. H. Barrett, "Air quality and public health impacts of UK airports. Part II: Impacts and policy assessment," *Atmos. Environ.*, vol. 67, pp. 184–192, Mar. 2013, doi: 10.1016/J.ATMOSENV.2012.10.017.

[44]   S. Sgouridis, P. A. Bonnefoy, and R. J. Hansman, "Air transportation in a carbon constrained world: Long-term dynamics of policies and strategies for mitigating the carbon footprint of commercial aviation," *Transp. Res. Part A Policy Pract.*, vol. 45, no. 10, pp. 1077–1091, Dec. 2011, doi: 10.1016/J.TRA.2010.03.019.

[45] R. Teoh, U. Schumann, A. Majumdar, and M. E. J. Stettler, "Mitigating the Climate Forcing of Aircraft Contrails by Small-Scale Diversions and Technology Adoption," *Environ. Sci. Technol.*, vol. 54, no. 5, pp. 2941–2950, Mar. 2020, doi: 10.1021/acs.est.9b05608.

[46] International Renewable Energy Agency, *Biofuels for Aviation: Technology brief*. International Renewable Energy Agency, 2017. Accessed: Mar. 25, 2019. [Online]. Available: www.irena.org

[47] Y. Bicer and I. Dincer, "Life cycle evaluation of hydrogen and other potential fuels for aircrafts," *Int. J. Hydrogen Energy*, vol. 42, no. 16, pp. 10722–10738, Apr. 2017, doi: 10.1016/j.ijhydene.2016.12.119.

[48] D. L. Daggett, R. C. Hendricks, R. Walther, and E. Corporan, "Alternate Fuels for Use in Commercial Aircraft," Apr. 2008, Accessed: Jan. 11, 2019. [Online]. Available: https://ntrs.nasa.gov/search.jsp?R=20080018472

[49] E. Nygren, K. Aleklett, and M. Höök, "Aviation fuel and future oil production scenarios," *Energy Policy*, vol. 37, no. 10, pp. 4003–4010, Oct. 2009, doi: 10.1016/J.ENPOL.2009.04.048.

[50] R. W. Stratton, "Life cycle assessment of greenhouse gas emissions and non-CO_2 combustion effects from alternative jet fuels," 2010, Accessed: Jan. 11, 2019. [Online]. Available: https://dspace.mit.edu/handle/1721.1/59694

[51] J. I. Hileman, P. E. Donohoo, and R. W. Stratton, "Energy Content and Alternative Jet Fuel Viability," *J. Propuls. Power*, vol. 26, no. 6, pp. 1184–1196, Nov. 2010, doi: 10.2514/1.46232.

[52] S. Blakey, L. Rye, and C. W. Wilson, "Aviation gas turbine alternative fuels: A review," *Proc. Combust. Inst.*, vol. 33, no. 2, pp. 2863–2885, Jan. 2011, doi: 10.1016/J.PROCI.2010.09.011.

[53] S. S. Jagtap, "Evaluation of blended Fischer-Tropsch jet fuel feedstocks for minimizing human and environmental health impacts of aviation," in *AIAA Propulsion and Energy 2019 Forum*, 2019. doi: 10.2514/6.2019-4412.

[54] German-Environment-Agency, "Power-to-Liquids Potentials and Perspectives for the Future Supply of Renewable Aviation Fuel," *German Environment Agency*, 2016. https://www.umweltbundesamt.de/sites/default/files/medien/377/publikationen/161005_uba_hintergrund_ptl_b arrierrefrei.pdf (accessed Mar. 10, 2019).

[55] H. Nojoumi, I. Dincer, and G. F. Naterer, "Greenhouse gas emissions assessment of hydrogen and kerosene-fueled aircraft propulsion," *Int. J. Hydrogen Energy*, vol. 34, no. 3, pp. 1363–1369, Feb. 2009, doi: 10.1016/J.IJHYDENE.2008.11.017.

[56] H. Kobayashi, A. Hayakawa, K. D. K. A. Somarathne, and E. C. Okafor, "Science and technology of ammonia combustion," *Proc. Combust. Inst.*, vol. 37, no. 1, pp. 109–133, 2019, doi: 10.1016/j.proci.2018.09.029.

[57] J. L. Toof, "A model for the prediction of thermal, prompt, and fuel NOX emissions from combustion turbines," *J. Eng. Gas Turbines Power*, vol. 108, no. 2, pp. 340–347, 1986, doi: 10.1115/1.3239909.

[58] P. Kumar, "An experimental and numerical study of NOx formation mechanisms in NH3-H2-Air flames," Iowa State University, 2012. Accessed: Dec. 28, 2019. [Online]. Available: https://pdfs.semanticscholar.org/88b2/4d4446889dd608775e933f93f7a95859c9f7.pdf

[59] K. Lokesh, "Techno-economic environmental risk analysis of advanced biofuels for civil aviation," Cranfield University, 2015. Accessed: Jan. 11, 2019. [Online]. Available: https://dspace.lib.cranfield.ac.uk/handle/1826/9243

[60] IATA, "Sustainable Aviation Fuels Sustainable Aviation Fuels: Fact Sheet 2," *International Air Transport Association*, 2020. https://www.iata.org/contentassets/d13875e9ed784f75bac90f000760e998/saf-technical-certifications.pdf (accessed Apr. 06, 2020).

[61] H. Wei, W. Liu, X. Chen, Q. Yang, J. Li, and H. Chen, "Renewable bio-jet fuel production for aviation: A review," *Fuel*, vol. 254. Elsevier Ltd, p. 115599, Oct. 15, 2019. doi: 10.1016/j.fuel.2019.06.007.

[62] N. Pavlenko, S. Searle, and A. Christensen, "The cost of supporting alternative jet fuels in the European Union," *International Council on Clean Transportation*. https://theicct.org/sites/default/files/publications/Alternative_jet_fuels_cost_EU_20190320.pdf (accessed Jul. 13, 2019).

[63] P. Schmidt, V. Batteiger, A. Roth, W. Weindorf, and T. Raksha, "Power-to-Liquids as Renewable Fuel Option for Aviation: A Review," *Chemie Ing. Tech.*, vol. 90, no. 1–2, pp. 127–140, Jan. 2018, doi: 10.1002/cite.201700129.

[64] B. Khandelwal, A. Karakurt, P. R. Sekaran, V. Sethi, and R. Singh, "Hydrogen powered aircraft: The future of air transport," *Progress in Aerospace Sciences*, vol. 60. Elsevier Ltd, pp. 45–59, 2013. doi: 10.1016/j.paerosci.2012.12.002.

[65] D. Verstraete, "Long range transport aircraft using hydrogen fuel," *Int. J. Hydrogen Energy*, vol. 38, no. 34, pp. 14824–14831, Nov. 2013, doi: 10.1016/j.ijhydene.2013.09.021.

[66] D. Verstraete, P. Hendrick, P. Pilidis, and K. Ramsden, "Hydrogen fuel tanks for subsonic transport aircraft," *Int. J. Hydrogen Energy*, vol. 35, no. 20, pp. 11085–11098, Oct. 2010, doi: 10.1016/j.ijhydene.2010.06.060.

[67] S. K. Mital, J. Z. Gyekenyesi, S. M. Arnold, R. M. Sullivan, J. M. Manderscheid, and P. L. N. Murthy, "Review of Current State of the Art and Key Design Issues With Potential Solutions for Liquid Hydrogen Cryogenic

Storage Tank Structures for Aircraft Applications," 2006. Accessed: Jan. 01, 2020. [Online]. Available: https://ntrs.nasa.gov/archive/nasa/casi.ntrs.nasa.gov/20060056194.pdf

[68] D. Verstraete, "On the energy efficiency of hydrogen-fuelled transport aircraft," *Int. J. Hydrogen Energy*, vol. 40, no. 23, pp. 7388–7394, Jun. 2015, doi: 10.1016/j.ijhydene.2015.04.055.

[69] M. Thoennes, A. Busse, and L. Eckstein, "Forecast of Performance Parameters of Automotive Fuel Cell Systems - Delphi Study Results," *Fuel Cells*, vol. 14, no. 6, pp. 781–791, Dec. 2014, doi: 10.1002/fuce.201400035.

[70] M. Delgado Gosálvez *et al.*, "Green Flying: Final Report," *TU Delft*, 2018. https://www.researchgate.net/publication/326294480_The_Greenliner_Green_Flying_Final_Report_DSE_Group_8 (accessed Jan. 02, 2020).

[71] A. F. B. Abu Kasim, M. S. C. Chan, and E. J. Marek, "Performance and failure analysis of a retrofitted Cessna aircraft with a Fuel Cell Power System fuelled with liquid hydrogen," *J. Power Sources*, vol. 521, p. 230987, Feb. 2022, doi: 10.1016/J.JPOWSOUR.2022.230987.

[72] S. Nicolay, S. Karpuk, Y. Liu, and A. Elham, "Conceptual design and optimization of a general aviation aircraft with fuel cells and hydrogen," *Int. J. Hydrogen Energy*, vol. 46, no. 64, pp. 32676–32694, Sep. 2021, doi: 10.1016/J.IJHYDENE.2021.07.127.

[73] E. G. Waddington, J. M. Merret, and P. J. Ansell, "Impact of LH2 Fuel Cell-Electric Propulsion on Aircraft Configuration and Integration," *AIAA Aviat. Aeronaut. Forum Expo. AIAA Aviat. Forum 2021*, 2021, doi: 10.2514/6.2021-2409.

[74] G. Vonhoff, "Conceptual Design of Hydrogen Fuel Cell Aircraft: Flying on hydrogen for a more sustainable future," Delft University of Technology, 2021. Accessed: Aug. 05, 2022. [Online]. Available: https://repository.tudelft.nl/islandora/object/uuid%3A8bd63dec-b67b-496b-92bc-3d5c07ff859f

[75] B. J. Brelje and J. R. R. A. Martins, "Aerostructural wing optimization for a hydrogen fuel cell aircraft," *AIAA Scitech 2021 Forum*, pp. 1–18, 2021, doi: 10.2514/6.2021-1132.

[76] F. Nicolosi, V. Marciello, and F. Orefice, "Conceptual Design of a Hydrogen-Propelled Aircraft with Distributed Electric Propulsion," Jun. 2022, doi: 10.2514/6.2022-3205.

[77] C. L. Pastra, G. Cinar, and D. N. Mavris, "Feasibility and benefit assessments of hybrid hydrogen fuel cell and battery configurations on a regional turboprop aircraft," Jun. 2022, doi: 10.2514/6.2022-3290.

[78] T. Dietl *et al.*, "POLARIS-DESIGN OF A LIQUID HYDROGEN TURBO-ELECTRIC TRANSPORT AIRCRAFT," 2018. doi: 10.25967/480344.

[79] T. Y. J. Druot, N. Peteilh, P. Roches, and N. Monrolin, "Hydrogen Powered Airplanes, an exploration of possible architectures leveraging boundary layer ingestion and hybridization," *AIAA Sci. Technol. Forum Expo. AIAA SciTech Forum 2022*, 2022, doi: 10.2514/6.2022-1025.

[80] PowerCell, "PowerCell S3," *PowerCell*, 2020. https://bumhan.com/wp-content/uploads/sites/126/2021/02/PowerCell-S3.pdf (accessed Aug. 16, 2020).

[81] HyPoint, "HyPoint," *H2-view*. https://www.h2-view.com/sponsorships/hypoint/ (accessed Sep. 28, 2022).

[82] S. West, "Decarbonizing Aviation A Climate Technology White Paper," *BloombergNEF*, 2022.

[83] EASA, "ICAO Aircraft Engine Emissions Databank," *EASA*, 2021. https://www.easa.europa.eu/domains/environment/icao-aircraft-engine-emissions-databank (accessed Aug. 16, 2020).

[84] National-Academies-of-Sciences-Engineering-and-Medicine, *Commercial aircraft propulsion and energy systems research: Reducing global carbon emissions*. National Academies Press, 2016. doi: 10.17226/23490.

[85] EASA, "TYPE-CERTIFICATE DATA SHEET for GE90 Series Engines," *EASA*, 2019. https://www.easa.europa.eu/downloads/7799/en (accessed Aug. 16, 2020).

[86] C. Winnefeld, T. Kadyk, B. Bensmann, U. Krewer, and R. Hanke-Rauschenbach, "Modelling and Designing Cryogenic Hydrogen Tanks for Future Aircraft Applications," *Energies*, vol. 11, no. 1, p. 105, Jan. 2018, doi: 10.3390/en11010105.

[87] P. Rompokos *et al.*, "Synergistic technology combinations for future commercial aircraft using liquid hydrogen," *J. Eng. Gas Turbines Power*, vol. 143, no. 7, Jul. 2021, doi: 10.1115/1.4049694/1095473.

[88] E. Fonseca, "Heat Recovery System for a Gas Turbine Engine," Apr. 07, 2011 Accessed: Jan. 11, 2019. [Online]. Available: https://patents.google.com/patent/US20140190162A1/en

[89] E. E. FONSECA, "HEAT RECOVERY SYSTEM FOR A GAS TURBINE ENGINE," May 2012, Accessed: Jan. 11, 2019. [Online]. Available: https://patentscope.wipo.int/search/en/detail.jsf?docId=WO2012057848

[90] C. A. Perullo, D. N. Mavris, and E. Fonseca, "An Integrated Assessment of an Organic Rankine Cycle Concept for Use in Onboard Aircraft Power Generation," in *Volume 2: Aircraft Engine; Coal, Biomass and Alternative Fuels; Cycle Innovations*, Jun. 2013, p. V002T01A028. doi: 10.1115/GT2013-95734.

[91] S. S. Jagtap, "Heat recuperation system for the family of shaft powered aircraft gas turbine engines," Oct. 14, 2014 Accessed: Jan. 11, 2019. [Online]. Available: https://patents.google.com/patent/US20180334959A1/en

[92] S. S. Jagtap, "Heat recuperation system for the family of shaft powered aircraft gas turbine engines," May 07, 2016 Accessed: Jan. 11, 2019. [Online]. Available:

https://patentscope.wipo.int/search/en/detail.jsf?docId=WO2016067303

[93] S. S. Jagtap, "An Apparatus for Exchanging Heat with Flow in an Annulus," *J. Eng. Sci. Technol. Rev.*, vol. 10, no. 1, pp. 173–176, 2017, Accessed: Jan. 11, 2019. [Online]. Available: http://www.jestr.org/downloads/Volume10Issue1/fulltext241012017.pdf

[94] D. Misirlis *et al.*, "INTERCOOLED RECUPERATED AERO ENGINE: DEVELOPMENT AND OPTIMIZATION OF INNOVATIVE HEAT EXCHANGER CONCEPTS," in *2nd ECATS Conference Making aviation environmentally*, 2016. Accessed: May 01, 2019. [Online]. Available: http://www.ecats-network.eu/uploads/2017/06/ECATS2016_2.10-Misirlis_etal.pdf

[95] R. McRoberts, J. M. Early, F. Morscheck, M. Price, and B. Korn, "Tanker Mission Implication on a Civil Aerial Refuelling Transport System's Benefit Evaluation," *J. Aircr.*, vol. 52, no. 1, pp. 320–328, Jan. 2015, doi: 10.2514/1.C032726.

[96] R. K. Nangia, "Highly Efficient Civil Aviation, Now via Operations - AAR & Challenges," in *2018 Aviation Technology, Integration, and Operations Conference*, Jun. 2018. doi: 10.2514/6.2018-3591.

[97] Verhagen, "Formation flight in civil aviation," TU Delft, 2015. Accessed: Jan. 11, 2019. [Online]. Available: https://repository.tudelft.nl/islandora/object/uuid:44cc6034-e974-4306-a540-9195a48322f8/datastream/OBJ/download

[98] "Distance from Seattle (SEA) to Miami (MIA)." https://www.airmilescalculator.com/distance/sea-to-mia/ (accessed Jan. 11, 2019).

[99] M. V Chester and A. Horvath, "Environmental assessment of passenger transportation should include infrastructure and supply chains," *Environ. Res. Lett.*, vol. 4, no. 2, p. 024008, Apr. 2009, doi: 10.1088/1748-9326/4/2/024008.

[100] S. S. Jagtap, "Sustainability assessment of hydro-processed renewable jet fuel from algae from market-entry year 2020: Use in passenger aircrafts," in *16th AIAA Aviation Technology, Integration, and Operations Conference*, Jun. 2016. doi: 10.2514/6.2016-4367.

[101] "The National Research Council of Canada joins partners to investigate aircraft contrails from biofuel blends - National Research Council Canada," *National Research Council Canada*, 2017. https://www.nrc-cnrc.gc.ca/eng/stories/2017/aero_biofuel_blends.html (accessed Jan. 16, 2019).

[102] K. Walker, "Canadian 100% biofuel flight tests show significant emission reductions | Eco-Aviation content from ATWOnline," *Air Transport World*, 2013. http://atwonline.com/eco-aviation/canadian-100-biofuel-flight-tests-show-significant-emission-reductions (accessed Jan. 16, 2019).

[103] M. Kousoulidou and L. Lonza, "Biofuels in aviation: Fuel demand and CO2 emissions evolution in Europe toward 2030," *Transp. Res. Part D Transp. Environ.*, vol. 46, pp. 166–181, Jul. 2016, doi: 10.1016/J.TRD.2016.03.018.

[104] ATR, "ATR successfully performs test flights with 100% SAF in one engine - ATR," *ATR*, Feb. 2022. https://www.atr-aircraft.com/presspost/atr-successfully-performs-test-flights-with-100-saf-in-one-engine/ (accessed Jul. 18, 2022).

[105] Rolls Royce, "Rolls-Royce - Rolls-Royce conducts first tests of 100% sustainable aviation fuel for use in business jets," *Rolls Royce*, 2021. https://www.rolls-royce.com/media/press-releases/2021/01-02-2021-business-aviation-rr-conducts-first-tests-of-100-precent-sustainable-aviation-fuel.aspx (accessed Jul. 18, 2022).

[106] Airbus, "First A380 powered by 100% Sustainable Aviation Fuel takes to the skies ," *Airbus*, 2022. https://www.airbus.com/en/newsroom/press-releases/2022-03-first-a380-powered-by-100-sustainable-aviation-fuel-takes-to-the (accessed Jul. 18, 2022).

[107] S. Menon, "How is the world's first solar powered airport faring? - BBC News," *BBC news*, Oct. 09, 2015. Accessed: Jan. 14, 2019. [Online]. Available: https://www.bbc.co.uk/news/world-asia-india-34421419

[108] D. Carrington, "Solar plane makes history after completing round-the-world trip | Environment | The Guardian," *The Guardian*, Jul. 26, 2016. Accessed: Jan. 14, 2019. [Online]. Available: https://www.theguardian.com/environment/2016/jul/26/solar-impulse-plane-makes-history-completing-round-the-world-trip

[109] U. of Cambridge, "Watts up - aeroplanes go hybrid-electric," *University of Cambridge*, 2014. https://www.cam.ac.uk/research/news/watts-up-aeroplanes-go-hybrid-electric (accessed Jan. 14, 2019).

[110] DLR, "Conceptual study for environment-friendly flight," *DLR*, 2020. https://www.dlr.de/en/latest/news/2020/02/20200504_conceptual-study-for-environment-friendly-flight (accessed May 26, 2021).

[111] A. Hern, "First ever plane with no moving parts takes flight | Science | The Guardian," *The Guardian*, Nov. 21, 2018. Accessed: Jan. 14, 2019. [Online]. Available: https://www.theguardian.com/science/2018/nov/21/first-ever-plane-with-no-moving-parts-takes-flight

[112] J. Korn, "Alice, the first all-electric passenger airplane, takes flight | CNN Business," *CNN*, 2022. https://edition.cnn.com/2022/09/27/tech/eviation-alice-first-flight/index.html (accessed Oct. 12, 2022).

[113] J. M. Cullen and C. Hall, "Engineering Fundamentals of Energy Efficiency," University of Cambridge, 2009. Accessed: Mar. 10, 2019. [Online]. Available:

https://www.repository.cam.ac.uk/bitstream/handle/1810/225127/Cullen 2009 PhD thesis.pdf?sequence=1&isAllowed=y

[114]   RAeS, "Air Travel - Greener by Design The Technology Challenge, Report of the Technology Sub-Group," 2003. Accessed: Mar. 10, 2019. [Online]. Available: https://www.aerosociety.com/Assets/Docs/About_Us/Greener By Design/GbD - 2003 The Tech Challenge.pdf

[115]   M. J. Benzakein, "What does the future bring? A look at technologies for commercial aircraft in the years 2035–2050," *Propulsion_and_Power Res.*, vol. 3, no. 4, pp. 165–174, Dec. 2014, doi: 10.1016/J.JPPR.2014.11.004.

[116]   F. Collier, "Concepts and technologies for Green Aviation," in *Green Engineering Masters Forum*, 2009. [Online]. Available: https://www.nasa.gov/pdf/395949main_collier.pdf

[117]   S. S. Jagtap, "Systems evaluation of subsonic hybrid-electric propulsion concepts for NASA N+3 goals and conceptual aircraft sizing," *Int. J. Automot. Mech. Eng.*, vol. 16, no. 4, pp. 7259–7286, 2019, doi: https://doi.org/10.15282/ijame.16.4.2019.07.0541.

[118]   H. Kim and M.-S. Liou, "Flow simulation and optimal shape design of N3-X hybrid wing body configuration using a body force method," *Aerosp. Sci. Technol.*, vol. 71, pp. 661–674, Dec. 2017, doi: 10.1016/J.AST.2017.09.046.

[119]   J. L. Felder, G. V. Brown, H. DaeKim, and J. Chu, "Turboelectric Distributed Propulsion in a Hybrid Wing Body Aircraft," 2011. Accessed: Aug. 19, 2020. [Online]. Available: https://ntrs.nasa.gov/citations/20120000856

[120]   A. Seitz *et al.*, "Concept validation study for fuselage wake-filling propulsion integration," *31st Congr. Int. Counc. Aeronaut. Sci. ICAS 2018*, 2018, Accessed: Aug. 19, 2020. [Online]. Available: https://research.chalmers.se/en/publication/508475

[121]   "Imagine travelling in this blended wing body aircraft - Innovation - Airbus." https://www.airbus.com/newsroom/stories/Imagine-travelling-in-this-blended-wing-body-aircraft.html (accessed Aug. 19, 2020).

[122]   "KLM and TU Delft join forces to make aviation more sustainable." https://news.klm.com/klm-and-tu-delft-join-forces-to-make-aviation-more-sustainable/ (accessed Aug. 19, 2020).

[123]   E. M. Greitzer *et al.*, "N+3 Aircraft Concept Designs and Trade Studies, Final Report, Volume 1," 2010. [Online]. Available: https://ntrs.nasa.gov/archive/nasa/casi.ntrs.nasa.gov/20100042401.pdf

[124]   T. Grönstedt *et al.*, "Ultra Low Emission Technology Innovations for Mid-Century Aircraft Turbine Engines," in *Volume 3: Coal, Biomass and Alternative Fuels; Cycle Innovations; Electric Power; Industrial and Cogeneration; Organic Rankine Cycle Power Systems*, Jun. 2016, p. V003T06A001. doi: 10.1115/GT2016-56123.

[125]   B. J. Brelje and J. R. R. A. Martins, "Electric, hybrid, and turboelectric fixed-wing aircraft: A review of concepts, models, and design approaches," *Prog. Aerosp. Sci.*, vol. 104, pp. 1–19, Jan. 2019, doi: 10.1016/J.PAEROSCI.2018.06.004.

[126]   C. Pornet and A. T. Isikveren, "Conceptual design of hybrid-electric transport aircraft," *Prog. Aerosp. Sci.*, vol. 79, pp. 114–135, Nov. 2015, doi: 10.1016/J.PAEROSCI.2015.09.002.

[127]   J. Mukhopadhaya and D. Rutherford, "Performance analysis of evolutionary hydrogen-powered aircraft," *International Council on Clean Transportation*, 2022. https://theicct.org/publication/aviation-global-evo-hydrogen-aircraft-jan22/ (accessed Jun. 04, 2022).

[128]   S. Job, M. Campbell, B. Hall, Z. Hamadache, and N. Kumar, "SUSTAINABILITY REPORT - The Lifecycle Impact of Hydrogen-Powered Aircraft," 2022. Accessed: Jun. 05, 2022. [Online]. Available: https://www.ati.org.uk/wp-content/uploads/2022/03/FZO-STY-REP-0005-FlyZero-Sustainability-Report.pdf

[129]   Droneii, "Pushing the Boundaries-Drone Energy Sources," *Drone Industry Insights*, 2017. https://www.droneii.com/wp-content/uploads/2017/06/Drone-Energy-Sources.pdf (accessed Aug. 19, 2020).

[130]   C. L. Nickol and W. J. Haller, "Assessment of the Performance Potential of Advanced Subsonic Transport Concepts for NASA's Environmentally Responsible Aviation Project," in *54th AIAA Aerospace Sciences Meeting*, Jan. 2016. doi: 10.2514/6.2016-1030.

[131]   E. Torenbeek, "Blended wing body and all-wing airliners." Accessed: Jan. 19, 2019. [Online]. Available: http://www.fzt.haw-hamburg.de/pers/Scholz/ewade/2007/EWADE2007_Torenbeek.pdf

[132]   N. B. Kuntawala, "Aerodynamic Shape Optimization of a Blended-Wing-Body Aircraft Configuration," University of Toronto, 2011. Accessed: Jan. 18, 2019. [Online]. Available: https://tspace.library.utoronto.ca/bitstream/1807/31289/6/Kuntawala_Nimeesha_B_201111_MASc_thesis.pdf

[133]   R. Liebeck, M. Page, and B. Rawdon, "Blended-wing-body subsonic commercial transport," in *36th AIAA Aerospace Sciences Meeting and Exhibit*, Jan. 1998. doi: 10.2514/6.1998-438.

[134]   S. Peigin and B. Epstein, "Computational Fluid Dynamics Driven Optimization of Blended Wing Body Aircraft," *AIAA J.*, vol. 44, no. 11, pp. 2736–2745, Nov. 2006, doi: 10.2514/1.19757.

[135]   N. Qin, A. Vavalle, A. Le Moigne, M. Laban, K. Hackett, and P. Weinerfelt, "Aerodynamic studies for blended wing body aircraft," in *9th AIAA/ISSMO Symposium on Multidisciplinary Analysis and Optimization*, 2002. doi:

10.2514/6.2002-5448.

[136] S. Siouris and N. Qin, "Study of the effects of wing sweep on the aerodynamic performance of a blended wing body aircraft," *Proc. Inst. Mech. Eng. Part G J. Aerosp. Eng.*, vol. 221, no. 1, pp. 47–55, Jan. 2007, doi: 10.1243/09544100JAERO93.

[137] M. A. Potsdam, M. A. Page, R. H. Liebeck, D. Mcdonnell, L. Aerospace, and C. Beach, "Blended wing body analysis and design," in *15th Applied Aerodynamics Conference*, 1997. doi: 10.2514/6.1997-2317.

[138] A. . Bolsunovsky *et al.*, "Flying wing—problems and decisions," *Aircr. Des.*, vol. 4, no. 4, pp. 193–219, Dec. 2001, doi: 10.1016/S1369-8869(01)00005-2.

[139] R. H. Liebeck, "Design of the Blended Wing Body Subsonic Transport," *J. Aircr.*, vol. 41, no. 1, pp. 10–25, Jan. 2004, doi: 10.2514/1.9084.

[140] D. Roman, R. Gilmore, and S. Wakayama, "Aerodynamics of high subsonic blended wing body configuations," in *41st Aerospace Sciences Meeting and Exhibit*, 2003. doi: 10.2514/6.2003-554.

[141] C. ¨ Osterheld, W. Heinze, and P. Horst, "Preliminary Design of a Blended Wing Body Configuration using the Design Tool PrADO," in *DGLR BERICHT 5*, 2001. Accessed: Jan. 18, 2019. [Online]. Available: http://citeseerx.ist.psu.edu/viewdoc/download?doi=10.1.1.69.7786&rep=rep1&type=pdf

[142] T. Pambagjo, K. Nakahashi, S. Obayashi, and K. Matsushima, "Aerodynamic design of a medium size blended-wing-body airplane," in *39th Aerospace Sciences Meeting and Exhibit*, Jan. 2001. doi: 10.2514/6.2001-129.

[143] N. Qin, A. Vavalle, A. Le Moigne, M. Laban, K. Hackett, and P. Weinerfelt, "Aerodynamic considerations of blended wing body aircraft," *Prog. Aerosp. Sci.*, vol. 40, no. 6, pp. 321–343, Aug. 2004, doi: 10.1016/J.PAEROSCI.2004.08.001.

[144] D. Roman, J. Allen, and R. Liebeck, "Aerodynamic design challenges of the Blended-Wing-Body subsonic transport," in *18th Applied Aerodynamics Conference*, Aug. 2000. doi: 10.2514/6.2000-4335.

[145] N. Qin, A. Vavalle, and A. Le Moigne, "Spanwise Lift Distribution for Blended Wing Body Aircraft," *J. Aircr.*, vol. 42, no. 2, 2005, doi: 10.2514/1.4229.

[146] A. Diedrich, J. Hileman, D. Tan, K. Willcox, and Z. Spakovszky, "Multidisciplinary Design and Optimization of the Silent Aircraft," in *44th AIAA Aerospace Sciences Meeting and Exhibit*, Jan. 2006. doi: 10.2514/6.2006-1323.

[147] R. Liebeck, "Blended Wing Body Design Challenges," in *AIAA International Air and Space Symposium and Exposition: The Next 100 Years*, Jul. 2003. doi: 10.2514/6.2003-2659.

[148] T. E. Pambagjo, K. Nakahashi, and K. Matsushima, "An Alternate Configuration for a Regional Transport Airplane.," *Trans. Jpn. Soc. Aeronaut. Space Sci.*, vol. 45, no. 148, pp. 94–101, 2002, doi: 10.2322/tjsass.45.94.

[149] V. Mukhopadhyay, "Blended Wing Body (BWB) Fuselage Structural Design for Weight Reduction," in *46th AIAA/ASME/ASCE/AHS/ASC Structures, Structural Dynamics and Materials Conference*, Apr. 2005. doi: 10.2514/6.2005-2349.

[150] D. Vicroy, "Blended-Wing-Body Low-Speed Flight Dynamics: Summary of Ground Tests and Sample Results (Invited)," in *47th AIAA Aerospace Sciences Meeting including The New Horizons Forum and Aerospace Exposition*, Jan. 2009. doi: 10.2514/6.2009-933.

[151] S. Wakayama and I. Kroo, "The challenge and promise of blended-wing-body optimization," in *7th AIAA/USAF/NASA/ISSMO Symposium on Multidisciplinary Analysis and Optimization*, Sep. 1998. doi: 10.2514/6.1998-4736.

[152] J. D. Flamm, K. James, and J. T. Bonet, "Overview Of ERA Integrated Technology Demonstration (ITD) 51A Ultra-High Bypass (UHB) Integration for Hybrid Wing Body (HWB) (Invited)," in *54th AIAA Aerospace Sciences Meeting*, Jan. 2016. doi: 10.2514/6.2016-0007.

[153] M. Stettner and R. Voss, "Aeroelastic, Flight Mechanic, and Handling Qualities of the MOB BWB Configuration," in *9th AIAA/ISSMO Symposium on Multidisciplinary Analysis and Optimization*, Sep. 2002. doi: 10.2514/6.2002-5449.

[154] E. R. Galea, L. Filippidis, Z. Wang, and J. Ewer, "Fire and evacuation analysis in BWB aircraft configurations: computer simulations and large-scale evacuation experiment," *Aeronaut. J.*, vol. 114, no. 1154, pp. 271–277, Apr. 2010, doi: 10.1017/S0001924000003717.

[155] P. Okonkwo and H. Smith, "Review of evolving trends in blended wing body aircraft design," *Prog. Aerosp. Sci.*, vol. 82, pp. 1–23, Apr. 2016, doi: 10.1016/J.PAEROSCI.2015.12.002.

[156] Siti Mardiana, "Modifying Research Onion for Information Systems Research," *Solid State Technol.*, vol. 63, no. 4, 2020, Accessed: Jul. 13, 2022. [Online]. Available: http://solidstatetechnology.us/index.php/JSST/article/view/4321

[157] A. Melnikovas, "Towards an Explicit Research Methodology: Adapting Research Onion Model for Futures Studies," *J. Futur. Stud.*, vol. 23, no. 2, pp. 29–44, 2018, doi: 10.6531/JFS.201812_23(2).0003.

[158] "Inductive or Deductive? Two Different Approaches." https://saylordotorg.github.io/text_principles-of-sociological-inquiry-qualitative-and-quantitative-methods/s05-03-inductive-or-deductive-two-dif.html (accessed Dec. 08, 2020).

[159] P.-J. Proesmans and R. Vos, "Comparison of Future Aviation Fuels to Minimize the Climate Impact of

Commercial Aircraft," Jun. 2022, doi: 10.2514/6.2022-3288.

[160] Airbus, "Airbus reveals new zero-emission concept aircraft," *Airbus*, 2020. https://www.airbus.com/en/newsroom/press-releases/2020-09-airbus-reveals-new-zero-emission-concept-aircraft (accessed Nov. 15, 2021).

[161] Carrie Hampel, "Airbus works on metallic tanks for liquid hydrogen," *Electrive.com*, 2021. https://www.electrive.com/2021/06/17/airbus-works-on-metallic-tanks-for-liquid-hydrogen/ (accessed Nov. 15, 2021).

[162] Hydrogen-Central, "Hamburg Testing use of Liquid Hydrogen in Aviation," *Hydrogen Central*, 2021. https://hydrogen-central.com/hamburg-testing-liquid-hydrogen-aviation/ (accessed Nov. 15, 2021).

[163] Airbus, "Airbus establishes Zero-Emission Development Centres in Germany and France," *Airbus*, 2021. https://www.airbus.com/en/newsroom/press-releases/2021-06-airbus-establishes-zero-emission-development-centres-in-germany-and (accessed Nov. 15, 2021).

[164] T. Hardingham-Gill, "Airbus to use A380 to test hydrogen-fueled engine | CNN Travel," *CNN*, 2022. https://edition.cnn.com/travel/article/airbus-test-hydrogen-fueled-engines-on-a380/index.html (accessed Jun. 23, 2022).

[165] M. Prewitz, A. Bardenhagen, and R. Beck, "Hydrogen as the fuel of the future in aircrafts – Challenges and opportunities," *Int. J. Hydrogen Energy*, vol. 45, no. 46, pp. 25378–25385, Sep. 2020, doi: 10.1016/J.IJHYDENE.2020.06.238.

[166] B. Yang, M. Mane, and W. A. Crossley, "An Approach to Evaluate Fleet Level CO2 Impact of Introducing Liquid-Hydrogen Aircraft to a World-Wide Network," Jun. 2022, doi: 10.2514/6.2022-3313.

[167] F. Svensson, "Potential of reducng the environmental impact of civil subsonic aviation by using liquid hydrogen," Cranfield University, 2005. Accessed: Jun. 17, 2022. [Online]. Available: https://dspace.lib.cranfield.ac.uk/handle/1826/10726

[168] D. Silberhorn, G. Atanasov, J.-N. Walther, and T. Zill, "ASSESSMENT OF HYDROGEN FUEL TANK INTEGRATION AT AIRCRAFT LEVEL," *Inst. Transp. Res.*, 2019.

[169] J. Hoelzen, D. Silberhorn, T. Zill, B. Bensmann, and R. Hanke-Rauschenbach, "Hydrogen-powered aviation and its reliance on green hydrogen infrastructure – Review and research gaps," *Int. J. Hydrogen Energy*, vol. 47, no. 5, pp. 3108–3130, Jan. 2022, doi: 10.1016/J.IJHYDENE.2021.10.239.

[170] W. F. Lammen, B. Peerlings, E. S. van der Sman, and J. Kos, "Hydrogen-powered propulsion aircraft: conceptual sizing and fleet level impact analysis," *Netherlands Aerospace Centre: NLR*, 2022. http://hdl.handle.net/10921/1587 (accessed Oct. 07, 2022).

[171] V. Cipolla, D. Zanetti, K. A. Salem, V. Binante, and G. Palaia, "A Parametric Approach for Conceptual Integration and Performance Studies of Liquid Hydrogen Short–Medium Range Aircraft," *Appl. Sci. 2022, Vol. 12, Page 6857*, vol. 12, no. 14, p. 6857, Jul. 2022, doi: 10.3390/APP12146857.

[172] A. Gomez and H. Smith, "Liquid hydrogen fuel tanks for commercial aviation: Structural sizing and stress analysis," *Aerosp. Sci. Technol.*, vol. 95, p. 105438, Dec. 2019, doi: 10.1016/j.ast.2019.105438.

[173] F. Troeltsch, M. Engelmann, F. Peter, J. Kaiser, M. Hornung, and A. E. Scholz, "Hydrogen powered long haul aircraft with minimized climate impact," *AIAA Aviat. 2020 FORUM*, p. 14, 2020, doi: 10.2514/6.2020-2660.

[174] V. Grewe *et al.*, "Assessing the climate impact of the AHEAD multi-fuel blended wing body," *Meteorol. Zeitschrift*, vol. 26, no. 6, pp. 711–725, 2017, doi: 10.1127/METZ/2016/0758.

[175] Airbus, "Liquid Hydrogen Fuelled Aircraft-System Analysis: CRYOPLANE Final Technical report," 2003. https://www.fzt.haw-hamburg.de/pers/Scholz/dglr/hh/text_2004_02_26_Cryoplane.pdf (accessed Dec. 30, 2019).

[176] D. Silberhorn *et al.*, "Climate Impact Reduction Potentials of Synthetic Kerosene and Green Hydrogen Powered Mid-Range Aircraft Concepts," *Appl. Sci. 2022, Vol. 12, Page 5950*, vol. 12, no. 12, p. 5950, Jun. 2022, doi: 10.3390/APP12125950.

[177] G. Onorato, P. Proesmans, and M. F. M. Hoogreef, "Assessment of hydrogen transport aircraft: Effects of fuel tank integration," *CEAS Aeronaut. J.*, vol. 1, pp. 1–33, Sep. 2022, doi: 10.1007/S13272-022-00601-6/TABLES/11.

[178] J. Huete, D. Nalianda, and P. Pilidis, "Impact of tank gravimetric efficiency on propulsion system integration for a first-generation hydrogen civil airliner," *Aeronaut. J.*, vol. 126, no. 1302, pp. 1324–1332, Aug. 2022, doi: 10.1017/AER.2022.60.

[179] J. Huete, D. Nalianda, and P. Pilidis, "Propulsion system integration for a first-generation hydrogen civil airliner?," *Aeronaut. J.*, vol. 125, no. 1291, pp. 1654–1665, Sep. 2021, doi: 10.1017/AER.2021.36.

[180] G. D. Brewer, *Hydrogen aircraft technology*. CRC Press, 2017. doi: 10.1201/9780203751480.

[181] Reinhard Faass, "CRYOPLANE," 2001. https://www.fzt.haw-hamburg.de/pers/Scholz/dglr/hh/text_2001_12_06_Cryoplane.pdf (accessed Dec. 28, 2019).

[182] A. Bauen, N. Bitossi, L. German, A. Harris, and K. Leow, "Sustainable aviation fuels status, challenges and prospects of drop-in liquid fuels, hydrogen and electrification in aviation," *Johnson Matthey Technol. Rev.*, vol. 64, no. 3, pp. 263–278, Jul. 2020, doi: 10.1595/205651320x15816756012040.

[183] I. A. Waitz., "Lecture: Breguet's range equation," *Lecture notes*, 2008. https://web.mit.edu/16.unified/www/FALL/Unified_Concepts/Breguet-Range-U2-notes-Fall08(2).pdf (accessed Aug. 27, 2020).

[184] A. K. Kundu, M. A. Price, and D. Riordan, *Conceptual Aircraft Design : an Industrial Perspective.*, First. John Wiley & Sons, Incorporated, 2019.

[185] M. R. Kirby, "A methodology for technology identification, evaluation, and selection in conceptual and preliminary aircraft design," Georgia Institute of Technology, 2001. Accessed: Dec. 17, 2019. [Online]. Available: https://pdfs.semanticscholar.org/3e8f/f5be8491a4f30f4dbb9edce1ff08cfd5b45a.pdf

[186] "GasTurb - GasTurb." https://gasturb.de/software/gasturb.html (accessed Apr. 10, 2020).

[187] J. Kurzke, "GasTurb 13 Design and Off-Design Performance of Gas Turbines," 2018.

[188] J. Kurzke, "GasTurb 13," *GasTurb GmbH*, 2017. https://gasturb.de/software/gasturb.html

[189] J. Kurzke and I. Halliwell, *Propulsion and Power: An Exploration of Gas Turbine Performance Modeling*. Springer International Publishing, 2018. doi: 10.1007/978-3-319-75979-1.

[190] P. P. Walsh and P. Fletcher, *Gas Turbine Performance*. Wiley, 2004. doi: 10.1002/9780470774533.

[191] D. Verstraete, "The Potential of Liquid Hydrogen for long range aircraft propulsion," Cranfield University, 2009. Accessed: Aug. 27, 2020. [Online]. Available: http://dspace.lib.cranfield.ac.uk/handle/1826/4089

[192] A. Goldmann *et al.*, "A Study on Electrofuels in Aviation," *Energies*, vol. 11, no. 2, p. 392, Feb. 2018, doi: 10.3390/en11020392.

[193] G. Kenway *et al.*, "Reducing Aviation's Environmental Impact Through Large Aircraft for Short Ranges," in *48th AIAA Aerospace Sciences Meeting Including the New Horizons Forum and Aerospace Exposition*, Jan. 2010. doi: 10.2514/6.2010-1015.

[194] K. Seeckt, "Aircraft Preliminary Sizing with PreSTo Re-Design of the Boeing B777-200LR Aircraft Preliminary Sizing with PreSTo," 2008.

[195] G. Dimitriadis, "Introduction to Aircraft Design: Aircraft Performance," *Université de Liège*, 2017. http://www.ltas-cm3.ulg.ac.be/AERO0023-1/ConceptionAeroPerformances.pdf (accessed Feb. 13, 2020).

[196] J. Henn *et al.*, "Environautics: AIAA Foundation Undergraduate Team Aircraft Design Competition 2009-10," 2010.

[197] PIANO-X, "Boeing 787 Dreamliner : Analysis," *PIANO-X*, 2005. https://www.lissys.uk/samp1/index.html (accessed Aug. 28, 2020).

[198] J. Roskam, *Airplane Design. Part I: Preliminary Sizing of Airplanes*. DAR Corporation, 2005.

[199] C. L. Nickol and L. A. McCullers, "Hybrid Wing body configuration system studies," in *47th AIAA Aerospace Sciences Meeting including the New Horizons Forum and Aerospace Exposition*, 2009. doi: 10.2514/6.2009-931.

[200] D. Scholz, "Drag Prediction," *Lecture notes*, 2017. https://www.fzt.haw-hamburg.de/pers/Scholz/HOOU/AircraftDesign_13_Drag.pdf (accessed Aug. 28, 2020).

[201] D. Raymer, *Aircraft Design: A Conceptual Approach, Sixth Edition*. Washington, DC: American Institute of Aeronautics and Astronautics, Inc., 2018. doi: 10.2514/4.104909.

[202] P. L. Varghese, "Weight and CG estimation," *Lecture notes University of Texas, Austin*, 1999. https://www.ae.utexas.edu/~plv955/class/aircraft/weights2.PDF (accessed Aug. 28, 2020).

[203] Z. Goraj, "Design and Optimisation of Fuel Tanks for BWB Configurations," *Arch. Mech. Eng.*, vol. 63, no. 4, pp. 605–617, Dec. 2016, doi: 10.1515/meceng-2016-0034.

[204] G. Polek, "HyPoint Extends Hydrogen Flight Range with New Ultralight Fuel Tanks," *FutureFlight*, Mar. 29, 2022. https://www.futureflight.aero/news-article/2022-03-29/hypoint-extends-hydrogen-flight-range-new-ultralight-fuel-tanks (accessed Jul. 22, 2022).

[205] J. Sjöberg, J. Smith, O. Haglund Nilsson, P. Emanuelsson, and S. Otlu, "Liquid Hydrogen Tanks for Low-Emission Aircraft," Chalmers University of Technology, 2021. Accessed: Aug. 03, 2022. [Online]. Available: https://odr.chalmers.se/handle/20.500.12380/302666

[206] Air-Liquide, "Hydrogen storage on board aeronef and ground infrastructure : Air Liquide Advanced Technologies-Workshop on aeronautical applications of fuel cell and hydrogen technologies," *FCH - CleanSky joint workshop*, 2015.

[207] Wessington-Cryogenics, "ISO VAC 40 LNG : 40 ft LNG Iso Container," *Wessington Cryogenics*, 2020. https://wessingtoncryogenics.com/products/liquefied-natural-gas-containers/iso-vac-40-lng/ (accessed Sep. 15, 2021).

[208] I. Dincer and C. Zamfirescu, "Sustainable Hydrogen Production," *Elsevier*, 2016. https://books.google.co.uk/books/about/Sustainable_Hydrogen_Production.html?id=c7h0BgAAQBAJ&redir_esc=y (accessed Aug. 28, 2020).

[209] Airbus, "A350 AIRCRAFT CHARACTERISTICS AIRPORT AND MAINTENANCE PLANNING," *Airbus*, 2020. https://www.airbus.com/sites/g/files/jlcbta136/files/2021-11/Airbus-Commercial-Aircraft-AC-A350-900-1000.pdf

[210] M. Burzlaff and I. D. Scholz, "Project Aircraft Fuel Consumption-Estimation and Visualization," 2017. doi:

10.7910/DVN/2HMEHB.

[211]   National-Academies-of-Sciences-Engineering-and-Medicine, *Commercial Aircraft Propulsion and Energy Systems Research*. Washington, D.C.: National Academies Press, 2016. doi: 10.17226/23490.

[212]   Airbus, "Airbus A350 XWB," *Airbus*, 2014. https://web.archive.org/web/20131129074833/http://www.airbus.com/aircraftfamilies/passengeraircraft/a350xwbfamily/technology-and-innovation/ (accessed Nov. 09, 2022).

[213]   M. Gerzanics, "FLIGHT TEST: Airbus A350-1000 takes growth in its stride | In depth | Flight Global," *Flight-Global*, 2018. https://www.flightglobal.com/in-depth/flight-test-airbus-a350-1000-takes-growth-in-its-stride/128532.article (accessed Nov. 09, 2022).

[214]   D. S. Gerren, "Design, Analysis, and Control of a Large Transport Aircraft Utilizing Selective Engine Thrust as a Backup System for the Primary Flight Control," *NASA*, 1995. https://ntrs.nasa.gov/api/citations/19960003535/downloads/19960003535.pdf (accessed Nov. 09, 2022).

[215]   Engineering-toolbox, "U.S. Standard Atmosphere," *Engineering-toolbox*, 2003. https://www.engineeringtoolbox.com/standard-atmosphere-d_604.html (accessed Aug. 27, 2020).

[216]   S. Pfeifer, "Airbus to test hydrogen-powered engine on A380 superjumbo," *Financial Times*, 2022. Accessed: Jul. 15, 2022. [Online]. Available: https://www.ft.com/content/3a5f7756-781a-418e-a151-0c87f85fa3df

[217]   R. Beck *et al.*, "Efficiency meets sky," *Joint NASA/DLR Aeronautics design challenge 2017-18*, 2018. https://www.dlr.de/dlr/Portaldata/1/Resources/documents/2018/TU_Berlin_EFFICIENCY_MEETS_SKY.pdf (accessed Jan. 19, 2020).

[218]   S. S. Jagtap, P. R. N. Childs, and M. E. J. Stettler, "Energy performance evaluation of alternative energy vectors for subsonic long-range tube-wing aircraft," *Transp. Res. Part D Transp. Environ.*, vol. 115, p. 103588, Feb. 2023, doi: 10.1016/J.TRD.2022.103588.

[219]   A. Silverstein and E. Hall, "Liquid hydrogen as a jet fuel for high-altitude aircraft," 1955. Accessed: Mar. 16, 2019. [Online]. Available: https://ntrs.nasa.gov/archive/nasa/casi.ntrs.nasa.gov/19630002665.pdf

[220]   A. Silverstein and E. Hall, "Liquid hydrogen as a jet fuel for high altitude aircraft." https://apps.dtic.mil/sti/pdfs/ADC051938.pdf (accessed May 03, 2021).

[221]   E. Obert, *Aerodynamic Design of Transport Aircraft*. 2009. Accessed: Sep. 02, 2020. [Online]. Available: http://ebooks.iospress.nl/book/aerodynamic-design-of-transport-aircraft

[222]   M. Ponater, S. Pechtl, R. Sausen, U. Schumann, and G. H. Hüttig, "Potential of the cryoplane technology to reduce aircraft climate impact: A state-of-the-art assessment," *Atmos. Environ.*, vol. 40, pp. 6928–6944, 2006, doi: 10.1016/j.atmosenv.2006.06.036.

[223]   D. Scholz, "Fuselage design," *Lecture notes*, 2017. https://www.fzt.haw-hamburg.de/pers/Scholz/HOOU/AircraftDesign_6_Fuselage.pdf (accessed Jan. 22, 2021).

[224]   Bijewitz J, Seitz A, and M. Hornung, "Architectural Comparison of Advanced Ultra-High Bypass Ratio Turbofans for Medium to Long Range Application," in *Deutscher Luft- und Raumfahrtkongress 2014*, 2014.

[225]   B. K. Kestner, J. S. Schutte, J. C. Gladin, and D. N. Mavris, "Ultra high bypass ratio engine sizing and cycle selection study for a subsonic commercial aircraft in the N+2 timeframe," in *Proceedings of the ASME Turbo Expo*, 2011, vol. 1, pp. 127–137. doi: 10.1115/GT2011-45370.

[226]   G. Corchero and J. L. Montañ, "An approach to the use of hydrogen for commercial aircraft engines," *Proc. Inst. Mech. Eng. Part G J. Aerosp. Eng.*, vol. 219, no. 1, pp. 35–44, 2005, doi: 10.1243/095441005X9139.

[227]   S. R. Turns, *An introduction to combustion : concepts and applications*. McGraw-Hill, 2012.

[228]   C. Marek, T. Smith, and K. Kundu, "Low Emission Hydrogen Combustors for Gas Turbines Using Lean Direct Injection," in *41st AIAA/ASME/SAE/ASEE Joint Propulsion Conference & Exhibit*, Jul. 2005. doi: 10.2514/6.2005-3776.

[229]   "Table of gaseous composition of dry air." https://eesc.columbia.edu/courses/ees/slides/climate/table_1.html (accessed Jan. 15, 2020).

[230]   D. N. Anderson, "EMISSIONS OF OXIDES OF NITROGEN FROM AN EXPERIMENTAL PREMIXED-HYDROGEN BURNER," Cleveland, Ohio, 1976. Accessed: Jan. 15, 2020. [Online]. Available: https://ntrs.nasa.gov/search.jsp?R=19760016183

[231]   N. A. Cumpsty, *Jet propulsion : a simple guide to the aerodynamics and thermodynamic design and performance of jet engines*. 2015.

[232]   P. Dagaut and M. Cathonnet, "The ignition, oxidation, and combustion of kerosene: A review of experimental and kinetic modeling," *Progress in Energy and Combustion Science*, vol. 32, no. 1. pp. 48–92, 2006. doi: 10.1016/j.pecs.2005.10.003.

[233]   D. J. Poferl and R. A. Svehla, "THERMODYNAMIC AND TRANSPORT PROPERTIES OF AIR AND ITS PRODUCTS OF COMBUSTION WITH ASTM-A-1 FUEL AND NATURAL GAS," 1973. Accessed: Jan. 15, 2020. [Online]. Available: https://ntrs.nasa.gov/search.jsp?R=19740004462

[234]   W. G. Vincenti and C. H. Kruger, *Introduction to physical gas dynamics*. Krieger, 1975.

[235]   C. Vallance, *An Introduction to Chemical Kinetics*. IOP Publishing, 2017. doi: 10.1088/978-1-6817-4664-7.

[236]   J. Seitzman, "Laminar Flame Speed," 2004.

http://seitzman.gatech.edu/classes/ae6766/PremixedLaminarFlames.pdf (accessed Jan. 11, 2020).

[237] J. Seitzman, "Premixed Flames: Propagation Limits and Stability," 2004. http://seitzman.gatech.edu/classes/ae6766/FlamePropagationLimits.pdf (accessed Jan. 11, 2020).

[238] S. S. Jagtap, "Assessment of feedstocks for blended alcohol-to-jet fuel manufacturing from standalone and distributed scheme for sustainable aviation," in *AIAA Propulsion and Energy 2019 Forum*, 2019. doi: 10.2514/6.2019-3887.

[239] S. S. Jagtap, "Comparative assessment of manufacturing setups for blended sugar-to-aviation fuel production from non-food feedstocks for green aviation," in *AIAA Propulsion and Energy 2019 Forum*, 2019. doi: 10.2514/6.2019-4332.

[240] G. Dahl and F. Suttrop, "Engine control and low-nox combustion for hydrogen fuelled aircraft gas turbines," *Int. J. Hydrogen Energy*, vol. 23, no. 8, pp. 695–704, Aug. 1998, doi: 10.1016/s0360-3199(97)00115-8.

[241] M. H. Sadraey, *Aircraft Design: A Systems Engineering Approach*. John Wiley and Sons, 2012. doi: 10.1002/9781118352700.

[242] J. P. Fielding, *Introduction to Aircraft Design*. Cambridge University Press, 2017. doi: 10.1017/9781139542418.

[243] E. Torenbeek, *Advanced Aircraft Design: Conceptual Design, Analysis and Optimization of Subsonic Civil Airplanes*. John Wiley and Sons, 2013. doi: 10.1002/9781118568101.

[244] E. S. Hendricks, "A multi-level multi-design point approach for gas turbine cycle and turbine conceptual design," Georgia Institute of Technology, 2017. Accessed: Oct. 17, 2019. [Online]. Available: https://smartech.gatech.edu/handle/1853/58212

[245] J. D. Mattingly, W. H. Heiser, and D. T. Pratt, *Aircraft Engine Design, Third Edition*. American Institute of Aeronautics and Astronautics, 2018. doi: https://doi.org/10.2514/4.105173.

[246] H. I. H. Saravanamuttoo, G. F. C. Rogers, H. Cohen, P. V. Straznicky, and A. C. Nix, *Gas Turbine Theory*, Seventh. Pearson, 2017. Accessed: Dec. 17, 2019. [Online]. Available: https://www.pearson.com/us/higher-education/program/Cohen-Gas-Turbine-Theory-7th-Edition/PGM1943364.html

[247] J. R. Quinlan and F. H. Gern, "Conceptual design and structural optimization of nasa environmentally responsible aviation (ERA) hybrid wing body aircraft," in *57th AIAA/ASCE/AHS/ASC Structures, Structural Dynamics, and Materials Conference*, 2016. doi: 10.2514/6.2016-0229.

[248] C. L. Nickol, "Hybrid wing body configuration scaling study," in *50th AIAA Aerospace Sciences Meeting Including the New Horizons Forum and Aerospace Exposition*, 2012. doi: 10.2514/6.2012-337.

[249] R. H. Thomas, C. L. Burley, and C. L. Nickol, "Assessment of the Noise Reduction Potential of Advanced Subsonic Transport Concepts for NASA's Environmentally Responsible Aviation Project," in *54th AIAA Aerospace Sciences Meeting*, Jan. 2016. doi: 10.2514/6.2016-0863.

[250] I. Dincer and C. Acar, "A review on potential use of hydrogen in aviation applications," *Int. J. Sustain. Aviat.*, vol. 2, no. 1, p. 74, 2016, doi: 10.1504/IJSA.2016.076077.

[251] M. A. Engines, "PW1100G-JM engine." https://www.mtu.de/maintenance/commercial-aircraft-engine-services/engine-portfolio-mro/narrowbody-and-regional-jets/pw1100g-jm/ (accessed Dec. 20, 2019).

[252] S. Liu and Y. C. Shin, "Additive manufacturing of Ti6Al4V alloy: A review," *Mater. Des.*, vol. 164, Feb. 2019, doi: 10.1016/j.matdes.2018.107552.

[253] S. C. Joshi and A. A. Sheikh, "3D printing in aerospace and its long-term sustainability," *Virtual Phys. Prototyp.*, vol. 10, no. 4, pp. 175–185, Oct. 2015, doi: 10.1080/17452759.2015.1111519.

[254] "Damage-Tolerant Fan Casings for Jet Engines." https://spinoff.nasa.gov/Spinoff2006/T_1.html (accessed Dec. 04, 2019).

[255] L. Liu *et al.*, "Ballistic impact testing and analysis of triaxial braided composite fan case material," in *Advanced Materials Research*, 2012, vol. 535–537, pp. 121–132. doi: 10.4028/www.scientific.net/AMR.535-537.121.

[256] R. Coroneos, "Structural Analysis and Optimization of a Composite Fan Blade for Future Aircraft Engine," 2012. Accessed: Dec. 04, 2019. [Online]. Available: https://ntrs.nasa.gov/archive/nasa/casi.ntrs.nasa.gov/20120013597.pdf

[257] J. A. Dicarlo, "Advances in SiC/SiC Composites for Aero-Propulsion," 2013. Accessed: Dec. 04, 2019. [Online]. Available: http://www.sti.nasa.gov

[258] F. Yin and A. Gangoli Rao, "Performance analysis of an aero engine with inter-stage turbine burner," in *Aeronautical Journal*, Nov. 2017, vol. 121, no. 1245, pp. 1605–1626. doi: 10.1017/aer.2017.93.

[259] T. Hinoki, E. Lara-Curzio, and L. L. Snead, "Mechanical properties of high purity SiC fiber-reinforced CVI-SiC matrix composites," *Fusion Sci. Technol.*, vol. 44, no. 1, pp. 211–218, 2003, doi: 10.13182/FST03-A336.

[260] "Tyranno Fiber® - UBE INDUSTRIES,LTD." https://www.ube.com/contents/en/chemical/continuous_inorganic_fiber/tyranno_fiber.html#h2_id_2 (accessed Dec. 04, 2019).

[261] I. Spitsberg and J. Steibel, "Thermal and Environmental Barrier Coatings for SiC/SiC CMCs in Aircraft Engine Applications*," *Int. J. Appl. Ceram. Technol.*, vol. 1, no. 4, pp. 291–301, Jan. 2005, doi: 10.1111/j.1744-7402.2004.tb00181.x.

[262] M. Wilkie and M. Lucas, "The effect of Ti-6Al-4V microstructure on the performance of ultrasonic soft tissue cutting tips," *Cit. Proc. Mtgs. Acoust*, vol. 32, p. 20010, 2017, doi: 10.1121/2.0000735.

[263] "Titanium Alloys for Aeroengine and Airframe Applications." https://www.azom.com/article.aspx?ArticleID=1569 (accessed Dec. 04, 2019).

[264] I. Inagaki, T. Takechi, Y. Shirai, and N. Ariyasu, "Application and Features of Titanium for the Aerospace Industry," 2014. Accessed: Dec. 04, 2019. [Online]. Available: https://www.nipponsteel.com/en/tech/report/nssmc/pdf/106-05.pdf

[265] United-Performance-Metals, "Properties of Nickel Alloy 718." https://www.upmet.com/sites/default/files/datasheets/718.pdf (accessed Dec. 04, 2019).

[266] I. Halliwell, "An Ultra-High Bypass Ratio Turbofan Engine for the Future," 2014. https://pdfslide.us/documents/undergraduate-team-engine-student-design-competition-2014-undergraduate.html (accessed Dec. 09, 2019).

[267] J. Li, X. Sun, Y. Liu, and V. Sethi, "Preliminary Aerodynamic Design Methodology for Aero Engine Lean Direct Injection Combustors," *Aeronaut. J.*, vol. 121, pp. 1087–1108, 2017, doi: 10.1017/aer.2017.47.

[268] "Pratt and Whitney PW1100G Geared Turbofan Engine | The Flying Engineer." http://theflyingengineer.com/flightdeck/pw1100g-gtf/ (accessed Dec. 06, 2019).

[269] R. K. Bansal, *A Textbook of Strength of Materials*. Laxmi Publications, 2010. Accessed: Dec. 06, 2019. [Online]. Available: https://books.google.co.uk/books?hl=en&lr=&id=2IHEqp8dNWwC&oi=fnd&pg=PT20&dq=strength+of+materials+I+beams+bansal&ots=TmqGqmnIL-&sig=_SdNlZ8NTO4L8Ub_Z_fHc_Q09Gg#v=onepage&q=I section&f=false

[270] I. Halliwell, "An Improved Engine for a High Altitude Long Endurance Unmanned Air Vehicle," *AIAA, ASME and IGTI*, 2012. https://files.asme.org/igti/33208.pdf (accessed Dec. 08, 2019).

[271] A. R. A. Talib, E. Gires, and M. T. Ahmad, "Performance Evaluation of a Small-Scale Turbojet Engine Running on Palm Oil Biodiesel Blends," 2014, doi: 10.1155/2014/946485.

[272] E. G. Tulapurkara, A. Venkattraman, and V. Ganesh, "AN EXAMPLE OF AIRPLANE PRELIMINARY DESIGN PROCEDURE-JET TRANSPORT," 2007. https://nptel.ac.in/content/storage2/courses/101106035/057_Appendix 10.2_(05-10-2013).pdf (accessed Dec. 07, 2019).

[273] Society-of-Robots, "High Altitude Balloon Tutorial: Measuring Humidity." https://www.societyofrobots.com/space_balloon_humidity_test.shtml (accessed Dec. 07, 2019).

[274] Skybrary, "BOEING 787-8 Dreamliner - SKYbrary Aviation Safety." https://www.skybrary.aero/index.php/B788 (accessed Dec. 07, 2019).

[275] Skybrary, "AIRBUS A350-900 - SKYbrary Aviation Safety." https://www.skybrary.aero/index.php/A359 (accessed Dec. 07, 2019).

[276] H. Gazzetta Junior, C. Bringhenti, J. Roberto Barbosa, and J. T. Tomita, "Real-Time Gas Turbine Model for Performance Simulations," *J. Aerosp. Technol. Manag. São José dos Campos*, vol. 9, no. 3, pp. 346–356, doi: 10.5028/jatm.v9i3.693.

[277] J. Bijewitz, A. Seitz, A. T. Isikveren, and M. Hornung, "Multi-disciplinary design investigation of propulsive fuselage aircraft concepts," *Aircr. Eng. Aerosp. Technol.*, vol. 88, no. 2, pp. 257–267, Mar. 2016, doi: 10.1108/AEAT-02-2015-0053.

[278] A. Manneville, "Propulsion System Concepts for Silent Aircraft," MIT, 2004. Accessed: Dec. 06, 2019. [Online]. Available: https://core.ac.uk/download/pdf/4385607.pdf

[279] J. W. Chapman, T. M. Lavelle, and J. S. Litt, "Practical Techniques for Modeling Gas Turbine Engine Performance." Accessed: Dec. 07, 2019. [Online]. Available: https://ntrs.nasa.gov/search.jsp?R=20170000884

[280] B. Roth and J. de Luis, "LOST THRUST METHODOLOGY FOR GAS TURBINE ENGINE PERFORMANCE ANALYSIS," in *ASME Turbo Expo 2005*, 2005. Accessed: Dec. 07, 2019. [Online]. Available: https://smartech.gatech.edu/bitstream/handle/1853/10606/GT-2005-68200.pdf

[281] A. Dankanich and D. Peters, "Turbofan Engine Bypass Ratio as a Function of Thrust and Fuel Turbofan Engine Bypass Ratio as a Function of Thrust and Fuel Flow Flow," 2017. Accessed: Dec. 07, 2019. [Online]. Available: https://openscholarship.wustl.edu/mems500https://openscholarship.wustl.edu/mems500/34

[282] E. Gamble, D. Terrell, and R. DeFrancesco, "Nozzle Selection and Design Criteria," Jul. 2004. doi: 10.2514/6.2004-3923.

[283] "First Law - Control Volumes - Energy Equation," *Ohio University website*, 2009. https://www.ohio.edu/mechanical/thermo/Intro/Chapt.1_6/Chapter4a.html (accessed Jan. 08, 2020).

[284] D. Wu, "Models, Optimal Performances and Sensitivies of Commercial Flight Trajectory in the Air Traffic System," UNIVERSITY OF MINNESOTA, 2012. Accessed: Jun. 10, 2022. [Online]. Available: https://conservancy.umn.edu/bitstream/handle/11299/144391/Wu_umn_0130E_13330.pdf?sequence=1&isAllowed=y

[285] M. Oak, A. Fabre, M. Delavenne, E. N. Van, E. Benard, and S. Defoort, "Spectral project - application of

FAST-OAD code to the conceptual design of a hydrogen fuelled commercial aircraft," *IOP Conf. Ser. Mater. Sci. Eng.*, vol. 1226, no. 1, p. 012027, Feb. 2022, doi: 10.1088/1757-899X/1226/1/012027.

[286] S. J. Ling, W. Moebs, and J. Sanny, "Heat Capacity and Equipartition of Energy." OpenStax, Sep. 15, 2016.

[287] C. L. Nickol, "Technologies and Concepts for Reducing the Fuel Burn of Subsonic Transport Aircraft," *NTRS - NASA Technical Reports Server*, 2012. https://ntrs.nasa.gov/citations/20120016006 (accessed Sep. 03, 2020).

[288] J. C. June, R. H. Thomas, and Y. Guo, "System Noise Prediction Uncertainty Quantification for a Hybrid Wing–Body Transport Concept," *AIAA J.*, vol. 58, no. 3, pp. 1157–1170, Mar. 2020, doi: 10.2514/1.J058226.

[289] "Commerce Business Daily," 1999. https://books.google.co.uk/books?id=EBFNWr5KWwEC&pg=RA12-PA23&lpg=RA12-PA23&dq=transport+jet+reserve+loiter+altitude+5000+ft&source=bl&ots=iY8FNdRIwg&sig=ACfU3U0KVdm9ammVUwkWXkYVsn6szXZKcg&hl=en&sa=X&ved=2ahUKEwjvpZ-ztMDnAhUNTcAKHabXBls4ChDoATABegQIChAB#v (accessed Feb. 07, 2020).

[290] Virginia Polytechnic Institute and State University, "Aircraft performance." http://www.dept.aoe.vt.edu/~lutze/AOE3104/climb.pdf (accessed Feb. 12, 2020).

[291] D. C. Garmendia, "A MULTI-DISCIPLINARY CONCEPTUAL DESIGN METHODOLOGY FOR ASSESSING CONTROL AUTHORITY ON A HYBRID WING BODY CONFIGURATION," Georgia Institute of Technology, Jul. 2015. Accessed: Sep. 02, 2020. [Online]. Available: https://smartech.gatech.edu/handle/1853/54328

[292] "LOCKHEED C-5A BL488.2 AIRFOIL (c5b-il)." http://airfoiltools.com/airfoil/details?airfoil=c5b-il (accessed Sep. 02, 2020).

[293] "KC-135 BL52.44 AIRFOIL (kc135a-il)." http://airfoiltools.com/airfoil/details?airfoil=kc135a-il (accessed Sep. 02, 2020).

[294] "BOEING-VERTOL VR-15 AIRFOIL (vr15-il)." http://airfoiltools.com/airfoil/details?airfoil=vr15-il (accessed Sep. 02, 2020).

[295] "Boeing 767 Aircraft Operations," 2013. https://studylib.net/doc/18499334/delta-virtual-airlines-boeing-767-aircraft-operations (accessed Jan. 25, 2019).

[296] S. R. Pereira, T. Fontes, and M. C. Coelho, "Can hydrogen or natural gas be alternatives for aviation? - A life cycle assessment," in *International Journal of Hydrogen Energy*, Aug. 2014, vol. 39, no. 25, pp. 13266–13275. doi: 10.1016/j.ijhydene.2014.06.146.

[297] Dassault-Systems, "3D CAD Design Software | SOLIDWORKS." Dassault Systems, 2019. Accessed: Feb. 17, 2020. [Online]. Available: https://www.solidworks.com/

[298] P. A. Jackson, *IHS Jane's all the world's aircraft : development & production*. Janes Information Group, 2014.

[299] Medium.com, "Boeing 777X: Dimensions matter," *Medium.com*, 2017. https://medium.com/o530-carris-pt-herald/boeing-777x-dimensions-matter-8e80dd601a83 (accessed Aug. 27, 2020).

[300] S. De Jong *et al.*, "Life-cycle analysis of greenhouse gas emissions from renewable jet fuel production," *Biotechnol. Biofuels*, vol. 10, no. 1, pp. 1–18, Mar. 2017, doi: 10.1186/S13068-017-0739-7/TABLES/4.

[301] INTERNATIONAL CIVIL AVIATION ORGANIZATION, "CORSIA Default Life Cycle Emissions Values for CORSIA Eligible Fuels," *INTERNATIONAL CIVIL AVIATION ORGANIZATION*, Mar. 2021. https://www.icao.int/environmental-protection/CORSIA/Documents/ICAO document 06 - Default Life Cycle Emissions - March 2021.pdf (accessed May 31, 2022).

[302] M. Prussi *et al.*, "CORSIA: The first internationally adopted approach to calculate life-cycle GHG emissions for aviation fuels," *Renew. Sustain. Energy Rev.*, vol. 150, p. 111398, Oct. 2021, doi: 10.1016/J.RSER.2021.111398.

[303] B. W. Kolosz, Y. Luo, B. Xu, M. M. Maroto-Valer, and J. M. Andresen, "Life cycle environmental analysis of 'drop in' alternative aviation fuels: a review," *Sustain. Energy Fuels*, vol. 4, no. 7, pp. 3229–3263, Jun. 2020, doi: 10.1039/C9SE00788A.

[304] Elisabeth van der Sman, Bram Peerlings, Johan Kos, Rogier Lieshout, and Thijs Boonekamp, "Destination 2050 – A route to net zero European Aviation - SEO Economisch Onderzoek," *NLR – Royal Netherlands Aerospace Centre*, 2021. https://www.seo.nl/en/publications/destination-2050-a-route-to-net-zero-european-aviation/ (accessed May 31, 2022).

[305] C. Koroneos, A. Dompros, G. Roumbas, and N. Moussiopoulos, "Advantages of the use of hydrogen fuel as compared to kerosene," *Resour. Conserv. Recycl.*, vol. 44, no. 2, pp. 99–113, May 2005, doi: 10.1016/J.RESCONREC.2004.09.004.

[306] S. V. Ratner, C. Yuri, and N. H. Hien, "Prospects of Transition of Air Transportation to Clean Fuels: Economic and Environmental Management Aspects," *Int. Energy J.*, vol. 19, no. 3, 2019, Accessed: May 30, 2022. [Online]. Available: http://www.rericjournal.ait.ac.th/index.php/reric/article/view/2084

[307] O. Siddiqui and I. Dincer, "A comparative life cycle assessment of clean aviation fuels," *Energy*, vol. 234, p. 121126, Nov. 2021, doi: 10.1016/J.ENERGY.2021.121126.

[308] T. Miller, "Environmental Assessments of Capital-Intensive Product Systems," *Yale Grad. Sch. Arts Sci. Diss.*, Apr. 2021, Accessed: Jun. 03, 2022. [Online]. Available:

https://elischolar.library.yale.edu/gsas_dissertations/240

[309] ANL, "Argonne GREET Publications," *Argonne National Laboratory*. https://greet.es.anl.gov/publications (accessed Jun. 08, 2022).

[310] Energy Information Administration, "Electricity," *Energy Information Administration, USA*, 2021. https://www.eia.gov/outlooks/aeo/pdf/04 AEO2021 Electricity.pdf (accessed Jun. 08, 2022).

[311] Nikita Pavlenko and Stephanie Searle, "Assessing the sustainability implications of alternative aviation fuels," *International Council on Clean Transportation*, 2021. https://theicct.org/publication/assessing-the-sustainability-implications-of-alternative-aviation-fuels/ (accessed Jun. 09, 2022).

[312] M. Schaefer and S. Bartosch, "Overview on fuel flow correlation methods for the calculation of NOx, CO and HC emissions and their implementation into aircraft performance software," *DLR*, 2013. https://www.researchgate.net/publication/271210746_Overview_on_fuel_flow_correlation_methods_for_the_calculation_of_NOx_CO_and_HC_emissions_and_their_implementation_into_aircraft_performance_software (accessed Jun. 14, 2022).

[313] Boeing, "777 Flight Crew Training Manual Qatar Airways," 2007. http://virtavia.online/wp-content/uploads/wpforo/attachments/1/975-B777-FCTM.pdf (accessed Jun. 16, 2022).

[314] "AIRBUS A350-900 - SKYbrary Aviation Safety." https://www.skybrary.aero/index.php/A359 (accessed Jan. 21, 2021).

[315] "What do you know about take-off speed? V1, Vr, and V2." https://www.aviationnepal.com/what-do-you-know-about-take-off-speed-v1-vr-and-v2/ (accessed Jun. 16, 2022).

[316] "Airbus A350-800 - Price, Specs, Photo Gallery, History - Aero Corner." https://aerocorner.com/aircraft/airbus-a350-xwb/ (accessed Jun. 16, 2022).

[317] Digital-Dutch, "1976 Standard Atmosphere Calculator," *Digital Dutch*, 1999. https://www.digitaldutch.com/atmoscalc/ (accessed Feb. 09, 2021).

[318] F. Caiazzo, A. Agarwal, R. L. Speth, and S. R. H. Barrett, "Impact of biofuels on contrail warming," *Environ. Res. Lett.*, vol. 12, no. 11, p. 114013, Nov. 2017, doi: 10.1088/1748-9326/AA893B.

[319] F. Svensson, "Potential of reducng the environmental impact of civil subsonic aviation by using liquid hydrogen," Cranfield University, 2005. Accessed: Jun. 17, 2021. [Online]. Available: http://dspace.lib.cranfield.ac.uk/handle/1826/10726

[320] D. Gielen, E. Taibi, and R. Miranda, "HYDROGEN: A RENEWABLE ENERGY PERSPECTIVE," *International Renewable Energy Agency*, 2019. https://www.irena.org/-/media/Files/IRENA/Agency/Publication/2019/Sep/IRENA_Hydrogen_2019.pdf (accessed Jul. 01, 2022).

[321] A. I. Osman *et al.*, "Hydrogen production, storage, utilisation and environmental impacts: a review," *Environ. Chem. Lett.*, vol. 20, no. 1, pp. 153–188, Feb. 2021, doi: 10.1007/S10311-021-01322-8.

[322] International Atomic Energy Agency, "Hydrogen Production Using Nuclear Energy," *International Atomic Energy Agency No. NP-T-4.2*, 2011. http://www.iaea.org/Publications/index.html (accessed Jul. 01, 2022).

[323] P. Spath, A. Aden, T. Eggeman, M. Ringer, B. Wallace, and J. Jechura, "Biomass to Hydrogen Production Detailed Design and Economics Utilizing the Battelle Columbus Laboratory Indirectly-Heated Gasifier," 2005. Accessed: Jul. 01, 2022. [Online]. Available: https://www.nrel.gov/docs/fy05osti/37408.pdf

[324] S. S. Jagtap, P. R. N. Childs, and M. E. J. Stettler, "Performance sensitivity of subsonic liquid hydrogen long-range tube-wing aircraft to technology developments," *Int. J. Hydrogen Energy*, vol. 50, pp. 820–833, Jan. 2024, doi: 10.1016/J.IJHYDENE.2023.07.297.

[325] S. S. Jagtap, P. R. N. Childs, and M. E. J. Stettler, "Conceptual design-optimisation of a future hydrogen-powered ultrahigh bypass ratio geared turbofan engine," *Int. J. Hydrogen Energy*, vol. 95, pp. 317–328, Dec. 2024, doi: 10.1016/J.IJHYDENE.2024.10.329.

[326] S. S. Jagtap, M. E. J. Stettler, and P. R. N. Childs, "Data in brief : Energy performance evaluation of alternative energy vectors for subsonic intercontinental tube-wing aircraft".

[327] S. Jagtap, A. Strehlow, M. Reitz, S. Kestler, and G. Cinar, "Model-Based Systems Engineering Approach for a Systematic Design of Aircraft Engine Inlet," in *AIAA SCITECH 2025 Forum*, 2025. doi: https://doi.org/10.2514/6.2025-1410.

[328] S. S. Jagtap, "Non-food feedstocks comparison for renewable aviation fuel production towards environmentally and socially responsible aviation," in *2019 AIAA Propulsion & Energy Forum*, 2019.

[329] B. Emerson, S. Jagtap, J. M. Quinlan, M. W. Renfro, B. M. Cetegen, and T. Lieuwen, "Spatio-temporal linear stability analysis of stratified planar wakes: Velocity and density asymmetry effects," *Phys. Fluids*, vol. 28, no. 4, p. 045101, Apr. 2016, doi: 10.1063/1.4943238.

[330] S. S. Jagtap, P. R. N. Childs, and M. E. J. Stettler, "Conceptual design-optimisation of a subsonic hydrogen-powered long-range blended-wing-body aircraft," *Int. J. Hydrogen Energy*, vol. 96, pp. 639–651, Dec. 2024, doi: 10.1016/J.IJHYDENE.2024.11.331.

[331] B. L. Emerson, S. Jagtap, and T. C. Lieuwen, "Stability Analysis of Reacting Wakes: Flow and Density Asymmetry Effects," in *53rd AIAA Aerospace Sciences Meeting*, Jan. 2015. doi: 10.2514/6.2015-0429.

[332] S. S. Jagtap, "Heat recuperation system for the family of shaft powered aircraft gas turbine engines," Oct. 29,

2014 Accessed: Jun. 29, 2019. [Online]. Available:
https://patents.google.com/patent/US20180334959A1/en?q=heat&q=recuperation&q=system&q=family&q=shaft&q=powered&q=aircraft&q=gas+turbine+engines&oq=heat+recuperation+system+for+the+family+of+shaft+powered+aircraft+gas+turbine+engines+uspto

[333] S. S. Jagtap, "Evaluation of technology and energy vector combinations for decarbonising future subsonic long-range aircraft," Imperial College London.

[334] S. S. Jagtap, M. E. J. Stettler, and P. R. N. Childs, "Data in brief : Performance sensitivity of subsonic liquid hydrogen long-range tube-wing aircraft to technology developments".

[335] S. S. Jagtap, M. E. J. Stettler, and P. R. N. Childs, "Data in brief : Conceptual design-optimisation of futuristic hydrogen powered ultrahigh bypass ratio geared turbofan engine".

[336] S. S. Jagtap, M. E. J. Stettler, and P. R. N. Childs, "Data in brief : Conceptual design-optimisation of a subsonic hydrogen-powered long-range blended-wing-body aircraft".

[337] S. S. Jagtap, "Aero-thermodynamic analysis of space shuttle vehicle at re-entry," *IEEE Aerosp. Conf. Proc.*, vol. 2015-June, Jun. 2015, doi: 10.1109/AERO.2015.7119253.

[338] S. Jagtap and S. Bhandari, "Solar Refrigeration," *Sardar Patel Int. Conf.*, 2012, [Online]. Available: https://papers.ssrn.com/sol3/papers.cfm?abstract_id=2103115

[339] S. Jagtap and S. Bhandari, "Solar Refrigeration using Triple Fluid Vapor Absorption Refrigeration and Organic Rankine Cycle," in *Sardar Patel International Conference SPICON 2012 Mechanical*, 2012.

[340] N. Komerath, S. Jagtap, and N. Hiremath, "Aerothermoelastic Tailoring for Waveriders," in *US Air Force Summer Faculty Fellowship Program*, 2014.

[341] S. S. Jagtap, "Exploration of sustainable aviation technologies and alternative fuels for future inter-continental passenger aircraft."

[342] S. S. Jagtap, "Identification of sustainable technology and energy vector combinations for future inter-continental passenger aircraft."

[343] T. Mommsen, "Airbus A320/321 Quick Change Market Analysis - A Case Study," *Master's Theses - Daytona Beach*, Dec. 1994, Accessed: Feb. 08, 2021. [Online]. Available: https://commons.erau.edu/db-theses/252

[344] R. Babikian, "THE HISTORICAL FUEL EFFICIENCY CHARACTERISTICS OF REGIONAL AIRCRAFT FROM TECHNOLOGICAL, OPERATIONAL, AND COST PERSPECTIVES," 2001. Accessed: Mar. 15, 2019. [Online]. Available: http://web.mit.edu/aeroastro/sites/waitz/publications/Babikian.Thesis.pdf

[345] Aerospaceweb, "Airbus A320 Short to Medium-Range Jetliner," *Aerospaceweb*, 2011. http://www.aerospaceweb.org/aircraft/jetliner/a320/ (accessed Feb. 09, 2021).

[346] B. Boling, Y. Liu, and E. Stumpf, "Understanding Fleet Impacts of Formation Flight," 2015.

[347] All-the-world's-aircraft, "BOEING 767-300 GENERAL MARKET FREIGHTER," *All the world's aircraft*, 2011. http://janes.migavia.com/usa/boeing/boeing-767-300.html (accessed Feb. 09, 2021).

[348] Boeing, "The Boeing 767-300 Freighter - The newest member of the Boeing Frieghter Family," *Boeing*, 2014. http://www.boeing.com/farnborough2014/pdf/BCA/bck-767_5_13_2014.pdf (accessed Feb. 09, 2021).

[349] R. Babikian, S. P. Lukachko, and I. A. Waitz, "The Historical Fuel Efficiency Characteristics of Regional Aircraft from Technological, Operational, and Cost Perspectives," 2001. http://web.mit.edu/aeroastro/sites/waitz/publications/Babikian.pdf (accessed Feb. 08, 2021).

[350] P. Lironi, "CF6-80C2 engine history and evolution," 2007.

[351] Butterworth-Heinemann, "Civil Jet Aircraft Design - Aircraft Data File - Boeing Aircraft," *Elsevier*, 2001. https://booksite.elsevier.com/9780340741528/appendices/data-a/table-3/table.htm (accessed Feb. 09, 2021).

[352] AIB-family-flights, "Airbus A350 family," *AIB-family-flights*, 2015. https://aibfamily.flights/Airbus-A350 (accessed Aug. 27, 2020).

[353] Modern-airliners, "Boeing 777 Specs, what makes this giant twin work?," *Modern-airliners*, 2017. https://modernairliners.com/boeing-777/boeing-777-specs/ (accessed Aug. 27, 2020).

[354] "Equivalent Diameter." https://www.engineeringtoolbox.com/equivalent-diameter-d_205.html (accessed Aug. 28, 2020).

[355] Airbus, "AIRBUS A380 AIRPLANE CHARACTERISTICS FOR AIRPORT PLANNING AC," *National Air Transportation Association*. https://www.nata.aero/agso/astgcache/f6a9e8b3-ab2e-4502-bedc-92f463486e22.pdf (accessed Aug. 28, 2020).

[356] "Malaysia Airlines Fleet Airbus A380-800 Details and Pictures | AirlinesFleet.com." https://airlinesfleet.com/malaysia-airlines-fleet-airbus-a380-800-details-and-pictures/ (accessed Aug. 28, 2020).

[357] "The Airbus A380 Vs Boeing 787 - Which Plane Is Best? - Simple Flying." https://simpleflying.com/airbus-a380-vs-boeing-787/ (accessed Aug. 28, 2020).

[358] R. Roedts, R. Somero, and C. Waskiewicz, "Airbus A380 Analysis."

[359] The-points-guy, "The 787 Dreamliner — What Are the Differences Between a -8, -9 and -10?," *The points guy*, 2018. https://thepointsguy.co.uk/news/differences-787-8-and-787-9-and-787-10/ (accessed Jan. 22, 2021).

[360] Modern-Airliners, "Douglas DC8," *Modern Airliners*, 2017. https://modernairliners.com/douglas-dc8/ (accessed Jan. 22, 2021).

[361]   S. Hoerner, *Fluid-dynamic Drag: Practical Information on Aerodynamic Drag and Hydrodynamic Resistance*. 1965. Accessed: Jan. 22, 2021. [Online]. Available: https://books.google.co.in/books/about/Fluid_dynamic_Drag.html?id=abU8AAAAIAAJ&redir_esc=y

[362]   G. L. Juste, "Hydrogen injection as additional fuel in gas turbine combustor. Evaluation of effects," *Int. J. Hydrogen Energy*, vol. 31, no. 14, pp. 2112–2121, Nov. 2006, doi: 10.1016/j.ijhydene.2006.02.006.

[363]   "The Hindenburg disaster - HISTORY." https://www.history.com/this-day-in-history/the-hindenburg-disaster (accessed Oct. 31, 2020).

[364]   S. Rondinelli, A. Gardi, R. Kapoor, and R. Sabatini, "Benefits and challenges of liquid hydrogen fuels in commercial aviation," *Int. J. Sustain. Aviat.*, vol. 3, no. 3, p. 200, 2017, doi: 10.1504/ijsa.2017.086845.

[365]   U. Schmidtchen, E. Behrend, H. W. Pohl, and N. Rostek, "Hydrogen Aircraft and Airport Safety," *Renew. Sustain. Energy Rev.*, vol. 1, no. 4, pp. 239–269, 1997, doi: 10.1016/S1364-0321(97)00007-5.

[366]   M. R. Swain, "Fuel Leak Simulation," in *Proceedings of the 2001 DOE Hydrogen Program Review, NREL/CP-570-30535*, 2001. Accessed: Dec. 27, 2019. [Online]. Available: https://www.cob.nl/wp-content/uploads/2018/01/Fuel_Leak_Simulation.pdf

[367]   M. Janic, "Is liquid hydrogen a solution for mitigating air pollution by airports?," *Int. J. Hydrogen Energy*, vol. 35, no. 5, pp. 2190–2202, Mar. 2010, doi: 10.1016/j.ijhydene.2009.12.022.

[368]   E. Baharozu, G. Soykan, and M. B. Ozerdem, "Future aircraft concept in terms of energy efficiency and environmental factors," *Energy*, vol. 140, pp. 1368–1377, Dec. 2017, doi: 10.1016/j.energy.2017.09.007.

[369]   T. F. Rahmes *et al.*, "Sustainable Bio-derived Synthetic Paraffinic Kerosene (Bio-SPK) jet fuel flights and engine tests program results," in *9th AIAA Aviation Technology, Integration and Operations (ATIO) Conference, Aircraft Noise and Emissions Reduction Symposium (ANERS)*, 2009. doi: 10.2514/6.2009-7002.

[370]   A. Zschocke, S. Scheuermann, and J. Ortner, "High Biofuel Blends in Aviation (HBBA): Final Report," *European Commission*. https://ec.europa.eu/energy/sites/ener/files/documents/final_report_for_publication.pdf (accessed Mar. 15, 2020).

[371]   J. I. Hileman *et al.*, "Near-term feasibility of alternative jet fuels," 2009. https://rosap.ntl.bts.gov/view/dot/18417 (accessed Mar. 31, 2020).

[372]   J. T. Edwards, L. M. Shafer, and J. K. Klein, "AIR FORCE HYDROPROCESSED RENEWABLE JET (HRJ) FUEL RESEARCH ," 2012. https://apps.dtic.mil/dtic/tr/fulltext/u2/a579552.pdf (accessed Mar. 31, 2020).

[373]   F. White, *Viscous Fluid Flow*. McGraw-Hill Science/Engineering/Math, 2005. Accessed: Feb. 13, 2020. [Online]. Available: http://www.amazon.com/Viscous-Fluid-McGraw-Hill-Mechanical-Engineering/dp/0072402318

[374]   A. H. Lefebvre and D. R. Ballal, *Gas Turbine Combustion: Alternative Fuels and Emissions*. 2010.

[375]   X. Hui, K. Kumar, C. J. Sung, T. Edwards, and D. Gardner, "Experimental studies on the combustion characteristics of alternative jet fuels," *Fuel*, vol. 98, pp. 176–182, Aug. 2012, doi: 10.1016/j.fuel.2012.03.040.

[376]   E. Corporan *et al.*, "Emissions characteristics of a turbine engine and research combustor burning a Fischer-Tropsch jet fuel," *Energy and Fuels*, vol. 21, no. 5, pp. 2615–2626, Sep. 2007, doi: 10.1021/ef070015j.

[377]   F. Wolters, R.-G. Becker, and M. Schaefer, "IMPACT OF ALTERNATIVE FUELS ON ENGINE PERFORMANCE AND CO2-EMISSIONS ," in *28TH INTERNATIONAL CONGRESS OF THE AERONAUTICAL SCIENCES* , 2012.

[378]   P. R. Tabrizian, "HOW TO SIMPLIFY INVERSE TRIGNOMETRY FORMULAS." https://math.berkeley.edu/~peyam/Math1ASu11/Handouts/Inverse Trig.pdf (accessed Feb. 12, 2020).

[379]   Karlijn de Vries, "Contribution of Sustainable Aviation Fuels Towards Net Zero 2050 – Using Life Cycle Analysis," University of Groningen, 2022. Accessed: Jul. 02, 2022. [Online]. Available: https://fse.studenttheses.ub.rug.nl/26595/1/IP_Final_upload.pdf

[380]   "Hydrogen Production: Natural Gas Reforming | Department of Energy." https://www.energy.gov/eere/fuelcells/hydrogen-production-natural-gas-reforming (accessed Jul. 10, 2022).

[381]   "Hydrogen Production: Biomass Gasification," *Hydrogen and Fuel Cell Technologies Office, Department of Energy, USA*. https://www.energy.gov/eere/fuelcells/hydrogen-production-biomass-gasification (accessed Jul. 05, 2022).

[382]   "Coke Oven Gas." http://compressormash.ru/en/products/compressible_gas/coke_oven_gas/ (accessed Jul. 10, 2022).

[383]   K. Yang *et al.*, "Hydrogen production via chemical looping reforming of coke oven gas," *Green Energy Environ.*, vol. 6, no. 5, pp. 678–692, Oct. 2021, doi: 10.1016/J.GEE.2020.06.027.

[384]   "U.S. Energy Information Administration - EIA - Independent Statistics and Analysis." https://www.eia.gov/todayinenergy/detail.php?id=5930 (accessed Jul. 10, 2022).

[385]   D. Y. Lee and A. Elgowainy, "By-product hydrogen from steam cracking of natural gas liquids (NGLs): Potential for large-scale hydrogen fuel production, life-cycle air emissions reduction, and economic benefit," *Int. J. Hydrogen Energy*, vol. 43, no. 43, pp. 20143–20160, Oct. 2018, doi: 10.1016/J.IJHYDENE.2018.09.039.

[386]   "Hydrogen Basics - Solar Production." http://www.fsec.ucf.edu/en/consumer/hydrogen/basics/production-solar.htm (accessed Jul. 10, 2022).

[387]   Viktor Sivertsson, "Hydrogen production using high temperature nuclear reactors : A feasibility study," 2010. Accessed: Jul. 08, 2022. [Online]. Available: https://uu.diva-portal.org/smash/get/diva2:303943/FULLTEXT01.pdf

[388]   Q. Dai, A. Elgowainy, J. Kelly, J. Han, and M. Wang, "Life Cycle Analysis of Hydrogen Production from Non-Fossil Sources," *Argonne National Laboratory*, 2016. https://greet.es.anl.gov/files/h2-nonfoss-2016 (accessed Jul. 05, 2022).

[389]   C. Acar and I. Dincer, "3.1 Hydrogen Production," *Compr. Energy Syst.*, vol. 3–5, pp. 1–40, Jan. 2018, doi: 10.1016/B978-0-12-809597-3.00304-7.

[390]   K. Tennakone, "Hydrogen from brine electrolysis: A new approach," *Int. J. Hydrogen Energy*, vol. 14, no. 9, pp. 681–682, Jan. 1989, doi: 10.1016/0360-3199(89)90046-3.

Appendix A

A.1. Thermodynamic cycle analysis of a turbofan engine

Table A.1. Thermodynamic cycle analysis input and output parameters at design point

	Jet-A	100% SPK	LH$_2$	LNG	LNH$_3$	Methanol	Ethanol
Cycle input parameters							
Fan pressure ratio	1.6	1.6	1.6	1.6	1.6	1.6	1.6
Fan polytropic efficiency	0.9	0.9	0.9	0.9	0.9	0.9	0.9
Compressor pressure ratio	18	18	18	18	18	18	18
Compressor polytropic efficiency	0.9	0.9	0.9	0.9	0.9	0.9	0.9
Ambient or engine inlet pressure (Pa)	101,325	101,325	101,325	101,325	101,325	101,325	101,325
Ambient or engine inlet temperature (K)	288	288	288	288	288	288	288
Turbine polytropic efficiency	0.9	0.9	0.9	0.9	0.9	0.9	0.9
BPR	5	5	5	5	5	5	5
Heat capacity ratio at engine cold sections	1.4	1.4	1.4	1.4	1.4	1.4	1.4
Specific heat capacity (constant pressure) at engine cold sections (J/kg)	1,005	1,005	1,005	1,005	1,005	1,005	1,005
Heat capacity ratio at engine hot sections*	1.313	1.313	1.316	1.314	1.314	1.311	1.311
Specific heat capacity (constant pressure) at engine hot sections (J/kg)*	1,212.14	1,212.14	1,243.09	1,221.32	1,251.69	1,229.21	1,229.21
Air to fuel ratio	50.00	51.04	138.89	57.87	21.53	23.03	31.48
Gas constant of combustion products (J/kg-K)*	289.04	289.04	298.21	291.58	299.31	291.78	291.78
LCV (MJ/kg)**	43.2	44.1	120.0	50.0	18.6	19.9	27.2
Fuel flow rate (kg/s)	0.89	0.88	0.31	0.77	2.01	1.92	1.40
Turbine cooling air fraction (%)	Zero	Zero	Zero	Zero	Zero	Zero	Zero
Cycle output							
Thrust (kN)	100	100	100	100	100	100	100
TSFC (g/kN-s)	8.9	8.8	3.1	7.7	20.1	19.2	14.0
TSEC (kJ/kN-s)	384.5	388.1	372.0	385.0	373.9	382.1	380.8
Fan inlet mass flow (kg/s)	268.1	268.1	260.4	265.8	259.3	265.3	265.3
HPT inlet temperature (K)	1,697	1,697	1,697	1,697	1,697	1,697	1,697
HPT inlet mass flow (kg/s)	44.7	44.7	43.4	44.3	43.2	44.2	44.2
LPT outlet temperature (K)	1049.4	1049.4	1065.5	1054.3	1069.8	1058.4	1058.4
LPT inlet mass flow (kg/s)	44.7	44.7	43.4	44.3	43.2	44.2	44.2

*source [192], ** source [33], [47]

A simple thermodynamic analysis of a turbofan engine is conducted for constant thrust production using different fuels under consideration. This is carried out using standard set of equation for gas-turbine engines that apply Brayton cycle, which can be found in resources [190], [231], [245], [246]. Table A.1 lists the thermodynamic cycle analysis input and output parameters at design point. Firstly, a baseline (Jet-A) engine performance is conducted for producing a target thrust of 100 kN and the fuel flow rate is iterated towards this objective, for fixed input component efficiencies, ambient pressure and temperature, and air to fuel ratio.

For a given alternative fuel, the input component efficiencies, and ambient pressure and temperature remain the same as that of Jet-A, but its air to fuel ratio is calculated by multiplying the air to fuel ratio of Jet-A case with the ratio of LCV of the alternative fuel and the LCV of Jet-A. The LCVs [33], [47] and properties of combustion gas [192] for all

fuel cases are known from the respective resources. For 100% SPK and ethanol, the properties of combustion gases are not known. It is assumed that the combustion gas properties of 100% SPK and ethanol are same as that of Jet-A and methanol, respectively. Similar to the Jet-A case, the fuel flow rate for engine powered by a given alternative fuel is iterated towards the objective of producing a target thrust of 100 kN.

A.2. Stepwise procedure of the range equation analysis at design point for the baseline and alternative fuel cases

Conventional jet fuel (Jet-A) case:

The methodology description is listed/summarised below as a stepwise process of the range equation analysis for Jet-A (baseline) case (based on Figure 4.1):

- Step 1: Use the known values of OEW, W_p, $W_{F,total}$ of the aircraft to estimate the aircraft GTOW (= OEW + $W_{F,total}$ + W_p).
- Step 2: Input the known lost fuel value, h, and η_o, for Jet-A aircraft being evaluated.
- Step 3: Calculate $W_{initial}$ and W_{final}
  $W_{initial}$ = (1 – lost fuel value) x GTOW
  W_{final} = GTOW – 0.9 x $W_{F,total}$
- Step 4: Calculate the aircraft L/D
- Step 5: Calculate the Jet-A aircraft range using Breguet's range equation (equation 4.1)

Alternative cryogenic fuel cases:

For alternative cryogenic fuel cases (based on Figure 4.2), the methodology is listed/summarised below as a stepwise process of the range equation analysis:

- Step 1: Guess a value (initial guess value of 1 kg) for $W_{F,total}$
- Step 2: The OEW for the alternative cryogenic fuel case is calculated based on the value of $W_{F,total}$ as additional fuselage structure is required to store the said fuel in cryogenic tanks.
- Step 3: The GTOW (= OEW + $W_{F,total}$ + W_p) is calculated for a given payload case
- Step 4: Is the GTOW<=MTOW of the aircraft?
- Step 5: If 'yes' to question in step 4, estimate the lost fuel value, h, and η_o, for the alternative fuelled aircraft under consideration.
- Step 6: After step 5, calculate $W_{initial}$ and W_{final}
  $W_{initial}$ = (1 – lost fuel value) x GTOW
  W_{final} = GTOW – 0.9 x $W_{F,total}$
- Step 7: After step 6, calculate the aircraft L/D (includes penalty due to additional fuselage requirement)
- Step 8: After step 7, calculate the aircraft range using Breguet's range equation (equation 4.1)
- Step 9: Does the calculated range of the alternative fuelled aircraft meet the target range of the Jet-A (baseline) aircraft?
- Step 10: If 'yes' to the question in step 9, then the aircraft is fixed/finalised
- Step 11: If 'no' to the question in step 9, then increase the guess for $W_{F,total}$ and execute step 1 to follow the steps thereafter
- Step 12: If 'no' to question in step 4, then restore values of all parameters from previous iteration (based on previous guess of $W_{F,total}$), and the aircraft is fixed/finalised.

Alternative non-cryogenic fuel cases:

For alternative non-cryogenic fuel cases (based on Figure 4.2), the methodology is listed/summarised below as a stepwise process of the range equation analysis:

- Step 1: Guess a value (initial guess value of 1 kg) for $W_{F,total}$
- Step 2: Does total fuel at mission start fit inside the wing tanks?
- Step 3: If 'yes' to question in step 2, the OEW of aircraft is same as that of the Jet-A aircraft case i.e., no additional fuselage.

- Step 4: If 'no' to question in step 2, estimate (and store) the fuel volume that fits inside the wing tanks and for the remaining fuel (calculate the) additional fuselage is required for storing non-cryogenic fuel tank. The OEW of aircraft is calculated based on this additional fuselage requirement.
- Step 5: Following step 3 or 4, the OEW for the alternative non-cryogenic fuel case is calculated.
- Step 6: The GTOW (= OEW + $W_{F,total}$ + W_p) is calculated for a given payload case
- Step 7: Is the GTOW<=MTOW of the aircraft?
- Step 8: If 'yes' to question in step 7, estimate the lost fuel value, h, and η_o, for the alternative fuelled aircraft under consideration.
- Step 9: After step 7, calculate $W_{initial}$ and W_{final}

    $W_{initial}$ = (1 – lost fuel value) x GTOW

    W_{final} = GTOW – 0.9 x $W_{F,total}$
- Step 10: After step 9, calculate the aircraft L/D (includes penalty due to additional fuselage requirement)
- Step 11: After step 10, calculate the aircraft range using Breguet's range equation (equation 4.1)
- Step 12: Does the calculated range of the alternative fuelled aircraft meet the target range of the Jet-A (baseline) aircraft?
- Step 13: If 'yes' to the question in step 12, then the aircraft is fixed/finalised
- Step 14: If 'no' to the question in step 12, then increase the guess for $W_{F,total}$ and execute step 1 to follow the steps thereafter
- Step 15: If 'no' to question in step 7, then restore values of all parameters from previous iteration (based on previous guess of $W_{F,total}$), and the aircraft is fixed/finalised.

A.3. Stepwise procedure of the range equation analysis at off-design points for the baseline and alternative fuel cases

Maximum permissible range estimation with full fuel tank:

The stepwise process shown in Figure 4.3 is as follows -
- Step 1: Use the fixed/designed aircraft where values of OEW, maximum $W_{F,total}$, and maximum payload weight are known for fuel under consideration. Begin with full fuel tank capacity for a given payload case (weight) within the maximum payload limit and estimate the aircraft GTOW (= OEW + $W_{F,total}$ (max.) + W_p).
- Step 2: Input the known lost fuel value, h, and η_o, for aircraft and fuel being evaluated.
- Step 3: Calculate $W_{initial}$ and W_{final}

    $W_{initial}$ = (1 – lost fuel value) x GTOW

    W_{final} = GTOW – 0.9 x $W_{F,total}$
- Step 4: Calculate the aircraft L/D
- Step 5: Calculate and record the aircraft range using Breguet's range equation (equation 4.1) with full fuel tank capacity for a given payload case (weight). This is the maximum permissible range for given payload case (with full fuel tank capacity).

Estimation of block energy consumption for given range and payload combination:

The stepwise process shown in Figure 4.4 is as follows -
- Step 1: Use the fixed/designed aircraft where values of OEW, maximum $W_{F,total}$, and maximum payload weight are known for fuel under consideration. For a given payload case (weight) within the maximum payload limit, select the aircraft range at which fuel performance needs to be evaluated (example: 5,000 km). This range selection should be within maximum range of aircraft for given payload, which is evaluated using schematic shown in Figure 4.3.
- Step 2: Begin with a guess value (initial guess value of 1 kg) for $W_{F,total}$.
- Step 3: The GTOW (= OEW + $W_{F,total}$ + W_p) is calculated for a given payload case
- Step 4: Use the lost fuel value, h, and η_o, for the fuel case under consideration.
- Step 5: Calculate $W_{initial}$ and W_{final}

    $W_{initial}$ = (1 – lost fuel value) x GTOW

    W_{final} = GTOW – 0.9 x $W_{F,total}$
- Step 6: Calculate the aircraft L/D

- Step 7: Calculate the aircraft range using Breguet's range equation (equation 4.1)
- Step 8: Does the calculated range of the aircraft meet the target (selected range) range (example: 5,000 km considered in step 1)?
- Step 9: If 'yes' to the question in step 8, then record the block fuel/energy consumption for given range and payload combination

    $W_{F,block} = 0.9 \times W_{F,total}$ (as discussed in section 4.3.3)
- Step 10: If 'no' to the question in step 8, then increase the guess within the maximum value of total fuel weight at mission start for given aircraft-fuel case and execute step 2 to follow the steps thereafter.

A.4. Validation of the used equations

A.4.1 Validation of Breguet's range equation

Two aircraft are considered for validation of Breguet's range equation. Each aircraft has two operational points of range and payload combinations. Overall, there are four validation points. Additionally, the lift to drag ratio estimation, which is an intermediate calculation step, is also validated for both aircraft. The two aircraft considered here are Airbus A320-200 and Boeing 767-300F. The A320-200 is a small narrow-body and single-aisle aircraft and the B767-300F is a small wide-body freighter aircraft. It is to be noted that both aircraft are small transport jets. The skin friction coefficient (C_f) for small transport jets is 0.0035 [195], in comparison with 0.003 for large transport jet (used in section 4.3.4). Table A.2 and Table A.3 below provide the characteristics of Airbus A320-200 and Boeing 767-300F aircraft, respectively, that are required for Breguet's range equation analysis.

Table A.2. Airbus A320-200 aircraft characteristics

Parameter	Units	Value	Reference
OEW	kg	44,200	[343]
MTOW	kg	73,500	[343]
Maximum payload	kg	16,565	[343]
Range at maximum payload	km	2,935	[343]
	nmi	1,585	[343]
Payload at maximum range	kg	10,341	[343]
Maximum range	km	5,181	[343]
	nmi	2,798	[343]
Cruise L/D	-	15 – 16	[344]
Overall efficiency	-	0.3	Calculated using [344]
Wing area	m² or ft²	122.4 or 1,317.5	[345], [346]
AR	-	9.5	[345], [346]
Cruise Mach	-	0.795	[345], [346]
Cruise altitude	ft or km	37,000 or 11.28	[345], [346]
Air density at cruise altitude	kg/m³	0.348	Calculated using [317]
Speed of sound at cruise altitude	m/s	295.07	Calculated using [317]

Table A.3. Boeing 767-300F aircraft characteristics

Parameter	Units	Value	Source
MTOW	kg	185,065	[347]
Maximum zero fuel weight (MZFW)	kg	140,160	[347]
Maximum payload (PL_{max})	kg	52,700	[348]
OEW (= MZFW - PL_{max})	kg	87,460	Calculated
Range with 40,823 kg payload	km	7,408	[347]
	nmi	4,000	[347]
Range with 50,800 kg payload	km	5,556	[347]
	nmi	3,000	[347]
Cruise *L/D*	-	15-16	Estimated using [349]
Overall efficiency (η_o)	-	0.34	Estimated using [211], [350]
Wing area	m^2 or ft^2	282.3 or 3,050	[351]
AR	-	7.99	[351]
Cruise Mach	-	0.8	[348]
Cruise altitude	ft or km	35,000 or 10.67	[348]
Air density at cruise altitude	kg/m^3	0.38	Calculated using [317]
Speed of sound at cruise altitude	m/s	296.54	Calculated using [317]

Table A.4. Airbus A320-200 and Boeing 767-300F aircraft performance validation

Parameter	Published	Calculated in this chapter	Prediction difference
Airbus A320-200			
Range with 16,565 kg payload (1)	2,935 km	3,054 km	+4.05%
L/D for (1)	15-16*	15.7	-
Range with 10,341 kg payload (2)	5,181 km	4,947	-4.52%
L/D for (2)	15-16*	15.48	-
Boeing 767-300F			
Range with 40,823 kg payload (3)	7,408 km	7,098 km	-4.19
L/D for (3)	15-16*	15.75	-
Range with 50,800 kg payload (4)	5,556 km	5,604	+0.86%
L/D for (4)	15-16*	15.86	-
* Typical cruise *L/D*			

For the A320-200 aircraft, η_o is not known directly. However, the cruise thrust specific fuel consumption (TSFC) of this aircraft is known to be ~17.5 mg/N-s from resource [349]. Using the definition of η_o,[flight speed/(TSFC x fuel

calorific value)] its value is estimated. The flight speed in cruise is 234 m/s [= 0.8 (Mach) x 295.54 (speed of sound)]. η_o is estimated to be 0.3 for A320-200 aircraft (as listed in Table A.2). Additionally, the cruise *L/D* for A320-200 is known to be (approximately) 15 – 16 [344]. The cruise *L/D* is plotted in a figure in resource [344], and so the exact value is not known. This approximate value of cruise *L/D* for A320-200 listed in Table A.2.

Similarly, for the B767-300F aircraft, η_o is not known directly. However, η_o of Boeing 747-400 aircraft is known to be ~0.34 from resource [211]. The B747-400 aircraft uses four CF6 – 80C2 engines and B767-300F uses two CF6 – 80C2 engines [350]. Hence, η_o of B767-300F aircraft is expected to be 0.34 and is listed in Table A.3. Additionally, the cruise *L/D* for B767-300F is not known directly. However, the cruise *L/D* of similar size/type aircraft viz. Airbus A310 and B767-300ER are known to be about 15 – 16 from resource [344]. The cruise *L/D* is plotted in a figure in resource [344], and so the exact value is not known. This approximate value of cruise *L/D* (of 15 – 16) is expected to be same for B767-300F aircraft and this value is listed in Table A.3. The required data for Breguet's range analysis of the above two aircraft are now known.

Table A.4 lists the Airbus A320-200 and Boeing 767-300F aircraft performance validation. As discussed before, each aircraft has two operational points of range and payload combinations, and overall, there are four validation points. According to the book by Kundu et al. [184] and thesis of Kirby [185], a prediction difference of ±5% is an acceptable/typical industry trend in the conceptual design phase or for low-order modelling. The above criteria of ±5% prediction difference is used for establishing confidence in the model. It can be observed from Table A.4 that Breguet's range equation for the estimation of range is accurate to within ±5%, which is acceptable for conceptual design phase or low-order modelling used in this chapter. Additionally, the cruise *L/D* for both aircraft at each of the four points agree with the published values.

A.4.2   Validation of aircraft wetted area prediction equation

The aircraft wetted area prediction equation needs to be tested for its accuracy while predicting the wetted area of recent or advanced/NextGen tube-wing aircraft. Two validation cases are conducted here. The first case is wetted area estimation of Boeing 787-8 aircraft. Piano-X is an aircraft analysis tool and PIANO-X data for this aircraft with take-off weight of 476,000 lb (215,910 kg) estimates the wetted area to be 19,533 ft^2 (1815 m^2) [197]. Substituting the take-off weight of 476,000 lb in equation 4.5 (aircraft wetted area prediction equation in section 4.3.4), the wetted area is calculated to be 19,756 ft^2 (1,835 m^2), compared to the wetted area estimate of 19,533 ft^2 known from PIANO-X data. The prediction difference between PIANO-X data and prediction by using equation 4.5 is +1.14%. The second case is wetted area estimation of an advanced tube-wing aircraft. The study by Nickol et al. [199] designs an advanced tube-wing aircraft for seating 300 passengers using FLOPS software. The GTOW of this aircraft is 503,350 lb (228,316 kg). Substituting this GTOW in equation 4.5, the wetted area is calculated to be 20,605 ft^2 (1914 m^2) compared to the wetted area estimation of 20,600 ft^2 by Nickol et al. study. Roskam's model is found to be highly accurate as the prediction difference is +0.024%. For both cases, Roskam's model is found to be accurate with a prediction difference well within the criteria defined (prediction difference of ±5%) for accuracy during the conceptual design phase or low-order modelling.

A.4.3   Validation of fuselage wetted area and weight prediction equation

Before using equation 4.6 (fuselage wetted area prediction equation) and equation 7 (fuselage weight prediction equation) from section 4.3.4, these need to be tested for their accuracy using the defined criteria. Piano-X data for B787-8 aircraft estimates the fuselage wetted area of 9,484 ft^2 (881 m^2) and 'fuselage group weight' of 44,917 lb (20,374 kg) [197]. For B787-8 aircraft, the values of d_f and l_f are 18.83 ft and 183.5 ft, respectively [197]. Substituting these values of d_f and l_f in equation 4.6, the fuselage wetted area is calculated to be 9,412 ft^2 (874 m^2), compared to the fuselage wetted area value of 9,484 ft^2 from Piano-X (prediction difference of -0.76%). Substituting this predicted fuselage wetted area of 9,412 ft^2 in equation 4.7, results in fuselage weight of 47,060 lb (21,346 kg) compared to the 'fuselage group weight' of 44,917 lb from Piano-X (prediction difference of +4.77%). The prediction difference using equation 4.6 and equation 4.7 are within the criteria defined (prediction difference of ±5%) for accuracy during the conceptual design phase or low-order modelling.

A.4.4   Validation of the LH_2 aircraft from the Clean Sky 2 – FCH joint project

An attempt is made below to replicate the long-range LH_2 aircraft design in the Clean Sky 2 - Fuel Cells and Hydrogen (FCH) joint project [34], where very few/limited design details or aircraft characteristics are revealed. It is known from the said project report that the long-range LH_2 aircraft from the Clean Sky 2 – FCH joint project seats 325

passengers and has a design range of 10,000 km, where the cryogenic tank η is 0.38 for an integral tank with double walled multi-layer insulation system [34], [206]. Using the model of the A350-1000 aircraft developed in the present chapter, an LH_2 powered large aircraft is designed for 325 passenger-payload (30,875 kg) with a target design range of 10,000 km and a cryogenic LH_2 tank η value of 0.38 is used. The aircraft performance characteristics of the said aircraft is listed in Table A.5. ΔL represents the additional fuselage length for accommodating the alternative fuel. It can be observed from Table A.5 that the magnitude of increase in LH_2 aircraft fuselage length calculated in this chapter and the published value in Clean Sky 2 – FCH joint project are similar for the same cryogenic tank η and passenger payload.

Table A.5. Comparison of LH_2 aircraft characteristics for passenger payload of 30,875 kg (325 passengers) between the Clean Sky 2 – FCH joint project and the present chapter

Fuel and study	Cryogenic tank η	Payload weight W_p (kg)	Fuselage length (m)	ΔL (m)	ΔL (%)	R (km)
LH_2 (Clean Sky 2 – FCH joint project [34])	0.38	30,875	-	-	30.00	10,000
LH_2 (Using present model)	0.38	30,875	93.99	21.74	30.09	10,000

A.5.   Results of the performance characteristics of aircraft powered by different fuels

A.5.1   Miscellaneous results of the performance characteristics at design point

The performance characteristics of Airbus A350-1000 aircraft modified for the use of alternative fuels (for same payload of 34,770 kg i.e., 366 passenger payload) is listed in Table A.6. The fuselage and aircraft modification data of Airbus A350-1000 aircraft for the use of alternative liquid fuels is listed in Table A.7. It is to be noted that the wing planform (area, span, and/or AR) is maintained constant for different fuel cases. This is similar to or in-line with the approach used in the Cryoplane study of minimal change to the wing planform, and the positive effects of this approach on the wing loading are observed later.

Table A.6. Airbus A350-1000 performance characteristics using alternative liquid fuels for passenger payload of 34,770 kg (366 passengers) for same wing area (465 m^2) and AR (9.12)

Fuel	h/g (km)	Cryogenic tank η	OEW (kg)	$W_{F,total}$ (kg)	GTOW (kg)	Fuel in fuselage tank (kg)	ΔL (m)	L/D	R (km)
Jet-A	4,404	-	155,129	126,101	315,999	-	-	18.63	13,870
100% SPK	4,496	-	155,314	123,320	313,404	5,178	0.25	18.57	13,870
LH_2	12,233	0.78	183,371	50,375	268,516	50,375	26.87	16.09	13,870
LNG Case 1	5,097	0.78	187,239	93,990	315,999	93,990	8.40	18.20	10,895
LNG Case 2	5,097	0.63	205,161	76,068	315,999	76,068	6.77	18.48	8,517
LNH_3	1,896	0.80	183,605	97,624	315,999	97,624	5.05	18.34	3,478
Methanol	2,029	-	155,191	126,037	315,999	1,809	0.08	18.52	5,943
Ethanol	2,773	-	155,202	126,027	315,999	2,111	0.10	18.57	8,421

As discussed in section 4.3.5, for LNG two cases are evaluated - the first LNG case uses a hypothetical (futuristic) η of 0.78 similar to LH_2 case and in the second LNG case a present-day value of η of 0.63 is used which is similar to the

values used in transportation of LNG fuel via trucks. The effect of LNG cryogenic tank η can be observed from Table A.6. With increasing η, the aircraft range and $W_{F,total}$ increases, and the OEW decreases.

Table A.7. Airbus A350-1000 fuselage and aircraft modification data for different alternative fuels for passenger payload of 34,770 kg (366 passengers) for same wing area (465 m²) and AR (9.12)

Fuel	l_f (m)	Fuselage structural weight $W_{Fuselage}$ (kg)	Fuselage wetted area $S_{wet,Fuselage}$ (m²)	Aircraft wetted area S_{wet} (m²)	Wing loading at take-off (kg/m²)	SEC (MJ/tonne-km)
Jet-A	72.25	29,484	1,208	2,445	679.6	10.17
100% SPK	72.5	29,596	1,212	2,450	674.0	10.15
LH_2	99.12	41,749	1,710	2,948	577.5	11.28
LNG C1	80.65	33,315	1,365	2,602	679.6	11.17
LNG C2	79.02	32,572	1,334	2,572	679.6	11.56
LNH_3	77.3	31,785	1,302	2,539	679.6	13.51
Methanol	72.33	29,521	1,209	2,447	679.6	10.93
Ethanol	72.35	29,527	1,210	2,447	679.6	10.54
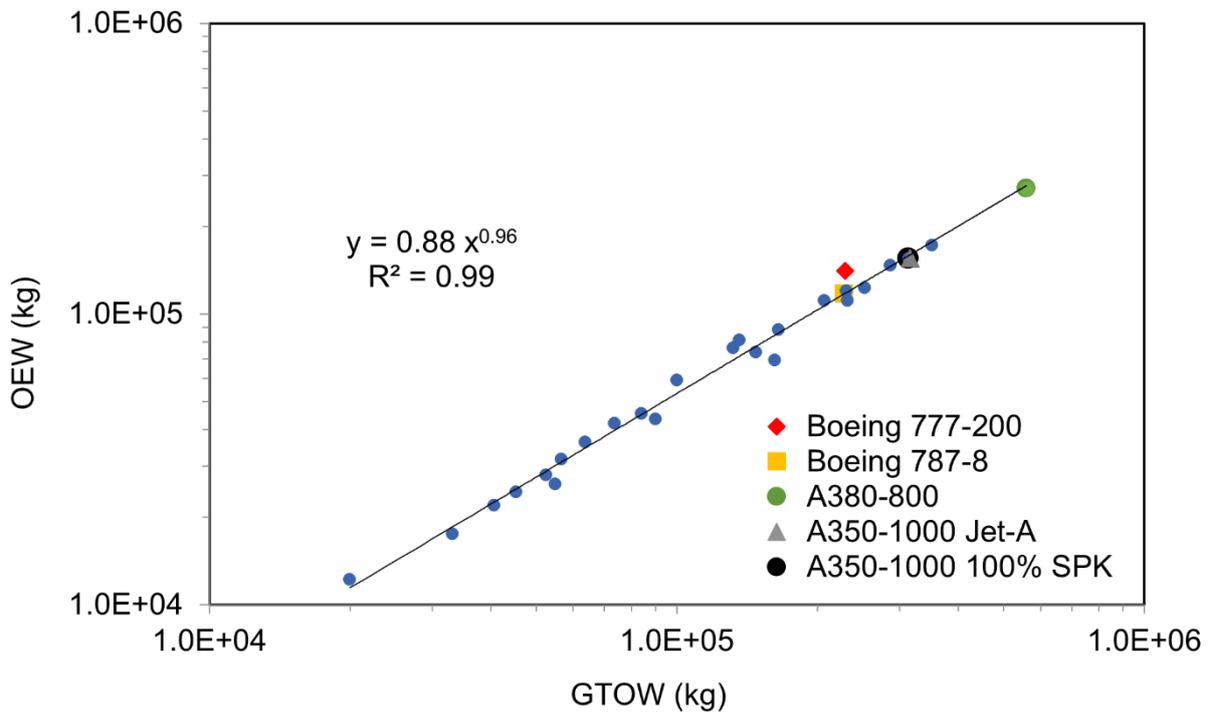
Figure A.1. Relationship between OEW and GTOW of 100% SPK from the present study and aircraft in service for facilitating weight sizing studies

It can be observed from Table A.6 that only 100% SPK and LH_2 powered aircraft are able to fly same range/distance (R) as that of the Jet-A aircraft (baseline) within the same limit of MTOW (of 316 tonnes). Since other alternative fuels have lower h as compared to Jet-A, higher quantity of fuel would be required (to be carried) on the aircraft for enabling the same range as that of the Jet-A aircraft. This also increases the OEW of the aircraft and resultantly the GTOW. Since the GTOW is structurally limited by the MTOW bound, limited fuel and corresponding OEW can be supported for a given aircraft structure (MTOW defined).

It should be noted that since LH_2 has 2.78 times higher gravimetric energy density as that of Jet-A, $W_{F,total}$ for LH_2 is lesser than that for Jet-A. The lower volumetric energy density of LH_2 fuel increases the fuselage length by 26.87 m (or by 37.2%) compared to Jet-A case. In this work, the 37.2% increase in LH_2 aircraft fuselage length compared to Jet-A case, penalizes the aircraft performance as the LH_2 aircraft fuselage weight increases to 41,749 kg from 29,484 kg, and L/D ratio decreases to 16.09 from 18.63. The associated increase in fuselage wetted area and aircraft wetted area can be observed from Table A.7.

Table A.8. OEW and GTOW data of aircraft in service and aircraft designed in this study [198], [298]

Aircraft	GTOW (kg)	OEW (kg)
727-200	83,824	45,359
737-200	52,390	27,955
737-300	56,472	31,720
747-200B	351,534	172,365
747-SP	285,763	147,417
757-200	99,790	59,157
767-200	136,078	81,230
DC8-Super 71	147,417	73,799
DC9-30	54,885	25,941
DC9-80	63,503	36,177
DC10-10	206,384	111,086
DC10-40	251,744	122,952
Lockheed L1011-500	231,332	111,357
Fokker F28-4000	33,112	17,546
Rombac-111-560	45,200	24,386
VFW-Fokker 614	19,958	12,179
Bae 146-200	40,596	21,999
A300-B4-200	164,999	88,500
A310-202	131,995	76,616
Ilyushin-Il-62M	162,000	69,400
Tupolev-154	90,000	43,499
Boeing 787-8	227,930	117,707
A380-800	559,993	270,012
A330-200	229,998	120,499
Airbus A320	73,498	42,100
Boeing 777-200	229,518	140,659
A350-1000 Jet-A	316,000	155,129
A350-1000 100% SPK	313,404	155,314

The cryogenic tank η used by Brewer [172], [180], [191] (η = 0.836) is of the similar order used in this work (η = 0.78). According to the book by Brewer [180], the LH_2 aircraft will have lower wing loading. Brewer [172], [180], [191] evaluates a double-decker 400 passenger LH_2 aircraft (18,500 km range). The wing (area) is subjected to modifications (wing structural weight and loading). The wingspan and wing area reduces from 87.7 m (Jet-A) to 66.2 m (LH_2 fuel) and from 698.7 m^2 (Jet-A) to 438.1 m^2 (LH_2 fuel), respectively. The AR (span^2/ area) reduces from 11 (Jet-A) to 10 (LH_2 fuel). The gross take-off weight of the Jet-A and LH_2 aircraft are known to be 476,230 kg and 249,400 kg, respectively. The wing loading at take-off of the Jet-A and LH_2 aircraft are calculated to be (476,230 kg/698.7 m^2 =) 681.6 kg/m^2 and (249,400 kg/438.1 m^2 =) 569.3 kg/m^2, respectively. Therefore, the wing loading of the double-decker 400 passenger LH_2 aircraft (18,500 km range) evaluated by Brewer [180] reduces by 16.5%, compared to the baseline Jet-A aircraft. In the present work, the wing planform (area, span and/or AR) is maintained constant for different fuel cases. This is similar to or in-line with the approach used in the Cryoplane study of minimal change to the wing planform. As observed from Table A.7, the wing-loading at take-off of the LH_2 aircraft (577.5 kg/m^2) modelled in this work reduces by 15% (similar to 16.5% reduction observed by Brewer), in comparison with the wing-loading of the Jet-A aircraft (679.6 kg/m^2).

For 100% SPK fuel, the extra fuel (in addition to the wing tank) required considering slightly lower volumetric energy density as compared to Jet-A, to meet the flight range of Jet-A aircraft within the MTOW limit of 316 tonnes, is small as compared to the fuel that fits in the wing tanks. Therefore, for 100% SPK, ΔL is 0.25 m which has an insignificant impact on the (wetted area) *L/D* performance. Figure A.1 shows the relationship between OEW and GTOW of 100% SPK from the present study and aircraft in service. It can be observed that the relationship between OEW and GTOW for the aircraft designed in this research is similar to that of aircraft in service. 100% SPK aircraft have similar (magnitude of) OEW and GTOW as that of Jet-A case. For compactness, only the names of recent aircraft in service and the aircraft designed in this research are mentioned in Figure A.1.

The data points in Figure A.1 comprise of small and medium size aircraft, LTA aircraft and large quad. All data points (OEW and GTOW data of aircraft in service and aircraft designed in this research), are listed in Table A.8. Additionally, the developed equation is useful during preliminary design or aircraft weight sizing process, and knowing either OEW or GTOW, the GTOW or OEW can be estimated.

A.5.2 LH$_2$ aircraft landing weight analysis

Considering an emergency situation, the landing weight of an aircraft is an important factor. The safe landing weight is dependent on the structural weight of the aircraft. Roskam [198] recommends 0.84 to be an average permissible ratio of the aircraft landing weight and the aircraft's permissible take-off weight, for a transport jet. In the event of an emergency landing immediately after take-off, the pilot performs fuel jettison or dumps the conventional Jet-A fuel in air so that the aircraft weight goes below its permissible landing weight. However, for an aircraft powered by hydrogen fuel, this highly flammable fuel cannot be dumped into the atmosphere. The present research uses the same MTOW limit (316 tonnes) for both Jet-A and LH$_2$ aircraft. As discussed earlier, for LH$_2$ fuel there is a net reduction in the aircraft GTOW of 15% from the permissible weight, or GTOW$_{LH2}$ = 0.85 MTOW. During engine start, taxi-out and take-off, LH$_2$ fuel will be consumed, and this would further reduce this aircraft weight. The GTOW of this LH$_2$ aircraft is similar to the average permissible landing weight of the baseline aircraft (structure). This means that there might not be a need to conduct fuel jettison of a highly flammable hydrogen fuel in the event of an emergency landing. This finding is of significance considering the safety issue associated with LH$_2$ use in a passenger aircraft.

A.5.3 Off-design point analysis

Figure A.4 shows the comparison of OEW/GTOW for Jet-A, 100% SPK, and LH$_2$ aircraft at different range and payload (load factor) combinations. It is to be noted that at the off-design points, the OEW for a given fuel case is constant and the GTOW (sum of OEW, payload weight, and $W_{F,total}$) varies with flight range/distance to be travelled. For a given payload/load factor case, the $W_{F,total}$ increases (and thus GTOW increases) with increasing range. LH$_2$ has higher gravimetric energy density than Jet-A (and 100% SPK) and hence relatively less fuel weight is added to the aircraft as compared to Jet-A case. Therefore, the drop in OEW/GTOW is steeper for Jet-A case (and 100% SPK) than LH$_2$ case with increasing range. This is observed despite the fact that the OEW of the LH$_2$ aircraft is more than that for the corresponding Jet-A aircraft. For 100% SPK, since the OEW is slightly higher (due to negative volumetric density effects that needs 0.25 m of additional fuselage) and the GTOW is slightly lower (due to positive gravimetric density effects) than Jet-A, OEW/GTOW is slightly higher than Jet-A at all load factor – range combinations.

It was observed from Figure 4.6 and Figure A.2 that for a given passenger – load factor case, LH$_2$ aircraft consumes more energy than Jet-A aircraft. LH$_2$ aircraft has a longer fuselage than the corresponding Jet-A aircraft, and therefore a penalty is observed on its aerodynamic performance. Figure A.5 shows the *L/D* comparison of different fuel cases at different range and load factor combinations. Figure A.6 and Figure A.7 show the lift coefficient (C_L) and drag coefficient (C_D) comparison of different fuel cases at different range and load factor combinations. It can be observed that for a given passenger – load factor case the *L/D* of LH$_2$ aircraft is lesser than the corresponding Jet-A aircraft. The GTOW of Jet-A aircraft is greater than the corresponding LH$_2$ aircraft. According to equation 4.4, the C_L for the Jet-A aircraft is expected to be greater, and this is observed in Figure A.6. Likewise, increasing the range increases the $W_{F,total}$ and thus the GTOW. Resultantly, C_L (or lift) increases with increasing range, and this is observed from Figure A.6. The C_D calculated here includes the parasitic and lift-induced drag (equation 4.2). For a given LH$_2$ aircraft case, the OEW is fixed at off-design points. Therefore, for a given aircraft, with increasing range the parasitic drag remains constant. As discussed above, C_L increases with increasing range and therefore the lift-induced drag also increases. Thus, for a given aircraft case, C_D increases with range. This is observed from Figure A.7. Overall, both C_L and C_D increase with range for a given aircraft case. For a given aircraft case, the increase in C_L is greater than the increase in C_D which results in a net

improvement of *L/D* with increasing range as observed in Figure A.5. For example: C_L at 13,870 km is 1.21 times C_L at 5,000 km whereas C_D at 13,870 km is 1.12 times C_D at 5,000 km for Jet-A 100% load factor; and C_L at 13,870 km is 1.07 times C_L at 5,000 km whereas C_D at 13,870 km is 1.04 times C_D at 5,000 km for LH_2 100% load factor. This results in 1.08 times increase and 1.03 times increase in L/D for Jet-A 100% load factor and LH_2 100% load factor respectively.

Figure A.2. SEC comparison for Jet-A, 100% SPK, and LH₂ aircraft ($\eta = 0.78$) at different range and payload (load factor) combinations

For 100% SPK, due to the slightly higher gravimetric energy density, the GTOW is lower than Jet-A. Thus, according to equation 4.4, the C_L for the 100% SPK aircraft is expected to be lower than Jet-A and this is observed in Figure A.6. Additionally, since the OEW is slightly higher (due to negative volumetric density effects that needs 0.25 m of additional fuselage), the parasitic drag is higher than Jet-A. However, the GTOW is slightly lower and thus the lift induced drag is smaller than Jet-A. Overall, the C_D for the 100% SPK aircraft is lower than Jet-A and this is observed in Figure A.7. Considering the effects of both C_L and C_D, the effect of lower GTOW of 100% SPK relative to Jet-A results in lower *L/D* and this is observed in Figure A.5.
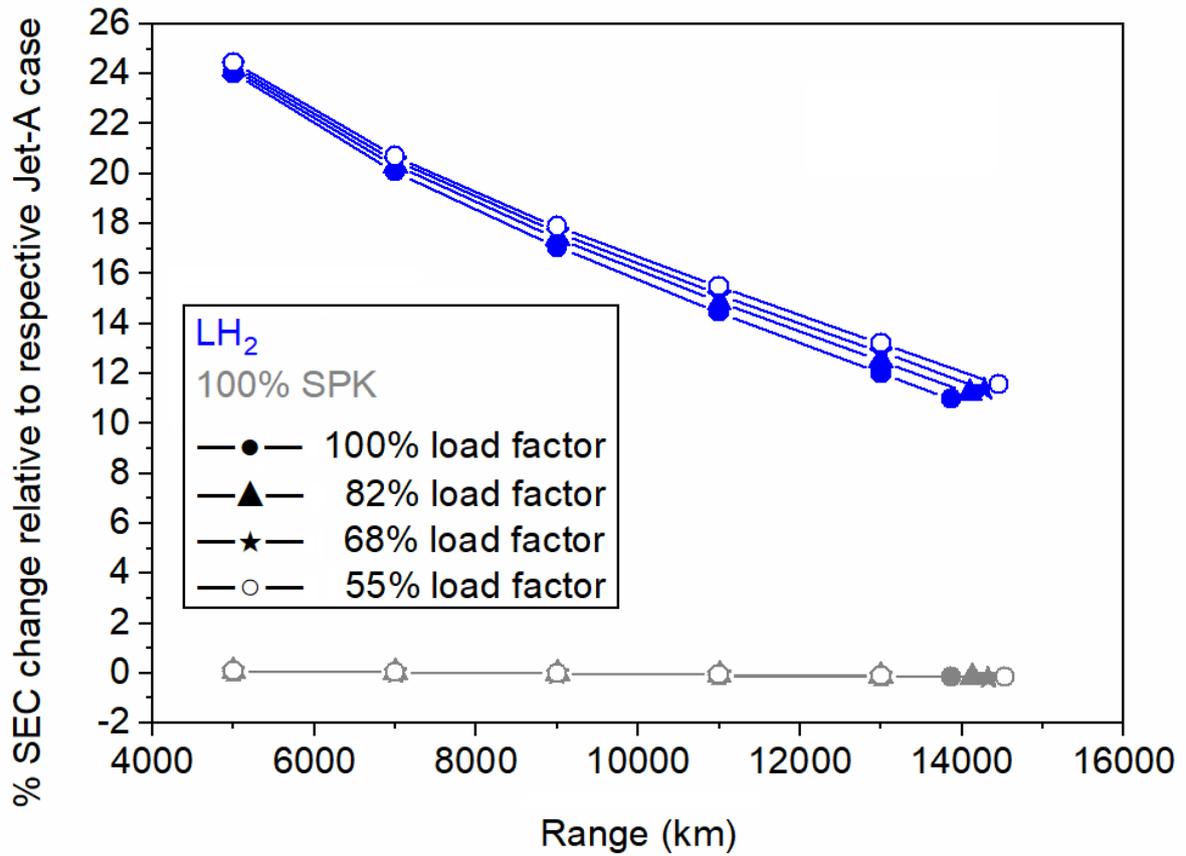
Figure A.3. Comparison of percent change in SEC for LH₂ ($\eta = 0.78$) and 100% SPK relative to the Jet-A aircraft at different range and payload (load factor) combinations
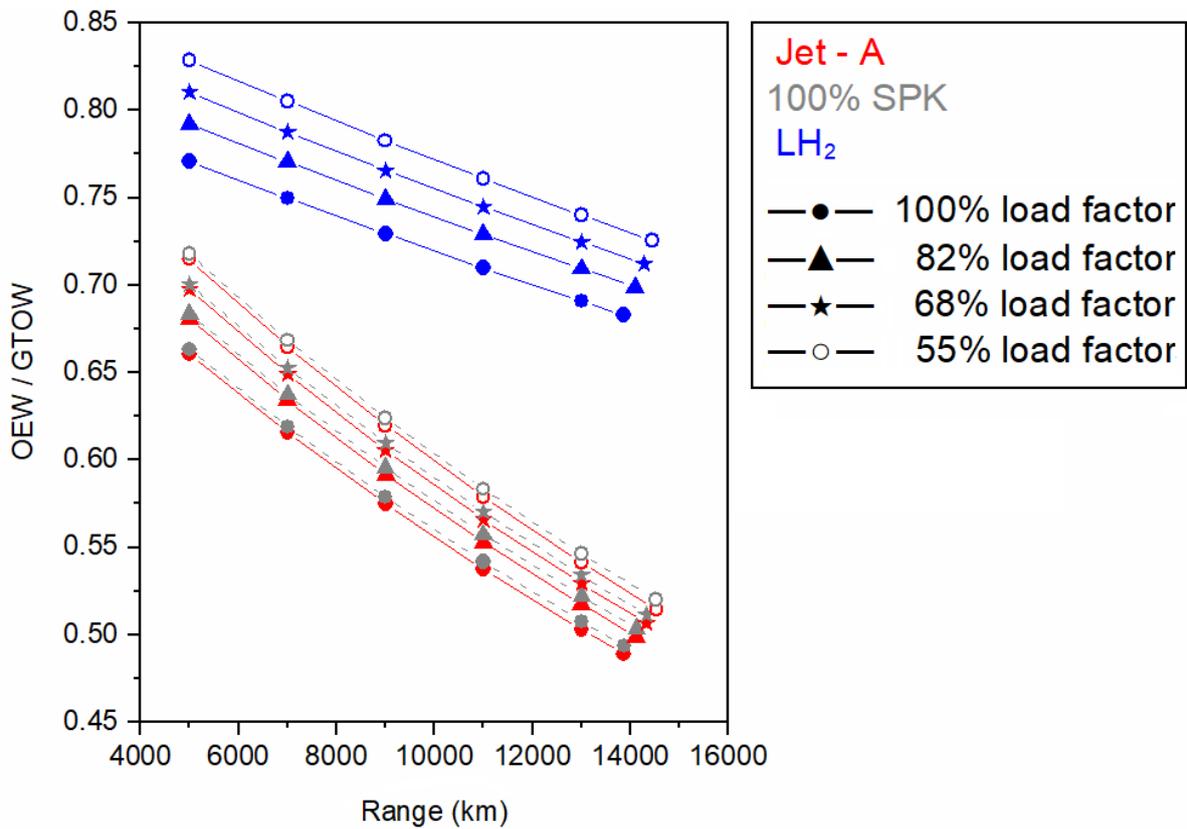
Figure A.4. Comparison of OEW/GTOW ratio for Jet-A, 100%, SPK and LH₂ aircraft ($\eta = 0.78$) at different range and payload (load factor) combinations
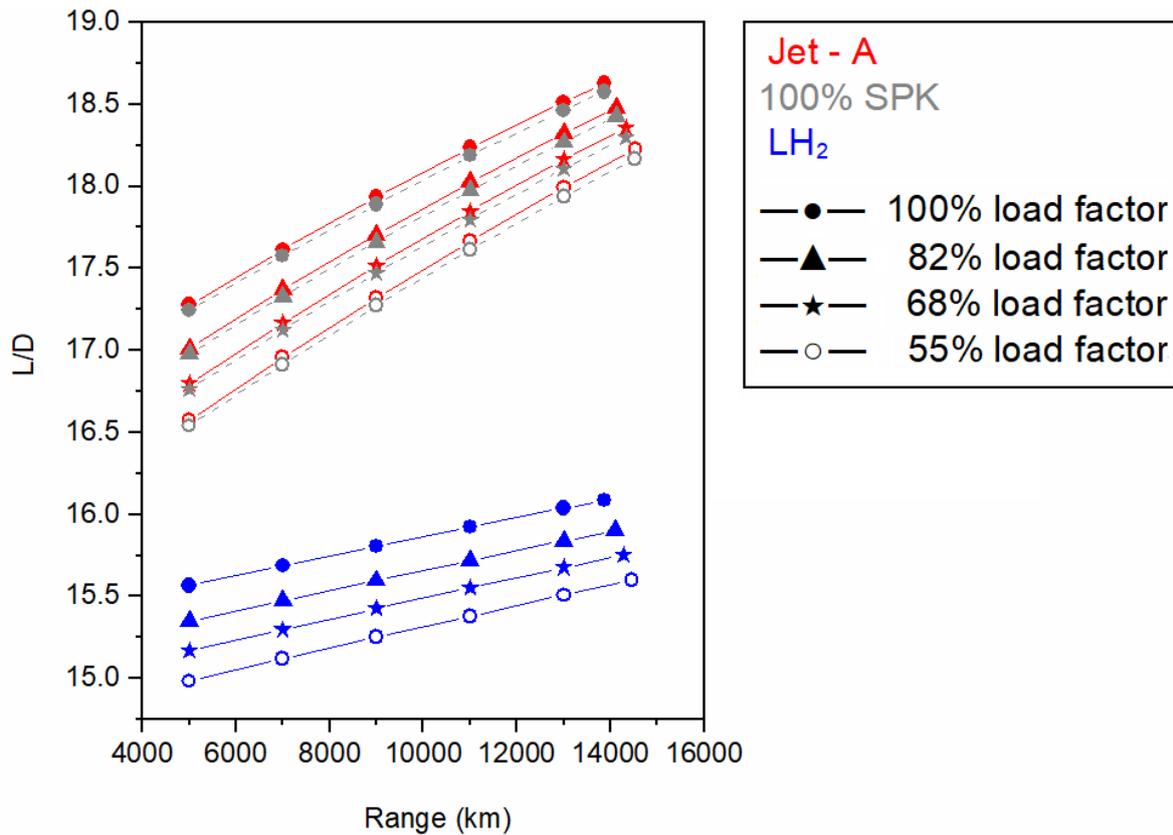
Figure A.5. Comparison of *L/D* for Jet-A, 100% SPK, and LH$_2$ aircraft ($\eta = 0.78$) at different range and payload (load factor) combinations
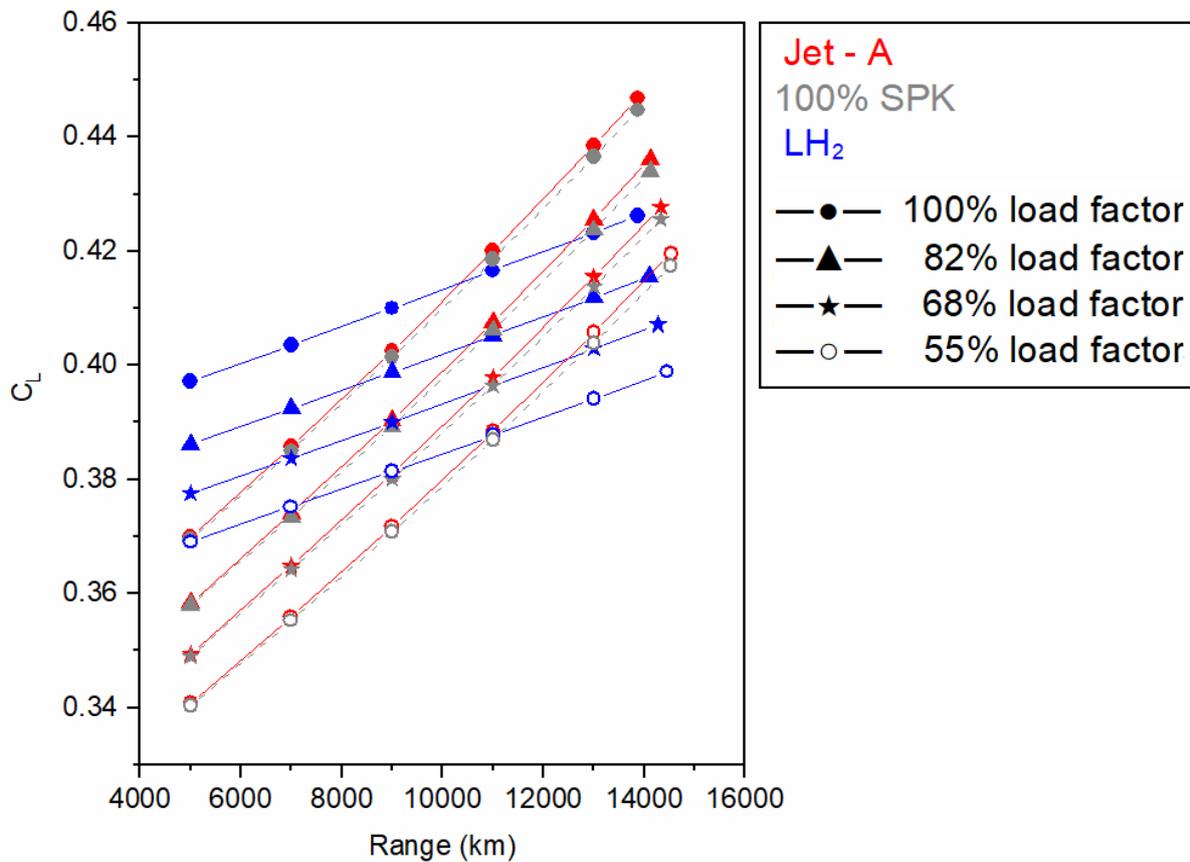
Figure A.6. Comparison of C$_L$ for Jet-A, 100% SPK, and LH$_2$ aircraft ($\eta = 0.78$) at different range and payload (load factor) combinations
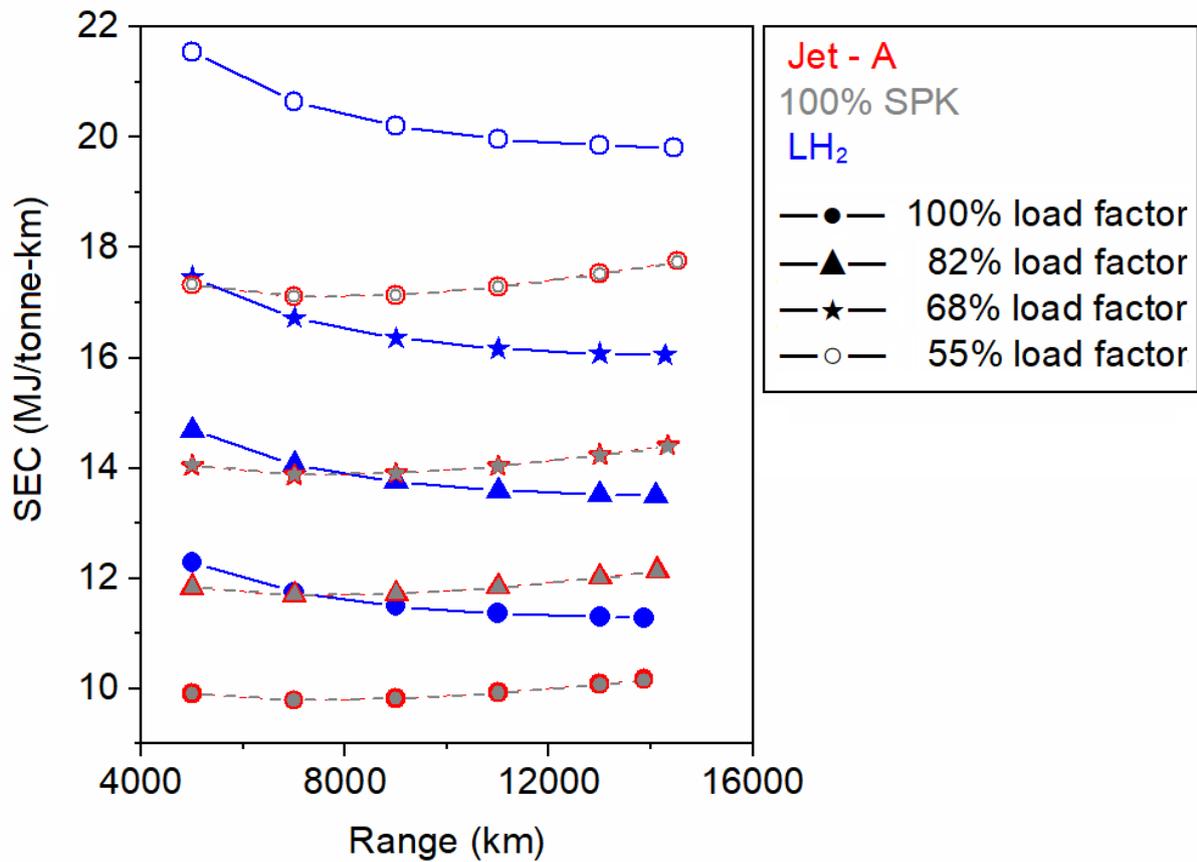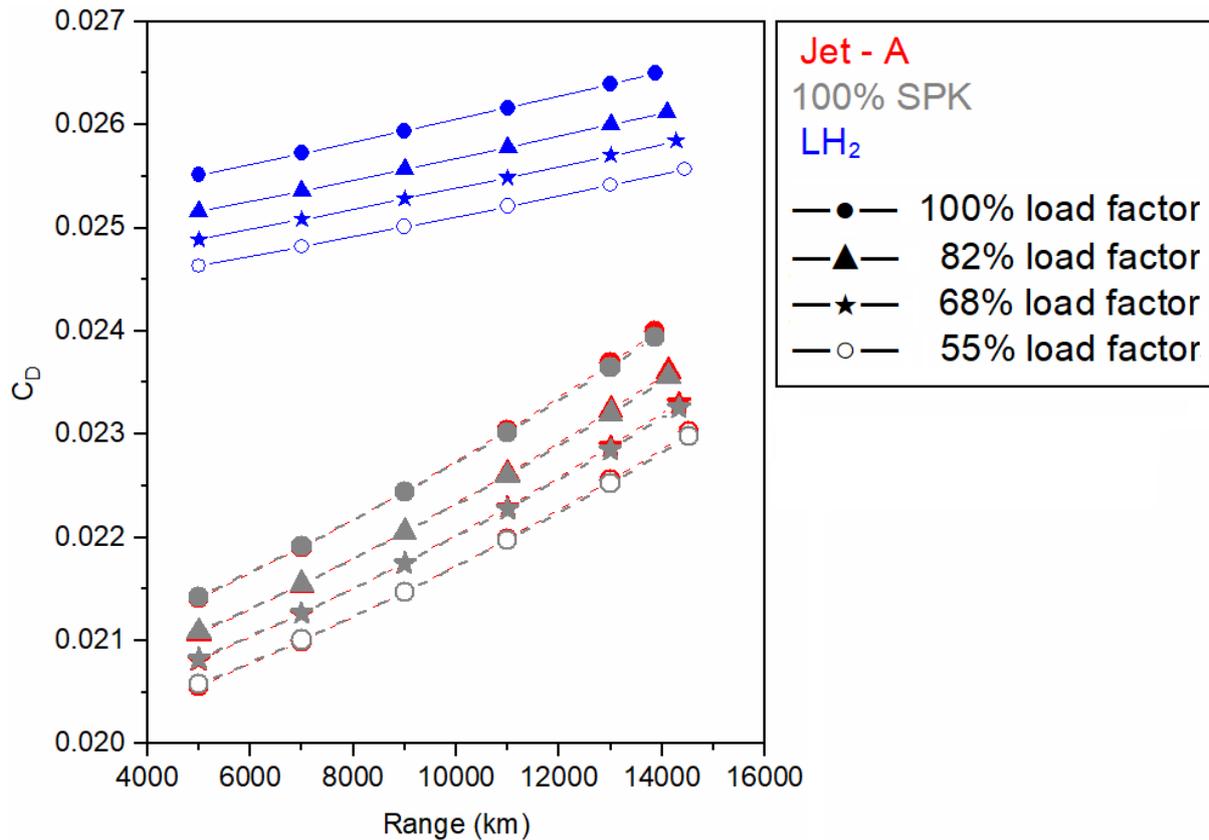
Figure A.7. Comparison of C_D for Jet-A, 100% SPK, and LH$_2$ aircraft ($\eta = 0.78$) at different range and payload (load factor) combinations

A.6.   Modified A350-1000 performance characteristics for 301 passengers powered by liquid hydrogen

The A350-1000 aircraft (366 passengers) is a single decker aircraft [352] and is similar to a Boeing 777-200 LR aircraft (301 passengers) for a 3-class configuration [353]. The significant difference between the two vehicles is that A350-1000 aircraft (72.25 m) is longer than Boeing 777-200 LR aircraft (63.7 m) for accommodating more passengers. As observed from section 4.4.1 and section A.5, fuselage length is a sensitive parameter for LH$_2$ aircraft which negatively impacts aircraft performance. The passenger seating of a Boeing 777-200 LR aircraft (301 passengers) for a 3-class configuration can be applied to A350-1000 aircraft (366 passengers 3-class configuration). This would enable use of approximately 8 m of fuselage length and thus the associated volume A350-1000 aircraft for storing LH$_2$ tanks and additional need of LH$_2$ tanks can be accommodated via increase in aircraft fuselage length.

In this section, the baseline case is A350-1000 aircraft (366 passenger seating capacity) that carries 301 passenger-payload. The effect of removal of 65 seats on OEW is assumed to be negligible. The calculation process remains similar to the procedure outlined in section 4.3 with the only difference that passenger payload weight changes from 34,770 kg (366 passengers) to 28,595 kg (301 passengers). Similarly, for the LH$_2$ A350-1000 aircraft with 28,595 kg payload (301 passengers) the calculation process remain similar except that 8 m of fuselage length and associated volume is now available to store LH$_2$ tanks. Therefore, the penalty on L/D and energy performance of LH$_2$ aircraft, observed in section 4.4.1 and section A.5, is expected to decrease.

Table A.9 shows the performance characteristics of modified A350-1000 for LH$_2$ use compared to original Jet-A A350-1000 aircraft for a payload of 28,595 kg (301 passengers). It is to be noted that for Jet-A case same fuel capacity is maintained as observed in the earlier case (section 4.4). Since the passenger payload has decreased from 34,770 kg (Table 4.3 and Table A.6) to 28,595 kg (Table A.9), the range has increased from 13,869 km to 14,125 km respectively, which is an expected trend. This is the typical design range for LTA aircraft such as Boeing 777-200 LR [130]. Additionally, for the LH$_2$ aircraft case, the total fuel requirement at mission start has reduced from 50,375 kg (Table A.6) to 47,645 kg (Table A.9) because of reduced penalty on aircraft via fuselage length. The increase in fuselage length has reduced from 26.87 m (Table A.6) to 17.42 m (Table A.9). It is to be noted that both cases (Table A.6, and Table A.9) have different payload conditions. Additionally, the L/D has improved from 16.09 (Table A.6) to 16.48 (Table A.9). The

associated increase in fuselage wetted area and weight, and aircraft wetted area can be observed from Table A.10. Moreover, there is an increase in the GTOW reduction from ~15% (Table 4.4 and Table A.6) to ~18% (Table A.9) for the LH$_2$ aircraft case.

Table A.9. Performance characteristics of modified A350-1000 for LH$_2$ use compared to original Jet-A A350-1000 aircraft for payload of 28,595 kg (301 passengers)

Fuel	OEW (kg)	W$_{f,total}$ (kg)	GTOW (kg)	Fuel in fuselage tank (kg)	ΔL (m)	L/D	R (km)
Jet-A	155,129	126,101	309,824	-	-	18.48	14,125
LH$_2$	178,284	47,645	254,524 *(-17.85%)*	47,645	17.42	16.43	14,125

Table A.10. A350-1000 fuselage and aircraft modification data for LH$_2$ fuel for passenger payload of 28,595 kg (301 passengers)

Fuel	Fuselage length (m)	Fuselage structural weight (kg)	Fuselage wetted area (m^2)	Aircraft wetted area (m^2)
Jet-A	72.25	29,484	1,208	2,445
LH$_2$	89.67	37,432	1,533	2,771

Table A.11. SEC performance of modified A350-1000 for LH$_2$ use compared to original Jet-A A350-1000 aircraft for payload of 28,595 kg (301 passengers)

Fuel	W$_p$ (kg)	h (MJ/kg)	W$_{f,block}$ (kg)	R (km)	SEC (MJ/t-km)
Jet-A		43.2	113,491	14,125	12.14
LH$_2$	28,595	120	42,881	14,125	12.74 *(+4.95%)*

Table A.11 provides SEC performance of the modified A350-1000 for LH$_2$ use compared to original Jet-A A350-1000 aircraft for payload of 28,595 kg (301 passengers). There is a ~5% increase in energy consumption between Jet-A case and LH$_2$ case. However, modifying the A350-1000 aircraft for 301 passenger seating has improved the energy efficiency as compared to A350-1000 LH$_2$ aircraft (366 passenger payload) observed in Table A.11. In the earlier example (Table 4.4 and Table A.6), the increase in energy consumption was ~11% which has now reduced to ~5% (Table A.11) due to above modifications.

A.7.   Airbus A380 aircraft conversion to an LH$_2$ powered aircraft

Based on the findings in section 4.4.1, a follow up study is undertaken for the modification and use of retired aircraft (by major airlines during 2020 lockdown) such as Airbus A380. This is in-line with recent efforts from Airbus to convert retired A380 aircraft into an LH$_2$ aircraft [216].

The fuselage/hydrogen tank volume is proportional to the square of the fuselage diameter. So far, through this research it is observed that fuselage length is a significant aspect for hydrogen aircraft. Considering the above points, very large aircraft like A380-800 that has a double-decker architecture or large fuselage diameter has the potential to reduce the increase in fuselage length for a hydrogen powered aircraft.

The A380-800 aircraft data is included in Table A.12. For the A380-800 aircraft (non-cylindrical or elliptical fuselage) the fuselage width and height are known to be 7.14 m and 8.4 m from (from Table A.12). The equivalent

diameter is calculated to be 7.8 m (using [354]). The fuselage length is known to be 70.4 m (from Table A.12). The fuselage wetted area of the A380-800 aircraft is calculated to be 15,907 ft² (1,478 m²) (using equation 4.6) and the fuselage weight is calculated to be 36,077 kg (using equation 4.7). Additionally, the A380-800 aircraft MTOW is known to be 1,254,430 lb (569 tonnes). Using equation 4.5 the A380-800 aircraft wetted area is calculated to be 40,986 ft² (3,808 m²).

Table A.12. Airbus A380-800 aircraft data

Parameters	Units	Value
Maximum take-off weight (MTOW)	kg	569,000 [355]
Maximum passengers in a 3-class configuration (double-decker)	-	486 [356]
Average weight of one passenger	kg	95 [210]
Passenger payload weight (W_p)	kg	46,170 (= 95 x 486)
Operating empty weight (OEW)	kg	270,364 [355]
Overall efficiency ($\eta_{overall}$)	-	0.38 [211]
Total fuel weight ($W_{f,total}$) at mission start for MTOW for given OEW with W_p (= MTOW – OEW – W_p)	kg	252,465
Fuselage length	m	70.4 [355]
Fuselage height	m	8.4 [355]
Fuselage width	m	7.14 [355]
Wing area	m²	845 [357]
AR	-	7.53 [358]

Table A.13. Data of original Airbus A380-800 aircraft (486 passengers 3-class layout) and modified LH₂ A380-800 aircraft (312 passengers 3-class layout)

Boeing 777-200 LR (301 passengers) [353]								
Passenger count								
Economy			Business class			First class		
227			58			16		
Original A380-800 aircraft (486 passengers 3-class layout) [356]								
Cabin width 7.14 m and fuselage length 70.4 m								
Deck	Passenger count			Passenger seating area (m²)			Passenger seating area per seat (m²/seat)		
	EC	BC	BS	EC	BC	BS	EC	BC	BS
Upper	66	66	-	78.2	173.53	-	1.19	2.63	-
Lower	346	-	8	279.89	-	39.13	0.81	-	4.89
Modified LH₂ A380-800 aircraft (312 passengers 3-class layout)								
Cabin width 7.14 m, 10.41 m of fuselage length available for LH₂ tanks								
Deck	Passenger count			Change in fuselage length (m)			Total change in fuselage length (m)		
	EC	BC	BS	EC	BC	BS	EC+BC		BS
Upper	-	60	-	-10.95	-2.20	+2.74	-13.15		+2.74
Lower	236	-	16						
EC: Economy class; BC: Business class; BS: Business suite								

In this section, three cases are analysed. The first case is the actual A380-800 aircraft with full passenger payload (486 passengers in a 3-class configuration). The second case is the A380-800 aircraft for 312 passenger-payload powered by Jet-A. The third case is the A380-800 aircraft modified for seating 312 passengers powered by LH₂. The modifications for the third case are disclosed below. These modifications are important particularly for utilising the aircraft volume for installing hydrogen tanks. Additionally, this is a doubledecker aircraft so the reduction in seating must be done carefully.

The A380-800 aircraft seats 486 passengers (3-class configuration) in total [356]. The upper deck seats 66 economy class passengers and 66 business class passengers. The lower deck seats 346 economy class passengers and 8

business suite passengers. This aircraft is modified to a 312 passenger seater aircraft such that it meets the at least the passenger seating of a Boeing 777-200LR aircraft (301 passengers [227 economy, 16 first (or business suite) and 58 business class] in a 3-class configuration) [353]. This is done by removing 66 seats from economy class and 6 seats from business class from the upper deck. Simultaneously, from the lower deck 110 seats from economy class are removed and 8 seats are added to business suite. Table A.13 provides the seat distribution and passenger seating area estimated from resource [356] for original A380-800 aircraft. It also includes the modified LH_2 A380-800 aircraft (312 passengers 3-class layout [236 economy, 16 business suite, 60 business class]) seat distribution with fuselage length estimation. Overall, 10.41 m of the aircraft fuselage length is available for the installation of LH_2 tanks.

The overall efficiency of A380-800 aircraft is known to be 0.38, see Table A.12. Using Table 4.1 (section 4.3), the overall efficiency of a hydrogen powered A380-800 aircraft is calculated to be 0.3919. The remaining parameters of the range equation are known from Table A.12 and the calculation process remain similar to the earlier two examples.

Table A.14. Performance characteristics of modified A380-800 for LH_2 use (312 passenger-payload) compared to original Jet-A A380-800 aircraft for 486 and 312 passenger-payload

Fuel	W_p (kg)	h/g (m)	OEW (kg)	$W_{f,total}$ (kg)	GTOW (kg)	ΔL (m)	L/D	R (km)
Jet-A	46,170 (486 PAX)	4,404	270,364	252,465	569,000	-	18.94	15,449
Jet-A	29,640 (312 PAX)	4,404	270,364	215,809	515,813	-	18.58	14,000
LH_2		12,233	309,625	78,440	417,705 (-19.02%)	14.03	17.07	14,000

Table A.15. A380-800 fuselage and aircraft modification data for LH_2 fuel

Fuel	Fuselage length (m)	Fuselage structural weight (kg)	Fuselage wetted area (m^2)	Aircraft wetted area (m^2)
Jet-A	70.4	36,077	1,478	3,808
LH_2	84.43	44,457	1,821	4,151

Table A.16. SEC performance of modified A380-800 for LH_2 use (312 passenger-payload) compared to original Jet-A A380-800 aircraft for 486 and 312 passenger-payload

Fuel	W_p (kg)	h (MJ/kg)	$W_{f,block}$ (kg)	R (km)	SEC (MJ/t-km)
Jet-A	46,170	43.2	227,219	15,449	13.76
			194,228	14,000	20.22
LH_2	29,640	120	70,596	14,000	20.41 (-0.96%)

Table A.14 shows the performance characteristics of the modified A380-800 aircraft for LH_2 use (312 passenger-payload) compared to original Jet-A A380-800 aircraft for 486 and 312 passenger-payload. The original Jet-A A380-800 aircraft for 486 passenger-payload at MTOW can travel ~15,450 km distance. For Jet-A 312 passenger-payload case, and typical LTA aircraft design range of 14,000 km would require less total fuel weight carried at mission start as compared to the 486 passenger-payload case (observed from Table A.14). For LH_2 312 passenger-payload case, the aircraft meets the similar range at ~20% reduced GTOW compared to the Jet-A 312 passenger-payload case and 26.6% reduction in GTOW compared to the aircraft MTOW of 569 tonnes. Table A.15 shows the A380-800 fuselage and aircraft

modification data for LH$_2$ fuel**.** For LH$_2$ 312 passenger-payload case less penalty is observed on fuselage length and *L/D* performance compared to earlier two aircraft examples.

Table A.16 shows SEC performance of modified A380-800 for LH$_2$ use (312 passenger-payload) compared to original Jet-A A380-800 aircraft for 486 and 312 passenger-payload. It can be observed that SEC of the modified A380-800 for LH$_2$ use (312 passenger-payload) has increased slightly (by ~1%) compared to the Jet-A A380-800 aircraft 312 passenger-payload case. This contrasts with the earlier two examples of A350-1000 LH$_2$ aircraft for 366 and 300 passenger payload cases where the increase in the energy consumption increased by ~11% and ~5% respectively compared to their respective reference Jet-A aircraft case. However, the absolute energy consumption of the modified A380-800 for LH$_2$ use (312 passenger-payload) is greater than A350-1000 LH$_2$ aircraft for 366 and 300 passenger payload cases. This aspect is discussed in the next section where the different LH$_2$ aircraft cases are compared.

A.8.   Comparison of different LH$_2$ aircraft cases

Figure A.8 provides the comparison of different LH$_2$ aircraft cases with their reference aircraft. For each of the three aircraft cases (A350-1000 366 and 301, and A380-800), the aircraft the energy consumption increases for LH$_2$ aircraft case primarily due to increase in the ratio of OEW and payload (PL) weight as compared to the Jet-A case. Of the three LH$_2$ aircraft case (A350-1000 366 and 301, and A380-800 312), using the A380-800 312 aircraft would cost the airlines/passengers more as compared to A350-1000 366 case. However, another aspect to be considered here is the A380 type aircraft acquisition cost which could be low considering that that the A380-800 aircraft have been retired by major airlines from their fleet during the 2020 lockdown. It is to be noted that the aircraft need to be redesigned for increasing the structural strength for longer fuselage for hydrogen tanks.
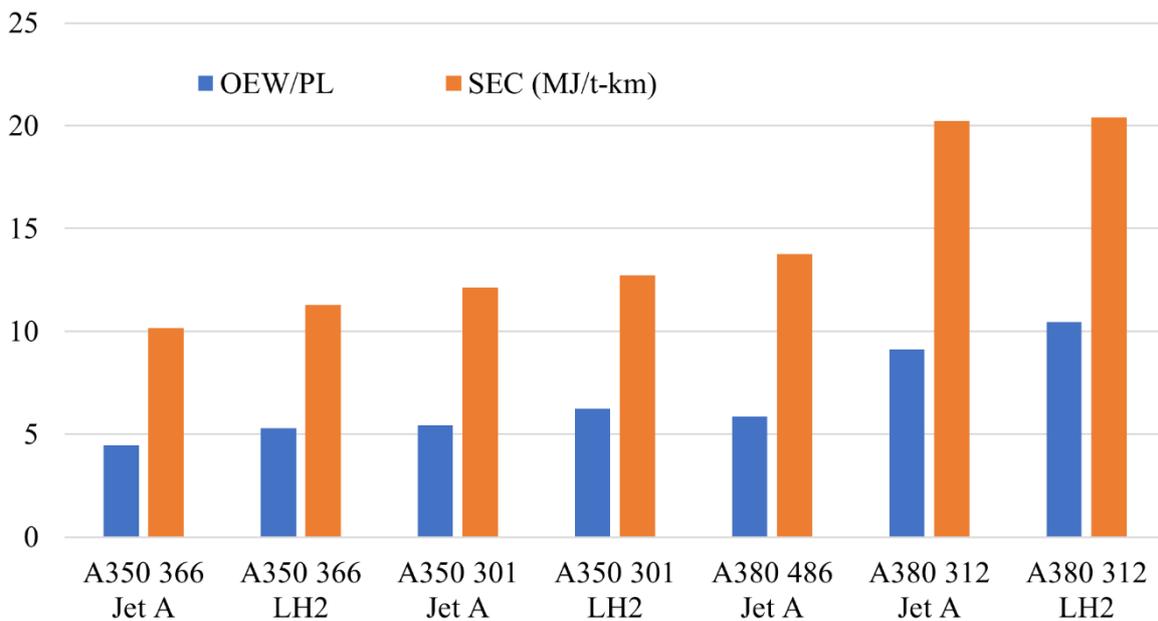
Figure A.8. Comparison of different LH$_2$ aircraft cases with their reference aircraft

Overall, unless the LH$_2$ fuel cost is extremely low (close to zero), A380-800 LH$_2$ aircraft could be economically infeasible compared to flying LH$_2$ A350-1000 366 or 301 aircraft cases considered in this research. Considering only the energy consumption, across all cases, hydrogen aircraft consumes more energy than their respective baseline Jet-A aircraft, due to increase in OEW. In general, future Jet-A fuel costs are uncertain, especially in a post pandemic time. Hydrogen fuel cost is completely dependent on the process through which it is manufactured. The other part of the operational cost is the incentive of using of clean alternative fuels such as hydrogen that emit zero carbon in the use-phase. Additionally, the production pathway of hydrogen also needs to be less carbon intense.

A.9. Discussion on four aspects

Fuselage length:

The fuselage fineness ratio (FR = length/diameter) of Boeing 777-200 ER and LR both are 10.27 (= 63.7/6.2), and that of Boeing 777-300 ER is (73.9/6.2 =) 11.92 [353]. The FR of Boeing 787-8, 787-9 and 787-10 are 9.69 (= 55.91/5.77), 10.75 (= 62/5.77) and 11.7 (= 67.48/5.77), respectively [359]. The FR of the baseline A350-1000 Jet-A aircraft is known to be 12.12 from Table 4.3. The FR of the LH_2 aircraft modelled in section 4.4.1 is (99.12/5.96 =) 16.63 (37.2% increase in fuselage length relative to baseline Jet-A aircraft). One of the interesting aircraft cases is the DC-8 Super 60, which has a slender fuselage and has the fineness ratio of 14.95 (= 55.75/3.73) [360]. Lastly, the FR of Concorde is 16.7 [223]. The Concorde is an exception because it was a supersonic aircraft and had special aerodynamic requirement as compared to the above sub-sonic aircraft. Slender fuselage (high FR) enables higher cruise Mach number flights as the drag divergence number increases [361]. LH_2 aircraft with longer fuselage could have several issues to be addressed. These aircraft could necessitate design and development for increasing the structural strength for the longer fuselage to prevent longitudinal failures. Particularly, longer fuselage for unchanged diameter (high FR) could imply increase in bending of the fuselage and associated stresses. Additionally, increase in fuselage length is associated with a shift in aircraft's centre of gravity. This could mandate an examination on the criteria for positioning of the landing gear and an evaluation on the required take-off and landing speeds to avoid tail-strikes. From a design viewpoint, a longer aircraft might not be safe from flight dynamics perspective. The empennage and control surfaces must be redesigned and/or recalibrated for stability. Moreover, considering an absolute scale, longer fuselage could affect take-off rotation, turning radius, operations at the airport, and could necessitate longer field length during take-off and landing. Therefore, significantly longer aircraft might not be readily compatible with present day airport infrastructure. The future airport planning/redesigning should consider these effects if significantly longer (than present) LH_2 aircraft are to enter in service.

Optimisation of aircraft:

In section 4.3.2.1 it was assumed that the thrust production for Jet-A and alternative fuels is the same. It is observed in section 4.4.1 that the LH_2 aircraft GTOW reduces by 15% respectively, and thus its thrust/weight ratio (*T/W*) will be greater than the baseline aircraft. The optimisation of the LH_2 aircraft is necessary considering that its GTOW significantly reduces, and this decreases the thrust requirement and energy consumption. According to studies by Dincer [250] and Nojoumi [55], for a LH_2 powered aircraft the thrust requirement reduces and the engine becomes smaller in size (engine weight savings). Reduction in thrust requirement reduces engine weight and associated fuel weight savings, which further reduces the GTOW. Therefore, for a significantly lighter LH_2 aircraft, optimisation is necessary considering that a similar *T/W* of the baseline aircraft is to be maintained for this aircraft.

Embodied emissions and energy:

The fuel cost of 100% SPK and LH_2 is completely dependent on the process through which they are manufactured. The other part of the operational cost is the incentive of using of clean alternative fuel such as hydrogen that emits zero carbon in the aircraft's operational phase. The production pathway of 100% SPK and LH_2 also needs to be less carbon intense. According to the Clean Sky 2 - FCH joint project report [34], PtL fuel might be a more cost-effective decarbonisation solution with an evolutionary tube-wing long-range aircraft instead of LH_2. PtL is same as 100% SPK i.e., has same fuel properties. It is to be noted that PtL fuel production uses hydrogen produced from electrolysis (using power produced from renewable energy). Considering process conversion losses in the PtL fuel production (from hydrogen) and that the future LH_2 powered tube-wing aircraft (implementing advanced aircraft technology) could be more energy efficient than present day tube-wing Jet-A aircraft, the LH_2 aircraft powered by hydrogen produced from renewable electricity could be more sustainable than PtL on a lifecycle basis.

Effect of technology:

Referring to section 4.3.1, Breguet range equation shows that the aircraft energy performance depends on the type of fuel used and advancements in (three) aircraft technology such as use of energy efficient engines and lighter materials and improved aerodynamics. Also, from section 4.3.5 and findings from section 4.4.1, it is observed that cryogenic tank η affects the aircraft energy performance. The effect of these four technology aspects on the long-range LH_2 powered LTA aircraft performance (such as its SEC) could be explored via a sensitivity analysis.

Appendix B

B.1   Global sensitivity analysis – miscellaneous results
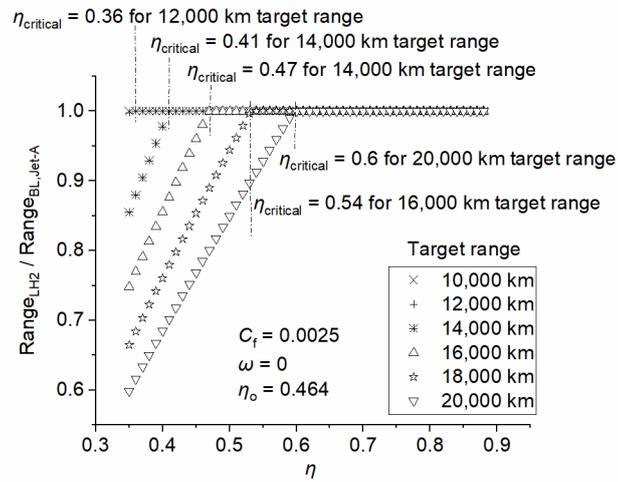
Figure B.1. Effect of design target range on $\eta_{critical}$ of the LH$_2$ aircraft
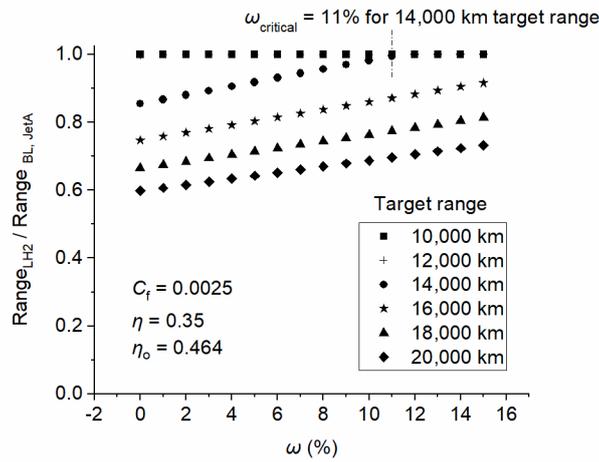
Figure B.2. Effect of design target range on $\omega_{critical}$ of the LH$_2$ aircraft
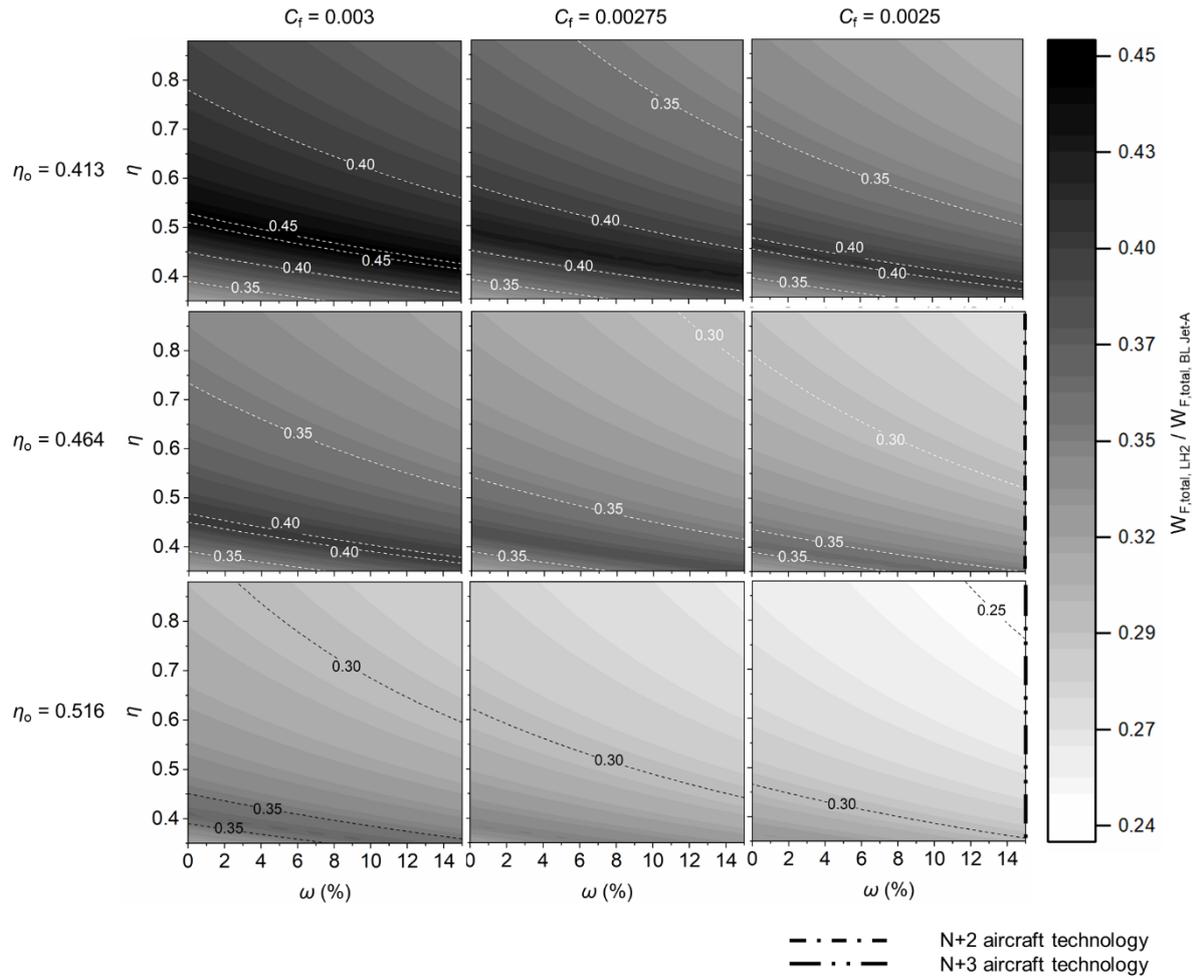
Figure B.3. Effect of gravimetric index (η), skin friction coefficient (C_f), overall efficiency (η_o), and OEW and fuselage weight reduction factor (ω) on the ratio of the total LH2 fuel weight carried at mission start ($W_{F,total,LH2}$) and (present-day) baseline (BL) Jet-A total fuel weight carried at mission start ($W_{F,total,BL\ Jet-A}$)
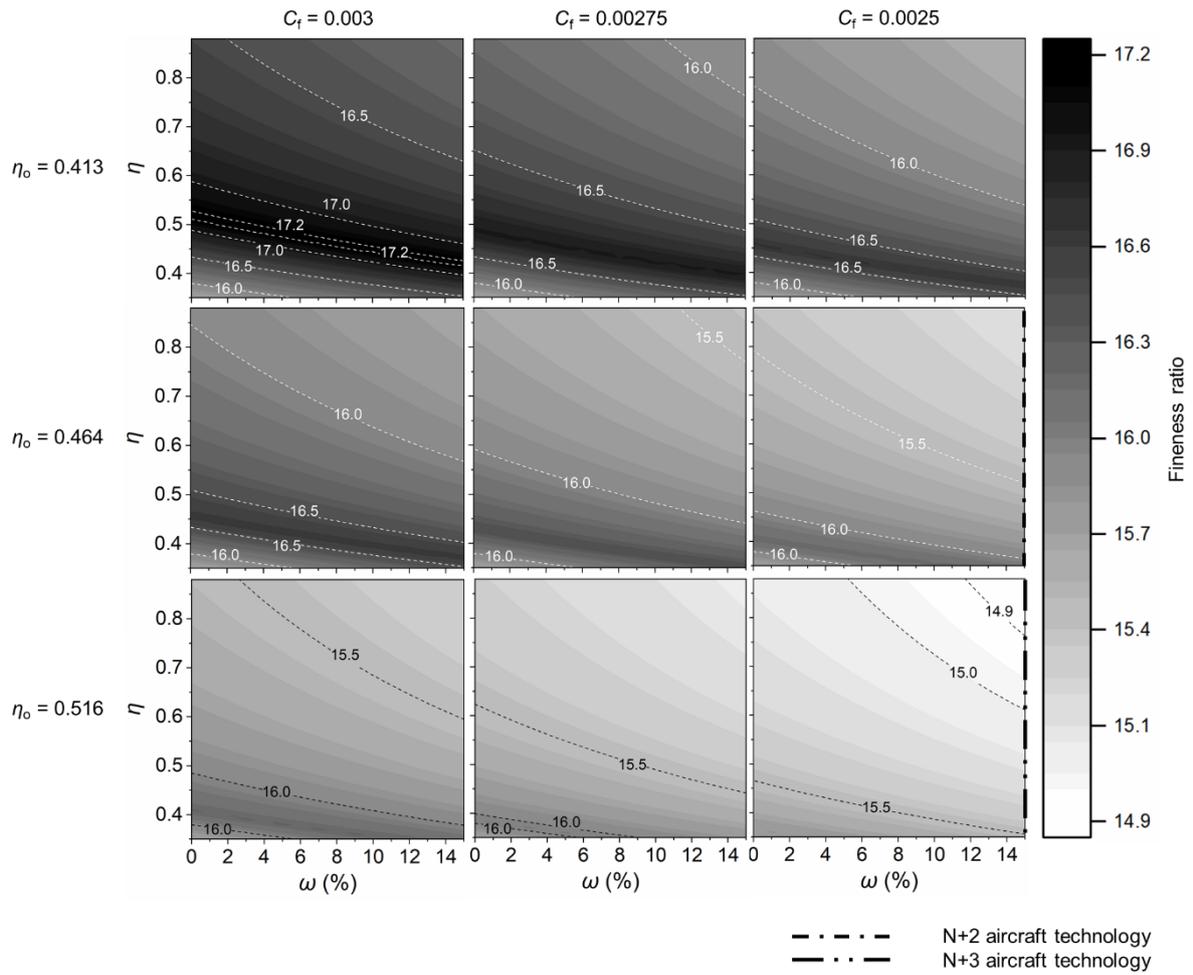
Figure B.4. Effect of η, C_f, η_o, and ω on the fuselage fineness ratio of the LH2 aircraft
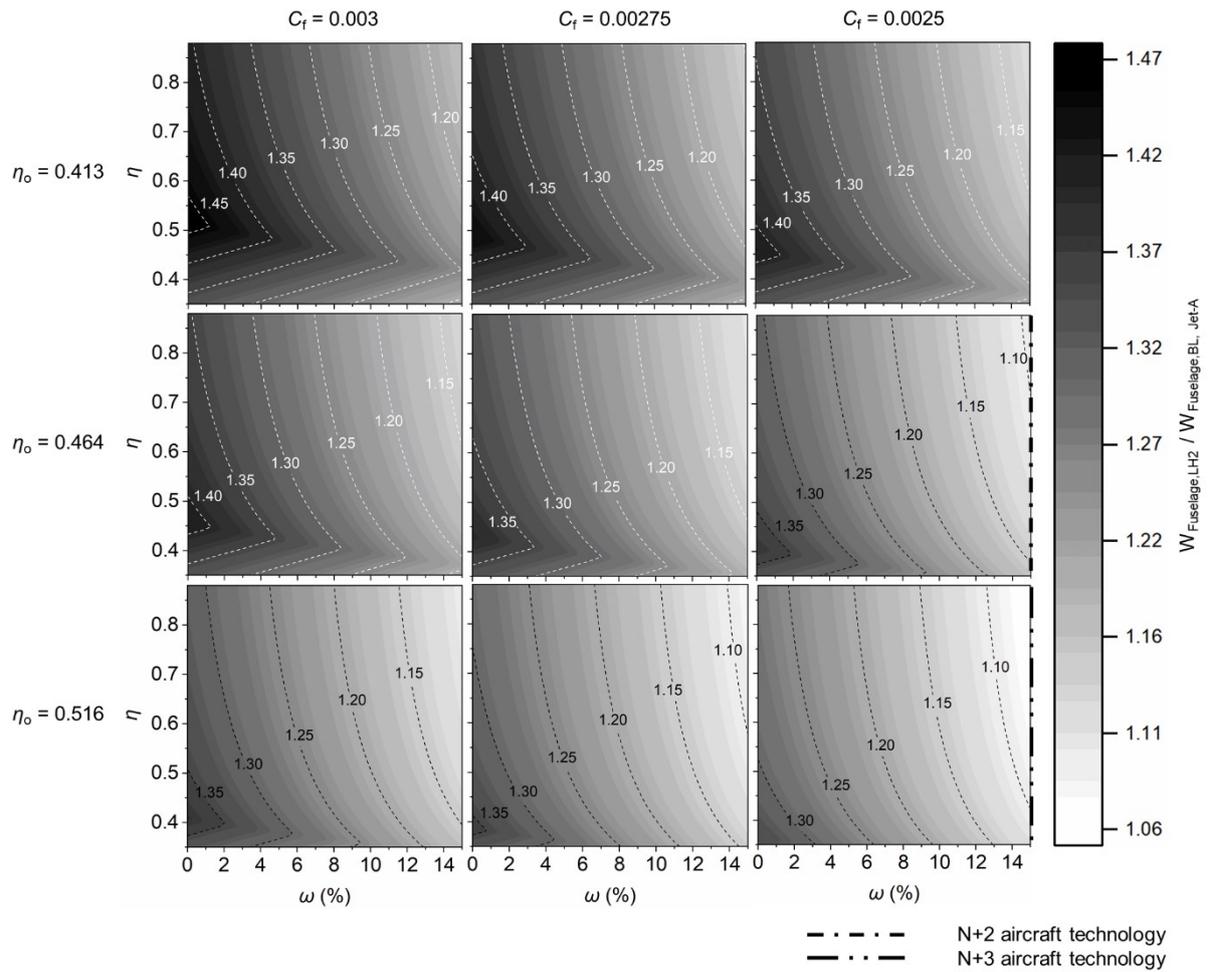
Figure B.5. Effect of η, C_f, η_o, and ω on the ratio of LH2 aircraft fuselage weight ($W_{Fuselage,LH2}$) and (present-day) baseline (BL) Jet-A aircraft fuselage weight ($W_{Fuselage,BL,Jet-A}$)
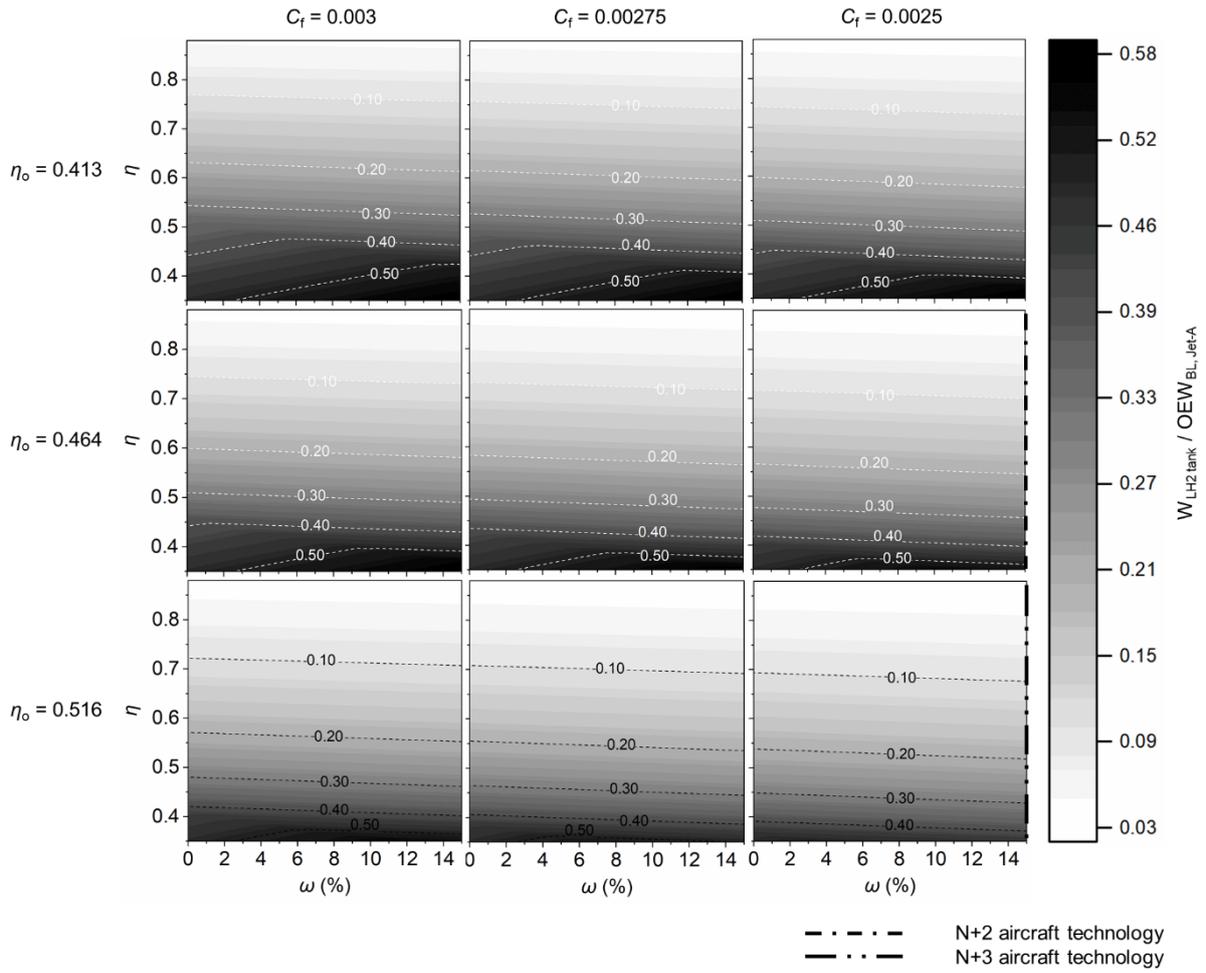
Figure B.6. Effect of η, C_f, η_o, and ω on the ratio of the LH$_2$ cryogenic tank weight (W$_{\text{LH2 tank}}$) and (present-day) baseline (BL) Jet-A aircraft OEW (OEW$_{\text{BL, Jet-A}}$)
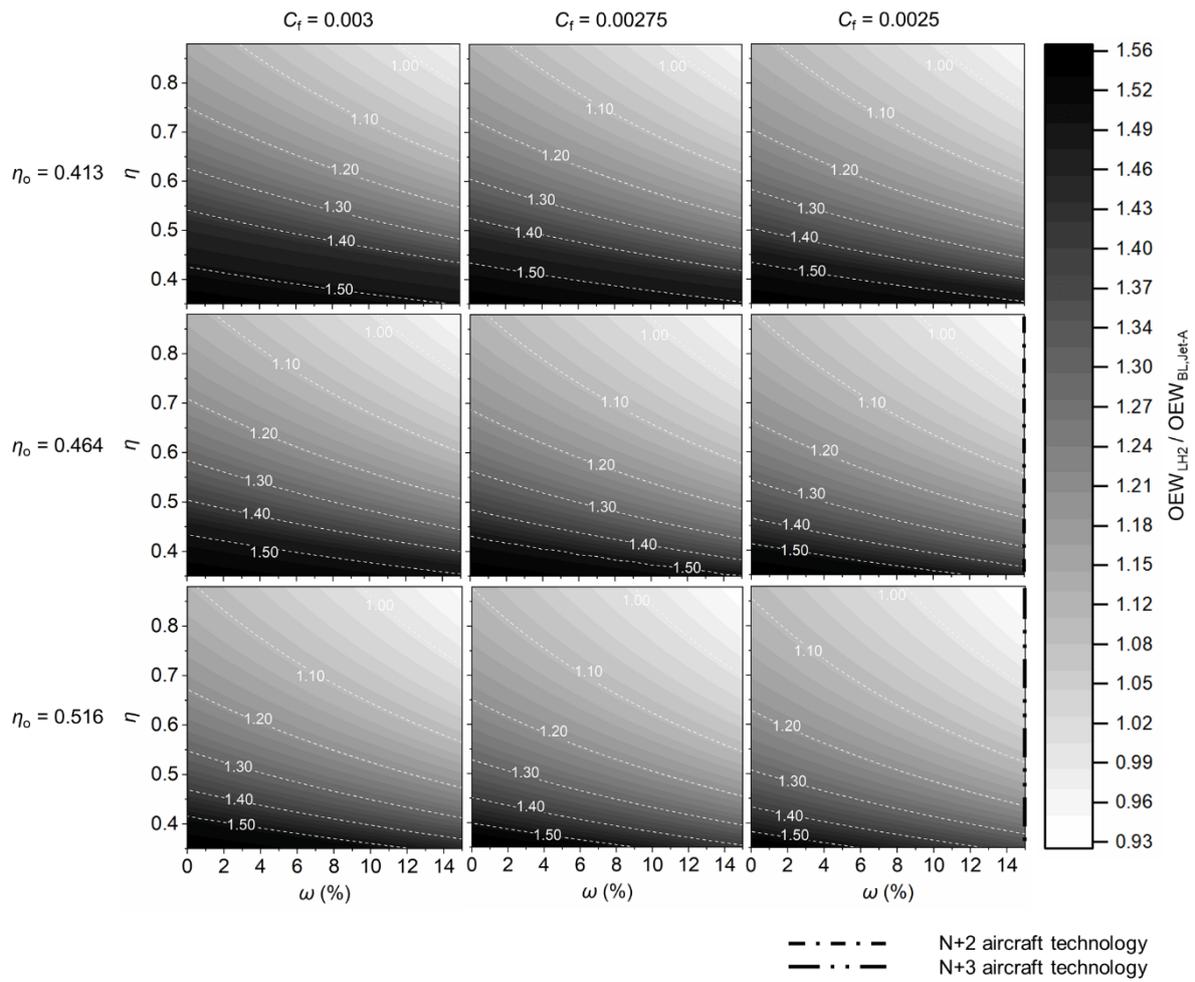
Figure B.7. Effect of η, C_f, η_o, and ω on the ratio of OEW of LH$_2$ aircraft (OEW$_{LH2}$) and OEW of (present-day) baseline (BL) Jet-A (OEW$_{BL, Jet-A}$) aircraft
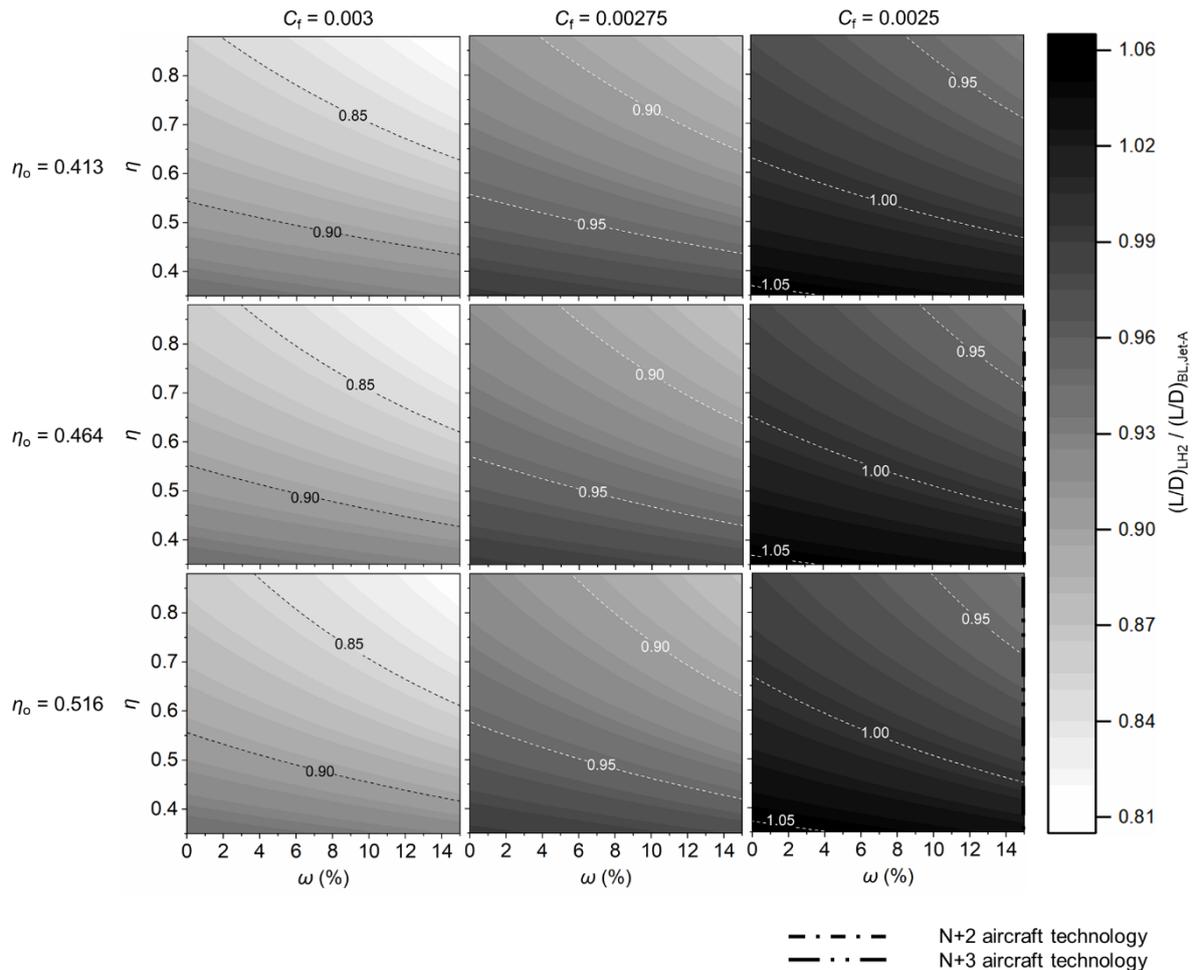
Figure B.8. Effect of η, C_f, η_o, and ω on the ratio of LH2 aircraft lift to drag ratio (L/D) LH2 and (present-day) baseline (BL) Jet-A aircraft lift to drag ratio (L/D)BL, Jet-A

B.2   Detailed author comments

Aircraft length –

The fuselage fineness ratio (FR = length/diameter) of Boeing 777-300 ER is (73.9/6.2 =) 11.92, and that of both Boeing 777-200 LR and ER is 10.27 (= 63.7/6.2) [218], [334], [353]. The FR of Boeing 787-10, 787-9 and 787-8 are 11.7 (= 67.48/5.77), 10.75 (= 62/5.77), and 9.69 (= 55.91/5.77), respectively [218], [359]. The FR of the baseline A350-1000 Jet-A aircraft is known to be 12.12 [218]. The FR of the LH2 aircraft modelled in Chapter 4 is (99.12/5.96 =) 16.63 (37.2% increase in fuselage length compared to the baseline Jet-A aircraft). From the global sensitivity analysis, the maximum and minimum FR is 17.23 (42.1% increase in fuselage length from baseline) and 14.85 (22.5% increase in fuselage length from baseline), respectively. The DC-8 Super 60 is an interesting case since it has a slender fuselage and FR of 14.95 (= 55.75/3.73) [218], [360]. Finally, the FR of Concorde is 16.7 [223]. The Concorde is an exception to the above list of FR since it was a supersonic aircraft, and has special aerodynamic needs relative to the sub-sonic civil aircraft. High FR or slender fuselage enables greater cruise Mach number flights because the drag divergence number increases [218], [361].

LH2 aircraft having longer fuselage poses several challenges [218]. These aircraft might need a complete engineering design and development for improving the structural strength to support a longer fuselage (for avoiding longitudinal fuselage failure). The longer fuselage especially with an unchanged diameter (high FR) might increase fuselage bending and related stresses. Also, fuselage length increase could move the location of aircraft's centre of gravity. As a result, an evaluation would be required for checking the criteria for landing gear positioning and an assessment on the necessary landing and take-off speeds for preventing tail-strikes. From a design perspective, a longer fuselage could be unsafe considering flight dynamics, and to provide stability the control surfaces and empennage should be recalibrated/redesigned.

Additionally, on an absolute scale, longer fuselage might require longer field length at landing and take-off and could have an effect on operations at the airport, turning radius, and operations at the airport [218]. Thus, there could be compatibility issues of the significantly longer aircraft, with current airport infrastructure. The above aspects need to be considered while designing and/or planning of future airport if such significantly longer LH_2 aircraft (relative to present-day aircraft) are to be operated.

Optimisation of aircraft –

In this study and previous study [218], it was/is assumed that the thrust production for alternative fuels (including LH_2) and Jet-A remains unchanged. It is observed in section 5.4.3 that the GTOW of the LH_2 aircraft decreases by up to 34% (maximum GTOW reduction), and therefore its thrust/weight ratio (T/W) will be higher as compared with the baseline Jet-A aircraft. The optimisation of the LH_2 aircraft is required accounting significant reduction in GTOW, thereby reducing the thrust requirement and thus the energy consumption. For a LH_2 powered aircraft, as per studies by Nojoumi [55] and Dincer [250], the thrust requirement decreases and causes the engine to become smaller in size leading to weight reduction. The thrust requirement reduction decreases engine weight and related reduction in fuel weight, which further decreases the GTOW [218]. Thus, for LH_2 aircraft where there is significant reduction in GTOW, optimisation is required for maintaining similar T/W of the baseline aircraft.

Other future technologies for enabling LH_2 aircraft –

The present aircraft structures (tube-wing) are designed to store Jet-A (type) fuel which fuel the gas turbine engines, and this combination only allows a limited retrofitting of alternative energy vectors such as LH_2 [86]. Novel and unconventional aircraft design architecture like BWB aircraft enables a more flexible integration of cryogenic hydrogen tanks [86]. This is because BWB aircraft has lesser wetted area to volume ratio compared to the tube-wing aircraft [132]. In other words, BWB aircraft has higher internal volume and better L/D compared to the conventional tube-wing aircraft. In the global sensitivity analysis, it was observed that improving the aerodynamics was one of the two technology aspect that can enable a successful and energy efficient large long-range LH_2 aircraft. Therefore, BWB is a promising and new aircraft architecture, and is expected to provide benefits in terms of better L/D performance, and LH_2 storage due to its higher internal volume, compared to tube-wing aircraft.

According to the Clean Sky 2 - Fuel Cells and Hydrogen (FCH) joint project report [34], "*LH₂ is technically feasible but less suitable for evolutionary long-range aircraft designs from an economic perspective*". PtL fuel might be a more cost-effective decarbonisation solution with an evolutionary tube-wing long-range large aircraft [34]. Innovative and novel aircraft architecture like BWB could change that for the use of LH_2 in large long-range flight but may be after 2040 (service entry) [34]. Revolutionary designs like BWB that enable significantly better integration of the LH_2 storage and have improved aerodynamics, and could be an effective solution for the decarbonisation of the future large long-range air transportation [34]. The limitation of such radically novel/unconventional aircraft is that they have an uncertain and long commercialization process [34]. Additionally, these require extended testing for ensuring the aircraft's aerodynamic stability in different flight conditions, and for optimising cabin design, manufacturing, and operations [34].

Embodied emissions and energy –

The cost of LH_2 and other alternative fuels depend on the pathway and/or feedstocks with which they are manufactured [218]. Another aspect of the operational cost is the incentive of operating the aircraft with clean alternative fuels like LH_2 that release zero carbon. The production pathway of the alternative fuels should be less carbon intense, and this would enable aviation's decarbonisation in a true sense.

As per the Clean Sky 2 - Fuel Cells and Hydrogen (FCH) joint project report [34], instead of LH_2, power-to-liquid (PtL) fuel (similar to SPK's fuel properties) could cost less and offer a decarbonisation solution to be used on an evolutionary tube-wing long-range aircraft. It is to be noted that hydrogen is an intermediate product in the PtL fuel manufacturing process (via electrolysis of water using the power generated from renewable energy) [218]. Accounting the conversion losses in the PtL fuel manufacturing (from hydrogen) and considering that LH_2 powered tube-wing aircraft using future technology could be 33% more energy efficient (known from the global sensitivity analysis) compared to the present day tube-wing Jet-A aircraft, the LH_2 aircraft powered by hydrogen manufactured from the renewable electricity might be more sustainable on lifecycle basis compared to PtL.

B.3   Literature review on other aspects of liquid hydrogen aviation

Hydrogen fired combustors:

Hydrogen combustion in gas turbine engine is more complex than just a simple FAR modification. It also depends on the geometry of combustor [362]. The addition of hydrogen to conventional fuels improves the engine performance, though the performance of using 100% hydrogen in conventional combustors is inferior to conventional fuels [64]. This drop in performance is because of combustors geometry being insufficient for the effective mixing of air and fuel. As discussed in section 6.2.2, the flame speed of hydrogen is greater than kerosene, where the conventional combustors are designed for the flame speeds of kerosene. Hydrogen combustion in a conventional combustor causes large diffusive flames where stoichiometric ratios are found in the flame vicinity. This causes very high temperatures and resultantly high NO_x emissions (ibid). These issues can be resolved by considering all flame attributes of combustion like combustion efficiency, flame stability, acoustics, and other crucial diagnostics, for the design of a hydrogen fired combustor. After considering these aspects, two novel combustor concepts have emerged through research-development, for the effective and efficient combustion of hydrogen such that its full potential can be utilised. The two concepts of hydrogen combustors that are likely to be future alternatives are: the lean direct injection (LDI) examined by Marek et al. [228]; and micro-mix concepts studied by Dahl and Suttrop [240]. These two designs have proven to be successful via actual combustion experiments. Both design/concepts are similar in their methodology. Both concepts establish that flashback is a primary concern with the desire of increasing fuel mixing [64]. In both designs, the hydrogen-air mixing strength is significantly enhanced for preventing the formation of large diffusion flames that result in higher NO_x emissions. By improving the mixing strength, the flame length reduces for desired combustion quality, with lower combustor residence time. NO_x depends on residence time and temperature. Enhancing the strength of mixing (or reducing the residence time) will result in very low NO_x emissions. The two concepts of hydrogen combustors are discussed as follows:

LDI combustor
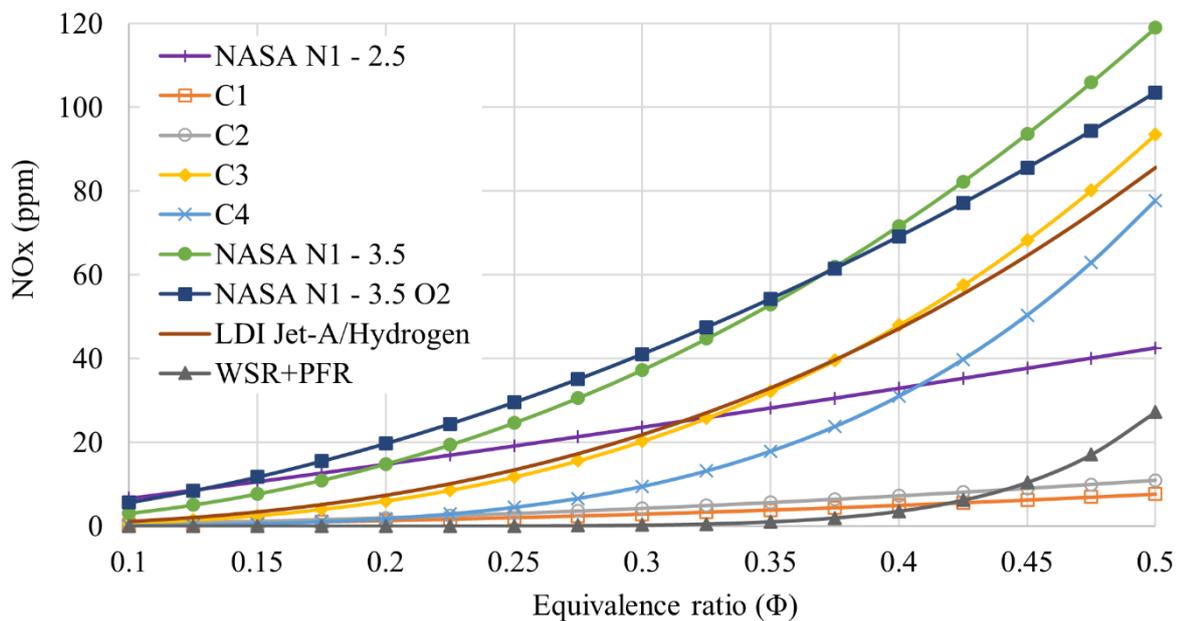
Figure B.9. Comparison of NO_x emission (ppm) for different LDI combustor configurations at combustor inlet temperature of 700 K, combustor inlet pressure of 6.8 atm., 4% fuel injector air flow pressure drop and 2 milliseconds of combustor residence time (created using correlations from Marek et al. [228])

Multiple configurations/types of LDI combustors were studied by Marek et al. [228] at NASA's Glenn research centre, which is capable of replicating typical conditions of gas turbine engine operations and ensuring reliability. A detailed discussion on combustion physics (for terms such as flame speed and quenching diameter) has been carried out previously and can be found in section 6.2.2. In the combustor, flashback is prevented by using a H_2 inlet tube of size lower than the quenching diameter for hydrogen. Marek et al. find that the performance of hydrogen LDI combustors is

outstanding as compared with the performance of advanced Jet-A LDI combustors. Different configurations of fuel injectors are studied in the LDI experiments by Marek et al. (the injector and combustor geometry details can be found in [228]). Figure B.9 provides a comparison of NO_x emission (ppm) for different LDI combustor configurations at combustor inlet temperature of 700 K, combustor inlet pressure of 6.8 atm., 4% fuel injector air flow pressure drop and 2 milliseconds of combustor residence time (using correlations from Marek et al.).

Referring to Figure B.9, using injector C3 produces similar NO_x emissions compared to LDI Jet-A, but it is an injector design that is simple, durable, and safe. The design of injector C4 is similar to the design of injector C3 but its NO_x emissions are lesser for equivalence ratios below 0.4 (or combustor temperature lower than 1,650 K). Injector C4 is durable and there is considerable radial mixing. C1 and C2 configurations have best performance in terms of NO_x emission reductions, both of which produce less than half of NO_x produced by LDI Jet-A combustor. The C1 injector failed during the experiments and therefore it could not be examined completely over the desired pressure range. C2 is unique in design, and it encourages very fast mixing. However, the durability and cooling of C2 was compromised as it resulted into a failure. All LDI examinations by Marek et al. are very stable. The LDI combustors result in reduced NO_x levels without any auto-ignition or flashback. Other combustor (computational) configuration like a well-stirred reactor (WSR) followed by a plug flow reactor (PFR), practically produce near-zero NO_x at equivalence ratios below 0.325, and it releases lower NO_x than C1 and C2 at equivalence ratios below 0.425.

Micro-mix combustor

The micro-mix combustor is studied by Dahl and Suttrop [240] for hydrogen combustion. The study demonstrates safe combustion of hydrogen with focused efforts on minimising the NO_x production. The objective of the study by Dahl and Suttrop was to convert the auxiliary power unit (APU) of A320 i.e., GTCP 36-300, such that it safely functions on hydrogen. The hydrogen combustor is designed using miniaturised diffusive combustion. This type of combustion improves the local mixing regions. Miniaturised diffusive combustion prevents the large diffusive flames (very high temperature zones) observed in hydrogen combustion carried out in conventional combustor. The enhanced mixing is a result of turbulence formations and the breakdown of eddies, which decreases the residence times, and the stoichiometric conditions are prevented.
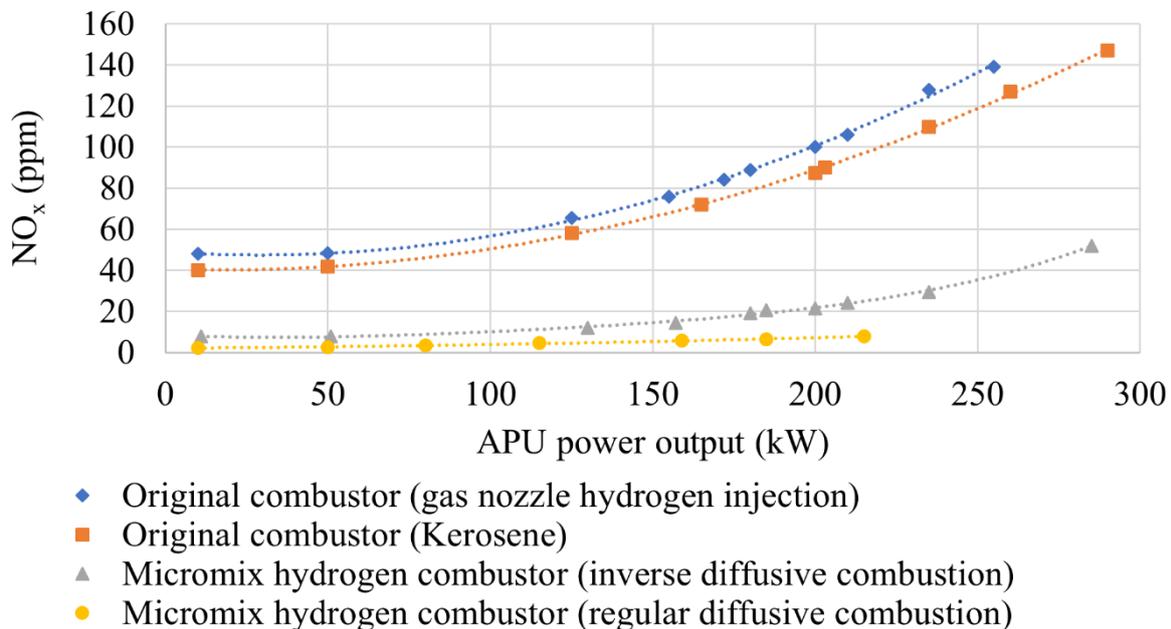
Figure B.10. Comparison of NO_x emissions performance of APU powered by conventional jet fuel and hydrogen fuel in conventional combustor and micro-mix combustor (data source [64], [240])

Figure B.10 shows the NO_x emissions performance comparison of APU powered by conventional jet fuel and hydrogen fuel in conventional combustor and micro-mix combustor (data source [64], [240]). The highest NO_x emissions are found in hydrogen combustion using conventional combustor, because of the large diffusive flames that tend to be at the stoichiometric conditions. High temperatures occur at stoichiometric conditions and NO_x emission production is

temperature dependent. The use of micro-mix combustor for hydrogen combustion produces lowest NO_x emissions because it principally prevents stoichiometric conditions through improvement in local mixing strength.

Safety aspects of LH_2 use

When one hears of aircraft using hydrogen, it is very natural to immediately recall the Hindenburg disaster [363]. Therefore, it is important to account the safety aspect because it is of paramount importance for civil aviation. It is to be noted that the flammable 'cloth' of the containment bag of the Hindenburg class airship is significantly different than the highly insulated, structurally more rigid, robust, and ergonomic tanks which are proposed for future LH_2 aircraft [364]. Compared to the conventional jet fuel, hydrogen cannot contaminate soil or water. LH_2 is much safer than gaseous (compressed) H_2 due to the lower pressure of LH_2 storage tanks, which decreases the likelihood of fatigue-induced structural failures [365]. Gaseous hydrogen has high potential to mix with air or other combustible sources to cause dangerous detonations in case of large leaks. A comparison of different fuels shows that LH_2 is the safest form of hydrogen-based fuel as it causes least damage in case of leaks. The important concerns related to the LH_2 fuel is hydrogen's tendency to escape from a storage enclosure. This is obviously unwanted as it results in loss of energy. In the event of a leak, hydrogen in reasonable quantity has the potential to cause asphyxiation.
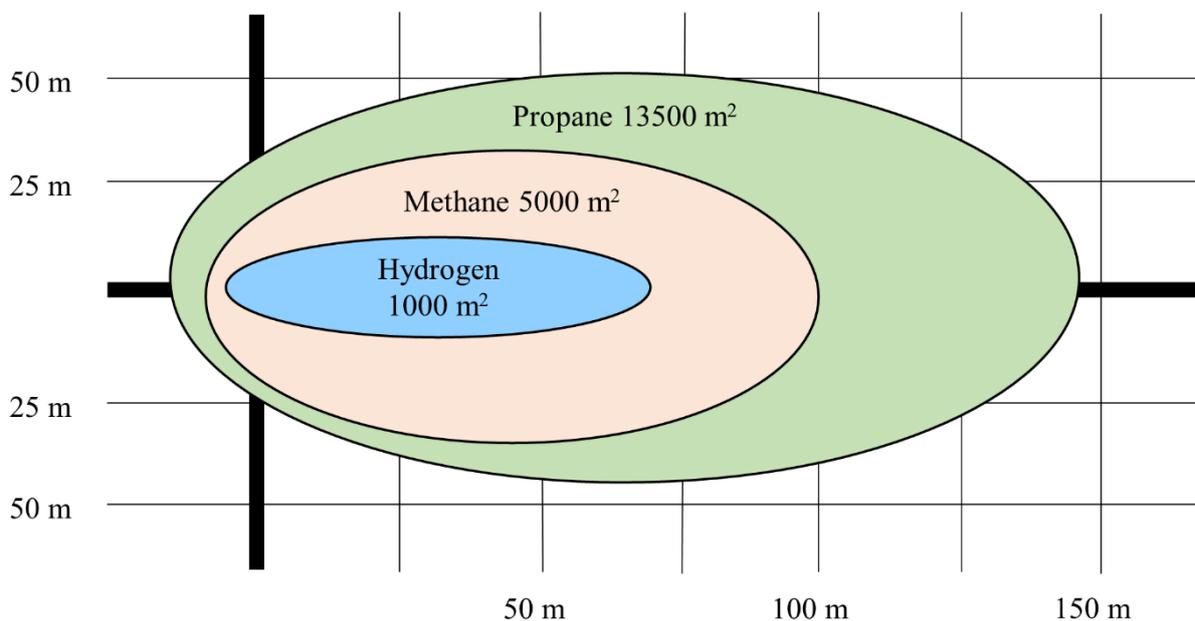
Figure B.11. Comparison of danger zones of spilled liquid gases (data source [181])

An experimental study by Swain [366] compared a gasoline fuel leak (which is similar to kerosene fuel/conventional jet fuel) with a hydrogen fuel leak in a car. Both fuels were ignited after a certain time period post leak-initiation for allowing both fuels to spread. As gasoline is a liquid fuel, it spreads in space. Hydrogen being the lightest gaseous fuel, its leak is localised in a small region. Hydrogen rises into the atmosphere in a controlled manner. The fuel is allowed to leak for 3 secs and ignited at 1 min (60 sec) from the beginning of the experiment. The study finds that hydrogen leak continues to burn in a control manner until the tank is empty [64]. On the other hand, gasoline leak (similar to conventional jet fuel) engulfs the vehicle completely in one minute. It is to be noted that this experimental study was conducted on a car and does not consider any moment on an aircraft as a result of a jet emission. Other safety concern is hydrogen leak and the gas/flame movement inside the aircraft/cabin.

A 'large' LH_2 leak when compared to other liquid fuels spreads less, which can be observed from Figure B.11. In Figure B.11 the spill is of 3.3 m^3 liquid gas with wind speed of 4 m/sec [181]. Hydrogen molecule (molecular weight of 2 g/mol) is the lightest of all fuels. In open atmosphere, hydrogen will rise rapidly thus there is a small danger zone if it gets spilled/leaked. Whereas other fuels like methane (molecular weight of 16 g/mol) and propane (molecular weight of 44 g/mol) spread farther along the ground (directly proportional to the molecular weight), as compared to hydrogen. Hydrogen will combust at concentrations significantly below the detonation limit [181]. There is no danger of detonation in free atmosphere and less risk of fire carpet formation (ibid).

Fuel metering systems and fuel purging during start-up and shutdown are required to enable effective and reliable combustion [64]. Purging is a very important system that must be incorporated with gaseous fuels avoiding all risks of flashback. Like any other fuel, the location of fuel lines must be delegated with care. It is to be ensured that the fuel pipes are far enough from areas of high temperatures and any other possible ignition source (ibid). The recommended way to extinguish such fires is by using a dry powder extinguisher [366]. However, if such fires are extinguished without turning off the fuel flow, it is likely that a combustible mixture may be formed that can further create more serious hazards [64]. Other gas turbine engine related safety measures and operations (like fuel purging, location of fuel lines, etc.) are discussed ahead in this section.

<u>Airport systems design and operations</u>

A challenge associated with LH_2 fuel is its delivery process and refuelling time. A conventional aircraft can be refuelled easily at the airport but when the fuel changes completely (to LH_2), new issues arise. These comprise of: LH_2 fuel transportation and its storage at the airports. The airports will need to be redesigned to enable regular operations of LH_2 powered aircraft [364]. Additionally, it must be ensured that necessary maintenance and support services are available. To meet the LH_2 fuel demand of aircraft operators, it is necessary to integrate LH_2 fuel systems that may include an integrated and dedicated supply chain and logistics. These can be fulfilled by setting an onsite hydrogen manufacturing unit or the adoption of infrastructure which can safely and securely store LH_2 reserves locally. For ensuring the economic viability of LH_2 fuel systems there should be sufficient demand by local aircraft operators. Additionally, multiple airports need to be equipped with LH_2 supply such that this alternative fuel can be commercially feasible for regular airline operations. As the implementation stage of LH_2 fuel systems at the airports begins (or fuel transition phase), airports should ensure seamless delivery of LH_2 fuel in conjunction with conventional jet fuel (ibid). It is anticipated that the larger airports will be the first to accommodate this new infrastructure since the first LH_2 aircraft will most likely be a long-range aircraft [367]. While planning future operational network it is necessary to consider the regions that have a strong LH_2 manufacturing infrastructure. Also, it is to be noted that while comparing LH_2 with conventional jet fuel, the refuelling process could consume more time because of lower density (or more fuel volume) of LH_2 [368].

The optimal fuel delivery systems for the future LH_2 aircraft will most likely include onsite LH_2 production [367]. The location of the storage tanks should be planned carefully. The piping insulation should be appropriate for transporting LH_2 at -253°C. It may consist of three pipes that satisfy the requirements, such as: transferring LH_2, collecting boiled off hydrogen, and allowing redundancy (ibid). Although hydrogen is not poisonous or corrosive, its cryogenic temperatures (LH_2) could cause injury to anyone who comes in contact with it. A local liquefier should be carefully designed (at the airports). The fuel system devices like connections, pumps, and accessories for LH_2 need specific arrangements because of the cryogenic conditions [364]. Personnel that are expected to be in the vicinity of such systems will need specialised training for preventing injuries and for measures to be taken after anyone gets injured due to the cryogenic accidents. The airports should incorporate procedures, policies, and technologies for economical and safe handling of LH_2. The risks can be reduced by carefully planning the LH_2 storage location along with the enforcement of minimum safety distances. Additionally, there should be efforts for intensifying security steps, enforcing strict scrutiny, and access-restriction to LH_2 storage units (ibid).

Airports contribute to 5% of the total air pollution of the aviation industry [367], ignoring journeys to the airport. This air pollution at the airport is caused by aircraft, passengers, freight, and airside/landside vehicle movements. The adoption of hydrogen fuel for ground vehicles will benefit the airport area as it will reduce GHG emissions and air pollution from the operational phase. Presently, the fuel delivery systems for the conventional jet fuel aircraft are large and in some cases, it can be quite complex. Typically, it comprises of a tank area which is within a reasonable distance from the airport apron. These tanks supply 1-3 days of fuel. This fuel is provided to the airport users through a system of underground pipes or trucks. Most large airports have underground piping for reducing congestion, and smaller or regional airports typically use fuel tankers for simplicity. These trucks are powered by conventional fuels and thus cause air pollution in the operational phase. It is proposed in a study by Schmidtchen et al. [365] that the distribution lines should have entrenched yet open plans that enable required venting of potentially dangerous hydrogen gas. The LH_2 fuel tanks should be protected from external elements which can be in the form of underground LH_2 tanks. More improvements to the airport-related aircraft pollution may come through the use of LH_2 powered APU. This can further result in aircraft weight reduction via the elimination of generators within the engine assembly [364]. Hydrogen combustion release only water vapour and small amount of NO_x emission. Hydrogen use in APU with specialised combustor called 'micro-mix' combustor significantly decreases the NO_x emission (by 75+%) as compared to the performance of both kerosene and

hydrogen combusted in the conventional combustor. Therefore, the operational phase air pollution from APU can be significantly reduced by combusting hydrogen in the low-NO_x (like micro-mix) combustors, as the only emission would be water vapour and ultra-low levels of NO_x.

<u>Engine operational issues for hydrogen use</u>

During engine start, hydrogen travels from the cryogenic tanks through the fuel lines to the combustor. Before this, the fuel lines are void of hydrogen and only air present there. With the presence of ambient air in the fuel lines there is a high risk of combustion at the moment when hydrogen interacts with air [64]. This could potentially lead to flash back during the engine start-up phase [the previously discussed aspect of (critical) quenching diameter for hydrogen fuel lines in section 6.2.2 is also relevant here]. This risk can be eliminated by purging the fuel lines with an inert gas. Nitrogen can be used as a cheap substitute for an inert gas. Additionally, there is a possibility of solidification of gases when they come in contact with cryogenic hydrogen which can impede fuel flow. The purging of fuel lines will also be necessary while shutting down the engine (ibid).

Hydrogen not only has a high energy density per unit mass but is also an excellent heat sink (can be used to cool components). The cooling capacity of hydrogen is about 4.9 times the cooling capacity of conventional jet fuel and approximately 2.8 times the cooling capacity of CH_4 [64]. Before the fuel enters the combustion chamber it should be preheated. This ensures that the fuel has completely vapourised during the condition maximum flow rate from the cryogenic tank. This can be safely and effectively performed by using a heat exchanger. Installation of fuel lines in the vicinity of engine hot sections is not recommended because any fuel leak will immediately result in high flammability risk. The use of a separate fluid in a heat exchanger will cool the hot sections of the engine, where the cryogenic hydrogen cools this separate fluid in the heat exchanger and in the process, hydrogen starts warming. Cooling the hot engine sections will help in the reduction of energy needed for combustion. This further ensures that the fuel will be fully in a gaseous state before injection. This increases component life and thermal efficiency, while benefiting from the heat sink potential of cryogenic hydrogen (as discussed above). Engine starting will need an electrical heater that increases the fuel temperature and after the engine reaches its idle rotational speed the heat exchanger becomes fully functional. Furthermore, a metering system is needed to be installed, as it can regulate the required liquid and gas fuel flow rate for different power settings (ibid).

B.4   Literature review on fuel properties of SPK and their operational impact

During the cultivation process, plants consume CO_2 from the atmosphere. These plants are then used as biomass source for extracting oil which are further refined chemically to produce SPK. Considering the lifecycle of this fuel, because CO_2 from the atmosphere is consumed during the cultivation of the feedstock, such SPK fuels have the potential to reduce the GHG emission on a fuel lifecycle basis [100]. Additionally, PtL which is another form of SPK has been reviewed in Chapter 2.

<u>Fuel properties</u>

Biomass based alternative aviation fuels can significantly reduce the lifecycle GHG emissions and provide economic benefits due to growth in fuel availability along with reduced fuel costs [369]. This motivated the formation of an industry-led team that carried out:
- Evaluation of sustainable feedstocks for biofuel production [369];
- Large-scale manufacturing of bio-jet fuel [369];
- Examination of fuel properties [369]; and
- Engine operability, performance, and emissions testing for the use of bio-jet fuel [369].

Table B.1 provides the summary of biomass derived 50% blended SPK testing on ground and in commercial flights. In these tests, only plant-based feedstocks were used by the team since the target of this exercise was to motivate similar or lesser life cycle GHG emissions as compared to Jet-A. As can be observed from Table B.1 that different industrial entities were involved in this joint research venture. The objective of this research was to examine the readiness levels of sustainable bio-jet fuels and to enable biofuel technology to mature (ibid).

Table B.1. Summary of biomass derived 50% blended SPK testing on ground and in commercial flights (source [369])

Aspect	Airlines		
	Continental Airlines	Japan Airlines	Air New Zealand
Engine	CFM International CFM56-7B	Pratt & Whitney JT9D-7R4G2	Rolls-Royce RB211-524G2-T
Aircraft	Boeing 737-800	Boeing 747-300	Boeing 747-400
Fuel provider for test flight	UOP	Nikki Universal/UOP	UOP
% SPK blend	50%	50%	50%
Biomass feedstock	2.5% algae and 47.5% jatropha	8% jatropha and algae, and 42% camelina	50% jatropha

Table B.2. Comparison of properties of Jet-A and SPK fuel (two approved blending % and neat fuel) (source [33], [51])

Property	Units	Jet-A	SPK		
			10%	50%	100%
Mass density	kg/L	0.802	0.798	0.780	0.757
Gravimetric energy density	MJ/kg	43.2	43.29	43.64	44.10
Volumetric energy density	MJ/L	34.65	34.52	34.02	33.38

Ideal carbon length $C_8 - C_{16}$
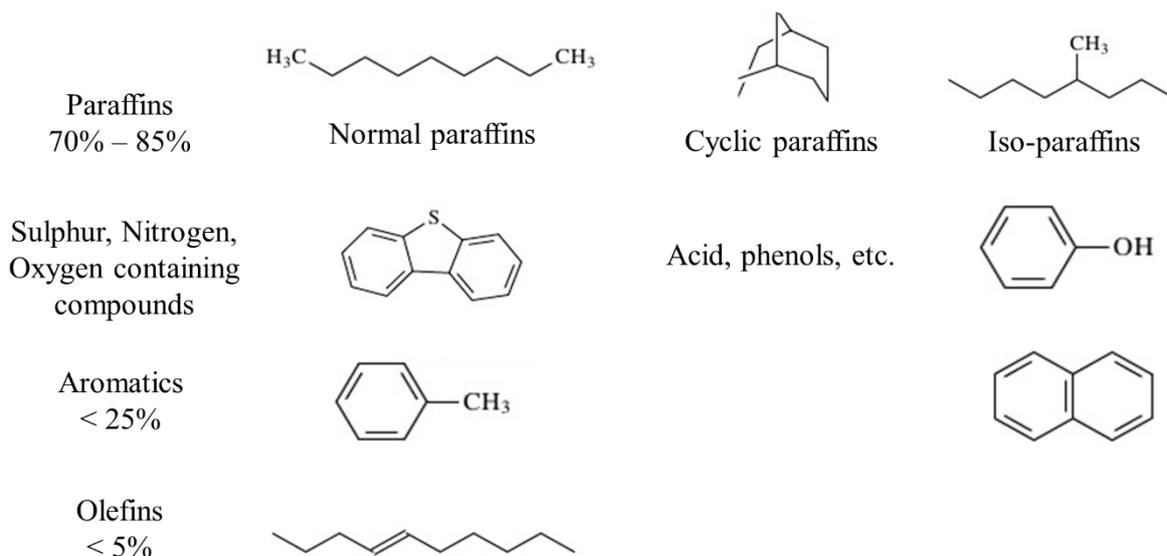
Figure B.12. Composition of the conventional jet fuel (information source [369])

The composition of the conventional jet fuel is shown in Figure B.12. The conventional jet fuel has a broad paraffin distribution, and the paraffin type and concentration is dependent on the crude oil and the refining process [369]. The properties of SPK depend on the source of bio-oil and fuel refining conditions (ibid). The manufacturing process of the SPK used for the engine and flight tests [369], is as follows:

i. The fuel manufacturing begins with bio-oil (free fatty acids and triglycerides) extraction from the cultivated biomass/feedstock,

ii. The impurities from the bio-oil are removed by standard oil-cleaning process,

iii. Thereafter, the bio-oil is converted to small-chain diesel-range paraffins using UOP's renewable jet process. During this process, bio-oil is deoxygenated, and any olefins are converted to paraffins by reaction with hydrogen. The deoxygenation process increases fuel's calorific value, and the termination of olefins and absence of hetero-atoms (S, O, and N) and metals improves the thermal stability of the fuel. Therefore, the SPK fuel has

slightly higher calorific value (both blended and 100%) and excellent thermal stability as compared to the conventional jet fuel (ibid).

iv. Thereafter, a second reaction isomerizes and cracks the diesel-range paraffins to branched jet-range paraffins. This results in a lower freezing point for the SPK fuel. Referring to Figure B.12, the first row i.e., paraffins, primarily represents the composition of SPK (ibid).

Table B.3. Properties of Jet-A and 100% SPK fuel (square brackets indicate reference number)

Properties	Units	ASTM test method	Jet-A	100% SPK
LCV	MJ/kg	D4529, D3338 or D4809	43.2 [33], [51], [369]	44.0 – 44.3 [369]
Viscosity at -20°C	mm^2/s	D445	8.0 [369]	3.336 – 3.663 [369]
Aromatics	vol %	D1319	25 [369]	0 – 0.3 [369]
Sulphur	Total mass %	D1266, D2622, D4294 or D5453	0.3 [369]	≤ 0.0001 [369]
Density	kg/L	D1298 or D4052	0.802 [33], [51]	0.757 [33], [51]
Hydrogen content	% mass	ASTM D3343 - 16	13.4 [369]	15 – 15.5 [369]
Initial Boiling Point	°C	D86/D2887	170 [370]	150 [370]
Flash Point	°C	D56 or D3828	38 [369]	41.0 – 46.5 [369]
Final boiling point	°C	D86	300 [369]	242 – 248 [369]
		D2887	300 [369]	251 – 256 [369]
Freezing point	°C	D5972, D7153, D7154 or D2386	-40 [369]	-63.5 to -54.5 [369]

The experimental study by Rahmes et al. [369] finds that SPK fuels comprise of normal (n-) and isomeric (iso-) paraffins, along with a small fraction of cycloparaffins. As per the study by Rahmes et al., the types and carbon numbers of the iso- and n-paraffin content of 100% SPK vary between C_9 and C_{15}. This is typically the range observed in conventional jet fuel (ibid). Additionally, the study by Rahmes et al. investigates for impurities in SPK fuel which have the potential to negatively impact the engine performance. These impurities comprise of 21 different metals along with oxygen, nitrogen, and sulphur compounds. The authors find that the blended SPK fuel is free from any traceable amounts of impurities. Additionally, the authors found that the impurity content in 100% SPK is below detection levels.

Table B.2 provides the comparison of properties between of Jet-A and SPK fuel. Table B.3 provides the comparison of properties between conventional jet fuel (Jet-A) and 100% SPK fuel. Most of the fuel properties in Table B.3 are from the study by Rahmes et al. [369], and others are taken from the study by Lokesh [59], Hileman et al. [51], and the GREET model [33], as indicated.

Effect of the fuel characteristics on maintenance, performance, and operability

The effects of characteristics of 100% SPK fuel on the performance, operability, maintenance, etc. of aircraft and engines, have not been quantified and reported in literature. The experimental examinations of biofuel (blended and 100% biofuel) by Rahmes et al. [369] report the quantitative fuel properties. However, this examination does not address the impacts of fuel properties on aspects such as engine operation and maintenance. Another investigation by Lokesh [59] only examines the qualitative effects of fuel properties on the performance of engine because of the lack of data on the engine impacts of use of 100% SPK [59]. All alternative fuels for civil aviation application are tested by institutions like ASTM, and the approval of these fuels is based on these tests [59]. The performance and thermal properties of the alternative fuels are studied and are designated as standard specifications. These, in general, can be classified into combustion and handling properties (ibid).

In general, the compatibility of 100% SPK fuel with today's aircraft engines and their impacts on engines can be evaluated via thorough experimental investigations [59]. Experimental studies using 100% SPK fuel in engines have been conducted by Rahmes et al. [369] but the impacts of the fuel properties on engine maintenance are not reported. There is a need for an experimental investigation that examines the effect of using 100% SPK fuel on engine maintenance, operability, and performance. These effects include: the need for hardware reconfigurations, and the impact on the mechanical life of aircraft engines [59]. The discussion below is completely qualitative in nature.

Effect of fuel properties on combustion characteristics

The vapour pressure of 100% SPK fuel is expected to be greater than Jet-A [59]. The fuel vapour pressure is a measure of its volatility. Therefore, 100% SPK fuel is expected to have higher volatility than Jet-A, which enables faster vaporisation post atomisation. This enhances the combustion efficiency. Additionally, FAR of 100% SPK fuel is lesser than Jet-A. Cumulatively, over one flight mission, leaner combustion of 100% SPK fuel reduces the fuel consumption (i.e., fuel savings) (FC) and can therefore reduce the GTOW of the aircraft (ibid).

An investigation by Lokesh [59], finds that 100% SPK demonstrate enhanced thermodynamic behaviour. As can be observed from Table B.3, the LCV (MJ/kg) of 100% SPK fuel is greater than Jet-A, and this effect is explored in Chapter 4. As can be observed from Table B.3, the viscosity of Jet-A is greater than 100% SPK fuel. The lesser viscosity of 100% SPK fuel enables formation of reduced droplet size as compared to Jet-A, thereby improving the efficiency of combustion and decreasing the combustion products such as PM, CO, and soot [59]. Additionally, as can be observed from Table B.3 the aromatic content of 100% SPK is significantly lesser than Jet-A, which reduces the VOC emission (ibid).

The study by Rahmes et al. [369] finds that the smoke number (SN) for Jet-A was significantly higher than SN for biofuel. The SN reduction for biofuel is attributable to the negligible aromatic content and a slightly greater hydrogen-to-carbon ratio of biofuel as compared to the conventional jet fuel. The authors noticed that there was an observable reduction in NO_x emission at high power for 100% biofuel as compared to the conventional jet fuel. Also, for blended biofuel the authors noticed a negligible decrease in NO_x, as compared to the conventional jet fuel.

According to the study by Lokesh [59], the engine using 100% SPK fuel can potentially qualify the LTO-NO_x certification process because it reduces the LTO-NO_x by 7 – 8% and such an advantage can be observed without necessarily considering the incentive (kink on the Committee on Aviation Environmental Protection (CAEP)/8) for fuel economy. This feature of 100% SPK fuel could potentially motivate more rigorous CAEP restrictions for the future. Resultantly, it will drive design and development of aircraft technology that is compatible with SPK fuel (ibid).

The density of a fuel is an important property for analysing its behaviour before and during combustion [59]. The fuel atomisation, mixing, and evaporation rates are dependent on the fuel density. The fuel spray characteristics such as droplet size are principally dependent on the fuel density (ibid). During combustion, the fuel density determines the concentration of the fuel near the flame. Improved fuel atomisation results in better mixing and evaporation rates, which is positive as the ignition is improved. As observed from Table B.3, 100% SPK has lesser mass density than Jet-A, and this improves combustion characteristics (ibid).

Effect of fuel properties on the fuel handling properties

The handling properties of a fuel are essentially its physico-chemical properties and these impact the fuel supply-chain and operational processes which comprise transportation, pipeline transfer, storage, and fuel injection point [59]. The handling properties studied below are fuel lubricity, vapour pressure, flash point, freezing point and viscosity, density, and aromatic content.

- *Fuel vapour pressure and flash point*

  The vapour pressure of 100% SPK fuel and resultantly its volatility, are expected to be higher than Jet-A as discussed above. Flash point of a fuel depends on the fuel volatility and density [59]. 100% SPK has higher flash point as observed in Table B.3, which is safer from handling perspective (ibid).

- *Fuel lubricity and thermal stability*

  100% SPK fuel has sufficient lubricity [59] and high thermal stability [371], [372]. High thermal stability enables the reduction of carbonaceous deposits in the fuel systems, which can potentially reduce maintenance [371]. According to both Syntroleum corporation and Honeywell UOP LLC, the HEFA-SPK fuel manufactured from their technology is suitable for Jet-Aircraft use [371].

- *Fuel freezing point and viscosity*

  It can be observed from Table B.3 that 100% SPK fuel has higher hydrogen content and lesser mass density than Jet-A. In terms of handling characteristics, this is advantageous as 100% SPK fuel can bear lesser temperature than Jet-A

before it freezes [59]. Therefore, as observed from Table B.3, the freezing point temperature of 100% SPK fuel is lesser than that of Jet-A.

In terms of fuel handling, viscosity is of paramount importance. The fuel transport through pumping line, storage, and aircraft fuelling, is governed by the fuel viscosity [59]. The viscosity of a liquid varies inversely with temperature [373]. Thus, the behaviour of liquid fuel at lesser temperatures has to be studied. The viscosity of 100% SPK fuel was measured at -20°C in the experimental study by Rahmes et al. [369] and it was found to be 3.336 – 3.663 mm^2/s as compared to the viscosity of Jet-A of 8 mm^2/s. This can be observed from Table B.3. The lesser viscosity of 100% SPK fuel as compared to Jet-A is advantageous considering the handling perspective especially at cruise conditions since it enables sufficient fuel fluidity [59].

- *Fuel density*

The fuel density is an important fuel property, especially considering the fuel handling perspective. The density governs the transfer of fuel to the storage units in the fuel supply-chain process [59]. Additionally, other aspects that are dependent on the fuel density are the fuel pumping and storage, aircraft refuelling, and aircraft's ability to travel a flight-range with a fixed tank (ibid). It can be observed from Table B.3 that the density of 100% SPK fuel is lesser than that of Jet-A. As can be observed from Table B.2, the gravimetric energy density and volumetric energy density of 100% SPK fuel is respectively higher and lower than Jet-A. The effect of both lower volumetric energy density and higher gravimetric energy density effect of 100% SPK, compared to Jet-A, was explored in Chapter 4.

- *Fuel aromatic content*

As observed from Table B.3, 100% SPK fuel has negligible aromatic content. Therefore, the aromatic concentration in blended SPK fuel will also be lesser than Jet-A fuel [369]. Aromatic compounds have carbon-to-carbon double bonds. Additionally, they have lesser hydrogen-to-carbon (H/C) ratio in comparison with paraffinic compounds for the same carbon number due to their cyclic form. Resultantly, 100% and blended SPK fuels have higher hydrogen-to-carbon ratios in comparison with Jet-A (ibid), which can be observed from Table B.3 where 100% SPK fuel has higher hydrogen content (% mass).

In Jet-A fuel, higher presence of aromatics result in the formation of 'gums' that gets deposited in the fuel lines and tanks and obstructs the fuel flow [59], [374]. The deposition of gums in the fuel lines and tanks increases the maintenance costs. As can be observed from Table B.3, lesser aromatic content of 100% SPK fuel is beneficial considering the handling and storage perspective (ibid).

In the current aircraft engines, the sub-systems are designed according to the properties of Jet-A i.e., the conventional fuel. In the current engines, certain rubber seals that prevent fuel leaks in the high pressure fuel system function because of the aromatic content of the fuel [59]. These seals swell and prevent the fuel leaks (ibid). Additionally, studies by Hui et al. [375], Blakey et al. [52], Daggett et al. [48], and Corporan et al. [376], recommend that the aromatic content requirement (specification) that was conceived about five decade ago should be reviewed and updated. Future aircraft that are designed for 100% SPK fuel operation can use compatible and NextGen elastomers, and/or synthetic aromatics/additives can be added to 100% SPK fuel that enable the required swelling of the seals [59], [371], [377].

It can be observed from Table B.3 that 100% SPK fuel have negligible aromatics as compared to Jet-A. Using 100% SPK fuel in the present-day engine might not swell the seals to desired levels and therefore might create a safety issue. In the current set-up, three types of seal materials are used. These comprise of fluorocarbon-O rings, nitrile compounds, and fluoro-silicone [59]. 50% blend of SPK fuel with JP-8 fuel increases the aromatic content by 7% by volume and it does not affect the Fluoro-silicone and Fluorocarbon-O rings, however, it shows desired levels of nitrile rubber swelling [59], [374]. Similar observations were made in the testing of 50% SPK fuel conducted by Rahmes et al. [369], however, there is a need for further examination of the impacts of aromatics (or lack of it in case of 100% SPK fuel) and other compounds on swelling of seals.

Operational impact of biofuel use

Flight tests using SPK

Test flights using blended SPK fuel from algae and camelina were successfully conducted [59], [101], [102]. Additionally, Lufthansa conducted a successful six-month flight-operation using 50% blended SPK fuel on Airbus A321 between Frankfurt and Hamburg, which did not reveal any technical or operational issues [59], [103].

Referring to Table B.1, in both of the flight tests by Continental airlines and Japan airlines using 50% SPK fuel, both the engine and aircraft performance were unaffected by the biofuel use [369]. In the flight test by Japan airlines, there were no obvious indications that the alternative fuel negatively impacted the engine response (ibid). Additionally, in the flight test by Air New-Zealand, there were no obvious indications of 50% SPK fuel affecting the engine operation (ibid). The hardware inspection after the Air New-Zealand test comprised of examination of the low-pressure fuel filter, fuel management system, 24 fuel nozzles, and fuel pump (ibid). Overall, in all three flight tests, 50% SPK fuel did not negatively impact any aircraft system. The authors recommend further exploration of aspects that will enable higher SPK fuel blends (>50%) as this can potentially provide environmental, performance, and economic advantages. The aspects that are recommended by the authors for further exploration include chemical composition, compatibility of materials, density, etc. According to IATA [60], currently the aviation sector is focused on producing sustainable 'drop-in' replacement fuels, and in future 100% biofuel has the potential to be a complete replacement to the conventional jet fuel. In recent years many test flights have been conducted on regional jet (ATR aircraft) [104], business jets [105], and LTA (A350) and VLTA (A380) [106], powered by 100% SPK primarily from HEFA pathway using waste biomass. From these test flights, no major issues were reported.

Engine testing using biofuel

As part of the ground testing, the performance of a Pratt and Whitney engine was evaluated in a test facility in Canada [369]. The engine testing comprised of operability (engine start, transient thrust properties, and flame-out), control, and performance. These tests were performed using 100% biofuel, 50% biofuel, and Jet-A-1 fuel (ibid). The biofuel used in this test comprised of iso- and n-paraffins, which was a diesel-range hydrotreated vegetable oil manufactured by Neste Oil (ibid). The authors observed that there was no engine degradation through operability, control, and performance or via hardware examination after the test. The authors observed that powering the engine with the biofuel did not cause performance deterioration. Following the testing, the engine was inspected for deterioration of components. More specifically, the authors observed that there were no: engine hardware deterioration and peculiar odours due to the use of the alternative fuel, during engine operations and handling (i.e., mixing of fuel blend, filling of tanks, etc.).

Effect on safety, reliability, and airline revenues

If there are any incompatibilities detected in the performance properties of alternative fuels, then the fuel is not acceptable for aircraft operations as 'fuel compatibility' with the hardware is a significant techno-economical parameter for engineers and related stakeholders (ibid). The fuel incompatibility could result in increase of maintenance cost and necessitate engine modifications/redesign, which may affect reliability and safety (ibid). Whenever alternative fuels are proposed to be used in gas turbine engines designed for conventional fuel, there is a need to study the compatibility of the alternative fuels with the engine and aircraft [59]. Such an investigation is of utmost importance because it drives the crucial aspects of the airline sector i.e., safety of passengers and techno-economic issues (technological reliability and airline profitability). In terms of passenger safety, the storage and handling properties of the alternative fuel should be ideal during different operational paths of the aircraft (ibid).

Table B.4. Details of different studies on LH$_2$ powered aircraft with the tank gravimetric index

Study	Application	Tank type	Tank and insulation material	η	λ	Year, Ref.
Multi-layer insulation						
Clean Sky 2 - Fuel Cells and Hydrogen joint project	19 passenger commuter aircraft with 500 km range	Integral	Double-wall evacuated tank with multi- layer insulation	0.25*	3**	2020 [34], [206]
Clean Sky 2 - Fuel Cells and Hydrogen joint project	80 passenger regional aircraft with 1,000 km range	Integral	Double-wall evacuated tank with multi- layer insulation	0.30*	2.33**	2020 [34], [206]
Clean Sky 2 - Fuel Cells and Hydrogen joint project	165 passenger (short-range) aircraft with 2,000 km range	Integral	Double-wall evacuated tank with multi- layer insulation	0.35*	1.86**	2020 [34], [206]
Clean Sky 2 - Fuel Cells and Hydrogen joint project	250 passengers (medium range) aircraft with 7,000 km range	Integral	Double-wall evacuated tank with multi- layer insulation	0.37*	1.70**	2020 [34], [206]
Clean Sky 2 - Fuel Cells and Hydrogen joint project	325 passenger (long-range) aircraft with 10,000 km range	Integral	Double-wall evacuated tank with multi- layer insulation	0.38*	1.63**	2020 [34], [206]
Foam insulation						
Cryoplane	Different aircraft categories (regional to very large aircraft)	Integral	Stainless steel tank with polymer foam insultation	-	-	[175], [181]
Winnefeld et al.	General application of cylindrical tanks	Non-integral	Aluminium alloy tank with polymer foam insulation	0.6 – 0.7*	0.667 – 0.429**	2018, [86]
Brewer (1991) summarised by Verstraete (2009)	-	Non-integral	Aluminium alloy tank with foam (polyurethane) insultation	0.9**	0.113*	1991, [191]
NACA/NASA	High-altitude (20 km) tube-wing reconnaissance aircraft	Integral	Stainless steel tank with plastic foam insulation	0.881 feasible (used 0.87)**	0.134 feasible (used 0.15)*	1955, [219], [220]
Delgado Gosálvez et al. (Greenliner design)	19 passenger commuter aircraft with 926 km range	Non-integral	Aluminium alloy tank with foam insultation	0.5*	1**	2018, [70]

Verstraete et al.	Regional tube-wing aircraft for 32 passengers and range of 2,100 km	Integral	Aluminium alloy tank with foam (polyurethane) insultation	0.658 – 0.71*	0.52 – 0.408**	2010, [66]
Gomez et al.	Tube-wing aircraft for 197 passengers and range of 9,000 km	Integral	Aluminium alloy tank with polyurethane insultation	0.826 (rear tank) and 0.741 (forward tank)**	0.21 (rear tank) and 0.35 (forward tank)*	2019, [172]
Brewer (1991) summarised by Gomez et al. (2019) and Verstraete (2009)	Tube-wing aircraft for 400 passengers and range of 10,190 km	Integral	Aluminium alloy tank with foam (polyurethane) insultation	0.836**	0.196*	1991, [172], [180], [191]
Beck et al.	Very large twin aisle BWB aircraft with design range 11,400 km for 531 passengers)	Non-integral	Aluminium alloy tank with polymer foam insulation	0.77*	0.299**	2018, [217]
Verstraete et al.	Large tube-wing aircraft for 550 passengers and range of 13,890 km	Integral	Aluminium alloy tank with foam (polyurethane) insultation	0.764 – 0.791*	0.308 – 0.264**	2010, [66]

*Published values
**Calculated values

Trend of engine technology development

Table B.5. Different efficiency metrics during cruise for engines entered in service till date (data source [211]) and engines modelled in this work

Aircraft	Effective propulsive efficiency	Core efficiency	Overall efficiency
B707	0.485	0.440	0.213
B727	0.585	0.440	0.257
MD80	0.615	0.450	0.277
B747-100	0.625	0.480	0.300
A300	0.650	0.500	0.325
B757	0.665	0.510	0.339
B747-400	0.680	0.500	0.340
B777	0.700	0.530	0.371
B787	0.715	0.550	0.393
A380	0.690	0.570	0.393
A350	0.710	0.563	0.400
Propfan	0.760	0.526	0.455
BWB UHB GTF Jet-A	0.752	0.605	0.469
BWB UHB GTF 100% SPK	0.752	0.605	0.477
BWB UHB GTF LH2 C1	0.750	0.626	0.485
BWB UHB GTF LH2 C2	0.756	0.631	0.455
BWB UHB GTF LH2 C3	0.756	0.641	0.400

Appendix C

C.1   Engine modelling validation cases

After proposing a model/methodology, it is important to try and test the model using published literature. This enables to establish the model's accuracy. By conducting validation cases, a scientific confidence is built on the proposed model. In this section, there are two validation cases, and these were primarily selected because of the sufficiency of data availability (one or multiple publications) to replicate the studies. According to the book by Kundu et al. [184] and thesis of Kirby [185], a prediction difference of ±5% is acceptable in the conceptual design phase. Therefore, for the two validation cases, this criteria of ±5% difference on engine metrics is used as a basis for establishing confidence in the model.

C.1.1.   Validation Case 1

Bijewitz et al. [224] design an UHB GTF engine for future aviation application in GasTurb 11 software. The engine data is only known for on-design point and hence this validation case is only limited to on-design point. Most of the data required for this validation case comes from study [224] and remaining information comes from another study of the same author [277] that considers same engine conditions.

Data known and methodology for case 1:

Table C.1. On-design data of GTF engine at TOC condition of 35,000 feet (10,668 m) altitude at Mach 0.78 modelled by Bijewitz et al. [224], [277]

Parameter	Value
Basic inputs	
BPR	19.4 [224]
Fan inlet Mach number	0.7 [277]
Fan inlet Hub/Tip Ratio	0.29 [277]
Intake pressure ratio	0.997 [277]
Core intake pressure ratio	0.99 [277]
Bleed and power off-take	None [224]
Number of fans, IPC, HPC, HPT, LPT stages	1, 3, 9, 2, 4 [224]
Gear ratio	4:1 [224]
TET or T_4	1,750 K [224]
Cooling flows	
Cooling flows	20% for HPT; 0% for LPT [224]
Constraints	
Thrust	56 kN [224]
OPR	60 [224]
Fan diameter	3.35 m
Performance parameters	
TSFC	12.67 g/s-kN [224]
Core efficiency	0.6 [224]
Propulsive efficiency	0.85 [224]
Thrust/engine mass flow	83 [224]
OR	OR
Engine mass flow	674.6 kg/s

The data known for the validation case 1 is summarised in Table C.1. The process of design-optimisation remains the same as discussed in the methodology section (6.4). Table C.1 also categorizes the data from the studies of Bijewitz et al. [224], [277] into inputs, cooling flows, constraints, and performance parameters. The design requirement here is to design a UHB GTF engine with a BPR of 19.4, OPR of 60, fan diameter 3.35 m, and to produce thrust of 56 kN at TOC point of 35,000 feet (10,668 m) altitude with Mach 0.78 [224].

The fuel used here is Jet-A, and cooling flows are 20% for HPT with uncooled LPT [224]. The number of fan, IPC, HPC, HPT, and LPT stages are 1, 3, 9, 2, and 4, respectively [224]. The fan inlet Mach number and hub/tip ratio are 0.7 and 0.29, respectively [277]. There is no power off-take and bleed [224]. The pressure ratios at engine inlet and core inlet are 0.997 and 0.99, respectively [277]. Bijewitz et al. [224] use conventional material in the engine except the fan, where they use PMC. The properties of conventional material (including gearbox technology) and PMC are known from Table 6.9 – Table 6.11. The above information/inputs need to be updated in the model described in the methodology section (6.4).

The component efficiency for each turbomachine is unknown through the studies of Bijewitz et al. [224], [277], and therefore all component efficiencies will be treated as design variables in the optimisation process, unlike the proposed model in section 6.4. For all these design variables, all minimum values are set to 0.85, the start-guess values are set to the values in Table 6.5 (present efficiencies) and the maximum values are set to values in Table 6.6 (future efficiencies at TOC point). Also, compared to the proposed model, the design TET and gear ratio are known to be 1,750 K and 4:1, respectively. Hence, these two parameters, which are design variables in the proposed model in section 6.4, will be removed as design variables as these values are fixed as per the known data/design requirement.

The design constraints (parameters) remain the same, except the change in their values. Thus, 56 kN of thrust is to be produced with an engine which has OPR of 60 and fan diameter of 3.35 m. Overall, the model described in the methodology section (6.4), remains unchanged (including all model inputs) except the changes/updates mentioned above as they are pertinent to replicate the studies of Bijewitz et al. [224], [277] listed in Table C.1. The methodology for this validation case is now completed, and the results are discussed below, along with a comparison of engine performance with the published values.

Validation case 1 results and discussion:

Table C.2. Comparison of on-design engine performance between the current model and study by Bijewitz et al. [224]

TOC		Bijewitz et al. [224]	Present model
		GasTurb 11	GasTurb 13
Mach, Altitude	- , m	0.78 at 10,668 m	0.78 at 10,668 m
Net Thrust	*kN*	*56*	*56.6*
Thrust difference with respect to Bijewitz et al. [224]	*%*	*-*	*+ 1.071*
OPR		*60*	*60*
BPR		*19.4*	*19.4*
Fan diameter	*m*	*3.35*	*3.35*
Number of Fan, IPC, HPC, HPT, LPT stages		1, 3, 9, 2, 4	1, 3, 9, 2, 4
Engine mass flow	kg/s	674.6	674.4
TSFC	g/kN-s	12.67	12.6744
TSFC difference with respect to Bijewitz et al. [224]	%	-	+ 0.035
Fuel consumption (FC)	kg/s	0.71	0.71
Gear ratio		4	4
Cooling flow	%	20	20
TET or T_4	K	1750	1750
Power off-take and bleed		None	None
Core efficiency		0.6	0.6
Propulsive efficiency		0.85	0.85
LPT inlet temperature	K	< 1,350	1,207.08

Table C.2 shows the comparison of on-design engine performance between the current model and study by Bijewitz et al. [224]. It can be observed from Table C.2 that the proposed model of Chapter 6 is able to replicate the study by Bijewitz et al. [224] with high accuracy (+0.035% difference in the TSFC values between both studies relative to Bijewitz et al. [224]) and meet all design requirements (italicised). The LPT inlet temperature in both cases is lower than 1,350 K which was a requirement for having uncooled LPT.

In terms of engine weight, the study by Bijewitz et al. [224] does not provide engine weight directly, instead it gives the total propulsion system weight (of 7,648 kg). Additionally, the breakdown of the total propulsion system weight into component weights, is not provided by Bijewitz et al. [224]. Moreover, it is not clear whether the total propulsion system weight (of 7,648 kg) is inclusive of engine mount weight. Therefore, there are two different engine weights estimated below in Table C.3: 1. Inclusive of weights of the bare engine, nacelle and inlet, and mount; 2. Inclusive of weights of the bare engine, nacelle, and inlet only. The bare engine weight is calculated using GasTurb 13 as discussed previously. The nacelle and inlet weight, and mount weight, both come from Table 6.2 i.e. from the NASA N+2 study by Nickol et al. [130]. It is to be noted that the engine weight calculation (with disk optimisation) is not as rigorous as discussed in the section 6.4, because the off-design points are not considered by Bijewitz et al. [224]. Therefore, disk weight optimisation, and resultantly the bare engine weight estimation, is just limited to the on-design point.

Table C.3. Comparison of total engine weights between the current model and study by Bijewitz et al. [224]

| | | First case: | | |
| | | PMC for fan section and conventional materials in other components | | |
		Bijewitz et al. [224]	Present model	% difference
Bare engine weight	kg	-	6,738	-
Total engine weight [1]	kg	7,648	7,651	+ 0.039
Total engine weight [2]	kg	7,648	7,514	- 1.752
		Second case:		
		PMC for fan section, CMC for hot sections and conventional materials in other components		
Engine weight	kg	-	6,629	-
Total engine weight [1]	kg	7,648	7,543	-
Total engine weight [2]	kg	7,648	7,406	-

[1] Inclusive of weights of the bare engine, nacelle and inlet, and mount.
[2] Inclusive of weights of the bare engine, and nacelle and inlet only

There are two different cases considered in Table C.3. The first case is the known case, where PMC material is used for the fan section and for other components conventional materials are used. Ideally, 'total propulsion system weight' should be the first type of weight calculation i.e. inclusive of weights of the bare engine, nacelle and inlet, and mount, and its estimation by the proposed model is highly accurate (well within the ±5% difference criteria) compared to the study by Bijewitz et al. [224]. Recalling the value of 1,750 K for the design-point TET i.e. at TOC point from the study by Bijewitz et al. [224], it would mean that at SLS conditions the TET would be of the order of 2,000K which is very high for conventional materials (used by Bijewitz et al. [224]) to withstand a successful engine operation. Bijewitz et al. [224] mention that their maximum limit for TET is 2,050 K. Clearly, it is necessary to use CMCs as these are the only materials that can withstand such high temperatures. Thus, a second case is considered and is listed in Table C.3, where PMC is used in fan, CMCs are used in hot sections, and conventional materials in other components. In the second case considered here, only the present model adheres to the changes (CMC use). The total engine weight of Bijewitz et al. [224], remains unchanged compared to the first case. The second case highlights the need to use CMCs in hot components, not only from realistic engine operability perspective but also its potential of engine weight reduction. Since this (second case) is a hypothetical or proposed case, there is no basis for a direct comparison of weights and thereby no validation process is conducted.

The thrust and TSFC values are estimated with +1.071% and +0.035% difference respectively. In terms of weights, the first type and the second type of total weight calculation have +0.039% and – 1.752% difference, respectively. These predictions fall well within the set criteria of prediction difference of ±5% from literature for a successful conceptual design. Overall, it is observed that the proposed model estimated the engine performance and weight, with a high accuracy in comparison with the study by Bijewitz et al. [224]. This concludes the first validation case. A second validation case is considered next, as a sanity check towards establishing confidence on the proposed model.

C.1.2.   Validation Case 2

Nickol et al. [130] design a UHB GTF engine powered by Jet-A for NASA N+2 timeframe, using the NPSS software. The engine data is only known for on-design point and one off-design point (of SLS). However, the component efficiencies are not known for both these points. Thus, the current validation case is limited only to on-design point with

three possible cases of component efficiencies. It is to be noted that this is the same study (Nickol et al. [130]) which is used as a reference study to establish the aircraft and engine design targets towards the objective of Chapters 6 and 7. The engine design requirement (on-design/TOC point only) of this validation case is exactly similar to the design requirements of the proposed model described in section 6.4, because these are based on same study by Nickol et al. [130].

Data known and methodology for case 2:

For this validation case, all known data is already included in section 6.4. The model setup remains unchanged except for few parameters discussed below. As discussed in detail in section 6.4, the stage counts of turbo-machineries are not known from the study by Nickol et al. [130]. Therefore, the selection of turbomachinery stage counts is based on three different studies, and this selection process is discussed previously in section 6.3.3.2. The number of Fan, IPC, HPC, HPT, and LPT stages are 1, 3, 9, 2, and 3, respectively, as listed in Table 6.7, and these are assumed to remain unchanged for this validation case. The model inputs remain the exact same except component efficiencies and materials. It is to be noted that in terms of materials, CMC is the only material known to be used in the study by Nickol et al. [130] in their engine design for hot sections. Therefore, it is assumed that conventional materials are used for all engine components except the combustor and HPT, where CMC is used. However, it is very likely that PMC 'might' be used in the engine fan section by Nickol et al. [130], though not considered in this validation case. Additionally, cooling flows, gear ratio and pressure ratios of compressors are unknown. 20% cooling flows are assumed, as mentioned also in section 6.4. Gear ratio, and pressure ratios of IPC and HPC, are treated as design variables in optimisation, which are exactly similar to the proposed model in section 6.4.

As mentioned above, the component efficiencies are not known from the study by Nickol et al. [130]. Therefore, at on-design point three cases of component efficiencies are used towards this validation case. In the first and second case, future component efficiencies and conventional component efficiencies are used, respectively. For both cases, the optimisation scheme also remains unchanged. In the third case, all component efficiencies will be treated as design variables in the optimisation process (similar to validation case 1), unlike the proposed model in section 6.4. For all these design variables (in the third case), all minimum values are set to 0.85, the start-guess values are set to the values in Table 6.5 (present efficiencies) and the maximum values are set to values in Table 6.6 (future efficiencies at TOC point). Additionally, in this third case, a constraint-target of TSFC (13.1543 g/kN-sec) is added to the model that enables the exact replication of NASA N+2 study by Nickol et al. [130]. By doing this, the exact component efficiencies can be found by reverse-engineering for a fixed/known target TSFC.

Overall, the model described in section 6.4, remains unchanged (including all model inputs) except the changes/updates mentioned above. The methodology for this validation case is now completed, and the results are discussed below, along with a comparison of engine performance with the published values.

Validation case 2 results and discussion:

Table C.4 provides the comparison of on-design/TOC engine performance and weights between the study by Nickol et al. [130] and three cases of the present model. The three cases are:
- 1st case: Future component efficiencies are used,
- 2nd case: Conventional component efficiencies are used,
- 3rd case: All component efficiencies are treated as design variables (future component efficiencies treated as the maximum limit for these design variables) in optimisation, with TSFC set as a design constraint-target (of 13.1543 g/kN-sec).

Table C.5 provides the comparison of component efficiencies between the three cases of the present model. It is to be noted that the component efficiencies listed for the 3rd case are the output of the optimisation process. It can be observed from Table C.5 that the proposed model (all three cases) exactly meets all design requirements (italicised). The LPT inlet temperature in all three cases of the present model are below 1,350 K, which was a requirement for having uncooled LPT.

It can be observed from Table C.4 that compared to the study by Nickol et al. [130], the TSFC and/or FC for: the 1st case is 5.737% lesser, the 2nd case is slightly higher (i.e. +0.875% difference), and 3rd case is equal (as TSFC was a constraint-target in the 3rd case) [0% error]. This is primarily because of the component efficiencies. The 1st case uses future component efficiencies, whereas 2nd case uses present day efficiencies, which results in the above-mentioned difference in TSFCs and/or the FC values. It can be observed from Table C.5 that there is less difference between the component efficiencies of 2nd case and 3rd case. It means that the present day component efficiencies are similar to the

optimum component efficiencies that enables the 3rd case to meet the exact TSFC and/or FC value of the study by Nickol et al. [130], and the TSFC and/or FC of 2nd case is similar/slightly higher (i.e. +0.875% difference) compared to the said study. Additionally, with the assumptions made here, it appears that the study by Nickol et al. [130] might have used present day component efficiencies.

Table C.4. Comparison of on-design/TOC (Mach 0.8 at 10,668 m) engine performance and weights between the study by Nickol et al. [130] and three cases of the present model

Parameters	Units	Nickol et al. [130]	1st case	2nd case	3rd case
Net thrust	*kN*	*55.603*	*55.603*	*55.603*	*55.603*
OPR		*60*	*60*	*60*	*60*
BPR		*17.65*	*17.65*	*17.65*	*17.65*
FPR		*1.35*	*1.35*	*1.35*	*1.35*
Fan diameter	*m*	*3.36296*	*3.36296*	*3.36296*	*3.36296*
Engine mass flow	kg/s	-	638.06	638.06	638.06
TSFC	g/kN-s	13.1543	12.3997	13.2694	13.1543
FC	kg/s	0.731	0.689	0.7378	0.7314
TSFC/FC difference with respect to Nickol et al. [130]	%	-	- 5.737	+ 0.875	0
Bare engine weight	kg	6,789	6,992	7,170	7,150
Bare engine weight difference with respect to Nickol et al. [130]	%	-	+ 2.99	+ 5.612	+ 5.317
Gear ratio		-	3.5	3.5	3.5
Cooling flow	%	-	20	20	20
Ratio of temperatures at turbine inlet and fan inlet (T_4/T_2)		-	6.844	7.06	7.05
Power off-take	kW	150	150	150	150
LPT inlet temperature	K	-	1,139	1,186	1,180

It can be observed from Table C.4 that the engine weights of the 1st case, 2nd case and 3rd case, compared to the engine weight from the study by Nickol et al. [130], are greater by approximately 200 kg (+2.99% difference), 380 kg (+5.61% difference), and 360 kg (+5.32% difference), respectively. These differences in engine weights are attributable to the unknowns from the study by Nickol et al. [130], such as:

- Engine materials,
- Turbo-machinery stage count,
- Gear ratio,
- Pressure ratios of IPC and HPC,
- Cooling flows, and
- Component efficiencies

Table C.5. Comparison of component polytropic efficiencies between the three cases of the present model

Components		Component polytropic efficiencies		
		1st case [123]	2nd case [188]	3rd case
Fan	Inner	0.928	0.910	0.902
	outer		0.904	0.912
IPC		0.925	0.920	0.920
HPC		0.912	0.910	0.908
HPT		0.944	0.890	0.896
LPT		0.956	0.922	0.925

The engine material selection has direct impact on the engine weight. CMC is the only material known to be used in the hot section of the engine modelled by Nickol et al. [130] and therefore assumption was made to use conventional materials in all components except HPT and combustor. As mentioned before, is very likely that PMC 'might' be used in the engine fan section by Nickol et al. [130] in their study. Additionally, parameters that are directly

linked to each other such as gear ratio, IPC and HPC pressure ratio, and turbomachinery stage count and efficiencies, all have a considerable impact on the engine weight. Moreover, cooling flows can significantly affect both the TSFC (directly) and weight (indirectly). Lastly, it is to be noted that the engine weight calculation (with disk optimisation) conducted here is not as rigorous as discussed in the section 6.4, because the off-design points are not considered here (as reasoned before while defining the scope of this validation case). Therefore, disk weight optimisation, and resultantly the bare engine weight estimation, is just limited to the on-design point.

In the first case, where the model uses future component efficiencies, the model predicts TSFC or FC and bare engine weight with -5.74% and +2.99% difference, respectively. For the second case, where the model uses present component efficiencies, the model predicts TSFC or FC, and bare engine weight with +0.875% and +5.612% difference, respectively. Lastly for the third case, where the model component efficiencies are set as design variables, the model predicts TSFC/FC and bare engine weight with 0% and +5.317% difference, respectively. As mentioned above, second and third case appear to be realistic and closer to study by Nickol et al. [130]. Therefore, for these two cases, it is observed that the proposed model estimates the engine TSFC and FC with high accuracy (<0.88% difference) as compared to the study by Nickol et al. [130]. These predictions are well within the set criteria of prediction difference of ±5% from literature for a successful conceptual design. In terms of engine weights, there is a lot of unknown information from the study of Nickol et al. [130], which is underscored and discussed above in detail. For the second and third case, there is a difference of +5.612% and +5.317% in bare engine weight, respectively. Despite these mentioned unknowns, the model predicts engine weights with reasonable accuracy. These predictions are similar in magnitude to the set criteria of prediction difference of ±5% from literature for a successful conceptual design. This concludes the second validation case.

C.1.3. Conclusion of the validation cases

The proposed model can successfully replicate the engine performance in both validation cases, considered in this section. It is observed that the success of the validation process is also dependent on the pool of the known information from the study to be replicated. In the first validation case, the proposed model predicted both engine performance and its weight with high accuracy, where both performance metrics and engine weight predictions fall well within the set criteria of prediction difference of ±5%. In the second validation case, the proposed model predicted the engine performance with high accuracy, and the accuracy of engine weight prediction was reasonable despite not knowing the critical engine design parameters from the study to be replicated i.e. study by Nickol et al. [130]. In the second case, TSFC and FC predictions are well within the set criteria of prediction difference of ±5% from literature for a successful conceptual design; and the bare engine weight prediction by the model, despite a plethora of identified unknowns, provided predictions that are similar in magnitude to the set criteria of prediction difference for a successful conceptual design. This can therefore be considered a satisfactory validation process. Overall, a strong confidence has now been developed on the proposed model, through this scientific procedure.

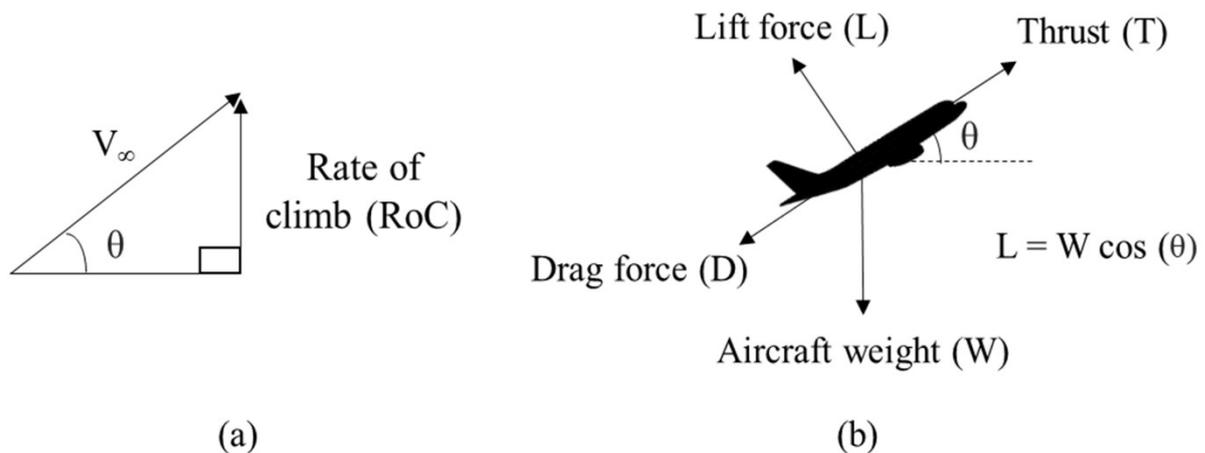### C.2   Service ceiling equation derivation

Figure C.1. Geometry of flight during climb and aircraft force balance diagram

$$\text{Rate of climb (RoC)} = \left(\frac{Power\ available - Power\ required}{Aircraft\ weight}\right) = \frac{TV_\infty - DV_\infty}{W}$$

Referring to Figure C.1 (a), $\text{RoC} = V_\infty \sin\theta$ and/or $\theta = \sin^{-1}\left(\frac{RoC}{V_\infty}\right)$

Substituting RoC definition into the above equation, $V_\infty\left(\frac{T-D}{W}\right) = V_\infty \sin\theta$

$\sin\theta = \left(\frac{T-D}{W}\right) = \frac{T}{W} - \frac{D}{W}$, referring to Figure C.1 (b), $W = \frac{L}{\cos\theta}$

$\sin\theta = \frac{T}{W} - \frac{D}{W} = \frac{T}{W} - \frac{\cos\theta}{L/D}$; substituting $\theta = \sin^{-1}\left(\frac{RoC}{V_\infty}\right)$ here, $\sin\theta = \frac{T}{W} - \frac{\cos\left(\sin^{-1}\left(\frac{RoC}{V_\infty}\right)\right)}{L/D}$

For a transport jet θ_{max} occurs at $(L/D)_{max}$, $\sin\theta_{max} = \frac{T}{W} - \frac{\cos\left(\sin^{-1}\left(\frac{RoC}{V_\infty}\right)\right)}{(L/D)_{max}}$

Substituting the relation $\frac{RoC}{V_\infty} = \sin\theta$, $\frac{RoC}{V_\infty} = \frac{T}{W} - \frac{\cos\left(\sin^{-1}\left(\frac{RoC}{V_\infty}\right)\right)}{(L/D)_{max}}$

Rearranging the above equation, $T = W\left(\frac{RoC}{V_\infty} + \frac{\cos\left(\sin^{-1}\left(\frac{RoC}{V_\infty}\right)\right)}{(L/D)_{max}}\right)$

Using trigonometry, $\cos(\sin^{-1}x) = \sqrt{1-x^2}$ [378]

$$T = W\left(\frac{RoC}{V_\infty} + \frac{\sqrt{1 - \left(\frac{RoC}{V_\infty}\right)^2}}{(L/D)_{max}}\right)$$

C.3 Aircraft weight and fuel consumption breakdown over flight mission

Using the aircraft weight sizing process detailed in section 7.4, the aircraft weight and the fuel consumption over the flight mission are calculated for the baseline case (Jet-A BWB aircraft), 100% SPK, and three cases of LH$_2$ aircraft. Tables C.6, C.7, C.8, C.9, and C.10 provide the FFs, aircraft weight and fuel consumption over one flight mission for Jet-A BWB aircraft, case 1 (LH$_2$), case 2 (LH$_2$), case 3 (LH$_2$), and 100% SPK, respectively. It can be observed that the ratio of the $W_{F,block}$ of Jet-A case and case 1, 2, and 3 is 3:1, 3.06:1, and 3.13:1, respectively.

Table C.6. Fuel fractions, aircraft weight and fuel consumption over flight mission of Jet-A BWB aircraft

No.	Segment	FF	Start weight	Fuel used
		-	kg	kg
1	Engine start and warm-up	0.9964	236,398	847
2	Taxi-out	0.9964	235,551	844
3	Take-off	0.9982	234,708	420
4	Climb	0.9975	234,287	584
5	Cruise	0.7474	233,704	59,035
6	Descent and approach	0.9964	174,669	626
7	Loiter	0.9846	174,043	2,678
8	Land, taxi-in and shutdown	0.9971	171,366	491
	Total	0.72	170,875 (weight of aircraft at the end of flight mission)	$W_{F,block} =$ 65,523

The ratio of gravimetric energy densities of LH$_2$ fuel and Jet-A is (120/43.2=) 2.78. The above ratio of the block fuel consumption of Jet-A aircraft and LH$_2$ aircraft is ~3:1 as compared to the ratio of the gravimetric energy densities of LH$_2$ and Jet-A of 2.78:1. This means that LH$_2$ aircraft design analysis, in general, cannot be just limited in terms of the effect of improved TSFC due to the use of a high gravimetric energy density fuel (like LH$_2$) in propulsion systems. The effect of the aircraft weight reduction (and thrust requirement reduction leading to smaller engines the resulting reduction in the engine weight) while carrying lesser weight of a high gravimetric energy density fuel (like LH$_2$), also contributes

to the above ratio of $W_{F,block}$ (of Jet-A aircraft and LH$_2$ aircraft) of ~3:1, though as observed the effect of improved TSFC is dominant. For 100% SPK cases (Table C.10), $W_{F,block}$ is of similar magnitude as that of Jet-A.

Table C.7. Fuel fractions, aircraft weight and fuel consumption over flight mission of LH$_2$ case 1

No.	Segment	FF	Start weight	Fuel used
		-	kg	kg
1	Engine start and warm-up	0.9987	195,325	244
2	Taxi-out	0.9987	195,080	244
3	Take-off	0.9994	194,837	122
4	Climb	0.9991	194,715	172
5	Cruise	0.8984	194,543	19,758
6	Descent and approach	0.9987	174,786	218
7	Loiter	0.9947	174,567	932
8	Land, taxi-in and shutdown	0.9990	173,635	174
	Total	0.89	173,461 (weight of aircraft at the end of flight mission)	$W_{F,block} =$ 21,863

Table C.8. Fuel fractions, aircraft weight and fuel consumption over flight mission of LH$_2$ case 2

No.	Segment	FF	Start weight	Fuel used
		-	kg	kg
1	Engine start and warm-up	0.9987	194,177	243
2	Taxi-out	0.9987	193,935	242
3	Take-off	0.9994	193,692	121
4	Climb	0.9991	193,571	170
5	Cruise	0.8998	193,401	19,384
6	Descent and approach	0.9987	174,018	218
7	Loiter	0.9947	173,800	923
8	Land, taxi-in and shutdown	0.9990	172,887	173
	Total	0.89	172,704 (weight of aircraft at the end of flight mission)	$W_{F,block} =$ 21,473

Table C.9. Fuel fractions, aircraft weight and fuel consumption over flight mission of LH$_2$ case 3

No.	Segment	FF	Start weight	Fuel used
		-	kg	kg
1	Engine start and warm-up	0.9987	192,677	241
2	Taxi-out	0.9987	192,436	241
3	Take-off	0.9994	192,196	120
4	Climb	0.9992	192,076	162
5	Cruise	0.9010	191,913	19,003
6	Descent and approach	0.9987	172,910	216
7	Loiter	0.9948	172,694	894
8	Land, taxi-in and shutdown	0.9990	171,800	172
	Total	0.89	171,628 (weight of aircraft at the end of flight mission)	$W_{F,block} =$ 21,049

Table C.10. Fuel fractions, aircraft weight and fuel consumption over flight mission of 100% SPK

No.	Segment	FF	Start weight	Fuel used
		-	kg	kg
1	Engine start and warm-up	0.9965	234,798	824
2	Taxi-out	0.9965	233,974	821
3	Take-off	0.9982	233,152	409
4	Climb	0.9976	232,743	568
5	Cruise	0.7514	232,175	57,727
6	Descent and approach	0.9965	174,449	612
7	Loiter	0.9849	173,837	2,623
8	Land, taxi-in and shutdown	0.9972	171,213	481
	Total	0.73	170,733 (weight of aircraft at the end of flight mission)	$W_{F,block} =$ 64,065

C.4 LH_2 BWB aircraft landing weight analysis

Considering an emergency situation, the landing weight of an aircraft is an important factor. The 'safe' landing weight is dependent on the structural weight of the aircraft. Roskam [198] recommends 0.84 to be an average permissible ratio of the aircraft landing weight and the aircraft GTOW, for a transport jet. In the event of an emergency landing immediately after take-off, the pilot performs fuel jettison or dumps the conventional jet fuel in air so that the aircraft weight goes below its permissible landing weight. However, in the case of an aircraft powered by LH_2, this highly flammable fuel cannot be dumped into the atmosphere in events of emergency landing. Since the present chapter uses the same airframe/structure from the study by Nickol et al. [130] [NASA N+2 BWB-GTF 301 PAX (Jet-A) aircraft], the permissible landing weight of Jet-A BWB aircraft, BWB LH_2 aircraft (all three cases), and NASA N+2 BWB-GTF 301 PAX (Jet-A) aircraft, are the same. Therefore, the GTOW of the NASA N+2 BWB-GTF 301 PAX (Jet-A) aircraft ($GTOW_{NASA}$) determines the average permissible landing weight for the said aircraft, Jet-A BWB aircraft and BWB LH_2 aircraft (all three cases). Table 7.13 lists the ratio of $GTOW/GTOW_{NASA}$ for Jet-A BWB aircraft and BWB LH_2 aircraft (all three cases). It can be observed that the $GTOW/GTOW_{NASA}$ ratios for case 1, 2, and 3 of BWB LH_2 aircraft are 0.806, 0.801, and 0.795, respectively. This means that with BWB LH_2 aircraft (all three cases), there is no need to conduct fuel jettison of a highly flammable hydrogen fuel in the event of an emergency landing, because its GTOW is lesser than the average permissible landing weight considering its structure. This finding is of great significance considering the safety issue associated with LH_2 use in an aircraft.

C.5   Weight sizing of BWB LNG aircraft

Similar to Chapter 4, two LNG cases are considered here for BWB powered by LNG (LCV of 50 MJ/kg and density 424 kg/m³ [47]). The first LNG case uses a hypothetical value of $\eta = 0.78$, similar to LH_2 case. In the second LNG case, a present-day (best) value of $\eta = 0.63$ is used, which is similar to the values used in transportation of LNG fuel via trucks [207]. In the LNG BWB aircraft weight sizing process, similar process schematic (Figure 7.5) and methodology discussed in section 7.4 is used for both LNG cases, as that used for (same thrust requirement) LH_2 case 1 (LNG has similar LCV on the order of Jet-A but has approximately half the Jet-A fuel density). This is based on the finding of Chapter 4. For both LNG cases, the fuel will be stored in the volume available as per the tanks designed for LH_2 case 1 in BWB wings, which has the maximum fuel volume storage requirement. The FF for Jet-A and both LNG cases are calculated according to the methodology discussed in section 7.4, and these are listed in Table C.11. The propulsion system is designed according to the methodology detailed in section 6.4 in Chapter 6 using GasTurb 13. Table C.12. lists the performance of propulsion system at different points in the flight mission profile for Jet-A and LNG (two cases) and their weights.

Table C.13 provides a comparison of BWB aircraft performance powered by Jet-A, LH_2, and LNG (both cases). The effect of LNG cryogenic tank η can be observed from Table C.13. With increasing η, the aircraft range and $W_{F,total}$ increases, and the OEW decreases. This is similar to the observation made in Chapter 4 for tube-wing LNG aircraft. For both LNG cases, the GTOW = MTOW (of BWB Jet-A structure) during the weight sizing process. Both BWB LNG cases

do not meet the design target range as the GTOW = MTOW and the weight sizing process ends, and no more fuel can be added to the aircraft despite the availability of the tank volume (similar to LH$_2$ case 1 which has highest volume requirement). For LNG C1 case which has highest cryogenic tank η of the two cases, the aircraft reaches a range of 12,052 km. Therefore, LNG is not identified as an alternative fuel even for use in an N+2 BWB aircraft (since target design range is not met).

Table C.11. FFs for Jet-A, and FFs for LNG cases

Segment	Operation	Modified FFs (Jet-A)	FFs (LNG C1)	FFs (LNG C2)
1	Engine start and warmup	0.9964	0.9969	0.9969
2	Taxi-out	0.9964	0.9969	0.9969
3	Takeoff	0.9982	0.9985	0.9985
4	Climb	0.9975	0.9979	0.9979
5	Cruise	0.7474	0.8504	0.8077
6	Descent	0.9964	0.9969	0.9969
7	Loiter	0.9846	0.9881	0.9879
8	Land, taxi-in, engine shutdown	0.9971	0.9975	0.9975
	Overall FF	0.72	0.83	0.79

Table C.12. Performance of propulsion system at different points in the flight mission profile for Jet-A and LNG (two cases) and their weights

		Units	Jet-A	LNG C1	LNG C2
Total propulsion systems weight		kg	12,319	12,319	12,319
TOC	Mach, altitude	- , m	0.8 at 10,668 m	0.8 at 10,668 m	0.8 at 10,668 m
	TSFC	g/kN-s	12.400	10.669	10.669
Cruise	Mach, altitude	- , m	0.84 at 10,668 m	0.84 at 10,668 m	0.84 at 10,668 m
	TSFC	g/kN-s	12.667	10.898	10.898
SLS	Mach, altitude	- , m	0 at 0 m	0 at 0 m	0 at 0 m
	TSFC	g/kN-s	5.124	4.409	4.409
Climb	Mach, altitude	- , m	0.47 at 5,334 m	0.47 at 5,334 m	0.47 at 5,334 m
	TSFC	g/kN-s	9.798	8.430	8.430
Loiter	Mach, altitude	- , m	0.6 at 1,500 m	0.6 at 1,500 m	0.6 at 1,500 m
	TSFC	g/kN-s	12.175	10.475	10.475

Table C.13. Comparison of BWB aircraft performance powered by Jet-A, LH$_2$, and LNG (both cases)

BWB	Cryogenic tank η	GTOW (kg)	OEW (kg)	OEW/GTOW$_{Jet-A}$	$W_{F,total}$ (kg)	$W_{F,block}$ (kg)	Cryogenic tank volume (m^3)	R (km)
Jet-A	-	236,398	110,150	0.466	72,678	65,523	-	13,890
LNG C1	0.78	236,398	126,588	0.535	56,241	50,704	132.65	*12,052*
LNG C2	0.63	236,398	137,591	0.582	45,238	40,784	106.7	*9,263*
LH$_2$ C1	0.78	195,325	117,505	0.497	24,250	21,863	341.6	13,890
LH$_2$ C2	0.78	194,177	116,790	0.494	23,818	21,473	335.5	13,890
LH$_2$ C3	0.78	192,677	115,760	0.49	23,348	21,049	329	13,890
100% SPK	-	234,798	110,169	0.466	71,061	64,065	-	13,890

Appendix D

D.1.   Fuel manufacturing process

D.1.1   Jet-A and 100% SPK

The fuel manufacturing process can be broadly broken down into four steps – raw material extraction, transportation of raw materials to the fuel refining unit, fuel refining, and fuel transportation to the storage facility.

Kerosene or jet fuel is manufactured from crude oil (fossil fuel). The extracted crude oil is transported to the refining plant where the crude oil undergoes refining, distillation, cracking, reforming, and separation [379]. During the production of kerosene several other co-products like petrol, gas oil, diesel oil, and residual oil are formed. After kerosene is manufactured, it is transported to the storage facility and/or airport.

In Chapter 8, four SPK production pathways are considered for evaluation – ATJ, STJ, HEFA, and FT. The production process of these four pathways is discussed below:

1. ATJ fuel is produced from alcohols that are sourced from sugar containing feedstocks and lignocellulosic biomass by fermentation [379]. In the ATJ production, alcohols are dehydrated, and water is removed to form hydrocarbon chains via oligomerisation. Later these are distilled for fractioning the hydrocarbons in terms of chain lengths or separate products (ibid).

2. STJ fuel is manufactured from biomass feedstocks that contain sugars [379]. When such feedstocks are fermented, hydrocarbons are formed which are further refined and catalytically improved to form SPK (ibid).

3. FT fuel is primarily manufactured from syngas which can be sourced from any carbon containing matter [379]. Coal and natural gas are presently used as common feedstocks for producing FT fuel. Syngas is commonly manufactured via gasification of lignocellulosic biomass feedstocks such as energy crops, municipal solid waste, and agricultural residues. The biomass undergoes chemical process at very high pressure and temperature in the presence of air and steam. The need for external electric power for the FT process is low. This is because during the FT conversion process, syngas is partly converted to wax and partly to produce electricity that is used for FT conversion process. The co-products of this process are utilised to make hydrogen that is required for hydrocracking of the wax formed during the process. This is followed by separation of products (ibid).

4. HEFA SPK is produced from feedstocks that contain renewable oil i.e., oil extracted from plants, waste greases, and animal fats [379]. Renewable oil has properties similar to jet fuel and conversion to SPK is an easy process. Such oils undergo hydrotreatment followed by hydrocracking to produce the required hydrocarbon chain. During this process the oxygen from oil is removed. The products are separated into naphtha, diesel, and jet fuel (ibid).

The present fuel readiness level of ATJ, STJ, FT, and HEFA are 7, 6 – 7, 7, and 9 respectively (ibid).

D.1.2   Hydrogen

- Natural gas

Hydrogen is produced from natural gas using process known as SMR, which is an endothermic process. At present, hydrogen is primarily produced using SMR process. In SMR, methane reacts with steam at high pressure (3–25 bar pressure) using a catalyst to produce carbon monoxide, hydrogen, and a small amount of carbon dioxide [380].

- Coal

Organic matter, for example coal, is converted to hydrogen, carbon dioxide, and CO at temperatures above 700°C without combustion, and this process is called as gasification [381]. Further CO reacts with water to form more hydrogen and carbon dioxide via water-gas shift reaction. Hydrogen is separated from the products using special membranes and/or adsorbers (ibid).

- COG

COG is formed when coal is heated to 1100°C without the presence of air. COG typically contains ethylene (5%), CO (10%), CH_4 (34%), and H_2 (51%) [382]. COG undergoes steam reforming followed with water-gas shift reaction to produce H_2 and CO_2 [383].

- By-product of NGL steam cracking

NGLs are hydrocarbons such as ethane, propane, butane, isobutane, and pentane [384]. Steam crackers convert hydrocarbon/NGLs to light olefins using thermal cracking process (converting long-chain hydrocarbon to short-chain hydrocarbons) to produce hydrogen as a by-product [385].

- Solar PV

The electricity produced from solar energy using PV system, is used for the electrolysis of water to produce hydrogen [386].

- Nuclear thermochemical cracking of water

Sulphur – Iodine process is a common thermo-chemical process used for splitting water to produce hydrogen [387]. The first step is called as Bunsen reaction where iodine and sulphur dioxide react with water at 120 °C to produce hydriodic acid and sulphuric acid. In the second step, sulphuric acid is decomposed to sulphur dioxide at high temperature (around 1,000 °C). In the final step, hydriodic acid is decomposed to produce iodine and hydrogen at above 300 °C (ibid).

- Nuclear high temperature gas reactor

A nuclear high temperature gas reactor is a graphite moderated and helium cooled reactor [387]. A heat exchange system is used to cool off the helium and heat up water to produce steam. Electricity is produced from the steam using turbines and hot water from the turbine outlet is electrolysed to produce hydrogen, using the electricity produced from turbine (ibid).

- Biomass

Hydrogen can be produced from biomass using gasification process which is described above. Since growing biomass reduces atmospheric carbon dioxide, the net carbon emissions of this process could be low, especially if carbon capture and storage technology is employed [381].

- Integrated fermentation

Hydrogen can be produced from biological routes that use sunlight (photosynthesis and photolysis), fermentative bacteria (dark fermentation i.e. no light), and electrolysis of organic matter via microbial metabolism with small external energy input (microbial electrolysis cell [MEC]) [388]. The effluent from the dark fermentation route is rich in organic matter and this could be utilised by MEC for producing additional hydrogen. This process is an integrated pathway that combines MEC and dark fermentation for hydrogen production (ibid).

- HTE with SOEC

HTE uses both electricity and thermal energy for splitting water employing SOEC and hydrogen is produced [389]. In this process, water is heated so that it evaporates which requires a high amount thermal energy. This thermal energy is provided either directly in the form of steam to the electrolyser or via an external heat input (ibid). The heat input could come from renewable energy source like solar, wind, nuclear, etc. and the embodied carbon for hydrogen production could be reduced. In Chapter 8, two electricity source types are studied – Nuclear HTGR and natural gas combined cycle.

- By-product of chlorine manufacturing plant

The electrolysis of a sodium chloride solution (brine) is called as the Chlor-alkali process [390]. Hydrogen gas is one of the co-products of this process along with chlorine and sodium hydroxide (ibid).

D.2. Other unintended environmental and social impacts – Resource consumption

Figure D.1 provides the comparison of fossil fuel use for different LH$_2$ and 100% SPK feedstock and pathways for 2020 and 2050 US energy mix scenarios. It can be observed that for the three identified LH$_2$ cases (Biomass w CS LUSME, Biomass w CS LBIGCC, and/or IF w CS), the use of fossil fuels is significantly greater (indicative of poor process efficiency) compared to Jet-A production (difference of order of magnitude).
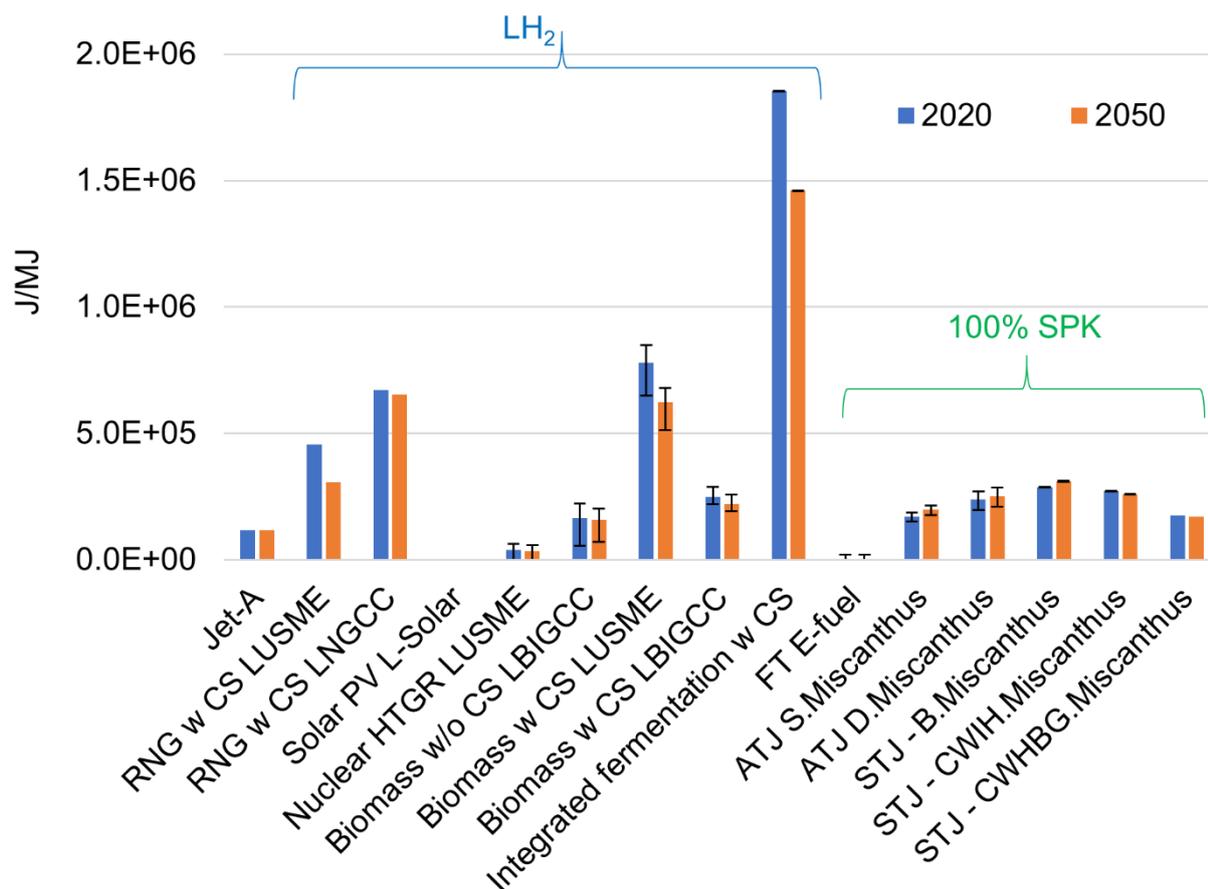
Figure D.1. Comparison of fossil fuel use for different LH$_2$ and 100% SPK feedstock and pathways for 2020 and 2050 US energy mix scenarios

The net WTWa CO_2 equivalent emissions are lower for these three cases due to the employment of carbon sequestration. The greater use of fossil fuels (indirectly) for producing LH$_2$ from the above three feedstocks/pathways compared to Jet-A, is an unintended natural resource (environmental) impact which none of the studies in literature have accounted. This greater (indirect) use of fossil fuels for the three feedstock/pathways is due to the poor manufacturing (supply-chain) process energy efficiency (from the point of cultivating crops to the point of producing hydrogen from biomass). This needs to be reduced for US based LH$_2$ production from the above three routes or could be lesser in regions that employ greater renewable energy resources (like European countries) for power production. This effect of greater renewable energy resources in the energy mix can be observed from Figure D.1 between 2020 and 2050 US energy mix scenarios. Additionally, the indirect use of fossil fuels can be reduced for the said three routes by improving the energy efficiency of fuel manufacturing and its supply chain. For 100% SPK cases, the fossil fuel use is greater than Jet-A but of the similar order.

Figure D.2 shows the comparison of water consumption for different LH$_2$ and 100% SPK feedstock and pathways for 2020 and 2050 US energy mix scenarios. It can be observed that for the three identified LH$_2$ cases (Biomass w CS LUSME, Biomass w CS LBIGCC, and/or IF w CS), the water consumption is significantly greater compared to Jet-A production due to the water required for cultivation of biomass feedstocks/crops. The greater use of water for producing LH$_2$ from the above three feedstocks/pathways compared to Jet-A, is an unintended resource (environmental and social) impact which none of the studies in literature have accounted. For biomass based 100% SPK cases, water consumption is greater than Jet-A due to the water required for crop cultivation.
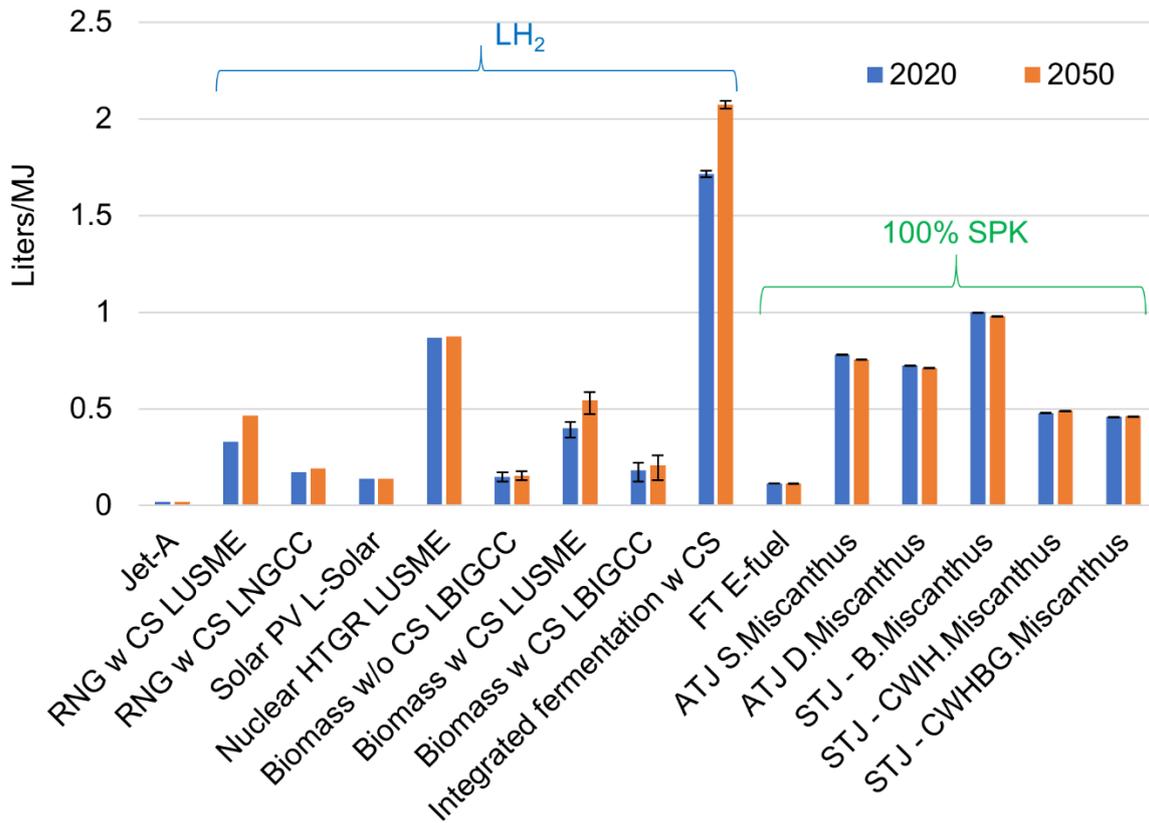
Figure D.2. Comparison of water consumption for different LH₂ and 100% SPK feedstock and pathways for 2020 and 2050 US energy mix scenarios

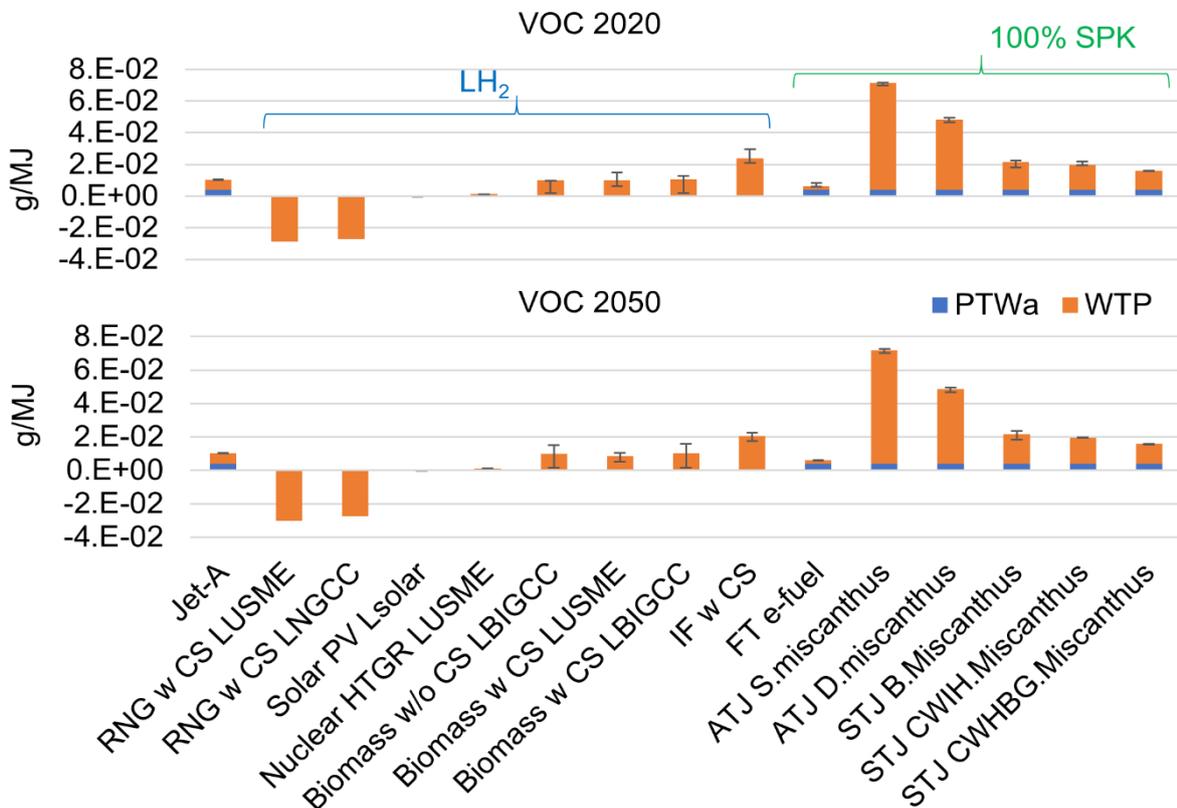## D.3. Other unintended environmental and social impacts – Emissions

Figure D.3. WTWa VOC emission comparison for different LH₂ and 100% SPK feedstock and pathways for 2020 and 2050 US energy mix scenarios including non-CO₂ effects
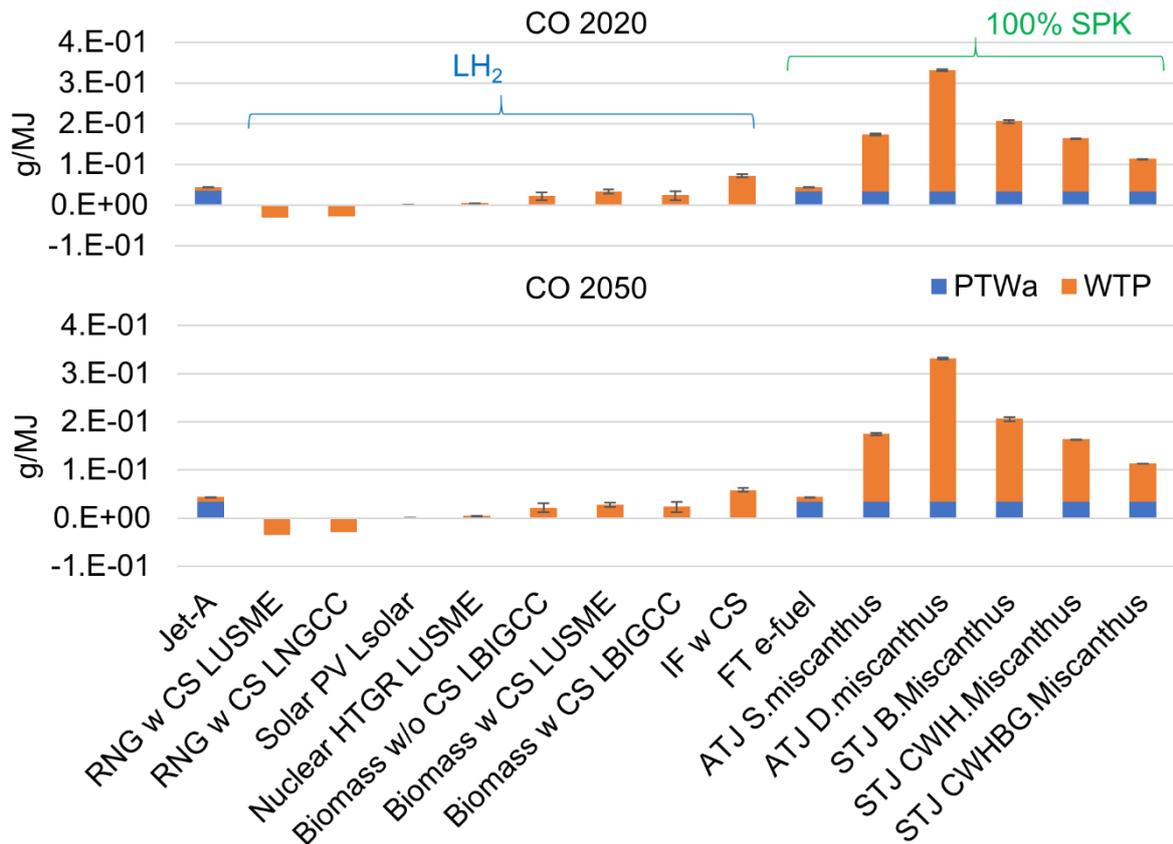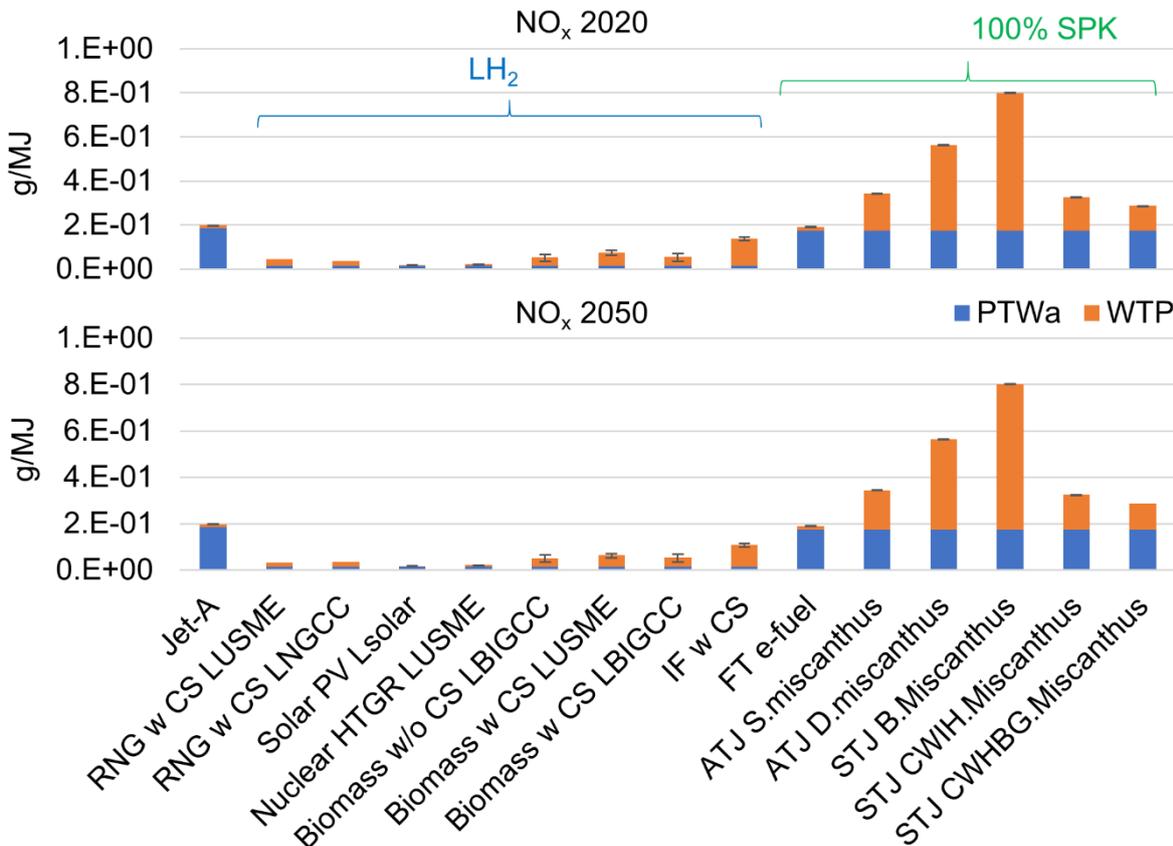
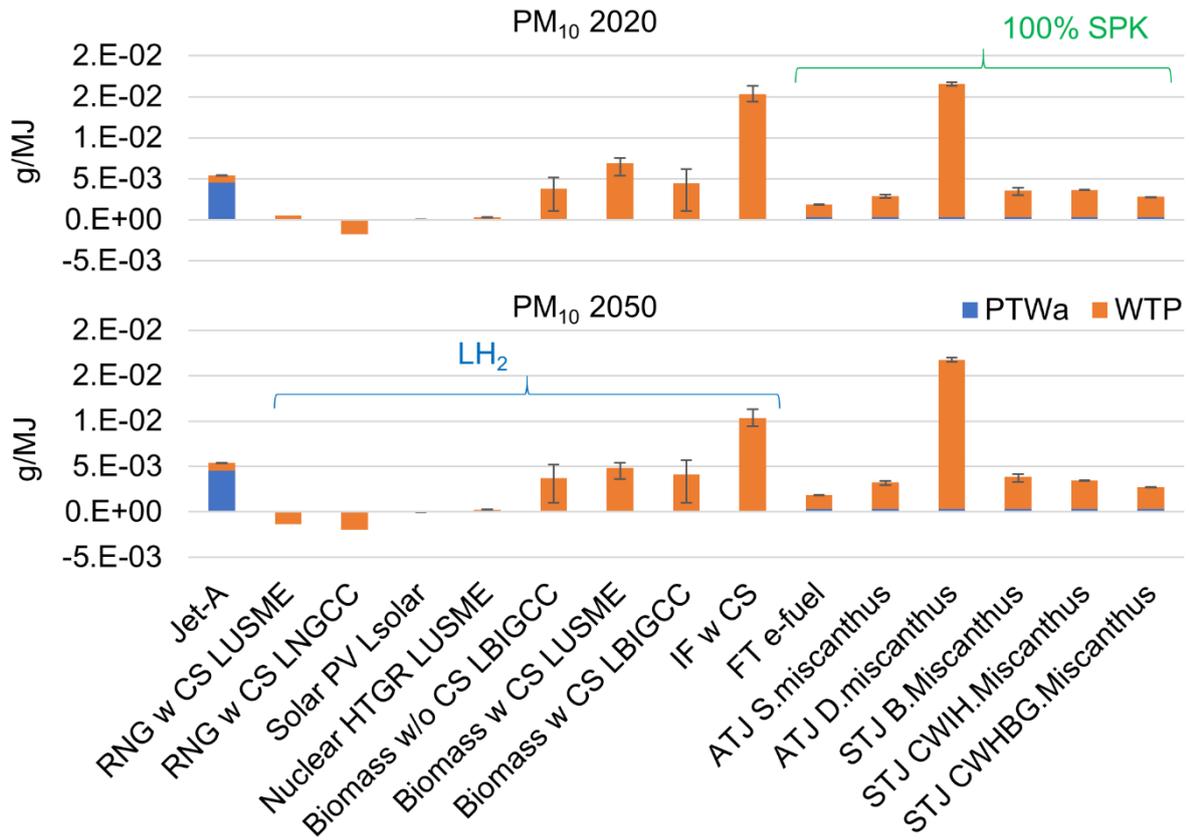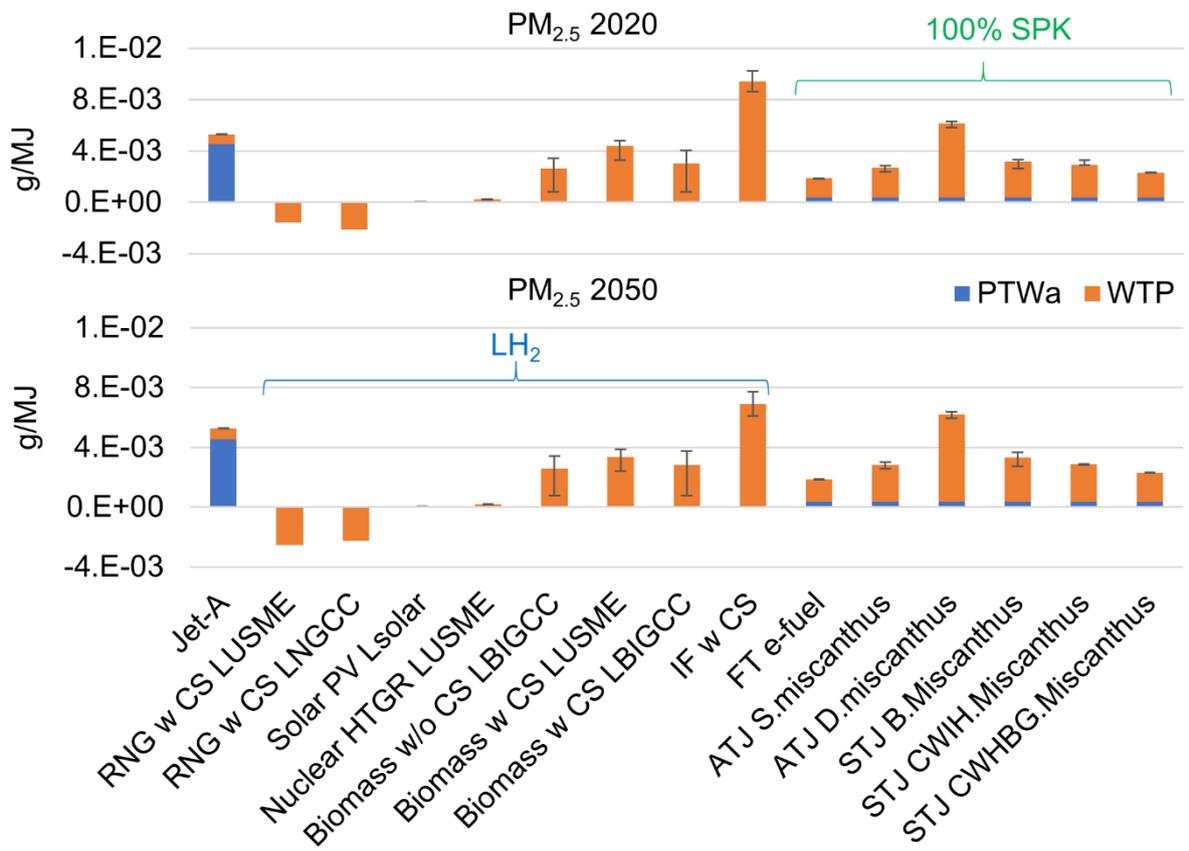**Figure D.4. WTWa CO emission comparison for different LH₂ and 100% SPK feedstock and pathways for 2020 and 2050 US energy mix scenarios including non-CO₂ effects**
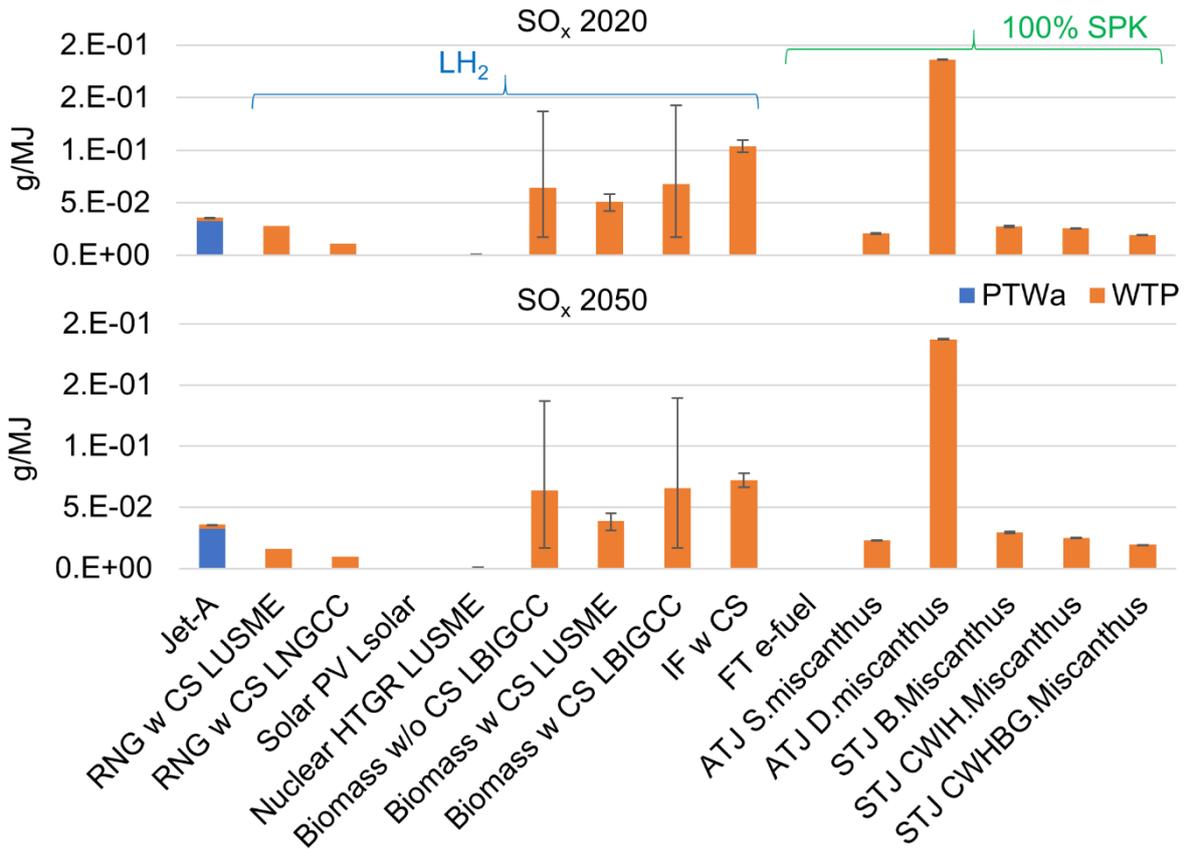

Figure D.5. WTWa NOₓ emission comparison for different LH₂ and 100% SPK feedstock and pathways for 2020 and 2050 US energy mix scenarios including non-CO₂ effects

Figure D.6. WTWa PM$_{10}$ emission comparison for different LH$_2$ and 100% SPK feedstock and pathways for 2020 and 2050 US energy mix scenarios including non-CO$_2$ effects

Figure D.7. WTWa PM$_{2.5}$ emission comparison for different LH$_2$ and 100% SPK feedstock and pathways for 2020 and 2050 US energy mix scenarios including non-CO$_2$ effects

Figure D.8. WTWa SO$_x$ emission comparison for different LH$_2$ and 100% SPK feedstock and pathways for 2020 and 2050 US energy mix scenarios including non-CO$_2$ effects
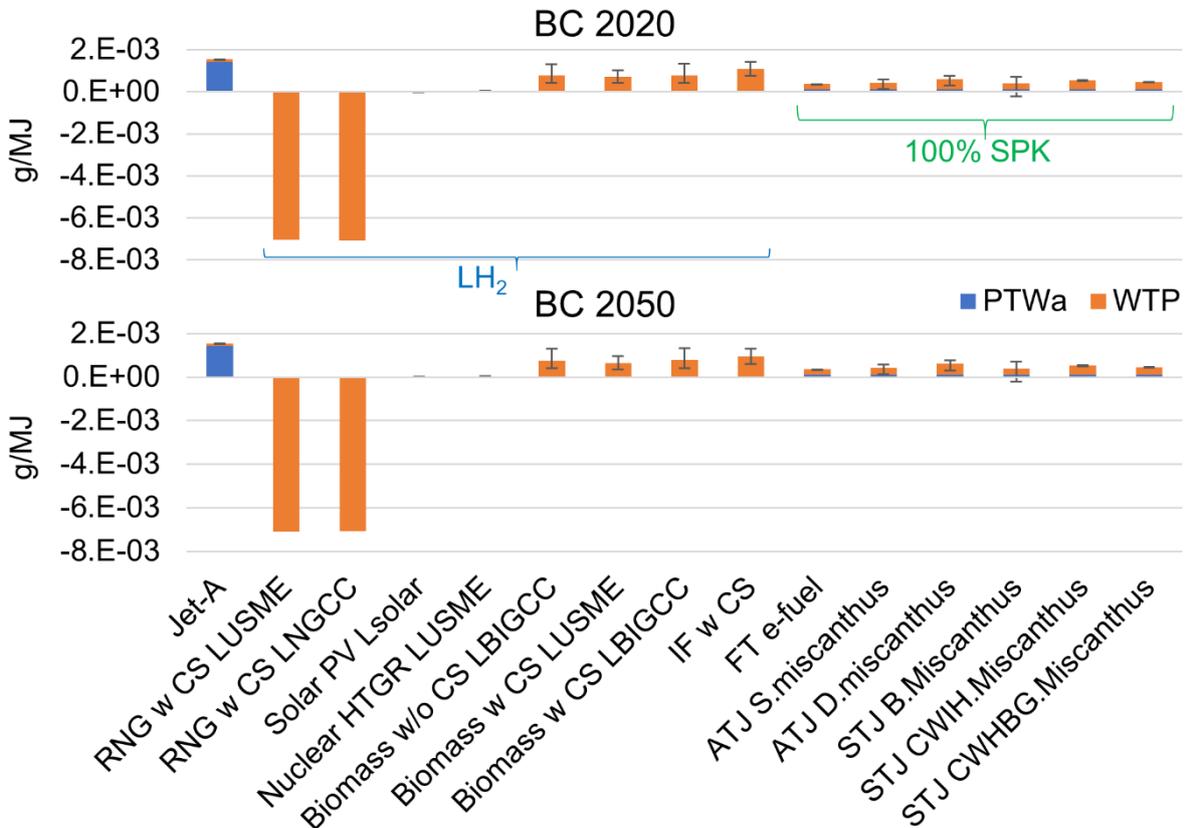

Figure D.9. WTWa BC emission comparison for different LH$_2$ and 100% SPK feedstock and pathways for 2020 and 2050 US energy mix scenarios including non-CO$_2$ effects
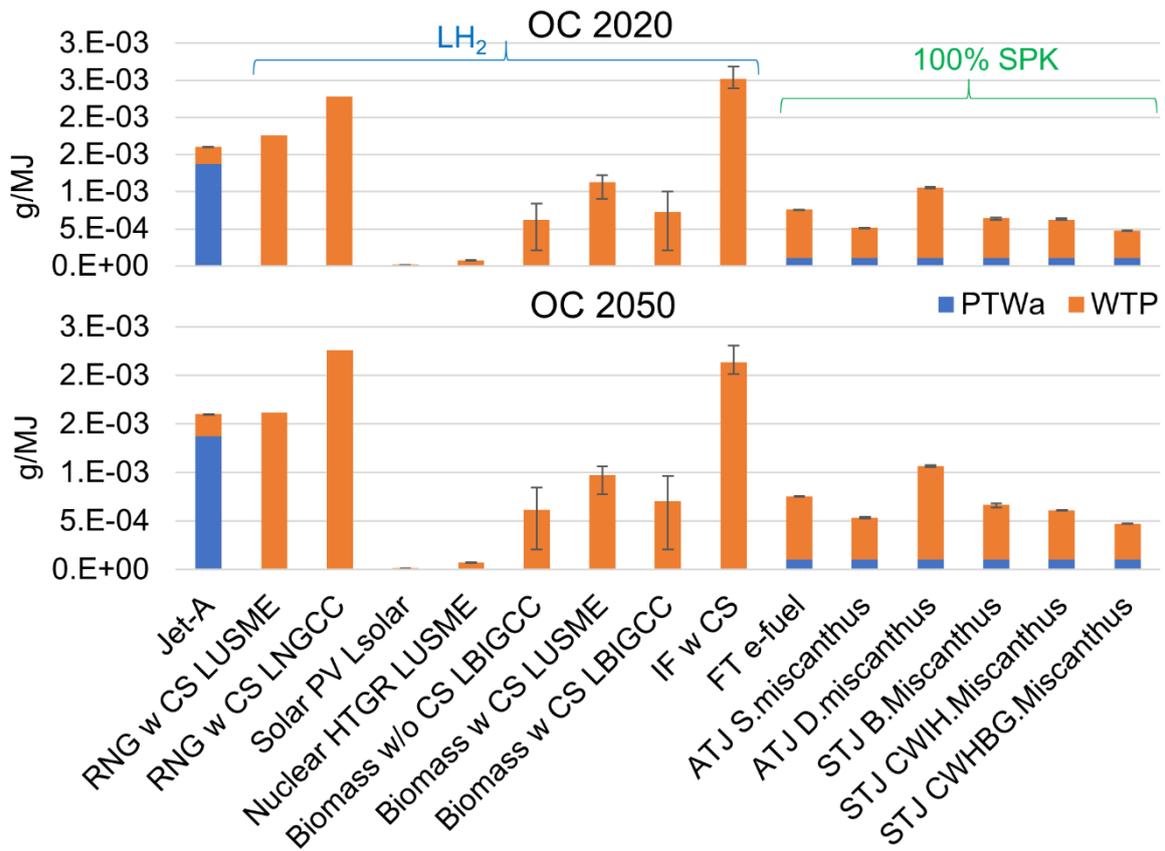
Figure D.10. WTWa OC emission comparison for different LH₂ and 100% SPK feedstock and pathways for 2020 and 2050 US energy mix scenarios including non-CO₂ effects